An Experimental Investigation into the Stress-Dependent Mechanical Behavior of Cohesive Soil with Application to Wellbore Instability

by

Naeem Omar Abdulhadi

Bachelor of Engineering in Civil and Environmental Engineering
University College London, University of London, England (2003)

Master of Science in Soil Mechanics and Environmental Geotechnics
Imperial College of Science, Technology and Medicine, University of London, England (2004)

Submitted to the Department of Civil and Environmental Engineering
in Partial Fulfillment of the Requirements for the Degree of

Doctor of Philosophy in Geotechnical and Geoenvironmental Engineering

at the

MASSACHUSETTS INSTITUTE OF TECHNOLOGY

September 2009

Signature of Author……
Department of Civil and Environmental Engineering
August 14, 2009

Certified by……
John T. Germaine
Senior Research Associate of Civil and Environmental Engineering
Thesis Supervisor

Certified by……
Andrew J. Whittle
Professor of Civil and Environmental Engineering
Thesis Supervisor

Accepted by...……
Daniele Veneziano
Chairman, Departmental Committee for Graduate Students

An Experimental Investigation into the Stress-Dependent Mechanical Behavior of Cohesive Soil with Application to Wellbore Instability

by

Naeem Omar Abdulhadi

Submitted to the Department of Civil and Environmental Engineering on August 14, 2009
in Partial Fulfillment of the Requirements for the Degree of
Doctor of Philosophy in Geotechnical and Geoenvironmental Engineering

ABSTRACT

This thesis investigates the mechanical behavior of cohesive soils with reference to the applications of wellbore instabilities through an extensive program of laboratory element and model borehole tests. The laboratory tests use Resedimented Boston Blue Clay (RBBC) as an analog test material.

Undrained triaxial shear tests have been performed on specimens that were K_0-consolidated to stress levels ranging from 0.15 to 10.0 MPa in both compression and extension shear modes. Compression tests were also performed on overconsolidated specimens.

Model borehole tests make use of two new automated, high pressure Thick-Walled Cylinder (TWC) devices to study the effects of the following parameters on the borehole response: mode of loading, specimen geometry, preshear lateral stress ratio, drainage conditions, consolidation stress level, stress history, and cavity volumetric strain rate. This testing program has been performed using small and large TWC devices with outer diameter, D_o=7.6cm and 15.2cm, respectively. Both devices allow for independent control of the vertical stress and the radial pressures acting on the inner and outer walls of the cylinder, as well as pore pressure.

The triaxial compression and extension test results demonstrate remarkable reductions in the undrained strength ratio (s_u/σ'_{vc}) with consolidation stress level, notable reduction in the stiffness ratio (E_u/σ'_{vc}), increase in the strain to mobilize the peak resistance (ε_f), and a significant decrease in the large strain friction angle (φ').

The model borehole data indicate that most of the reduction in cavity pressure occurs at volume strains less than 5% before the borehole becomes unstable. Increases in outer diameter and strain rate lead to a reduction in the minimum borehole pressure. The initial cavity stiffness ratio decreases as consolidation stress level increases. Drained tests have larger cavity strain at a given cavity pressure and lower minimum pressure than the undrained tests. The borehole closure curves were analyzed using a framework originally developed for interpreting undrained shear properties in model pressuremeter tests (Silvestri, 1998). Backfigured undrained strength ratios from these analyses range from s_u/σ'_{vc}=0.19-0.21 corresponding to an average between the measured triaxial compression and extension strength ratios. The relationship between s_u/σ'_{vc} and overconsolidation ratio is consistent with element tests.

Thesis Supervisor: John T. Germaine
Title: Senior Research Associate of Civil and Environmental Engineering

Thesis Supervisor: Andrew J. Whittle
Title: Professor of Civil and Environmental Engineering

ACKNOWLEDGEMENTS

I would like to express my deep appreciation and sincere gratitude to my thesis supervisor, Dr. John Germaine, for his continuous guidance, assistance, and motivation throughout my years at MIT. Dr. Germaine taught me a great deal about laboratory testing and soil behavior and was always available when I needed him. I greatly admire his experimental talents and problem solving skills. It has been a pleasure and great honor to work with him.

I would like to thank Professor Andrew Whittle, also my thesis supervisor, for the valuable contributions he provided throughout my work. His technical insights and meticulous review of my thesis are greatly appreciated.

I am indebted to Professors Herbert Einstein and Brian Evans for serving as members of my doctoral committee and for their helpful comments.

The MIT Wellbore Instability Project was sponsored by BP America Inc., Houston, and by the BP-MIT Major Projects Program. Dr. Steve Willson is the technical monitor for the project and has provided much valuable assistance for this research.

I am very grateful to Stephen Rudolph for his friendship and expert fabrication of the experimental equipment. His assistance with the machining has been instrumental to the success of this research project.

My gratitude also extends to Sheila Fay, Andre Dixon, Kris Kipp, Jeanette Marchocki, Patty Glidden, and the staff of the CEE department for their assistance and friendship.

Several colleagues deserve recognition for helping me with the laboratory work. Thanks to Safia Moniz for performing the triaxial extension tests. I am also grateful to Ray Janeiro, John Grennan, and Cullin Jones for their help with the equipment lifting and specimen preparation.

I would like to acknowledge my geotechnical friends and officemates: Antonios Vytiniotis, Nick Kontopoulos, Gonzalo Corral, Sherif Akl, Ray Janeiro, Bruno Silva, Maria Nikolinakou, Rita Sousa, Dimitrios Iliadelis, Kartal Toker, and Alejandro Abrams. Special thanks to Alessia Ferrari for her sincere friendship and for sharing the exciting and enjoyable times with me in Boston.

Many thanks to my ‘gang’ outside MIT: Carl Nehme, Tarek Hamade, JP Mondalek, Gaylee Saliba, and Raed Nasr, for their companionship. My appreciation also extends to my dear friends in London and back home.

Finally, I am most thankful to my parents, Omar and Malak, and to my sisters, Dina and Noura. They were always there to provide guidance, encouragement, consolation, courage, and inspiration. I gain my strength and dedication from their unconditional love and support.

My father dedicated his PhD thesis to my grandfather, Naim A. Abdulhadi

I am proud to dedicate this thesis to my father,

Omar N. Abdulhadi

Table of Contents

List of Tables

List of Figures

List of Symbols

AC	Alternating Current
A/D	Analog-to-Digital Converter
BASIC	Beginner's All-purpose Symbolic Instruction Code
BBC	Boston Blue Clay
CAD	Anisotropically Consolidated Drained Shear Test
CAU	Anisotropically Consolidated Undrained Shear Test
CF	Clay Fraction
CID	Isotropically Consolidated Drained Shear Test
CIU	Isotropically Consolidated Undrained Shear Test
CK_0U	K_0-Consolidated Undrained Shear Test
CK_0UC	K_0-Consolidated Undrained Compression Test
CK_0UDSS	K_0-Consolidated Undrained Direct Simple Shear Test
CK_0UE	K_0-Consolidated Undrained Extension Test
CL	Low Plasticity Clay
CR	Virgin Compression Ratio
CRS	Constant Rate of Strain
CU	Consolidated Undrained Test
D/A	Digital-to-Analog Converter
DC	Direct Current
DCDT	Direct Current Displacement Transducer
DSC	Directional Shear Cell Test
DSS	Direct Simple Shear Test
ESE	Effective Stress Envelope
ESP	Effective Stress Path
LIR	Load Increment Ratio
LVDT	Linear Variable Differential Transformer
MADC	Multi-Channel Analog to Digital Converter
MIT	Massachusetts Institute of Technology
NC	Normally Consolidated
NSP	Normalized Soil Parameter
OC	Overconsolidated
OCR	Overconsolidation Ratio
PC	Personal Computer
PID	Proportional-Integral-Derivative
PSC	Plane Strain Compression Shear Test
PSE	Plane Strain Extension Shear Test
PVC	Pressure-Volume Controller
RBBC	Resedimented Boston Blue Clay
SR	Swelling Ratio
TC	Triaxial Compression Shear Test
TE	Triaxial Extension Shear Test
TSHC	Torsional Shear Hollow Cylinder Test
TTA	True Triaxial Apparatus

TWC	Thick-Walled Cylinder
TX	Triaxial
USR	Undrained Strength Ratio (s_u/σ'_{vc})
UU	Unconsolidated Undrained Compression Test
SHANSEP	Stress History and Normalized Soil Engineering Properties
TSP	Total Stress Path
VCL	Virgin Compression Line

A (A_f)	Skempton's pore pressure parameter (at failure)
a’	Cohesion intercept
a, a’	Inner radius, deformed inner radius
B	Skempton's pore pressure parameter
b	Intermediate principal stress ratio
b, b’	Outer radius, deformed outer radius
C_c	Compression index
C_k	Permeability change index
C_s	Swelling index
C_α	Secondary compression index
$C_{\alpha\varepsilon}$	Secondary compression ratio
c_v	Coefficient of consolidation
c’	Cohesion intercept
D_i	Internal diameter
D_o	Outer diameter
E_u	Undrained secant Young’s modulus
E_{uMAX}	Undrained secant Young’s modulus (maximum)
e	Void ratio
e_0	Initial void ratio
G_s	Specific gravity
G_i	Initial shear modulus
H	Height
I_p	Plasticity index
K	Lateral coefficient of earth pressure
K_0	Coefficient of lateral earth pressure at rest
K_{0NC}	Coefficient of lateral earth pressure at rest for NC soil
K_c	Lateral coefficient of earth pressure at end of consolidation
k_v	Vertical hydraulic conductivity
L	Length
m	OCR exponent in SHANSEP equation for undrained strength ratio
m_v	Coefficient of volume change
p, p’	Average effective stress, $(\sigma_1 + \sigma_3) / 2$, $(\sigma'_1 + \sigma'_3) / 2$
p_h	Average effective stress in the horizontal plane
p_i	Internal pressure
p_m	Mean effective stress, $(\sigma_1 + \sigma_2 + \sigma_3) / 3$
p_o	Outer pressure
q	Shear stress, $(\sigma_1 - \sigma_3) / 2$

q_h	Shear stress in the horizontal plane
q_u	Unconfined compressive strength
R	Current pressuremeter radius
R_0	Initial pressuremeter radius
r^2	Coefficient of determination
r, r’	Radial coordinate, deformed radius
S	Undrained strength ratio for NC soil in SHANSEP equation
S_i	Initial Saturation
s_u	Undrained shear strength
t	Time
t_p	Time to end of primary
u, Δu	Pore pressure, change in pore pressure
u_e	Excess pore pressure
u_s	Shear induced pore pressure
u_0	Pore (back) pressure at start of shearing
V, ΔV	Current volume, change in volume
V_0	Initial volume
w	Water content
w_L	Liquid limit
w_p	Plastic limit

β	Size parameter
ε	Strain
ε_a	Axial strain
ε_{cav}	Cavity volumetric strain
ε_f	Strain at peak shear stress
ε_v	Specimen volume strain
ε_r	Radial strain
ε_θ	Circumferential (hoop) strain
ε_0	Pressuremeter strain
$\acute{\varepsilon}$	Strain rate
$\acute{\varepsilon}_a$	Axial strain rate
$\acute{\varepsilon}_{cav}$	Cavity volumetric strain rate
φ, φ’	Friction angle, effective friction angle
φ'_p	Effective friction angle at peak
φ'_{mo}	Effective friction angle at maximum obliquity
γ	Shear strain
γ_a	Shear strain at inner radius
γ_b	Shear strain at outer radius
γ_r	Shear strain at radius r
γ_w	Unit weight of water
ν	Poisson’s ratio
ρ	Density
ρ_c	Compression index
χ	Distortion parameter

σ_v, σ'_v	Vertical stress, vertical effective stress
σ_h, σ'_h	Horizontal stress, horizontal effective stress
σ_{h0}	Initial horizontal stress
σ_r	Radial stress
σ_{ri}	Radial stress at inner wall
σ_{ro}	Radial stress at outer wall
σ_{r0}	Initial radial stress (at end of consolidation)
σ_θ	Circumferential (hoop) stress
σ_p	Preconsolidation pressure
σ'_v	Vertical effective stress
σ'_{vc}	Vertical consolidation effective stress
σ'_{vm}	Maximum vertical consolidation effective stress
σ_1, σ_2, σ_3	Principal stresses
σ_{oct}	Mean octahedral stress
τ	Shear stress
τ_a	Shear stress at inner radius
τ_b	Shear stress at outer radius
τ_r	Shear stress at radius r

1 INTRODUCTION

1.1 PROBLEM STATEMENT

Shallow oil reservoirs at depths less than 1,000 m are situated within weak rock formations. Most of these formations are poorly lithified and more properly classified as 'strong soils' (very hard clays and lightly cemented granular materials). The wells are bored within reservoir and overburden rocks that are much weaker and more deformable than those encountered at more typical deep reservoirs (greater than 3,000 m). Most existing wellbores pass vertically through these upper weak sediments and are usually successfully cased and cemented to mitigate effects of minor near-surface soil disturbance. In contrast, shallow field development concepts rely on a small number of surface drilling locations, with high-angle wells drilled with complex directional trajectories. In these situations control of the drilling operations is closely related to an understanding of wellbore instability mechanisms.

Wellbore stability methods commonly employed in the design of deep wells are based on assumptions appropriate to the strength and deformation characteristics of well lithified rock formations (e.g., shales, sandstones and mudstones). These materials fail in a quasi-brittle manner (e.g., Santarelli & Brown, 1989), creating classic borehole breakout failure patterns in the rock. The accuracy of these conventional models has been verified by model experiment (e.g., Ewy & Cook, 1990; Haimson & Song, 1993, 1998) and comparison with actual field drilling results (e.g., Edwards et al., 2004).

There are no comparable prediction methods for evaluating the stability of shallow boreholes drilled in very hard soils and poorly lithified rock formations. These materials are expected to undergo large plastic deformations (borehole squeezing), creating a more extensive zone of disturbance around the borehole. There have been surprisingly few experimental studies to evaluate systematically the strength and deformation properties of soils in the relevant range of consolidation pressures, 1 – 10 MPa (exceptions include work on sands by Yamamuro & Lade, 1996; Coop & Willson, 2003; and on clays by Bishop et al., 1965; Petley, 1994; Amorosi & Rampello, 2007 among others) and no model tests on borehole stability. Prior analytical

studies (e.g., Yu & Rowe, 1999) are based on simplified constitutive models of soil shear behavior.

The present research addresses the problem of wellbore instability in soils through a program of experimental measurements that includes element and model borehole tests conducted using resedimented clay over a wide range of consolidation stresses. This thesis describes the testing material and equipment used to carry out the experimental program, presents the results of the element and model borehole tests, and analyzes the test results by using principles of soil mechanics and soil behavior.

1.2 MIT WELLBORE INSTABILITY PROJECT

The work conducted for this thesis was part of a four year research project at MIT sponsored by BP to address the issue of wellbore instability mechanisms in strong soils. The project was motivated by shallow field developments in onshore prospects in the North Slope of Alaska (e.g., Schrader Bluff and Ugnu reservoir units) and deepwater environments in the Gulf of Mexico (e.g., Great White field). The overall goal of this research is to develop reliable methods for evaluating the stability of wellbores in soils and the development of appropriate design methodologies for these geological environments.

The project comprises an integrated program of analytical modeling, supporting laboratory experiments, and evaluation of predictive capabilities. The numerical modeling activities, carried out by doctoral candidate Sherif Akl, make use of advanced elasto-plastic constitutive models developed previously at MIT (e.g., MIT-E3, Whittle & Kavvadas, 1994). The model parameters are directly calibrated from laboratory high pressure element tests, while finite element simulations of borehole stability are evaluated and refined using data from laboratory model borehole tests. The numerical analyses also address the influence of the inclination angle on wellbore deformations and effects of partial drainage on wellbore stability.

This thesis encompasses the experimental investigation conducted for the MIT wellbore instability project including: a) a series of 1-D consolidation and undrained triaxial shear tests to evaluate the effect of consolidation stress level on the effective stress-strain-strength properties of the soil under uniform stress state; and b) Thick-Walled Cylinder (TWC) tests with

independent control of the vertical stress and radial pressures acting on the inner and outer walls of the hollow cylindrical test specimen to study stability of a vertical wellbore at reduced scale.

Results from this research project are presented in a Technical Progress Report (Abdulhadi et al., 2008), a Final Technical Report in progress (Whittle et al., 2010), a PhD thesis in progress (Akl, 2010), and this thesis.

1.3 THESIS SCOPE AND OBJECTIVES

This thesis has two main objectives. The first objective is to gain an improved understanding of the elemental mechanical behavior of cohesive soils at elevated consolidation stresses (up to 10 MPa). The laboratory tests use Resedimented Boston Blue Clay (RBBC) as an 'analog' test material. The stress level dependence of the consolidation and shear properties of RBBC is investigated through an extensive experimental program of 1-D Constant Rate of Strain (CRS) consolidation as well as K_0-consolidated undrained triaxial compression and extension tests under various stress histories. The program also seeks to enhance the experimental capabilities for testing cohesive soils at high confining pressures in the triaxial apparatus.

The second objective is to gain insight into the response of RBBC to non-uniform stress state simulating the stress conditions around a model borehole. This research specifically investigates the role of the following factors on the model borehole behavior: mode of loading, specimen geometry, lateral stress ratio, drainage conditions, consolidation stress level, stress history, and strain rate. The results of these investigations are expected to provide insight into the significance of these variables. In addition, an analysis of the measured results outlines the fundamental behavior of model boreholes in the TWC apparatus.

The model borehole experimental program necessitates the design and construction of two automated, high pressure TWC devices for different specimen sizes. The new equipment were also evaluated to assess their performance.

1.4 ORGANISATION OF THE THESIS

This thesis is organized in seven chapters, with the intention of presenting the reader with a complete picture of the problem investigated: relevant background, experimental details, and finally presentation and analysis of the results.

Chapter 2 provides the pertinent background information needed for the current research program. This chapter begins with a discussion of the wellbore stability problem and the types of borehole instabilities typically encountered during drilling. It then covers fundamental aspects of soil behavior during undrained shear deformation that are related to this research including properties at high confining pressures, normalized shear behavior, and strength anisotropy. It continues with a review of prior experimental research on model boreholes using the Thick-Walled hollow Cylinder (TWC) apparatus. The chapter also presents the interpretation methods used for the pressuremeter tests which are later used to interpret the model borehole tests (Chapter 6).

Chapter 3 presents an overview of Resedimented Boston Blue Clay (RBBC), the test material used in the entire testing program. The chapter summarizes the resedimentation procedure used to prepare individual test specimens, the index properties of the soil, and provides extensive background on its engineering properties. In particular, the current knowledge on the consolidation and undrained shear behavior of RBBC is reviewed in some detail. The intent of this effort is to summarize the reference database that this research complements and demonstrate that the behavior is typical of that of many natural soils.

Chapter 4 provides a complete description of the experimental equipment used to perform the tests presented in this thesis. This includes the existing low pressure and modified high pressure triaxial devices, as well as the two new high pressure TWC (small and large diameter) apparatuses developed for this research project. The control system hardware, software, measurement instrumentation, and the data acquisition system are all described. This chapter also evaluates the new testing equipment and reviews testing procedures.

Chapter 5 presents the results of the K_0-consolidated undrained triaxial testing program on RBBC. The testing program consists primarily of triaxial compression and extension tests in which specimens are consolidated to different consolidation stresses. The stress level effects are investigated at three well-defined stress histories for the compression tests while the extension

tests include only normally consolidated specimens. In addition, there is a section summarizing and analyzing the K_0-consolidation results.

The results of the model borehole experimental program using the TWC apparatus are presented and analyzed in Chapter 6. The program investigates the role of several parameters on the model borehole behavior. This chapter begins by describing the results of a baseline reference model borehole test. It then presents the results of the experimental program, treating each of the variables investigated separately. Finally, Chapter 6 provides a comprehensive analysis of the results using pressuremeter-type interpretation.

A summary of the results and of the main conclusions drawn from the analysis is contained in Chapter 7, which also presents recommendations for future research.

2 BACKGROUND

2.1 INTRODUCTION

As mentioned in Chapter 1, the main purpose of this research is to improve our understanding of the behavior of 'strong soils' under simulated wellbore in situ conditions. The term 'strong soils' is used in this thesis to describe unlithified materials (mainly cohesive) with unconfined compressive strengths, q_u = 1.0 – 8.0 MPa. According to the soil classification proposed by Terzaghi & Peck (1948), these materials are classified as hard-very hard clays (i.e., q_u > 0.4 MPa). On the other hand, using the classification system for intact rock (Deere & Miller, 1966), strong soils can be described as very low strength rock materials (i.e., q_u < 30.0 MPa). The mechanical properties of strong soils are somewhat between those of soft rocks and soils, and researchers neither in rock mechanics nor in soil mechanics have performed extensive testing to study them. Although there has been a growing interest in the behavior of weak rocks in the past twenty years with regards to the application in oil industry (e.g., Steiger & Leung, 1988; Nakken et al., 1989; Wu et al., 1990; Marsden et al., 1996 among others), there is still a lack of knowledge of the mechanical behavior of strong soils/weak rocks.

Instabilities in hard rock occur around underground openings (such as boreholes, shafts or tunnels) when the redistributed stresses are greater than the strength of the material. These instabilities depend on the geometry of the openings, properties of the rock, and in situ stresses among other factors. Hard rocks tend to be more brittle, with little ability to deform and carry load after the peak stress has been reached. The brittleness tends to decrease with decreasing confining pressure. Softer rocks and strong soils are normally more ductile, i.e., they have larger ability to deform and carry load beyond their elastic limit. The brittle-ductile transition depends on the stress level and hence, depth of the formation.

Stress-induced instabilities are evident in underground excavations as well as wellbores. In underground excavations, many types of failure mechanisms have been observed. Barton (1987) indicated that hard brittle rocks under very high anisotropic stress can be expected to fail by successive development of extension fractures, while soft porous rocks under high anisotropic stress can be expected to fail by the interaction of log spiral-like shear surfaces.

Wellbore instability mechanisms are affected by the depth of the oil reservoir. In deep reservoirs at depths greater than 3,000 m, the wells are located within strong lithified rock. These materials fail in a brittle manner creating borehole breakouts. In contrast, shallow wells are drilled in weaker and more deformable formations (e.g., strong soils) and therefore expected to undergo large plastic deformation and borehole squeezing.

The chapter begins with a discussion of the wellbore stability problem. This covers the different types of borehole instabilities typically encountered during drilling and describes the borehole stability analysis used in design.

Section 2.3 reviews fundamental soil behavior aspects during undrained shear deformation that are related to this research. It presents a brief summary of previous experimental research on cohesive soils and mudrocks at high confining pressures and discusses the concept of normalized behavior and its application in clays and shales. In addition, a short introduction to soil anisotropy is provided.

Section 2.4 presents a very concise summary of prior experimental research on scaled, model boreholes using the Thick-Walled hollow Cylinder (TWC) apparatus. This section surveys the multitude of tests carried out on hard brittle rocks as well as the very few tests performed on soft ductile shales.

The mode of shearing in the model borehole test is identical to the one produced by the pressuremeter test. The pressuremeter test is a popular in situ cavity expansion test often used to obtain geotechnical properties for design purposes. The interpretation methods for evaluating the undrained shear strength and stress-strain behavior are well established for saturated clays. Model pressuremeter tests have also been performed in the laboratory using hollow cylinder devices. These tests resemble closely to the model borehole tests; the main difference is that the cylindrical cavity expands in the pressuremeter test while in model borehole test the cavity contracts. Under the conditions of plane strain and undrained shearing, the interpretation methods established for cavity expansion are applicable to cavity contraction, since the problem becomes fully strain controlled. Section 2.5 presents an overview of the interpretation methods used for the pressuremeter test in the field as well as in the laboratory. The current research makes use of these methods to interpret the model borehole tests.

2.2 WELLBORE STABILITY

2.2.1 Introduction

Wellbore instability during drilling is of great importance in the oil and gas industry. It causes the process of drilling a wellbore to be slowed down and the cost of the well to exceed the experts' predictions. Financial losses due to wellbore failure are estimated to cost over $1 billion per year and amount to typically 5-10% of drilling costs in exploration and production (Dussaeault, 1994). Most instabilities of practical importance occur in shale or mudrocks; predominantly in the overburden, but sometimes also within the reservoir. These rocks are one of the most abundant materials on the uppermost layer of the earth's surface and make up about 75% of sedimentary basins (Hornby et al., 1994).

Borehole instability problems have been encountered for as long as wells have been drilled. Several new challenges have appeared in last twenty years, making the stability issue more critical and requiring better understanding of the associated geomechanics. For example, there has been an increasing demand by the industry for more sophisticated well trajectories. Highly deviated, multilateral and horizontal wells are attractive, since a single production platform can then produce from a much larger area of the reservoir, this can reduce the number of platforms required to produce a given field. However, wellbore instability is more common in deviated than in vertical boreholes. Other situations where borehole stability problems may be expected are during infill drilling in depleted reservoirs, when drilling in tectonically active areas, and in deep and geologically complex surroundings. Deep water drilling is a special challenge. Due to the high cost of drilling in such environments, additional time lost on borehole instability has an extra high price.

A particular challenge that this research is addressing is the drilling of wells in shallow oil reservoirs at depths less than 1,000 m. These reservoirs are situated within formations that are poorly lithified (strong soils). The wells are drilled within relatively weak and deformable reservoir and overburden rocks and therefore expected to undergo large plastic deformation, creating a more extensive zone of disturbance around the borehole. Shallow field developments also entail drilling deviated wells with complex trajectories.

The following subsection presents the types of borehole instabilities typically encountered during drilling. Section 2.2.3 describes the borehole stability analysis used in design.

2.2.2 Types of Borehole Instabilities

A formation at depth exists under a state of compressive in situ stresses. When a borehole is drilled, the stresses in the vicinity of the borehole are redistributed as the support previously provided by the removed material must now be provided by the shear resistance within the soil/rock mass and by the mud pressure in the borehole. Bradley (1979) grouped the different borehole instabilities into the following three types (these types of instability are shown in Figure 2-1):

i) Hole closure due to plastic flow of rock into the borehole (ductile unloading). This mechanism requires the development of a zone of plastic shear strains around the borehole and involves little loss of shear strength within the material.

ii) Hole enlargement or borehole breakout (Bell & Gough, 1979) due to brittle failure of the rock around the wellbore (brittle unloading). This condition initiates when the shear strength of the rock is mobilized at the wellbore.

iii) Accidental hydraulic fracture due to tensile splitting of the rock from excess mud pressure (brittle loading).

The first type of instability may occur in soft (plastic) formations such as weak shales and salt. It will result in a high friction between the drilling tool and the wall of the borehole and may cause loss of the tool and part or all of the borehole during drilling, or may damage the casing of the borehole during production. The second type of instability normally takes place in brittle rocks. The problem resulting from this type of instability includes poor directional control, difficulty in removing the cuttings, and poor cementing. Borehole breakout generally leads to ovalization of the hole and is of use in determination of in situ stress. It is widely accepted that the orientation of breakout indicates the direction of minimum in situ stress. However the relation between the depth of breakout and magnitude is inconclusive (Zoback et al., 1985). Finally, the third type of instability will lead to severe loss of drilling fluid to the formation via the fractures (induced or existing), resulting in lost time as well as increased cost and often leads

to well control problems, experienced as kick (rapid increase in well pressure) or an underground blow out. This is an operational problem, partly because the mud is expensive, and partly because there is a limit to the amount of mud available on the rig.

2.2.3 Borehole Stability Analysis

Figure 2-2 shows a schematic of a procedure for borehole stability analysis presented by Fjaer et al. (2008). This figure highlights in simple terms the main steps involved in borehole stability analysis. The input data required for the analysis are material mechanical properties, in situ stresses, pore pressure, and the well trajectory. Only the parameters listed in the first row of boxes are required for a "simple" analysis. For a more advanced analysis, chemical, thermal, plastic, anisotropic and time dependent features are added. In most cases these effects are simply added by superimposing poroelastic, thermoelastic, and osmotic contributions to the borehole stresses.

The main product of borehole stability analyses is the drilling mud weight window (i.e., the range of permitted mud weights associated with stable drilling). Drilling mud is the 'blood line' of wells and serves two main purposes: the first is to prevent flow of pore fluid into the well and/or hole instabilities. The second purpose is to transport drill cuttings to the surface. The mud weight window is governed by the hole collapse, the pore pressure, and the fracture gradient[1] profiles. The weight window is used to design and control drill procedures. The minimum permitted mud weight may be estimated from a material mechanical prospective. Soil/rock mechanics models are employed to estimate borehole failure. These models can vary from simple linear elastic theories (used to estimate stresses that initiate failure in brittle materials) to more complex elasto-plastic models that describe deformations around the wellbore (and include properties such as small-strain non-linearity and anisotropy). It is also necessary to keep the minimum mud weight above the pore pressure gradient in order to prevent influx of fluids (in particular gas). The maximum permitted mud weight needs to be below the fracture gradient to prevent loss of fluid to the formation by flow into existing or induced fractures (lost circulation). The well may be designed after these limits are established. It should be mentioned that the mud

[1] Pressure gradient or equivalent mud weight refers to a pressure at a given depth converted to a density value, i.e., $\rho=p/gD$; where ρ is the pressure gradient, p is the pressure at depth D, and g is the acceleration of gravity.

weight window tends to get smaller with increasing well inclination. Note that the mud chemistry may also affect the mechanical integrity of the formation near the well and hence, the stability of the borehole.

Well design involves more than borehole stability. The purpose of the well is to reach a certain target to ensure optimum drainage of a reservoir or reservoir zone. The suggested hole trajectory required to reach the target then has to be evaluated in order to see if it is drillable, and then the drilling process has to be optimized to reduce costs by drilling fast, and by using as few casing strings as possible. This is critical at large depths as the number of casing strings has to be kept low, since the casing diameter decreases for each new string.

Figure 2-3 illustrates the role of wellbore stability analysis in well design. After estimating the pore pressure gradient and the in situ horizontal and vertical gradients (full lines p, h, and v respectively in the figure), the collapse and fracture gradients (dotted lines c and f respectively) are calculated using soil/rock mechanics principles combined with the measured material mechanical properties. Subsequently, the mud weight gradient (dashed line m) is planned within the permitted mud weight window. It is not possible to drill the entire section with one mud weight; a casing has to be set to seal off the upper part of the wellbore before continuing with an increased mud weight in the lower part. The mud weight and the casing program are essentially the two main tools available to achieve stable wellbores.

2.3 MECHANICAL BEHAVIOR UNDER UNIFORM STRESSES

2.3.1 Introduction

The experimental program presented in this thesis comprises undrained triaxial and model borehole tests conducted using Resedimented Boston Blue Clay (RBBC) at vertical consolidation effective stresses, σ'_{vc} = 0.15 – 10 MPa. This section reviews fundamental soil behavior aspects during undrained shear that are most relevant to this work. Section 2.3.2 presents a concise summary of previous experimental research on hard clays at high pressures in triaxial compression. Section 2.3.3 discusses the normalization concept and its application in clays and shales. Section 2.3.4 gives a brief introduction to anisotropy in soils.

2.3.2 Mechanical Behavior of Hard Clays at High Pressures

In order to better understand the fundamental behavior of strong soils that are encountered in shallow field developments, the strength and deformation properties of the material in the relevant stress levels should be recognized. Moreover, these properties are essential for constitutive models used in analytical investigations to accurately predict the stability of the wellbore. The characteristic stress levels pertinent to shallow oil field developments (less than 1,000 m) range from 1 to 10 MPa. These correspond to much higher pressures than those normally used in testing soils in the laboratory. There are a multitude of data on soils at low effective stresses ($\sigma'_{vc} < 1$ MPa) and the effective stress-strain-strength properties are well established. However, there have been very few experimental studies to evaluate systematically the strength and deformation properties of clays in the relevant range of consolidation pressures.

In contrast to soils, the effect of confining pressure on the mechanical properties of rocks is much better understood. For example, a series of triaxial tests performed by Handin & Hager (1957) and Paterson (1978) on sedimentary rocks at room temperatures and various confining pressures ranging from 0.1 to 200 MPa demonstrated that the ultimate strength and ductility increases with increasing confining pressure. They also illustrated that the confining pressure inhibits fracturing and increases the tendency for the stress-strain curve to continue rising up to large strains with steeper slope, i.e., there is greater extent and degree of strain hardening at high confining pressure. Handin (1966) also gave extensive tables of rock strengths.

One of the earliest undrained triaxial shear tests on clays at relatively high confining pressures was performed by Bishop et al. (1965) on intact London Clay. These tests were carried out at effective stresses up to 2 MPa. Petley (1994) also conducted triaxial tests on London Clay but at much higher confining pressures (up to 30 MPa). In addition, the behavior of samples of Boom Clay in the triaxial at effective stresses between 0.9 and 5.4 MPa has been investigated by Horsemen et al. (1993) and Taylor & Coop (1993). Leddra et al. (1991) tested samples of Kimmeridge Clay to investigate undrained shear deformation at confining pressure between 0.5 and 10 MPa. Marsden et al. (1992) performed triaxial tests on Weald Clay at effective stresses up to 23 MPa. More recently, Amorosi & Rampello (2007) conducted undrained triaxial tests on Vallericca Clay at vertical effective stresses up to 6.7 MPa. All these studies were conducted on unweathered intact natural clay samples.

One of the main disadvantages of testing intact clays is that there is no control over the preconsolidation pressure (σ'_p) and therefore, tests consolidated to stresses lower than σ'_p in the triaxial are bound to be overconsolidated. Furthermore, if σ'_p is low then very large strains are required to reach high consolidation stresses. Consolidation of intact samples to stresses much higher than the in situ stresses tends to largely erase the initial microstructural features (Amorosi & Rampello, 2007). Therefore, the task of investigating the effect of stress level at different stress histories over a wide range of stresses in intact materials becomes more difficult. It is also worth noting that the test specimens in the above studies, except those conducted by Amorosi & Rampello (2007), were isotropically consolidated before being sheared undrained in the triaxial.

Some of the very few undrained triaxial tests carried out using reconstituted clays at intermediate and high pressures include the work by Yassir (1989) on mud volcano clays (up to 50 MPa), Burland (1990) on Todi Clay (up to 1.5 MPa), and Berre (1992) on artificial clay shale (up to 20 MPa). Berre (1992) prepared artificial clay shale samples by mixing Moum Clay and Kaolinite (the mixture had CF = 58%, w_L = 60%, and I_p = 37%). The specimens were consolidated in the oedometer to vertical effective stress, σ'_p = 32 MPa, before being unloaded and dismounted. Two triaxial specimens were cut from the oedometer specimen and stress path consolidated with K = 0.7 in the triaxial cell to consolidation effective stress, σ'_{vc} = 20 MPa (i.e., overconsolidation ratio, OCR = 1.6). The tests were sheared undrained in compression and the results were compared with natural clay shale tests with similar stress histories and preshear consolidation stresses. The results illustrated that the natural shales, which have lower void ratios, were also characterized by higher undrained shear strength and lower vertical strain at failure than the artificial clay shales. The artificial specimens showed a pronounced barrel shape with little sliding along the main failure plane while for the natural specimens most of the displacements occurred along one or two very distinct failure planes. Berre indicated that the artificial clay shale may be considered as the uncemented version of the natural clay shale.

Yassir (1989) performed an extensive investigation on the undrained shear behavior of three reconstituted volcanic clays (collected from mud volcanoes in Taiwan and Trinidad) at different consolidation stresses. The samples tested were prepared by consolidating a vacuumed slurry in an oedometer to vertical effective stress, σ'_p = 2.5 MPa. Triaxial specimens were trimmed from the oedometer specimen and then reconsolidated in the triaxial cell to consolidation stress levels higher than the initial batch preconsolidation pressure (i.e., OCR=1).

Figure 2-4 shows the shear stress-strain behavior ($q = (\sigma_1-\sigma_3)$ versus ε_a) for a low plasticity mud volcano clay (CL) from Taiwan (CF = 33%, w_L = 35%, and I_p = 14%) where specimens TA and TF were isotropically consolidated to σ'_{vc} = 50 and 5 MPa respectively and specimens TC, TD and TE were stress path consolidated with K = 0.6 to σ'_{vc} = 68, 20, and 34 MPa (i.e., $p'_m = (\sigma'_1+2\sigma'_3)/3$ = 50, 15, and 25 MPa) respectively. All tests reach a maximum shear strength followed by very little or no strain softening (i.e., reduction in deviatoric stress with increasing strain). The non-existent peak in the anisotropically consolidated tests is probably due to the very high consolidation pressures. The figure also shows that the two isotropic tests have higher strain at failure than the anisotropic tests. The normalized shear strength (s_u/σ'_v) range from 0.24 to 0.28 for the anisotropic tests with no clear trend with stress level. Figure 2-5 shows the effective stress paths in Cambridge stress space ($q = (\sigma_1-\sigma_3)$ versus $p' = (\sigma'_1+2\sigma'_3)/3$) for the same tests. The mean effective stress p' decreases steadily with increasing q for all the tests indicating contractive undrained shear behavior. The failure envelope reached at the end of the tests appears to be slightly curved, with the gradient gradually reducing with increasing effective stress.

There are a number of factors that tend to influence the form and position of the failure envelope such as stress level, OCR, and soil structure. Burland (1990) reviewed the behavior of different natural and reconstituted clays at stress levels up to 2 MPa and concluded that four fundamental failure envelopes can be described (see Figure 2-6): 1) a peak strength envelope for natural intact clays; 2) post rupture strength envelope, representing the end of dramatic and rapid strain softening in intact samples after reaching the peak strength; 3) 'intrinsic' critical state strength envelope, defined by the failure of reconstituted samples; this envelope was interpreted as being a basic property that is independent of the undisturbed state of the material, which provides a good basis for the comparison of the properties of different materials; and 4) residual strength envelope, which refers to the minimum strength after very large shearing displacements. Burland (1990) indicated that the peak strength of stiff intact natural clays is often significantly greater than the reconstituted counterpart at the same void ratio due to interparticle bonding. The drop in strength from peak to post rupture is largely due to the breaking of these bonds. Figure 2-6 shows that the post rupture strength lies very close to the intrinsic strength line. Strength reduction from post rupture to residual takes place gradually as the clay particles become aligned during sliding. Note that the intrinsic critical state line is assumed to be linear with zero cohesion for normally consolidated clays while for overconsolidated clays the peak failure line lies above

the critical state line; it is curved and often shows a cohesive intercept. Burland suggested that the failure envelopes, with the possible exception of the intrinsic critical state and residual envelopes, have a non-linear form.

Petley (1999) reviewed the behavior of various intact clays in the triaxial compression during undrained shear at effective stresses ranging from 1 to 50 MPa and proposed an "extension" to the work of Burland (1990) to incorporate the behavior of clays at effective stresses up to 50 MPa. Figure 2-7 shows the conceptual diagram of the three envelopes proposed by Petley (1999). The figure shows that the peak strength envelope has a non linear form, with the gradient steadily reducing with increasing effective stress. The post rupture envelope appears to have a linear form at low confining pressures but at high pressures the gradient reduces with increasing effective stress. Finally, there is the residual strength envelope, which is suggested to be linear even up to 50 MPa. However, it must be noted that the low pressure tests were in most cases overconsolidated while the high pressure tests were normally consolidated. Therefore, the shape of the envelopes (peak and post rupture) is not strictly due to the influence of stress level alone but also due to the stress history of the soil. Petley (1999) indicated that the linear residual envelope is not attained except at very high strains for low confining pressures while at very high effective stresses, however, it is the main deformation envelope. After reaching the peak strength, the samples strain soften to the post rupture envelope. This envelope intersects the peak envelope at the junction with the residual line.

It should be noted that none of the experimental studies presented above examined systematically the effect of stress level on the effective stress-strain-strength properties of clays as function of stress history.

2.3.3 Normalized Behavior

The Normalized Soil Parameter (NSP) concept is based on the empirical observation that the results of laboratory tests on clay samples having the same overconsolidation ratio, but different consolidation stresses, and therefore different preconsolidation pressures, exhibit similar properties (i.e., strength, stress-strain, pore pressure parameters, moduli, etc) when normalized with respect to the consolidation stress (Ladd & Foott, 1974). This concept has a significant practical value as it provides a useful framework for comparing and relating the behavioral characteristics of different cohesive soils and has led to the development of the

SHANSEP (Stress History and Normalized Soil Engineering Properties) design method (Ladd & Foott, 1974). Moreover, the NSP is also the basis of other frameworks of soil behavior, such as the Critical State Soil Mechanics (Schofield & Wroth, 1968) and the "simple" clay (Ladd, 1960), as well as analytical soil models such as the Modified Cam Clay (Roscoe & Burland,1968) and MIT-E3 (Whittle & Kavvadas, 1994). It is worth noting that in Chapter 5 the principle of normalization is evaluated for RBBC over a wide range of consolidation stresses using the triaxial device.

The SHANSEP method is applicable to uniform cohesive soils that have been mechanically overconsolidated or are truly normally consolidated (i.e., in situ OCR = 1) and maintain the same basic structure during loading beyond in situ stresses and therefore exhibit behavior that can be normalized by preshear consolidation stresses. This method is not intended to be used in cemented, highly sensitive clays or in drying crust of a soil deposit. The technique can be used in either drained or undrained conditions, but is often used to describe the undrained shear in triaxial compression and extension, plane strain compression and extension, and in direct simple shear tests. The premise of this technique is that the in situ stress history can be simulated in the laboratory that will provide accurate predictions of the in situ soil behavior at various OCRs. Thus, while the actual stresses are different between the laboratory and field, the SHANSEP method predicts identical behavior for a given OCR. The new stress history is achieved by 1-D (K_0) consolidation well past the preconsolidation pressure, σ'_p, into the virgin compression range to some new maximum stress, σ'_{vm} (points A or B in Figure 2-8; $\sigma'_{vm} \geq 1.5 - 2\ \sigma'_p$). For OCRs greater than unity, the soil is mechanically overconsolidated by K_0 swelling (points C or D); it is assumed that regardless of the physical mechanisms causing the in situ overconsolidation, all overconsolidated soil will behave in the same way.

Figure 2-9 shows typical results of a SHANSEP test program results for AGS plastic marine clay with three modes of shearing (triaxial compression and extension and direct simple shear), which can be represented by the equation:

$$\frac{s_u}{\sigma'_{vc}} = S \cdot (OCR)^m \tag{2.1}$$

where S is the undrained strength ratio for the normally consolidated clay, and m is the slope of the regression line.

A program of laboratory consolidation and CK_0U shear tests is used to determine the σ'_p versus depth profile and to measure the S and m parameters for the soil deposit. Once effective overburden stresses are computed, an OCR versus depth profile can be established and Equation 2.1 used to compute the shear strength variation with depth. This will provide information on the soil's anisotropy since the dependence of Equation 2.1 on stress system is also determined. When applied appropriately, this methodology can be a valuable analysis and design tool.

Another common method for determining in situ shear strengths from laboratory tests is the Recompression technique (Bjerrum, 1973). This method attempts to overcome the effects of sample disturbance by 1-D reconsolidating the specimen to the in situ vertical effective stress (σ'_{vo}). Because sample disturbance results in a reduced initial recompression stress-strain modulus, as Figure 2-8 shows, a lower water content results when the specimen is reconsolidated to σ'_{vo} in the laboratory. Thus, the validity of the Recompression method depends to a large extent upon the resulting water content reduction (Berre & Bjerrum, 1973). This method is more valid for highly structured, highly overconsolidated, or cemented soils that retain much of their small strain (less than 1%) stiffness with appropriate sampling, i.e., block samples (Ladd, 1991).

Few attempts have been made to investigate the possibility of normalizing the undrained shear strength behavior of clay shales and the applicability of SHANSEP to clay shales (e.g., Steiger & Leung, 1991; Gutierrez et al., 2008). Clay shales are fine grained soft rocks (clay fraction, CF > 50%) that are formed in sedimentary basins by diagenetic processes, which turn young clay sediments into cemented and lithified shales. They exhibit behavior that is intermediate of soft clays and hard cemented rocks (Johnston & Novello, 1994). Gutierrez et al. (2008) assembled a database of consolidated undrained (CU) triaxial test results on 25 types of clay shales from different locations and with various degrees of diagenesis and cementation. The porosity values for the 25 clay shales ranged from 62.5% to about 15%. The apparent preconsolidation stress was determined either experimentally (e.g., Casagrande's procedure) or by correlations with index tests (e.g., unconfined compressive strength). Figure 2-10 shows the normalized undrained shear strength in compression versus OCR for the 25 types of clay shales. The results show an approximately linear relationship between the log (s_u/σ'_{vo}) and log (OCR) indicating that the SHANSEP equation might be suitable for shales. The authors suggest that the normalization procedure can be applicable to clay shales with void ratios as low as 0.18.

However, the normalized undrained shear strength of more lithified samples is higher than younger uncemented samples because of higher values of the apparent preconsolidation pressure.

2.3.4 Soil Anisotropy

As mentioned previously, the experimental program conducted in this research comprises elemental triaxial compression and extension tests, as well as model borehole closure tests. The mode of shearing in these three tests is different which leads to variations in the stress-strain-strength properties due to anisotropy. The change in soil behavior with direction of loading (i.e., anisotropy) can arise from several factors, such as the depositional environment and the consolidation stress-strain history of the soil and also due to subsequent changes in the loading conditions.

Definitions for the various components of anisotropy have been discussed extensively (e.g., Casagrande & Carillo, 1944; Hansen & Gibson, 1949; Ladd et al., 1977; Jamiolkowski et al., 1985; Ladd, 1991). Ladd (1991) stated that the initial anisotropy (inherent and initial shear stress) denotes differences in the stress-strain-strength response of a K_0-consolidated soil with variations in the applied principal stress direction. Inherent anisotropy arises from a preferred soil structure developed during 1-D (K_0) deposition. Initial shear stress anisotropy describes the directionally dependent undrained response of soils whenever shearing starts from an anisotropic initial state of stress (i.e., $K_0 \neq 1$). It is also important to consider the influence of evolving anisotropy, which describes how the initial cross anisotropic properties of the K_0-consolidated soil change due to subsequent stressing and straining.

When comparing laboratory shear devices available for testing, two variables are commonly used to describe the basic differences in the applied stress system (Germaine, 1982): 1) direction of the applied major principal stress relative to the vertical (depositional) direction denoted by the δ angle; and 2) the relative magnitude of the intermediate principal stress defined by $b = (\sigma_2 - \sigma_3)/(\sigma_1 - \sigma_3)$. Figure 2-11 shows the combinations of b and δ that can be achieved by laboratory shear devices, these being triaxial compression and extension (TC/TE), plane strain compression and extension (PSC/PSE), direct simple shear (DSS), true triaxial apparatus (TTA), torsional shear hollow cylinder (TSHC), and the directional shear cell (DSC).

The triaxial device is one of the most commonly used shear devices to evaluate the stress-strain-strength behavior of soils because of its relative simplicity for testing and in the

interpretation of results. In addition, drainage conditions can be well controlled and the results are generally consistent and repeatable. The triaxial cell is used to test solid cylinders by applying an all around fluid pressure to the specimen and imposing a deviatoric load (positive or negative) in the axial direction. Consolidation can be isotropic or 1-D. However, the major principal stress can act only axially or radially, resulting in two possible b-δ combinations: 1) b = 0 and δ = 0° for triaxial compression (TC); and 2) b = 1 and δ = 90° for triaxial extension (TE).

The modes of shearing in borehole closure and pressuremeter tests are essentially the same. In both tests, the major and minor principal stresses are acting in the horizontal direction at failure while the intermediate principal stress is acting in the vertical direction. Therefore, the direction of the major principal stress, δ = 90°, while b can vary from 0 – 1 since the intermediate principal stress can vary between the major and minor principal stresses. In principle, the soil exhibits isotropic properties in the horizontal plane, due to the K_0-stress history and hence, the mode of loading (i.e., borehole expansion or contraction) should not affect the measured stress-strain response. Germaine (1980) indicated that considerations of anisotropic behavior suggest that the stress path followed during the pressuremeter test should lead to strengths less than those obtained for vertical loading (i.e., δ = 0° such as TC) and larger than TE. Moreover, Aubeny (1992) demonstrated using the MIT-E3 model that the predicted undrained strength ratios (s_u/σ'_v) in the pressuremeter shear mode are similar to those measured in the DSS mode (the DSS shear mode tends to give an "average" strength between the TC and TE, as illustrated in Section 2.3.3).

2.4 PREVIOUS EXPERIMENTAL STUDIES ON MODEL BOREHOLES

2.4.1 Introduction

The use of Thick-Walled hollow Cylinders (TWC) with cavities of circular cross section is a standard procedure for testing rocks under a system of non uniform stress state. The TWC test can be used to experimentally simulate the stress conditions around a model borehole in the laboratory. This section covers previous experimental research on scaled model boreholes. A large number of tests have been carried out on hard and brittle rocks to investigate the stability of boreholes and examine breakout failure patterns. On the other hand, very few model borehole tests have been conducted on soft shale and none on strong soils. Section 2.4.2 presents a

summary of prior experimental research on hard brittle rock. Section 2.4.3 discusses the mechanical behavior of soft ductile shale in the TWC test.

2.4.2 Hard Brittle Rock

The work carried out by Adams (1912) was one of the earliest studies to use the hollow cylinders for rock testing. He subjected specimens of Solenhofen Limestone and Westerly Granite to pressure up to 180 MPa and observed failure by spalling on the inner surfaces. The limestone specimens showed clearly a well developed spiral fracture surface radiating out from the inner surface. King (1912) discussed Adams results and predicted possible fracture systems depending upon the applied external pressures.

Since these early investigations, hollow cylinders have been used to study the mechanical behavior under inhomogeneous stress conditions, especially to study strength behavior under multiaxial stress state. For instance, hollow cylinders of several different rock types and different ratios of external to internal radii were tested in hydrostatic compression by Robertson (1955). Specimens with ratios of less than three failed by what Robertson termed "trap door" collapse, while those with ratios greater than three failed by spalling. The fracture surfaces resembled very closely the equiangular spiral predicted by King (1912). Robertson also noted that the onset of spalling appeared to coincide with a sudden yielding at the elastic limit of the specimens. Hoskins (1969) described experiments in which he tested five different rock types under various conditions of applied internal and external pressures. Depending upon the stress system used, fracture occurred on conical, spiral or helical surfaces. In particular, Hoskins's results showed that failure always started at the inner surfaces where the deformation was greatest. The deformation is decreased rapidly away from the inner surface in specimens not taken to complete failure. Gay (1973) used hollow cylinders with both circular and non circular holes in order to study the growth of fractures around the holes. The rock types were an isotropic sandstone and anisotropic argillaceous quartzite. He observed that failure around circular holes initiated by shearing at diametrically opposite points and spalling continued at these loci until the opening was sufficiently large for ultimate collapse of specimens to occur. The TWC specimens of limestone subjected to axisymmetric loading on the external diameter under plane strain conditions were used to simulate tunnel excavation (Daemen & Fairhurst, 1971). It was observed that in the initial stages of failure, fine dust particles were loosed from the wall of the borehole.

Experiments where both equal and unequal external stresses were applied to large rectangular blocks with predrilled circular holes have been conducted by Mastin (1984) and Haimson & Herrick (1985) to investigate the relationship between borehole and in situ stresses. It was found that borehole breakouts were directly related to the state of stress and occurred in two diametrically opposed zones along the borehole wall in the direction of the least horizontal stress. Ewy & Cook (1989) tested hollow cylinders of Berea Sandstone, to simulate and observe the deformation, fracture and failure around underground openings. Santarelli (1987) and Haimson & Song (1998) also conducted extensive model borehole tests on sandstones to investigate the breakout failure patterns. Kutter & Rehse (1996) performed true triaxial tests on hollow cylinder specimens of sandstone. The results confirmed those reported above.

2.4.3 Soft Ductile Rock

Although mudrock and shale horizons make up over 75% of the formations drilled during hydrocarbon exploitation, and approximately 20% of lost time may be attributed to problems encountered within them, only a small number of TWC tests have been conducted on soft shale, although such tests would produce invaluable information on the wellbore failure mechanisms in shale formations. The studies performed by Wu (1991) and Marsden et al. (1996) at Imperial College (Rock Mechanics Research Group) on soft smectite shale are some of the very few TWC investigations on weak rock. This section presents some of the results obtained from these studies since they are relevant to the work performed in this research.

Wu (1991) performed a series of consolidated undrained (CU) TWC tests on intact specimens of Fullers Earth (stiff clay/mudstone from the UK with soapy texture consisting of almost 100% Ca smectite). The TWC specimen had outer diameter, D_o = 10 cm, inner diameter, D_i = 2.5 cm, and length, L = 20 cm. Internal and external membranes were used to seal the specimen, which was allowed to drain to the top and bottom. External lateral deformations were measured at two normal directions using a pair of cantilever devices while the mean borehole deformations were measured using a borehole displacement transducer, which is based on a cantilever principle. The test procedures involve back pressure saturation followed by B value check, isotropic consolidation, and undrained borehole drawdown at a rate of 0.5 MPa/minute, with the sample being maintained in axial plane strain, at a constant external cell pressure.

In total, four TWC tests were performed on the smectite shale to simulate two drilling depths (with two tests being conducted for each depth). Figure 2-12 shows results during undrained borehole closure for test HC1, which was isotropically consolidated to 30 MPa with a back pressure of 20 MPa (i.e., effective stress is 10 MPa). Figure 2-13 shows results during undrained borehole closure for test HC4, which was isotropically consolidated to 20 MPa with a back pressure of 15 MPa (i.e., effective stress is 5 MPa). The curves of the internal bore pressure and the measured undrained pore pressure versus the borehole displacement are presented in the figures. The figures show that closure in the sample commenced with a relatively stiff, slightly non linear behavior prior to yield, followed by a softer, near linear behavior as the bores displaced and ultimately collapsed. Wu explains that as the borehole pressure decreased below the yield pressure, the deviatoric components of stress within the sample increased and failure propagated from the internal borehole surface towards the outer boundary of the sample. Ultimately the failure reached this outer surface and the whole sample began to collapse. The measured pore pressures appeared to rapidly increase with an initial reduction in the borehole pressure until the yield point then continued to increase at a slower rate during collapse before decreasing when it equals the bore pressure.

Figures 2-14 and 2-15 show the borehole pressure versus the external displacements measured across two orthogonal diameters for tests HC1 and HC4 respectively. In general, the curves are of similar form to those of the borehole closures versus borehole pressures. However, despite symmetry in the sample geometry and boundary conditions, sample HC1 (Figure 2-14) began to dilate across one of its diameters at yield, leading to an asymmetry which continued through to collapse.

Wu reports that the yield and onset of failure in all tests was somewhat sudden and occurred after the borehole pressures were reduced by only few MPa. Moreover, the pressure reductions needed to initiate failure appeared to be independent of initial test conditions. He also explains that as failure developed, shear surfaces formed as conjugate pairs resulting in lenticular failure patterns running along and consistently oriented along the length of each sample. The failure patterns form equi-angle spiral surfaces which confirms that the failure mechanism around model wellbores to be one of shear (Figure 2-16). Visual inspection of the deep seated failure surfaces showed them to be very smooth and highly polished. Wu noted that the patterns and failures generated in these tests are not to be confused with the breakouts often seen on more

competent rocks, such as sandstones (e.g., Santarelli, 1987). In the case of breakouts, failure is localized and occurs in proximity to the borehole, whereas the shear surfaces observed in this study were not localized, were continuous, and were accompanied by large borehole closures and shear displacements.

Although these studies provided useful insights into the behavior of soft ductile shale, the investigations were fairly limited and did not address important aspects such as stress history, boundary conditions, strain rate, drainage conditions among others.

2.5 PRESSUREMETER TESTING

2.5.1 Introduction

The model borehole tests performed using the TWC device bears a close resemblance to the pressuremeter test. In both tests, the soil that is consolidated in the vertical direction is being sheared in the horizontal plane as a cylindrical cavity expands or contracts. The pressuremeter is a device for applying uniform pressure to the walls of a borehole and from the measurements of stress and deformation, soil property interpretation can be made. The basic design consists of a deformable, cylindrical pressuremeter probe with a flexible membrane, which is expanded laterally to pressurize the surrounding soil[2]. The main soil properties obtained from this test for saturated clays include the undrained shear strength, shear modulus, and in situ horizontal stress.

The pressuremeter is unique among in situ tests used in geotechnical site characterization in that there exists a sound theoretical basis for deriving the complete stress-strain-strength properties of the surrounding soil directly from the measurements. There are several well established interpretation methods dealing with the analysis of the pressuremeter test in saturated clays, each using the basic assumptions of axial symmetry and plane strain, soil homogeneity, isotropy, and undrained conditions. Among the various methods proposed, the approaches of Baguelin et al. (1972), Palmer (1972), and Ladanyi (1972) are prevalent, where no prior knowledge of the constitutive properties is required. Section 2.5.2 presents an overview of these methods for interpreting the in situ pressuremeter test. It must be noted that there exist several

[2] Note that hydraulic fracture cannot be induced using the pressuremeter device since the fluid is contained within a membrane.

other interpretation methods that are based on idealized behavior (e.g., Gibson & Anderson, 1961; Prevost & Hoeg, 1975; Windle & Wroth, 1977; Houlsby & Withers, 1988) which will not be discussed in this section.

Model pressuremeter tests have been performed in the laboratory by expanding hollow cylindrical specimens to investigate the response of saturated clayey soils under controlled conditions and to assess the effect of various parameters, such as testing procedure, loading rate, and partial soil consolidation, on the expansion curves (e.g., Palmer & Mitchell, 1972; Juran & BenSaid, 1987; Anderson et al., 1987; Penumadu & Chameau, 1997; Silvestri et al., 2005). However, the expansion of the cavity of a hollow cylinder is different from the expansion of a cylindrical cavity in an infinite medium, and therefore to deduce stress-strain curves from the hollow cylinder tests using an infinite boundary assumption can be misleading, particularly at high strains. Silvestri (1998) proposed a method to obtain the exact solution to the problem of expanding a cavity in a thick-walled cylinder of clay, under plane strain and undrained conditions. Note that under these conditions, the interpretation methods established for cavity expansion of hollow cylinders are applicable to undrained model borehole tests performed on clays where the cavity is contracting, since the problem remains fully strain controlled. Section 2.5.3 discusses the interpretation methods used for the model pressuremeter test performed in the laboratory.

2.5.2 Interpretation of the In Situ Pressuremeter Test

The methods discussed in this section assume that the pressuremeter expansion can be analyzed as a plane strain problem, that the effective stress-strain relationship is unique for all locations in the soil mass, and that the expansion occurs sufficiently rapidly that there is no migration of pore water within the soil mass, and hence the clay is subjected to undrained shearing. Under these conditions, the problem is fully strain controlled and changes in volume of the pressuremeter can be related to the natural (Hencky) strains in the soil mass as follows:

$$\varepsilon_r = -\varepsilon_\theta = -\frac{1}{2}\ln\left\{1 - \frac{\Delta V}{V}\left(\frac{R}{r}\right)^2\right\} \tag{2.2}$$

where ε_r and ε_θ are the radial and circumferential strain respectively, $\Delta V/V$ is the current volumetric strain; $\Delta V = (V-V_0)$ is the volume of fluid injected into the pressuremeter, V is the

current volume, V_0 is the initial volume, R is the current pressuremeter radius, and r is the radial coordinate.

Pressuremeter data are often reported in terms of a pressuremeter strain, $\varepsilon_0 = \Delta R/R_0$, which can be related directly to the current volumetric strain:

$$\left(\frac{\Delta V}{V}\right) = 1 - \frac{1}{(1+\varepsilon_0)^2} \tag{2.3}$$

Baguelin et al. (1972), Palmer (1972), and Ladanyi (1972) independently developed methods for computing the shear stress-strain-strength of the clay from pressuremeter measurements. The authors assume that all points in a horizontal plane are initially at the same state of stress and exhibit homogeneous, but not pre-defined, stress-strain properties. The shear stress, $\tau = (\sigma_r - \sigma_\theta)/2$, in the soil adjacent to the pressuremeter is given by:

$$\tau = \frac{1}{2}\varepsilon_0(1+\varepsilon_0)(2+\varepsilon_0)\frac{dP}{d\varepsilon_0} \tag{2.4}$$

where P is the expansion pressure. For small strains this reduces to:

$$\tau = \varepsilon_0 \frac{dP}{d\varepsilon_0} \tag{2.5}$$

Equations 2.4 and 2.5 describe the complete stress-strain behavior of the soil, and the shear strength is equated with the maximum shear stress. Palmer (1972) extended the analysis to obtain an expression for the current shear stress in terms of the current cavity pressure and cavity strain:

$$\tau = \frac{dP}{d\left(\ln\frac{\Delta V}{V}\right)} \tag{2.6}$$

The stress-strain behavior is obtained by numerical differentiation of the pressure-volumetric strain curve, as shown in Figure 2-17.

2.5.3 Effect of Lateral Boundary on Interpretation of Model Pressuremeter Test

When cavity expansion tests are performed in the laboratory using thick-walled cylindrical samples of saturated clays, the analysis of Baguelin et al. (1972), Palmer (1972), and Ladanyi (1972) cannot be used because of the finite size of the soil cylinders, as discussed, for example, by Juran & BenSaid (1987). Juran & BenSaid suggest that to obtain the shear stress-strain curve

of the soil from the expansion curve of a hollow cylinder, it is necessary to know in advance the constitutive properties of the material. However, Silvestri (1998) shows that it is possible to obtain the shear curve of clays without having to make any assumption regarding their constitutive properties, as long as undrained and plane strain conditions are maintained. The theory used is based on the solution of Nadai (1950). This section summarizes the formulation proposed by Silvestri (1998).

In a hollow cylinder of clay stressed symmetrically around its axis uniformly along the length, the radial, circumferential, and the axial directions are the principal directions of stress and strain. Since strains of finite magnitude are considered, it is necessary to distinguish the distance r of a point in the original unstrained condition and corresponding r' of the same material element in the strained cylinder, and similarly the inner and outer radii a and b before and a' and b' after distortion has occurred. As a consequence, the natural shear strains at r = a, r, and r = b are equal to the following expressions:

$$\gamma_a, \gamma_r, \gamma_b = \ln\left(\frac{a'^2}{a^2}, \frac{r'^2}{r^2}, \frac{b'^2}{b^2}\right) \tag{2.7}$$

Silvestri introduced a distortion parameter $\chi = (a'/a)^2$. The natural circumferential strain at the inner surface r' = a' of the cylinder being equal to

$$\varepsilon_\theta = \ln\left(\frac{a'}{a}\right) = \frac{1}{2}\ln\chi \tag{2.8}$$

Because the material is incompressible and plane strain conditions prevail throughout the soil mass, one must have

$$r'^2 - a'^2 = r^2 - a^2 \tag{2.9}$$

$$b'^2 - a'^2 = b^2 - a^2 \tag{2.10}$$

If $\beta = a^2/b^2$, and $\beta_r = a^2/r^2$ then using Equations 2.9 and 2.10 yields

$$\left(\frac{a'}{a}\right)^2 = \chi \tag{2.11}$$

$$\left(\frac{b'}{b}\right)^2 = 1 - \beta + \beta\chi \tag{2.12}$$

$$\left(\frac{r'}{r}\right)^2 = 1 - \beta_r + \beta_r \chi \tag{2.13}$$

And from Equation 2.7,

$$\gamma_a = \ln \chi \tag{2.14}$$

$$\gamma_b = \ln(1 - \beta + \beta\chi) \tag{2.15}$$

$$\gamma_r = \ln(1 - \beta_r + \beta_r \chi) \tag{2.16}$$

Silvestri (1998) showed that the complete stress-strain curve could be obtained from the undrained plane strain expansion of a hollow cylinder by means of the following relationship:

$$\tau_a = \chi(\chi - 1)\frac{dP}{d\chi} + \frac{\chi}{1 - \beta + \beta\chi}\tau_b \tag{2.17}$$

where τ_a and τ_b are the shear stress (i.e., $(\sigma_r - \sigma_\theta)/2$) generated at the inner and outer radii respectively, and $dP/d\chi$ is the slope of the expansion curve, where P is the internal expansion pressure. Equation 2.17 is based on a solution obtained by Nadai (1950).

For the special case of pressuremeter testing in the field, $b/a = \infty$ and $\tau_b = 0$, and Equation 2.17 reduces to

$$\tau_a = \chi(\chi - 1)\frac{dP}{d\chi} \tag{2.18}$$

which is essentially the same equation as that obtained by Baguelin et al. (1972), Palmer (1972), and Ladanyi (1972). Silvestri indicates that because the shearing process is undrained and the soil is subjected throughout the same type of loading, that is, bi-axial loading in a plane strain without rotation of principal stresses, there is a unique shear stress-strain relationship operating throughout the soil mass, for as long as the material remain homogeneous (Baguelin et al.,1972, 1978; Palmer, 1972; Ladanyi, 1972). These particular conditions imply that it becomes possible to consider a shear stress-strain curve of any shape when looking at either the pressuremeter problem or the hollow cylinder problem.

The shear strain γ_a, generated at the face of the cavity, is related to the volume of injected fluid ΔV, necessary to expand the cavity, through the following relationship:

$$\gamma_a = \ln \chi = \ln\left(\frac{a'}{a}\right)^2 = \ln\left(1 + \frac{\Delta V}{V_0}\right) \tag{2.19}$$

where V_0 is the initial volume of the cavity, prior to expansion test. Figure 2-18 shows an example of this analysis on TWC cavity expansion test where $\beta = a^2/b^2 = 0.04$. Figure 2-18a shows the measured net cavity pressure (p_i-u_0; where u_0 is the pore pressure at the start of shearing) versus cavity volumetric strain ($\Delta V/V_0$). The expansion curve in Figure 2-18a has been modified to have net cavity pressure versus distortion parameter (χ), and the results are shown in Figure 2-18b. The interpreted shear stress-strain curve is obtained by first calculating the slope of the expansion curve in Figure 2-18b and then using Equation 2.17. The results are shown in Figure 2-18c. The undrained shear strength (s_u) is equated with the maximum shear stress (τ_{MAX}), that is s_u = 113 kPa.

Silvestri (1998) also showed that the radial and circumferential stresses, σ_r and σ_θ, generated at a distance r from the centre of the cavity are given by the following relationships:

$$\sigma_r = \sigma_{h0} + \int_{\gamma_b}^{\gamma_r} \frac{\tau d\gamma}{(e^\gamma - 1)} \tag{2.20}$$

$$\sigma_\theta = \sigma_r - 2\tau = \sigma_{h0} + \int_{\gamma_b}^{\gamma_r} \frac{\tau d\gamma}{(e^\gamma - 1)} - 2\tau \tag{2.21}$$

where σ_{h0} is the initial total horizontal pressure acting both inside and outside the hollow cylinder, τ is the shear stress, and γ is the natural shear strain. Hence, the radial, circumferential and shear stresses can be determined at various distances from the centre of the cavity and for different levels of cavity strain. Analysis of stress distributions are particularly valuable for determination of the gradual spreading of failure zones and the stress paths experienced by different soil elements around the probe. Total stress paths for shear in the horizontal plane are given by: $p_h = [(\sigma_r + \sigma_\theta)/2]$ and $q_h = \tau = [(\sigma_r - \sigma_\theta)/2]$.

Several researchers have used this method to interpret model pressuremeter tests performed in the laboratory (e.g., Degue, 1998; Diab, 2001; Silvestri et al., 2005). The current research makes use of this method to interpret the results of the undrained model borehole experimental program using the TWC apparatus (Chapter 6).

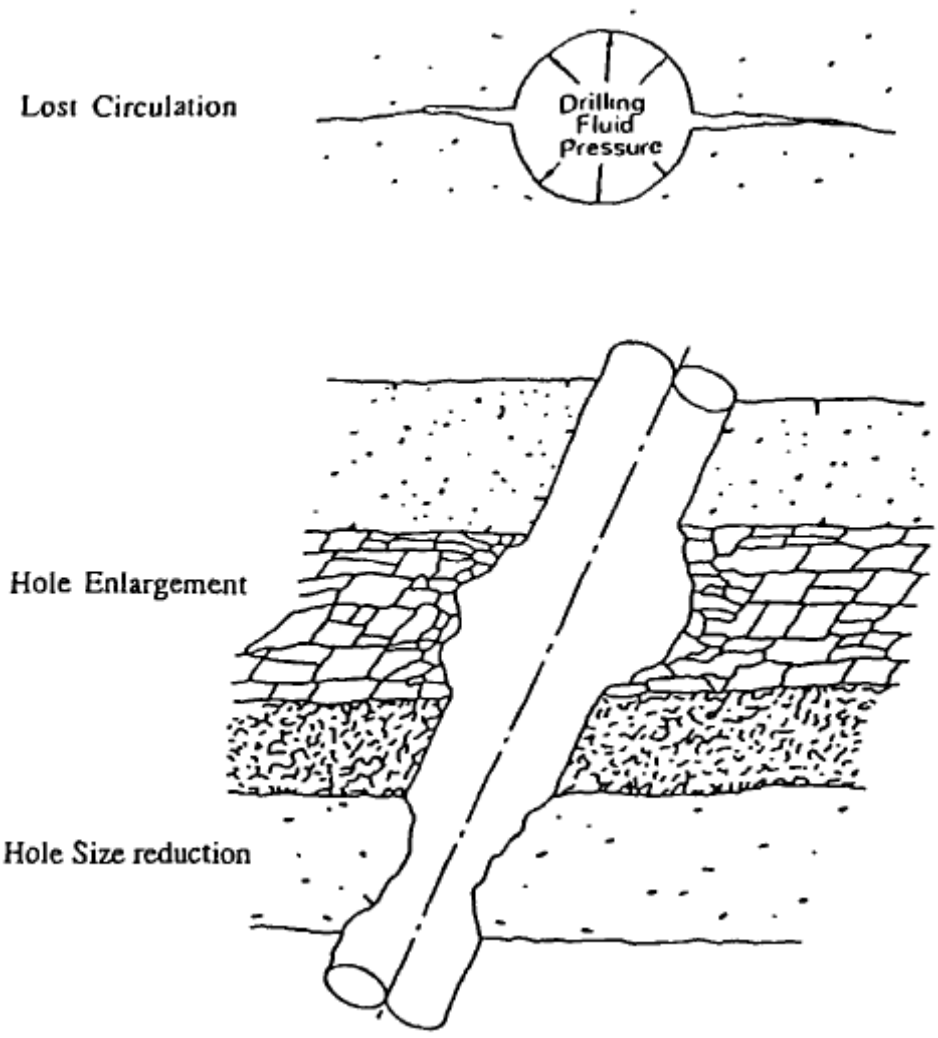

Figure 2-1: Types of stability problems during drilling (from Bradley, 1979)

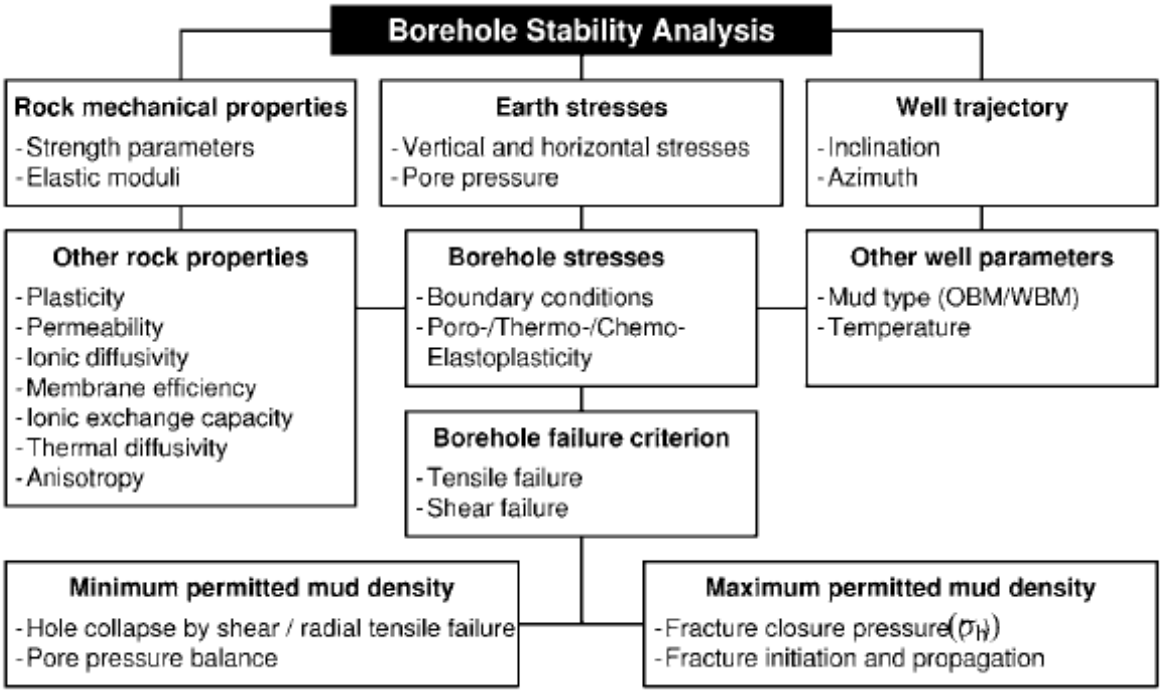

Figure 2-2: Schematic showing a procedure of borehole stability analysis (from Fjaer et al., 2008)

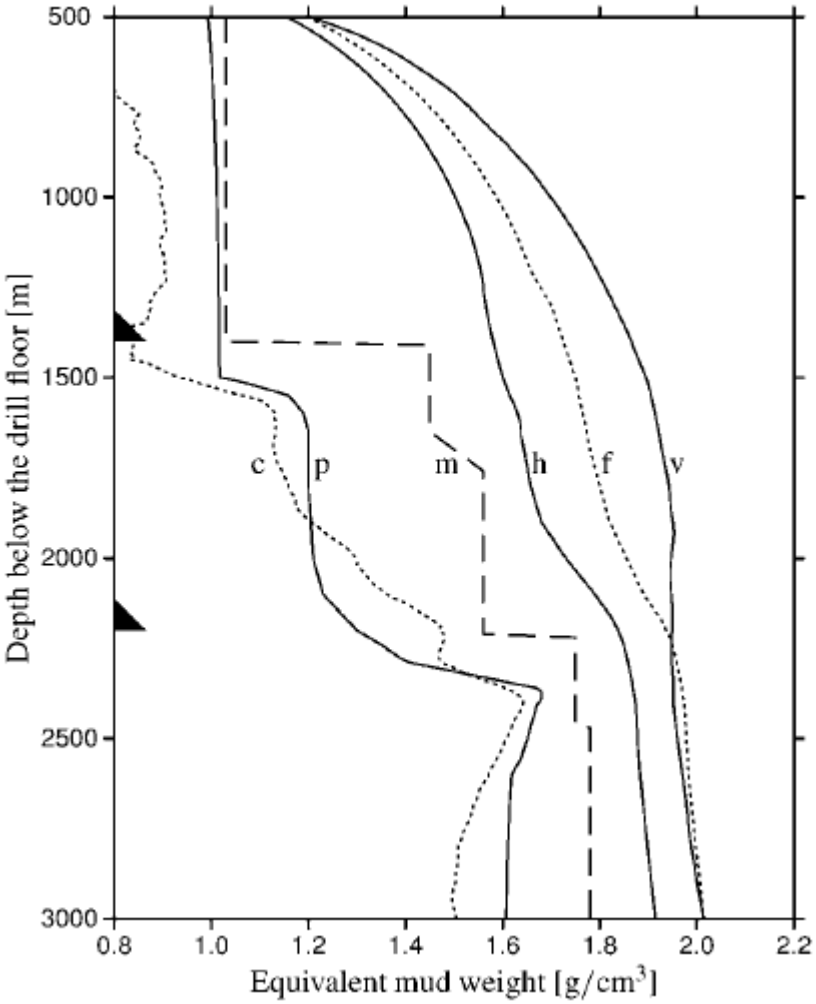

Figure 2-3: Example of a stability chart for a well from the Norwegian Continental Shelf (From Fjaer et al., 2008). The full lines are, from left to right, the estimated pore pressure gradient (p), the minimum horizontal stress gradient (h), and the overburden stress gradient (v). The dotted lines are the estimated collapse gradient (c), and the fracturing gradient (f), while the dashed line is the planned mud weight gradient (m). Casing shoes are indicated by the black triangles

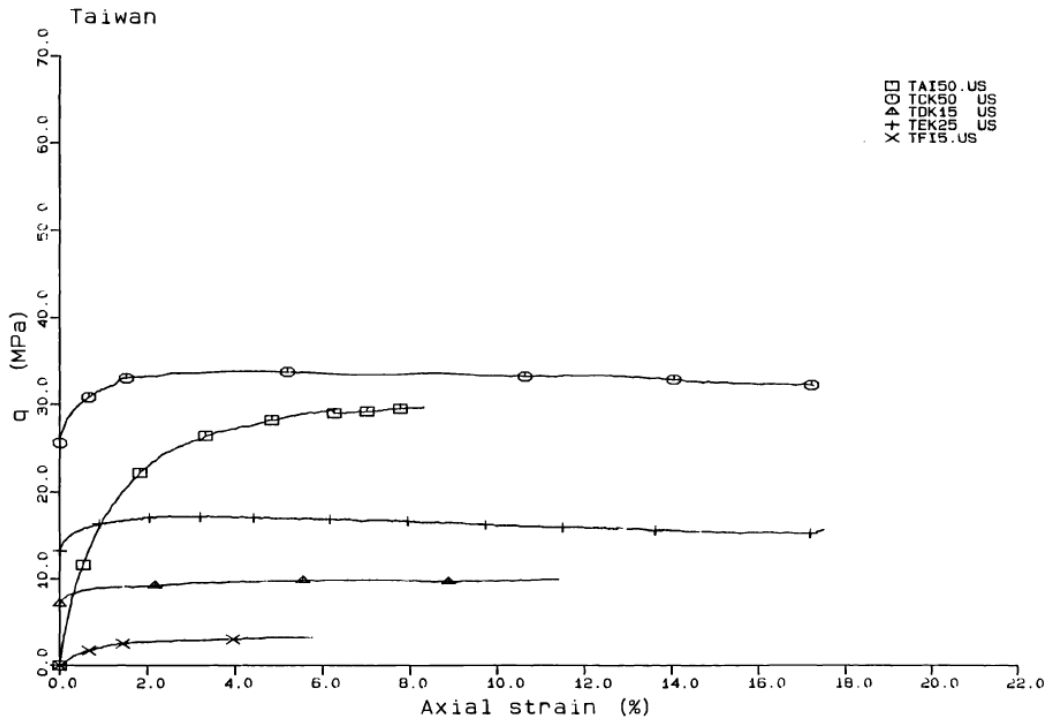

Figure 2-4: Stress-strain behavior in undrained triaxial compression for volcano clays from Taiwan (from Yassir, 1989)

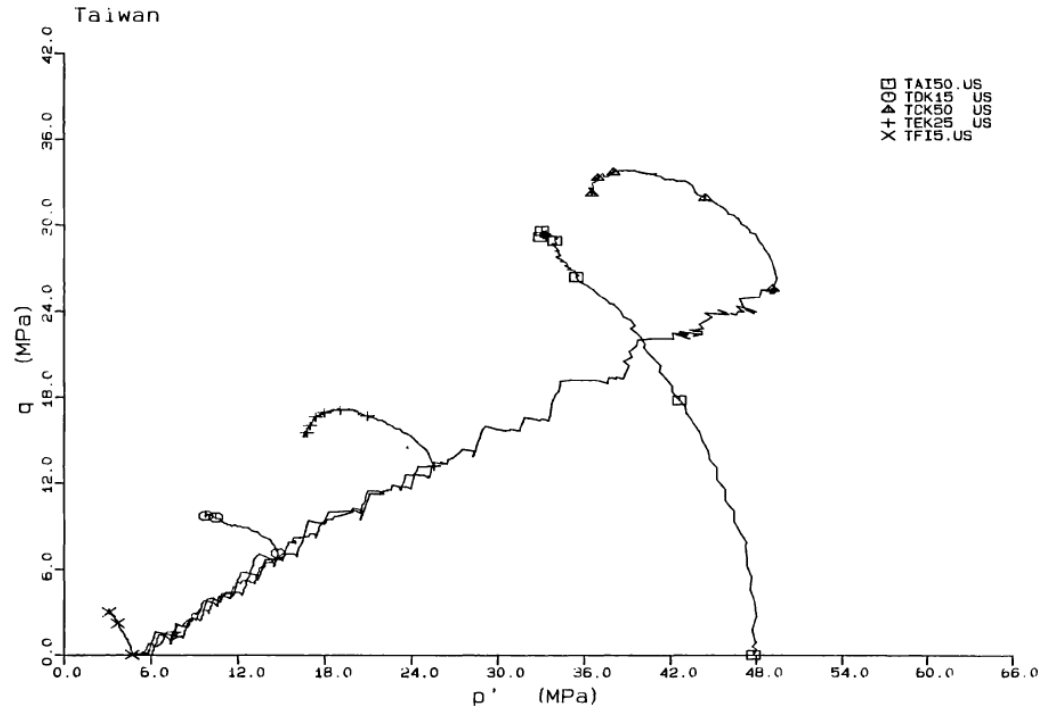

Figure 2-5: Effective stress paths in undrained triaxial compression for volcano clays from Taiwan (from Yassir, 1989)

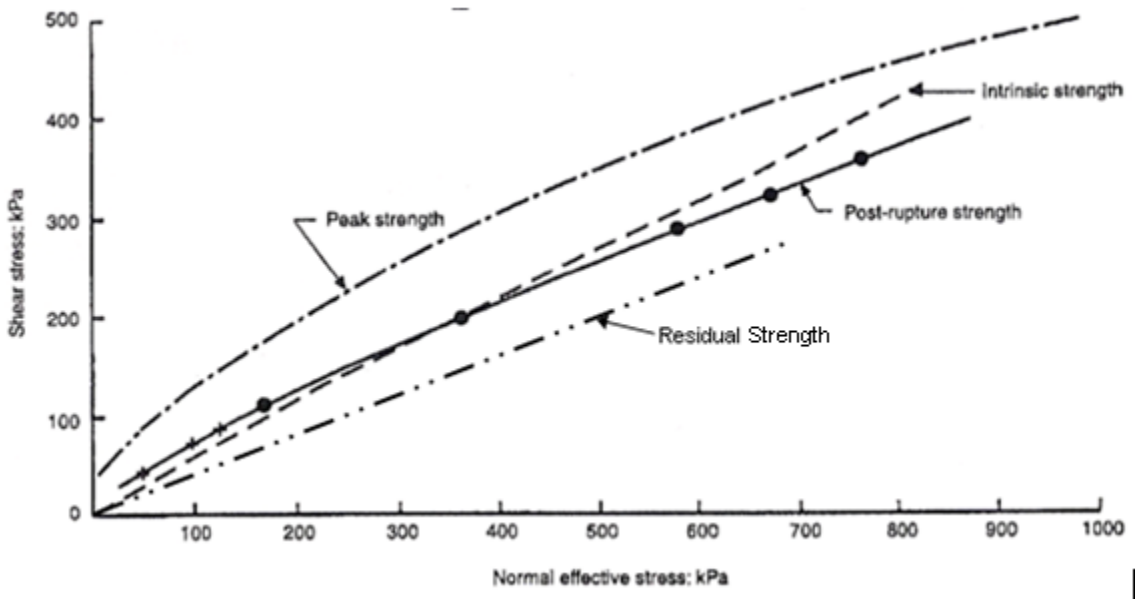

Figure 2-6: Failure envelopes for clays (from Burland, 1990)

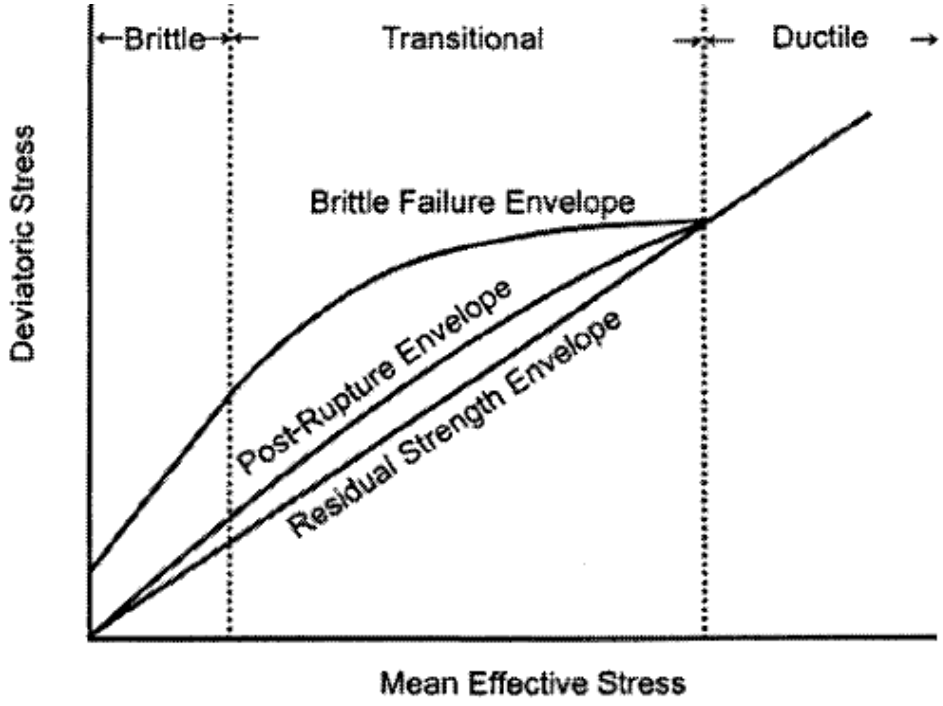

Figure 2-7: Conceptualized failure envelopes for clays (from Petley, 1999)

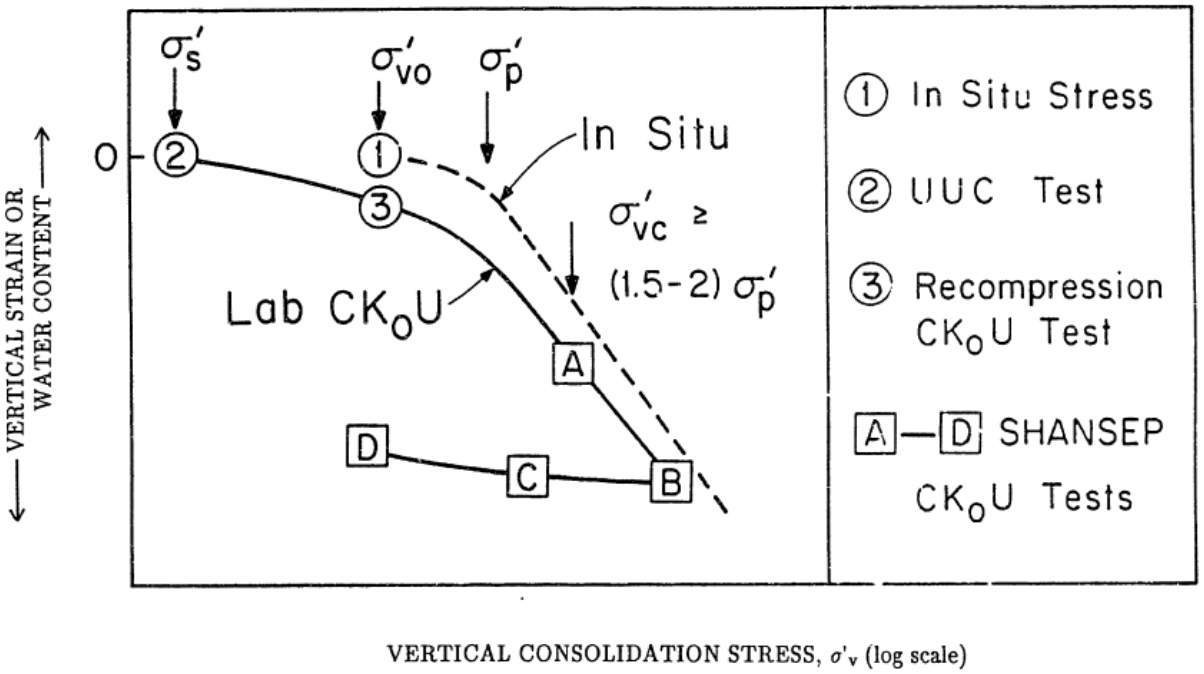

Figure 2-8: Consolidation procedure for laboratory CK_0U testing (from Ladd, 1991)

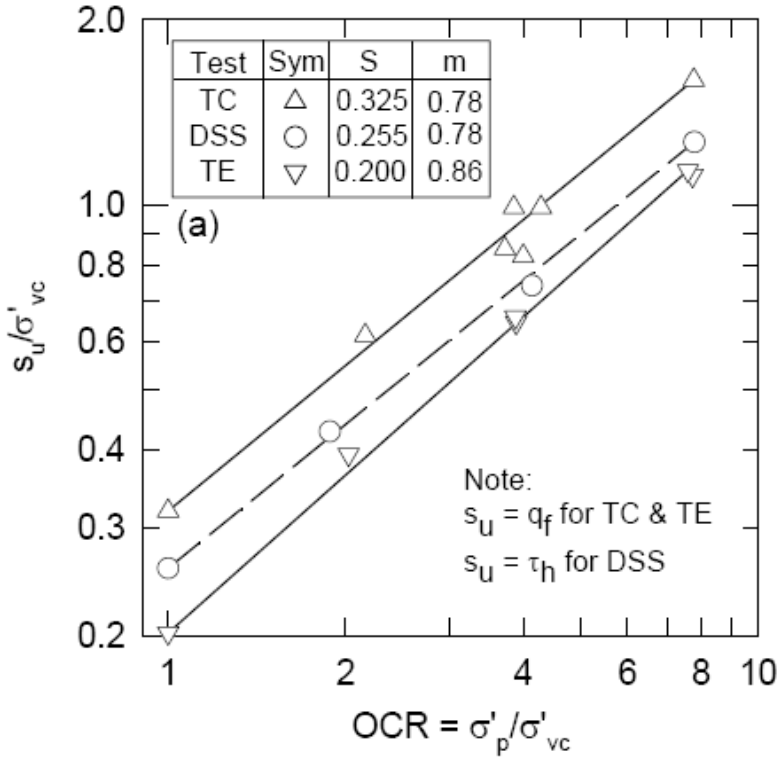

Figure 2-9: Normalized undrained shear strength versus OCR for AGS Plastic Marine Clay via SHANSEP (from Koutsoftas & Ladd, 1985)

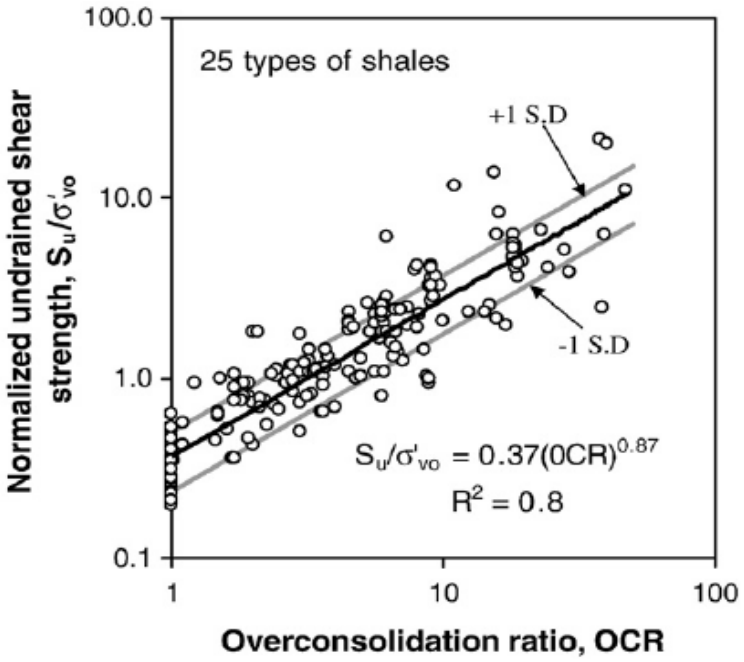

Figure 2-10: Normalized undrained shear strength versus OCR for 25 different types of shales (from Gutierrez et al., 2008)

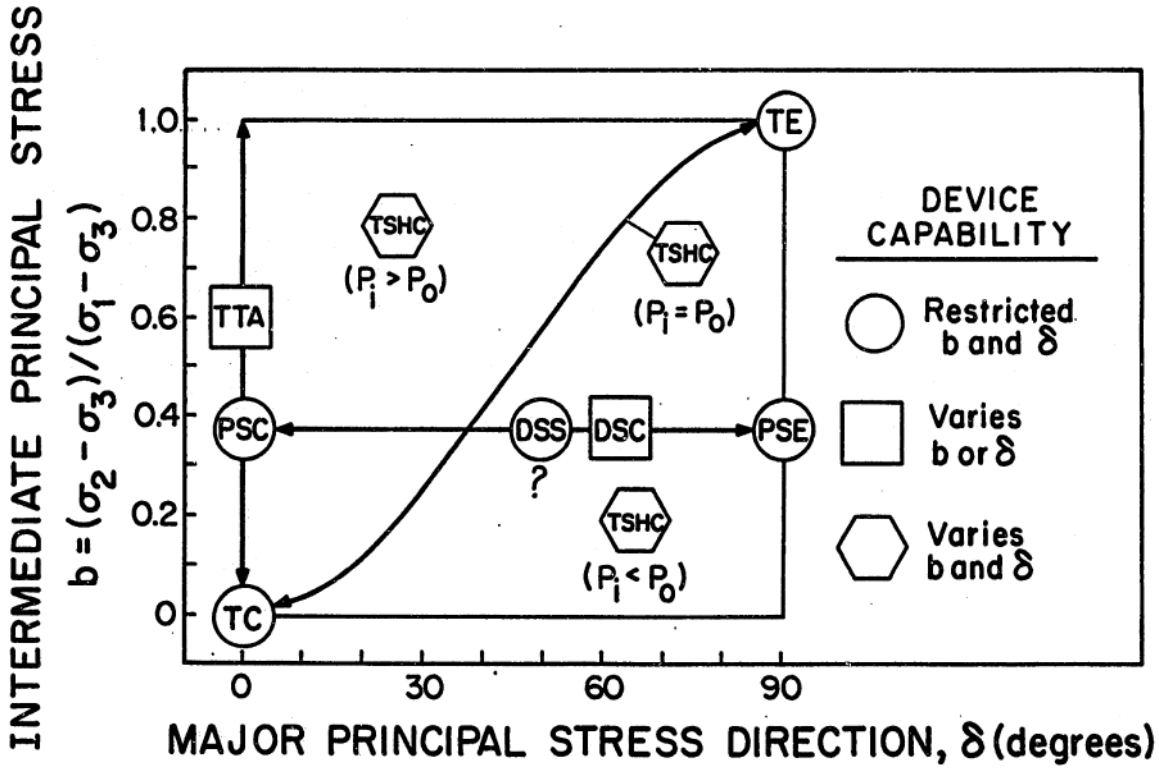

Figure 2-11: Stress systems achievable by shear devices for CK_0U testing (from Ladd, 1991 after Germaine, 1982)

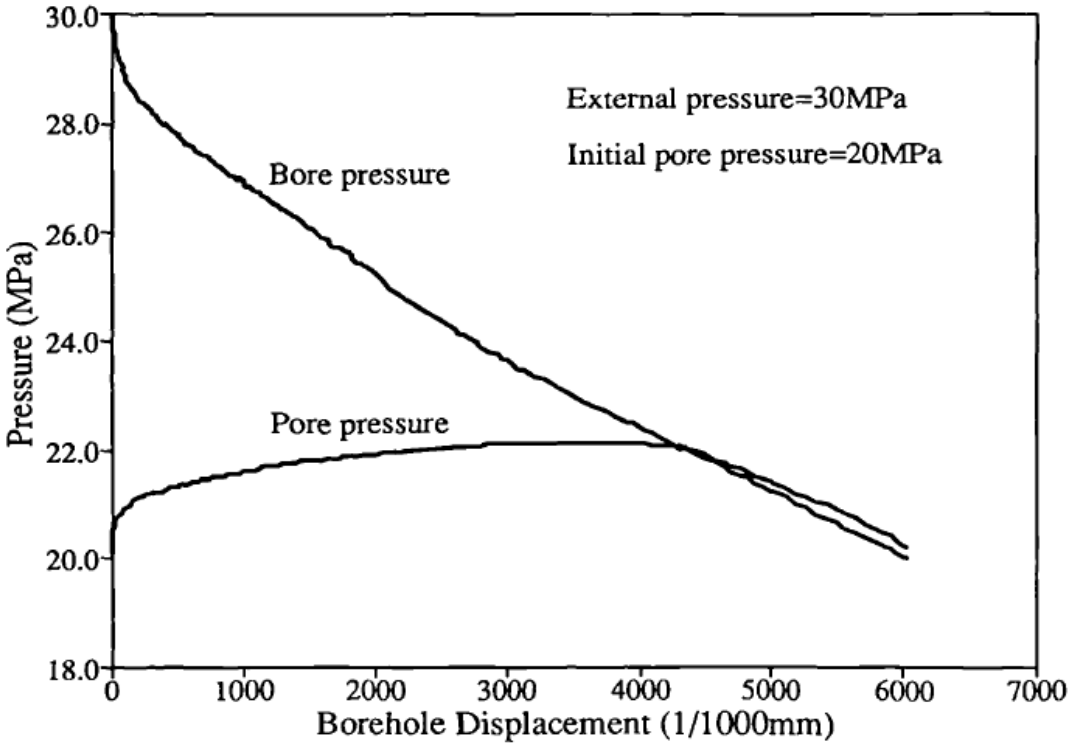

Figure 2-12: Borehole and pore pressures versus borehole closure for HC1 (from Wu, 1991)

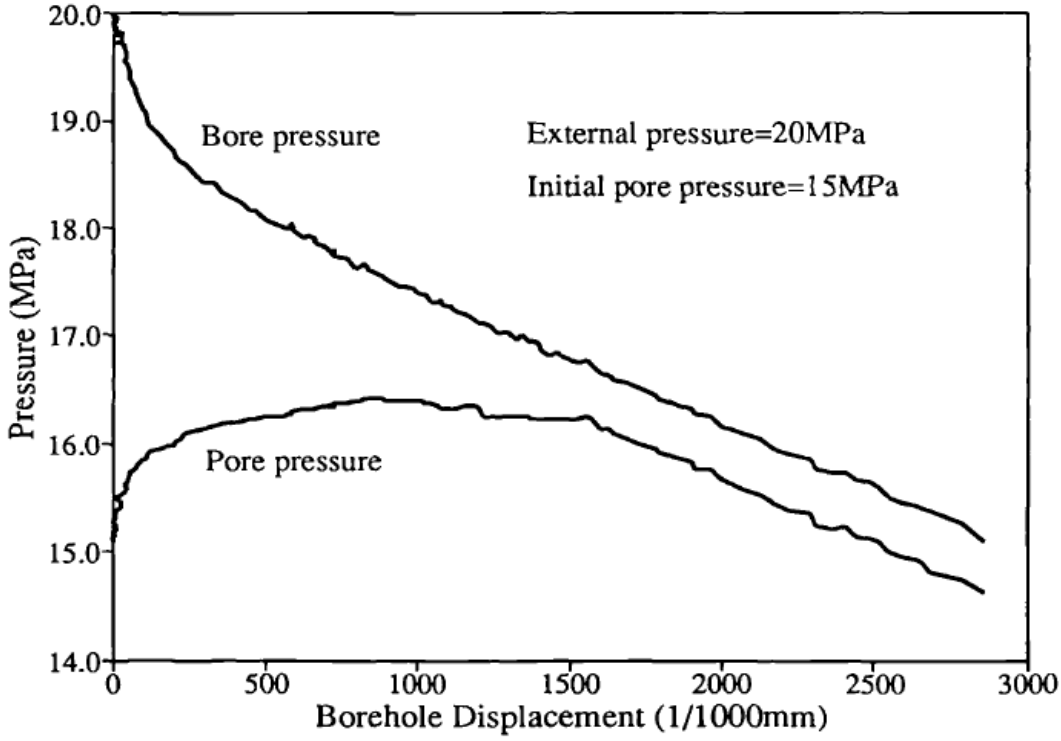

Figure 2-13: Borehole and pore pressures versus borehole closure for HC4 (from Wu, 1991)

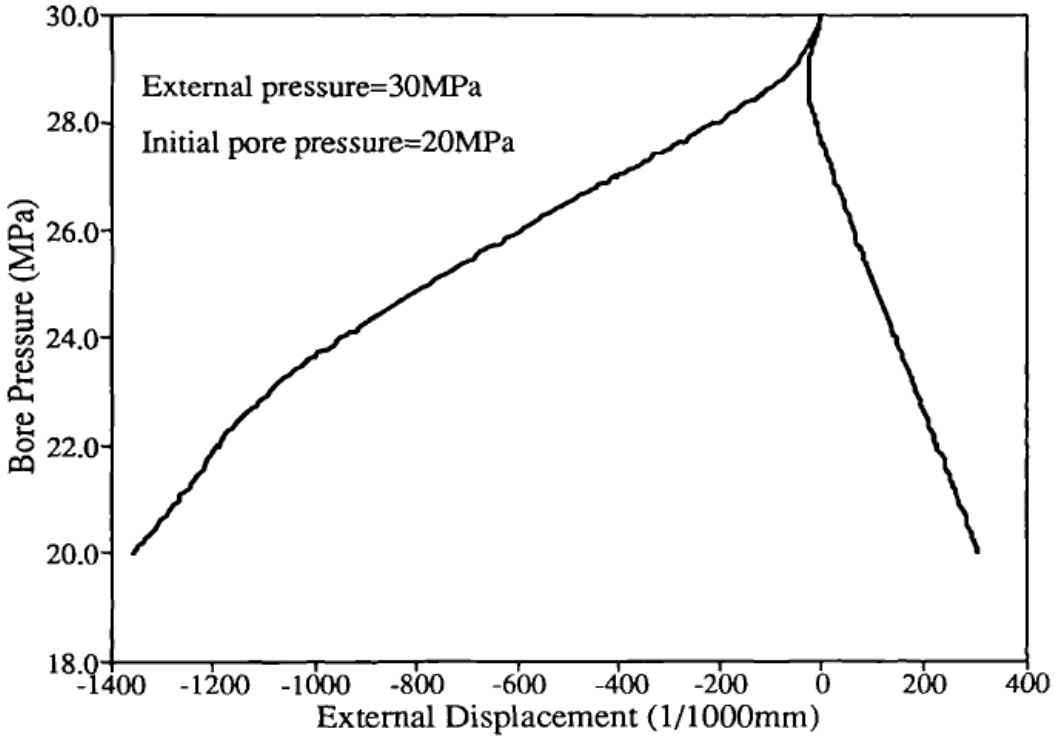

Figure 2-14: Borehole pressure versus external displacements for HC1 (from Wu, 1991)

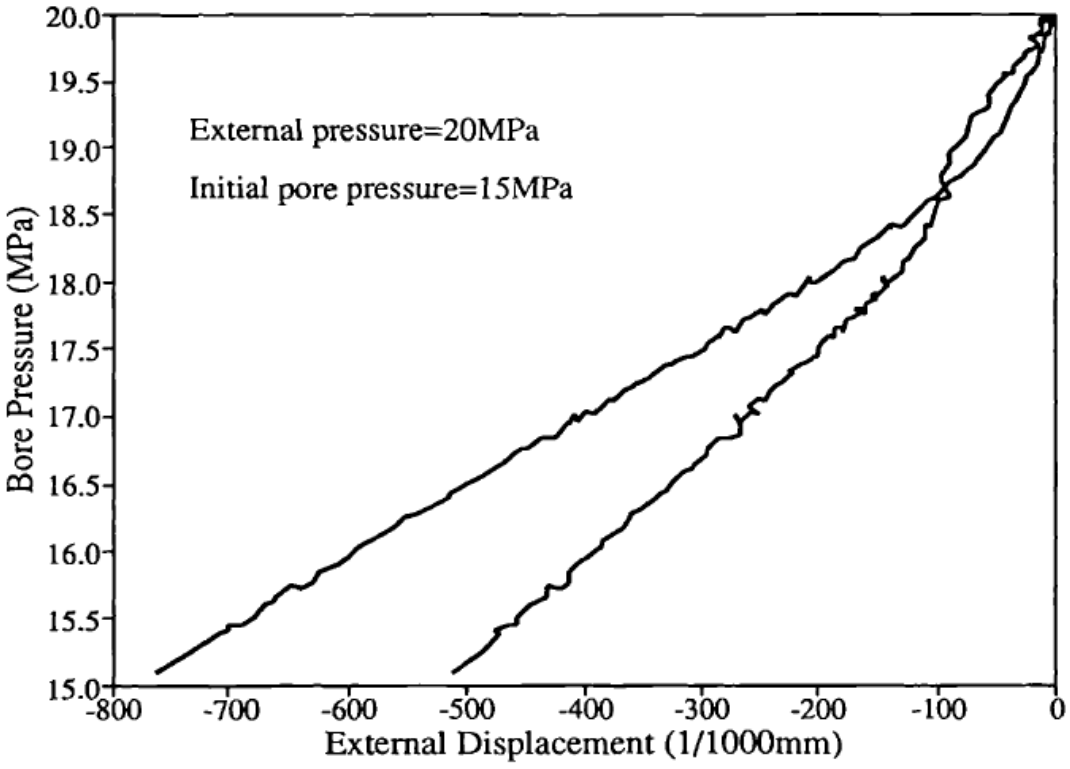

Figure 2-15: Borehole pressure versus external displacements for HC4 (from Wu, 1991)

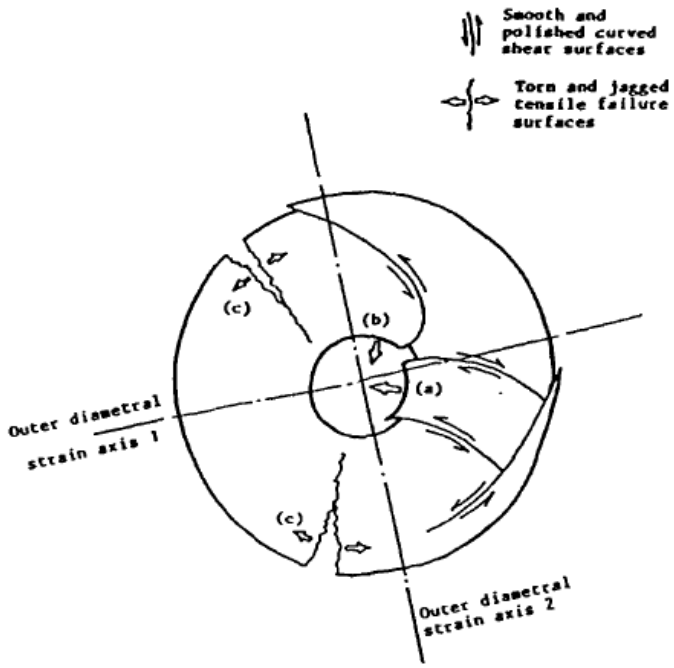

Figure 2-16: Collapse mechanism in the specimen of TWC test (from Wu, 1991)

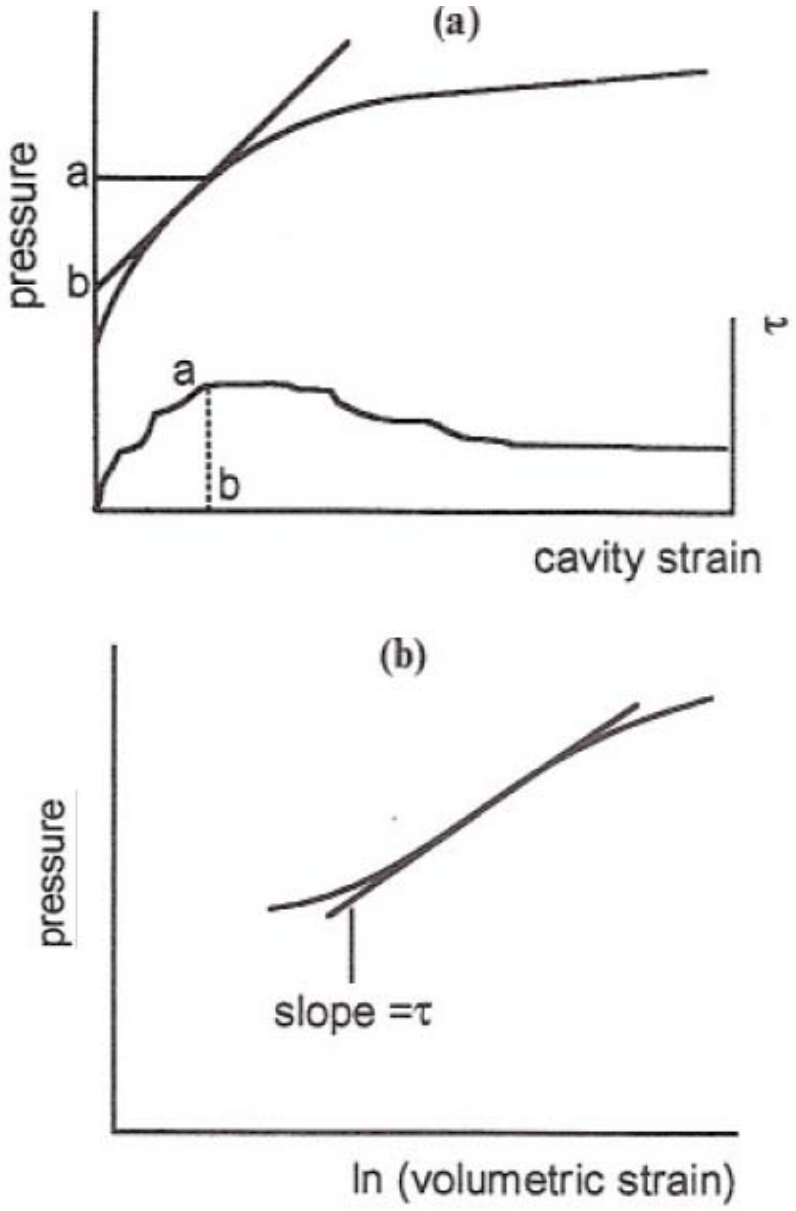

Figure 2-17: Derivation of shear stress for in situ pressuremeter test from curves of pressure against a) cavity strain, and b) volumetric strain

a)

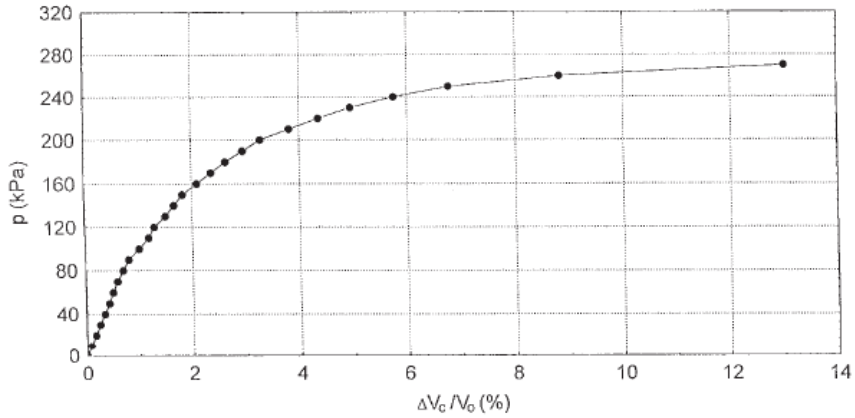

b)

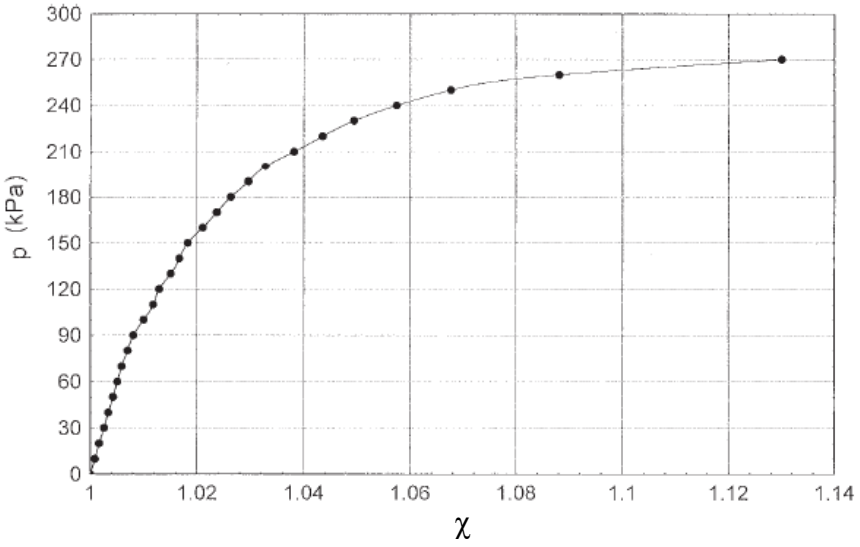

c)

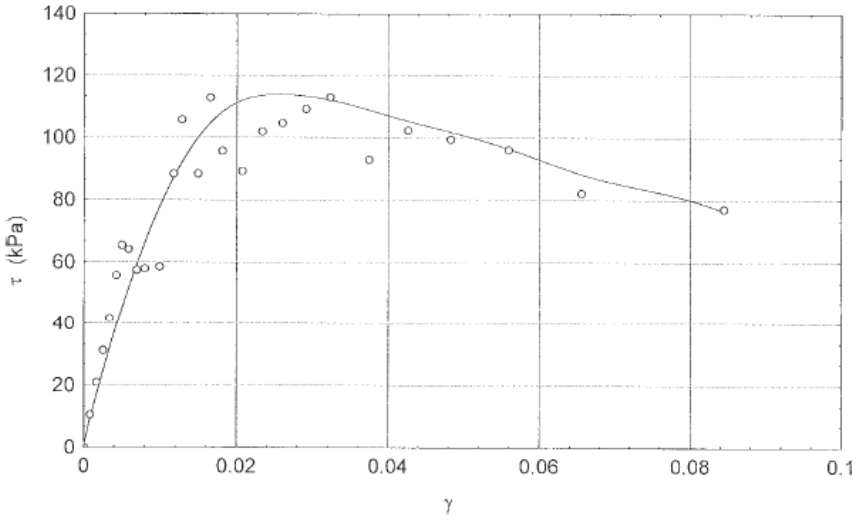

Figure 2-18: Derivation of shear stress for model pressuremeter test: a) net applied cavity pressure versus cavity volumetric strain; b) net applied cavity pressure versus distortion parameter; c) shear stress-strain (from Silvestri, 1998)

3 RESEDIMENTED BOSTON BLUE CLAY

3.1 INTRODUCTION

This chapter presents an overview of Resedimented Boston Blue Clay (RBBC), the test material employed in the current experimental program. RBBC is prepared by resedimenting natural Boston Blue Clay (BBC), an illitic glacio-marine clay of low plasticity (CL) and medium sensitivity. BBC was deposited in the Boston basin about 12,000 to 14,000 years ago following the Wisconsin glacial period (Kenney, 1964).

RBBC has several attractive features that make it an excellent reference material for research purposes. Its engineering properties are very similar to many natural, uncemented clay deposits, including stress-strain-strength anisotropy, low to medium sensitivity, significant strain rate dependency, and fairly typical consolidation characteristics. Since RBBC has been studied at MIT since 1961, there is an extensive database on the engineering properties of this material. Furthermore, the resedimentation process virtually eliminates spatial variability among specimens and provides uniform samples with well-defined, one-dimensional stress history. Along with its local relevance, complete saturation, and virtually infinite supply represent the key characteristics which have made this soil an ideal research material to investigate fundamental aspects of soil behavior without having to take into account the variability of natural soils. In addition, the well-defined and repeatable behavior of RBBC has also made it an asset in the development and proofing of new laboratory shear devices, as well as in the modification of existing apparatuses.

There has been extensive analytical research to model the properties of RBBC since the three generalized constitutive models formulated at MIT (MIT-E1 Kavvadas, 1982; MIT-E3 Whittle, 1987; MIT-S1 Pestana, 1994) have all been comprehensively validated using the wide database for RBBC. This provides a very useful source of information on soil behavior under a variety of testing conditions. Moreover, a number of projects were carried out at MIT, including this one, where the work comprised an integrated program of laboratory experiments on RBBC, numerical model calibration and validation.

Table 3-1 summarizes the research performed on RBBC since the 1960's (extended from Santagata, 1998). Although the use of laboratory resedimentation at MIT was pioneered by Wissa (1961), it was Bailey who first resedimented BBC in 1961. RBBC has been used in laboratory element tests as well as model tests. Element tests were conducted using the triaxial apparatus (e.g., Varallyay, 1966; Bensari, 1983; Sheahan, 1988, 1991; Santagata, 1994, 1998; Abdulhadi, 2009), plane strain device (e.g., Dickey, 1967; Bovee, 1968), Direct Simple Shear (DSS) device (e.g., Malek, 1987; DeGroot, 1989; Ahmed, 1990; Ortega, 1992), Constant Rate of Strain (CRS) device (e.g., Force, 1998; Gonzalez, 2000), and Directional Shear Cell (DSC) device (e.g., Germaine, 1982; Seah, 1990). On the other hand, model tests on RBBC include work performed by Kinner (1970) on the behavior of strip footings, and evaluation of the performance of suction caissons (Cauble, 1996) among others. The current research focuses on model borehole tests together with undrained triaxial shear and CRS 1-D consolidation element tests.

Natural BBC is present throughout the Boston area and varies in thickness from 20 to 40 m. While the depositional history and general characteristics of BBC are similar throughout the Boston area, some variability can be expected in soil from different locations, and thus in the resedimented BBC made from these different natural sources. The properties of the clay depend on several factors, for example, the particle size distribution, the chemistry of the pore fluid and the mineralogy.

The origin of the natural material employed to manufacture RBBC defines the batch series, and to this day BBC has been obtained from four different locations and therefore four series of RBBC exist. The material used in this thesis is from Series IV, obtained in 1992 from the base of an excavation for MIT's Biology Building (Building #68). Approximately 2500 kg of soil was obtained at a depth of about 12 m, with an in situ overconsolidation ratio ranging from 1.3 to 4.3 (Berman, 1993). The soil was processed as described in Section 3.2.2, and the dry powder was stored in sealed 40 gallon containers (Cauble, 1996). This study used about 2 containers while there are still 6 full containers left. Previous tests from 1988-1994 used Series III BBC, which was obtained by augering from a depth of 23 m during construction of parking garage near Kendall Square in Cambridge.

The resedimentation procedure, initiated in the early 1960's, has gradually been refined and improved through the years. The most significant improvement was made by Germaine (1982)

who refined the resedimentation technique to produce fully saturated and uniform samples of RBBC. The soil cake produced from this technique was trimmed into smaller pieces and stored to be used for a number of tests. This research introduces a new manufacturing procedure as each consolidometer is used to prepare an individual test specimen. The equipment and manufacturing procedure are discussed in Section 3.2. The effect of the consolidometer side-wall friction on the uniformity of the specimens is also briefly addressed in this section.

Section 3.3 presents the batch data for RBBC. This includes consolidation characteristics and material index properties including grain size distribution, Atterberg limits, specific gravity, and salt concentration data. These data are important to verify that the material from a new source exhibits characteristics similar to that of the soil previously used.

Since RBBC has been used at MIT for over 45 years, its behavior as a function of stress history and stress system is well documented. Thus a database exists that permits comparison with new experimental results. Section 3.4 provides a summary of the mechanical behavior of RBBC. This section addresses the behavior during K_0-consolidation, and during undrained shear in triaxial compression and extension and in direct simple shear, which are relevant to the current research. The results presented in this section are limited to the tests performed on RBBC Series III and IV.

3.2 RESEDIMENTATION PROCEDURE

3.2.1 Introduction

Batches of BBC are prepared by one-dimensionally consolidating a dilute slurry of soil in a cylindrical container (consolidometer). The earlier methods (e.g., Ladd & Varallyay, 1965) produced partially saturated samples that were subsequently saturated using a 200 kPa back pressure. Germaine (1982) substantially refined this technique to produce fully saturated, uniform samples of RBBC with salt concentration of 16 g/l. Further modifications were introduced by Seah (1990) to increase productivity, improve sample uniformity, and to allow continuous monitoring of the consolidation process.

All these techniques produced a large soil cake that was trimmed into smaller pieces (depending on project requirements) and stored for use in a number of tests. The technique

developed by Germaine (1982) uses an apparatus that consists of three major components: an upper mixing chamber where the rotating blades mix the powder with 100% water content under vacuum; a lower free fall chamber and a stainless steel consolidometer which receives the sprayed slurry and consolidates the soil. A schematic of this apparatus is shown in Figure 2-1. After consolidation is completed, the soil cake (30 cm in diameter and about 12.5 cm tall) is removed from the consolidometer, carefully trimmed and prepared for storage (Santagata, 1998). Each batch produced using this technique was given a number (typically numbered in sequence), and the index and engineering properties are often referenced to the batch number.

The following subsections present the procedure presently used to manufacture RBBC and discuss the effect of side-wall friction on the uniformity of the samples.

3.2.2 New Resedimentation Procedure

A new resedimentation procedure has been developed in order to produce individual test specimens. Three types of consolidometers were used to prepare specimens for triaxial, small and large diameter Thick-Walled Cylinder (TWC) tests. The triaxial consolidometer (Figure 3-2) was adapted from an oedometer apparatus. It has a stainless steel sleeve with 6.5 cm diameter and 20 cm height. The consolidation containers for the TWC consolidometers are clear plexiglass tubes (Figures 3-3 and 3-4). The small TWC tube has a 7.6 cm diameter and 45.7 cm height, while the large TWC tube has 15.2 cm diameter and 63.5 cm height. There are at least two consolidometers for each type in order to prepare batches of RBBC concurrently and hence, maximize the production process.

The manufacturing procedure of RBBC can be divided into four main steps: processing, deposition, consolidation, and sample extrusion and preparation:

a) Material Processing

The natural BBC was softened with tap water and mixed into a thick slurry. The slurry was then passed through a #10 US standard sieve to remove all non-natural material, gravel, coarse sand, and large shell fragments and oven-dried at 60°C in preparation for grinding. The dried material was ground to 95% passing a #100 US sieve by the Sturtevant Company using a roller mill. Finally, the material was manually randomized by two blending operations. The dry powder (RBBC Series IV) was stored in sealed 40 gallon containers (Cauble, 1996).

b) Deposition

The dry soil powder is thoroughly mixed with de-aired water (to achieve a water content of 100%) in order to produce a homogenous soil slurry without lumps. Note that this water content is about double the liquid limit (43 – 47 %) and agrees with the recommendations of Burland (1990). This results in a workable yet stable slurry (i.e., no free water at the surface). Sodium chloride is added to the slurry (to achieve a concentration of 16 g/l) in order to produce a flocculated particle structure and to prevent segregation of soil particles during sedimentation. Hence, the resulting soil structure is similar to that of natural BBC. The slurry is then vacuumed to get rid of the entrapped air bubbles using the setup shown in Figure 3-5. The flask used to vacuum the slurry has two lines: one line is connected to the vacuum pump (water aspirator) while the second line is used to pull the slurry from the adjacent container. The slurry is effectively de-aired as it drops into in the vacuum flask. Subsequently, the de-aired slurry is gradually placed in the consolidometer from bottom to top using a funnel with a long tube to minimize air entrapment as shown in Figure 3-6. Note that the walls of the triaxial consolidometer are greased with high vacuum grease while the walls of the TWC consolidometer are cleaned with silicone oil to minimize friction during consolidation and extraction of the soil from the consolidometer.

The consolidation of the RBBC slurry takes place in a rigid-walled consolidometer. The general setup of the consolidometer involves a tube (consolidometer wall) sitting on a base porous stone in a bath of water as illustrated in Figure 3-3. A smaller porous stone (diameter equal to the inside diameter of the tube) topped with filter paper is located inside the tube and separates the soil slurry from the base stone to prevent extrusion of the slurry. Another porous stone and filter paper lay on top of the slurry and a top cap is placed over the stone. The soil consolidates by applying load at the top through a piston.

c) Consolidation

The soil slurry is loaded incrementally, with a load increment ratio, $\Delta\sigma_v/\sigma_v = 1$, to a prescribed maximum vertical effective stress then unloaded to overconsolidation ratio (OCR) of 4. At OCR = 4 the soil is close to hydrostatic effective stress conditions (i.e., $K_0 = \sigma'_h/\sigma'_v \approx 1.0$) and therefore, the shear strains due to sample extrusion from the consolidometer are minimal, as confirmed by the work performed by Santagata (1994). Hence RBBC samples have essentially

no sample disturbance. The first few load increments in the consolidometer (up to 0.1 MPa) are applied using dead weights (e.g., Figure 3-3b). The consolidometer is then placed in a purpose-built load frame and is loaded by an air pressure actuator to achieve higher consolidation stresses (e.g., Figure 3-7). Throughout this consolidation phase, the vertical deformation is measured by a single displacement transducer (LVDT) to mark the end of primary consolidation and to establish the compression behavior of the slurry. Each load increment is maintained at least until the end of primary consolidation as determined by Casagrande log time method (typically 1 - 2 days for triaxial test specimens; 3 - 4 days for small diameter TWC test specimens; 5 - 8 days for large diameter TWC test specimens), while the maximum stress is held for one cycle of secondary compression (typically 2 days). The consolidation process in the consolidometer, which has double drainage, lasts from 3 to 4 weeks for the triaxial test specimens, 4 to 6 weeks for the small diameter TWC test specimens, and from 6 to 9 weeks for the large diameter TWC test specimens depending on the stress level. Additional information on the batch consolidation behavior is presented in Section 3.3.3.

The RBBC soil prepared for the triaxial tests is resedimented to maximum vertical stress of 0.1 MPa when the low pressure triaxial apparatus is used and to maximum vertical stress of 1.0MPa when the high pressure triaxial apparatus is used. However, the soil prepared for the TWC tests is consolidated to stresses proportional to those used in the TWC apparatus to reduce consolidation time in the apparatus and to minimize the subsequent consolidation strains in the test specimen. This is an important design consideration as the TWC apparatus setup has a rigid top drainage line that cannot accommodate large strains.

d) Sample Extrusion and Preparation

After consolidation is completed, the soil is removed from the consolidometer and prepared for testing. The triaxial and small TWC soil specimens are extruded from the consolidometer by slowly pushing the specimen out while holding the wall, taking advantage of the lubricant on its interior. If the soil is consolidated to high stresses (greater than 1 MPa), a hydraulic jack is used to extrude the soil. As for the large TWC consolidometer, a load frame with sizeable clearance to accommodate the consolidometer setup is employed to extract the soil specimen from the plexiglass tube.

The specimens prepared for the triaxial tests require trimming of the outside surface to the final diameter (3.6 cm) after extrusion. This is done using a wire saw and a mitre box. On the other hand, the soil prepared for the TWC tests is consolidated in smooth plexiglass tubes with an inside diameter equal to the diameter of the TWC test specimen and therefore eliminates the need for trimming the specimen after extrusion. Consequently, the ends of the specimen are shaved off and the soil is cored using a drill press to create a hollow cylinder specimen before mounting on the apparatus (this process is explained in more detail in Chapter 4).

3.2.3 Evaluation of Specimen Uniformity

As the soil sample consolidates in the consolidometer, the vertical stress at the base of the specimen can be less than that at the top due to side friction along the wall. This can affect the uniformity of the soil sample. Also, side friction can create variations in the batch radially, since differential settlement may occur across the specimen. Germaine (1982) and Seah (1990) evaluated the quality of the RBBC samples prepared in the large consolidometer (i.e., 30 cm diameter consolidometer). Uniformity of individual batches was confirmed by measuring the variation of water content throughout the specimen, using x-ray diffraction pattern on different samples and air drying of vertical and radial slices to check for stratification. Results from all these procedures verified that the batches were indeed uniform.

The RBBC specimens used in this research were prepared in consolidometers with altered dimensions. Moreover, the TWC test specimens were extracted from the consolidometer and cored with no trimming of the outer wall prior to test setup. As a result, the effect of the wall friction from these new consolidometers on the sample uniformity has been carefully evaluated. Table 3-2 shows the dimensions and areas (surface and cross section) of the consolidometer samples used in this research compared to the large consolidometer soil cake produced in previous years. The table also includes information on the small plexiglass triaxial consolidometer which is used to prepare triaxial test specimens without trimming the outside surface (i.e., inside diameter of consolidometer tube is 3.6 cm). This consolidometer was employed by some researchers (e.g., Mazzei, 2008) and was used in this study to evaluate the effect of side friction on the untrimmed specimen after extrusion. Figure 3-8 shows the setup for the small plexiglass triaxial consolidometer.

The table indicates that the four consolidometers used to prepare individual test specimen have greater height to diameter (at end of batch consolidation) and surface area to cross sectional area ratios than the large consolidometer used in the past. This suggests that the side friction is more critical in these new consolidometers. On the other hand, the batch consolidation data presented in Section 3.3.3 show very small variation in the compression behavior between the RBBC soil specimens prepared in the three consolidometers used in this research. These results also agree well with previous research where the large consolidometer was used.

For the triaxial test, a substantial portion of the outside surface is trimmed and therefore the test is performed on a specimen from the core of the soil batch. As a result, the triaxial consolidation and shear results agree very well with previous results for specimens trimmed from the large consolidometer soil cake. Measurements of water content throughout the triaxial specimen also confirm uniformity.

In the case of the TWC specimens, the outside surface is not trimmed after extrusion. The side friction due to consolidation and removal of the soil from the consolidometer might create slightly disturbed and smeared outer layer. Specimen coring can also smear the inside wall of the specimen. It is possible that the consolidation results are affected as the specimen may well incorporate some disturbed and weaker portions. Nevertheless, reconsolidation of the specimen in the TWC apparatus to higher stresses (than the initial maximum consolidation pressure in the consolidometer) ensures that the specimen is uniform before shearing. This was confirmed by comparing the consolidation and shear results of two K_0-consolidated undrained triaxial compression (CK_0UC) tests on RBBC where one specimen was prepared in the standard triaxial consolidometer while the second was prepared in the small plexiglass triaxial consolidometer (without trimming of the outside surface). The test results are presented in Figures 3-9 to 3-14. Both specimens were consolidated to the same stress in the consolidometer (0.1 MPa) and triaxial apparatus (0.35 MPa). Figures 3-9 and 3-10 show the second phase of consolidation (prior to shearing in the triaxial). At the final consolidation stress, σ'_{vc} = 0.35 MPa, the two specimens have almost identical void ratio, but slightly different K_0 stress and axial strain (K_0 trend with vertical stress is shown in Figure 3-11). Their undrained shear stress-strain response (Figures 3-12 and 3-13) is practically identical, with both tests having the same strain to peak, strength, and shear resistance at large strains. The small difference in the effective stress paths at the beginning of shearing (Figure 3-14) reflects the variation in preshear K_c.

3.3 BATCH DATA

3.3.1 Introduction

The properties of natural BBC vary widely over the Boston area even though the basic mineralogy of the clay is thought to be the same. Therefore, each time new material is obtained for resedimentation, it is necessary to perform several index and engineering tests to verify that the soil is sufficiently similar to the prior material. Another purpose is to obtain basic engineering properties needed to characterize any cohesive soil that is used for research. Resedimentation of BBC at MIT has produced close to 70 recorded batches of testing material for a variety of projects. This has generated an extensive database of material index and engineering properties. Table 3-3 summarizes the specific gravity, Atterberg limits, clay fraction and salt concentration values reported for RBBC used in research since 1961 (Series I, II and III). Table 3-4 lists the index data for Series IV RBBC used in this research.

In general, the index properties are quite consistent (with the exception of Series Ia RBBC). Specific gravity does not vary very much, ranging from 2.75 to 2.79. The Atterberg limits, however, change quite significantly among the different series. The plastic limit variation between 18 and 23% is relatively small compared with the 33 to 46% range for the liquid limits (lower liquid limits for the older batches). This variation is primarily due to the amount of clay size fraction in the soils which varies between 35 and 58%. The soil classification for all RBBC, including the earlier batches, is low plasticity (CL) clay. The salt concentration generally varied between 8 to 24 g/l.

The following subsections summarize the index properties for RBBC Series IV used throughout the experimental program presented in this thesis. Consolidation data from the original batch resedimentation process are also presented.

3.3.2 Index Properties for Series IV RBBC

Figure 3-15 shows the grain size distribution for series IV BBC powder obtained from the hydrometer test. The distribution shows that the soil has a fine fraction (% passing #200 sieve) greater than 98% and an average clay fraction (% less than 2μm) of 56%. The fine fraction and clay fraction agree with previous data for RBBC IV but are slightly higher than the respective data from RBBC III (90-95% and 46-56% respectively).

Atterberg limits were performed on the BBC powder (using distilled water) to check the index properties of the clay. The liquid limits were determined using the Casagrande cup, and the plastic limits using the "rolling" method (ASTM Standard D4318). The current batch has average plastic limit, w_p = 23.5±1.1%, liquid limit, w_L = 46.5±0.9% and plasticity index, I_p = 22.7±1.2%. These results are within the standard deviation of the values reported by Cauble (1996) for RBBC IV. The liquid limit and plasticity index data for RBBC IV are plotted on the plasticity chart in Figure 3-16 confirming the classification of RBBC as a low plasticity clay (CL).

Measurements of specific gravity G_s for Series IV RBBC yielded an average value of 2.81, which is same value obtained by Cauble (1996) but slightly higher than previous research. However, this value is within the expected range for illitic clays (G_s = 2.60 to 2.84 for illite; Lambe and Whitman, 1968).

Salt content was measured using the conductivity method recommended by Martin (1970) and calibrated against a KCL standard. The average value determined for Series IV RBBC was 12.5±1.5 g/l. As discussed in section 3.2.2, salt is added to the soil slurry during resedimentation.

Organic content by combustion yielded a value of 4.4% for Series IV RBBC (Cauble, 1996). These data are not available for previous series of RBBC.

3.3.3 Consolidation Behavior

Since the soil slurry is incrementally loaded in the consolidometer and the loads and resulting displacements are known, the one-dimensional behavior can be analyzed as in a standard incremental oedometer test. The consolidation process for the soil slurry starts with a very low vertical consolidation stress increment (about 1 kPa), and goes up to a maximum vertical stress of 1 MPa for the triaxial test specimens and up to a maximum stress of 6 MPa for the TWC test specimens. This study has produced more than 40 triaxial test specimens, about 20 small diameter TWC test specimens, and 2 large TWC test specimens. The batch consolidation data for the soil prepared in each type of consolidometer were almost identical and therefore the "typical" results (i.e., results from a representative consolidometer test) for the three consolidometers are presented here. Table 3-5 summarizes pertinent batch consolidation characteristics.

The end of primary consolidation for the soil batches prepared in the three consolidometers is different as the dimensions (drainage length) vary. In general, the time to reach end of primary is extremely long (several days) for the first few increments, and therefore the increments were sometimes placed before the end of primary is reached in order to reduce the time of consolidation. At vertical consolidation stresses greater than 0.02 MPa, the end of primary is reached in reasonable time and a full settlement-time curve could then be analyzed. Figure 3-17 shows typical settlement-(log)time curves at a vertical consolidation stress increment of 0.03MPa for the soil prepared in the triaxial, small and large TWC consolidometers. The figure shows that the end of primary (obtained using the log-time method) is about 14 hours for the triaxial test specimen, 72 hours (3 days) for the small TWC test specimen and about 180 hours (7.5 days) for the large TWC test specimen. The respective settlements are 0.8 cm, 1.4 cm and 1.9 cm. Note that the transition from primary to secondary compression is different in the three consolidometers. Figure 3-18 shows the normalized settlement-(log)time curves (degree of consolidation versus t/t_{100}, where t_{100} is time to reach end of primary) for the three consolidometers compared with Terzaghi's theory of one-dimensional consolidation. The figure clearly illustrates that the theory kicks in earlier and generally over predicts the settlement until reaching 100 % consolidation.

Figure 3-19 shows typical compression curves in axial strain (ε_a) versus vertical consolidation stress (σ_v) space for RBBC soil prepared in the three consolidometers. The measured water content at the end of batch consolidation was used with measured heights to back-calculate the water content and void ratio at the end of each prior increment (assuming 100% saturation). Figure 3-20 shows the compression curves in void ratio (e) versus vertical consolidation stress space. The results indicate very small variation in the behavior between the three consolidometers. In general, the compression index, C_c (= $\Delta e/\Delta \log \sigma'_v$), decreases with increasing vertical stress from C_c = 0.5 - 0.55 at σ_v = 0.02 - 0.03 MPa to C_c = 0.35 - 0.45 at σ_v = 0.6 - 1.0 MPa. These values agree with batch consolidation data from previous research on RBBC Series III and IV (e.g., Cauble, 1996; Seah, 1990).

Figure 3-21 shows the coefficient of consolidation, c_v (calculated using the log-time method) versus vertical consolidation stress during each batch consolidation increment for RBBC soil prepared in the three consolidometers. The results show that the value of c_v increases

with stress level from about c_v = 6x10^{-4} cm^2/s at σ_v = 0.003 MPa to c_v = 34x10^{-4} cm^2/s at σ_v = 4.0MPa for the three consolidometers. Both the magnitude of c_v and the trend with stress level is consistent with previous consolidometer tests on RBBC Series III and IV (Cauble, 1996; Seah, 1990; Sheahan, 1991). Seah (1990) and Sheahan (1991) found that c_v values obtained from the log-time method and those from the square root of time method during batch consolidation increment are approximately the same since the specimens are large (long drainage lengths) and the pore water pressure dissipation time is relatively long. This is not observed in one-day incremental oedometer tests with 2 cm height samples.

Figure 3-22 shows void ratio versus vertical hydraulic conductivity (k_v) for the RBBC consolidometer tests. The hydraulic conductivity was calculated from $k_v = m_v \cdot c_v \cdot \gamma_w$, where m_v is the coefficient of volume change ($\Delta\varepsilon/\Delta\sigma'_v$) and γ_w is the unit weight of water. The figure illustrates that the values of k_v obtained from the three consolidometers are in good agreement. The figure also shows that the hydraulic conductivity decreases with decreasing void ratio and hence increasing consolidation stress. The hydraulic conductivity reduces from approximately k_v= 1x10^{-6} cm/s at σ_v = 0.005 MPa (e= 1.85) to around k_v = 1.3x10^{-8} cm/s at σ_v = 6 MPa (e= 0.6). The value of C_k (= Δe/Δlogk) for the three tests is not constant over this stress range; C_k decreases with increasing stress level from C_k = 0.63 - 0.65 at low consolidation stresses to C_k = 0.57 - 0.59 at high stresses. Once again, this behavior is consistent with prior consolidometer testing (Seah, 1990).

3.4 ENGINEERING BEHAVIOR OF RBBC

3.4.1 Introduction

This section presents a summary of the most important engineering properties of RBBC available from previous research studies. The focus of this section is to provide a clear picture of the behavior of RBBC in the stress range 0.2 – 1.0 MPa for comparison with triaxial and CRS test results presented in Chapter 5 where the effect of stress level on the consolidation and shear behavior is investigated. Moreover, these results will be used as a reference in discussing the TWC test results presented in Chapter 6.

Section 3.4.2 summarizes the compression, consolidation, and flow characteristics derived from 1-D (i.e., K_0) consolidation tests. Section 3.4.3 provides an overview of the general undrained shear behavior of RBBC. This section discusses the undrained stress-strain-strength behavior in triaxial compression and extension as well as the direct simple shear. The results presented in these sections are limited to the tests performed on RBBC Series III and IV, which have very similar properties.

3.4.2 One-Dimensional Consolidation Behavior

The compression behavior of RBBC is examined from previous testing programs using results from incrementally loaded oedometer and CRS consolidation tests and from the 1-D consolidation phase in triaxial and DSS shear devices. Figure 3-23 shows the compression curves (ε_a-logσ'_v) obtained from the K_0-consolidation phase at constant rate of strain of seven triaxial tests performed on RBBC IV specimens (Force, 1998). Figure 3-24 shows the compression curves in e-logσ'_v space. The tests were consolidated in the apparatus to maximum vertical effective stress of about 1 MPa (~ 10 ksc), in which the corresponding strain was about 18%. The initial void ratio for the seven tests ranges only between 1.20 and 1.22. The figure provides an example of the excellent repeatability in the behavior of RBBC. It can be seen that there is a well defined yield at the preconsolidation pressure (σ'_p = 0.10 - 0.12 MPa) imposed in the consolidometer. In the unloading portion, the curve is much steeper, but becomes steeper with increasing OCR. Similar behavior is observed from the oedometer and CRS tests (Seah, 1990; Sheahan, 1991; Force, 1998).

The virgin consolidation line of the normally consolidated RBBC is more or less linear with approximately constant gradient in the range of stresses 0.2 - 0.5 MPa. At higher stresses the curve displays more of an S-shape. The compression ratio, CR (= $\Delta\varepsilon_a/\Delta$log$\sigma'_v$), generally varies from 0.155 to 0.180 in the stress range 0.2 - 0.8 MPa (Seah, 1990; Santagata, 1994). The swelling ratio, SR, defined as the average slope of the swelling line (in ε_a-logσ'_v space) over at least one log cycle reduction in effective stress, is approximately an order of magnitude smaller than CR. The value of SR increases with OCR from about SR = 0.011 at OCR of 2 to SR = 0.019 at OCR of 8 (Ahmed, 1990).

Figure 3-25 shows the variation in coefficient of consolidation obtained from triaxial CRS tests performed on RBBC IV specimens (Force, 1998). The results were interpreted using the standard linear theory (Wissa et al., 1971). The value of c_v was computed from $c_v = k_v/m_v\gamma_w$ where k_v and m_v are directly measured. In general, c_v decreases with vertical effective stress in the recompression range (i.e., for $\sigma'_v \leq \sigma'_p$; where $\sigma'_p \approx 0.1$ MPa [1 ksc] was imposed in the consolidometer) and then drops abruptly at σ'_p. In the normally consolidated region, c_v tends to increase with increasing consolidation stress level. The tests show c_v increasing from a minimum value of about $c_v = 20x10^{-4}$ cm^2/sec at $\sigma'_v = 0.2$ MPa (2 ksc) to $c_v = 40x10^{-4}$ cm^2/sec at $\sigma'_v = 0.9$ MPa (9 ksc). These parameters agree well with the values obtained from the batch consolidometer tests.

Figure 3-26 shows that the vertical hydraulic conductivity decreases with decreasing void ratio and hence increasing stress level (Force, 1998). The hydraulic conductivity reduces from approximately $k_v = 2 \times 10^{-7}$ at $\sigma'_v = 0.2$ MPa (2 ksc) to around $k_v = 3 \times 10^{-8}$ at $\sigma'_v = 1$ MPa (10 ksc). The average value of C_k is about 0.489. Again, these values are in good agreement with the batch consolidation data.

Ahmed (1990) and Force (1998) examined the effect of strain rate on the consolidation behavior in the CRS consolidation devises. The strain rates investigated range from very slow (0.07 %/hr) to very fast (12.71 %/hr). Force noted that the generated excess pore pressure increases with increasing strain rate in an approximately linear manner while the ratio of excess pore pressure to total stress varies between 0.2% and 30%. She also reported that the compression curves fall within a narrow band for all tests in which the faster tests tend to shift very slightly to the right (which increases σ'_p slightly). The hydraulic conductivity is hardly affected by the strain rate with the exception of the very fast test and the coefficient of consolidation values also agree well once the soil is normally consolidated.

The values of coefficient of earth pressure at rest (K_0) can be obtained from lateral stress oedometer and feedback-controlled 1-D consolidation in the triaxial shear cell. Figure 3-27 shows the typical trend of K_0 with vertical effective stress during consolidation for two triaxial tests performed by Santagata (1994). These results show that K_0 decreases during re-loading to the pre-consolidation pressure ($\sigma'_p \approx 0.1$ MPa [1 ksc]) and then increases. Once the soil is consolidated well into the virgin compression region $K_0 = K_{0NC}$ remains fairly stable.

Prior studies using triaxial (Sheahan, 1991; Santagata, 1994) and lateral stress oedometer devices (O'Neill, 1985) have found that the lateral earth pressure ratio of RBBC varies with OCR and can be well described by a power law relation first proposed by Schmidt (1966):

$$K_0 = K_{0NC}(OCR)^n \tag{3.1}$$

where for RBBC the exponent n ≈ 0.426.

Santagata (1994, 1998) observed limited variability in the results for K_{0NC} between 0.44 and 0.52 for RBBC III and IV. Sheahan (1991) and Seah (1990) ran a number of triaxial tests on RBBC III and found K_{0NC} = 0.488±0.009 and 0.522±0.005 respectively. Force (1998) obtained values K_{0NC} = 0.52±0.01 from triaxial tests on RBBC IV.

For the overconsolidated shear tests on RBBC, the specimen in the triaxial is unloaded or swelled following stress path consolidation (instead of K_0-consolidation) to the desired OCR based on an estimate of preshear K_0 at that OCR using Equation 3.1. This is because the lash-back in the triaxial load frame during load reversal tends to change the strain reading which in turn can affect the specimen area if the K_0-consolidation algorithm is used.

Data on the secondary compression behavior of RBBC has been reported by Cauble (1993) and by Sheahan (1991), based on K_0-consolidated DSS and triaxial tests, respectively. For normally consolidated RBBC both Cauble and Sheahan report $C_{\alpha\varepsilon} = d\varepsilon_a/d\log t$ = 0.0028±0.0005. Hence, the ratio $C_{\alpha\varepsilon}/CR$ (or $C_{\alpha e}/C_c$) reported is 0.0173±0.0042. Seah (1990) obtained a slightly higher value (~ 0.02) from a series of incremental oedometer tests. These data are well below the range observed by Mesri and Castro (1987) for a variety of inorganic soft clays (0.04±0.01) and are also on the low side of the data previously reported by O'Neill (1985) for RBBC II (0.036±0.004).

3.4.3 Undrained Shear Behavior

3.4.3.1 Introduction

The shearing behavior of RBBC has been studied by a number of researchers at MIT. The following subsections provide an overview of the general undrained shear behavior of this material in 1-D consolidated-undrained (CK_0U) triaxial compression and extension as well as

direct simple shear. The results are presented in normalized form[3] as this provides a very convenient format for presenting and evaluating clay behavioral characteristics. Note that in Chapter 5 the principle of normalization is evaluated for RBBC over a wide range of consolidation stresses using the triaxial device.

There is an extensive database on the normalized behavior of RBBC in different shear modes and at various values of OCR. Figure 3-28 shows the variation of the undrained strength ratio, USR (= s_u/σ'_{vc}), versus the overconsolidation ratio for the triaxial compression (Sheahan, 1991; Santagata, 1994), triaxial extension (Sheahan, 1991) and direct simple shear (Ahmed, 1990) for RBBC III. This relationship can be represented by the SHANSEP equation:

$$\frac{s_u}{\sigma'_{vc}} = S \cdot (OCR)^m \tag{3.2}$$

where S is the undrained strength ratio for the applicable shearing mode for the normally consolidated clay, and m is the slope of the regression line.

The SHANSEP parameters (S and m) for the three modes of shearing are summarized in Figure 3-28. Overall, increasing OCR produces an increase in the normalized strength in all three modes of shear. Note that the normalized strength of NC RBBC in DSS is only 60% of the strength measured in the triaxial compression, but is 54% higher than the strength found in the triaxial extension. The large difference in the behavior as a function of shear mode is indicative of the anisotropic behavior of RBBC. However, this difference decreases slightly with OCR.

Section 3.4.3.2 presents the undrained triaxial compression results carried out by Sheahan (1991) and Santagata (1994). This section is drawn primarily from Santagata (1998). Section 3.4.3.3 presents the undrained triaxial extension results performed by Sheahan (1991). Section 3.4.3.4 presents the direct simple shear results carried out by Ahmed (1990). All these tests were performed on RBBC III. Also note that these studies have operated at confining pressures less than 1.2 MPa (~12 ksc).

[3] The normalized behavior and SHANSEP method are explained in Chapter 2.

3.4.3.2 Triaxial Compression

The typical K_0-consolidated undrained triaxial compression (CK_0UC) behavior of normally consolidated (NC) and overconsolidated (OC) RBBC in the stress range 0.2 – 0.6 MPa is illustrated in the following figures. Figure 3-29 shows the shear stress ($q = (\sigma_1-\sigma_3)/2$) normalized to the maximum vertical consolidation stress (σ'_{vm}) versus the axial strain (ε_a) at nominal OCR's of 1, 2, 4, and 8 (Santagata, 1994). The four tests were conducted at a standard rate of 0.5 %/hr. The results show that the NC behavior is characterized by a peak (normalized shear strength, $s_u/\sigma'_{vm} = 0.33$) at small strain ($\varepsilon_a = 0.15\%$) followed by significant post peak softening. The normalized shear stress at $\varepsilon_a = 10\%$ drops to 0.25, which is about 75% of the peak strength. As OCR increases, the peak value of strength normalized to the maximum vertical stress decreases (the strength normalized to the preshear vertical consolidation stress increases), the strain softening decreases, and the axial strain at failure increases.

The corresponding normalized effective stress paths using the MIT stress space ($q/\sigma'_{vm} = (\sigma_1-\sigma_3)/2\sigma'_{vm}$ versus $p'/\sigma'_{vm} = (\sigma'_1+\sigma'_3)/2\sigma'_{vm}$) are shown in Figure 3-30 (Santagata, 1994). The results show that as OCR increases, the preshear K_0 increases while the post peak travel decreases. It can also be seen that the stress paths approach a common failure envelope at large strains. The effective stress failure envelope for triaxial compression can be deduced from the large database obtained by Sheahan (1991) and Santagata (1994) on NC and OC RBBC specimens. The linear regression through the data for shear stress versus average effective stress at maximum obliquity normalized by the maximum past pressure yields the following:

$$\frac{q}{\sigma'_{vm}} = 0.009 + \frac{p'}{\sigma'_{vm}} \cdot \sin(31.06°) \tag{3.3}$$

where $a' = 0.009$ is the intercept normalized to σ'_{vm}, and $\varphi'_{mo} = 31.06°$ is the friction angle at maximum obliquity.

The excess pore pressure ($u_e = \Delta u-\Delta\sigma_3$) and shear induced pore pressure ($u_s = \Delta u-\Delta\sigma_{oct}$) normalized to the vertical consolidation stress (σ'_{vc}) versus axial strain for the tests presented above are shown in Figures 3-31 and 3-32 respectively (Santagata, 1994). The figures show that the excess and shear induced pore pressures continue to increase throughout the test for NC soil. As OCR increases, the shear induced pore pressure decreases beyond 0.5-1.0% strain, and the excess pore pressure development decreases which becomes increasingly negative. This causes a

transition from a fully contractive behavior for OCR = 1 to entirely dilatant shear behavior at OCR = 8. The pore pressures generated can also be used to explain the shape of the stress paths shown in Figure 3-30. For example, the initial vertical portion of the NC stress path is due to very little shear induced pore pressures until reaching the peak or yield surface where thereafter will continue yielding with greater development of shear induced pore pressures up to the constant volume condition resulting in a significant decrease in p' and significant post-peak softening.

The undrained strength ratio varies with OCR as shown in equation 3.2. The values of S and m for triaxial compression tests on RBBC are 0.33±0.01 and 0.71 respectively based on the data by Sheahan (1991) and Santagata (1994). They also report that the friction angle at peak is $\varphi'_p = 25.4 \pm 1.1$.

Santagata (1994) also found that the undrained strength ratio of the K_0-normally consolidated RBBC is correlated with the preshear lateral stress ratio (K_{0NC}). Figure 3-33 shows the decreasing trend of undrained strength ratio with the lateral stress ratio for the data collected by Sheahan (1991) and Santagata (1994) in the stress range 0.2 – 0.6 MPa. Note that the data shown in the plot are from K_0-consolidated tests as well as from stress path tests performed to specific K values to investigate this trend. The equation of the regression through the data points is:

$$USR = 0.55 - 0.47 \cdot K_{0NC} \tag{3.4}$$

As noted above, the strain at failure (ε_{af}) tends to increase with increasing OCR. Figure 3-34 shows the strain at failure versus OCR (Santagata, 1994). The strain at failure for NC RBBC occurs at very small stains (0.10 - 0.22%). As OCR increases to 2, 4 and 8 the strain at failure increases to approximately 1%, 3% and 6% respectively.

Figure 3-35 shows curves of the undrained secant Young's modulus normalized to the vertical consolidation stress (E_u/σ'_{vc}) versus axial strain on a log-log plot for NC and OC RBBC (Santagata, 1994). As the measurements were performed employing external LVDT's the estimates of the stiffness are considered reliable only above 0.01 - 0.05%. The figure shows that the soil exhibits strong non-linearity from the very beginning of shear and that the decrease in stiffness is particularly marked once the soil reaches failure due to the large amount of post peak strain softening. The normalized stiffness increases as OCR increases at all strain levels but seem

to fall within a narrow band for OC soil (OCR = 2, 4, 8). Santagata (1998) also indicated that the undrained modulus is stress level dependent since it does not exhibit a perfect normalized behavior (as illustrated in Figure 3-35). She proposed the following equation linking the initial stiffness of RBBC to void ratio and consolidation stress level for OCR 1, 2, 4 and 8:

$$E_{uMAX} = 273 \cdot e^{-2.44} \cdot \sigma'^{0.44}_{vc} \ (MPa) \tag{3.5}$$

Sheahan (1991) investigated the effect of strain rate on the undrained shear behavior of NC and OC (OCR = 2, 4, 8) RBBC in triaxial compression. The triaxial apparatus used in the study had lubricated ends and the pore pressure was measured at the specimen mid-height. The four nominal strain rates investigated are 0.05, 0.5, 5 and 50 %/hr. The effect of strain rate on the stress-strain curves (small strains) of NC RBBC is shown in Figure 3-36. The results show that increasing the strain rate from 0.05 %/hr to 50 %/hr tends to increase the normalized strength from around 0.30 to 0.37, increase the post peak strain softening, and increase the initial stiffness. The corresponding stress paths in Figure 3-37 show that the peak friction angle increases with strain rate while the envelope formed by the stress states at maximum obliquity is independent of strain rate. The shear induced pore pressures tend to be suppressed with increasing strain rate as shown in Figure 3-38. The increase in undrained strength with strain rate appears to be caused by the increase in frictional resistance combined with the suppression of shear induced pore pressures. Similar trends are observed in OC RBBC, but the rate dependence decreases with increasing OCR especially at lower strain rates.

The effect of strain rate on the undrained strength ratio versus OCR relationship (SHANSEP equation) in CK_0U triaxial compression for RBBC is shown in Figure 3-39. The SHANSEP parameters for each strain rate are also shown in the figure. An increase in strain rate causes S to increase and m to decrease since the NC undrained strength increases with strain rate while the rate sensitivity decreases with OCR.

3.4.3.3 Triaxial Extension

While a reasonable amount of data exists on undrained compression behavior, there is a serious lack of reliable undrained extension data on RBBC. Test results in triaxial extension has been reported by Ladd and Varallyay (1965), Fayad (1986), and Sheahan (1988, 1991). The results presented in this section are from K_0-normally consolidated undrained triaxial extension

(CK_0UE) tests performed by Sheahan (1991) on NC and OC RBBC. Figure 3-40 shows the shear stress normalized to the vertical consolidation stress (σ'_{vc}) versus axial strain for two tests at OCR of 1 and 4 conducted at the standard rate of 0.5 %/hr. The specimens had lubricated ends and the pore pressure was measured at specimen mid-height. The figure shows that the NC soil reaches peak shear strength of 0.13 at axial strain of 12.2%. Note that the normalized strength is significantly lower while the strain at failure is much higher than the triaxial compression test. For the OCR = 4 test, the normalized strength is 0.4 while the axial strain at failure occurs at about 13%. The relationship between undrained strength ratio and OCR is shown in Figure 3-28. The values of S and m for triaxial extension tests on RBBC are 0.13 and 0.82 respectively based on these data.

Figure 3-41 shows the corresponding stress paths normalized to the maximum vertical consolidation stress (σ'_{vm}). The effective stress for NC RBBC decreases during shear (indicating contractive behavior) until it reaches a minimum effective stress and then begins to dilate back up the effective stress envelope. On the other hand, the effective stress path for the OCR = 4 test follows a slope approximately parallel to the total stress path until reaching the effective stress envelope at which point begins to dilate, increasing in effective stress at approximately constant obliquity until failure. The figure shows that both tests reach a common failure envelope yielding a friction angle at maximum obliquity of about 35°. The friction angle at peak is very similar to the maximum obliquity (~35°).

Figure 3-42 shows the normalized excess pore pressure and Figure 3-43 shows the normalized shear induced pore pressure for the two tests. The excess pore pressure plot shows a continuous increase during the test until reaching the peak then drops slightly. The shear induced pore pressure for the NC soil has a similar trend to the excess pore pressure as it increases during shearing then drops slightly. For the OCR = 4 test, the shear induced pore pressure is suppressed where it is around zero until 1% axial strain then rises to maxima before dropping again.

The normalized secant Young's modulus versus axial strain is shown in Figure 3-44. The normalized modulus for NC RBBC in extension is higher than in compression ($E/\sigma'_{vc} = 550$ in extension versus $E/\sigma'_{vc} = 450$ for compression at axial strain of 0.01%). As in the compression tests, the normalized stiffness increases as OCR increases. However, it should be noted that the estimates of stiffness are not very reliable since the measurements were performed employing external LVDT's and the specimens had lubricated ends.

Sheahan also investigated the effect of strain rate on the undrained shear behavior of NC and OC (OCR = 4) RBBC in triaxial extension. The three nominal strain rates investigated are 0.05, 0.5 and 50 %/hr. Figure 3-45 shows the effect of strain rate on the stress-strain curves of NC RBBC. Figure 3-46 shows the corresponding stress paths and Figure 3-47 shows the shear induced pore pressures. The figures demonstrate that the effect of strain rate on the shear behavior in triaxial extension is relatively small. This is because the pore pressures generated in extension are not large (the effective stress path is close to the total stress path in extension). The effect of strain rate is also small for OC RBBC.

3.4.3.4 Direct Simple Shear

This section presents results from a series of K_0-normally consolidated undrained direct simple shear (CK_0UDSS) tests performed by Ahmed (1990) on NC and OC RBBC using the Geonor DSS apparatus. Figure 3-48 plots the horizontal shear stress (τ_h) normalized to the vertical consolidation stress (σ'_{vc}) versus the shear strain (γ) at OCR of 1, 2, 3.25, 8, 15, and 32. All the specimens have the same maximum past pressure of about 1.2 MPa (12 ksc). Moreover, the specimens were sheared at a constant rate of strain of approximately 5 %/hr. The plot shows that the NC soil reaches a peak of about 0.195 (normalized shear strength) at shear strain of about 7% then strain softens. The plot also indicates a consistent increase in the normalized undrained shear strength accompanied with increase in shear strain at failure as OCR increases. The undrained strength ratio versus OCR relationship is shown in Figure 3-28. The SHANSEP parameters for DSS tests on RBBC are S = 0.20 and m = 0.74 - 0.82 based on the results obtained by Ahmed.

The corresponding stress paths in Figure 3-49 plot the horizontal shear stress versus the vertical effective stress required to maintain constant volume, both normalized to the maximum vertical consolidation stress (σ'_{vm}). The NC effective stress path indicates a contractive behavior (decreasing vertical effective stress) and represents the State Boundary Surface for the DSS mode of shearing. Hence, the stress paths for the OC tests climb up to this boundary reaching the envelope at the peak shear resistance and then follow the curve while strain softening and eventually reaching maximum obliquity. The angle of shear stress obliquity, $\psi = \tan^{-1}(\tau/\sigma'_v)$, reaches 24.1° at peak while $\psi = 30.7°$ at very large shear strains.

Figure 3-50 plots the normalized pore pressure ($\Delta u/\sigma'_{vc}$) versus the shear strain for all tests. The data demonstrate that significant positive pore pressures are developed during the test for the NC specimen while moderately OC specimens initially develop negative pore pressures which gradually become less negative (and even positive) with straining. However, highly overconsolidated specimens develop large negative pore pressures which start becoming less negative in the vicinity of the peak shear resistance and remain negative even until very large strains.

Ahmed also investigated the effect of stress level on the normalized undrained shear behavior for DSS tests on NC RBBC. Figure 3-51 shows the normalized stress-strain curves for tests at consolidation stresses ranging from 1.5 ksc to 12 ksc (~0.15 – 1.2 MPa). The plot illustrates a slight decrease in normalized strength from 0.202 at σ'_{vc} = 1.5 ksc to 0.194 at σ'_{vc} = 12 ksc. This is also shown in Figure 3-52 where the normalized strength is plotted against the vertical consolidation stress for 23 CK_0UDSS tests on NC RBBC performed by a number of researchers. In addition to decreasing the normalized strength, increasing stress level tends to increase the shear strain at failure, decrease the normalized pore pressure, and decrease the value of ψ angle at maximum obliquity from 50.1° at σ'_{vc} = 1.5 ksc to 28.3° at σ'_{vc} = 12 ksc.

Series	Year	Researcher	Topic	Tests Performed
I	1961	Bailey	Effect of salt concentration on undrained shear strength	-
	1963	Jackson	Thixotropy	Triaxial
	1964	Varallyay	Influence of stress system on undrained strength	Triaxial
	1965	Ladd	Use of pressure transducer to measure soil pressure	-
	1965	Preston	Sample disturbance	Triaxial
	1966	Braathen	Disturbance effects on undrained strength	Triaxial
	1967	Dickey	Developpment of plane strain device	Plane Strain Device
	1967	Rixner	Behavior in plane strain at OCR 1, 2, 4	Plane Strain Device
	1968	Bovee	Behavior in plane strain at OCR 1, 2, 4	Plane Strain Device
	1970	Kinner	Behavior of strip footings during undrained loading	Model footing tests
II	1982	Germaine	Cross-anisotropic behavior at OCR 4	DSC, Triaxial
	1984	Bensari	Stress-strain and yielding behavior	Triaxial
	1985	O'Neill	Anisotropy of Thixotropic clay	DSC, Triaxial
	1986	Fayad	Volumetric and undrained behavior	Triaxial
	1987	Malek	Behavior under cyclic loading	DSS
III	1988	Walbaum	Investigation of sample disturbance	DSS
	1988	Sheahan	Modification of computer controlled triaxial apparatus	Triaxial
	1989	DeGroot	Behavior in undrained multidirectional DSS at OCR 1	DSS
	1990	Ahmed	Normalized behavior in DSS	DSS
	1990	Seah	Anisotropy at OCR 1	DSC
	1991	Ting	Performance of sand drains	Model testing
	1991	Sheahan	Time dependent material	Triaxial
	1992	Ortega	Computer automation of DSS	DSS
	1993	Cauble	Cyclic and post-cyclic behavior in simple shear	DSS
	1994	Santagata	Simulation os sampling disturbance in soft clays using triaxial tests	Triaxial
IV	1994	Sinfield	Simulation of sampling and effects on compression and shear	CRS, Triaxial
	1996	Cauble	Behavior of model suction caisson	Model caisson
	1998	Santagata	Pre-failure behavior	Triaxial
	1998	Force	Strain rate selection in triaxial tests	CRS
	2000	Gonzalez	Investigation of CRS consolidation	CRS
	2009	Abdulhadi	Stability of boreholes	Triaxial, Model BH
	2009	Moniz	Normalized behavior in triaxial extension	Triaxial

Table 3-1: Overview of previous studies performed using RBBC

Consolidometer	Specimen Dimensions (cm)		Height to Diameter ratio	Surface Area (cm^2)	Cross Sectional Area (cm^2)	Surface to Cross Section Area ratio
	Diameter	Height*				
Triaxial	6.5	9.0	1.4	183.8	33.2	5.5
Small TWC	7.6	18.2	2.4	434.5	45.4	9.6
Large TWC	15.2	29.0	1.9	1384.8	181.5	7.6
Large Consolidometer	30.5	12.5	0.4	1197.7	730.6	1.6
Small Triaxial (Plexiglass)	3.6	8.8	2.7	99.5	9.6	10.3

* Estimates of final height are based on soil batches consolidated to vertical stress of 1 ksc.

Table 3-2: Dimensions and areas of consolidometer specimens

Year	Researcher	Series	Source Batch	G_s	w_l	w_p	I_p	Clay Frac. <2μm (%)	Salt (g/l)
1961	Bailey	Ia	MIT	2.77	30.0	17.5	12.5	40	2-3
			1139		34.7	17.7	17.0		35
1963	Jackson				36.2	19.5	16.7		16.7
1964	Varallyay		S4		32.6	19.5	13.1		
			S5		33.3	20.4	12.9	35	16.8
			S6		32.8	20.3	12.5		16.0
1965	Ladd, R.S.	Ib		2.77	45	22	23		16
1965	Preston		S1	2.77	45.6	23.4	22.2	35	24
1966	Braathen		S2	2.77	45.4	23.1	22.3		22
1967	Dickey				34.5	23.9	19.6		
1970	Kinner		100	2.78	43.5	19.6	23.9	50	
			150		43.5	19.6	23.9		
			200		38.1	17.8	20.3	52	8
			300		39.7	21.6	18.1		10
			400		39.4	21.3	18.1	52	10
			800		41.5	19.5	22.0	48	16
			900		41.2	18.7	22.5	54	16
			1000		41.1	19.5	22.6	58	16
			1100		42.0	20.6	21.4		16
			1200		40.2	18.6	21.6	48	16
			M101		40.7	19.6	21.1	52	
			M104		40.3	19.6	20.7		
			M107		41.3	19.6	21.7		
			M200		42.3	18.5	23.8	52	
			M400		39.8	18.9	20.9	47	
1971	Ladd et al.		160	2.78	38.1	17.8	20.3		8
			1300		42.1	22.1	20.0		16
			1500		43.8	20.6	23.2		16
1984	Bensari	II	105	2.75	47.6	23.3	24.3		16
			111	2.75	47.1	24.9	22.2		16
1985	O'Neill		105-112	2.78	41.3	22.1	19.2	52	16
1989	Seah	III	200-207	2.78	45.2	21.7	23.5	58	16
1991	Sheahan		210,214, 216		45.6	21.4	24.2		
1993	Cauble		217-218	2.78	37.0	21.3	15.7		
1994	Santagata		219-220		40.4	20.9	19.5		

Table 3-3: Index properties of RBBC from Series I - III (after Cauble, 1996)

Year	Researcher	Batch	w_l (%)	w_p (%)	I_p (%)	G_s	Clay fraction (%)	Salt g/L
1994	Zriek	powder	46.4	22.5	23.9	2.78	60.1	
1994	Sinfield	powder	47.0	23.8	23.2	2.79		
		402	46.8	22.4	24.4			
		403	47.2	23.3	23.9			
1996	Cauble	powder				2.81		
		401	46.7	21.8	24.9			
		404	47.4	21.9	25.5			10.4
		405	45.2	22.1	23.1			10.0
		406	45.0	22.6	22.4		57.6	12.5
		407	44.6	23.0	21.6		57.8	13.1
		408	44.7	23.9	20.8		58.7	10.1
		409	45.4	24.0	21.4		56.8	13.0
		410	46.6	25.0	21.6			13.4
		411	46.7	24.5	22.2		56.9	10.2
		413	45.5	24.3	21.2			9.7
		414	46.3	24.3	22.0			12.0
		415	46.1	24.7	21.4			10.5
		416	46.7	24.0	22.7			12.9
		417	47.2	24.5	22.7			13.2
1998	Santagata	418						
		419	47.8	23.3	24.5			
1998	Force	420	45.2	22.6	22.6			
2009	Abdulhadi	powder	46.5	23.5	23.0	2.81	56.0	11.1

Table 3-4: Index properties of RBBC for Series IV

Stress Level (MPa)	H (cm)			e			c_v (x 10^{-4} cm^2/s)		
	Triaxial	Small TWC	Large TWC	Triaxial	Small TWC	Large TWC	Triaxial	Small TWC	Large TWC
0.003	-	36.79	49.33	-	2.018	1.952	-	8.040	5.583
0.005	15.87	34.84	48.37	1.857	1.858	1.895	8.014	7.389	8.164
0.009	15.26	33.57	46.03	1.747	1.754	1.755	5.344	8.854	6.185
0.018	14.41	32.38	43.47	1.594	1.656	1.601	8.297	11.001	10.741
0.030	13.77	30.86	40.86	1.478	1.532	1.445	10.080	15.724	11.764
0.075	12.75	28.68	38.86	1.300	1.353	1.325	15.755	19.316	14.123
0.16	11.75	26.84	36.19	1.115	1.201	1.165	16.395	18.240	15.647
0.35	11.33	25.02	34.26	1.040	1.052	1.050	19.947	21.784	22.076
0.63	10.91	24.29	31.64	0.964	0.992	0.894	24.786	23.567	20.887
1.0	10.45	23.18	30.39	0.880	0.901	0.819	26.868	27.991	25.681
2.0	-	21.37	28.12	-	0.753	0.712	-	32.493	28.645
4.0	-	19.81	-	-	0.624	-	-	33.522	-

Stress Interval (MPa)	C_c			m_v (m^2/MN)			k_v (x 10^{-8} cm/s)		
	Triaxial	Small TWC	Large TWC	Triaxial	Small TWC	Large TWC	Triaxial	Small TWC	Large TWC
0.003 - 0.005	-	0.550	0.543	-	25.362	9.151	-	183.71	73.24
0.005 - 0.009	0.495	0.432	0.431	12.592	8.602	9.216	65.97	74.67	55.88
0.009 - 0.018	0.597	0.325	0.459	9.158	4.206	4.842	74.50	45.37	50.99
0.018 - 0.030	0.552	0.473	0.529	3.664	2.789	2.885	36.21	43.00	33.27
0.030 - 0.075	0.409	0.450	0.497	1.538	1.420	1.556	22.67	26.90	21.54
0.075 - 0.16	0.463	0.498	0.485	0.658	0.762	0.828	10.58	13.63	12.70
0.16 - 0.35	0.453	0.499	0.439	0.194	0.409	0.407	3.80	8.74	8.81
0.35 - 0.63	0.344	0.487	0.521	0.153	0.098	0.269	3.71	2.27	5.51
0.63 - 1.0	0.409	0.467	0.343	0.116	0.144	0.104	3.06	3.96	2.63
1.0 - 2.0	-	0.495	0.359	-	0.084	0.062	-	2.69	1.87
2.0 - 4.0	-	0.425	-	-	0.039	-	-	1.29	-

Table 3-5: Summary of typical batch consolidation behavior in the consolidometer for RBBC IV

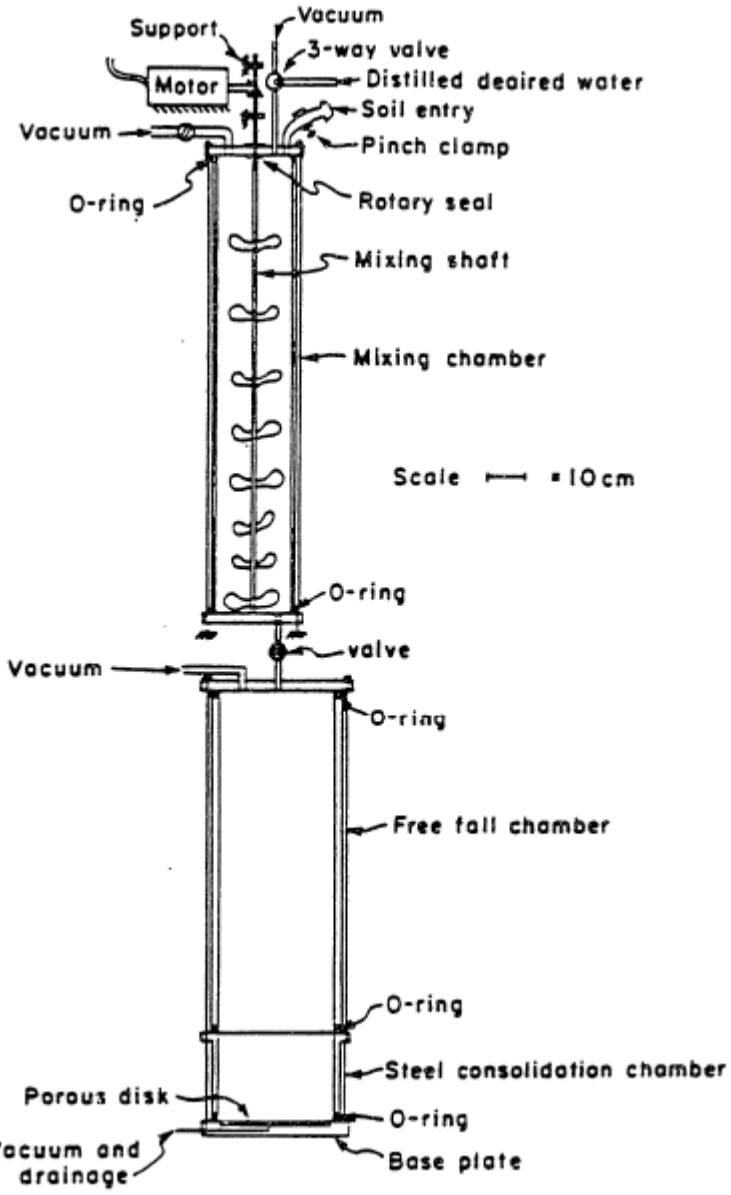

Figure 3-1: Schematic of equipment used to resediment BBC (after Germaine, 1982)

a)

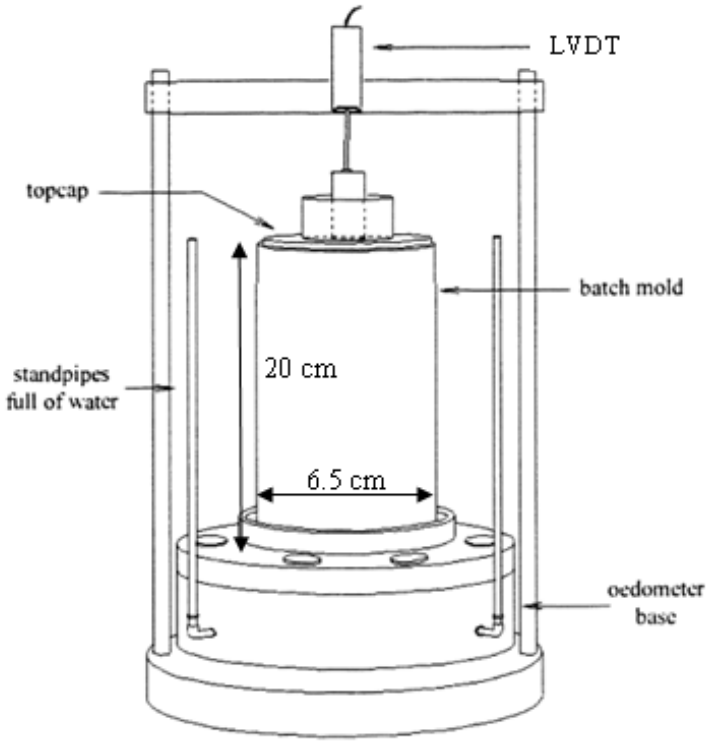

b)

Figure 3-2: Triaxial consolidometer setup: a) schematic, b) photograph

a)

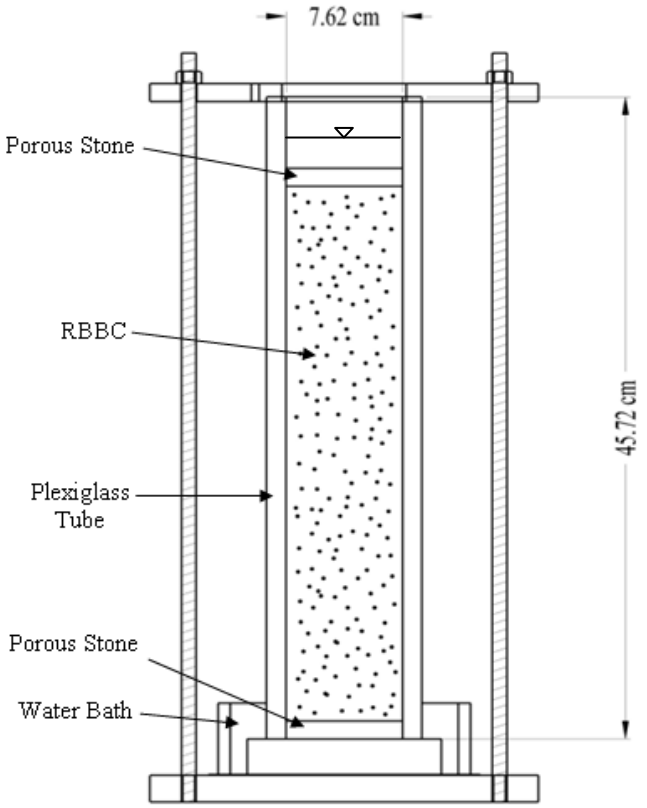

b)

Figure 3-3: Small TWC consolidometer setup: a) schematic, b) photograph

a)

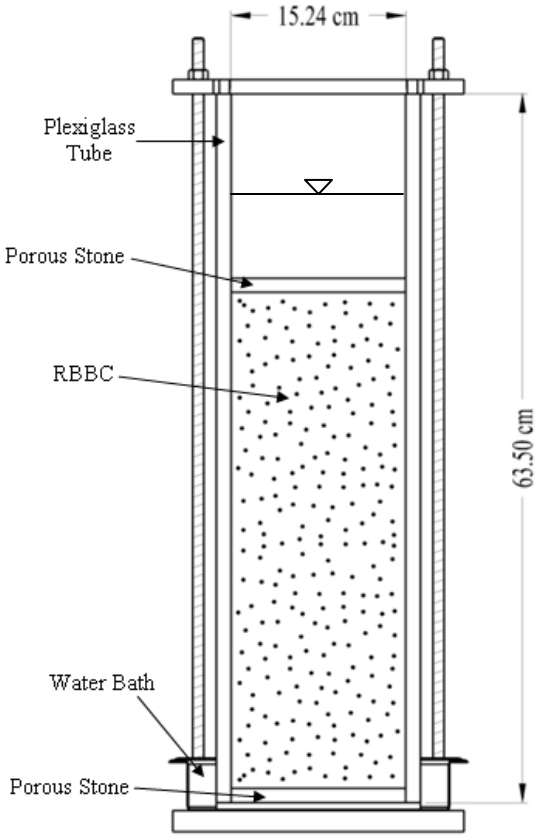

b)

Figure 3-4: Large TWC consolidometer setup: a) schematic, b) photograph

Figure 3-5: Vacuum setup used to de-air the RBBC slurry

Figure 3-6: Pouring of RBBC slurry into small TWC consolidometer

Figure 3-7: Consolidation of RBBC soil in small TWC consolidometer using high capacity load frame

Figure 3-8: Small plexiglass triaxial consolidometer setup

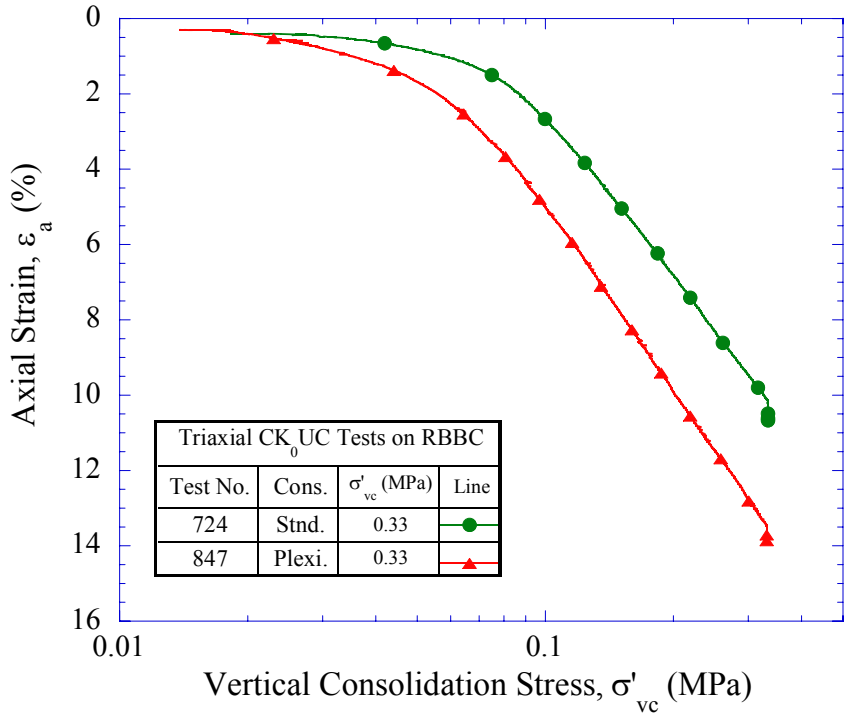

Figure 3-9: Comparison of compression curves (ε_a-logσ'_v) measured in the triaxial cell for RBBC prepared in standard and small plexiglass consolidometers

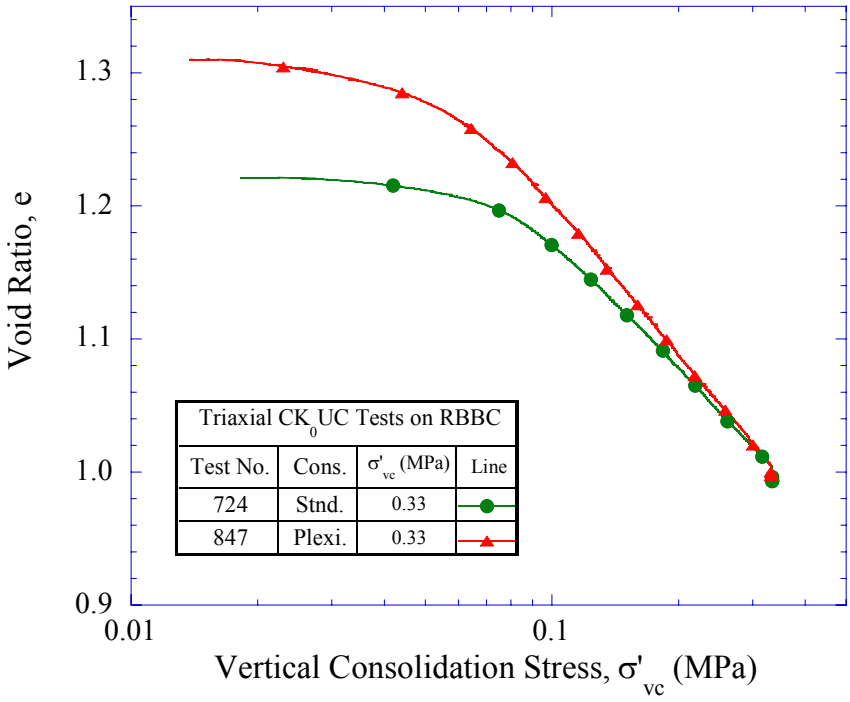

Figure 3-10: Comparison of compression curves (e-logσ'_v) measured in the triaxial cell for RBBC prepared in standard and small plexiglass consolidometers

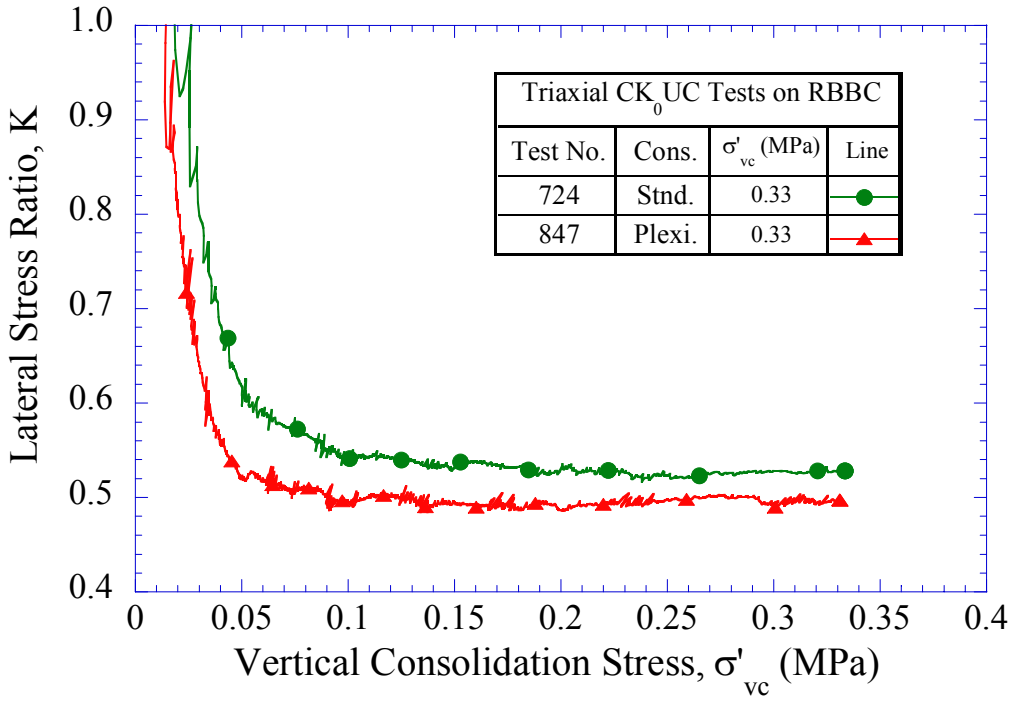

Figure 3-11: Comparison of lateral stress ratio measured in the triaxial cell for RBBC prepared in standard and small plexiglass consolidometers

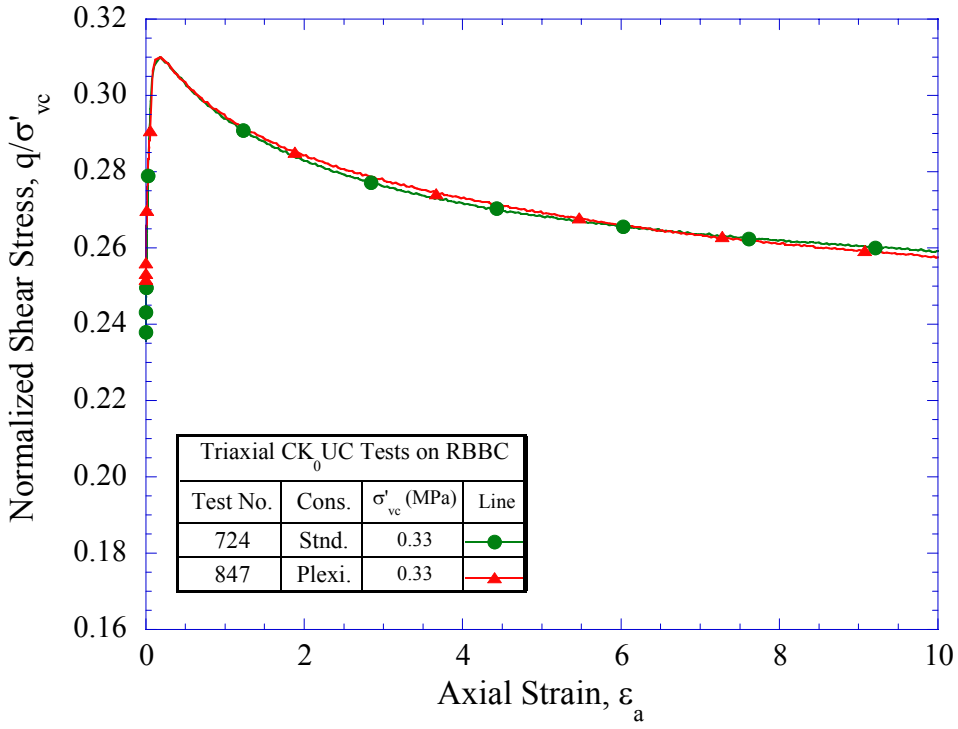

Figure 3-12: Comparison of shear stress-strain curves measured in the triaxial cell for RBBC prepared in standard and small plexiglass consolidometers

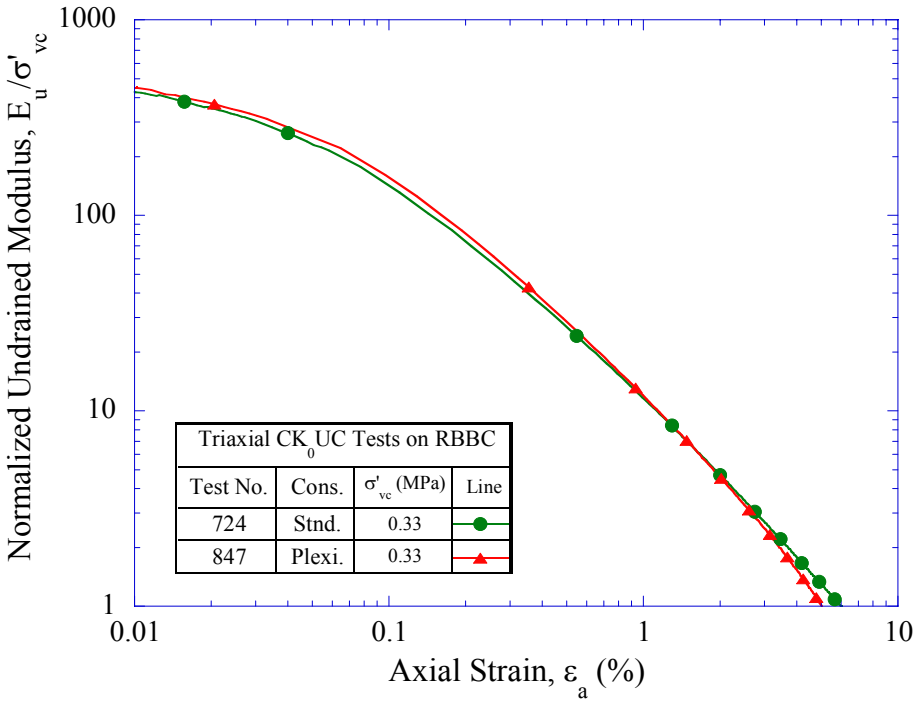

Figure 3-13: Comparison of undrained modulus measured in the triaxial cell for RBBC prepared in standard and small plexiglass consolidometers

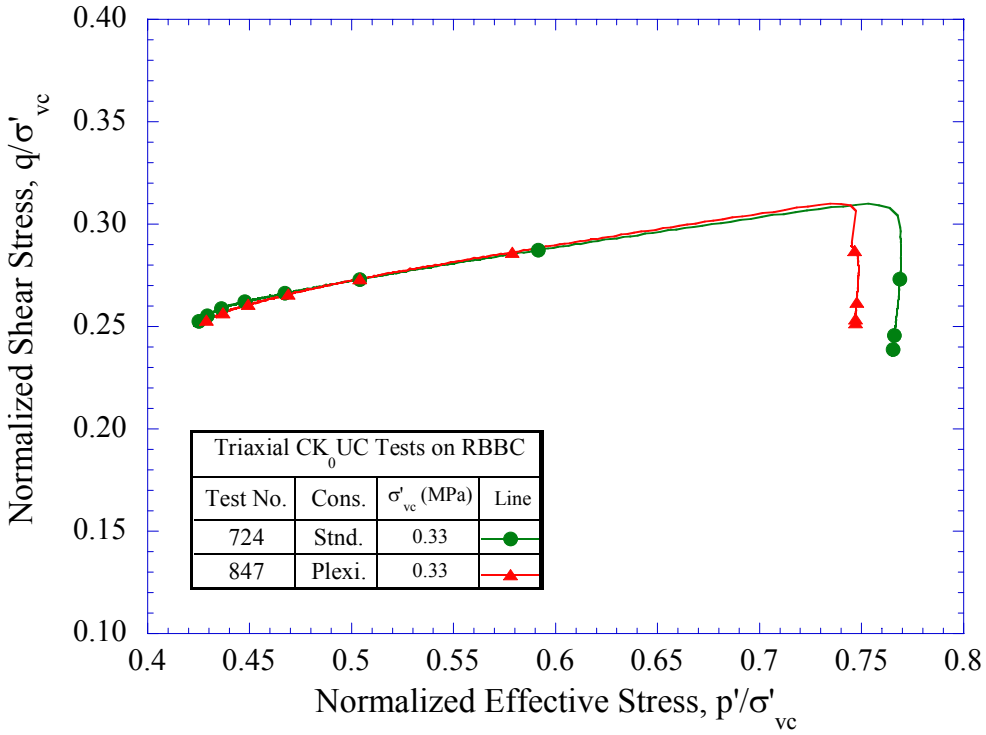

Figure 3-14: Comparison of effective stress paths measured in the triaxial cell for RBBC prepared in standard and small plexiglass consolidometers

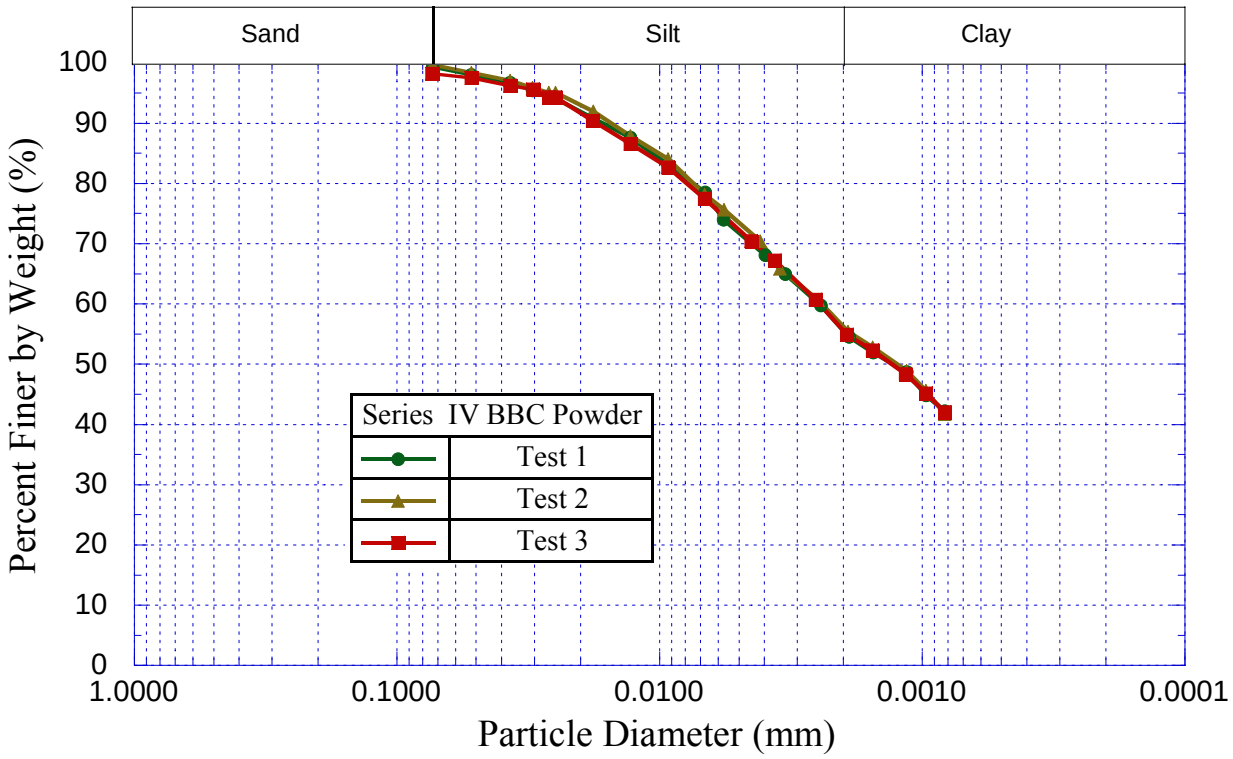

Figure 3-15: Results of grain size analyses for Series IV BBC powder

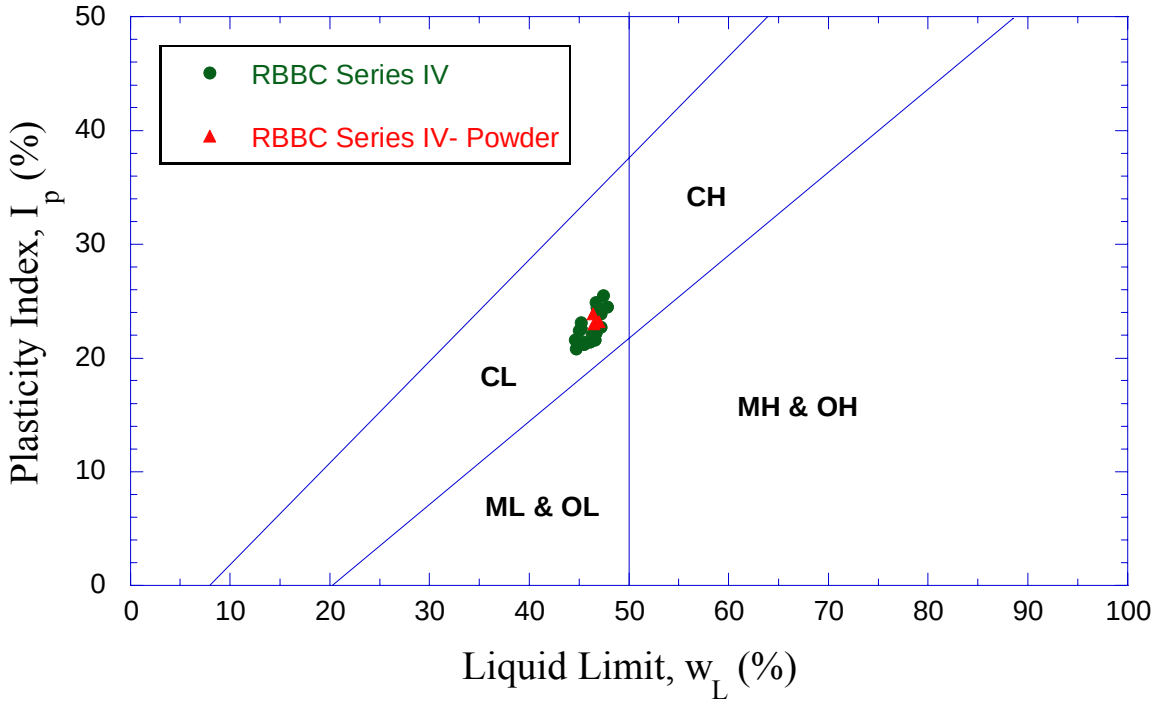

Figure 3-16: Plasticity chart showing data for RBBC Series IV

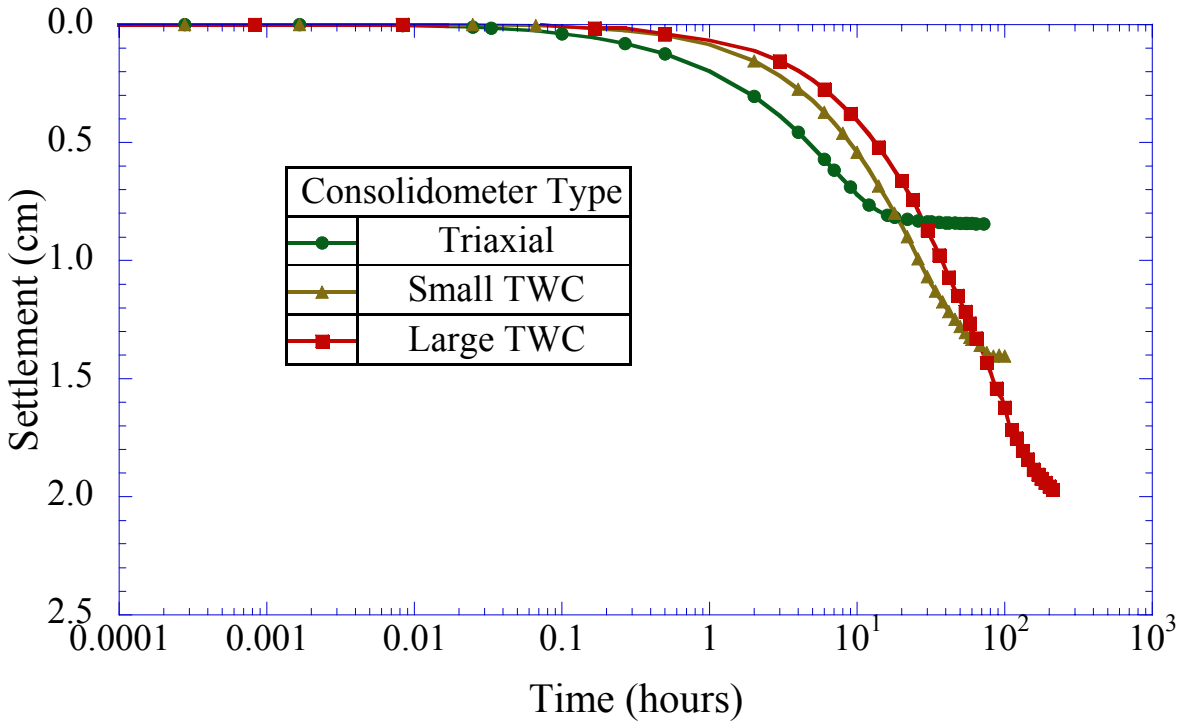

Figure 3-17: Settlement-time curves for 0.03 MPa stress increment for RBBC in the consolidometer

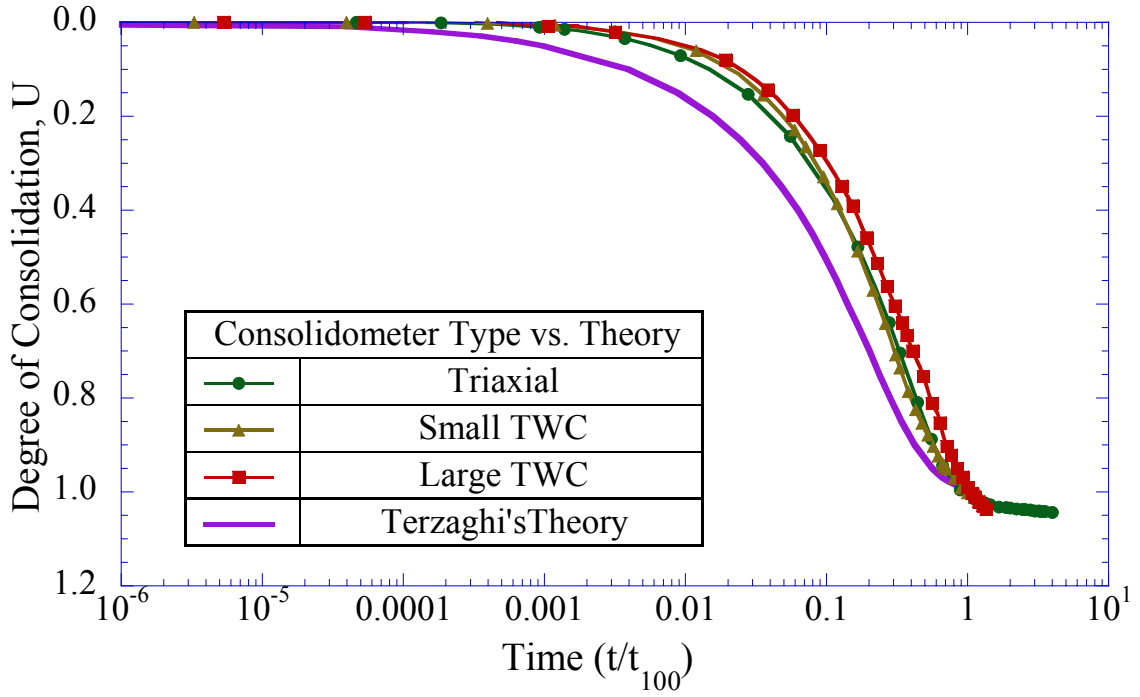

Figure 3-18: Normalized settlement-time curves for 0.03 MPa stress increment for RBBC in the consolidometer compared with the theoretical curve

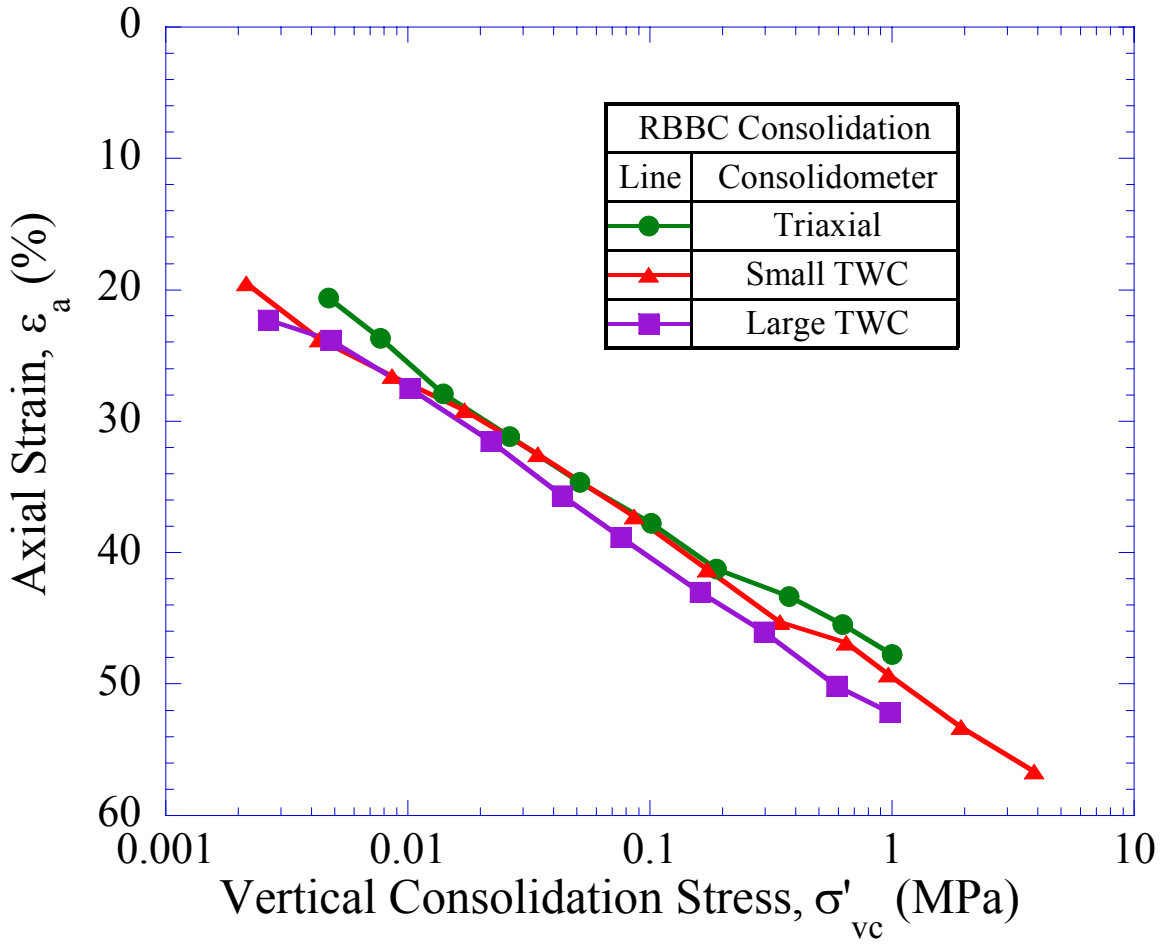

Figure 3-19: Compression behavior in ε_a-logσ'_v space for RBBC in the consolidometer

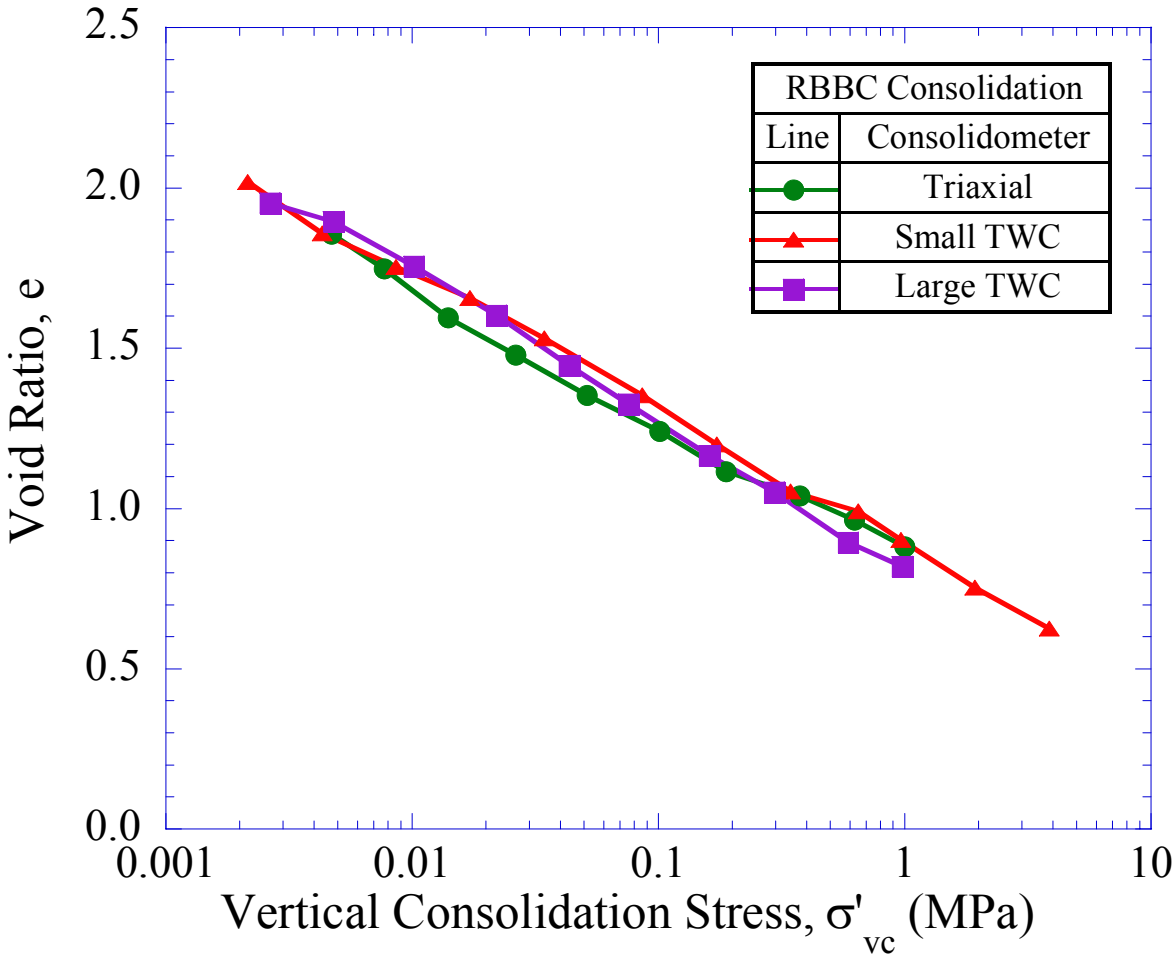

Figure 3-20: Compression behavior in e-logσ'_v space for RBBC in the consolidometer

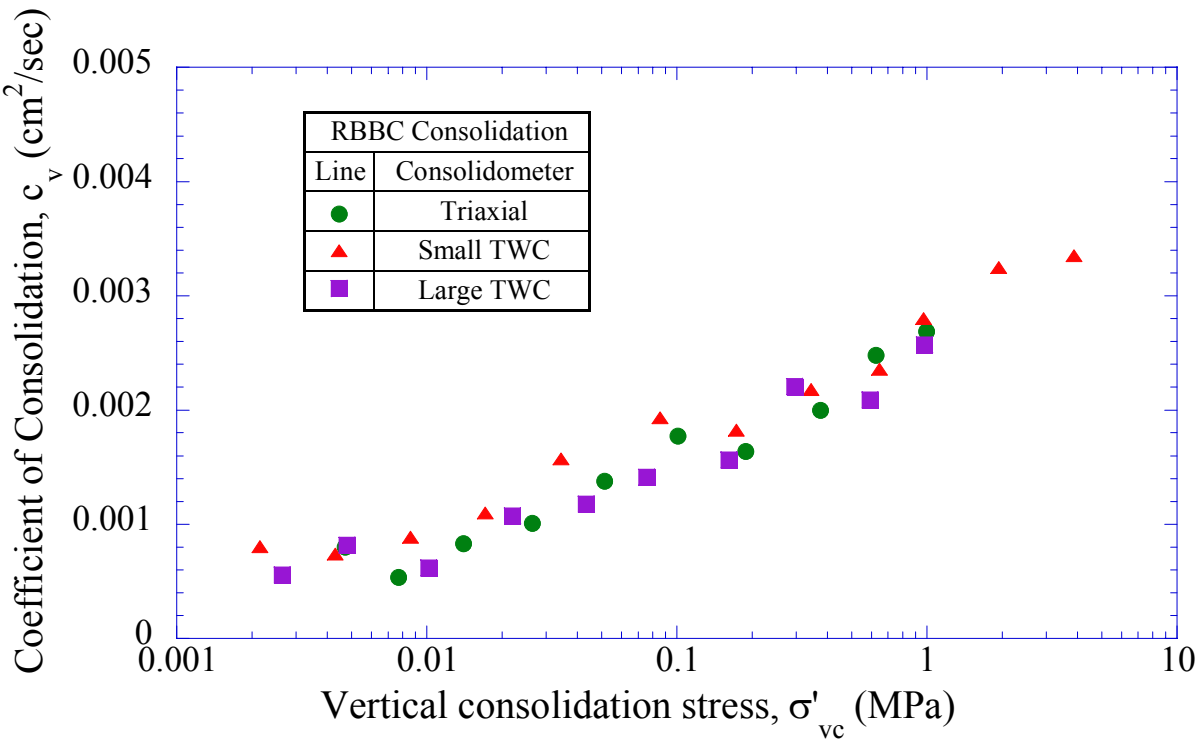

Figure 3-21: Coefficient of consolidation versus stress level for RBBC consolidometer tests

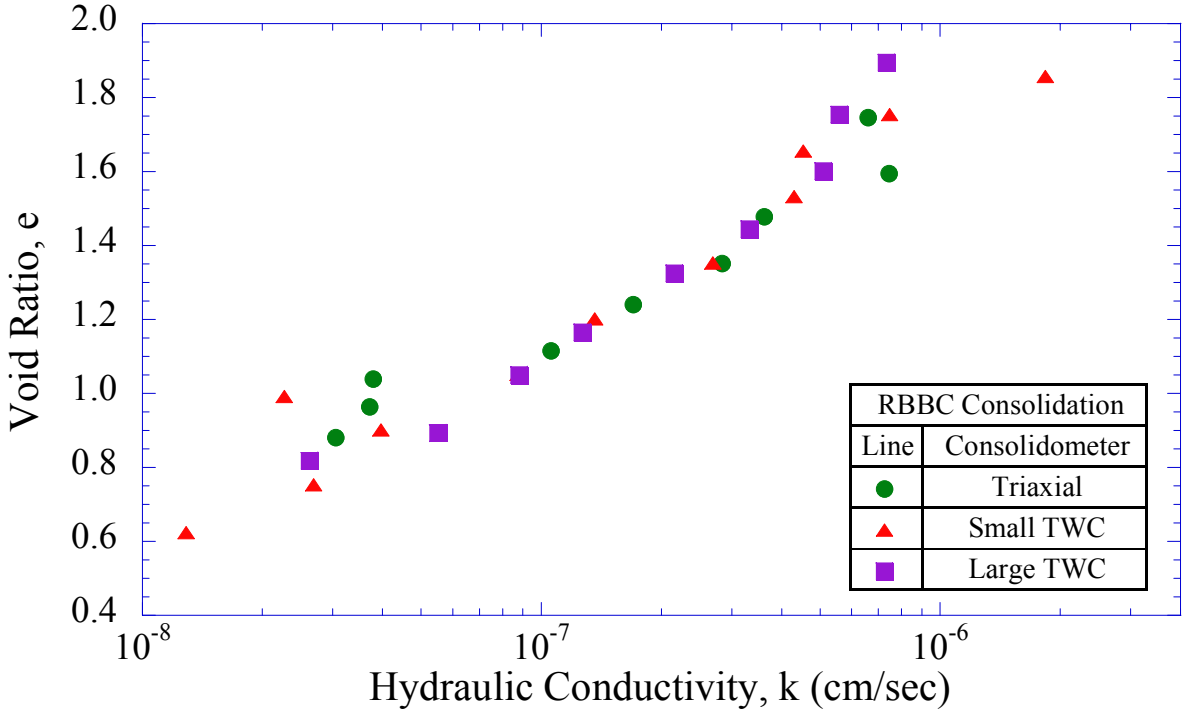

Figure 3-22: Void ratio versus hydraulic conductivity for RBBC consolidometer tests

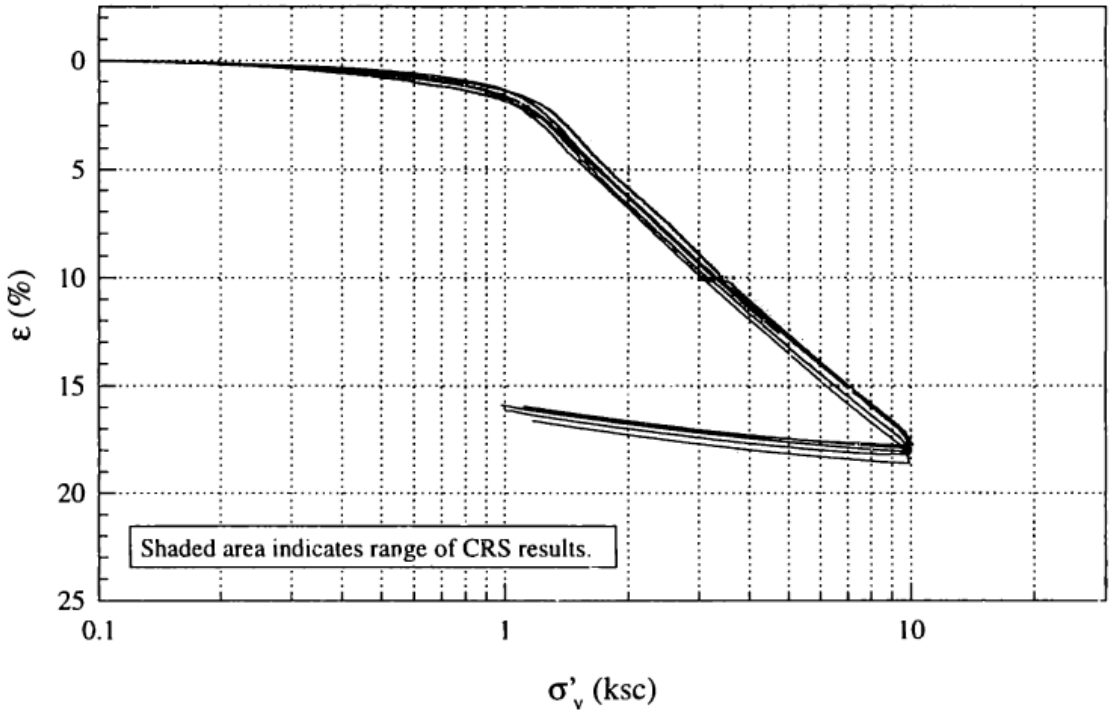

Figure 3-23: Compression curves in ε_a-logσ'_v space of K_0-consolidation of RBBC IV in the triaxial apparatus (Force, 1998)

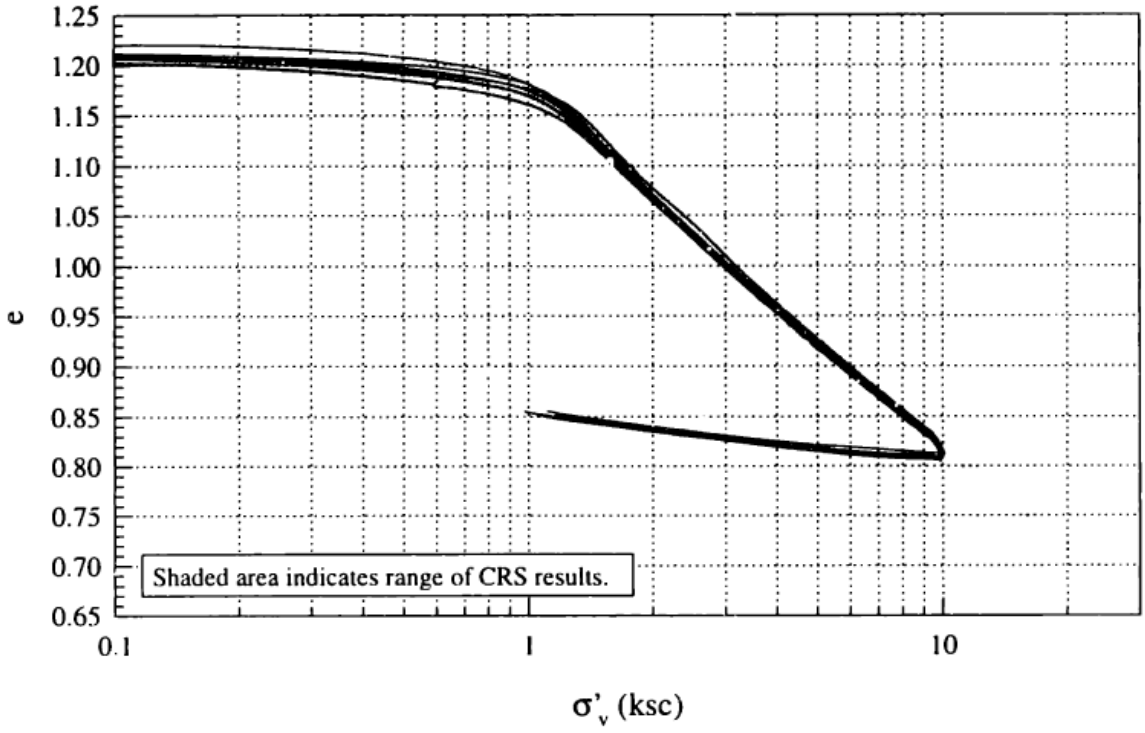

Figure 3-24: Compression curves in e-logσ'_v space of K_0-consolidation of RBBC IV in the triaxial apparatus (Force, 1998)

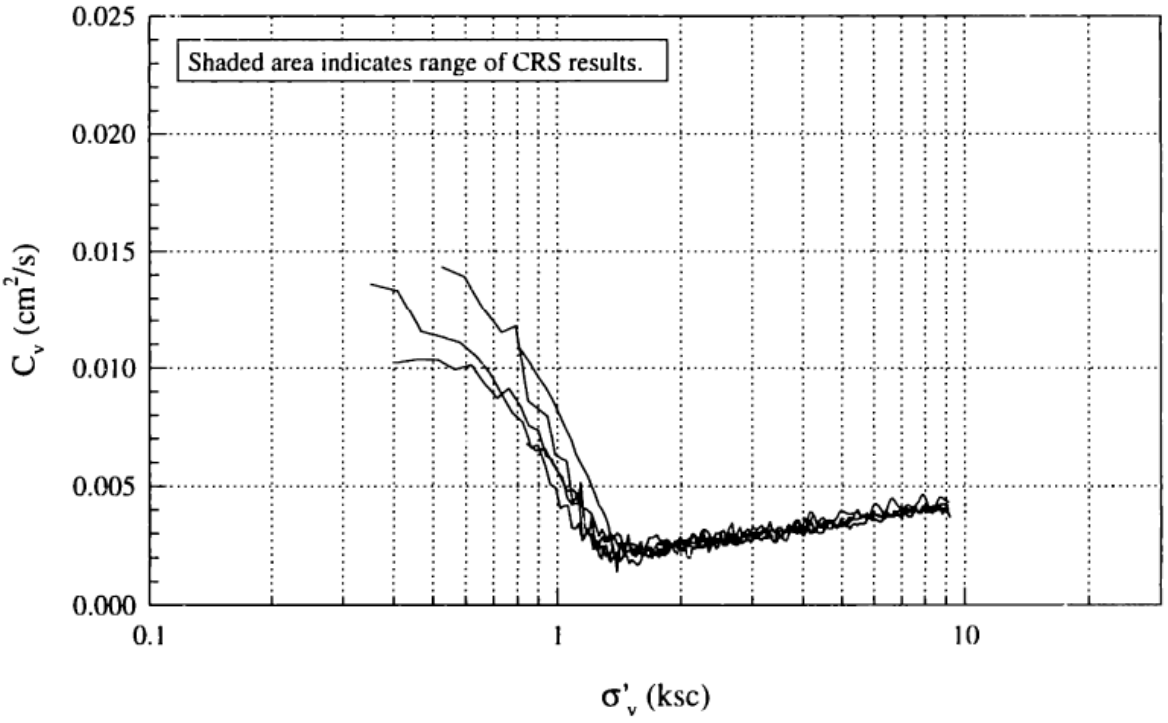

Figure 3-25: Coefficient of consolidation for K_0-consolidation of RBBC IV in the triaxial apparatus (Force, 1998)

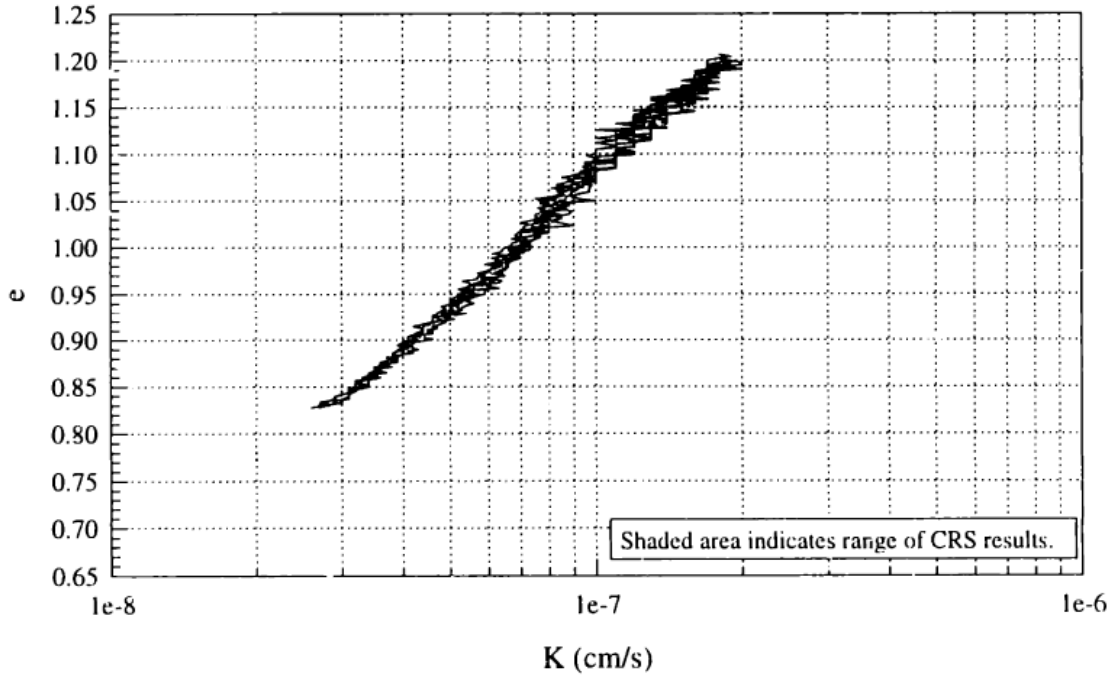

Figure 3-26: Hydraulic conductivity of K_0-consolidation of RBBC IV in the triaxial apparatus (Force, 1998)

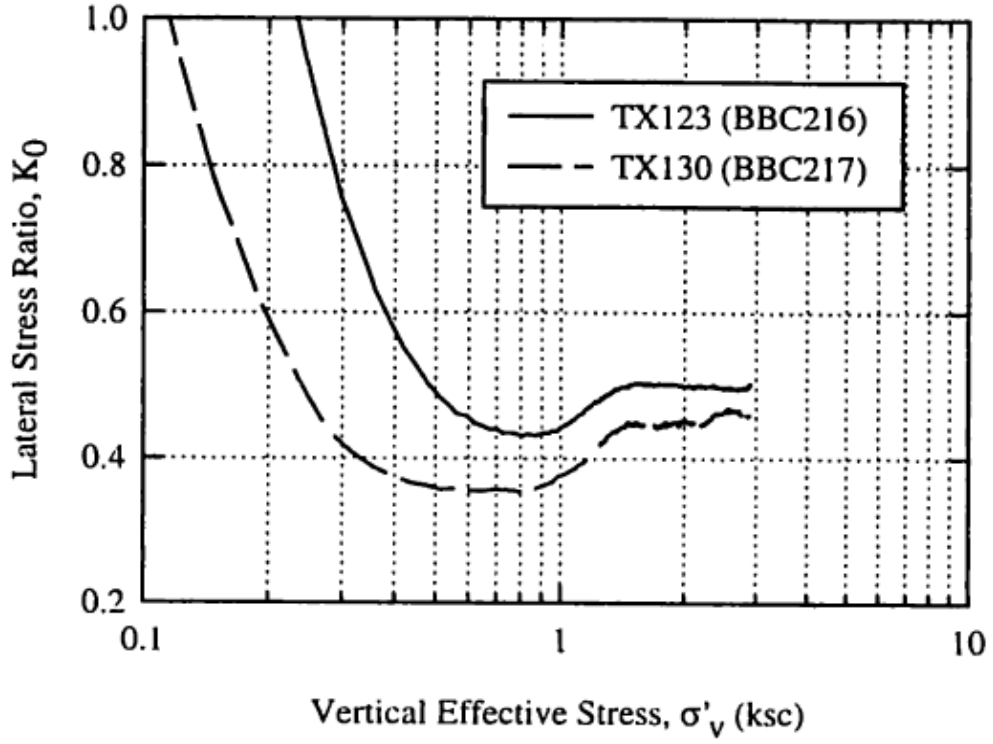

Figure 3-27: Lateral stress ratio versus vertical stress during K_0-consolidation of RBBC III (Santagata, 1994)

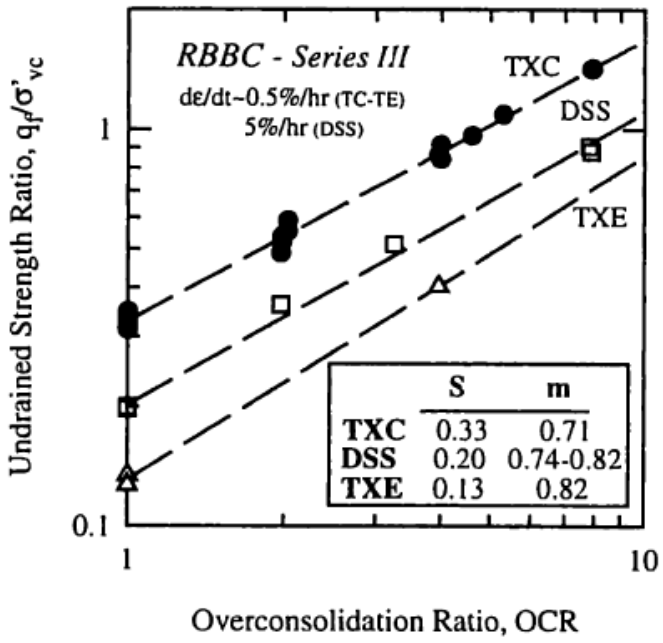

Figure 3-28: Undrained strength ratio versus OCR from Ck_0U tests in triaxial compression, extension, and direct simple shear (Santagata, 1998)

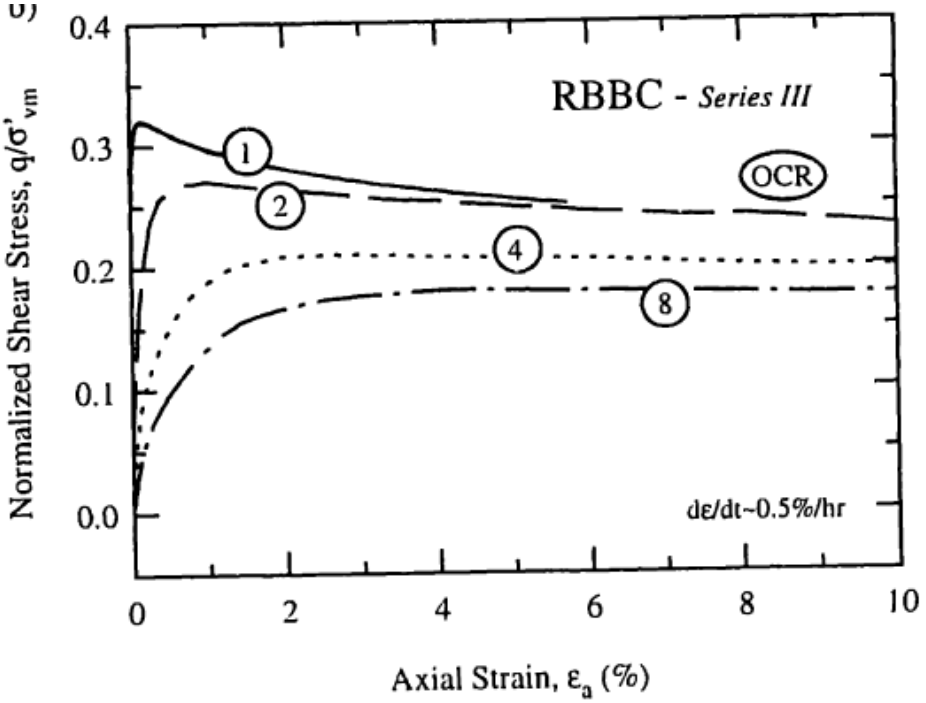

Figure 3-29: Normalized shear stress-strain behavior of RBBC III (OCR = 1, 2, 4, 8) in undrained triaxial compression (Santagata, 1994)

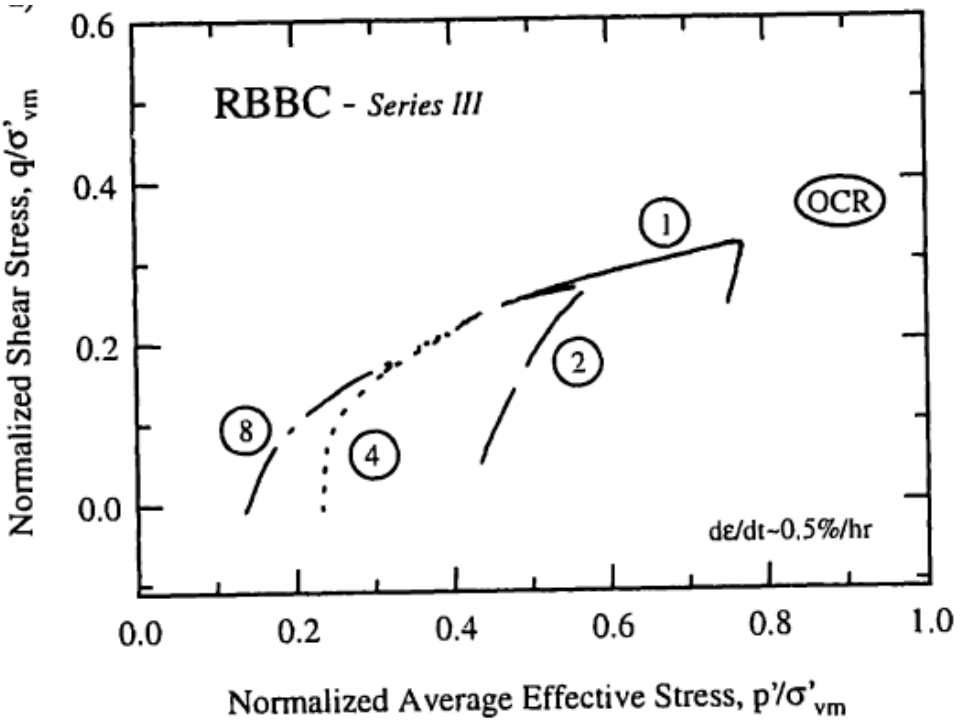

Figure 3-30: Normalized effective stress paths of RBBC III (OCR = 1, 2, 4, 8) in undrained triaxial compression (Santagata, 1994)

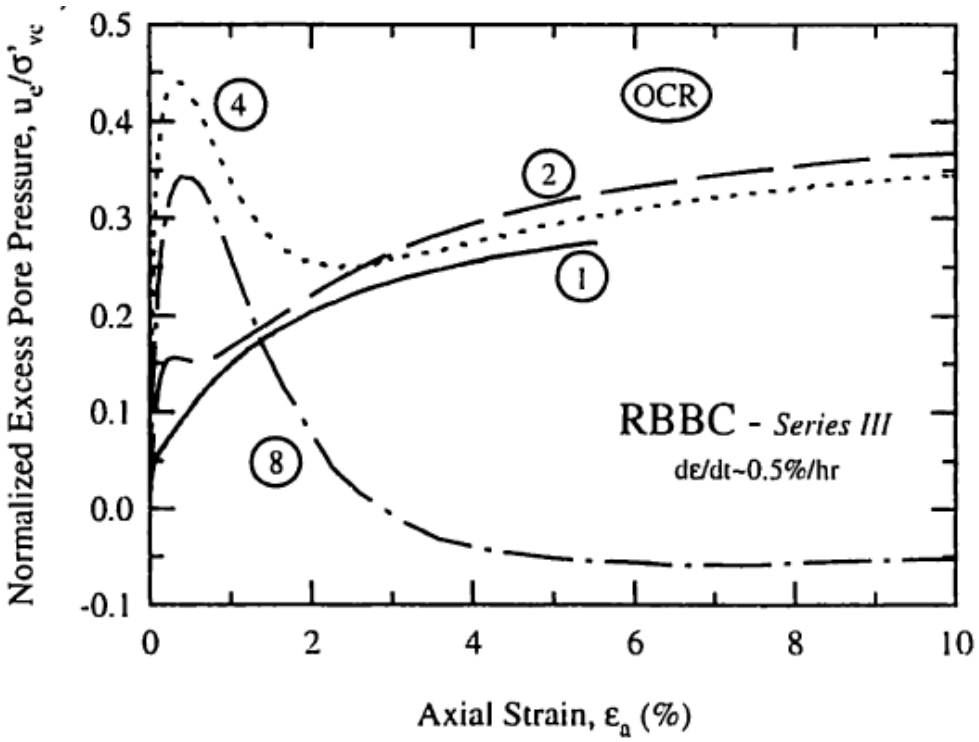

Figure 3-31: Normalized excess pore pressures of RBBC III (OCR = 1, 2, 4, 8) in undrained triaxial compression (Santagata, 1994)

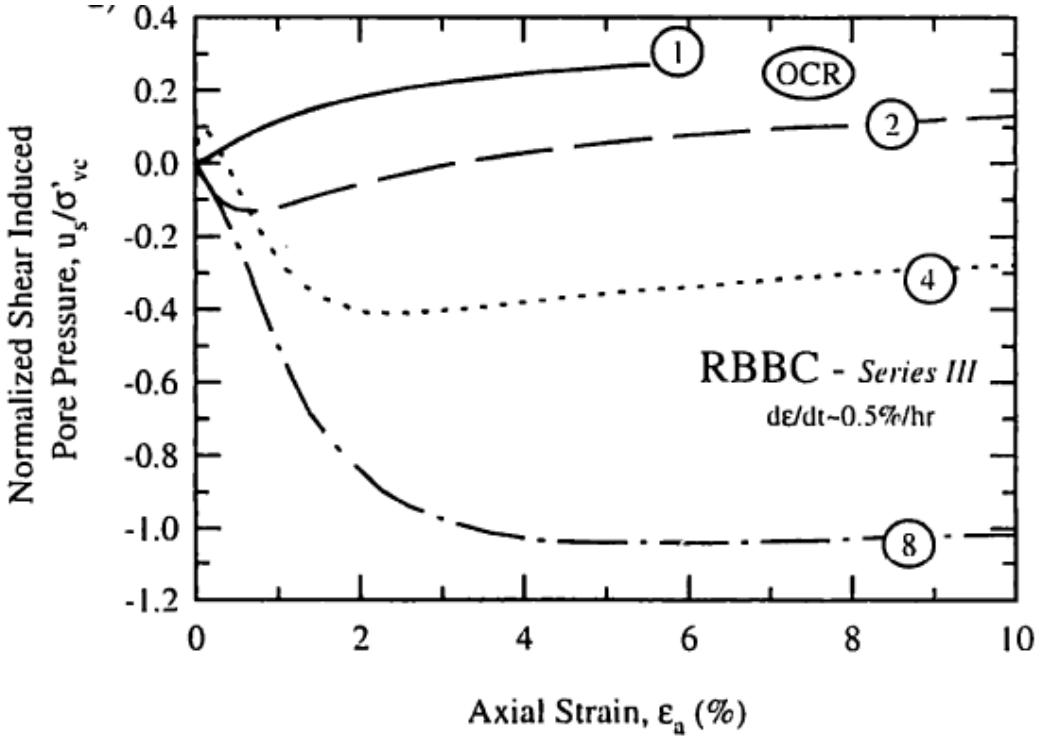

Figure 3-32: Normalized shear induced pore pressures of RBBC III (OCR = 1, 2, 4, 8) in undrained triaxial compression (Santagata, 1994)

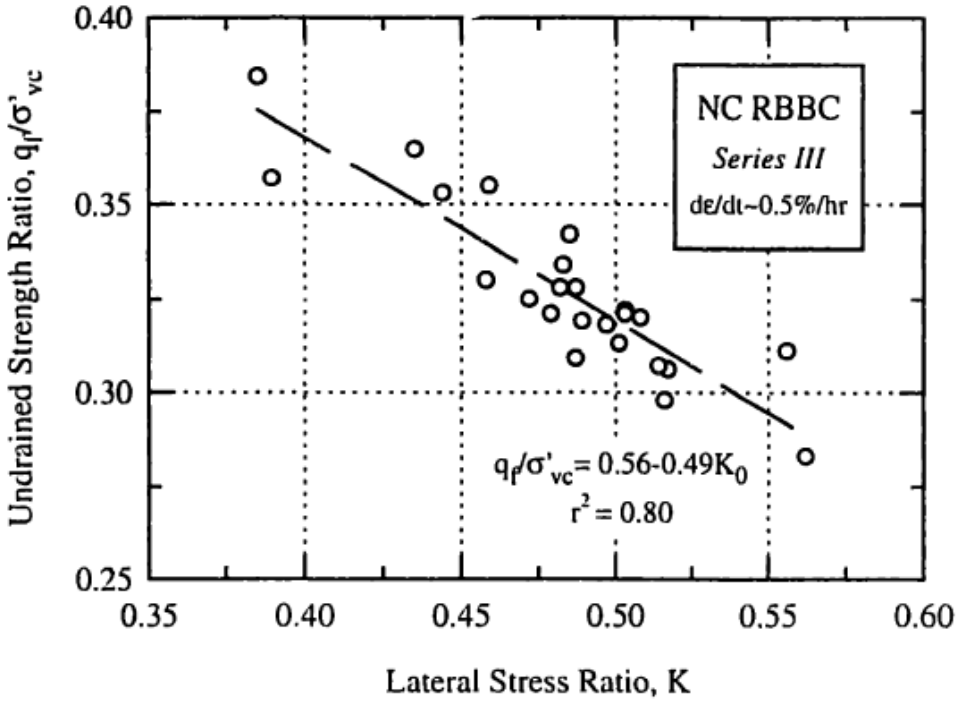

Figure 3-33: Undrained strength ratio versus lateral stress ratio for CK_0UC tests on NC RBBC III (Santagata, 1994)

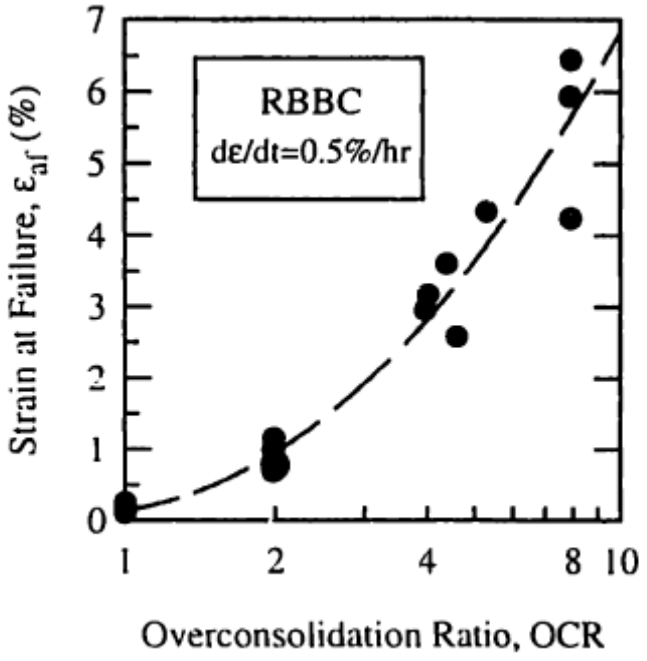

Figure 3-34: strain at failure versus OCR for RBBC III (Santagata, 1994)

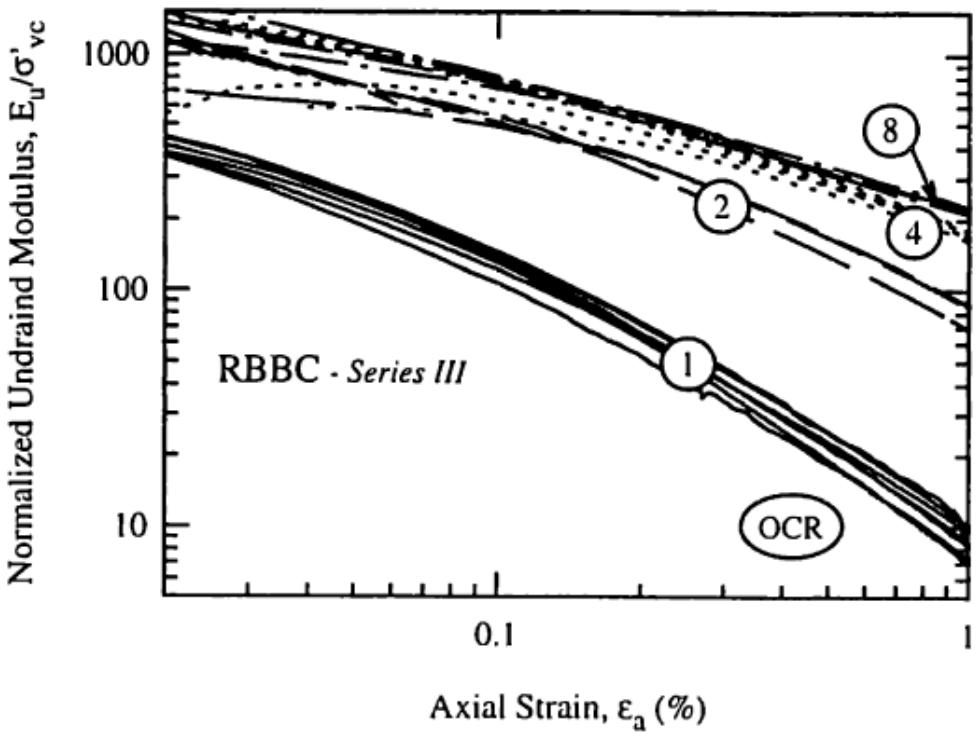

Figure 3-35: Normalized undrained secant modulus versus axial strain for RBBC III in triaxial compression (Santagata, 1994)

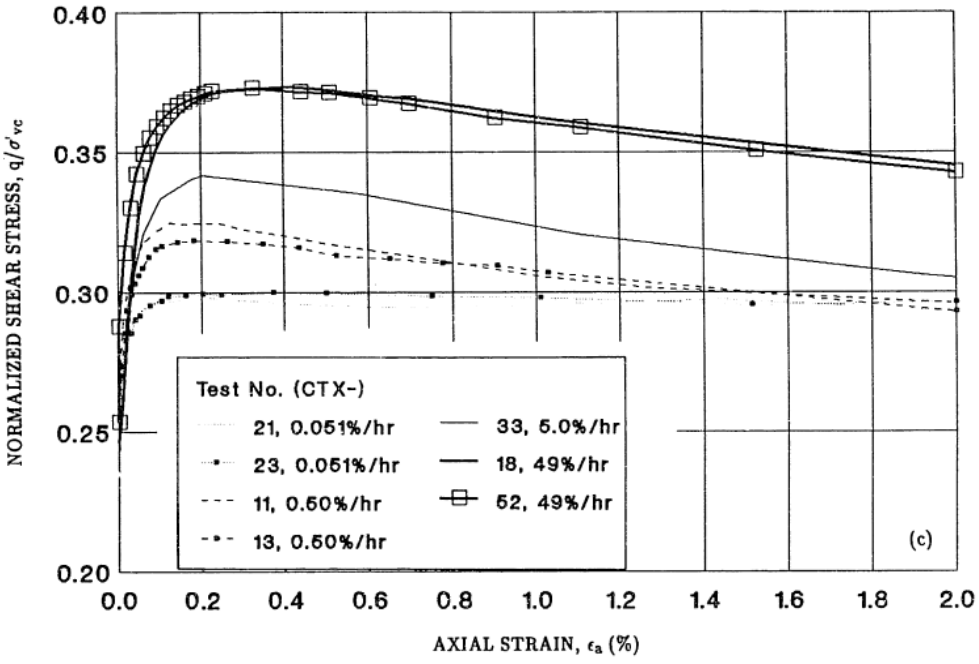

Figure 3-36: Effect of strain rate on normalized stress-strain curves (small strains) of NC RBBC III in undrained triaxial compression (Sheahan, 1991)

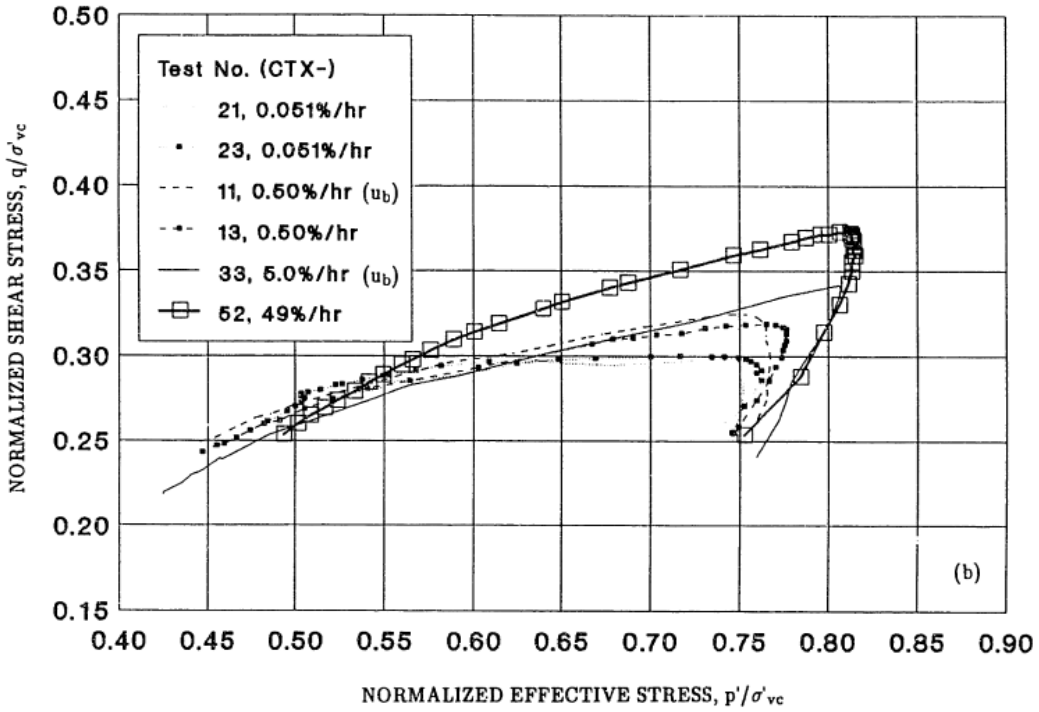

Figure 3-37: Effect of strain rate on normalized stress paths of NC RBBC III in undrained triaxial compression (Sheahan, 1991)

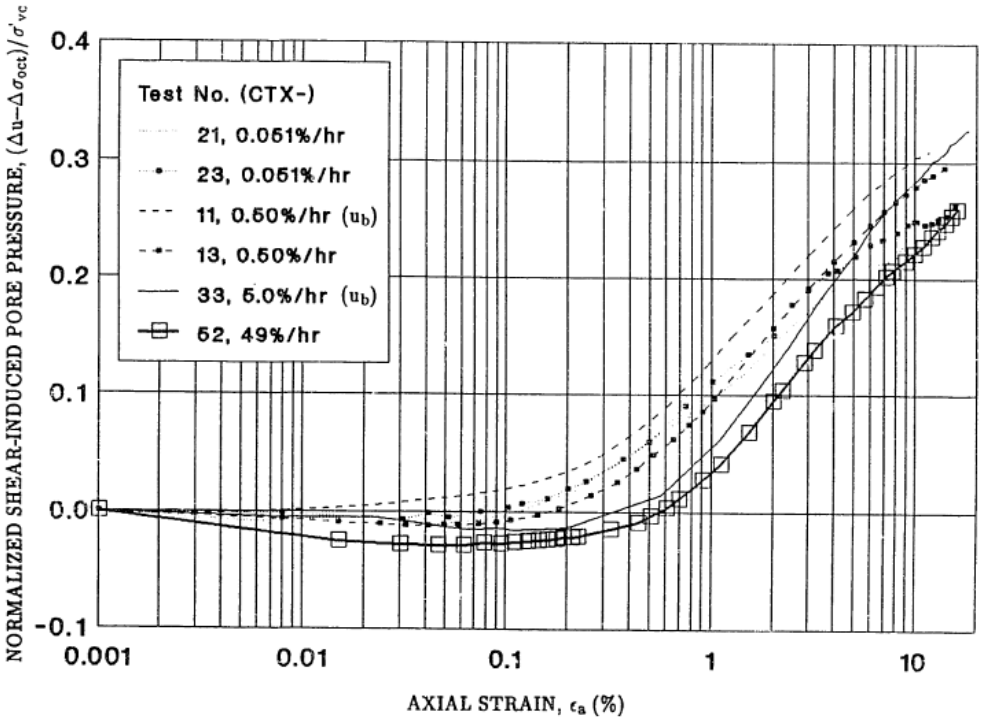

Figure 3-38: Effect of strain rate on normalized shear induced pore pressure of NC RBBC III in undrained triaxial compression (Sheahan, 1991)

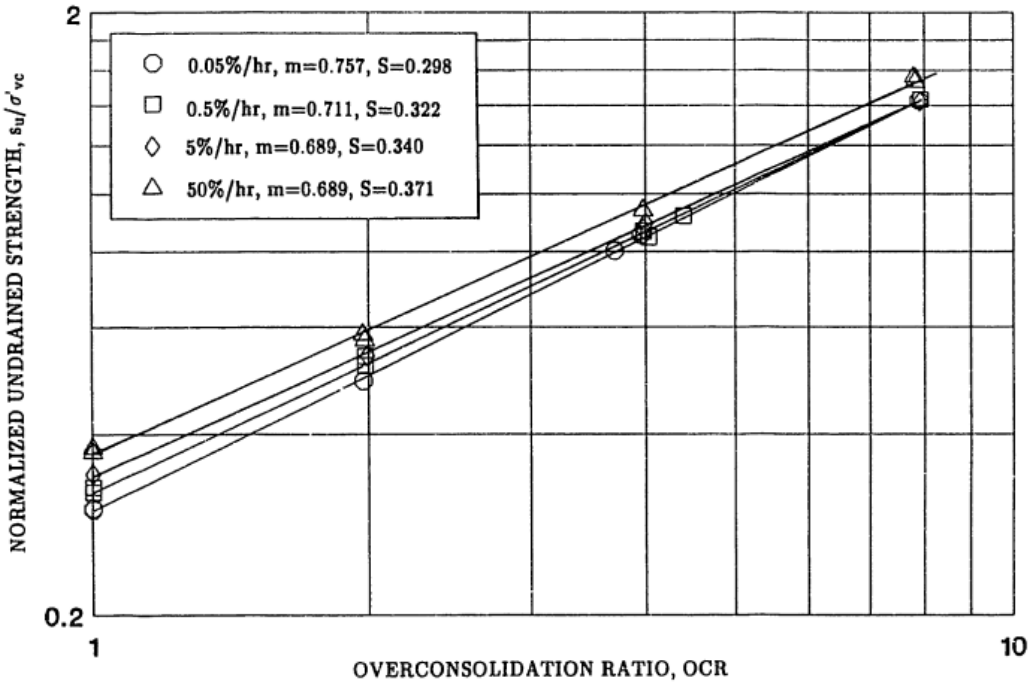

Figure 3-39: Effect of strain rate on undrained strength ratio versus OCR relationship in CK_0U triaxial compression for RBBC III (Sheahan, 1991)

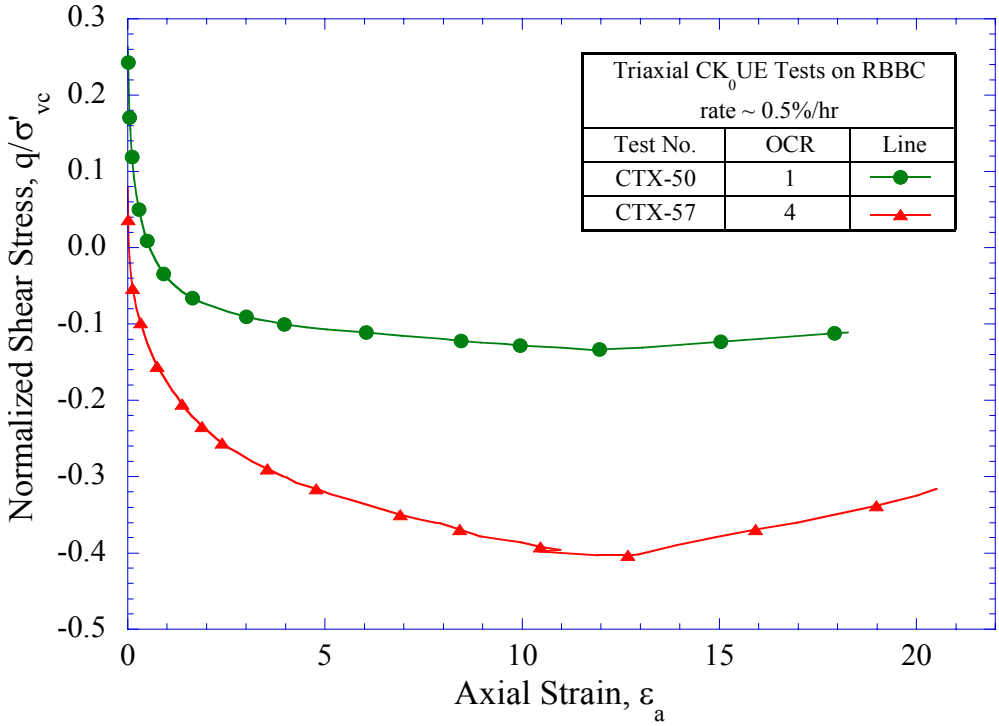

Figure 3-40: Normalized shear stress-strain behavior of RBBC III (OCR = 1, 4) in undrained triaxial extension (Sheahan, 1991)

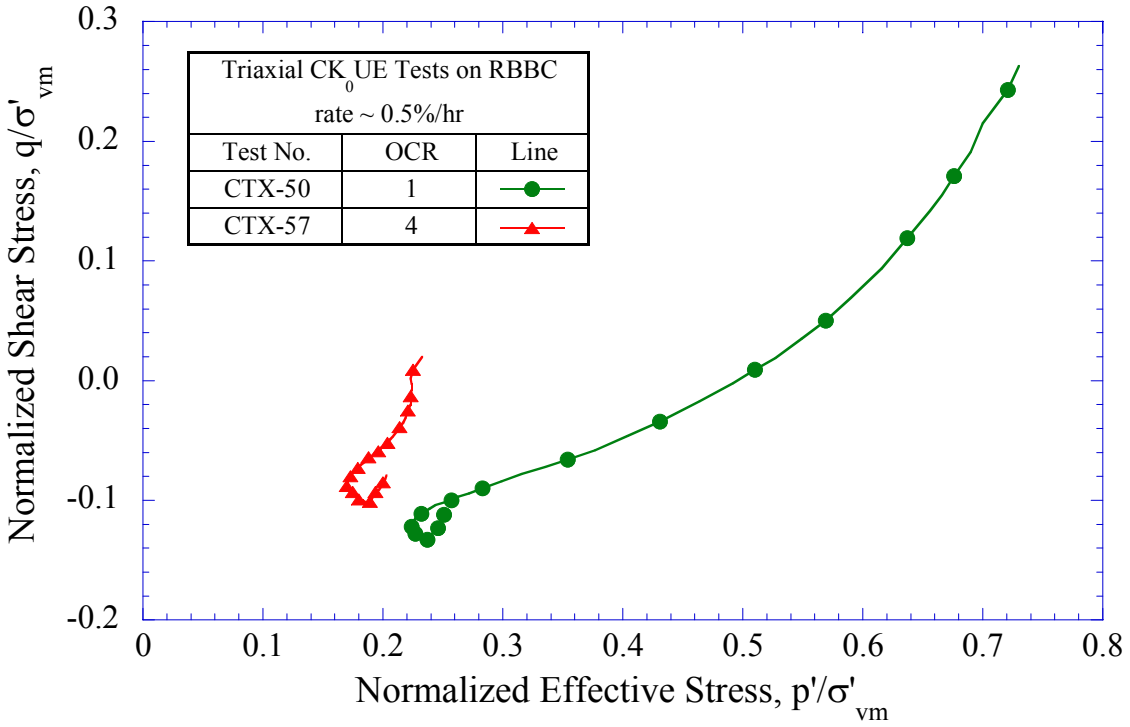

Figure 3-41: Normalized effective stress paths of RBBC III (OCR = 1, 4) in undrained triaxial extension (Sheahan, 1991)

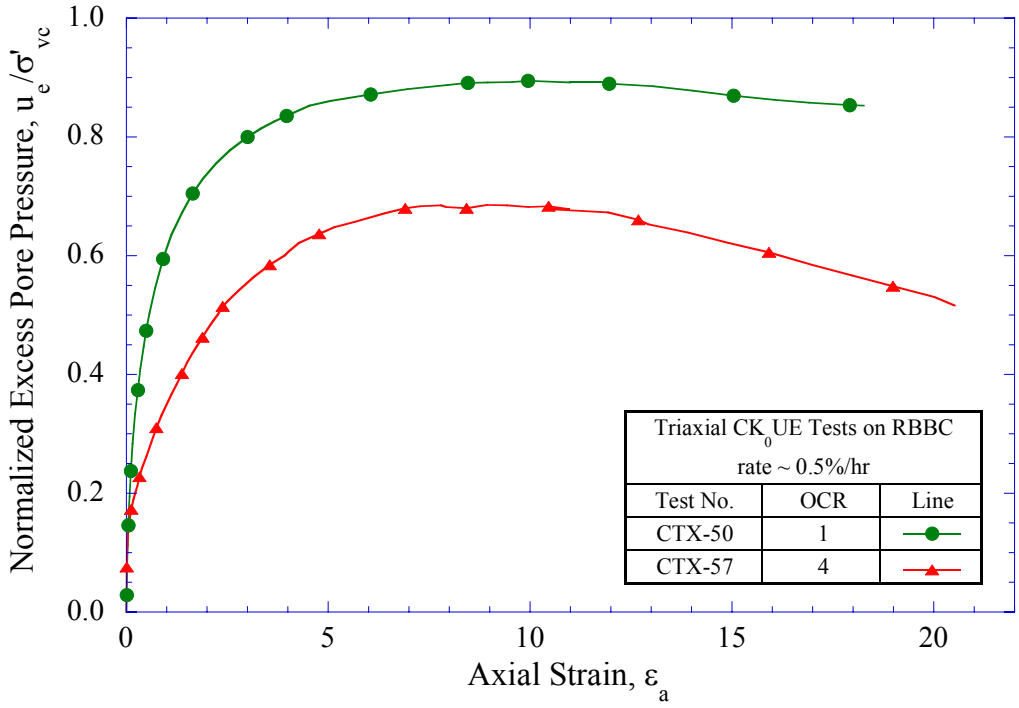

Figure 3-42: Normalized excess pore pressures of RBBC III (OCR = 1, 4) in undrained triaxial extension (Sheahan, 1991)

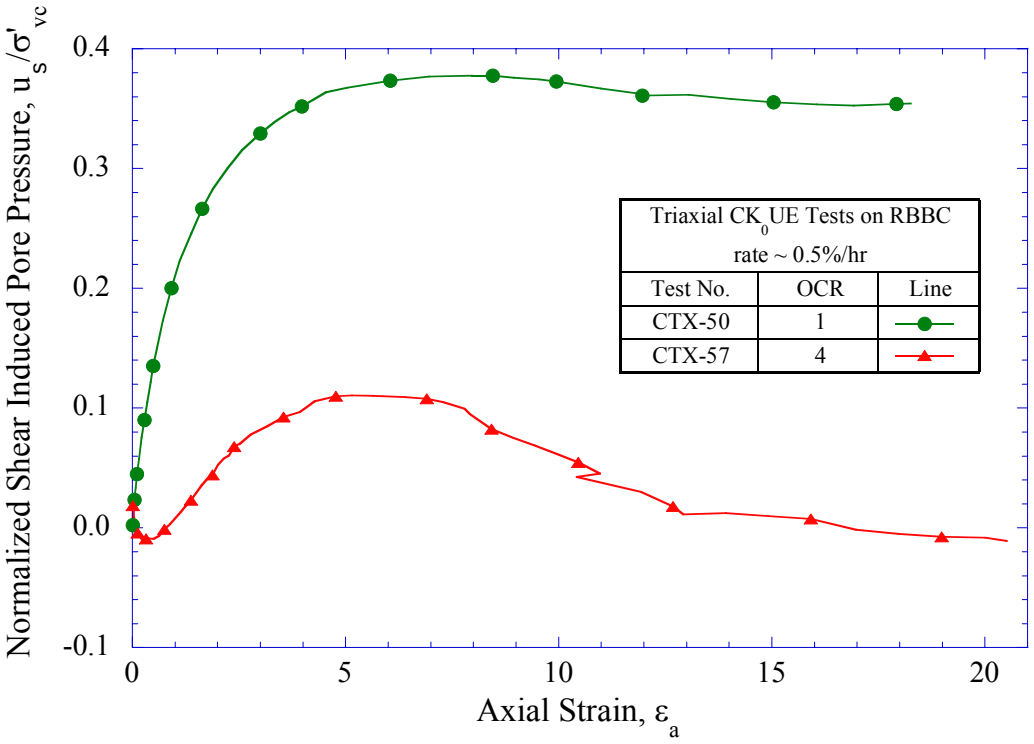

Figure 3-43: Normalized shear induced pore pressures of RBBC III (OCR = 1, 4) in undrained triaxial extension (Sheahan, 1991)

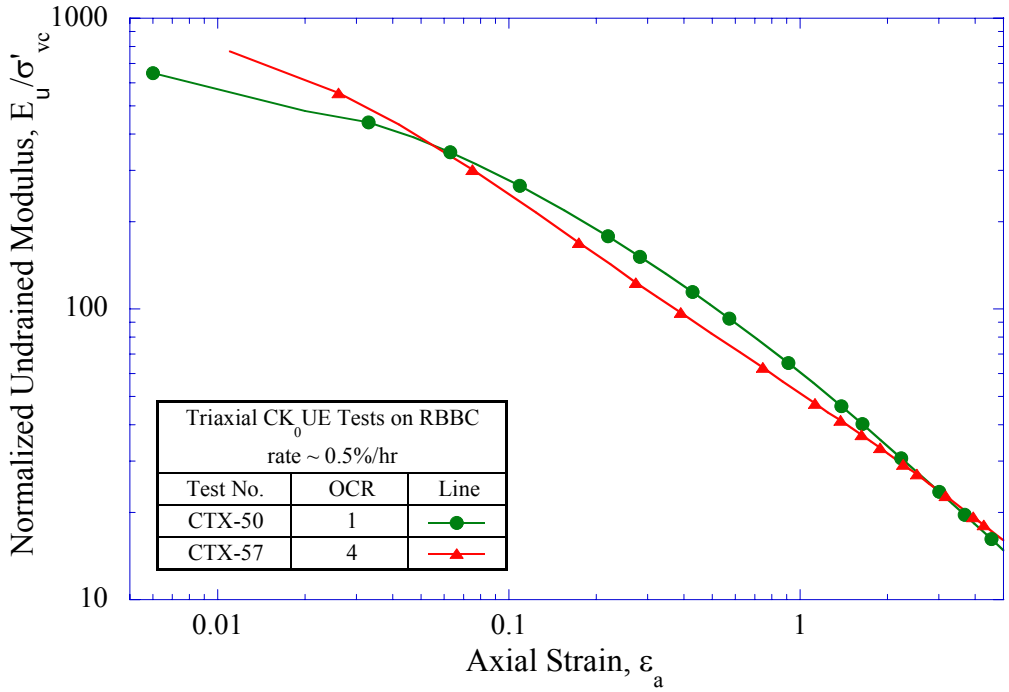

Figure 3-44: Normalized undrained secant modulus versus axial strain for RBBC III in undrained triaxial extension (Sheahan, 1991)

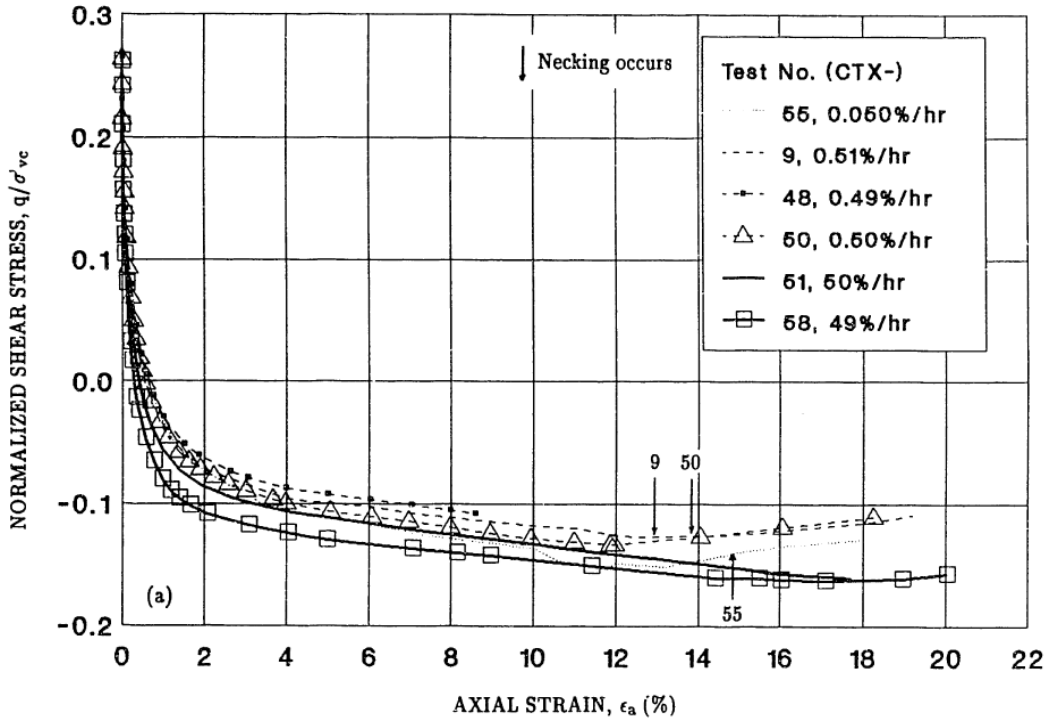

Figure 3-45: Effect of strain rate on normalized stress-strain curves of NC RBBC III in undrained triaxial extension (Sheahan, 1991)

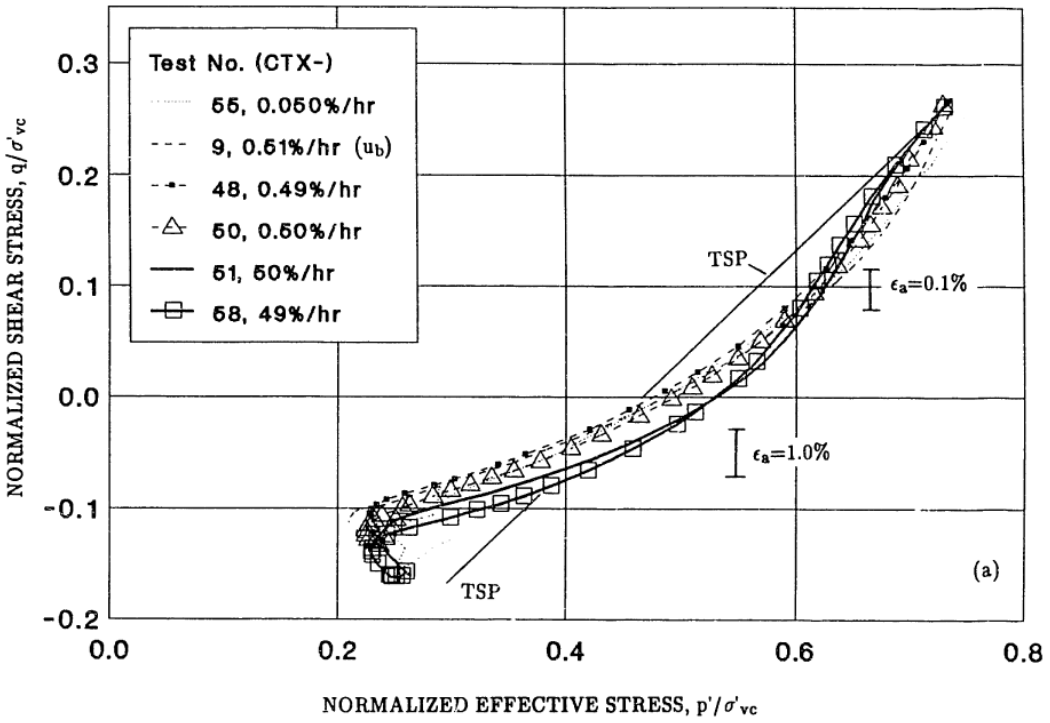

Figure 3-46: Effect of strain rate on normalized stress paths of NC RBBC III in undrained triaxial extension (Sheahan, 1991)

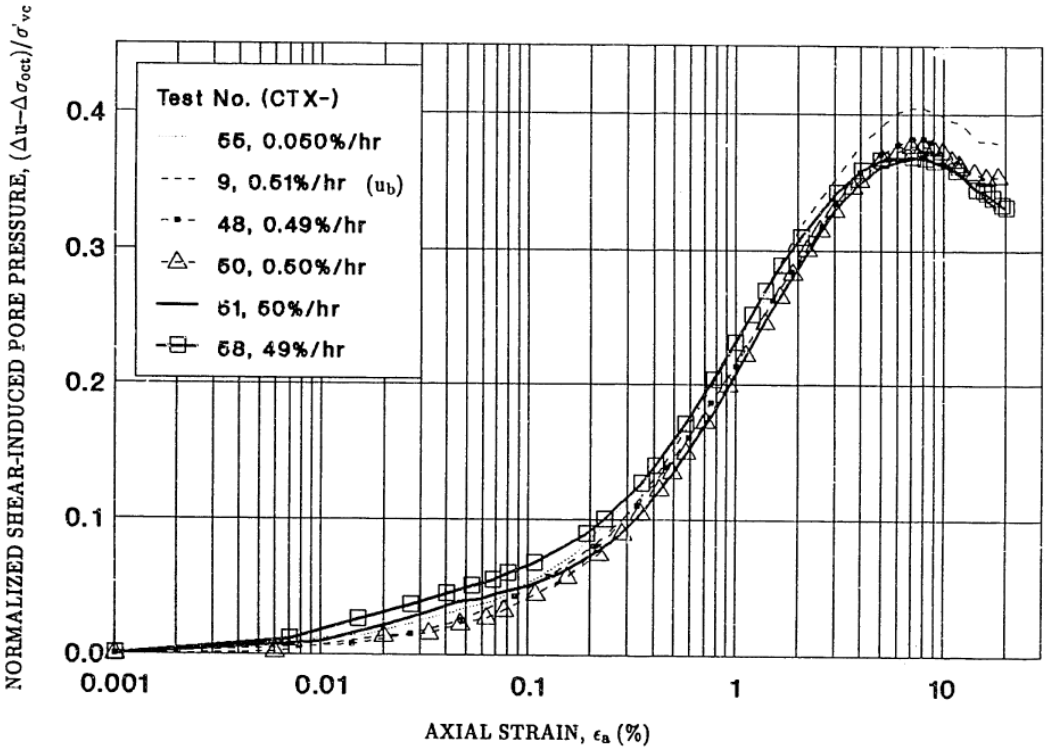

Figure 3-47: Effect of strain rate on normalized shear induced pore pressure of NC RBBC III in undrained triaxial extension (Sheahan, 1991)

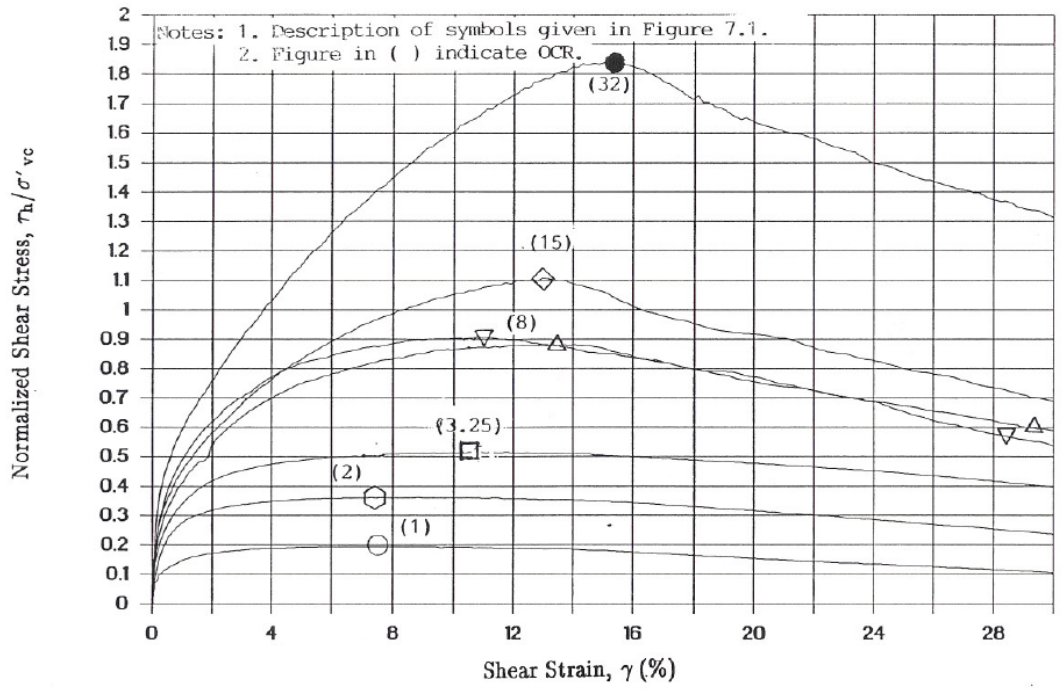

Figure 3-48: Normalized shear stress-strain behavior of RBBC III (OCR = 1, 2, 3.25, 8, 15, 32) in undrained direct simple shear (Ahmed, 1990)

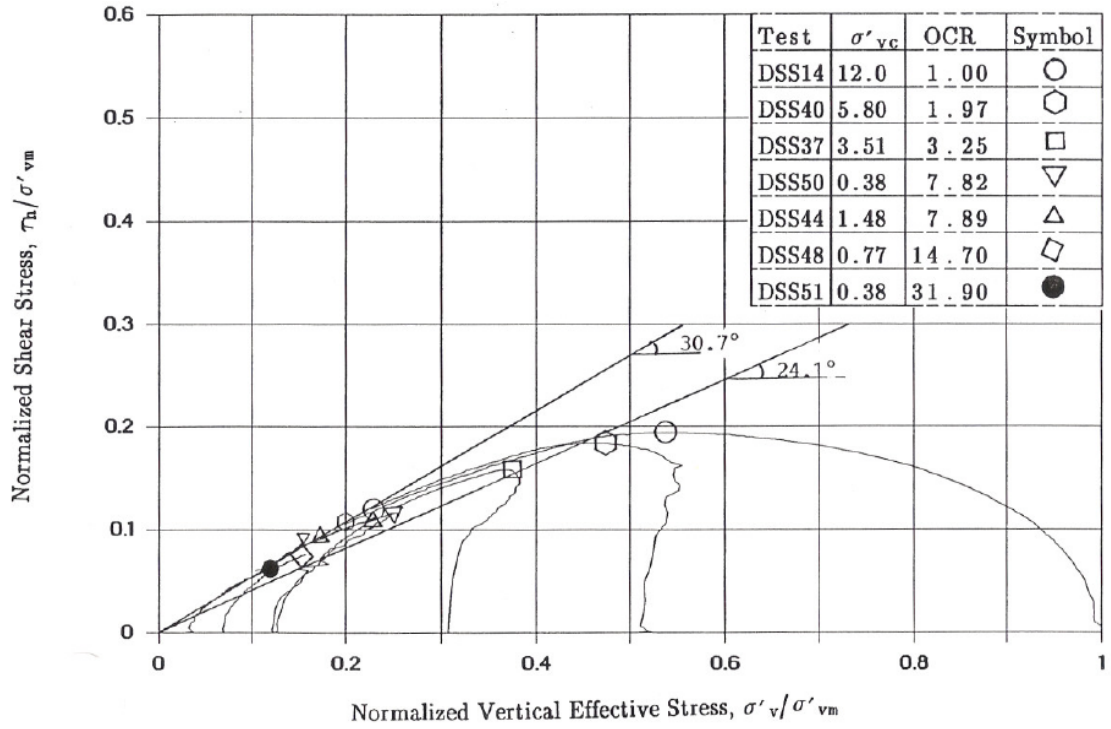

Figure 3-49: Normalized effective stress paths of RBBC III (OCR = 1, 2, 3.25, 8, 15, 32) in undrained direct simple shear (Ahmed, 1990)

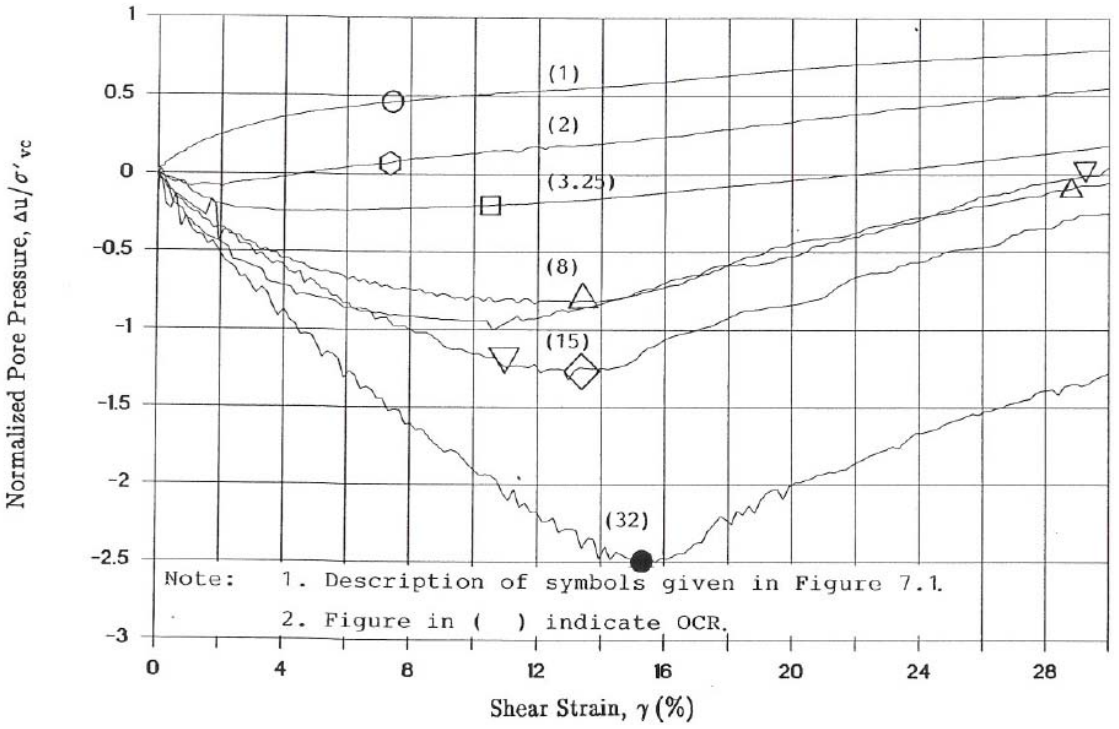

Figure 3-50: Normalized pore pressures of RBBC III (OCR = 1, 2, 3.25, 8, 15, 32) in undrained direct simple shear (Ahmed, 1990)

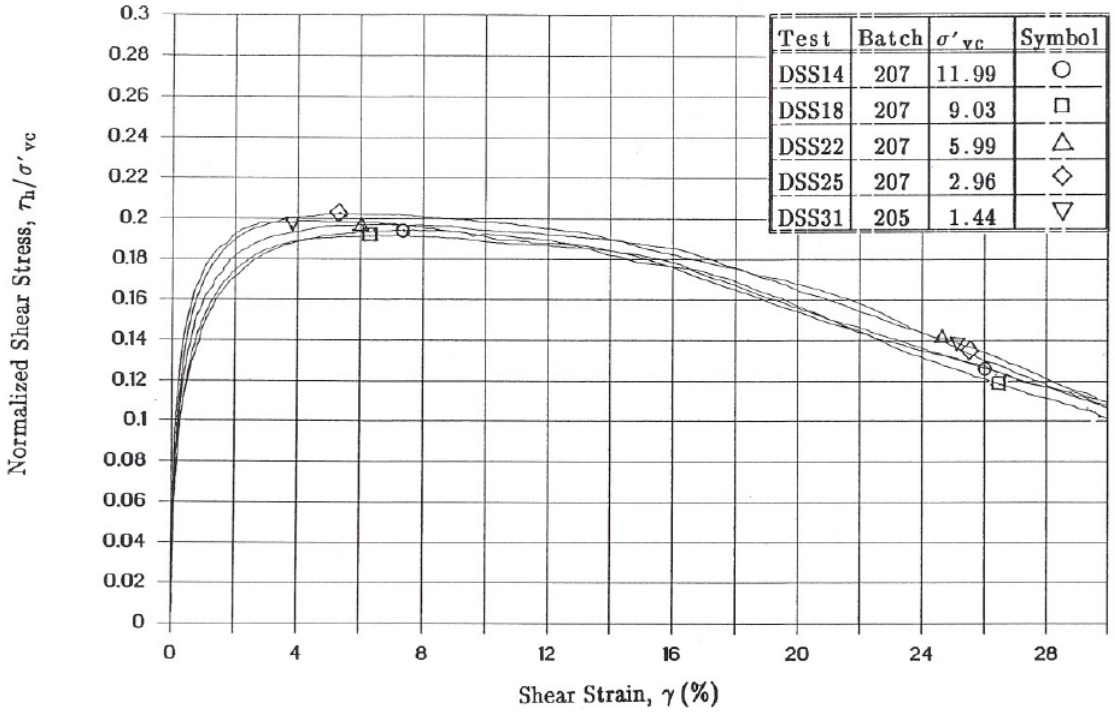

Figure 3-51: Effect of stress level on normalized stress-strain curves of NC RBBC III in undrained direct simple shear (Ahmed, 1990)

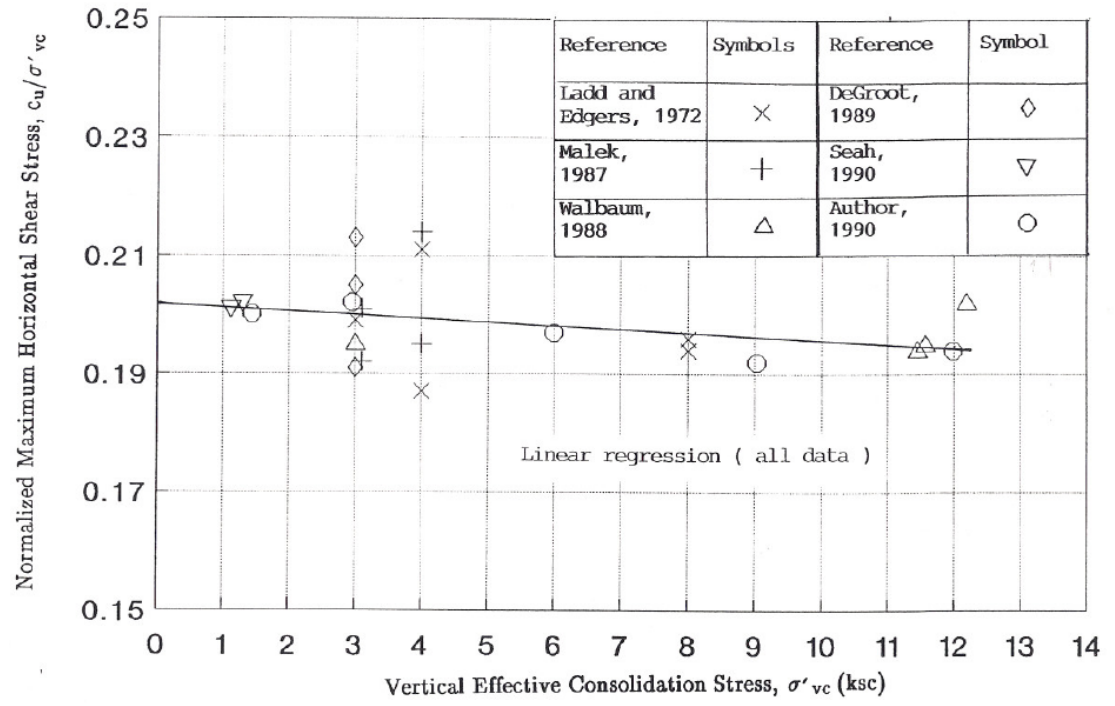

Figure 3-52: Undrained strength ratio versus stress level for NC RBCC III in undrained direct simple shear (Ahmed, 1990)

4 EQUIPMENT AND TESTING PROCEDURES

4.1 INTRODUCTION

This chapter describes the testing equipment and procedures used to perform the experimental program. Triaxial and Constant Rate of Strain (CRS) devices were employed in this research to investigate the effect of stress level on the 1-D consolidation and undrained shear properties. In addition, model borehole tests were performed using custom-built Thick-Walled hollow Cylinder (TWC) apparatuses to study the stability of boreholes.

The CRS consolidation tests were performed on small diameter specimens (D = 3.6 cm) consolidated to vertical consolidation effective stresses of 10 MPa using the Trautwein consolidometer device. The tests were consolidated at a strain rate of 2 %/hour and the results were interpreted using the standard linear theory (Wissa et al., 1971). The apparatus, testing procedures and interpretation method for this test are well documented (e.g., Force, 1998; Gonzalez, 2000) and therefore will not be discussed in this chapter.

The triaxial tests were performed using the MIT automated stress path triaxial cells which provide high quality results. Two types of triaxial cells were used: 1) the low pressure triaxial cell with a plexiglass chamber, and 2) the high pressure triaxial cell with a steel chamber. The maximum confining pressure that the low pressure apparatus can sustain is about 1.5 MPa while the high pressure apparatus was designed to operate at confining pressure up to 20 MPa. Both devices use test specimens with diameter, D = 3.6 cm, and height, H = 8.1 cm. The low pressure tests were performed using the automated triaxial apparatus originally developed by Sheahan (1991). The high pressure apparatus, originally developed by Anderson (1991) for testing frozen and unfrozen sands, was modified in this study for cohesive soils.

The automated, high pressure TWC apparatuses were developed as part of this research at MIT to experimentally simulate the stress conditions around a model borehole. The TWC testing program was carried out in two phases using two different devices. Phase 1 TWC tests have been performed on relatively small specimens with outer diameter, D_o = 7.6 cm, inner diameter, D_i = 2.5 cm, and height, H = 15.2 cm, while Phase 2 tests used larger specimens with dimensions D_o = 15.2 cm, D_i = 2.5 cm, and H = 22.8 cm, in order to enhance the boundary conditions. The

small diameter TWC apparatus was adapted from an existing high pressure triaxial apparatus where major modifications were made to both the top cap and pedestal in order to accommodate thick-walled cylindrical specimens of clay. The system capabilities were also increased from 3-axis control (cell pressure, back pressure, and axial load) to 4-axis control (cell pressure, back pressure, cavity pressure, and axial load). The high pressure apparatus for the large diameter TWC specimens was fully designed and fabricated for this project.

An overview of the triaxial (low and high pressure) and TWC (small and large diameter) testing equipment employed to perform the experimental program is presented in Section 4.2. This section highlights the main components inside the test chamber and provides a description of the overall system for each of the testing devices.

Since the equipment used to carry out the tests are automated, a description of the control system that performs the various stages of the test is provided in Section 4.3. This includes the measurement instrumentation, control system hardware, and software as well as the data acquisition system.

Evaluation of new testing equipment through experimental measurements is required in order to assess the reliability and the accuracy of the test results. In this research, the high pressure triaxial apparatus was modified and two new thick-walled hollow cylinder devices were developed. Section 4.4 evaluates the new testing systems for their ability to control the test processes, as well as the effectiveness of the various equipment modifications.

A complete description of the test procedures for cohesive soils is presented in Section 4.5. All samples tested for this thesis came from batches of Series IV Resedimented Boston Blue Clay (RBBC). Particular emphasis is placed on the description of the TWC test procedures since this test is performed for the first time at MIT.

4.2 OVERVIEW OF TESTING EQUIPMENT

4.2.1 Introduction

The triaxial and TWC testing devices used in the present study have the same system layout, which is based on previous technology that was first used to automate triaxial testing at MIT (Sheahan, 1991). Figure 2-1 shows a schematic of the standard computer controlled triaxial

testing apparatus used in the MIT Geotechnical Laboratory for testing cohesive soils. The system combines existing testing equipment (e.g., load frame, triaxial cell, etc.) with some innovative components (e.g., analog-to-digital converter, electronic motor control system, etc.). The automated triaxial and TWC testing devices incorporate six basic components: 1) the test chamber; 2) the system for load application comprising the pressure volume controllers and the loading frame; 3) the motors, motor controllers and drivers; 4) the instrumentation package including the power supply and all the transducers; 5) the personal computer based control system; and 6) the central data acquisition system.

This section discusses the first two components for each of the testing devices employed in this research. The other four components are discussed in the subsequent section (Section 4.3). Section 4.2.2 presents the MIT automated stress path triaxial cells. This covers the low pressure and high pressure test devices. The small and large diameter MIT automated stress path TWC apparatuses are presented in Section 4.2.3.

4.2.2 MIT Automated Stress Path Triaxial Cells

4.2.2.1 Low Pressure Triaxial Cell

The low pressure tests were carried out using the existing triaxial apparatus in the MIT Geotechnical Laboratory. The main features of this apparatus are presented in this section. A more complete description of the MIT automated stress path triaxial cells can be found in Sheahan (1991), Sheahan & Germaine (1992) and Santagata (1998).

The triaxial apparatus has a plexiglass chamber with a pressure capacity limit of 1.5 MPa. The chamber contains the specimen and sets the boundary conditions. It incorporates internal posts, base pedestal, top and bottom drainage, a fixed top cap, and a compact shear-beam load cell (500 lb [2.2 kN] capacity) located within the chamber for direct measurement of the axial deviator force. Figure 4-2 shows a schematic of the chamber and Figure 4-3 shows a photograph of the apparatus. The soil specimen is sealed using two thin impermeable membranes (unlubricated latex Trojan brand condom) fixed with O-rings. The use of an internal load cell eliminates the effects of piston seal friction on the load measurement. The electrical connections for the load cell are driven through the base of the cell. The load cell is connected to the loading

piston that rides through a low friction, linear bearing with O-ring seal. Piston movement is monitored with an externally mounted LVDT.

The chamber is filled using Dow-Corning "200 fluid", 20 centistokes silicone oil. This particular silicone oil exhibits extremely low viscosity under a wide range of temperatures, is optically transparent and does not degrade the seals or the latex membranes used in testing. The oil was initially selected to limit leakage over the course of the test, but also offers the added benefit of being nonconductive which is essential when locating electronic devices (such as the load cell within the chamber).

The entire system is axially loaded through the use of a 1 Tonne [9.8 kN] capacity bench-top Wykeham Ferrance screw driven loading frame with adjustable gear ratios. MIT-designed Pressure-Volume Controllers (PVC; see Section 4.3.3.1) are used to control the cell and back (pore water) pressures. The specimen volume changes are computed from LVDT's monitoring the motion of the back pressure PVC (see Section 4.3.2). Both the cell and back pressures are monitored with high performance diaphragm type (200 psi [1.4 MPa] capacity) pressure transducers that are located on the base of the cell to reduce system compliance.

The triaxial chamber, the load frame and the two pressure-volume controllers are housed inside an environmental enclosure within the main testing room. The enclosure and the rest of the apparatus are located inside an air-conditioned laboratory.

4.2.2.2 High Pressure Triaxial Cell

The high pressure triaxial testing apparatus was originally built for frozen soil research by Anderson (1991) and subsequently modified by Swan (1994) and Da Re (2000). The apparatus had an oversized base pedestal and top cap to accommodate radial deformations during shearing. The lubricated end platens were replaced in this study with standard frictional platens (i.e., 3.6cm diameter) and porous stones were located at the top and bottom to facilitate drainage and measurement of pore pressures.

The system, which is designed to operate at confining pressures up to 20 MPa, has a steel chamber which mates to the apparatus base. Figure 4-4 shows a schematic of the high pressure triaxial chamber and Figure 4-5 shows a section view of the apparatus. The triaxial chamber encloses the soil specimen, base pedestal, floating top cap, top and bottom drainage and an

internal shear-beam load cell. The top drainage line is made of copper tubing to minimize system compliance while it is coiled to increase flexibility and enable sufficient axial strains during consolidation and shearing (Figure 4-4). The valves and pressure transducers are located at the triaxial base to reduce system compliance. Furthermore, copper tubing and ball valves are employed also to minimize compliance and limit pressure loss in the loading system. The chamber is filled with Dow-Corning low viscosity silicone oil (which is essential since an internal load cell is used). Figure 4-6 shows a photograph of the high pressure triaxial apparatus.

The soil specimen in the high pressure triaxial apparatus was initially sealed with two thin membranes (unlubricated condom). This works well for tests at low confining pressures. However, leakage through the membranes was observed for tests with confining pressure exceeding 3 MPa. As a result, the two thin membranes were replaced with one thick commercial latex membrane (0.31 mm thick) and one thin membrane. This new arrangement enabled the device to be used for tests consolidated to the maximum vertical effective stress of 10 MPa (i.e., confining pressure up to 6 MPa).

The axial load is applied to the specimen via a 2.54 cm diameter hardened steel piston to which a 2,000 lb [8.9 kN] internal load cell is attached. The piston enters the top of the chamber through a double O-ring seal. Piston movement is continuously monitored by an externally mounted LVDT. The bottom of the load cell mates with the floating top cap on the specimen via an alignment device (Figure 4-5).

In order to impose triaxial state of stress to the specimen, the triaxial apparatus is linked to three PVC's. As in the case of the low pressure triaxial apparatus, two PVC's are used to control the cell and back (pore water) pressures. The volume change of the specimen is computed from LVDT's monitoring the motion of the back pressure PVC piston. The cell and pore pressures are measured using 1,000 psi [7 MPa] capacity pressure transducers. The Third PVC is used in this case to apply a vertical axial force to the specimen. It is directly attached to a 9 Tonne [89kN] hydraulic ram that converts fluid pressure to axial force, and thus moves the entire triaxial apparatus up against the load frame. The same low viscosity silicone oil used for the cell chamber is used as the hydraulic fluid in the PVC. Improvements were made to the control system to implement PID (proportional-integral-derivative) control algorithm in order to achieve and maintain a constant rate of strain during consolidation and shearing as described in Section 4.3.3.2.

Since the steel chamber is attached to the triaxial base outside the load frame, the base is disconnected from the PVC lines and the apparatus setup takes place on a mobile cart (Figure 4-6). Hence, after placing the apparatus back in the load frame and attaching the PVC lines, the water lines are saturated by applying vacuum to remove the air and then flushed with water.

The high pressure triaxial system is also housed inside an environmental enclosure within the main testing room as shown in Figure 4-7. The enclosure and the rest of the apparatus are located inside an air-conditioned laboratory.

4.2.3 MIT Automated Stress Path TWC Cells

4.2.3.1 Small Diameter TWC Cell

The small diameter TWC apparatus was adapted from an existing high pressure triaxial apparatus where major modifications were made to both the top cap and base pedestal to accommodate thick-walled cylindrical specimens of clay. The resulting automated high pressure apparatus allows for independent control of the vertical stress and the radial pressures acting on the inner and outer walls of the cylinder, as well as the pore pressure (4-axis control).

The TWC apparatus has a steel chamber that allows it to operate at confining pressures up to 20 MPa. Only the chamber and base were reused from the existing triaxial apparatus while the plumbing and all the other internal components were fabricated for this new device. Figure 4-8 shows a schematic of the small diameter TWC chamber and Figure 4-9 shows a section view of the apparatus. The chamber encloses the TWC specimen, base pedestal, top and bottom drainage, floating top cap, top and bottom annular platens, and annular porous stones. The base pedestal incorporates two conduits; a back pressure line connected to the specimen (pore water pressure inside the soil specimen) and an internal cavity line connected to the inner bore cavity. The TWC soil specimen is sealed with internal and external latex membranes. The external membrane is a commercial 0.31 mm thick membrane while the internal membrane is a custom made 0.63 mm thick membrane (North American Latex Corporation). The top and bottom annular platens are used to seal the internal cavity membrane with the use of O-rings. Figure 4-10 shows a schematic of the internal membrane seal. These annular platens are screwed to the pedestal and top cap where an O-ring seal prevents the cavity fluid from reaching the water lines connected to the specimen. The top cap has a drainage conduit and a bleeding screw to fill the internal cavity with

oil without trapping air, this screw is then tightened to completely isolate the cavity from the external cell. The specimen is allowed to drain to the top and bottom, and filter paper strips are applied to the outer surface to accelerate drainage. All the internal parts described are made of brass because they supply water to the specimen. Note that the pedestal, the top cap and the annular platens have the same diameter as the specimen. The top drainage line is made of copper to minimize system compliance while it incorporates few spirals at the top to accommodate some axial deformation during the test. In addition, copper tubing and ball valves are employed in the apparatus to minimize compliance and limit pressure loss in the loading system. The system is filled using Dow-Corning "200 fluid" silicone oil. Figure 4-11 shows a photograph of the small diameter TWC apparatus.

The axial load is applied to the specimen via a 25 mm diameter hardened steel piston which enters the top of the chamber through a double O-ring seal. The axial load is measured using an external shear-beam load cell. An external load cell is used instead of an internal one since the "outsized" TWC specimen occupies most of the space inside the chamber. The load cell, which is attached to the upper crossbar on the load frame, connects with the top of the loading piston by means of a ball bearing to minimize the eccentric loading. A 10,000 lb [44.5 kN] load cell was used in the highest stress level test (σ'_v = 10 MPa) while a 2,000 lb [8.9 kN] load cell was used for all the other tests. Piston movement is continuously monitored by an externally mounted LVDT.

The entire system is axially loaded through the use of a 2 Tonne [19.6 kN] capacity bench-top Mossco-Oslo (Type TP-2) screw driven loading frame. The external cell and the back (pore water) pressures are controlled using two PVC's. A third PVC was added to control the internal cavity pressure. An LVDT attached to the PVC monitors the piston displacement and hence, measures the volume changes. Volume changes in the specimen, external cell chamber and internal cavity bore are all monitored during the test. The external cell, internal cavity, and back pressures are measured using 2,000 psi [14 MPa] capacity diaphragm type pressure transducers. A more detailed description of the transducers is provided in Section 4.3.2. Modifications were made to the control system software to incorporate the borehole closure subroutine (see Section 4.3.3.2).

The TWC apparatus setup takes place on a mobile cart which requires the PVC lines to be disconnected for each test. Hence, after placing the apparatus back in the load frame and

connecting the PVC lines, the water lines are saturated by applying vacuum to remove the air and then flushed with water.

The TWC device and the three pressure-volume controllers are housed inside an environmental enclosure within the main testing room as shown in Figure 4-12. The enclosure and the rest of the apparatus are located inside an air-conditioned laboratory.

4.2.3.2 Large Diameter TWC Cell

The large diameter TWC apparatus was fully designed and fabricated for this project. The system required the fabrication of the apparatus chamber, four PVC's with high volume and pressure capacities, a new control box, local data acquisition system, custom-made membranes, refurbishment of existing high capacity load frame, new manifold and tubing. The resulting automated high pressure apparatus allows for independent control of the vertical stress and the radial pressures acting on the inner and outer walls of the cylinder.

The large diameter TWC chamber comprises a base with a manifold, large volume cell, internal chamber parts, external posts, and top plate. With the exception of the external posts, all the other parts are made of aluminum. However, since aluminum reacts with water, the entire apparatus was hard coated (2.5 microns thick Sanford Hardcoat with Nickel Acetate seal, Duralectra-CHN). This system is designed to operate at confining pressures up to 10 MPa. The general layout of this apparatus resembles closely the small diameter TWC apparatus. Figure 4-13 shows a schematic of the large diameter TWC chamber and Figure 4-14 shows a section view of the apparatus. The chamber encloses the TWC specimen, base pedestal, top and bottom drainage, floating top cap, top and bottom annular platens, and annular porous stones. The base pedestal incorporates the back (pore water) pressure line which is linked to the specimen. The apparatus base has a conduit for the internal cavity, a conduit for the top drainage line and a conduit for the external cell. The TWC soil specimen is sealed with internal and external latex membranes. Both membranes are custom made 0.63 mm thick membranes. The top and bottom annular platens are used to seal the internal cavity membrane with the use of O-rings (Figure 4-10). These platens are screwed to the pedestal and top cap where an O-ring seal prevents the cavity fluid from reaching the water lines connected to the specimen. The top cap has a drainage conduit and a bleeding screw to fill the internal cavity with oil without trapping air, this screw is then tightened to isolate the cavity from the external cell. Filter paper strips are applied to the

outer surface to accelerate drainage. Note that the pedestal, the top cap and the annular platens have the same diameter as the specimen. Copper tubing and ball valves are employed in the apparatus to minimize compliance and limit pressure loss in the loading system. However, the tubing for this apparatus is larger (0.635 cm diameter versus 0.317 cm for the previous devices) to provide more fluid capacity. The rigid top drainage line (made of copper) includes a few spirals at the top to allow for some axial deformation during the test. Figure 4-15 shows a photograph of the large diameter TWC apparatus. The system is filled using Dow-Corning "200 fluid" low viscosity silicone oil.

The load frame used to apply the axial load is Tetrahedron MTP-14 compression press (22.7 Tonne [223 kN] capacity). This hydraulic load frame (originally used for a heat press) was refurbished and modified for this study. A new PVC was attached to the existing hydraulics of the load frame (in order to convert the fluid pressure generated by the PVC to axial force) such that the entire apparatus can be moved up against the load frame. The pressure capacity of the PVC is about 10 MPa which translates to approximately 100 kN axial load in this load frame (diameter of load frame piston is about 11 cm). The available stroke of the load frame piston is roughly 20 cm. The axial load is applied to the specimen via a 50 mm diameter hardened steel piston which enters the top of the TWC chamber through a double O-ring seal. The load is measured using an external hydraulic load cell connected to 1,000 psi [7 MPa] capacity pressure transducer. This load cell has a capacity of 50,000 lb [223 kN]. Piston movement is continuously monitored by an externally mounted LVDT.

Three new purpose-built pressure volume controllers with high pressure and volume capacities are used to control the external cell, internal cavity, and back pressures (see Section 4.3.3.1). These pressures are measured using 1,000 [7 MPa] capacity diaphragm-type pressure transducers. The displacement of the piston is monitored using a string pot (linear position transducer) to measure the volume changes in the external cell, internal cavity, and specimen.

The apparatus setup for the large diameter TWC also takes place on a mobile cart and, therefore, the water lines are saturated by applying vacuum to remove the air and then flushed with water after placing the apparatus in the load frame.

The large diameter TWC apparatus is not housed inside an environmental enclosure. However, the apparatus is located inside an air-conditioned laboratory where the temperature is

reasonably constant (~ 25±1 °C). Figure 4-16 shows a photograph of the large TWC system in the laboratory.

4.3 COMPUTER CONTROL AND DATA ACQUISITION SYSTEMS

4.3.1 Introduction

As mentioned above, a large effort has been invested by the MIT Geotechnical Laboratory over the past 20 years into automating the strength testing equipment. The process of automating existing equipment, termed *adaptable automation* by Sheahan & Germaine (1992), involves the modification of existing manual system components to permit automation, as well as the addition of innovative new components to complete the system automation and increase flexibility and quality control. Automation also offers the added benefit of dramatic reduction in labor. The first application of this concept, which resulted in the development of the automated stress path triaxial cells, is described in more detail by Sheahan (1991) and Sheahan & Germaine (1992). The automation of other laboratory devices followed such as the high pressure triaxial cell (Andersen, 1991), the direct simple shear devise (Ortega, 1992) and a special Caisson Element Test (CET) cell (Cauble, 1996).

Automated control is carried out using a PC and a control program written in QBASIC. The program is task specific and able to perform all phases of the test from initial pressure up and saturation to the consolidation and shear phases. In the TWC tests, the original triaxial control software was slightly modified to incorporate the borehole closure subroutine.

The essential ingredient for automation is the feedback control loop for the driving systems of the apparatus. In essence, the electric transducers measure the actual specimen stress-strain state; these transducers signals are fed into the computer and converted to engineering units; software compares this actual state with a pre-scheduled time history of specimen stress-strain state; a software control algorithm is used to compute what action needs to be taken by the electric motors to keep the stress-strain state on schedule; and signals are sent to the motors to carry out the corrective action. Thus, closed-loop feedback control uses direct measurements in an iterative scheme to maintain specified time histories of the parameters being measured (Sheahan et al., 1990).

Both the hardware and software components of the control system cooperate in order to conduct the feedback control loop. The hardware includes the computer equipment, electronic signal converters, driver interfaces, and instrumentation. The software consists of the computer programs that generate the signals necessary to operate the driving system. Section 4.3.2 describes the instrumentation used in the tests. Section 4.3.3 provides a description of the control system hardware and software. Section 4.3.4 discusses the data acquisition system.

4.3.2 Measurement Instrumentation

An array of transducers is used to measure physical quantities during the test, all of which use a common input voltage of approximately 5.5 volts Direct Current (DC) from a regulated power supply. All instrumentation signals and the input voltage are monitored and logged by a central data acquisition system. The transducers used in this study can be categorized as follows: pressure transducers, load cells, axial displacement transducers, and volume change transducers. The measurements obtained and the means of obtaining them in the low and high pressure triaxial tests and the small and large diameter TWC tests are listed in Tables 4-1, 4-2, 4-3 and 4-4 respectively. These tables also include a summary of the calibration factors along with the resolution and stability of the transducer signals as measured by the central data acquisition system (see Section 4.3.4.2). The four categories of transducers are described here.

e) Pressure Transducers

The cell and back (pore water) pressures in the triaxial and TWC tests as well as the internal cavity pressure in the TWC tests are measured by Data Instruments AB/HP type pressure transducers. These transducers measure absolute pressures by the deflection of a steel diaphragm instrumented with strain gages. The low pressure triaxial apparatus employs two 200 psi [1.4 MPa] pressure transducers while the high pressure triaxial apparatus uses two 1,000 psi [7 MPa] transducers. On the other hand, the small diameter TWC employs three 2,000 psi [14 MPa] pressure transducers and the large diameter TWC uses three 1,000 psi [7 MPa] transducers.

f) Load Cells

The load cells used in the triaxial and small diameter TWC devices are Data Instruments JP type shear beam load cells. This type of load cell is an S-shaped steel section instrumented with strain gauges. The triaxial devices employ internal load cells while the TWC devices use external

ones due to the limited space inside the TWC chamber. The low pressure triaxial apparatus uses a 500 lb [2.2 kN] load cell while the high pressure triaxial and small diameter TWC devices employ 2,000 lb [8.9 kN] load cells. Only the highest stress level test performed in the small diameter TWC apparatus used a 10,000 lb [44.5 kN] load cell.

The load cell employed in the large diameter TWC apparatus is a hydraulic load cell that is part of the Tetrahedron MTP-14 load frame. It consists of a flat pancake cylinder (25 cm outside diameter) containing hydraulic oil. Pressure within the cylinder is monitored thru a 1,000 psi [7 MPa] Data Instruments AB/HP type pressure transducer. The load cell has a capacity of 50,000 lb [223 kN].

g) Axial Displacement Transducers

The specimen's axial displacement in the triaxial and TWC devices is measured externally using a Linear Variable Differential Transformer (LVDT) manufactured by Trans-Tek Inc. (Series 240). These transducers have a linear range of about 2.5 cm. The LVDT tube generates a magnetic field through which a ferromagnetic core moves. The core, when displaces axially through the LVDT tube, produces an output voltage change directly proportional to the displacement.

h) Volume Change Transducers

The volume change of the specimen in the triaxial and TWC tests and the volume change of the internal cavity and external cell in the TWC tests are determined by measuring the displacement of the piston in the PVC cylinder using either an LVDT (for the triaxial and small diameter TWC devices) or a string pot (for the large diameter TWC device). The area of the piston is calibrated and remains constant through its stroke; volume change equals displacement times calibrated piston area. The LVDT used in the standard PVC's is a Trans-Tek Series 240 displacement transducer. The linear range of these transducers is 10 cm. The string pot (linear position transducer) used in the large diameter TWC PVC's is manufactured by Celesco (SP1 type). As movement occurs, the extension of the wire rope rotates an internal capstan and sensing device (precision potentiometer) to produce an electrical output signal proportional to the wire rope extension. The range of this device is 30 cm.

4.3.3 Control System

4.3.3.1 Control System Hardware

The main function of the control system hardware is to convey electronic information along the digital feedback control loop that operates the driving systems. Figure 4-17 shows a schematic drawing of the control system hardware components. The output from the transducer is sent to an analog to digital (A/D) converter, which converts this continuous, variable analog signal into a digital form (number of bits) that the computer can understand. The A/D converter is the heart of a circuit board that is placed in an expansion slot in the computer. The triaxial and TWC apparatuses uses the multichannel analog to digital converter device (MADC) developed at MIT by Sheahan (1991) for computer automated triaxial testing. A low cost high precision alternative to commercial A/D circuit boards, the MADC was designed specifically to allow a minimum 18 bit resolution during signal conversion from analog to digital. The key element of the MADC is the Analog Devices AD1170 analog to digital converter, which performs the basic function of translating analog signals in volts to digital signals in bit counts (see Section 4.3.4.1).

A PC with an Intel processor and expansion slots for the MADC and digital to analog boards houses the control system software and determines the new command signal to be sent to the driving system to control the test phase. A monitor is used with the computer to display values of the measured variables during testing to allow the user to interface with the control software.

The command signal generated by the software is converted back into an analog signal through a digital to analog (D/A) converter board that is located within the computer. The D/A converter used is a commercial board (12 bit resolution with a 10 volt range) sold by Strawberry Tree Inc.

From the D/A card, the analog command signals are sent via a motor driver to the electric motor. The motor drives the piston of the mechanical load frame to apply axial load or the piston of the PVC to apply pressure (which can be converted to axial load in the hydraulic load frame). The mechanical load frames are employed in the low pressure triaxial and small diameter TWC devices and are driven by Electro-craft motor Model E286. The MIT-designed PVC's are used to control the external cell, internal cavity, and back pressures as well as to apply axial force in the hydraulic load frames (high pressure triaxial and large diameter TWC devices). It consists of a

motor driven ball screw actuator (manufactured by Duff-Norton) that converts the rotary motion of the motor into linear motion of a piston that displaces fluid from a cylinder. The triaxial and small diameter TWC devices used the existing standard PVC's in the MIT Geotechnical Laboratory. These PVC's use 0.5 Tonne actuators (driven by Electro-craft motor Model E372/352) and have a volume capacity of about 45 cm^3 and pressure capacity of 14 MPa. The large diameter TWC apparatus, however, employed new purpose-built PVC's which use 2 Tonne actuators (driven by Electro-craft motor Model E286) and have a volume capacity of about 613 cm^3 (i.e., 13 times the standard PVC) and pressure capacity of approximately 10 MPa. Figure 4-18 shows a schematic of the high capacity pressure-volume controller.

The driving system causes a perturbation according to the command signal received, thus completing the feedback control loop. A new cycle begins once the MADC converts a new analog signal from the transducer.

4.3.3.2 Control System Software

The control software, which is written in the QBASIC programming language, consists of programs which assist the user in setting up the system for testing, and those for test control. The software was originally written for the MIT automated stress path triaxial cell and is generally under continuous modification. The standard triaxial tests used revision 5.3 (Germaine, 2006). This revision was modified for the high pressure triaxial tests to incorporate PID control. The TWC tests also used revision 5.3 but a module for the cavity closure was added as described below.

The system setup software includes the master and setup programs. The master program is a menu-driven program that can operate the motors in a step-wise or continuous mode. Both the step increment and rotational speed can be varied. In addition, the transducer readings and input voltage can be displayed on the monitor. This program is mostly used to setup the equipment. The setup program generates the data input file of test parameters to be used by the control program. Specimen dimensions, correction factors, transducer zeros and calibration factors are all entered in an on-screen format. This program chains to the test control program.

The control program consists of separate modules that perform the various phases of the test. The basic modules are undrained initial pressure-up, back pressure saturation, hold stress (current or target values), B-value check, consolidation along any stress path or K_0 consolidation,

and drained or undrained shear. The control program begins by setting up the computer keyboard, analog to digital conversion card, the control motors and obtains an initial set of readings for all transducers. The user then starts a particular phase by choosing one of the control modules from an on-screen menu.

The PID (proportional-integral-derivative) control algorithm was incorporated in the control system of the high pressure triaxial apparatus to maintain a constant axial strain rate. This was essential since the relatively slow strain rates employed during consolidation and shear when testing cohesive soil with the hydraulic load frame (compared to the rates for sand that was used in this device) required the axial PVC motor to operate at very low rotational speeds which resulted in erratic performance. In the PID algorithm, the proportional control generates a control action that is proportional to the difference between the reference value and the target value. The integral control changes the controller output by an amount related to the integral of the error signal. The derivative control bases the control response on the rate of change of the error signal. Combining these three forms of feedback control results in a control algorithm that can be implemented in the triaxial testing control program. This combination reduces the steady state error to zero and often yields satisfactory dynamic response. As a result, the implementation of the PID control algorithm for strain rate allows the axial actuator to apply the desired constant deformation rate for tests with rates as slow as 0.1 %/hr. The modified control software (revision 6.2) employed in the high pressure triaxial tests is provided in Appendix A.

For the TWC test, a module for undrained cavity closure was added in the control program. In order to use this program, the user must first switch the pore PVC motor plug with the cavity PVC motor plug in the control box and the connectors of the pore pressure and specimen volume transducers with the connectors of the cavity pressure and volume transducers in the main transducer box connected to the PC. This is because the current system can only control three motors at the same time (note that the pore pressure reading is only monitored during undrained borehole closure). The program also prompts the user to enter the calibration factors and zero values for the cavity pressure and volume transducers. In the cavity closure module, the algorithm applies a constant cavity volume strain rate while keeping the external cell pressure and axial stress constant. Hence, the user needs to input the cavity volume strain rate and the final strain level before starting the program. Once this strain level is reached, the computer holds the internal cavity, external cell and axial stresses constant. The computer displays on the

monitor the values of the axial stress, cell pressure and cavity pressure along with the axial and cavity volumetric strains. Readings from the pore pressure and cell volume transducers are not fed into the PC but are monitored on the central data acquisition system. The control software for the TWC test (revision 7.1), which is also used in the standard low pressure triaxial test, is provided in Appendix B.

4.3.4 Data Acquisition System

4.3.4.1 AD1170 Data Acquisition Card

The testing equipment described above includes two data acquisition systems; a local one at the personal computer used for control purposes, and a central system used to collect all the data in the MIT Geotechnical laboratory for subsequent analysis. The local data acquisition system makes use of a high quality (MIT-designed) analog to digital conversion card which is built around Analog Devices model AD1170 high resolution, programmable integrating converter (Analog Devices Inc.). The AD1170 offers independently programmable integration time (from 1 ms to 350 ms) and allows the user to specify any resolution from 7 to 22 bits. Usable resolution is typically limited to 18 bits due to measurement and calibration noise error. This translates into a maximum resolution of 0.0024 mV which provides ample sensitivity for closed loop digital calculations. The high degree of signal averaging provided by the AD1170 helps eliminate the anomalies in the signal due to noise and thus provides a more reliable and repeatable representation of the quantity to be measured.

4.3.4.2 Central Data Acquisition System

The central system is based on a 486 microprocessor PC driven by Windows based software interfaced with an expanded channel Hewlett Packard HP3497A data acquisition unit which uses very low noise integrating analog to digital converter. This system has a 5.5 digit integrating analog to digital converter with auto-ranging amplification to four voltage scales (0.1, 1, 10, 100V). Currently the system is configured to monitor 140 channels simultaneously while providing analog to digital conversion and data storage at rates up to 1 Hz. This high quality low noise system also makes its possible to directly measure the load cell, pressure transducers, and displacement transducers without any signal amplification. The resolutions and the stability of

transducer signals as measured by the central data acquisition system in the triaxial and TWC testing devices are summarized in Tables 4-1 to 4-4.

4.4 EVALUATION OF NEW TESTING EQUIPMENT

4.4.1 Introduction

This section evaluates the performance and capabilities of the new testing equipment developed for the current research. Section 4.4.2 evaluates the high pressure triaxial apparatus. Section 4.4.3 assesses the small diameter TWC apparatus while Section 4.4.4 evaluates the large diameter TWC apparatus.

4.4.2 High Pressure Triaxial Apparatus

The high pressure triaxial apparatus was modified to test cohesive soils at high pressures. Triaxial testing of clays at elevated pressures up to $\sigma'_v = 10$ MPa has not previously been done at MIT. Therefore, the system components and test results are examined to evaluate the performance of this apparatus.

The high pressure triaxial cell incorporates an internal load cell in order to measure the actual vertical load applied by the axial piston on the test specimen (thus eliminating the effect of load system friction). An experiment was carried out to see if the load cell is sensitive to the confining pressure (i.e., to see if it's zero value shifts when the confining pressure increases or decreases). Figure 4-19 shows the results for two cycles of loading and unloading. It appears that the submersion of the load cell in the cell oil affects slightly the zero reading (from 0 to -7 N). Also, the loading in the first cycle to cell pressure of about 5.5 MPa (maximum confining pressure reached in the experimental program) increases the load cell reading by 1 N and the unloading by another 1 N. The second cycle does not seem to affect the load cell reading. The shift in zero value due to the submersion in the cell oil is nontrivial and needs to be corrected before starting the test. However, the shift in the zero value observed in the first cycle over the wide range of confining pressure translates to less than 2 kPa axial stress on the specimen. So it can be concluded that for all practical purposes, the load cell can be assumed to be insensitive to the confining pressure for the calculations in this research. The error introduced in the vertical

stress is negligible and no correction will be made for the very slight shift observed in the zero of the load cell.

Leakage problems are possible in the high pressure triaxial apparatus due to the high confining pressures and long duration of the tests. Two types of leakage can occur, internal and external. External leakage can be reduced by minimizing fittings and valves in the pore system, ensuring that ball valves are used and converting all connections to Swagelok type. Internal leakage through the membrane is normally controlled by selecting the right type of confining fluid and membranes. Although silicon oil was used as the cell fluid, initial triaxial tests performed at high confining pressures (greater than 3 MPa) experienced internal leakage through the membrane. The soil specimens in these tests were sealed with two thin membranes (latex condom). Consequently, it was decided to replace the two thin membranes with one thick commercial latex membrane (0.31 mm thick) and one thin membrane fixed with three O-rings at the top and bottom. This arrangement was checked with a dummy rubber specimen in the triaxial apparatus. The maximum confining cell pressure applied to the dummy was 6 MPa. The drainage valves were closed and therefore any increase in the measured pore pressure value indicates an internal leakage. However, the pore pressure measurement was stable and no trace of silicon oil was observed on the specimen after removing it from the apparatus confirming that the silicon oil did not permeate through the membrane.

A closed-loop PID control algorithm was incorporated in the control system of the high pressure triaxial to maintain a constant axial strain rate of 0.15 %/hr as mentioned in Section 4.3.3.2. However, the strain rate did not reach a constant value until approximately 0.1-0.2 % axial strain. The peak strength of normally consolidated soil in triaxial compression generally occurs at small axial strains (~ 0.2 %). The significance of this slightly delayed control of strain rate was investigated by examining different initial shearing rates ($\dot{\varepsilon}$ = 0.1 – 0.2 %/hr) and the results illustrated that the strength and modulus are essentially not affected. In addition, the results presented below for a test conducted in the high pressure triaxial apparatus compared with a similar one in the low pressure triaxial apparatus (where the strain rate was perfectly controlled) prove that the PID control is satisfactory.

In order to make sure that the high pressure triaxial apparatus is performing adequately and yielding reasonable results, a K_0-consolidated undrained triaxial compression (CK_0UC) test on RBBC at low pressure was conducted to simulate a matching test performed in the low pressure

triaxial apparatus and the results were compared. Figure 4-20 shows the compression curves for the two tests consolidated to maximum vertical effective stress of 0.33 MPa in the triaxial apparatus. Both soil specimens were first resedimented to the same batch stress in the consolidometer (σ'_v = 0.1 MPa) and therefore have the same preconsolidation pressure. The figure shows that the test performed in the high pressure apparatus (TX787) produced a higher sampling effective stress (the value of σ'_v at the beginning of consolidation) and slightly higher strain around the preconsolidation pressure than the test performed in the low pressure apparatus (TX724). This is believed to be due to differences in the specimen setup since a dry setup was employed in the high pressure device (pore lines were saturated using vacuum) while a wet setup was used in the low pressure device (see section 4.5.2 for details on test procedures). Figure 4-21 shows the lateral stress ratio (K_0) versus stress level. The consolidation results in general show comparable behavior of the 2 tests. The normalized shear stress-strain curves are shown in Figure 4-22. The figure indicates that the strength and the axial strain at failure are the same for the two tests. Figure 4-23 shows the normalized stress paths and Figure 4-24 shows the normalized undrained secant modulus versus axial strain. These results show that the shear behavior is almost identical. Therefore, it is concluded that the results from the high pressure triaxial apparatus are reasonable. It must be noted that an additional 2 matching tests were performed in the low and high pressures devices at consolidation stress of 1 MPa and the consolidation and shear properties were also very similar.

Note that the high pressure triaxial apparatus does not have capabilities for axial extension and therefore tests unloaded to OCR > 4 and triaxial extension tests cannot be performed in this device.

4.4.3 Small Diameter TWC Apparatus

After developing the small diameter TWC apparatus, the system was proof tested using a wooden dummy specimen and natural Boston Blue Clay (BBC) specimens from Shelby tubes. Tests employing the wooden dummy were carried out to validate the overall system and confirm the performance of various parts such as the PVC's, tubing connections, valves, and apparatus cell at high confining pressures. The first test experienced a minor internal leak which was believed to be from an O-ring seal. Consequently, more vacuum grease was applied to the platens and additional O-rings were used to seal the external (3 O-rings each end) and internal (2

O-rings each end) membranes which appeared to solve the leak problem. The proof test with the wooden dummy also confirmed the adequate control of the cell pressure, cavity pressure and axial load after modifying the "gain" values in the computer control software. If a small gain value (number of steps per change in pressure) is used, the system software corrects sluggishly. When the gain is too large, the system continually overshoots or undershoots the target resulting in unstable oscillation.

Proof tests with Shelby tube BBC samples were performed primarily to validate the consolidation and borehole closure phases of the TWC test. In addition, these tests were essential to get acquainted with the new apparatus and to establish the correct test procedures. The diameter of the Shelby tube is close to the outer diameter of the small TWC specimen and therefore the soil was simply extruded from the tube, cored to create the cavity, and then assembled in the TWC apparatus. A total of 5 tests were performed on natural BBC specimens. The soil was isotropically consolidated to relatively low pressures (up to 0.3 MPa) since the preconsolidation pressure of the natural material was quite low (0.1 - 0.2 MPa). The undrained borehole closure test was performed by drawing out cavity fluid using the manual control for the cavity PVC while keeping the external cell pressure constant. The pore pressure readings were monitored throughout this procedure. Testing on RBBC specimens was only initiated after confirming the adequate control of the test and establishing a workable testing program.

Cavity deformations are measured in the TWC apparatus by determining the amount of fluid expelled from the cavity using the pressure-volume controller. This measurement is affected by system compliance (e.g., compressibility of cavity fluid, tubing etc.) especially for the tests consolidated to high pressures. This was evaluated by performing a test on aluminum dummy specimen. Figure 4-25 shows the cavity pressure versus volume of fluid expelled from the cavity for 2 cycles of unloading. The maximum cavity pressure is 5.5 MPa which is the highest confining pressure reached in the small diameter TWC tests. The external cell pressure was kept constant at 5.5 MPa during the test. The figure shows that reducing the cavity pressure from 5.5 MPa to 0.6 MPa tends to expel about 2 cm^3 of cavity fluid (which is equivalent to 2.5% cavity volumetric strain based on the initial cavity volume in the small TWC specimen which is approximately 80 cm^3). It must be noted that that the axial compression was minimal during this procedure. This result is significant and therefore all small diameter TWC tests on RBBC were corrected for system compliance as explained in Section 4.5.3.7.

The external cell, internal cavity, and pore pressures are measured using 2,000 psi [14 MPa] capacity pressure transducers in the small diameter TWC apparatus. The confining pressures employed in the TWC tests range from 0.1 MPa to 5.5 MPa. The generated pore pressures during shearing generally do not exceed 1.5 MPa. According to Table 4-3, the resolution of the pressure transducers is about 0.15 kPa while the stability is 1.5 kPa, as measured by the central data acquisition system. In the lowest pressure tests (σ'_v = 0.15 MPa), the resolution of the test data in is not ideal. However, for all the other tests where the vertical effective stress is equal or greater than 1.5 MPa (19 out of 21 tests), the high capacity pressure transducers produce acceptable readings.

4.4.4 Large diameter TWC Apparatus

Like the small diameter TWC apparatus, the large diameter TWC system was proof tested using a plastic dummy specimen and pottery clay. In addition, the pottery clay was used as a trail "soil". Tests using the plastic dummy were performed in the new apparatus to validate the overall system at high pressures and to check for internal and external leaks. Confining pressure up to 6 MPa and axial loads up to 80 kN were checked, which are larger than the pressures and loads reached in the testing program performed in this apparatus. In addition, the gain values were adjusted in the control software to ensure adequate control of the cell pressure, cavity pressure, and axial load in the large apparatus. No leaks were observed in the apparatus and PVC's during this proof test.

Proof tests with pottery clay samples (Sheffield Pottery Inc.) were performed primarily to validate the consolidation and borehole closure phases of the TWC test. It is vital to ensure that the system can apply constant strain rates during consolidation and shearing and is able to control the stresses effectively before testing RBBC samples. The soil was consolidated to relatively low pressures (up to 0.15 MPa) in the apparatus to minimize strains. The undrained borehole closure test was performed by drawing out cavity fluid at a constant rate using the cavity PVC while keeping the external cell pressure and axial stress constant. After confirming that these procedures were performed suitably, tests on RBBC specimens were performed.

System compliance was also investigated in the large diameter TWC apparatus by performing a test on aluminum dummy specimen. Figure 4-26 shows the cavity pressure versus cavity volumetric strain for 2 cycles of unloading. The maximum cavity pressure is 3.5 MPa

which is the highest confining pressure reached in the large diameter TWC tests. The external cell pressure was kept constant at 3.5 MPa during the test. The figure shows that as the cavity pressure reduces from 3.5 ksc to 0.5 MPa, the volume expelled from the cavity was about 2.4 cm^3 (which is equivalent to about 2.3% cavity volumetric strain based on the initial cavity volume in the large TWC specimen which is approximately 115 cm^3). The axial compression measured was small during the test. This result is nontrivial and therefore all the large diameter TWC tests performed on RBBC samples were corrected for system compliance.

The axial load in the large diameter TWC apparatus is applied through a hydraulic load frame and is measured using a 50,000 lb [223 kN] capacity load cell. However, the axial loads measured in the TWC tests do not exceed 50 kN. According to Table 4-4, the resolution of the load cell is about 2.19 N while the stability is 21.9 N, as measured by the central data acquisition system. This stability translates to only 0.001 MPa axial stress on the large diameter specimen. So for all practical purposes, the axial load measurement is considered to be reasonable.

4.5 TESTING PROCEDURES

4.5.1 Introduction

The procedures for the triaxial tests performed in the standard MIT automated stress path triaxial cells are well established and documented (e.g., Sheahan, 1991; MIT subject 1.37: Geotechnical Measurements and Exploration – Assignment 9). The testing procedures for the high pressure triaxial tests are somewhat similar to the standard low pressure device with some minor differences especially in the apparatus setting up. Section 4.5.2 provides a brief description of the testing procedures for the high pressure triaxial tests. Since the TWC tests were performed for the first time at MIT, novel testing procedures were established for this new device. Section 4.5.3 provides a detailed description of the testing procedures for the TWC tests, from specimen preparation to specimen removal after test completion. In addition, a discussion of the corrections used in the reduction process is provided.

4.5.2 High Pressure Triaxial Test

The triaxial specimens prepared for testing in the high pressure triaxial apparatus were first consolidated to σ'_v = 1 MPa in the laboratory. Although the resultant clay is quite stiff, it was

possible to trim the specimen using the miter box and wire saw. Specimen dimensions and mass are determined and samples for water content are taken before mounting the specimen on the base pedestal.

The specimen preparation takes place on a mobile cart where a dry setup was adopted to prevent the specimen from swelling. This requires semi-dry porous stones, dry filter nylons, and no water left on the top cap and bottom pedestal in the triaxial cell. Nylon filters and porous stones are located above and below the specimen and a floating top cap is placed at the top. The end platens and stones are covered with latex membrane protectors before placing the commercial thick membrane using a membrane stretcher. This membrane is fixed with 2 O-rings at the top and bottom and another thin membrane (Trojan condom), already located around the pedestal, is rolled up over the top cap and sealed with O-rings. The top drainage line, which spirals around the specimen, is then attached to the apparatus base and top cap. An alignment device is used to make sure the top cap is perfectly aligned with the soil specimen during the setup process.

The cell steel chamber is put onto the cell base and the whole apparatus is placed in the load frame. The cell is filled with oil and the pressure and displacement transducers are attached. The cell fluid is then slightly pressurized (~ 50 kPa) and the water lines are vacuumed to remove the air then flushed with water.

After applying an initial isotropic stress increment (~ 200 kPa) and measuring the sampling effective stress, the specimen is back pressure saturated to 300 kPa in increments of 50 kPa while keeping this measured effective stress constant and deviatoric load zero. The B-value check is then performed with a cell pressure increment of 25 kPa.

All triaxial tests were K_0-consolidated to the required stress at a strain rate of 0.15 %/hr and left for 24 hrs of secondary compression. This rate is slow enough to prevent significant excess pore pressure in the specimen. The K_0-consolidation algorithm compares the axial and volume strains and adjusts the cell pressure accordingly to ensure zero lateral strain condition. If the specimen is to be unloaded or swelled to an effective vertical consolidation stress (σ'_{vc}) smaller than the maximum vertical stress (σ'_{vm}), stress path unloading to the desired OCR is performed with strain rate of 0.1 %/hr followed by another 24 hrs of aging. Stress path unloading requires

specifying the target vertical and horizontal stresses (i.e., preshear K_0) which can be estimated using the following equation first proposed by Schmidt (1966):

$$K_0 = K_{0NC}(OCR)^n \tag{4.1}$$

where for RBBC the exponent n ≈ 0.426.

Before starting the shearing phase, the drainage valves are closed and a leak check is performed. If no internal leak is detected, undrained shearing is commenced where the specimen is sheared at a constant strain rate of 0.5 %/hr in compression or extension mode. This rate is sufficiently slow to ensure that the pore pressures generated during shearing are fully redistributed across the RBBC specimen (i.e., uniform pore pressures). The test is terminated after reaching 10 - 12% axial strain during shearing if sheared in compression and after reaching 20% strain if sheared in extension.

The consolidation and shear raw data are reduced using a QBASIC program originally written by Sheahan (1991). The engineering values are determined for axial strain, volume strain, pore pressure, and vertical and radial effective stresses. During consolidation, these calculations are based on the initial specimen dimensions and incorporate corrections for the specimen area and the stiffness of the membranes. However, during the shear phase of the triaxial, the calculations are based on the preshear specimen dimensions while the membrane correction is still based on the setup dimensions of the specimen. Note that the parabolic area correction was used during triaxial compression while the cylindrical area correction was used during triaxial extension. This reduction procedure is standard practice for all triaxial tests run at MIT and is reported in detail by Sheahan (1991).

4.5.3 TWC Test

4.5.3.1 Specimen Preparation

As explained in chapter 3, the TWC specimens are consolidated in the resedimentation consolidometer to stresses proportional to those used in the TWC apparatus to reduce consolidation time in the testing device and to minimize the consolidation strains during the test (since a rigid top drainage line is used). The specimen is then unloaded to OCR = 4, where the stress state is approximately hydrostatic and the shear strains due to the removal from the

consolidometer are minimal. A hydraulic jack is used to extrude the small diameter TWC specimens from the plexiglass consolidometer while the large diameter TWC specimens are extruded using a load frame with sizeable clearance to accommodate the consolidometer setup. After extruding the soil specimen from the consolidometer, it is placed in a split mold and locked with hose clamps. Note that the soil specimen has outside diameter equal to the diameter of the consolidometer and therefore does not require trimming. Only the ends of the specimen are trimmed using a tree saw as shown in Figure 4-27. These ends are used to obtain the water content of the soil. The specimen is then cored using a drill press where a succession of four different metal drill bit sizes (12.7, 19.05, 23.8 & 25.3 mm) is used to create the cavity. The difference between the last two diameters is selected to be small in order to minimize disturbance of the final surface of the annular soil specimen. The drills and the scene of drilling are shown in Figure 4-28. This method of creating the cavity was examined by measuring the variation of water content across the specimen wall, visual inspection of the inside wall, and air drying of thin cross sections. Results from all these procedures verified that a smooth and clean inside surface was obtained without substantial smearing along the inner wall of the model bore. Once a hollow cylindrical specimen is prepared, its dimensions and mass are measured.

4.5.3.2 Specimen Setup

Since the RBBC specimens are pre-consolidated to high stresses in the consolidometer and then unloaded to OCR = 4, high suction potential and reaction with water are expected. Therefore, a dry setup method is adopted to prevent the specimen from swelling. This requires semi-dry porous stones, dry filter paper, and no water left on the top cap and bottom pedestal in the TWC cell. The first step in setting up the TWC specimen is to fix one end of the internal membrane on the bottom annular platen using 2 O-rings. The annular platen is then screwed to the base pedestal and the porous stone disc and filter nylon are placed on it. The internal membrane is collapsed using a plastic tube (where the diameter of the tube is smaller than the diameter of the inner bore of the specimen) to enable mounting the soil specimen on the platen without messing up the inner surface as shown in Figure 4-29. Another annular filter nylon and porous stone disc are located on top of the specimen before placing the top annular platen and fixing the other end of the internal membrane with 2 O-rings. The top cap is then screwed to the top annular platen.

Paper filter strips are used in the TWC tests to accelerate drainage. The filter strips are located vertically around the perimeter on the specimen where each strip has several horizontal cuts to minimize resistance during borehole closure. Ten filter strips (1.3 cm wide each) are placed around the small diameter TWC specimen while 12 filter strips (2.0 cm wide each) are located around the large diameter TWC specimen. Vacuum grease is applied to the end caps and protective rubber membranes are located around the caps and stones (filter strips are placed under the protective membranes). The external membrane (only one) is then placed using a membrane stretcher and is fixed with 3 O-rings at the top and bottom. Finally, the internal cavity is filled with oil and the vent screw in the top cap is tightened before attaching the top drainage line to the top cap and apparatus base.

The cell chamber is put onto the cell base and the whole apparatus is placed in the load frame. After connecting the PVC lines and the pressure transducers to the apparatus base, the cell is filled with oil and the zero values of all transducers are obtained. The cell fluid is slightly pressurized (confining pressure not exceeding the expected sampling effective stress, σ'_s, where $\sigma'_s \approx 0.2 - 0.25\ \sigma'_p$ – see below) and the water lines are saturated by applying vacuum to remove the air then flushed with distilled water.

4.5.3.3 Initial Pressure-Up and Saturation

With the drainage valves closed, an initial isotropic stress increment is applied in order to obtain a positive pore pressure in the soil specimen. The specimen is allowed to equilibrate overnight before measuring the sampling effective stress. For the RBBC specimens, $\sigma'_s \approx 0.2 - 0.25\ \sigma'_p$ imposed in the consolidometer which indicates good quality specimens (i.e., minimal sampling disturbance).

All tests are back pressure saturated to 400 kPa by increasing the cell, cavity, and back pressures in increments of 50 kPa (each increment is left for 30 minutes) while maintaining the measured σ'_s constant and the deviatoric load zero. This process is essential to make sure that the specimen and pore lines are fully saturated. Readings of the axial and volumetric strains are recorded for quality control purposes. In general, all the tests were saturated with minimal changes in strain readings (again confirming the high quality of the test specimens).

After reaching the required back pressure, the specimen is allowed to equilibrate for few hours before performing the B-value ($\Delta u/\Delta\sigma_3$) check. This is done by increasing the cell and

cavity pressures by 30 kPa and measuring the undrained pore pressure response inside the specimen.

4.5.3.4 Consolidation

The first few tests in the small diameter TWC apparatus were isotropically consolidated before deciding to stress path consolidate the specimens instead. The stress path consolidation option in the computer control program allows the user to consolidate the soil along any stress path. In the TWC tests, the soil specimens are consolidated to a pre-defined target value, K_{0NC} = 0.55, based on information from the triaxial test program. The internal cavity and external cell are connected during this procedure (i.e., same pressure).

The soil is stress path consolidated at a strain rate of 0.3 %/hr in two stages. The first stage starts from the hydrostatic condition and approaches a target value, K = 0.55 at $\sigma'_v = 0.8\ \sigma'_p$. This ensures that the specimen does not yield during this first stage of reconsolidation. The second stage involves stress path consolidation at K = 0.55 to the specified stress level ($\sigma'_{vm} = 1.5\ \sigma'_p$). The specimen is left for 24 - 48 hrs with the stresses held constant to allow the specimen volume strain to stabilize prior to unloading or proceeding to borehole closure.

If the specimen is to be unloaded or swelled to an effective vertical consolidation stress (σ'_{vc}) less than the maximum vertical stress (σ'_{vm}), stress path unloading to the desired OCR is performed with strain rate of 0.2 %/hr followed by another 24 hrs of aging. Equation 4.1 is used to determine the preshear K_0 value needed to perform this procedure.

4.5.3.5 Borehole Closure

Mechanisms of instability are introduced by reducing the internal cavity pressure within the model bore while keeping the external cell pressure and axial stress constant[4]. Cavity pressure reduction is performed by drawing out cavity fluid using the pressure-volume controller at a constant cavity volumetric strain rate. The tests are terminated at 20% cavity volumetric strain.

The borehole closure procedure is either performed in fully drained or "undrained" conditions. The "undrained" tests (i.e., no external drainage of pore fluid) are performed over

[4] One test was performed by increasing the external cell pressure while keeping the internal cavity pressure and axial stress constant. In addition, two tests were performed by increasing the internal cavity pressure (pressuremeter mode) while keeping the external cell pressure and axial stress constant.

relatively short time periods while reading the pore pressures inside the specimen. Most of the undrained TWC tests were sheared at an average cavity volumetric strain rate of 10 %/hr[5]. As mentioned in Section 4.3.3.2, the user must physically switch the pore PVC motor plug with the cavity PVC motor plug in the control box and the connectors of the pore pressure and specimen transducers with the connectors of the cavity pressure and volume transducers in the main transducer box that is connected to the PC. The program also prompts the user to enter the calibration factors and zero values for the cavity pressure and volume transducers. Finally, the user needs to input the cavity volume strain rate and the final strain level before starting the program. The borehole closure algorithm applies a constant cavity volume strain rate while keeping the external cell pressure and axial stress constant. Note that keeping the axial stress constant requires the axial load to be reduced in order to compensate for the reduction in the internal cavity pressure acting on the underside of the top cap. Once the required strain level is reached, the computer holds the internal cavity, external cell, and axial stresses constant. The computer displays on the monitor the values of the axial stress, cell pressure, cavity pressure, axial strain, and cavity volumetric strain. Readings from the pore pressure and cell volume transducers are not fed into the PC but are monitored on the central data acquisition system.

Drained tests require unloading the cavity pressure at sufficiently slow rate in order to ensure no development of excess pore pressure in the specimen. These tests are performed at cavity volumetric strain rate of 0.2 %/hr. Since the drained borehole closure procedure involves control of four parameters (internal cavity pressure, external cell pressure, axial stress, and back pressure) whereas the current control system can only control three, a second computer and controller are used to control the test. Like the undrained tests, the transducer readings of the cell pressure, cavity pressure, axial stress, axial strain, and cavity volumetric strain are sent to the main computer. The second computer controls the back pressure while reading the specimen volumetric strain and the cell volumetric strain.

4.5.3.6 Specimen Removal

At the completion of each test, the cell and cavity pressures are released, the transducers are removed, the PVC lines are disconnected and the cell chamber is drained using air pressure.

[5] Two tests were sheared at rates of 0.5 and 60 %/hr to investigate the effect of strain rate.

The apparatus is then placed on the mobile cart and the cell chamber is removed. The top drainage line and the cavity vent screw are disconnected and the cavity oil is drained by applying vacuum. The excess cell oil on the specimen and apparatus base is cleaned using paper towels. The top cap is detached and the external membrane and filter paper strips are carefully removed from the specimen. The top annular platen is then removed after releasing the 2 O-rings for the internal membrane. When the specimen has been removed from the cell, the specimen outer diameter is measured at the top, middle, and bottom using a caliper. The specimen is then cut into four pieces and the internal diameter is measured at both ends of each piece. Figure 4-30 shows the sliced TWC specimen after the test. Cracks in the inside wall are also mapped if present. The soil pieces are left to dry on the laboratory bench before archiving.

4.5.3.7 Corrections

The consolidation and BH closure raw data for the TWC tests are reduced using Microsoft Office Excel. The engineering values are determined for axial strain, specimen volume strain, cavity volume strain, pore pressure, vertical stress, and radial stresses acting on the inner and outer walls of the specimen. The following corrections are made during data reduction for the TWC tests.

a) Sensors

Measurement instrumentation used in this study was all electronic with excellent hysteresis, non-linearity and repeatability characteristics. Pressure and force transducers are extremely rigid so that compressibility in the instrumentation is not an issue. Linear calibration factors were used in all cases and found to be consistent over long periods of time. Transducers zero values were recorded before every test and used for data reduction.

b) System Compliance

Cavity deformations are measured in the TWC apparatus by determining the amount of fluid expelled from the cavity using the cavity PVC. As explained in Section 4.4, system compliance affects this measurement especially for the tests consolidated to high pressures. Tests performed in the small and large diameter TWC devices on aluminum dummy specimens are shown in Figure 4-25 and Figure 4-26 respectively. The calibration curves obtained from these tests are used to correct for the cavity volume strain in the TWC tests for RBBC specimens.

c) Membrane Resistance

The internal membrane in the TWC tests resists specimen deformation during borehole closure. The following expression is used to correct the radial stress acting on the internal wall of the specimen due to membrane resistance. This expression is adapted from the one used in the triaxial tests (Germaine & Ladd, 1988).

$$\Delta\sigma_r = \frac{4tE}{D_i}\left(\frac{\varepsilon_{cav}}{3}\right) \tag{4.2}$$

where t = initial membrane thickness

E = Young's modulus of rubber (1.5 MPa)

D_i = initial bore diameter

ε_{cav} = cavity volumetric strain

For example, the value of $\Delta\sigma_r$ at the end of the borehole closure procedure in the TWC test (i.e., when ε_{cav} = 20%) is about 10 kPa. Although this correction might be significant for the low pressure tests, the effect is relatively small on the intermediate and high pressure tests. Note that no correction is made to the axial force and external radial stress due to the membrane resistance since the values are very small.

d) Piston Friction and Area Correction

Since the TWC tests employ external load cells, a correction must be made for the axial loading piston friction and area. The small and large diameter TWC devices use a double O-ring seal for the axial piston which generates high friction forces. The friction correction is estimated by measuring the force required to push the piston into the cell. This was performed for all the TWC tests before starting the consolidation procedure to ensure contact between the piston and the top cap. The friction force is something like 150 N in the small diameter TWC device while in the large TWC device is about 300 N.

The effective piston area is obtained from tests where the cell pressure is varied and the uplift force is measured using the load cell; effective piston area is simply the uplift force divided by the cell pressure. The measured effective piston area is equal to 5.5 cm^2 and 20.5 cm^2 in the small and large diameter TWC devices respectively.

e) Axial Strain

The axial force is kept constant during the borehole closure procedure and as a result some axial deformations occur. The changes in the axial strain must be taken into account in the cavity strain calculation. The volume expelled due to change in specimen height is equal to the axial deformation times the area of the cavity. This value is subtracted from the cavity total volume change measured using the cavity PVC. In other words, the corrected cavity volumetric strain ($\varepsilon_{cav(corrected)}$) is equal to the measured volume strain (ε_{cav}) minus the axial strain (ε_a) assuming cylindrical deformation. For example, the axial strain measured during shearing is about 1 % which translates to 1 % cavity volumetric strain at the end of the test. The cavity radial strain at the specimen mid-height can be computed from the corrected cavity volumetric strain. Assuming uniform (cylindrical) deformation, the radial strain is basically the cavity volumetric strain (after correction) divided by 2. A radial strain based on a parabolic deformation tends to give higher values than the uniform assumption at a given cavity pressure.

Note that the cavity volumetric strain calculation is based on the preshear cavity volume, (i.e., the volume of the cavity after taking into account the axial strain during consolidation assuming cylindrical deformation).

Measurement	Device	Calibration Factor	Range	Resolution	Stability
Axial Strain	External LVDT	2.481 cm/v/v	2.5 cm	±0.0006% (0.1 mV)	±0.006% (1 mV)
Specimen Volume	Volume Strain LVDT	23.848 cm^3/v/v	45 cm^3	±0.0005% (0.1 mV)	±0.005% (1 mV)
Cell Pressure	Pressure Transducer	68.5 MPa/v/v	1.4 MPa	0.01 kPa (0.001 mV)	0.1 kPa (0.01 mV)
Pore Pressure	Pressure Transducer	68.8 MPa/v/v	1.4 MPa	0.01 kPa (0.001 mV)	0.1 kPa (0.01 mV)
Axial Load	Internal Load Cell	65.867 kN/v/v	2.2 kN	0.01 N (0.001 mV)	0.1 N (0.01 mV)

Table 4-1: Characteristics of instrumentation used in low pressure triaxial apparatus.

Note: Resolution and stability based on central data acquisition system, calculations based on specimen dimensions.

Measurement	Device	Calibration Factor	Range	Resolution	Stability
Axial Strain	External LVDT	3.295 cm/v/v	2.5 cm	±0.0007% (0.1 mV)	±0.007% (1 mV)
Specimen Volume	Volume Strain LVDT	22.078 cm^3/v/v	45 cm^3	±0.0005% (0.1 mV)	±0.005% (1 mV)
Cell Pressure	Pressure Transducer	345.56 MPa/v/v	7 MPa	0.06 kPa (0.001 mV)	0.6 kPa (0.01 mV)
Pore Pressure	Pressure Transducer	347.23 MPa/v/v	7 MPa	0.06 kPa (0.001 mV)	0.6 kPa (0.01 mV)
Axial Load	Internal Load Cell	291.891 kN/v/v	8.9 kN	0.05 N (0.001 mV)	0.5 N (0.01 mV)

Table 4-2: Characteristics of instrumentation used in high pressure triaxial apparatus.

Note: Resolution and stability based on central data acquisition system, calculations based on specimen dimensions.

Measurement	Device	Calibration Factor	Range	Resolution	Stability
Axial Strain	External LVDT	2.0685 cm/v/v	2.5 cm	±0.0003% (0.1 mV)	±0.003% (1 mV)
Specimen Volume	Volume Strain LVDT	39.276 cm^3/v/v	45 cm^3	±0.0001% (0.1 mV)	±0.001% (1 mV)
Cell Volume	Volume Strain LVDT	39.451 cm^3/v/v	45 cm^3	±0.0001% (0.1 mV)	±0.001% (1 mV)
Cavity Volume	Volume Strain LVDT	17.079 cm^3/v/v	45 cm^3	±0.0004% (0.1 mV)	±0.004% (1 mV)
Cell Pressure	Pressure Transducer	691.57 MPa/v/v	14 MPa	0.13 kPa (0.001 mV)	1.3 kPa (0.01 mV)
Pore Pressure	Pressure Transducer	804.42 MPa/v/v	14 MPa	0.15 kPa (0.001 mV)	1.5 kPa (0.01 mV)
Cavity Pressure	Pressure Transducer	-694.0 MPa/v/v	14 MPa	0.13 kPa (0.001 mV)	1.3 kPa (0.01 mV)
Axial Load	External Load Cell	301.777 kN/v/v	8.9 kN	0.06 N (0.001 mV)	0.6 N (0.01 mV)
Axial Load	External Load Cell	1408.995 kN/v/v	44.5 kN	0.26 N (0.001 mV)	2.6 N (0.01 mV)

Table 4-3: Characteristics of instrumentation used in small diameter TWC apparatus.

Note: Resolution and stability based on central data acquisition system, calculations based on specimen and apparatus dimensions.

Measurement	Device	Calibration Factor	Range	Resolution	Stability
Axial Strain	External LVDT	2.499 cm/v/v	2.5 cm	±0.0002% (0.1 mV)	±0.002% (1 mV)
Specimen Volume	Volume Strain LVDT	684.554 cm^3/v/v	615 cm^3	±0.0003% (0.1 mV)	±0.003% (1 mV)
Cell Volume	Volume Strain LVDT	684.206 cm^3/v/v	615 cm^3	±0.0003% (0.1 mV)	±0.003% (1 mV)
Cavity Volume	Volume Strain LVDT	384.888 cm^3/v/v	170 cm^3	±0.006% (0.1 mV)	±0.06% (1 mV)
Cell Pressure	Pressure Transducer	-345.89 MPa/v/v	7 MPa	0.06 kPa (0.001 mV)	0.6 kPa (0.01 mV)
Pore Pressure	Pressure Transducer	-348.85 MPa/v/v	7 MPa	0.06 kPa (0.001 mV)	0.6 kPa (0.01 mV)
Cavity Pressure	Pressure Transducer	-346.17 MPa/v/v	7 MPa	0.06 kPa (0.001 mV)	0.6 kPa (0.01 mV)
Axial Load	External Load Cell	11820.73 kg/v/v	223 kN	2.19 N (0.001 mV)	21.90 N (0.01 mV)

Table 4-4: Characteristics of instrumentation used in large diameter TWC apparatus.

Note: Resolution and stability based on central data acquisition system, calculations based on specimen and apparatus dimensions.

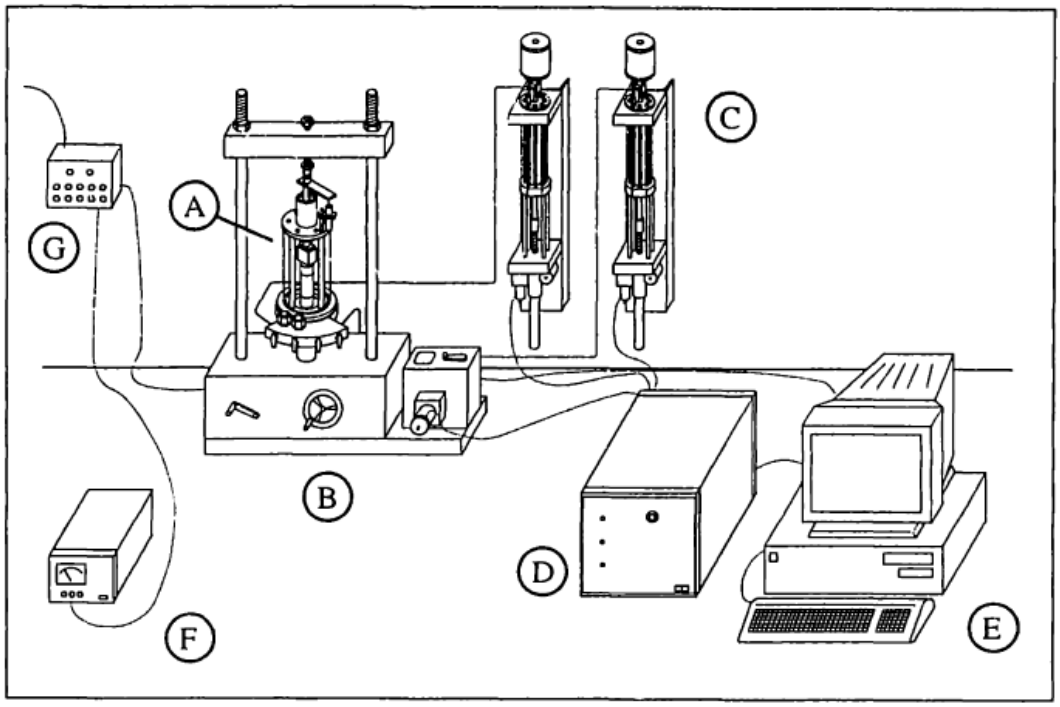

A - Triaxial Cell
B - Load Frame
C - Pressure/Volume Controllers
D - Motor Control Box
E - Personal Computer
F - DC Power Supply
G - Data Acquisition Channels

Figure 4-1: Schematic of MIT automated stress path triaxial cell (from Santagata, 1998)

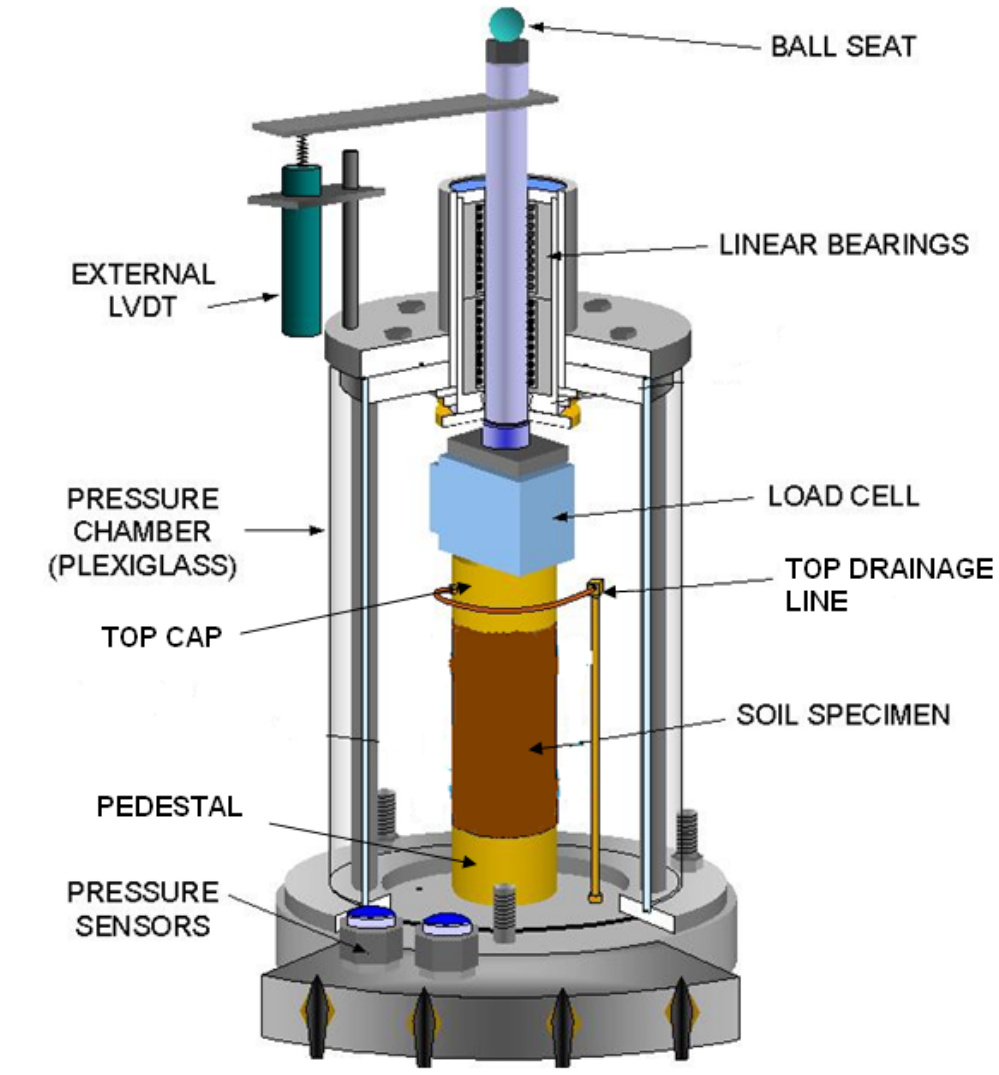

Figure 4-2: Schematic of low pressure triaxial chamber (from Santagata, 1998)

Figure 4-3: Photograph of the low pressure triaxial apparatus

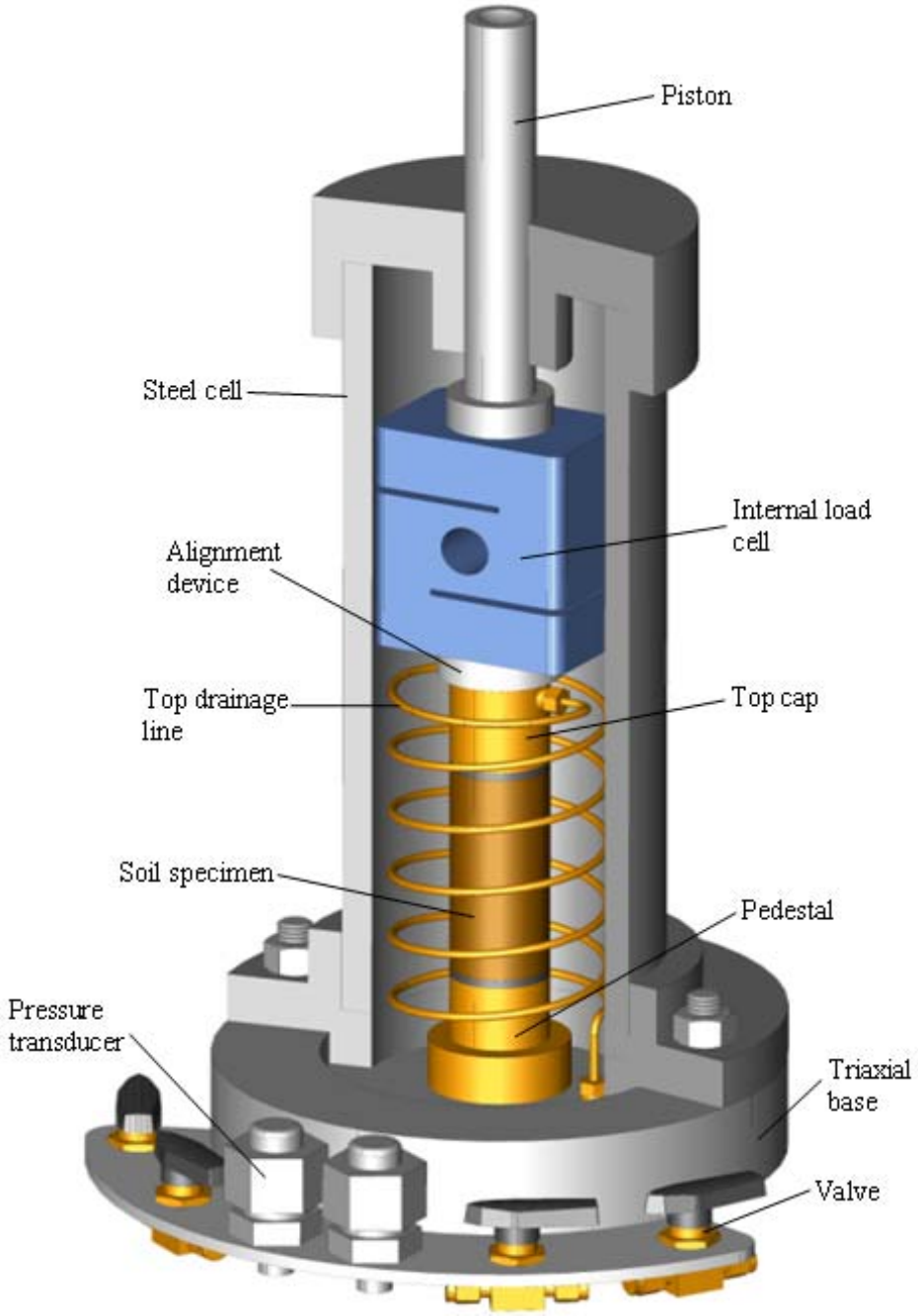

Figure 4-4: Schematic of high pressure triaxial chamber

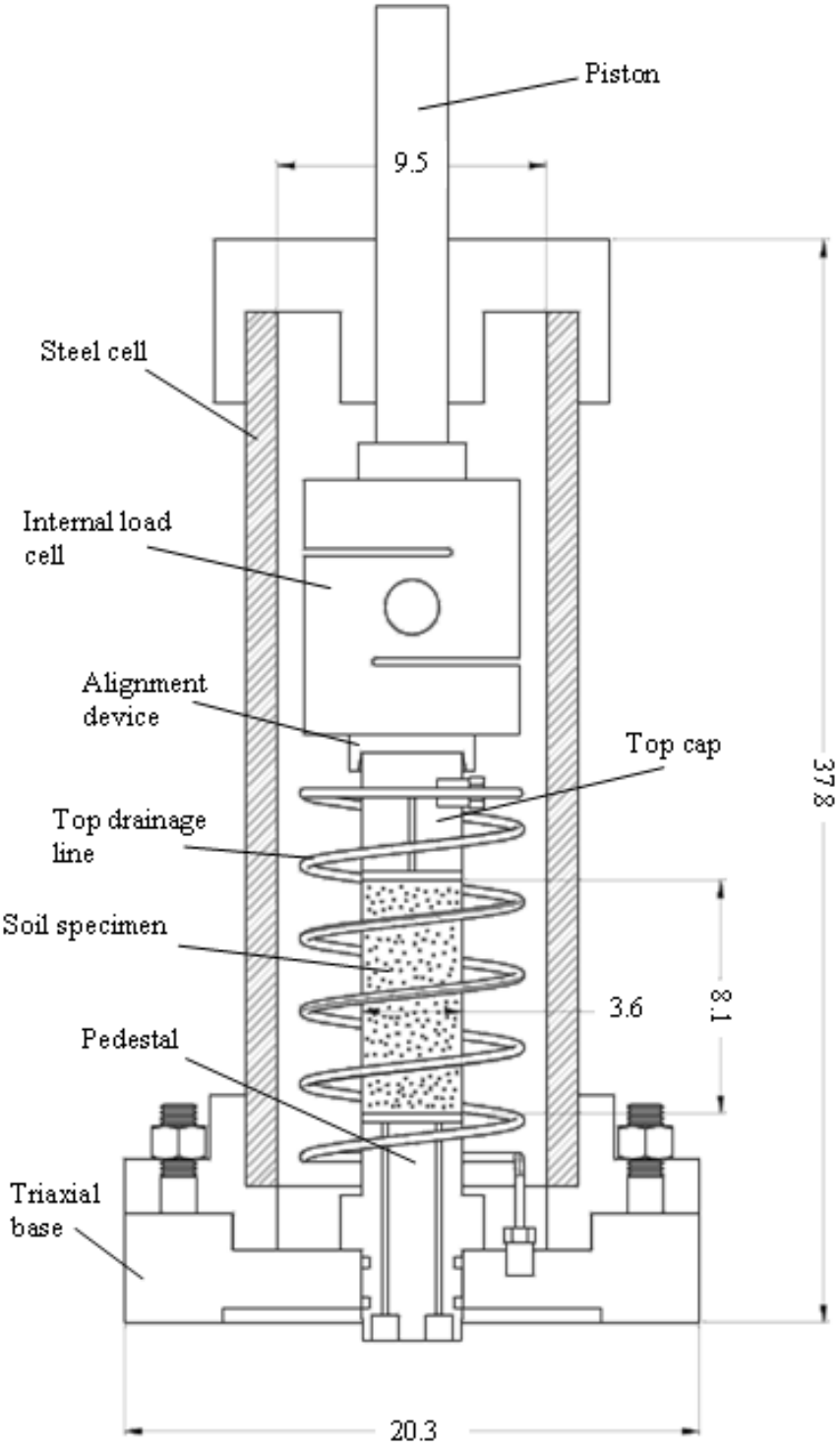

Figure 4-5: Section view of high pressure triaxial apparatus (dimensions in cm)

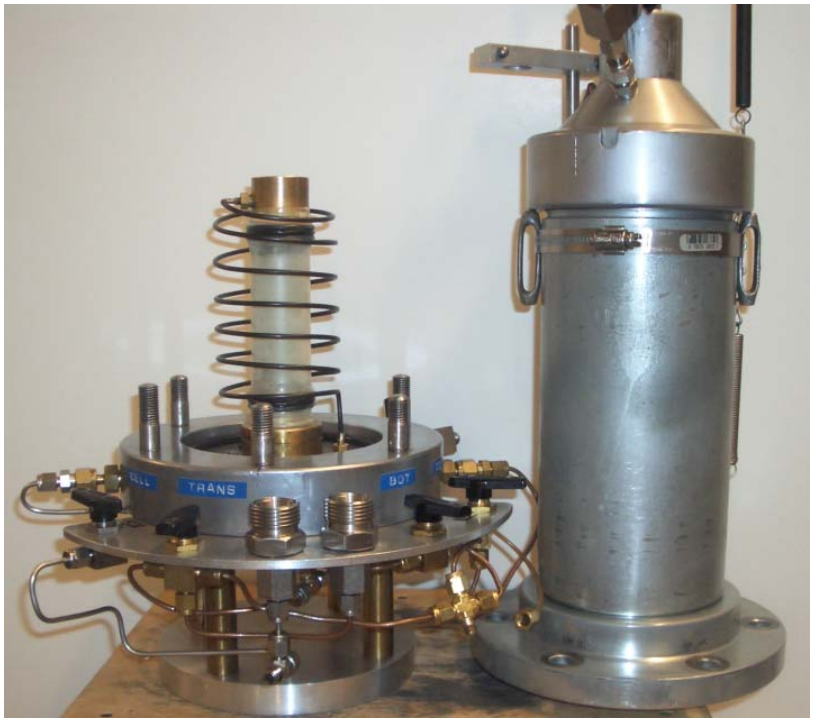

Figure 4-6: Photograph of the high pressure triaxial base and steel chamber

Figure 4-7: Photograph of the high pressure triaxial system inside the environmental enclosure

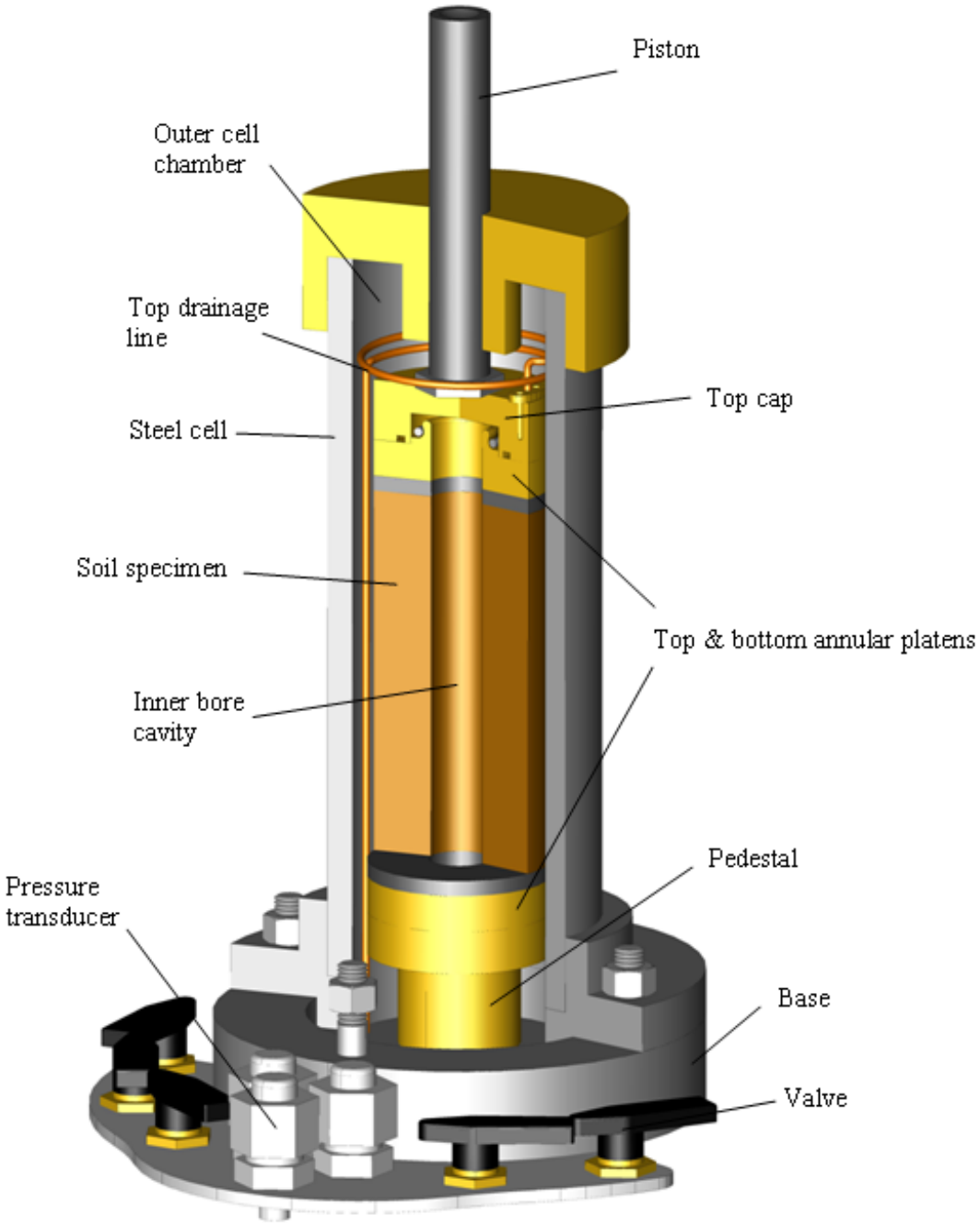

Figure 4-8: Schematic of small diameter TWC chamber

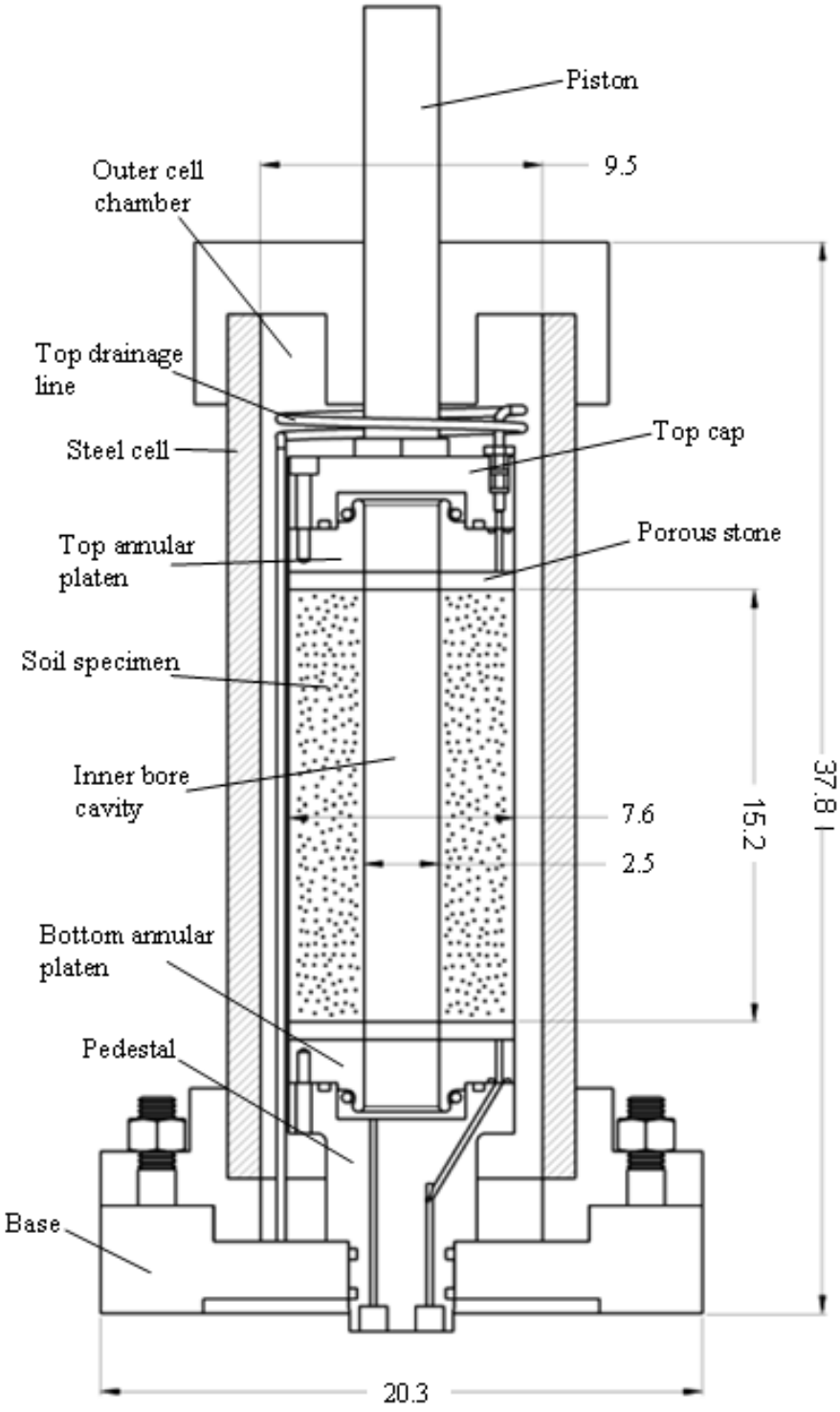

Figure 4-9: Section view of small diameter TWC apparatus (dimensions in cm)

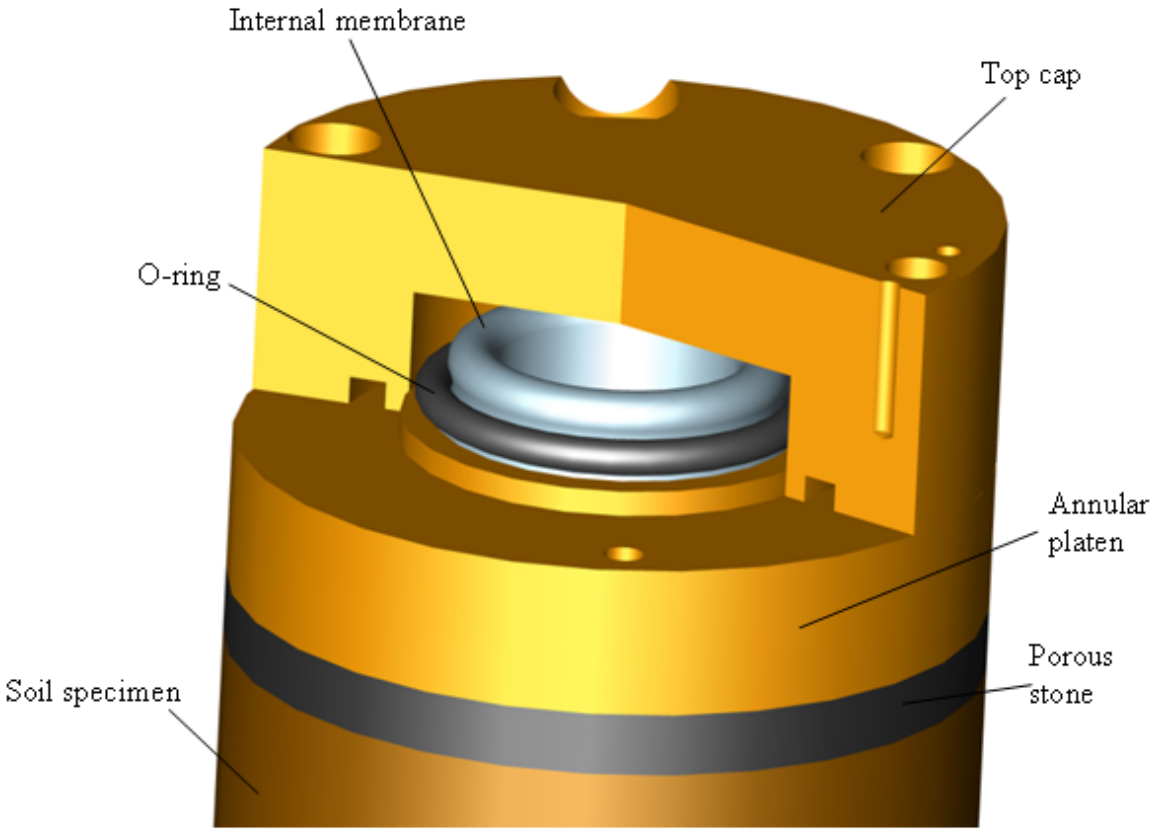

Figure 4-10: Schematic showing internal membrane seal

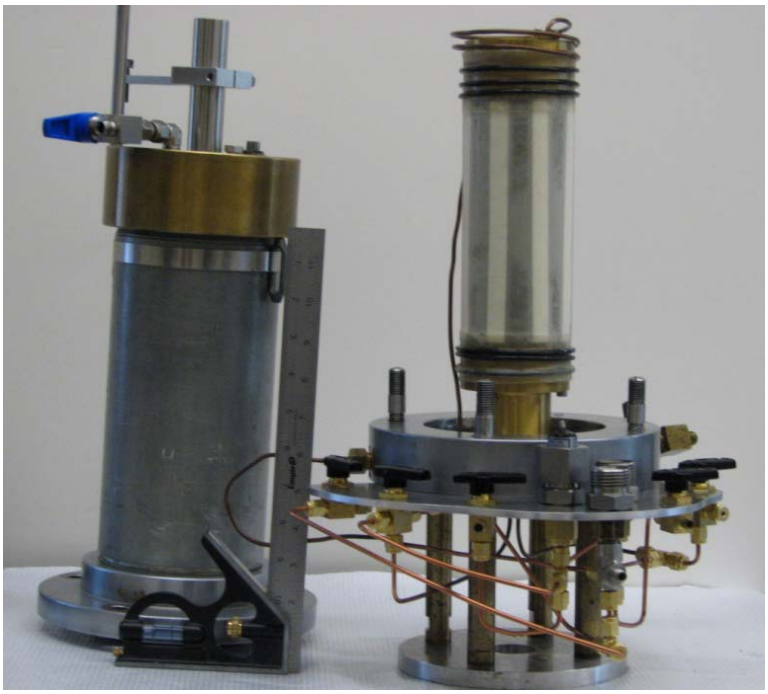

Figure 4-11: Photograph of the small diameter TWC base and steel chamber

Figure 4-12: Photograph of the small diameter TWC system inside the environmental enclosure

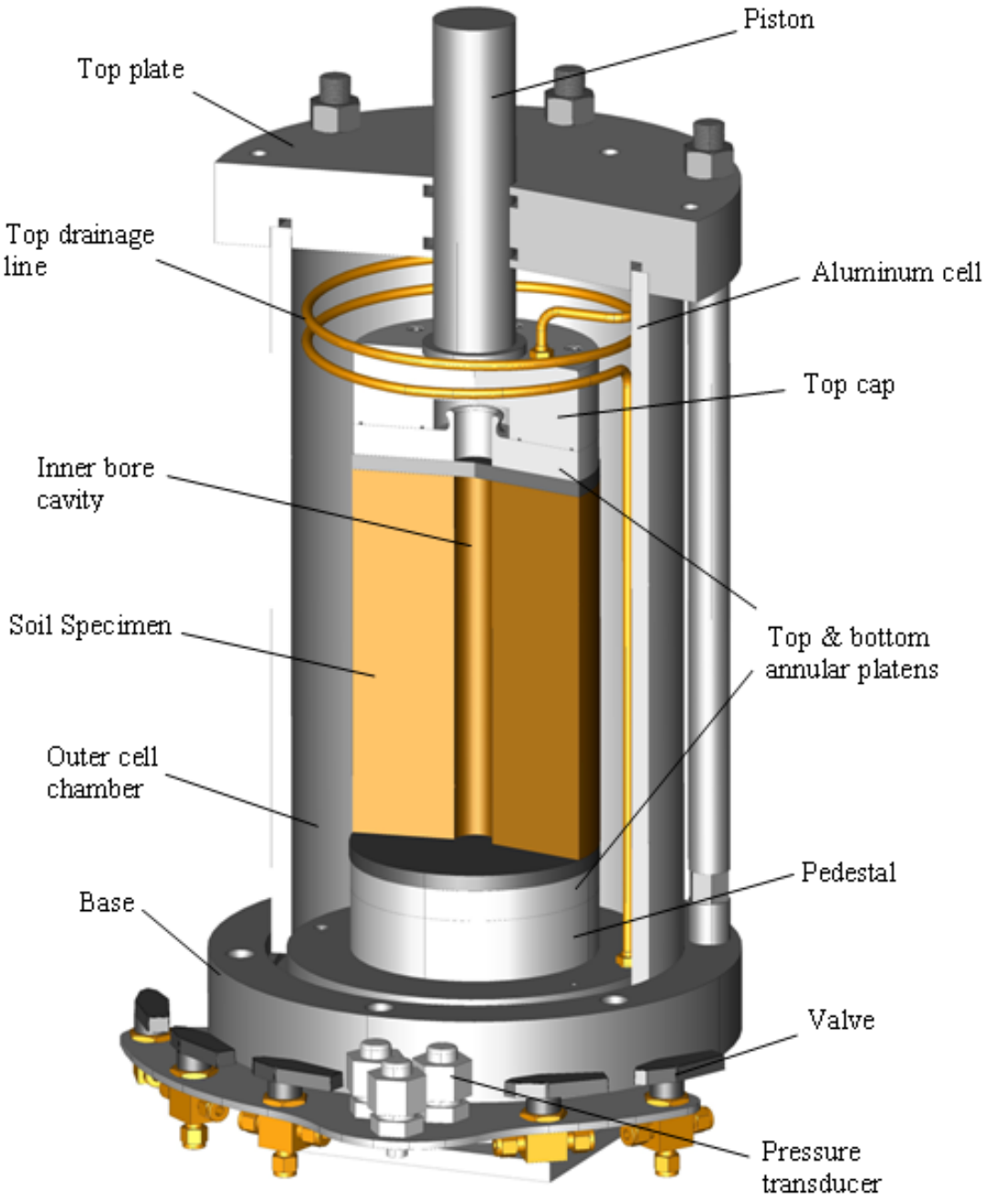

Figure 4-13: Schematic of large diameter TWC chamber

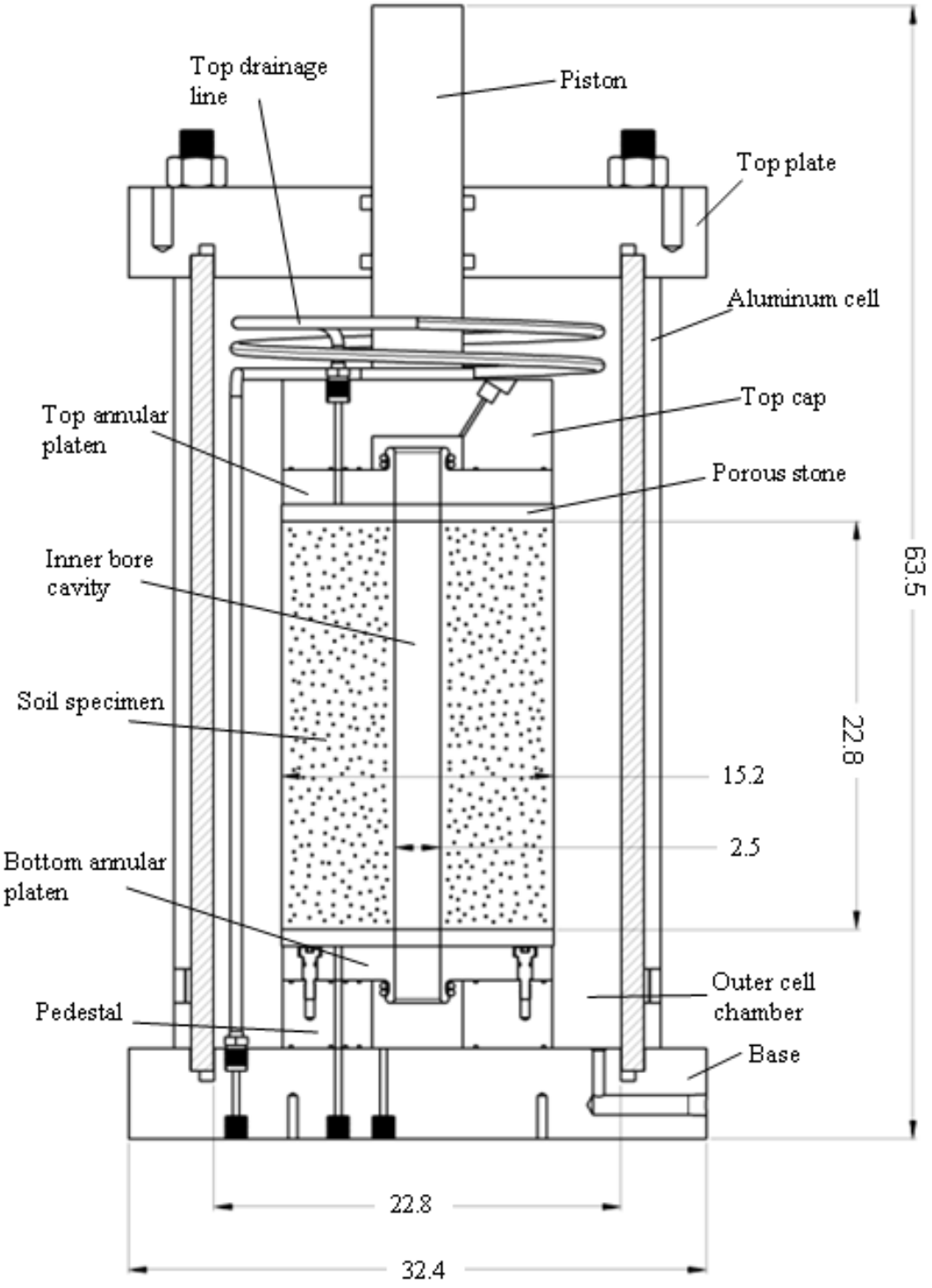

Figure 4-14: Section view of large diameter TWC apparatus (dimensions in cm)

Figure 4-15: Photograph of the large diameter TWC apparatus

Figure 4-16: Photograph of the large diameter TWC system

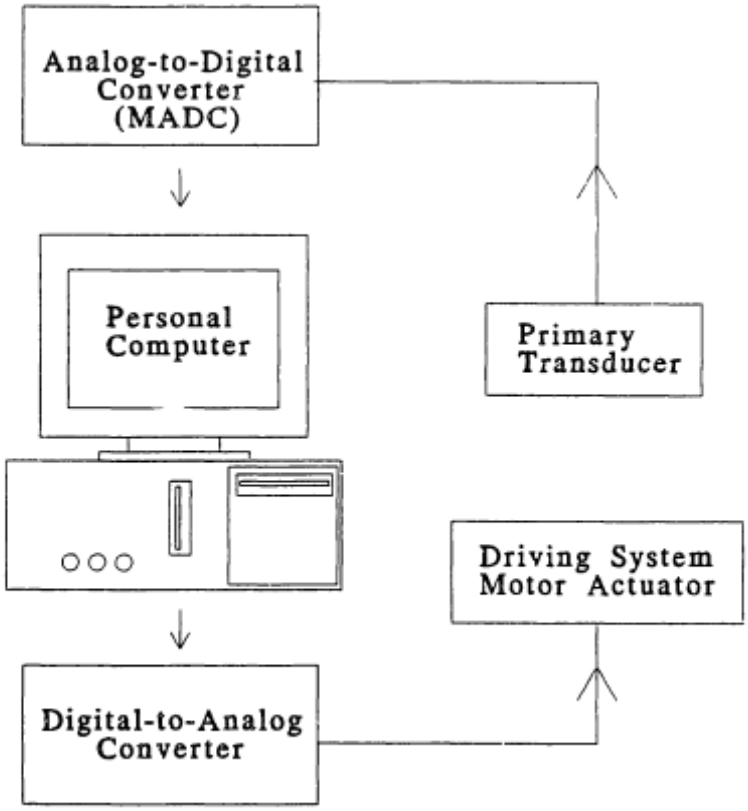

Figure 4-17: Schematic drawing of the control system hardware components

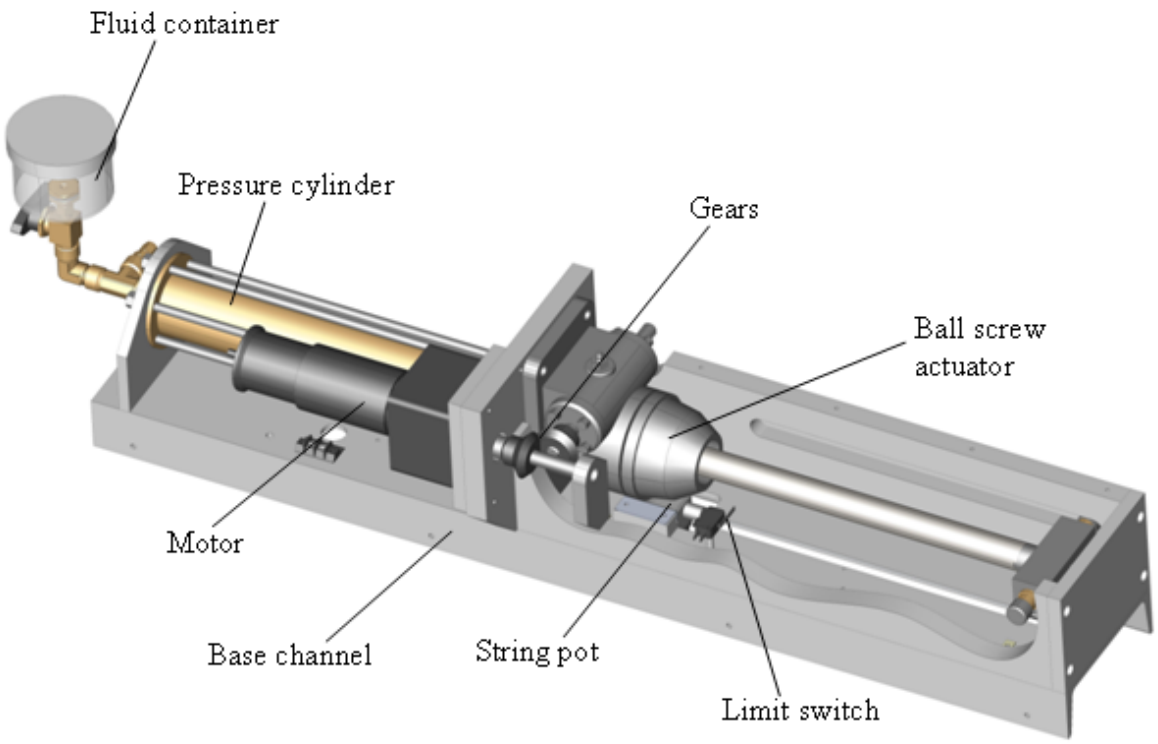

Figure 4-18: Schematic of high capacity Pressure-Volume Controller (PVC) for large diameter TWC apparatus

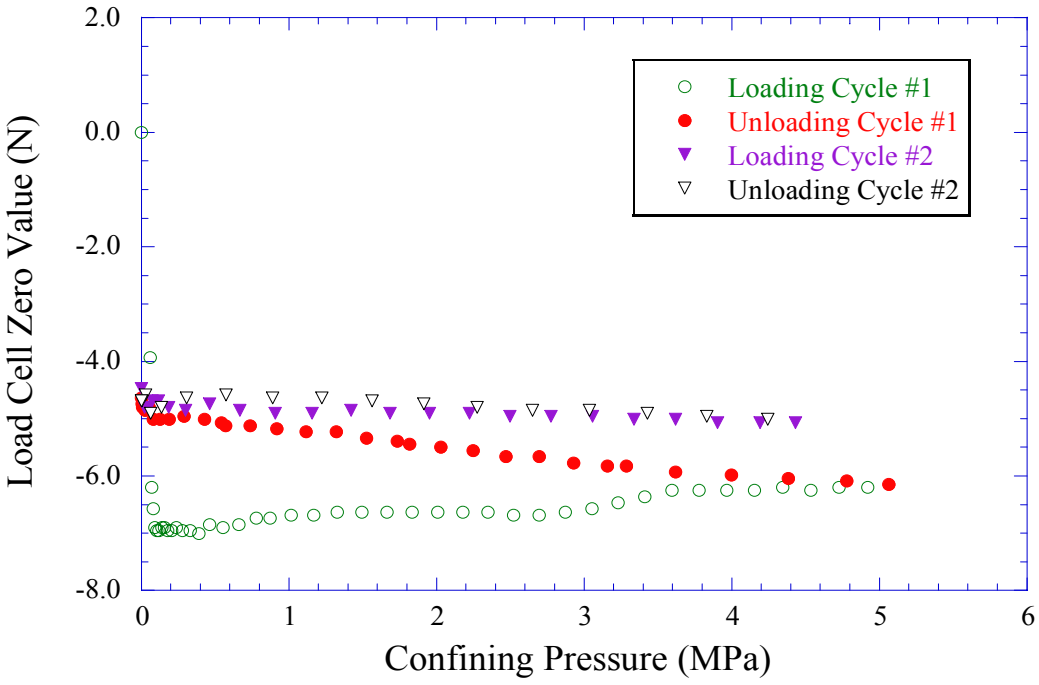

Figure 4-19: Influence of the confining pressure on the zero value of the internal load cell

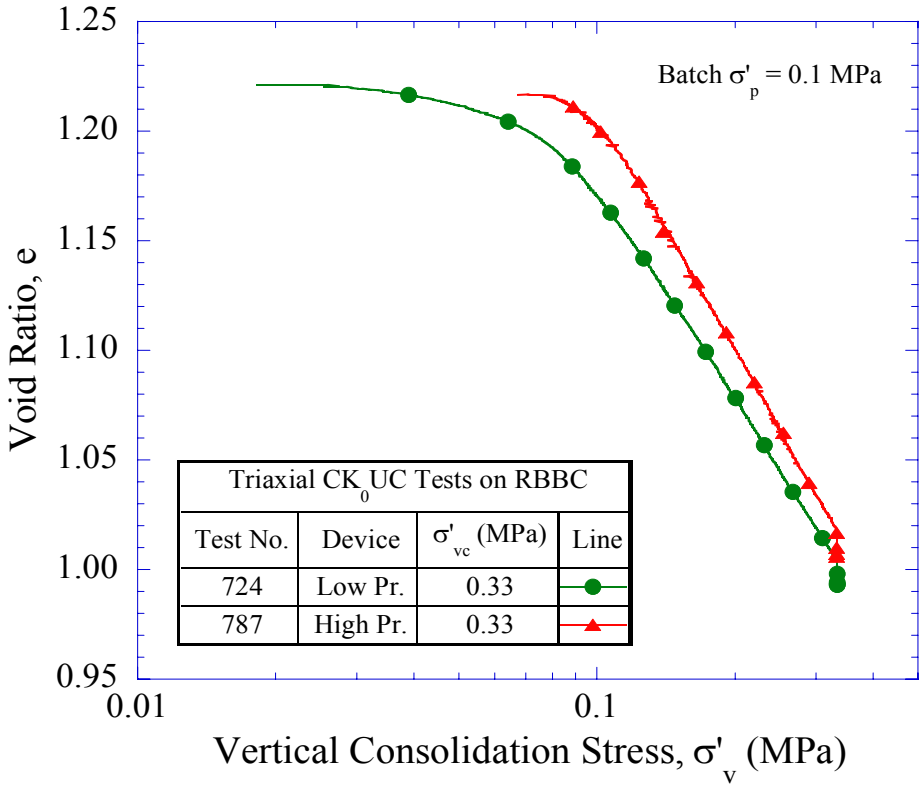

Figure 4-20: Comparison of compression curves measured in the low pressure and high pressure triaxial devices on RBBC

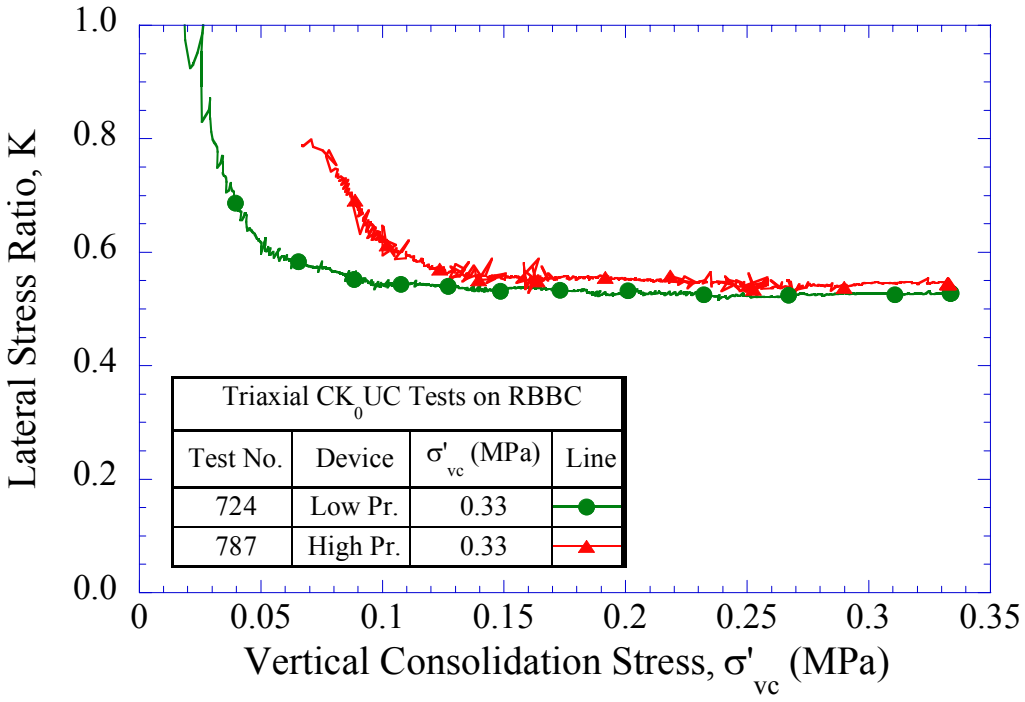

Figure 4-21: Comparison of lateral stress ratio measured in the low pressure and high pressure triaxial devices on RBBC

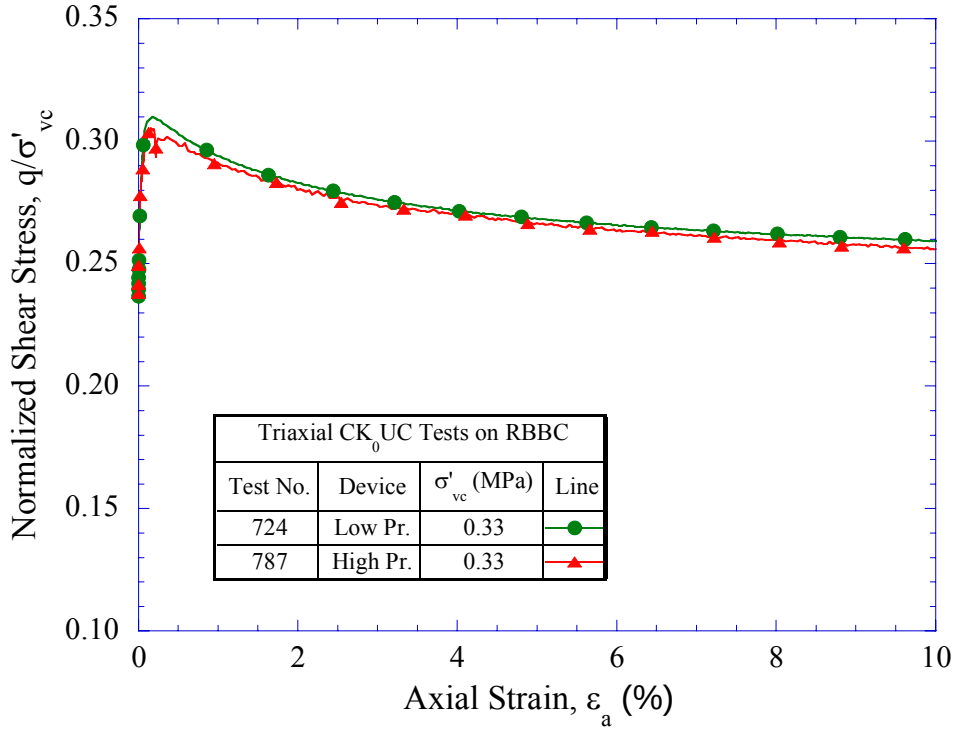

Figure 4-22: Comparison of shear stress-strain measured in the low pressure and high pressure triaxial devices on RBBC

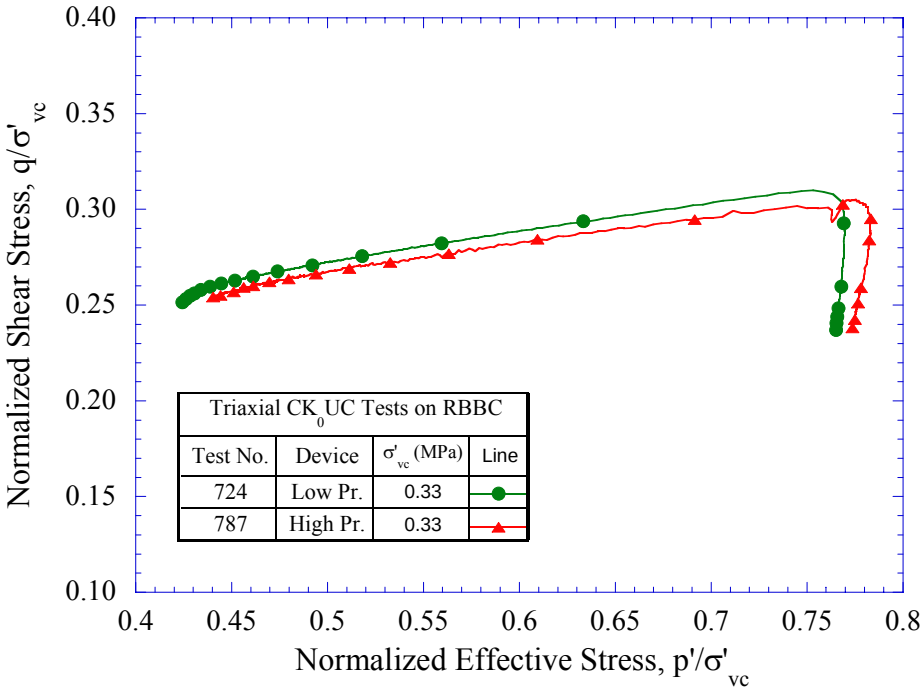

Figure 4-23: Comparison of effective stress paths measured in the low pressure and high pressure triaxial devices on RBBC

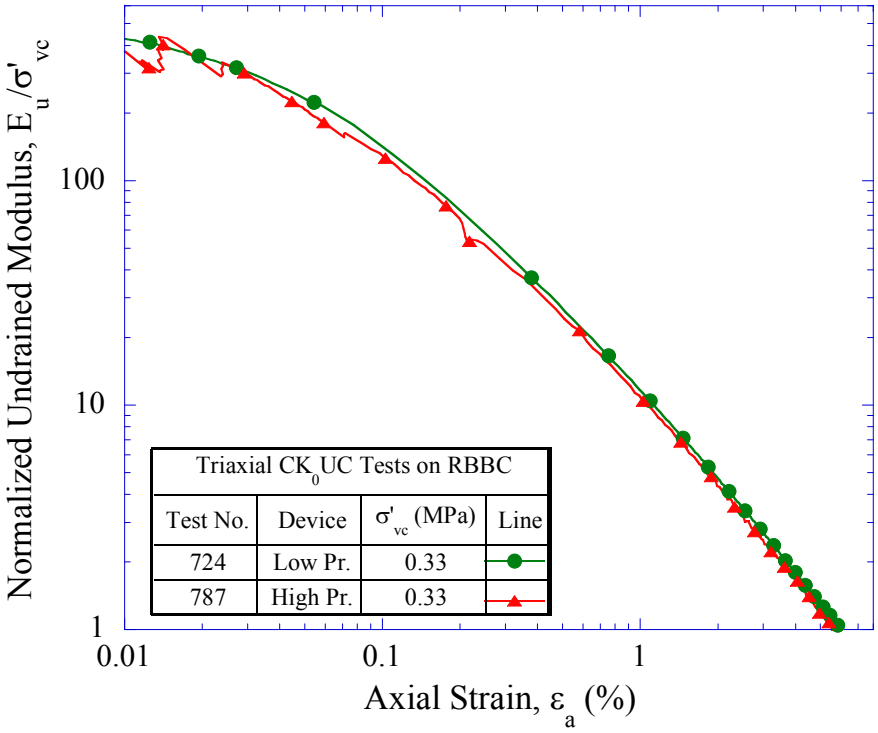

Figure 4-24: Comparison of undrained modulus measured in the low pressure and high pressure triaxial devices on RBBC

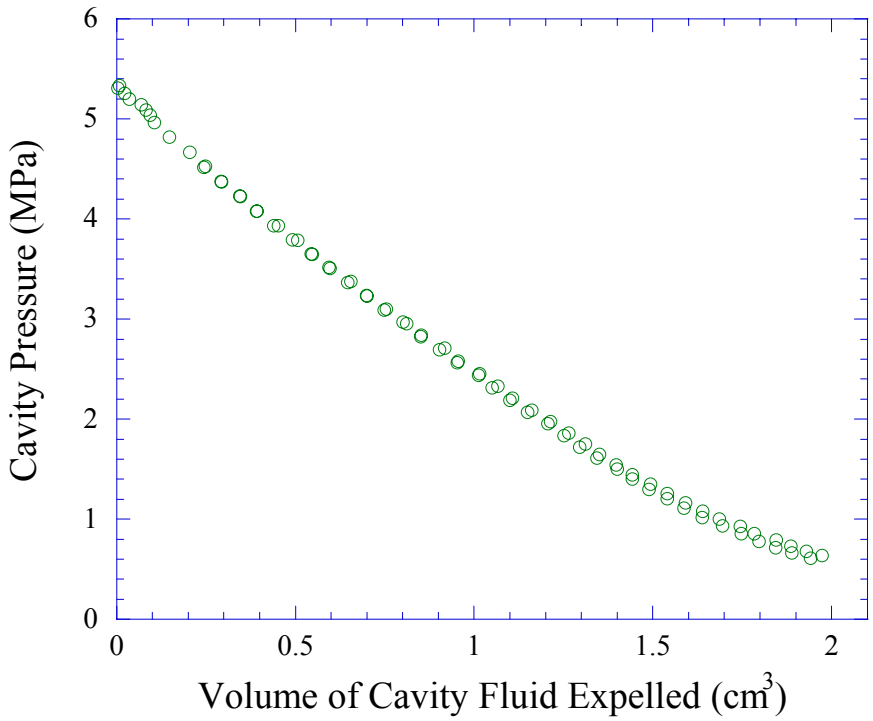

Figure 4-25: Influence of system compliance on the cavity pressure-strain measured in the small diameter TWC apparatus

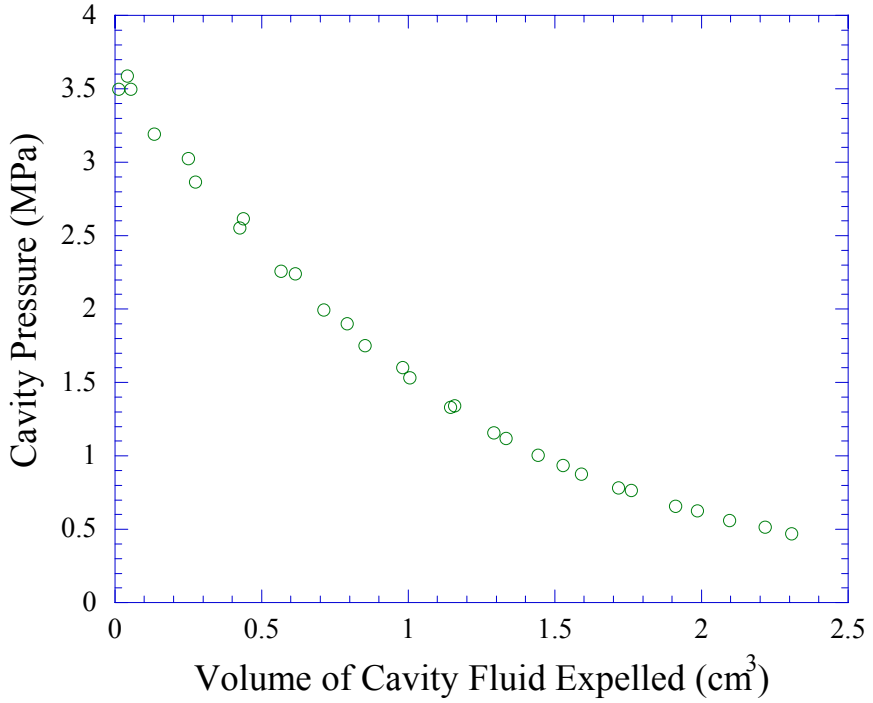

Figure 4-26: Influence of system compliance on the cavity pressure-strain measured in the large diameter TWC apparatus

Figure 4-27: Cutting the ends of the small diameter TWC specimen using a tree saw

Figure 4-28: Coring of cavity for small diameter TWC specimen using drill press

Figure 4-29: Collapsing of internal membrane using plastic tube in the small diameter TWC apparatus

Figure 4-30: Sliced small diameter TWC specimen after test

5 ELEMENTAL MECHANICAL BEHAVIOR

5.1 INTRODUCTION

The purpose of the elemental testing program is to obtain a better understanding of the mechanical behavior of Resedimented Boston Blue Clay (RBBC) at elevated consolidation pressures (simulating shallow reservoir wellbore stresses) and to investigate the effect of stress level on the 1-D consolidation and normalized[6] undrained shear properties of the material. This chapter presents the results from a series of Constant Rate of Strain (CRS) and K_0-consolidated undrained (CK_0U) triaxial tests conducted using RBBC at maximum vertical consolidation stresses ranging from 0.15 to 10.0 MPa.

Section 5.2 presents the compression, consolidation, and flow characteristics of RBBC. These results are obtained from CRS tests and from the 1-D consolidation phase of each triaxial test prior to undrained shearing.

The results from K_0-consolidated undrained triaxial compression (CK_0UC) tests on normally consolidated (NC) and overconsolidated (OC) specimens are presented in Section 5.3. The triaxial compression test series were intended to provide a fairly detailed study of cohesive soil stress level effects at three well defined stress histories. A total of 35 triaxial compression tests were performed as part of this experimental program. Of these, 14 tests experienced experimental problems and hence, are not reported.

Section 5.4 summarizes and compares the results for the NC and OC CK_0UC triaxial tests on RBBC. The purpose of the section is to integrate the observations made in the previous section in an attempt to gain an overall understanding of stress level effects as a function of stress history. It sums up the shear stress-strain and effective stress behavior, and looks at the stress level dependence of the SHANSEP equation in triaxial compression.

The results from K_0-consolidated undrained triaxial extension (CK_0UE) tests on NC specimens are presented in Section 5.5. These tests were performed by Safia Moniz (Moniz, 2009), an MEng student who investigated the normalized behavior of RBBC in triaxial extension

[6] See Chapter 2 for Normalized Soil Parameter concept.

at consolidation stress levels up to 2 MPa. The extension test series do not provide the same level of systematic study as that in the compression tests, but are intended to give initial insight on the effects of stress level in this mode of shearing.

5.2 ONE-DIMENSIONAL CONSOLIDATION BEHAVIOR

5.2.1 Introduction

Prior to undrained shear test phases, all triaxial specimens were K_0-consolidated using the MIT automated stress path triaxial cells (described in Chapter 4). In addition, three CRS tests were performed using the Trautwein consolidometer device. This section presents the K_0-consolidation results from these tests.

Table 5-1 summarizes the phase relations and pertinent consolidation characteristics for the three CRS tests. Table 5-2 lists for each triaxial test reported, the test type, the apparatus, the phase relations, the preconsolidation pressure, the applied K_0-consolidation stress history, and pertinent consolidation properties.

Section 5.2.2 presents the results from the CRS tests. Section 5.2.3 presents the consolidation results from the triaxial compression tests performed in this research.

5.2.2 Constant Rate of Strain Tests

Three CRS tests were performed on small diameter RBBC specimens (D = 3.6 cm) consolidated to a maximum vertical consolidation effective stress, σ'_{vm} = 10 MPa. The tests were consolidated at a strain rate of 2 %/hour such that the resultant base pore pressure ratio, $u_b/\sigma_v \approx$ 2-3%, is well within the range prescribed for standard linear interpretation of consolidation properties (Wissa et al., 1971).

Figure 2-1 shows the compression curves in conventional ε_a-logσ'_v space for the three tests. The figure provides an example of the excellent repeatability in the behavior of RBBC. It can be seen that the shape of the compression curves is characterized by a well defined break corresponding approximately to the batch preconsolidation pressure ($\sigma'_p \approx$ 0.1 MPa; see below). The axial strain at the maximum stress of 10 MPa (after one cycle of secondary compression) is about 32%. Figure 5-2 shows the compression curves in e-logσ'_v space. The initial void ratio for

the three tests is about 1.2 while the void ratio at σ'_v = 10 MPa is about 0.5. Pestana & Whittle (1995) proposed using loge-logσ'_v as an alternative space for presenting the compression behavior of soils over a wide range of stresses. Figure 5-3 shows the compression curves in this space.

Table 5-1 shows that the preconsolidation pressures, which are determined using the strain energy method (Becker et al, 1987), range from 0.108 to 0.120 MPa. These values are slightly higher than the nominal maximum pressure of 0.1 MPa applied in the batch consolidometer. This is believed to be due to the secondary compression ("aging") during batch consolidation at the maximum stress.

The virgin consolidation line of the normally consolidated RBBC is not perfectly linear in any of the three figures discussed above (i.e., the slope of the compression line changes with stress level) and appears to display more of an S-shape at higher stresses. Figure 5-4 shows the tangent compression and swelling ratios (CR and SR respectively) versus stress level. The figure demonstrates that the compression ratios decrease from about 0.18 - 0.2 at σ'_v = 0.2 MPa to 0.13 at σ'_v = 10 MPa. However, the rate of decrease reduces with stress level. The values of CR at low pressures (less than 1 MPa) are consistent with prior studies on RBBC while the values at high stresses are lower than what have been previously reported. Figure 5-5 shows SR as a function of the stress level. The figure illustrates that the swelling ratios are approximately an order of magnitude smaller than CR. As OCR increases from 1 to 4, SR increases slightly from 0.012 to 0.015. These values fall within the range reported from previous studies on RBBC. The compression index (ρ_c), defined by the slope of the compression curve in loge-logσ'_v space, also changes with stress level as it increases from about 0.16 at low stresses to 0.25 at high stresses.

Figure 5-6 shows the variation in the vertical coefficient of consolidation (c_v) obtained from the three CRS tests. In general, c_v decreases with vertical effective stress in the recompression range until the preconsolidation pressure is reached, drops abruptly, and then begins to rise with increasing stress level in the normally consolidated region. All three tests show c_v increasing from a minimum value of 15×10^{-4} cm^2/sec at σ'_v = 0.2 MPa to a range of 30 - 50×10^{-4} cm^2/sec at σ'_v = 10 MPa. However, this change in c_v is relatively small over such a wide range of consolidation stresses. It should be noted that the rate of pore pressure equilibration in the undrained triaxial shear tests is influenced by c_v of the material (Bishop & Henkel, 1962).

Therefore, the small change in c_v indicates that the pore pressure readings in the undrained triaxial shear tests performed at the standard rate of 0.5 %/hr are expected to be reliable at all pressures. The values of c_v and the trend with stress level are consistent with the results presented in Chapter 3 for the batch consolidometer tests and previous studies on RBBC at the relevant stresses.

Figure 5-7 shows that the vertical hydraulic conductivity (k_v) decreases with decreasing void ratio (i.e., with increasing consolidation stress). The hydraulic conductivity reduces from approximately 1 x 10^{-7} at e = 1.1 (σ'_v = 0.15 MPa) to around 3 x 10^{-9} at e = 0.53 (σ'_v = 10 MPa). This relationship appears to have more of a bi-linear form within the stress levels considered. Table 5-1 shows that the value of C_k (= $\Delta e / \Delta \log k$) for the three tests varies with stress level as it decreases from a range of 0.457 - 0.506 at low consolidation stresses (up to 1 MPa; e ≈ 0.8) to a range of 0.231 - 0.335 at higher stresses. The values of k_v (and hence C_k) are in agreement with the batch data at similar stress levels, as shown in Figure 5-8. The figure also illustrates that the batch consolidometer tests at very low stress increments yields higher C_k values than the above CRS test results. The values of C_k measured for the batch at low stresses range from 0.581 to 0.651. On the other hand, the values of C_k obtained at high pressures in the CRS are lower than any previous results reported on RBBC. Figure 5-9 shows the ratio of C_c/C_k versus stress level for the CRS tests. The values appear to have a relatively narrow range C_c/C_k = 0.7 - 1.2 (where $C_c = C_k$ is needed for validity of Terzaghi linear consolidation theory).

5.2.3 Triaxial Tests

All triaxial tests were K_0-normally consolidated at a constant strain rate of about 0.15 %/hr to a stress level greater than 1.5 times the batch preconsolidation pressure then left for 24 hrs of laboratory aging. The K_0-consolidation algorithm ensures zero lateral strain by adjusting the cell pressure to keep the axial and volume strains equal. If the specimen is to be unloaded to an effective vertical consolidation stress (σ'_{vc}) less than the maximum vertical stress (σ'_{vm}), stress path unloading to the desired OCR is performed (using the empirical equation given by Equation 4.1) with strain rate of 0.1 %/hr followed by another 24 hrs of aging.

Figure 5-10 shows the compression curves in ε_a-logσ'_v space for all NC triaxial tests (OC tests not included for clarity). The specimens were consolidated to maximum vertical effective consolidation stresses, σ'_{vm} = 0.15 - 10 MPa. The tests performed in the low pressure triaxial

apparatus were first resedimented to maximum vertical stress of 0.1 MPa in the consolidometer, while those performed in the high pressure triaxial device were first resedimented to 1.0 MPa. Therefore, the preconsolidation stresses (σ'_p) obtained in the triaxial were roughly 0.1 MPa and 1.0 MPa. This was done in order to minimize consolidation strains in the triaxial apparatus. The maximum axial strains reached in both apparatuses were about 18% (after one cycle of secondary compression). Note that the low and high pressure triaxial devices can accommodate about 30% axial strain due to equipment restrictions (for specimens with standard initial height of 8.1 cm) and since at least 10% axial strain is needed during triaxial compression shearing then the maximum allowable strain during consolidation is about 20%.

Figure 5-11 shows the compression behavior in e-logσ'_v space for all NC and OC (OCR = 2 & 4) triaxial tests. The initial void ratio for the low pressure tests range from 1.21 – 1.27 while for the high pressure triaxial tests from 0.85 – 0.88. The results show excellent agreement and repeatability among test specimens. Figure 5-12 shows the compression behavior in the triaxial compared to a 1-D consolidation test performed in the CRS device (CRS905). Overall, the curves from the two tests agree very closely. This agreement indicates that the rate of consolidation in the triaxial tests was adequate and that reasonably small excess pore pressures were generated during consolidation.

The interpreted preconsolidation pressure obtained using the strain energy method (Becker et al, 1987) ranges from 0.093 to 0.108 MPa for the low pressure tests and from 0.979 to 1.231 MPa for the high pressure tests, as seen in Table 5-2. These values bound the imposed pressures of 0.1 and 1.0 MPa applied in the consolidometer for the low pressure and high pressure tests, respectively. The variation in σ'_p could be attributed to the secondary compression ("aging") during batch consolidation at the maximum stress (which tends to increase σ'_p), the skin friction from the batch consolidometer sleeve (which tends to decrease σ'_p), and/or simply inexact application of the maximum vertical stress (especially if the load frame is used to apply the load).

The virgin compression ratio (CR) was determined at different stress levels for each test and the results are presented in Table 5-2. The table illustrates that the CR values range from 0.147 to 0.168 over the stress range of 0.15 – 10 MPa. However, no clear trend is observed with stress level. In addition, the compression curves in the conventional e-logσ'_v and ε_a-logσ'_v

spaces appear to have an approximately linear trend. This behavior is slightly different than the CRS test results, where CR decreases with stress level. It is not clear what causes this difference in trends between the two tests. For all OC tests, the swelling ratio (SR) values were determined by connecting the compression curve point at the end of loading and at the end of unloading (both after secondary compression); this is called the secant SR value. Table 5-2 shows that the value of SR range from 0.011 – 0.022, which is an order of magnitude smaller than CR.

Data on the coefficient of earth pressure at rest (K_0) can be obtained from feedback-controlled 1-D consolidation in the triaxial cell. Figure 5-13 shows the variation in K_0 with vertical stress during consolidation for all NC triaxial tests. These results show that K_0 decreases during the initial loading within the overconsolidated region until reaching the preconsolidation pressure (about 0.1 and 1.0 MPa respectively for low and high pressure tests) and then plateaus. Once the soil is consolidated well into the virgin compression region, K_0 remains fairly stable. The value of K_0 in the virgin compression region is referred to as the normally consolidated value $K_{0NC.}$ The trend of K_0 during 1-D consolidation from the triaxial results obtained in this study is slightly different than the trend discussed in Chapter 3 from previous studies on RBBC (e.g. Santagata, 1994; Sheahan, 1991). Santagata (1994) reported that K_0 decreases during reloading to a value lower than K_{0NC} then increases to a constant value once in the virgin compression region. This plunge in K_0 value before reaching the preconsolidation pressure was not observed in any of the triaxial tests performed in this study. However, it should be noted that the two studies mentioned above were performed on RBBC Series III (while this research used RBBC Series IV) and that different resedimentation procedures were used in the current research (see Chapter 3).

Table 5-2 shows that the values of K_{0NC} at maximum stress obtained from the triaxial tests range from 0.518 to 0.564. This variation in the preshear K is clearly linked to the consolidation stress level, as shown in Figure 5-14. The figure demonstrates that K_0 increases from 0.518 at σ'_v = 0.15 MPa to about 0.564 at σ'_v = 10 MPa. This increase is significant, especially given the fact that the preshear value of K_0 appears to dramatically affect the values of undrained strength, as reported by Santagata (1994) and discussed in the following section. While the values of K_0 at low pressures are within the range reported from previous studies on RBBC, the values obtained at high pressures are larger than anything previously reported.

5.3 UNDRAINED TRIAXIAL COMPRESSION – RESULTS

5.3.1 Introduction

This section presents results from triaxial tests in which NC and OC specimens were sheared undrained in compression at a constant axial strain rate of 0.5 %/hr after K_0-consolidation (and swelling in the case of OC tests) to vertical consolidation effective stresses, σ'_{vc} = 0.05 – 10 MPa. Two-thirds of the triaxial program consisted of tests on NC specimens, where a total of 14 successful tests were performed. Of these, 7 tests were performed in the low pressure (up to 1 MPa) triaxial apparatus (MIT02) while the other 7 tests were performed in the high pressure (up to 10 MPa) triaxial apparatus (MIT07). Two of the high pressure tests (TX787 & TX788) were performed to mimic similar tests in the low pressure device, and since the results were almost identical[7], the test results are not presented in this chapter. Section 5.3.2 presents the CK_0UC (NC) test results. Tests on mechanically overconsolidated specimens were performed to evaluate the effect of stress history on undrained stress level effects. In total, 3 tests (2 high pressure and 1 low pressure) were performed at nominal OCR = 2, and 4 tests at OCR = 4 (3 high pressure and 1 low pressure). Sections 5.3.3 and 5.3.4 present the CK_0UC tests results for OCR of 2 and 4 respectively.

Tables 5-3 and 5-4 list for each NC and OC test respectively, the test number and type, the apparatus, the preshear consolidation conditions, and the pertinent stress-strain-strength parameters at peak shear stress and at maximum obliquity. Note that the friction angle (φ') values represent a measure of the obliquity (σ'_v/σ'_h) at peak and at maximum obliquity; these values do not necessarily define the Mohr-Coulomb effective stress envelope for the OC tests (where the envelope is better fitted using an apparent cohesion intercept). The summary tables also indicate whether a shear plane formed during undrained shear.

[7] This was demonstrated in Chapter 4 (Section 4.4.2) and the results are summarized in Table 5-3.

5.3.2 Behavior of NC RBBC

5.3.2.1 Shear Stress-Strain Behavior

Figure 5-15 shows the shear stress-strain behavior ($q = (\sigma_1-\sigma_3)/2$ versus ε_a) for the NC CK_0UC tests. The results show that the peak undrained shear strength (s_u) is mobilized at relatively small strain levels ($\varepsilon_a \leq 1\%$) followed by some post peak softening. The undrained shear strength is reached with fairly small shear stress increment and increases with stress level as summarized in Figure 5-16. It can be seen that the general correlation is more or less linear, as suggested by the Normalized Soil Parameter (NSP) concept.

Figures 5-17, 5-18 and 5-19 show, in more detail, the normalized shear stress-strain behavior (q/σ'_{vc} versus ε_a), with the axial strain shown on linear (large strains), linear (small strains) and logarithmic scales, respectively. These figures illustrate that the preshear consolidation stress level has a pronounced effect on the normalized strength and shape of the stress-strain curves. The peak undrained strength ratio ($USR = s_u/\sigma'_{vc}$) decreases with increasing vertical consolidation effective stress as summarized in Figure 5-20. The results show that the undrained strength ratio decreases from 0.326 at low stresses to about 0.281 at high stresses. Note that the normalized strengths at low stresses are in agreement with prior studies on NC RBBC from CK_0UC tests (e.g., Sheahan, 1991). A slight leveling off in the s_u/σ'_{vc} - σ'_{vc} relationship is apparent at high consolidation stresses. However, it is likely that the USR trend with stress level is linked to variations in K_{0NC}. As discussed in Section 5.2.3, the value of K_{0NC} increases with increasing stress level. Figure 5-21 shows the USR versus the preshear value of K_{0NC}. The data are quite consistent and confirm that small changes in K_{0NC} have an important effect on the normalized undrained strength properties. The equation of the regression through the data points can be used to describe the relation between K_{0NC} and s_u/σ'_{vc}:

$$USR = 0.84 - 1.01 \cdot K_{0NC} \tag{5.1}$$

These results are consistent with prior experience for RBBC (Santagata, 1994), although the regression coefficients proposed are slightly different[8].

The shear stress-strain data (Figures 5-17, 5-18 and 5-19) also demonstrate that the behavior becomes more ductile as stress level increases. Larger strains are required to mobilize

[8] The regression equation proposed by Santagata (1994) is presented in Chapter 3 (Section 3.4.3.2).

the peak resistance and the post peak strain softening generally decreases with increasing vertical consolidation effective stress. As shown in Figure 5-22, the strain at failure increases from about 0.16% at low stresses to 1.05% at high stresses. Furthermore, consolidation stress level also tends to affect the post peak portion of the stress-strain curves. The degree of strain softening can be represented by the brittleness, which is the ratio of the undrained strength to the large strain shear resistance of the soil. In order to be consistent, the shear resistance at $\varepsilon_a = 10\%$ was taken as the large strain resistance. Figure 5-23 summarizes the brittleness versus stress level. The figure indicates that brittleness generally decreases from around 1.27 at low stresses to 1.12 at high stresses. The post peak portions of the stress-strain curves are not parallel and tend to intermingle especially for the intermediate and high pressure tests.

It must be noted that failure planes developed in the high pressure tests (those consolidated to vertical consolidation stresses in excess of 4 MPa; see Table 5-3) while the mode of failure in the low pressure tests involve only bulging of the specimens. Figure 5-24 shows a picture for 2 NC RBBC specimens after triaxial compression shearing illustrating the modes of failure for the low pressure and high pressure triaxial tests. In general, shear planes are not expected to form in NC specimens where the behavior is fully contractive. However, failure planes have been previously reported for NC specimens (e.g., Burland, 1990), especially if the consolidation is 1-D, since the induced fabric may be more prone than isotropically consolidated samples to the formation of slip surfaces.

5.3.2.2 Stiffness

Figure 5-25 shows curves of the undrained secant Young's modulus normalized to the vertical consolidation stress (E_u/σ'_{vc}) versus axial strain (on a log-log scale) for the NC RBBC. As the measurements were performed employing external LVDT's the estimates of the stiffness are considered reliable only above 0.01 - 0.05%. In general, the figure shows that the soil exhibits strong non-linearity and yielding occurs at small strains. The decrease in stiffness is particularly marked once the soil reaches failure due to the large amount of post peak strain softening. The results also suggest stress level dependence as the curves tend to be suppressed with increasing stress level. Hence, the maximum value of the normalized stiffness (E_{uMAX}/σ'_{vc}) decreases as stress level increases. In addition, the high pressure tests show a more linear initial

response than the low pressure tests. Note that the stiffness curves are not parallel and tend to interrelate at higher strains.

Figure 5-26 shows the normalized undrained modulus versus stress level at different strain levels. Once again, this plot demonstrates that the stiffness behavior of the clay is affected by the consolidation stress level, as the data do not exhibit a unique, normalized response. There is a clear decreasing trend in the normalized undrained modulus with increasing effective stress especially at small strains. However, it has already been shown that the stiffness is not well normalized by the consolidation stress level (e.g., Santagata, 1998)[9].

5.3.2.3 Effective Stress Behavior

Figure 5-27 shows the effective stress paths using the MIT stress space ($q = (\sigma_1-\sigma_3)/2$ versus $p' = (\sigma'_1+\sigma'_3)/2$) from the triaxial compression test series on NC RBBC. Pore pressure measurements were made at the base of the specimen in all cases. The results shows that the stress paths, which are all similar in shape, start from the K_0-consolidation line and rise to the peak strength then continue to shear with decreasing average effective stress (i.e., increasing excess pore pressure) until reaching the failure envelope.

Figures 5-28 and 5-29 show the corresponding normalized effective stress paths (q/σ'_{vc} versus p'/σ'_{vc}) in full view of the stress space and in close up view respectively. The figures show clearly the change in pore pressure development during the test where there is little pore pressure generation up to a yield point followed by much greater development of pore pressures. Peak shear conditions coincide with a yield condition in the low pressure tests, but the peak point moves further down the stress path as consolidation stress increases. The peak strength is evidently linked to the consolidation stress ratio. At large strains there is a pervasive difference in the stress obliquity (q/p') and hence, a common linear failure envelope is not reached. However, there seems to be a clear trend between the stress path end points and stress level, as illustrated in Figure 5-29. Table 5-3 lists the values of effective stress parameters at peak and maximum obliquity.

[9] The relationship linking the initial stiffness to consolidation stress level proposed by Santagata (1998) is presented in Chapter 3 (Section 3.4.3.2).

Figure 5-30 shows the variation in friction angle at peak and maximum obliquity with stress level. The results show that the secant friction angle at peak shear strength (φ'_p) varies only slightly; the friction angle decreases from $\varphi'_p = 26°$ at $\sigma'_{vc} = 0.15$ MPa to $\varphi'_p = 23°$ at $\sigma'_{vc} =$ 1MPa, then increases slightly to $\varphi'_p = 24°$ at $\sigma'_{vc} = 10$ MPa. This is related to the fact that the peak point moves down the stress path as stress level increases (i.e., normalized shear and average stresses at peak decrease). On the other hand, the friction angle at large strains shows a significant stress level dependence with the effective friction angle at maximum obliquity (φ'_{mo}) decreasing from 39.4° at low stresses to 29.2° at high stresses. The values of φ'_{mo} obtained in the past for RBBC from tests consolidated to vertical consolidation stresses ranging from 0.2 to 0.7MPa varied only between 33° to 36°. The reduction in large strain friction angle with stress level is significant and has not been previously observed for RBBC.

The pore pressures generated to peak, often expressed by the pore pressure Skempton parameter A ($=(\Delta u-\Delta\sigma_3)/(\Delta\sigma_1-\Delta\sigma_3)$) at peak shear stress ($A_f$), versus stress level is shown in Figure 5-31. The A_f value essentially indicates the orientation of the average effective stress at peak relative to its preshear stress value. The figure shows that A_f increases with stress level from about 0.5 at low stresses to a value of 1.2 at high stresses. These values are larger at high stress levels since the axial strain at failure increases with stress and hence the generated pore pressures are greater as indicated below. Also, as the peak point moves down the stress path, the A_f value increases.

The excess pore pressures ($u_e = \Delta u-\Delta\sigma_3$) generated during shear normalized to the vertical consolidation stress (σ'_{vc}) for the NC tests are shown in Figure 5-32. The results illustrate that the normalized excess pore pressure increases continuously throughout shear before leveling off. Increasing stress level tends to push down the normalized pore pressure curves.

Since the triaxial specimens are saturated, any change in octahedral stress ($\sigma_{oct}=(\sigma_1+2\sigma_3)/3$) should result in an equal pore pressure change, and thus no change in the effective stresses which control soil behavior. Therefore, to isolate the pore pressure due to changes in shear stress alone the shear induced pore pressure ($u_s = \Delta u-\Delta\sigma_{oct}$) is plotted. This essentially removes the effect of total stress path and starting K_0. Note that u_s is a property of the soil. Figure 5-33 plots the shear induced pore pressure normalized to the vertical consolidation stress versus axial strain. The progressively positive pore pressures generated throughout shearing indicate that the NC RBBC has a fully contractive behavior. Like the excess pore pressure plot, the normalized shear induced

pore pressures are increasingly suppressed as stress level increases. The decreasing trend of normalized pore pressures with stress level at different strain levels is clearly illustrated in Figure 5-34.

5.3.3 Behavior of OCR=2 RBBC

5.3.3.1 Shear Stress-Strain Behavior

Figure 5-35 shows the stress-strain behavior for the three CK_0UC tests performed on specimens with nominal OCR=2. The curves are characterized by a peak followed by some post peak softening. Figure 5-36 summarizes the peak undrained shear strength versus the preshear consolidation stress (σ'_{vc}). Figures 5-37, 5-38 and 5-39 present the normalized shear stress-strain behavior (q/σ'_{vc} versus ε_a), with the axial strain shown on linear (large strains), linear (up to ε_a=4%) and logarithmic scales, respectively. The undrained strength ratio (s_u/σ'_{vc}) decreases slightly with consolidation effective stress level. Figure 5-40 shows that USR drops from 0.55 at low stresses to about 0.49 at high stresses. Figure 5-41 shows that USR is also somewhat correlated with the preshear lateral stress ratio K_c. Note that the OC specimens were unloaded using the empirical method governed by Equation 4.1 and based on K_0 at the end of virgin consolidation (i.e., K_{0NC}).

Like the normally consolidated specimens, the stress-strain curves for OCR=2 tests exhibit a more ductile behavior with increasing stress level. Figure 5-42 shows that the strain at failure increases from about 0.9% in the low pressure test to around 2.35% at high stresses. The brittleness (s_u/(q at ε_a=10%)) decreases slightly from 1.11 to 1.07 with increasing vertical consolidation stress, as illustrated in Figure 5-43. The post peak portions of the stress-strain curves start off more or less parallel and then diverge at high strains.

The high pressure test (TX846) developed a failure plane during shearing while the other 2 specimens failed by bulging.

5.3.3.2 Stiffness

The normalized secant modulus (E_u/σ'_{vc}) as a function of axial strain for the OCR=2 RBBC test series is shown in Figure 5-44 (on log-log scale). It must be noted that the LVDT measurements at the beginning of shearing in the overconsolidated tests require some

manipulation to eliminate effects of load frame mechanical problems. Due to the backlash in the axial loading gear system during load reversal, the initial strain measurements are slightly affected and hence, a correction was made to the data.

The results suggest stress level dependence as the curves tend to be suppressed with increasing stress level. There is an apparent decreasing trend in the maximum stiffness (E_{uMAX}/σ'_{vc}) measured at small strains and then the curves converge at higher strains. This is also illustrated in Figure 5-45, which shows the normalized secant modulus versus effective stress level at different strain levels.

5.3.3.3 Effective Stress Behavior

The effective stress paths from the triaxial compression test series on RBBC with nominal OCR=2 are shown in Figure 5-46. Figures 5-47 and 5-48 show the corresponding normalized effective stress paths (q/σ'_{vc} versus p'/σ'_{vc}) in full view of the stress space and close up view, respectively. The effect of stress level is to shift the initial part of the stress paths to the right and push down the peak point and post peak portions. As a result, the effective friction angle at peak and maximum obliquity vary with consolidation stress level, as illustrated in Figure 5-49. The figure shows that φ'_p decreases from 32.9° to 29.1° while φ'_{mo} decreases from 39.4° to 30.0° as stress level increases (assuming zero cohesion intercept). Note that it is not possible to accurately determine a failure envelope with a cohesion intercept since this envelope appears to have a non-linear form, with the gradient steadily reducing with increasing effective stress.

Figure 5-50 shows that the Skempton pore pressure parameter A at peak shear stress (A_f) increases only slightly from 0.30 to 0.31 with increasing stress level. The values of A_f do not vary significantly since the preshear effective stress states and the generated pore pressures at peak (discussed below) are similar in the three tests.

Figure 5-51 depicts the normalized excess pore pressure generated during shear with strain. Like the NC tests, only positive excess pore pressure are generated and the general pattern in all tests involve an increase to a local maxima, decrease until approximately ε_f, then increase again during strain softening. Increasing stress level tends to suppress the normalized excess pore pressure curves.

The normalized shear induced pore pressures, shown in Figure 5-52, increase slightly then decrease to a minimum at about ε_f, before increasing again as the material strain softens. The shear induced pore pressures are also suppressed as stress level increases, but the minimum value does not seem to be greatly affected. This is also illustrated in Figure 5-53, where the normalized pore pressures are more or less the same at ε_a = 1% (corresponding roughly to the minimum u_s) but then the effect of stress level is evident at higher strains. The pore pressures response indicates that the OCR=2 RBBC specimens are somewhat neutral between contractive and dilatant undrained shear behavior.

5.3.4 Behavior of OCR=4 RBBC

5.3.4.1 Shear Stress-Strain Behavior

Figure 5-54 shows the stress-strain behavior for the four CK_0UC tests performed on specimens with nominal OCR=4. The data indicate that the peak undrained shear strength increases with increasing preshear consolidation stress (σ'_{vc}), as summarized in Figure 5-55. Figures 5-56, 5-57 and 5-58 present the normalized shear stress-strain behavior (q/σ'_{vc} versus ε_a), with the axial strain shown on linear (large strains), linear (up to ε_a=6%) and logarithmic scales, respectively. Figure 5-59 plots the undrained strength ratio (s_u/σ'_{vc}) variation with stress level. The USR decreases significantly from 0.95 at low stresses to about 0.77 at high stresses. The variations in USR are also associated to the preshear K_c, as illustrated in Figure 5-60. Note that the OC specimens were unloaded using the empirical method. If shear planes appeared during the test, it was always well after the peak shear stress was reached (see Table 5-4)

The strain at peak stress (ε_f) varied as in Figure 5-61. Increasing the stress level increased ε_f noticeably; from about 3.2% at low stresses to 5.5% at high stresses. However, it is difficult to pick a peak strength in these tests because of the shape of the stress-strain curves (i.e., the peak in these curves is not well defined like the NC tests). Consequently, strain softening of the stress-strain curves is quite mild. Figure 5-62 shows that brittleness (s_u/(q at ε_a=10%)) decreases only from about 1.04 to 1.01 with increasing vertical consolidation stress.

5.3.4.2 Stiffness

Figure 5-63 shows curves of normalized undrained secant Young's modulus (E_u/σ'_{vc}) versus axial strain on a log-log plot for the OCR=4 RBBC. Reasonable modulus results were obtained only beyond 0.05%, since the measurements were performed employing an external LVDT. The results show that the curves tend to be pushed down with increasing stress level. A summary of the normalized secant modulus at different strain levels versus the preshear consolidation stress is presented in Figure 5-64. It is clear from this plot that the normalized initial stiffness decreases with increasing stress level. However, all curves tend to converge at higher strains.

5.3.4.3 Effective Stress Behavior

The effective stress paths from the triaxial test series on RBBC with nominal OCR=4 are shown in Figure 5-65. Figures 5-66 and 5-67 show the full view and a close up view of the normalized effective stress paths (q/σ'_{vc} versus p'/σ'_{vc}), respectively. The normalized stress paths for the four tests start from similar preshear stress states and rise towards the effective stress envelope with comparable paths until reaching the peak stress at different locations.

Figure 5-68 shows the variation in friction angle at peak and maximum obliquity with stress level. The φ'_p decreases from 34.6° to 30.4° while φ'_{mo} decreases from 35.5° to 30.0° as stress level increases (assuming zero cohesion intercept). Note that the difference between φ'_p and φ'_{mo} gets smaller as OCR increases. Like the OCR=2 tests, it is difficult to determine a failure envelope with a cohesion intercept because of the non-linear nature of the envelope with increasing effective stress.

The dependence of the A parameter at peak (A_f) on the stress level appears to be minimal, as illustrated in Figure 5-69, with A_f increasing only from 0.12 to 0.18 as vertical consolidation stress increases.

Excess pore pressure generation with strain (Figure 5-70) initially increases before decreasing and reaching a minimum in the range of ε_f for each test. After reaching a minimum, these pore pressures increase slightly with additional strains. Although increasing stress level does not seem to affect the initial local maxima in the normalized excess pore pressure curves, the subsequent minima and the rate of post peak pore pressure increase are influenced by the

level of the preshear consolidation stress; high pressure tests have a higher minimum value and lower rate of pore pressure increase than the lower pressure tests.

Figure 5-71 illustrates the normalized shear induced pore pressure generation with strain. The pore pressures increase slightly to a positive value then decrease to a negative minimum, before increasing again during strain softening. The shear induced pore pressures become increasingly negative with decreasing stress level. This is also illustrated in Figure 5-72 , which shows the normalized pore pressures versus effective stress level at different strain levels. At this nominal OCR, the undrained shear behavior is ultimately dilatant.

5.4 UNDRAINED TRIAXIAL COMPRESSION – SUMMARY

5.4.1 Introduction

This section provides a summary and comparison of the results for NC and OC RBBC from CK_0UC triaxial tests, integrating the effects of stress history and consolidation stress level. The CK_0UC test series were intended to provide a comprehensive study of cohesive soil stress level effects (σ'_{vm} = 0.15 – 10.0 MPa) at three well defined stress histories (OCR = 1, 2 and 4). The following subsections highlight the most important aspects of the soil behavior as a function of the vertical consolidation stress level and the preshear stress history.

5.4.2 Shear Stress-Strain Behavior

Figure 5-73 shows the normalized shear stress-strain behavior (q/σ'_{vm} versus ε_a) from OCR=1, 2 and 4 CK_0UC tests performed at low and high stress levels (σ'_{vm} = 0.2 and 10 MPa). Note that the shear stress is normalized with σ'_{vm}, the maximum vertical consolidation stress. The results show that as OCR increases, the peak value of strength normalized to the maximum vertical stress decreases (the strength normalized to the preshear vertical consolidation stress increases), the post peak strain softening decreases, and the axial strain at failure increases. Increasing the stress level has similar effects; the normalized strength decreases, strain softening decreases, and axial strain at failure increases. These aspects are discussed in more detail below.

Figure 5-74 shows the normalized undrained shear strength (s_u/σ'_{vm}) versus the maximum consolidation stress (σ'_{vm}) for all OCRs. It is clear that there is a smooth and consistent trend of

decreasing s_u/σ'_{vm} with increasing stress level for each OCR which appears to be more sensitive at lower stresses. There are several factors that affect the normalized strength such as the preshear K_c value, the pore pressures at peak (e.g., A_f), and the peak friction angle (φ'_p). The previous sections illustrated that the normalized strength generally decreased as the preshear K_c increased. Note that the value of the lateral stress ratio K_c also tends to increase with increasing stress level, as shown in Figure 5-14. The association between the normalized strength and K_c is expected to be stronger in the NC specimens than the OC soil since a relatively small shear stress increment is required to attain the peak stress state from the preshear stress state. The relationship between the normalized strength and the preshear K_c is consistent with the observation of Santagata (1994) for NC RBBC.

The strain at peak shear stress (ε_f) for all CK_0UC tests versus OCR is shown in Figure 5-75. The strain at peak appears to be a function of the stress level and stress history. Increasing OCR from 1 to 4 increases ε_f from 0.15% to 3% in the low pressure tests, and from 1% to 5% in the high pressure tests. On the other hand, increasing stress level tends to increase ε_f from 0.15% to 1% at OCR=1 and from 3% to 5% at OCR=4.

The post peak loss of soil shear resistance with continued straining (strain softening) generally decreases with increasing OCR and stress level. The degree of strain softening, represented by the brittleness (s_u/(q at ε_a=10%)), for all OCRs versus maximum vertical stress is illustrated in Figure 5-76. Lack of brittleness represents the soil's ability to maintain a larger proportion of its peak shear resistance with continued deformation. Increasing stress level or OCR enhances this ability. Note that the increase in axial strain at peak and the decrease in strain softening with increasing stress level are coherent with previous studies at high pressures, as discussed in Chapter 2.

5.4.3 Stiffness

Figures 5-77 and 5-78 show curves of the undrained secant Young's modulus normalized to the vertical consolidation stress, σ'_{vc} and σ'_{vm} (E_u/σ'_{vc} and E_u/σ'_{vm}) respectively, versus axial strain on a log-log plot for the NC and OC RBBC at low and high stress levels (σ'_{vm} = 0.2 and 10MPa). Figure 5-77 shows that E_u/σ'_{vc} increases with increasing OCR. The NC soil has a consistently smaller normalized stiffness than the OC clay and exhibits the strongest non-linearity from the very beginning. Figure 5-78 shows the undrained secant Young's modulus

normalized to the maximum vertical consolidation stress (E_u/σ'_{vm}) versus axial strain for the same tests. The tests with the same σ'_{vm} start out with comparable initial modulus (E_{uMAX}/σ'_{vm}). However, the NC soil yields at smaller strains and stiffness degrades faster than the OC soil and hence, E_u/σ'_{vm} is lower at higher strains. The curves for RBBC with OCR = 2 and 4 fall within a narrow band at large strains. The effect of stress level is also evident as the figures show that increasing stress level tends to suppress the stiffness curves and generate a more linear initial response.

5.4.4 Effective Stress Behavior

Figures 5-79 and 5-80 present the effective stress paths normalized to the maximum vertical consolidation stress (q/σ'_{vm} versus p'/σ'_{vm}) from OCR = 1, 2 and 4 CK_0UC tests performed at low pressure (σ'_{vm} = 0.2 MPa) and high pressure (σ'_{vm} = 10 MPa) respectively. The figures illustrate that the NC and OCR=2 RBBC specimens ultimately contract during shearing, while those at OCR=4 ultimately dilate. At each stress level, the stress paths from the three stress histories approach a common failure envelope at large strains. However, the failure envelope at low stresses has a friction angle at maximum obliquity, φ'_{mo} = 33.66°, and normalized cohesion intercept, c'/σ'_{vm} = 0.018, while the failure envelope at high stresses has a friction angle at maximum obliquity, φ'_{mo} = 26.81°, and normalized cohesion intercept, c'/σ'_{vm} = 0.032.

Figure 5-81 shows the stress states at peak shear stress in MIT stress apace normalized to σ'_{vm} for all CK_0UC tests. The friction angle at peak (φ'_p) tends to increase with increasing OCR (assuming zero cohesion intercept). Moreover, φ'_p decreases slightly with increasing stress level at each OCR (assuming zero cohesion intercept), as illustrated in Figures 5-30, 5-49 and 5-68, suggesting that the peak failure envelope is non-linear. Figure 5-82 shows the stress states at maximum obliquity in MIT stress space normalized to σ'_{vm} for all CK_0UC tests. The figure demonstrates some scatter in the data points primarily due to variations in the preshear consolidation stress level, with the friction angle at maximum obliquity decreasing from $\varphi'_{mo} \approx$ 35° at low pressures to $\varphi'_{mo} \approx$ 27° at high pressures. It can be seen that determining a common failure envelope with a constant friction angle and a cohesion intercept for this data set is challenging due to the apparent non-linear form of the envelope. It must be noted that the variation observed in the large strain maximum obliquity friction angle with stress level has not been previously observed for RBBC. Moreover, this result contradicts prior knowledge of soil

behavior, where the large strain friction angle of clays is assumed to be constant, as discussed in Chapter 2.

Figure 5-83 shows the effective stress paths during shearing in e-log p' space for OCR=1 and 4 RBBC specimens at high pressure (σ'_{vm} = 10 MPa). The average effective stress decreases in the NC specimen and increases in the OCR=4 specimen during shearing at constant void ratio (no drainage allowed) until eventually reaching the critical state line. The critical state is an ultimate condition in which plastic shearing could continue indefinitely without changes in volume or effective stresses. Figure 5-84 presents the large strain stress states obtained at end of undrained shearing in e-log p' space for NC and OC RBBC from all CK_0UC tests. The figure also shows the K_0-consolidation line from 2 triaxial tests. All data points appear to lie on a unique critical state line approximately parallel to the K_0-consolidation line.

The pore pressures generated to peak, often expressed by the pore pressure Skempton parameter A at peak shear stress (A_f), decreases as OCR increases. However, A_f increases with increasing stress level at each OCR, as indicated in Figures 5-31, 5-50 and 5-69. The excess pore pressures remain positive at the three stress histories, and increasing stress level tends to suppress them. Figure 5-85 shows the normalized shear induced pore pressure (u_s/σ'_{vc}) generation with strain for RBBC (OCR = 1, 2 and 4) at low and high stress levels (σ'_{vm} = 0.2 and 10 MPa). In all cases, the pore pressures initially increase indicating contractive behavior. The NC soil remains contractive throughout shearing, while OCR=2 specimens tend to dilate and then contract again with increasing strain. The pore pressure decreases beyond 0.5% strain for OCR=4 clay and ultimately dilates with shearing. As stress level increases, the pore pressures are suppressed in OCR = 1 and 2. However, the pore pressures increase (becomes less negative) when consolidation stress increases for OCR=4 soil.

5.4.5 SHANSEP Equation in Triaxial Compression

The SHANSEP[10] equation is based on normalized behavior; clay specimens having the same overconsolidation ratio exhibit similar properties (i.e., strength, stress-strain, pore pressure parameters, etc.) when normalized with respect to the consolidation stress. The previous sections examined the effect of consolidation stress level on the normalized undrained shear properties of

[10] See Chapter 2 for details on SHANSEP design method and equation.

RBBC in triaxial compression. Since these tests were performed at three different OCRs, the SHANSEP equation parameters can be evaluated.

Figure 5-86 shows the undrained strength ratio (s_u/σ'_{vc}) versus OCR for all CK_0UC tests performed in the experimental program. The equation of the regression through all the data points show that the SHANSEP parameters S and m are equal to 0.296 and 0.741 respectively (r^2=0.979). However, the figure shows some scatter which appears to be related to the consolidation stress level. Figure 5-87 shows the undrained strength ratio (s_u/σ'_{vc}) versus OCR for selected CK_0UC tests at maximum consolidation stress, σ'_{vm} = 0.2, 0.6, 2 and 10 MPa. The OCR = 2 and 4 tests consolidated to σ'_{vm} = 0.6 MPa were obtained from Sheahan (1991). The Figure also summarizes the SHANSEP parameters (S and m) obtained from regression analyses. In all cases, r^2 was equal or greater than 0.999, indicating excellent conformity of the data to the fitted equation.

As illustrated in prior sections, the normalized strength decreases with increasing stress level in all three stress histories. This explains why the value of the slope m varies only slightly with stress level (m ranges between 0.74 and 0.77). The value of S (corresponding to the NC s_u/σ'_{vc}) decreases from 0.314 to 0.281 as stress level increases. The parameter S at σ'_{vm} = 0.2 MPa agrees with previous results for RBBC in triaxial compression (performed at low stresses). The value of m, however, is slightly higher than previously quoted values for RBBC. This is believed to be due to matching data points from tests with different σ'_{vm} in the past (i.e. higher OCR tests were consolidated to higher σ'_{vm}) while the data in Figure 5-87 clearly show consistently higher (and perhaps unique) m in tests with the same σ'_{vm}.

It can be concluded that the SHANSEP equation accurately models the undrained strength variations with OCR at distinct stress levels, but the equation parameters are stress level dependent. Note that these are the first data to show the reliable trends in S and m in the SHANSEP equation as a function of stress level.

5.5 UNDRAINED TRIAXIAL EXTENSION

5.5.1 Introduction

This section presents results from triaxial tests in which NC specimens were sheared in undrained extension at a constant axial strain rate of 0.5 %/hr after K_0-consolidation to vertical consolidation effective stresses, σ'_{vc} = 0.15 – 2 MPa. These tests were performed by Moniz (2009) under close supervision by the author. Out of a total of 8 tests, only 4 were successful and are reported in this section. One test (TX870) was terminated at ε_a=9.3%, but is reported since the data to that point are considered valuable. All these tests were performed in the low pressure triaxial apparatus (MIT02). The purpose of the extension tests was to gain an initial insight on the stress level effects in this mode of shearing.

The phase relations and the applied K_0-consolidation stress history for the triaxial extension tests are reported in Table 5-2. The preshear conditions and stress-strain-strength parameters at peak and at maximum obliquity are summarized for each test in Table 5-5. Note that the axial strains reported in Table 5-5 are negative while in the figures the strains are positive to facilitate analysis.

5.5.2 Shear Stress-Strain Behavior

Figure 5-88 shows the shear stress-strain behavior for the four CK_0UE tests performed on NC RBBC. The results show that the peak shear strength is reached at large strains followed by slight strain softening. The peak undrained shear strength increases with stress level as summarized in Figure 5-89.

Figures 5-90, 6-91 and 5-92 present the normalized shear stress-strain behavior (q/σ'_{vc} versus ε_a). Figure 5-90 shows the full view of the stress-strain curves with the axial strain shown on linear scale, Figure 5-91 shows a close up view of the curves, and Figure 5-92 shows the full view with the axial strain presented on logarithmic scale. The effect of stress level is evident in these figures which also confirm the decreasing trend of the undrained strength ratio, as depicted in Figure 5-93. The USR reduces from 0.173 to 0.153 with increasing consolidation stress level. Although the strength for the low pressure test (TX870) is not reported, it can be seen from the stress-strain curves that it is consistently higher than the other tests up to the termination point (ε_a=9.3%). It must be noted that the reported strengths are slightly higher than previous results on

RBBC at similar low consolidation stresses (e.g., Ladd & Varallyay, 1965; Sheahan, 1991). However, these studies were performed with different test conditions; Ladd & Varallyay (1965) used higher strain rates during shearing while Sheahan (1991) employed lubricated end platens. Figure 5-94 compares the USR values obtained from triaxial extension tests for NC RBBC with than those obtained from compression tests. The extension tests have much lower USR than the compression tests. This large difference in strengths between the two modes of shearing is indicative of the anisotropic behavior of RBBC.

In general, the extension test specimens tend to fail by necking followed by the development of a failure plane. When necking begins, the cylindrical area correction used in the reduction program cannot accurately account for the area reduction in the neck and hence, the results after necking are not very reliable. It is believed that necking occurred after the peak stress in the extension tests reported in this study and therefore the shear strengths are considered reliable.

Figure 5-95 shows that the strain at failure is not noticeably linked to the consolidation stress level. The strain at failure obtained in these tests ranged between 13.7% and 14.9%.

5.5.3 Stiffness

Figure 5-96 shows the normalized undrained secant Young's modulus versus axial strain (on a log-log scale) for the NC RBBC from the triaxial extension tests. Like the overconsolidated tests, the backlash in the load frame gear system during load reversal affects the initial strain measurements. Although a correction was made to the data, the initial portion of the curves remains not very well defined, as shown in Figure 5-96.

The figure illustrate that the soil exhibits non-linearity from the beginning of shear. The results also suggest stress level dependence as the curves tend to be suppressed with increasing stress level. There is a clear decreasing trend in the maximum stiffness (E_{uMAX}/σ'_{vc}) measured at small strains and then the curves converge at higher strains, indicating little stress level dependence. This is also illustrated in Figure 5-97, which shows the normalized secant modulus versus effective stress level at different strain levels. Note that the modulus values for NC RBBC obtained from extension tests are slightly higher than those obtained from compression tests (E_{uMAX}/σ'_{vc} = 260 in extension versus E_{uMAX}/σ'_{vc} = 120 in compression at σ'_{vc} = 2 MPa).

5.5.4 Effective Stress Behavior

The effective stress paths from the triaxial extension test series on NC RBBC are shown in Figure 5-98. The stress paths start from the K_0-consolidation line and progress with decreasing shear stress to the hydrostatic stress state, then increase with reversal of stress direction until reaching the failure envelope. The average effective stress decreases continuously throughout shearing. This decrease in the average effective stress indicates that the specimen is contractive until reaching a minimum effective stress at or near to maximum obliquity then begins to dilate along the failure envelope (p' increases slightly once the stress path hits the failure envelope). Figures 5-99 and 5-100 show the full view and a close up view of the normalized effective stress paths (q/σ'_{vc} versus p'/σ'_{vc}), respectively. The variation in the starting point of the stress paths is due to the preshear K_{0NC} effect. The stress paths then come together during shearing suggesting that K_{0NC} is no longer significant. Finally, the effective stress paths reach the failure envelope at different stress states demonstrating that the envelope is stress level dependent, as shown in Figure 5-100.

Figure 5-101 shows the variation in friction angle at peak and maximum obliquity with stress level for NC RBBC from triaxial extension and compression tests. Note that the peak stress and maximum obliquity occur at very similar strains in triaxial extension and therefore the friction angles for both conditions are comparable. The values of φ'_{mo} in CK_0UE tests decreases from 43.1° at low stresses to 31.2° at high stresses. The reported friction angle for the low pressure test (TX870) was obtained at ε_a=9.3% and could have been even slightly higher if the peak/maximum obliquity conditions were reached. The friction angles at low stresses are in agreement with previous studies on RBBC. However, they remain higher than those obtained from compression tests at low pressures, as shown in Figure 5-101. As consolidation stress level increases (up to 2 MPa), the friction angles in triaxial compression and extension tests tend to converge.

The excess pore pressures ($u_e = \Delta u - \Delta\sigma_3$; where $\Delta\sigma_3 = \Delta\sigma_h$) generated during shear normalized to σ'_{vc} for the NC tests are shown in Figure 5-102. The pore pressures decrease initially before increasing with additional strains. In general, the measured u_e is small because the effective stress path is close to the total stress path in these tests. There does not seem to be any particular trend in the excess pore pressure curves with the preshear stress level.

Figure 5-103 depicts the normalized shear induced pore pressures generation with strain. The figure shows that the pore pressures increase rapidly at the beginning and then reaches a steady state at large strains. The positive value of u_s throughout shearing indicates that the NC RBBC has a fully contractive behavior. Increasing stress level tends to push down the normalized shear induced pore pressure curves. These pore pressures are in agreement with the compression tests.

Test No.	w_0 (%)	e_0	σ'_p (MPa)	σ'_{vm} (MPa)	CR (Stress Range in MPa)				SR (Stress Range in MPa)		C_k (Stress Range in MPa)	
					0.2 - 0.3	0.6 - 0.8	1.0 - 2.0	7.0 - 9.0	9.0 - 8.0	4.0 - 3.0	0.2 - 2.0	2.0 - 10.0
CRS905	43.1	1.21	0.118	10.10	0.182	0.156	0.143	0.134	0.013	0.015	0.491	0.319
CRS910	42.7	1.20	0.120	10.15	0.188	0.154	0.139	0.130	0.011	0.015	0.506	0.335
CRS912	43.1	1.21	0.108	10.10	0.170	0.144	0.133	0.127	0.013	0.016	0.457	0.231

Table 5-1: Summary of CRS consolidation results

Test No. / Cell	Test Type	Initial			At Max. Stress		Preshear				CR (Stress Range in MPa)				SR (Secant)
		w_0 (%)	e_0	σ'_p (MPa)	σ'_{vm} (MPa)	$K_{0(NC)}$	σ'_{vc} (MPa)	OCR	e	K_c	0.15 - 0.3	0.6 - 0.8	1.5 - 3.0	6.0 - 9.0	
TX724 MIT02	CK_0UC (NC)	43.16	1.22	0.096	0.333	0.528	0.333	1.00	0.99	0.528	0.153	-	-	-	-
TX727 MIT02	CK_0UC (NC)	43.72	1.22	0.101	0.964	0.546	0.964	1.00	0.83	0.546	0.157	0.155	-	-	-
TX732 MIT02	CK_0UC (NC)	43.61	1.22	0.094	0.142	0.518	0.142	1.00	1.12	0.518	~ 0.148	-	-	-	-
TX741 MIT02	CK_0UC (NC)	44.13	1.23	0.103	0.478	0.536	0.478	1.00	0.94	0.536	0.165	-	-	-	-
TX748 MIT02	CK_0UC (NC)	45.23	1.26	0.093	0.817	0.542	0.817	1.00	0.86	0.542	0.157	0.152	-	-	-
TX757 MIT02	CK_0UC (NC)	45.21	1.27	0.095	0.670	0.542	0.670	1.00	0.90	0.542	0.157	0.147	-	-	-
TX762 MIT02	CK_0UC (NC)	43.04	1.21	0.105	0.189	0.523	0.189	1.00	1.09	0.523	0.167	-	-	-	-
TX787 MIT07	CK_0UC (NC)	42.80	1.23	0.106	0.332	0.538	0.332	1.00	1.01	0.538	0.163	-	-	-	-
TX788 MIT07	CK_0UC (NC)	34.95	1.00	0.432	0.972	0.542	0.972	1.00	0.83	0.542	-	1.610	-	-	-
TX793 MIT07	CK_0UC (NC)	30.34	0.88	0.999	5.870	0.556	5.870	1.00	0.60	0.556	-	-	0.159	0.156	-
TX798 MIT07	CK_0UC (NC)	29.56	0.86	1.091	1.954	0.540	1.954	1.00	0.74	0.540	-	-	0.166	-	-
TX803 MIT07	CK_0UC (NC)	30.13	0.85	1.142	3.908	0.543	3.908	1.00	0.64	0.543	-	-	0.168	-	-
TX811 MIT07	CK_0UC (NC)	30.52	0.87	1.102	7.822	0.550	7.822	1.00	0.55	0.550	-	-	0.162	0.158	-

Table 5-2: Summary of consolidation results for triaxial tests

Test No. / Cell	Test Type	Initial			At Max. Stress		Preshear				CR (Stress Range in MPa)				SR (Secant)
		w_0 (%)	e_0	σ'_p (MPa)	σ'_{vm} (MPa)	$K_{0(NC)}$	σ'_{vc} (MPa)	OCR	e	K_c	0.15 - 0.3	0.6 - 0.8	1.5 - 3.0	6.0 - 9.0	
TX829 MIT07	CK_0UC (NC)	29.94	0.86	1.205	9.743	0.564	9.743	1.00	0.53	0.564	-	-	0.165	0.153	-
TX831 MIT07	CK_0UC (OC)	30.43	0.88	1.157	5.835	0.541	1.429	4.08	0.63	0.997	-	-	0.159	0.163	0.020
TX840 MIT07	CK_0UC (OC)	30.62	0.87	1.231	9.742	0.561	2.398	4.06	0.56	1.000	-	-	0.162	0.156	0.022
TX843 MIT07	CK_0UC (OC)	30.60	0.87	0.979	1.934	0.540	0.469	4.13	0.76	0.980	-	-	0.154	-	0.016
TX846 MIT07	CK_0UC (OC)	30.42	0.87	1.103	9.743	0.544	4.846	2.01	0.53	0.731	-	-	0.163	0.157	0.020
TX849 MIT07	CK_0UC (OC)	30.54	0.87	1.049	1.937	0.549	0.958	2.02	0.75	0.740	-	-	0.156	-	0.017
TX854 MIT02	CK_0UC (OC)	43.65	1.22	0.097	0.191	0.520	0.094	2.04	1.09	0.701	0.159	-	-	-	0.011
TX859 MIT02	CK_0UC (OC)	44.23	1.23	0.108	0.191	0.513	0.046	4.20	1.12	0.920	0.164	-	-	-	0.012
TX870 MIT02	CK_0UE (NC)	42.98	1.21	0.101	0.141	0.509	0.141	1.00	1.11	0.509	-	-	-	-	-
TX872 MIT02	CK_0UE (NC)	43.64	1.22	0.097	0.967	0.548	0.967	1.00	0.81	0.548	-	-	-	-	-
TX904 MIT02	CK_0UE (NC)	43.08	1.21	0.109	0.413	0.535	0.413	1.00	0.98	0.535	-	-	-	-	-
TX909 MIT02	CK_0UE (NC)	43.76	1.23	0.102	1.961	0.545	1.961	1.00	0.71	0.545	-	-	-	-	-

Table 5-2: (continued) Summary of consolidation results for triaxial tests

Test No. Cell	Test Type	Conditions			At Peak Shear Stress					At Max Obliquity				Comments
		σ'_{vc} (MPa)	OCR	K_c	ε_a (%)	q/σ'_{vc}	p'/σ'_{vc}	A_f	φ'_p	ε_a (%)	q/σ'_{vc}	p'/σ'_{vc}	φ'_{mo}	
TX724 MIT02	CK_0UC (NC)	0.333	1.00	0.528	0.178	0.310	0.752	0.581	24.29°	10.574	0.244	0.420	35.52°	
TX727 MIT02	CK_0UC (NC)	0.964	1.00	0.546	0.335	0.288	0.736	0.799	22.98°	11.042	0.237	0.446	32.14°	
TX732 MIT02	CK_0UC (NC)	0.142	1.00	0.518	0.165	0.326	0.748	0.574	25.87°	10.470	0.267	0.421	39.39°	
TX741 MIT02	CK_0UC (NC)	0.478	1.00	0.536	0.252	0.297	0.746	0.668	23.48°	11.632	0.239	0.433	33.53°	
TX748 MIT02	CK_0UC (NC)	0.817	1.00	0.542	0.284	0.292	0.742	0.734	23.17°	10.443	0.237	0.443	32.37°	
TX757 MIT02	CK_0UC (NC)	0.670	1.00	0.542	0.223	0.292	0.750	0.666	22.92°	11.410	0.236	0.441	32.41°	
TX762 MIT02	CK_0UC (NC)	0.189	1.00	0.523	0.154	0.313	0.751	0.556	24.60°	9.691	0.256	0.431	36.42°	
TX787 MIT07	CK_0UC (NC)	0.332	1.00	0.538	0.158	0.305	0.775	0.479	23.17°	11.383	0.239	0.425	34.22°	
TX788 MIT07	CK_0UC (NC)	0.972	1.00	0.542	0.367	0.289	0.742	0.734	22.91°	11.174	0.234	0.457	31.03°	
TX793 MIT07	CK_0UC (NC)	5.870	1.00	0.556	0.938	0.281	0.699	1.201	23.73°	9.329	0.243	0.499	29.16°	Failure plane at ε_a=12.9%
TX798 MIT07	CK_0UC (NC)	1.954	1.00	0.540	0.404	0.290	0.727	1.037	23.48°	9.749	0.245	0.476	30.98°	
TX803 MIT07	CK_0UC (NC)	3.908	1.00	0.543	0.584	0.286	0.711	1.127	23.71°	8.980	0.247	0.491	30.26°	Failure plane at ε_a=13.3%
TX811 MIT07	CK_0UC (NC)	7.822	1.00	0.550	0.931	0.283	0.696	1.203	24.02°	8.746	0.252	0.512	29.46°	Failure plane at ε_a=11.4%
TX829 MIT07	CK_0UC (NC)	9.743	1.00	0.564	1.048	0.282	0.693	1.224	23.98°	8.374	0.249	0.511	29.22°	Failure plane at ε_a=10.9%

Table 5-3: Summary of CK_0UC (NC) triaxial tests

Test No. Cell	Test Type	Conditions			At Peak Shear Stress					At Max Obliquity				Comments
		σ'_{vc} (MPa)	OCR	K_c	ε_a (%)	q/σ'_{vc}	p'/σ'_{vc}	A_f	φ'_p	ε_a (%)	q/σ'_{vc}	p'/σ'_{vc}	φ'_{mo}	
TX831 MIT07	CK_0UC (OC)	1.429	4.08	0.997	5.188	0.773	1.528	0.162	30.41°	7.381	0.757	1.512	30.03°	Failure plane at ε_a=9.8%
TX840 MIT07	CK_0UC (OC)	2.398	4.06	1.000	5.350	0.781	1.507	0.177	31.30°	7.946	0.774	1.502	30.89°	Failure plane at ε_a=12.23%
TX843 MIT07	CK_0UC (OC)	0.469	4.13	0.980	4.790	0.810	1.531	0.169	31.92°	9.341	0.784	1.486	31.83°	
TX846 MIT07	CK_0UC (OC)	4.846	2.01	0.731	2.351	0.488	1.004	0.309	29.11°	7.466	0.454	0.908	30.03°	Failure plane at ε_a=9.9%
TX849 MIT07	CK_0UC (OC)	0.958	2.02	0.740	2.042	0.494	0.999	0.312	29.62°	9.674	0.450	0.850	31.95°	
TX854 MIT02	CK_0UC (OC)	0.094	2.04	0.701	0.897	0.549	1.013	0.300	32.85°	10.347	0.495	0.780	39.42°	
TX859 MIT02	CK_0UC (OC)	0.046	4.20	0.920	3.178	0.951	1.675	0.122	34.59°	10.253	0.913	1.572	35.51°	

Table 5-4: Summary of CK_0UC (OC) triaxial tests

Test No. Cell	Test Type	Conditions			At Peak Shear Stress					At Max Obliquity				Comments
		σ'_{vc} (MPa)	OCR	K_c	ε_a (%)	q/σ'_{vc}	p'/σ'_{vc}	A_f	φ'_p	ε_a (%)	q/σ'_{vc}	p'/σ'_{vc}	φ'_{mo}	
TX870 MIT02	CK_0UE (NC)	0.141	1.00	0.509	Not Reached					Not Reached				Test aborted at ε_a=9.3%
TX872 MIT02	CK_0UE (NC)	0.967	1.00	0.548	-13.721	-0.157	0.284	0.142	33.44°	-12.981	-0.156	0.282	33.61°	
TX904 MIT02	CK_0UE (NC)	0.413	1.00	0.535	-14.982	-0.173	0.278	0.128	38.31°	-13.933	-0.172	0.274	38.89°	
TX909 MIT02	CK_0UE (NC)	1.961	1.00	0.545	-14.663	-0.153	0.297	0.096	31.18°	-14.663	-0.153	0.297	31.18°	

Table 5-5: Summary of CK_0UE (NC) triaxial tests

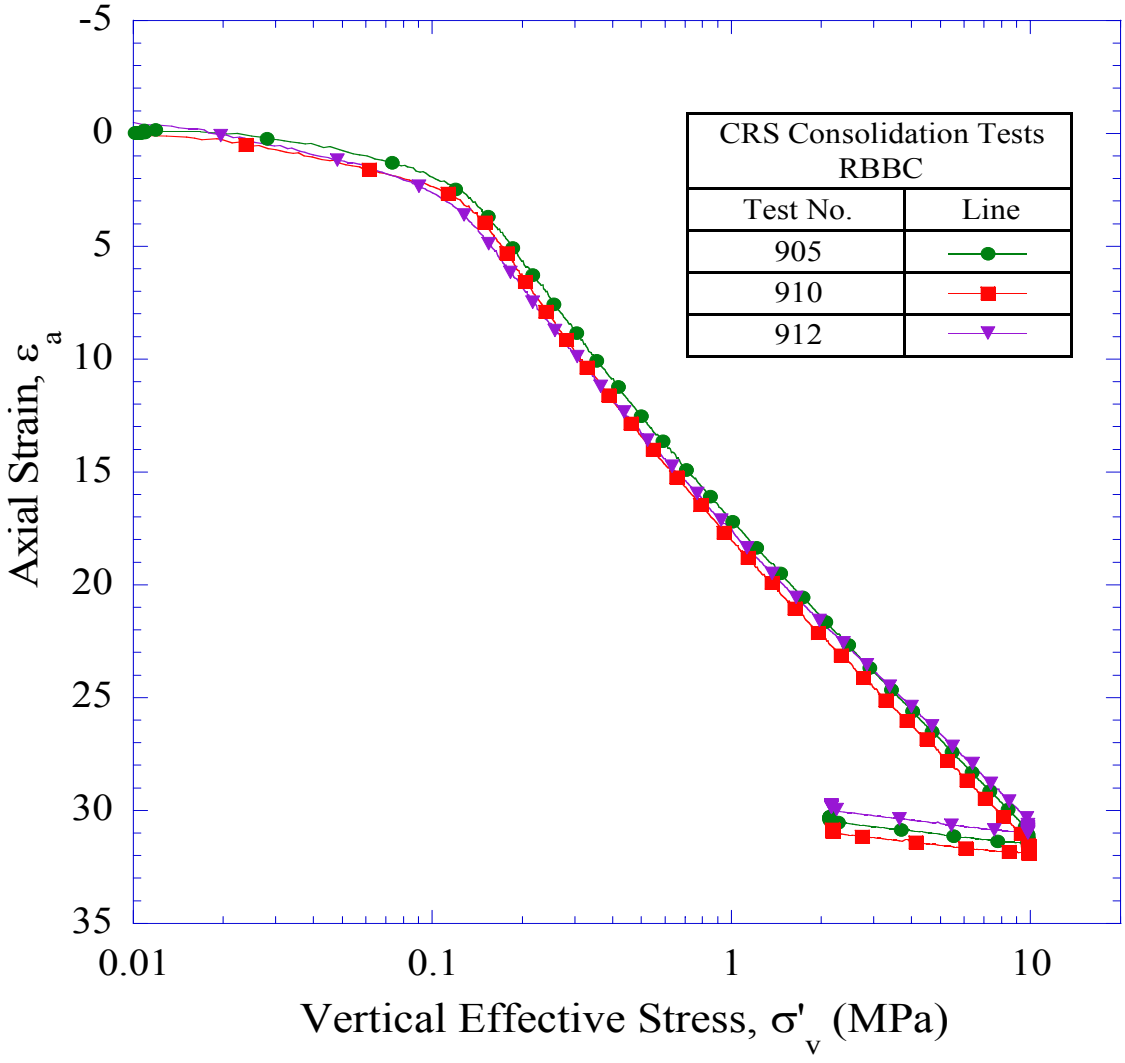

Figure 5-1: Compression behavior in ε_a-logσ'_v space for RBBC from CRS tests

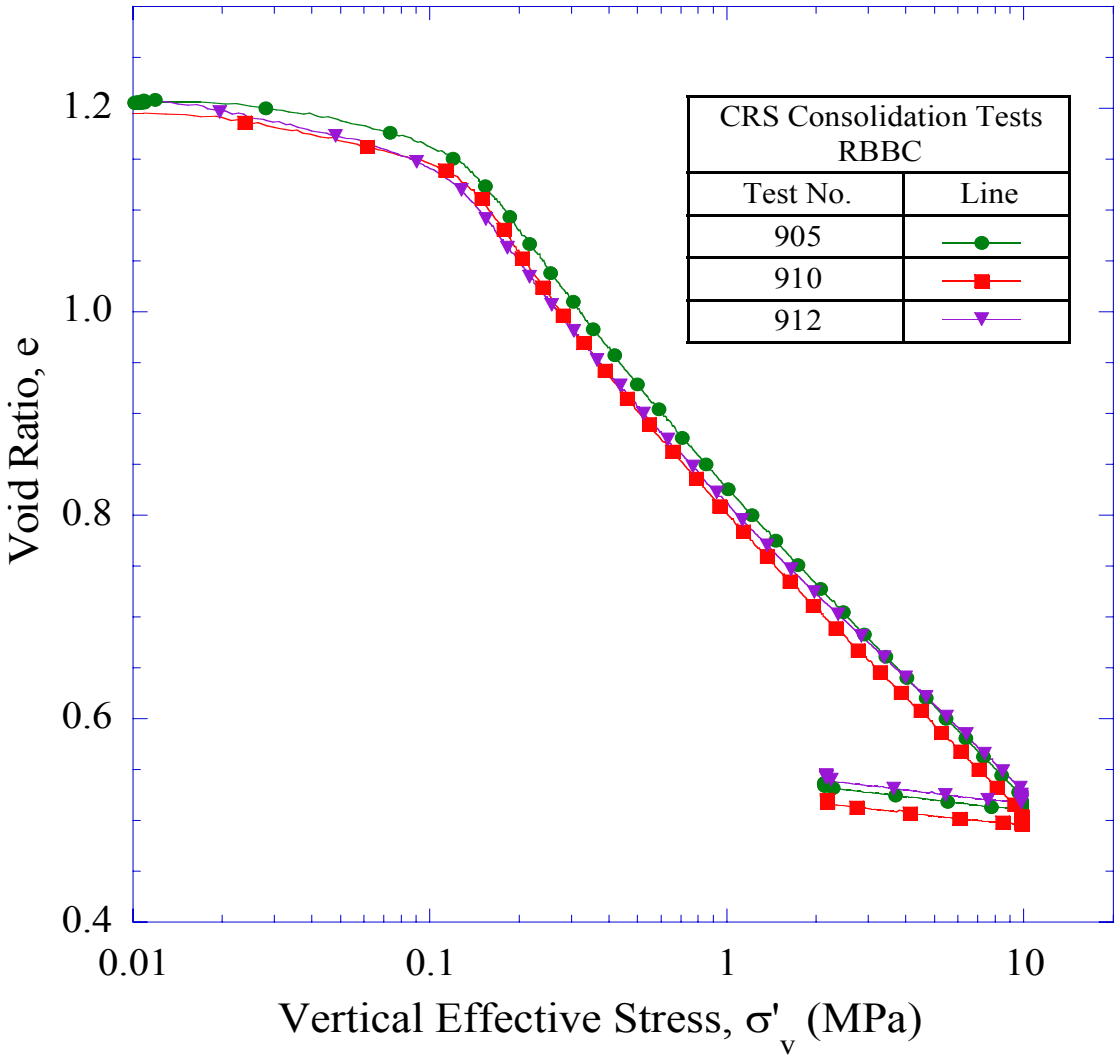

Figure 5-2: Compression behavior in e-logσ'_v space for RBBC from CRS tests

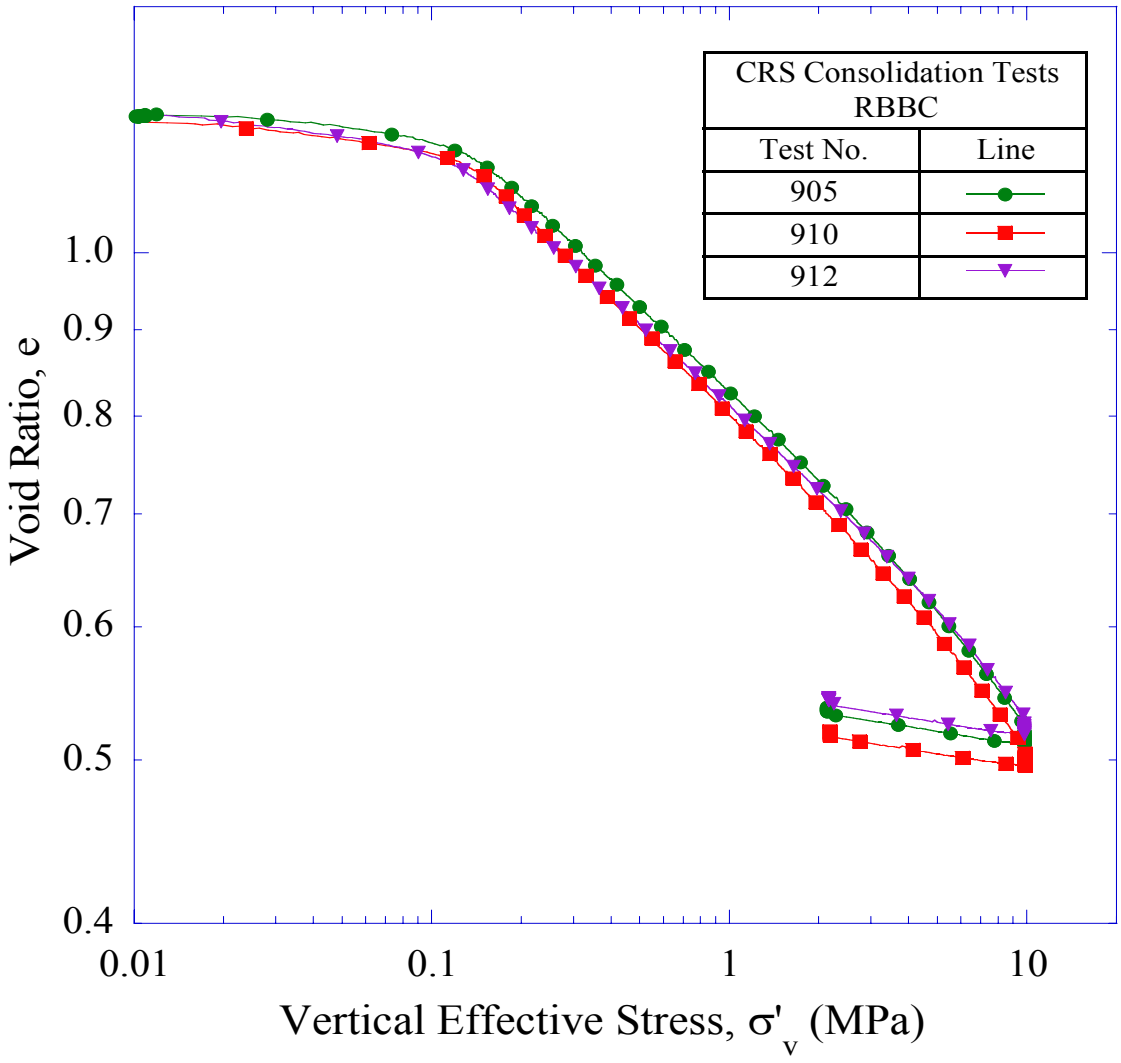

Figure 5-3: Compression behavior in loge-logσ'_v space for RBBC from CRS tests

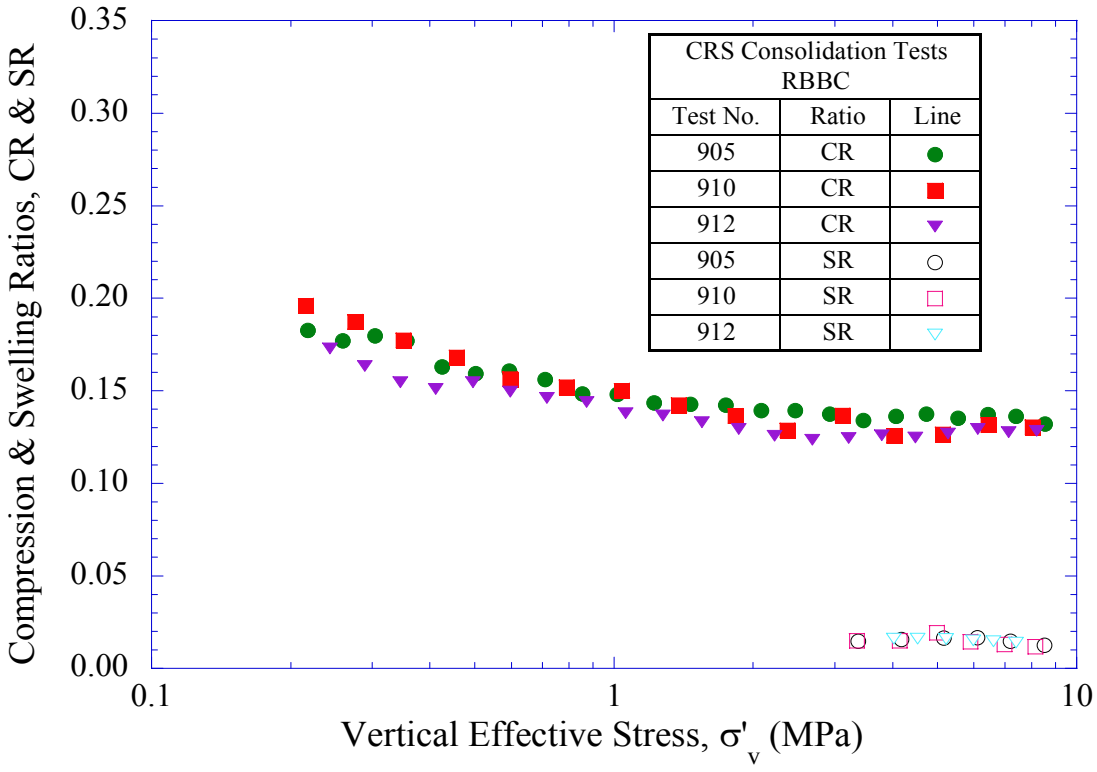

Figure 5-4: Compression and swelling ratios versus stress level for RBBC from CRS tests

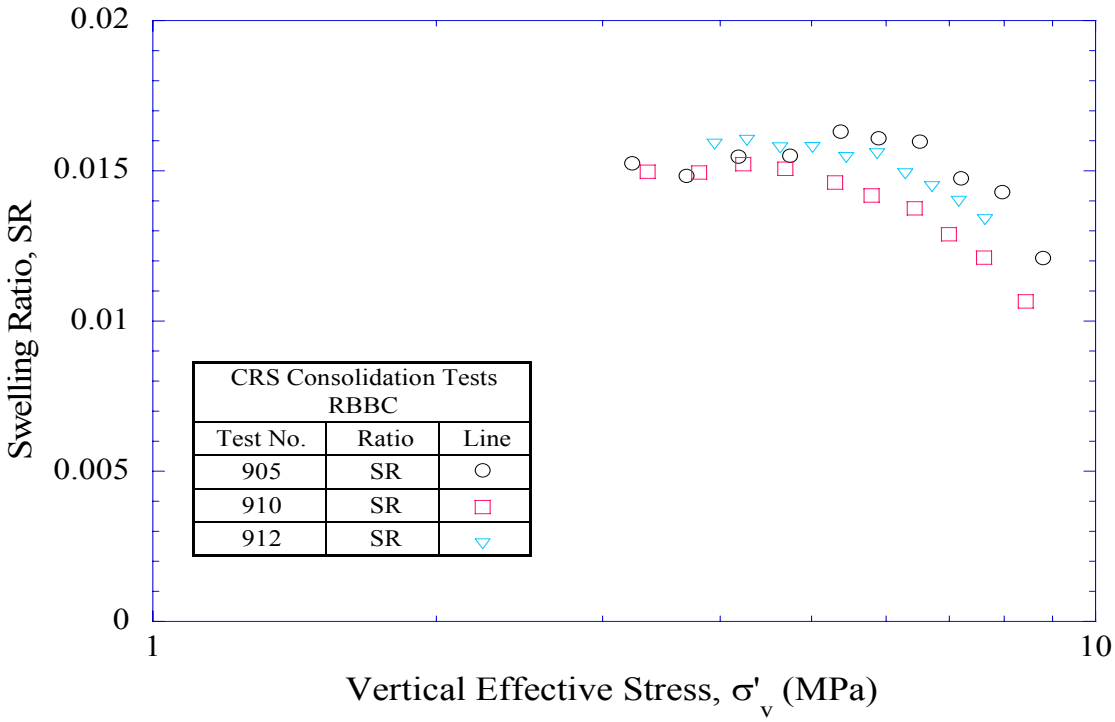

Figure 5-5: Swelling ratio versus stress level for RBBC from CRS tests

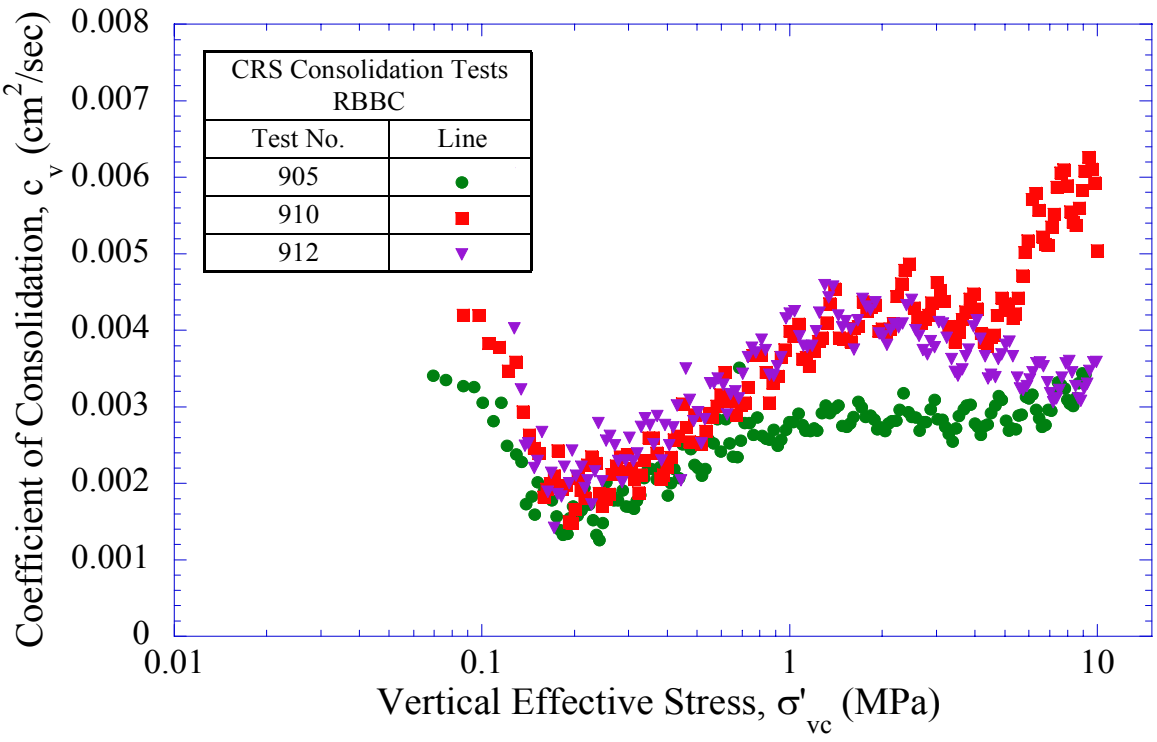

Figure 5-6: Coefficient of consolidation versus stress level for RBBC from CRS tests

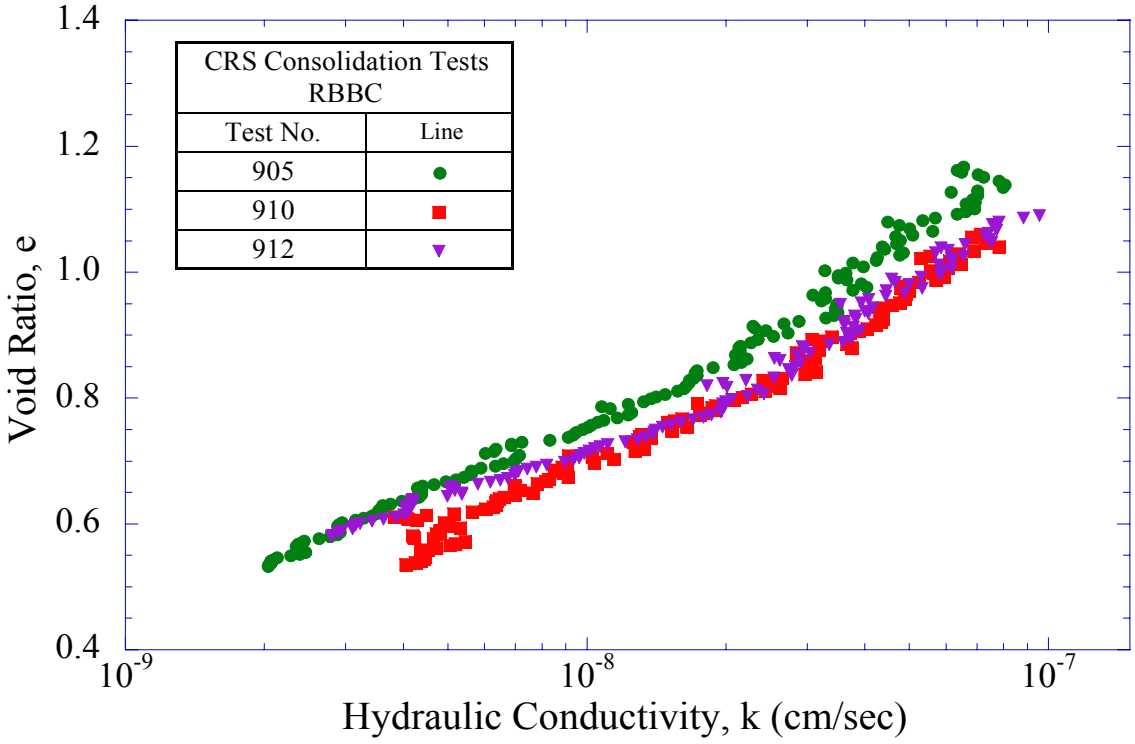

Figure 5-7: Void ratio versus hydraulic conductivity for RBBC from CRS tests

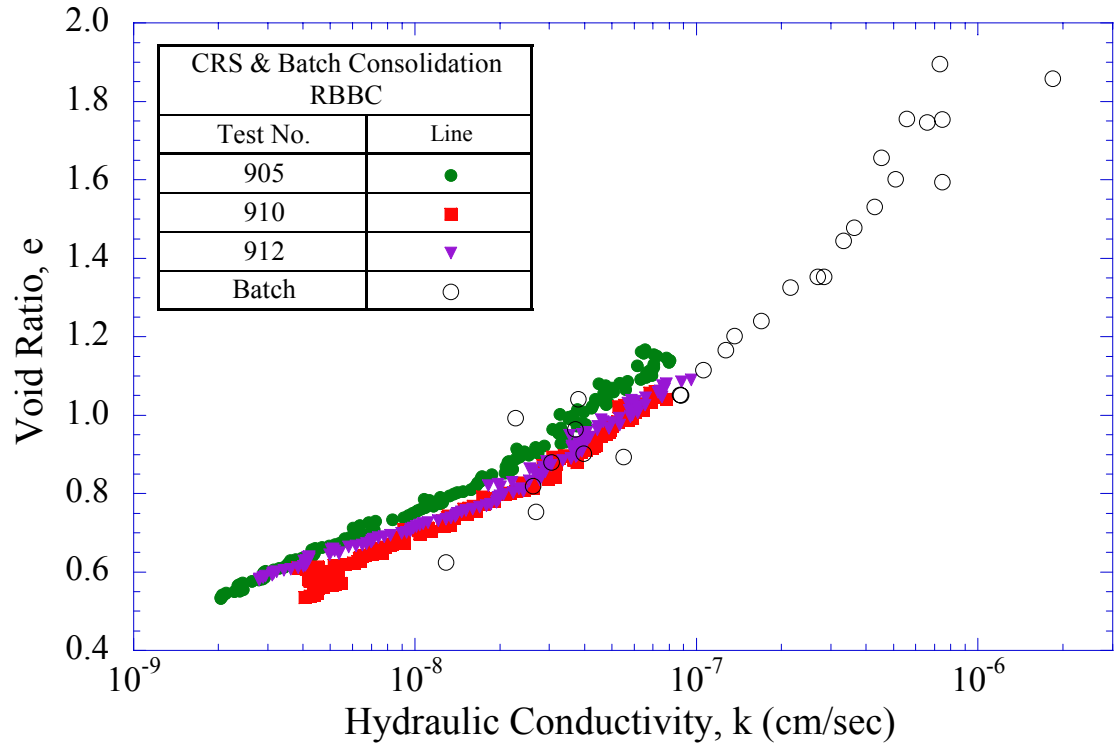

Figure 5-8: Void ratio versus hydraulic conductivity for RBBC from CRS and batch tests

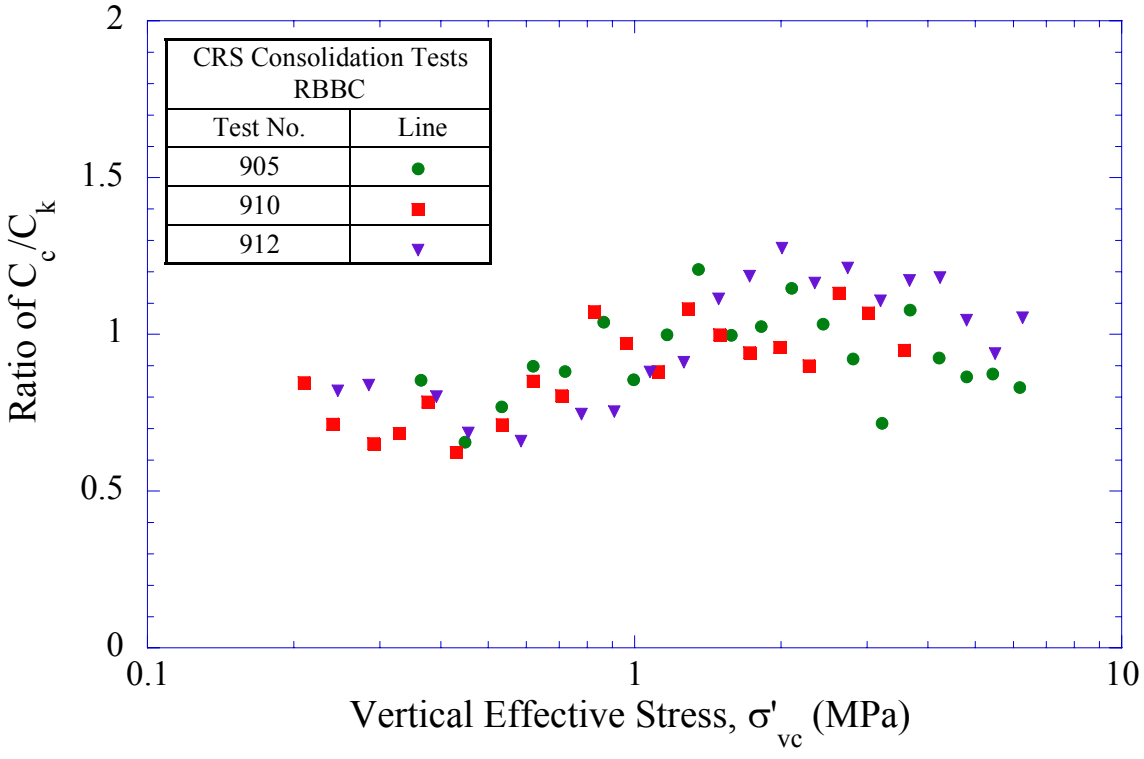

Figure 5-9: Ratio of C_c/C_k versus stress level for RBBC from CRS tests

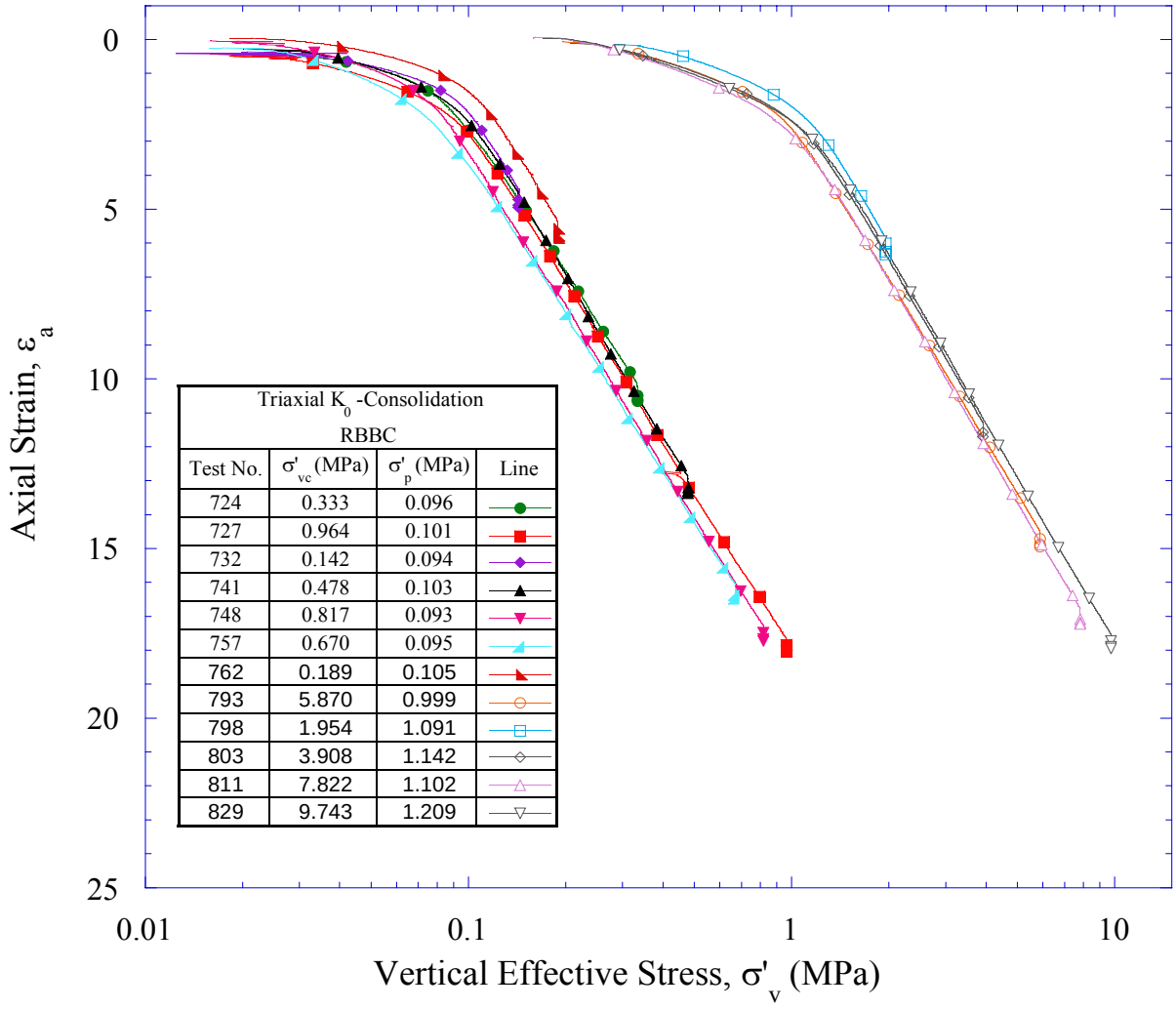

Figure 5-10: 1-D compression behavior in ε_a-logσ'_v space for RBBC from NC triaxial tests

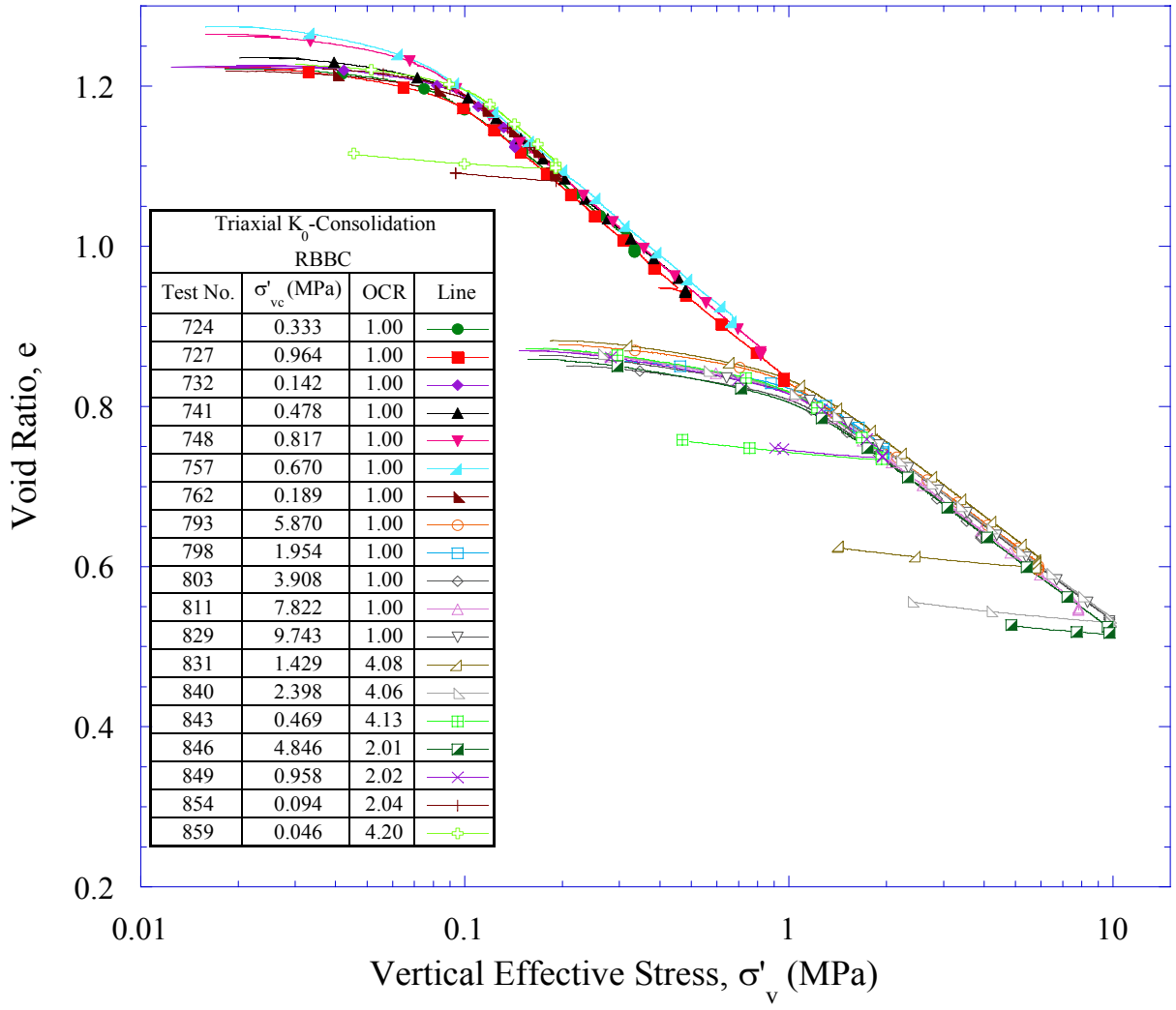

Figure 5-11: 1-D compression behavior in e-logσ'_v space for NC and OC RBBC from all triaxial tests

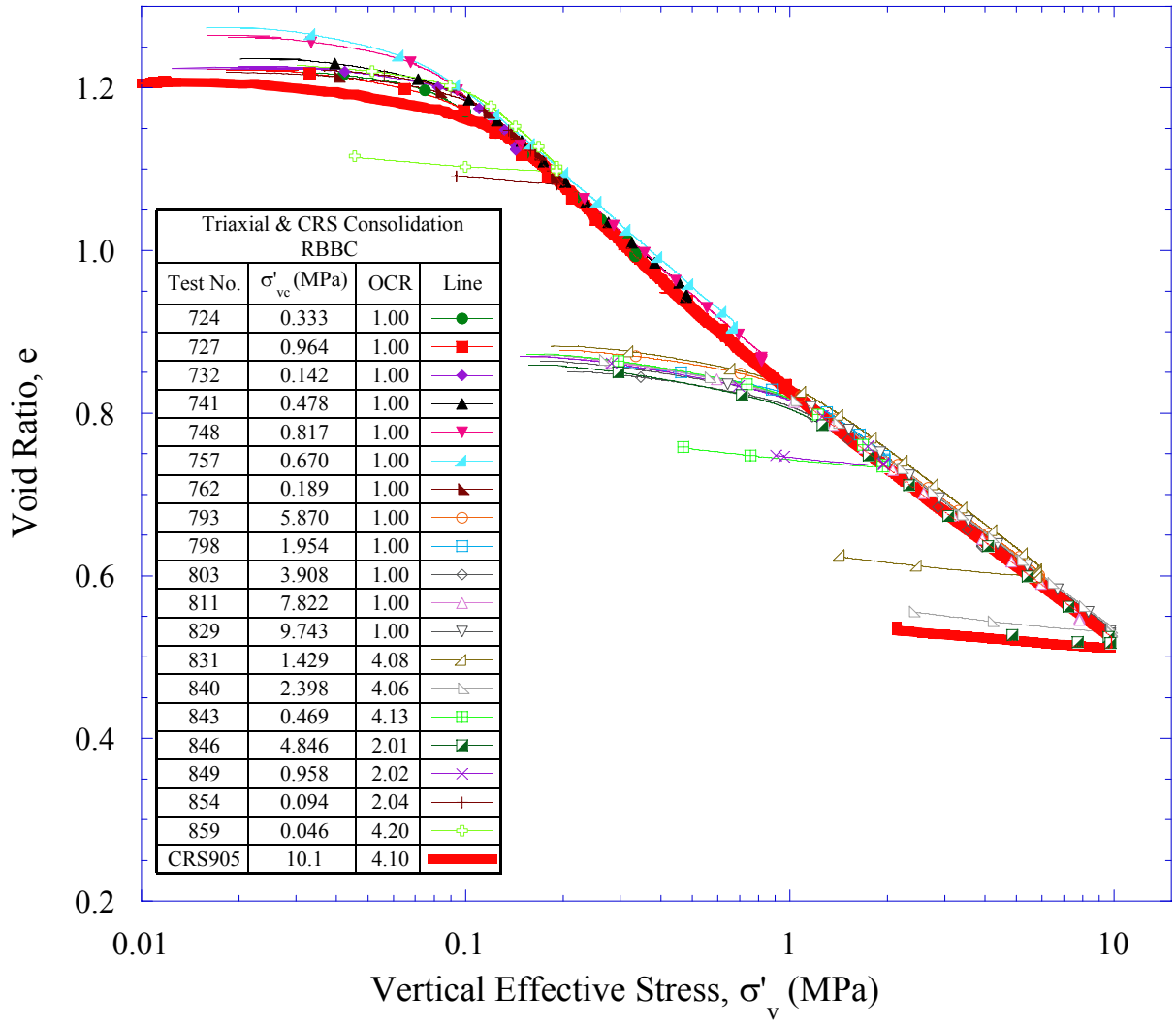

Figure 5-12: 1-D compression behavior in e-logσ'_v space for NC and OC RBBC from all triaxial tests compared with the CRS test

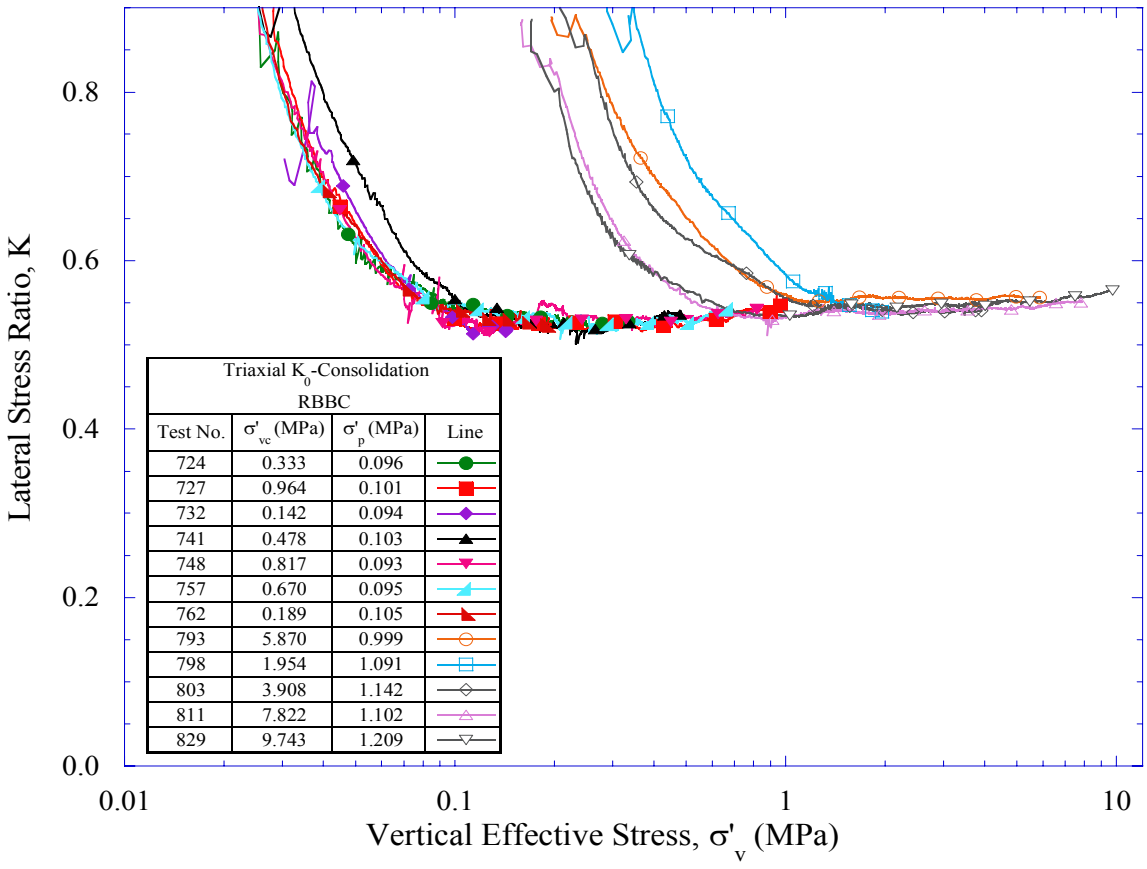

Figure 5-13: Lateral stress ratio versus stress level for RBBC from NC triaxial tests

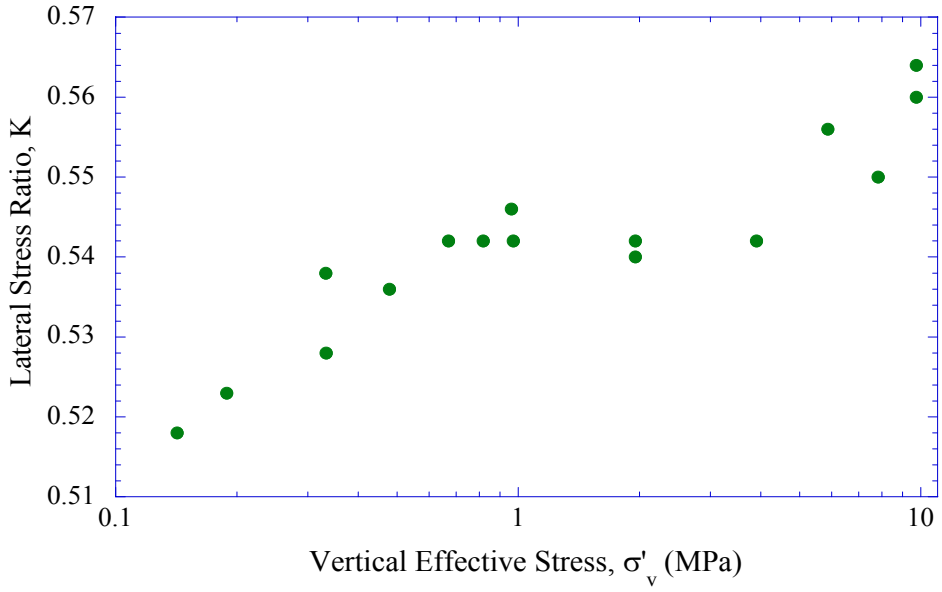

Figure 5-14: Lateral stress ratio at the end of virgin consolidation versus stress level for RBBC from NC triaxial tests

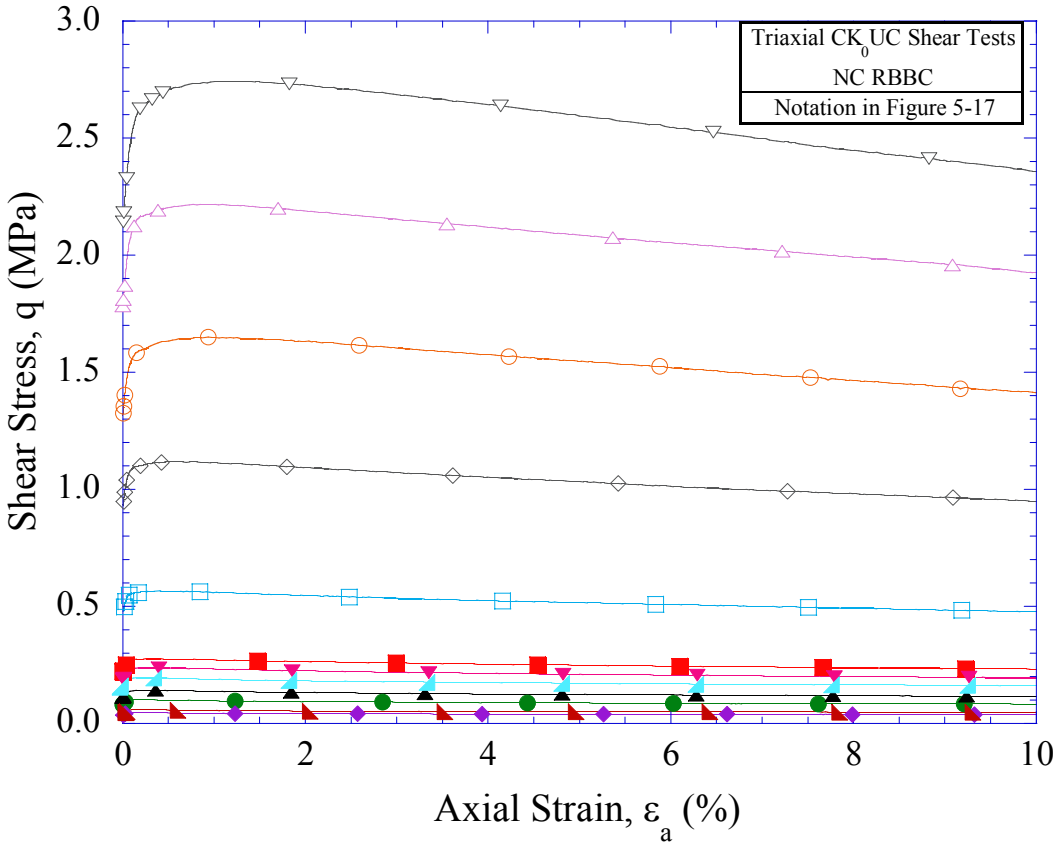

Figure 5-15: Stress-strain curves for NC RBBC from CK_0UC triaxial tests

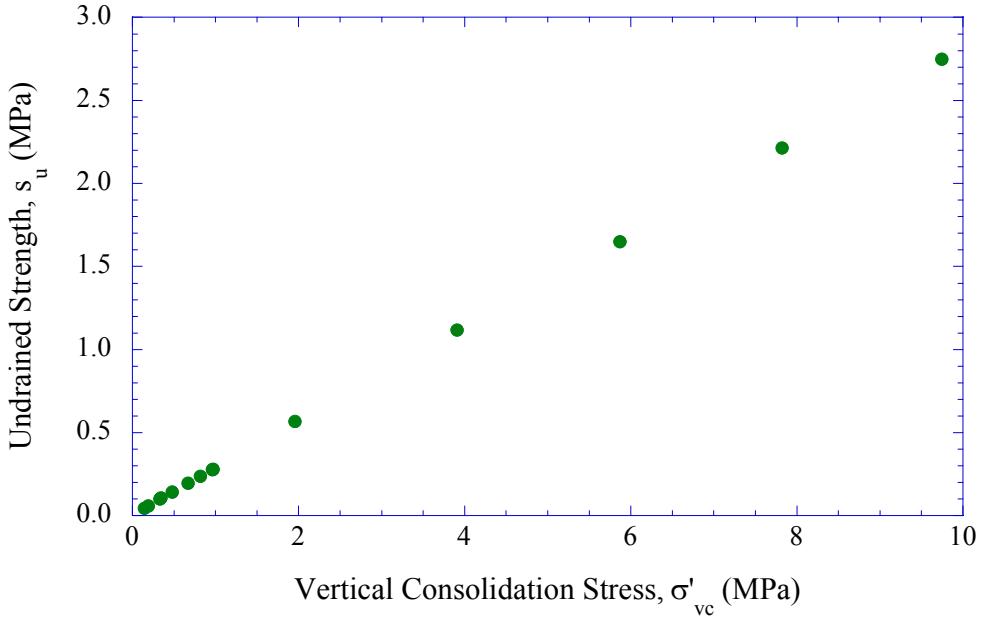

Figure 5-16: Undrained shear strength versus stress level for NC RBBC from CK_0UC triaxial tests

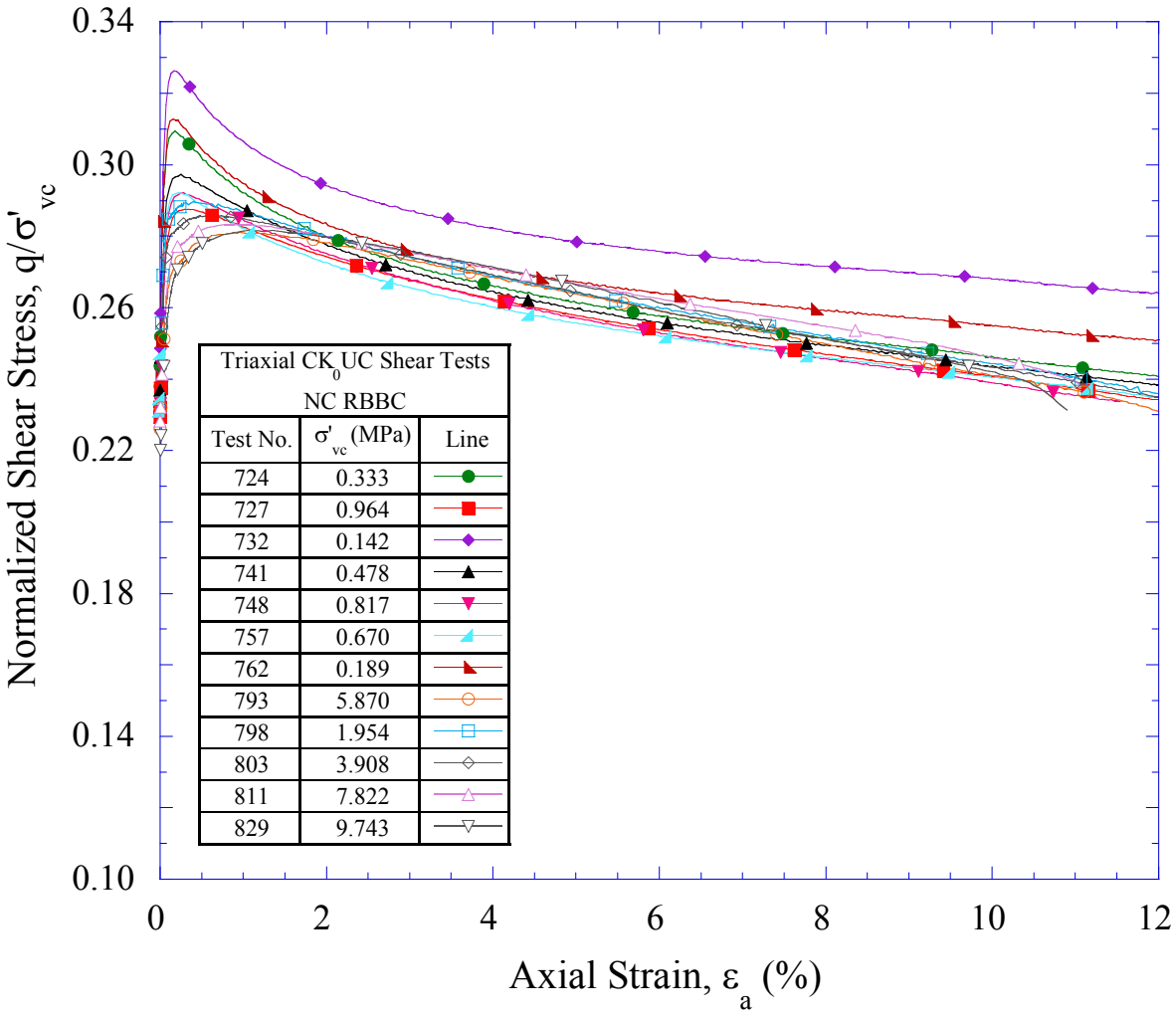

Figure 5-17: Normalized stress-strain curves for NC RBBC from CK_0UC triaxial tests

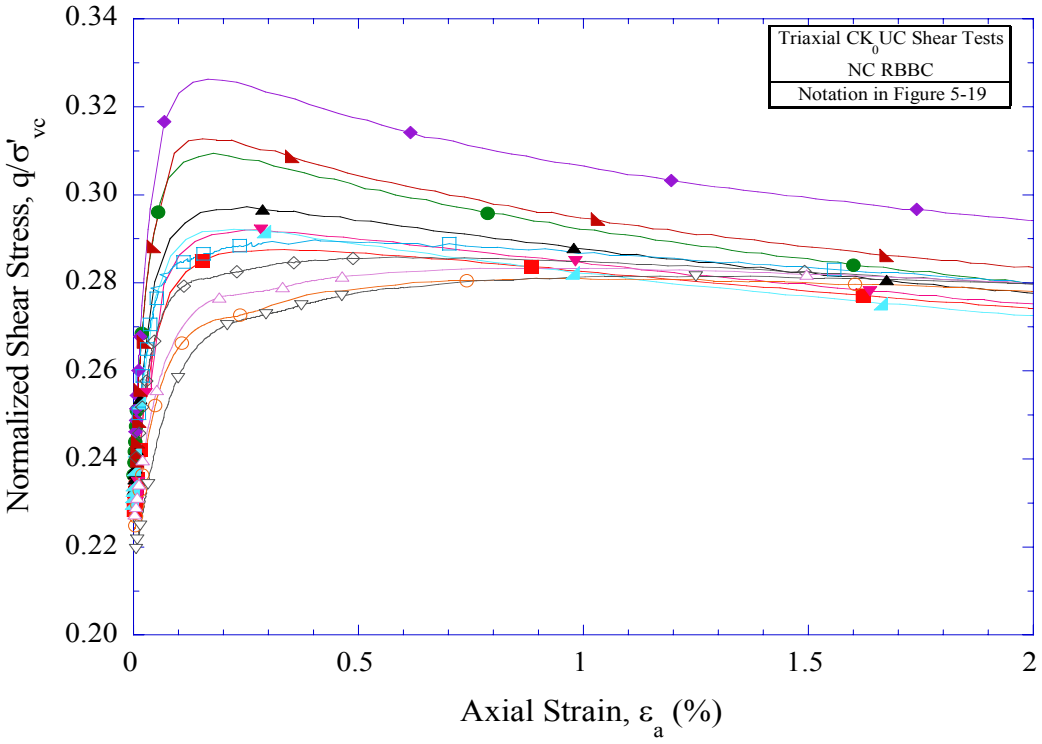

Figure 5-18: Normalized stress-strain curves (small strains) for NC RBBC from CK_0UC triaxial tests

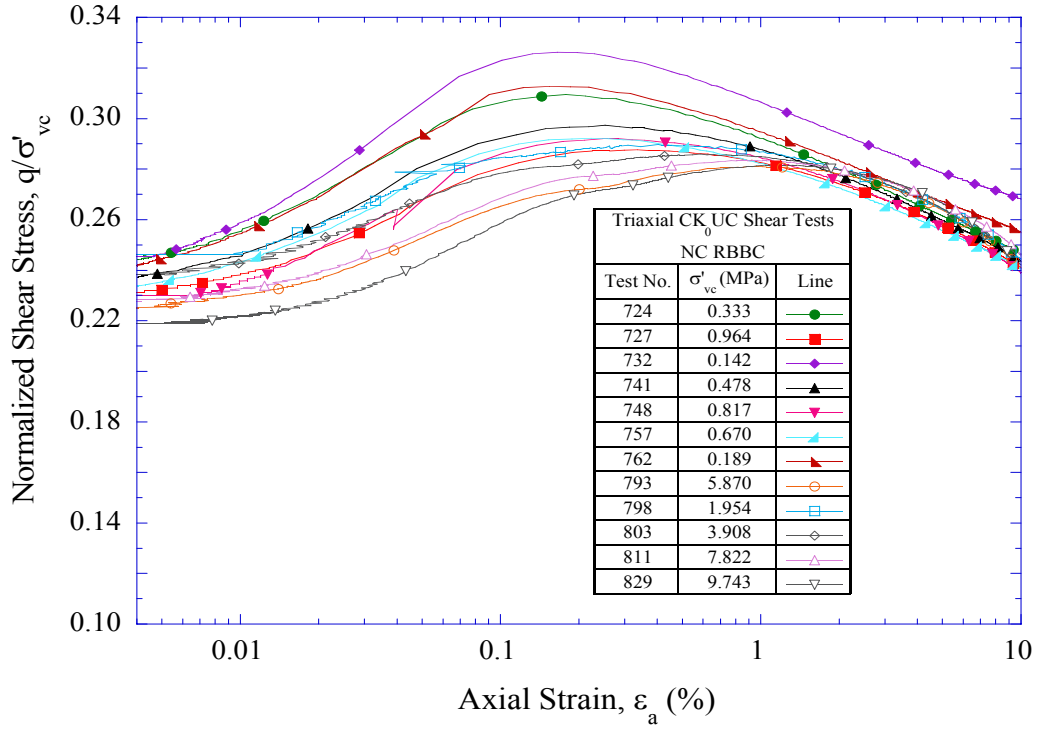

Figure 5-19: Normalized stress-(log) strain curves for NC RBBC from CK_0UC triaxial tests

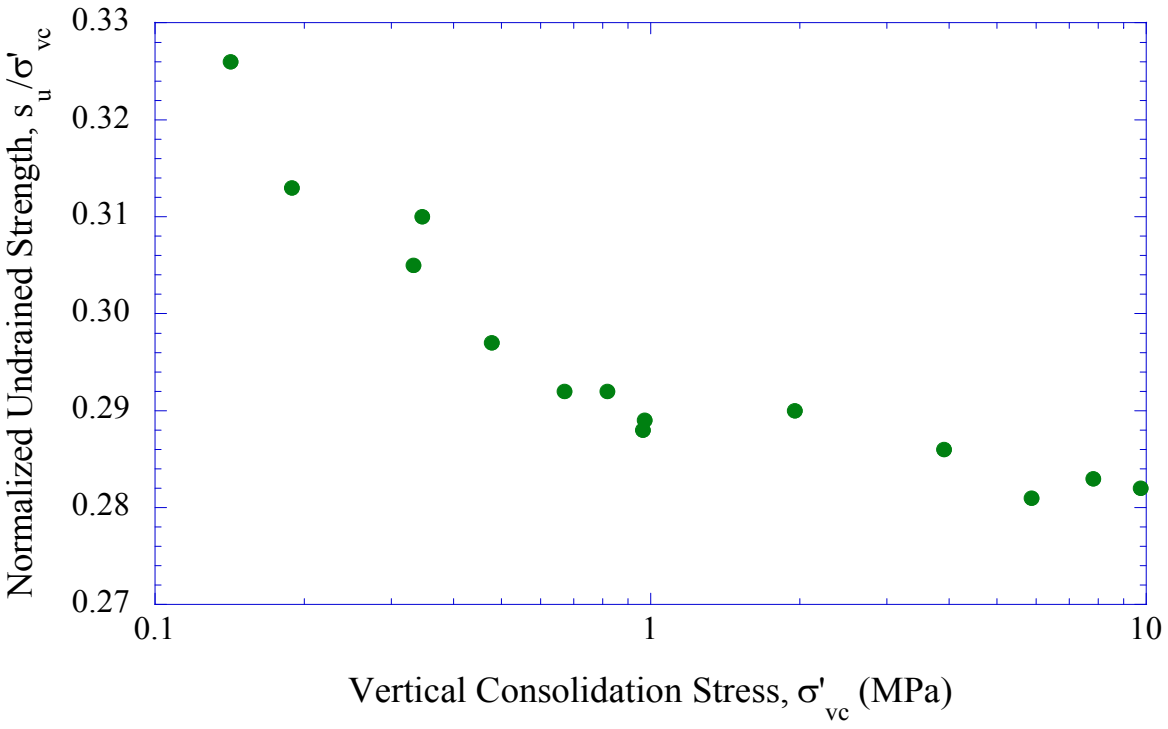

Figure 5-20: Normalized undrained shear strength versus stress level for NC RBBC from CK_0UC triaxial tests

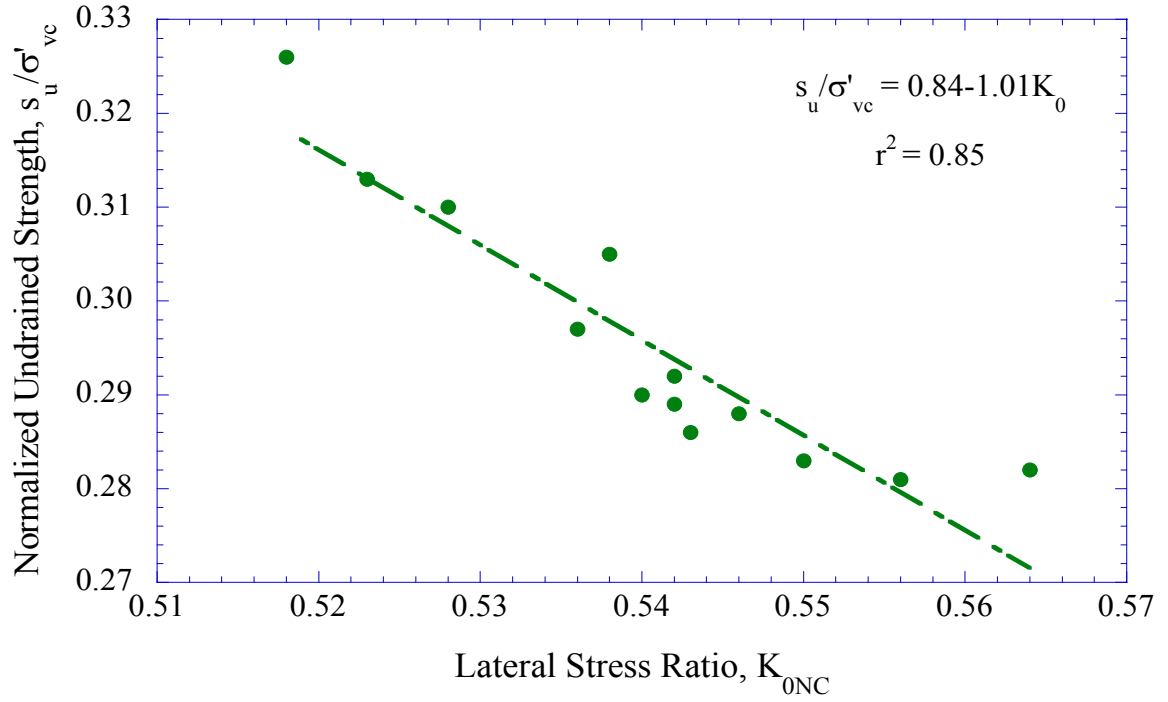

Figure 5-21: Normalized undrained shear strength versus lateral stress ratio for NC RBBC from CK_0UC triaxial tests

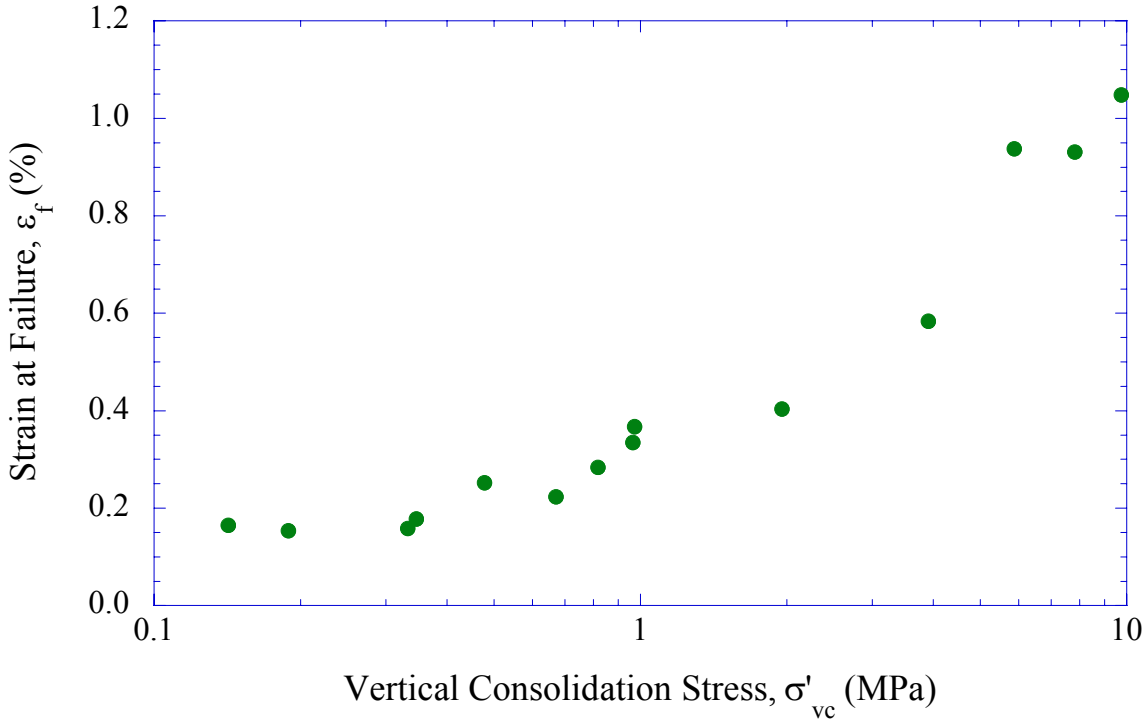

Figure 5-22: Strain at failure versus stress level for NC RBBC from CK_0UC triaxial tests

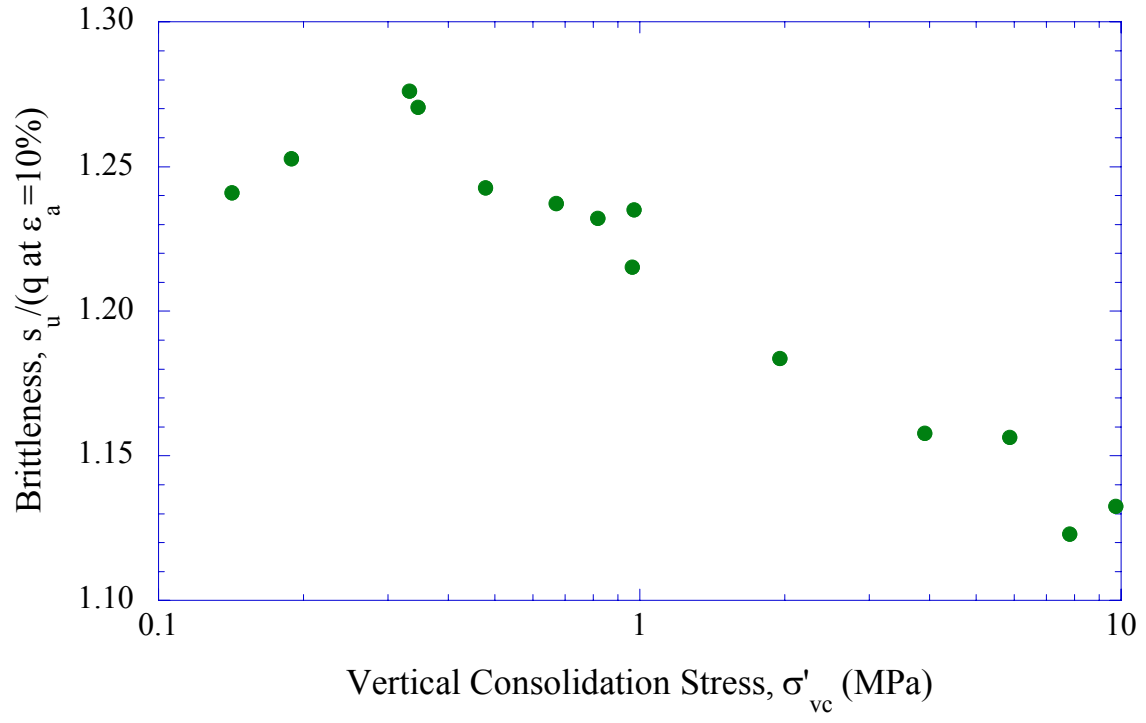

Figure 5-23: Brittleness versus stress level for NC RBBC from CK_0UC triaxial tests

Figure 5-24: A picture of NC RBBC specimens after CK_0UC triaxial testing showing bulging mode of failure for low pressure test (left) and slip surface for high pressure test (right)

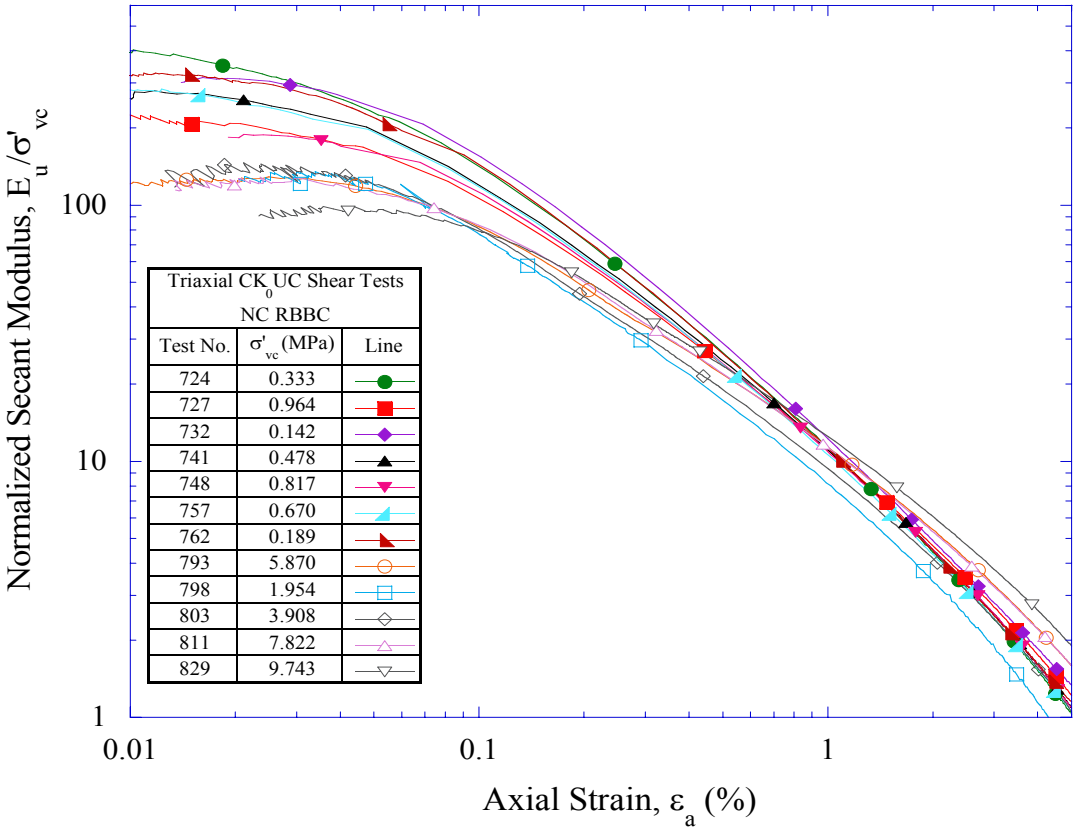

Figure 5-25: Normalized undrained secant modulus versus axial strain for NC RBBC from CK_0UC triaxial tests

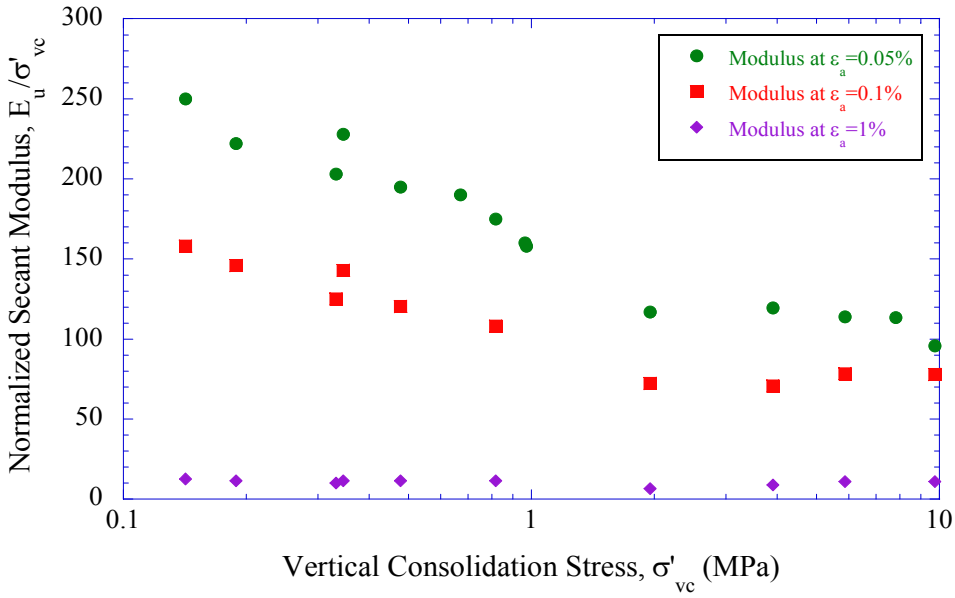

Figure 5-26: Normalized undrained secant modulus versus stress level for NC RBBC from CK_0UC triaxial tests

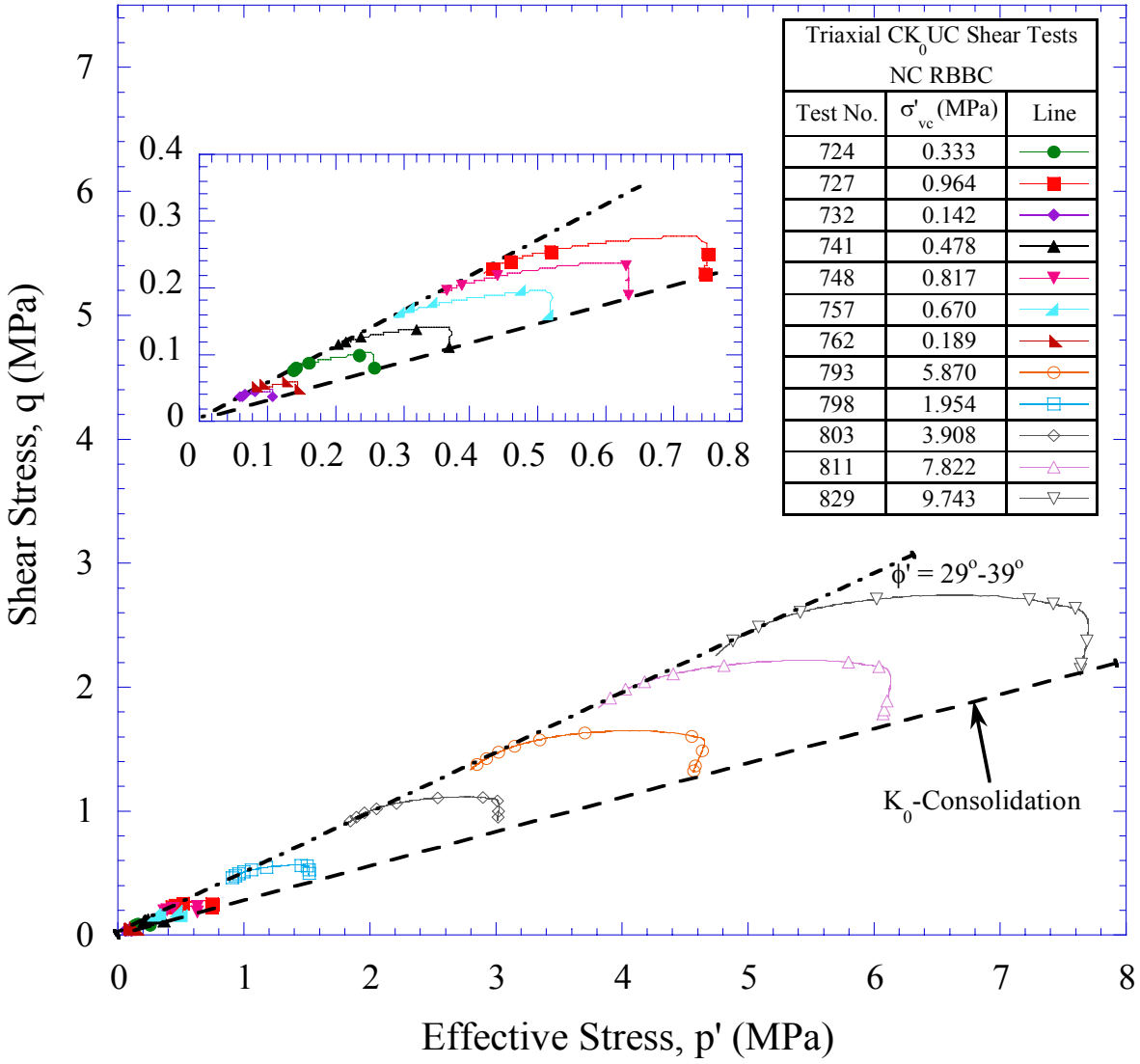

Figure 5-27: Effective stress paths for NC RBBC from CK_0UC triaxial tests

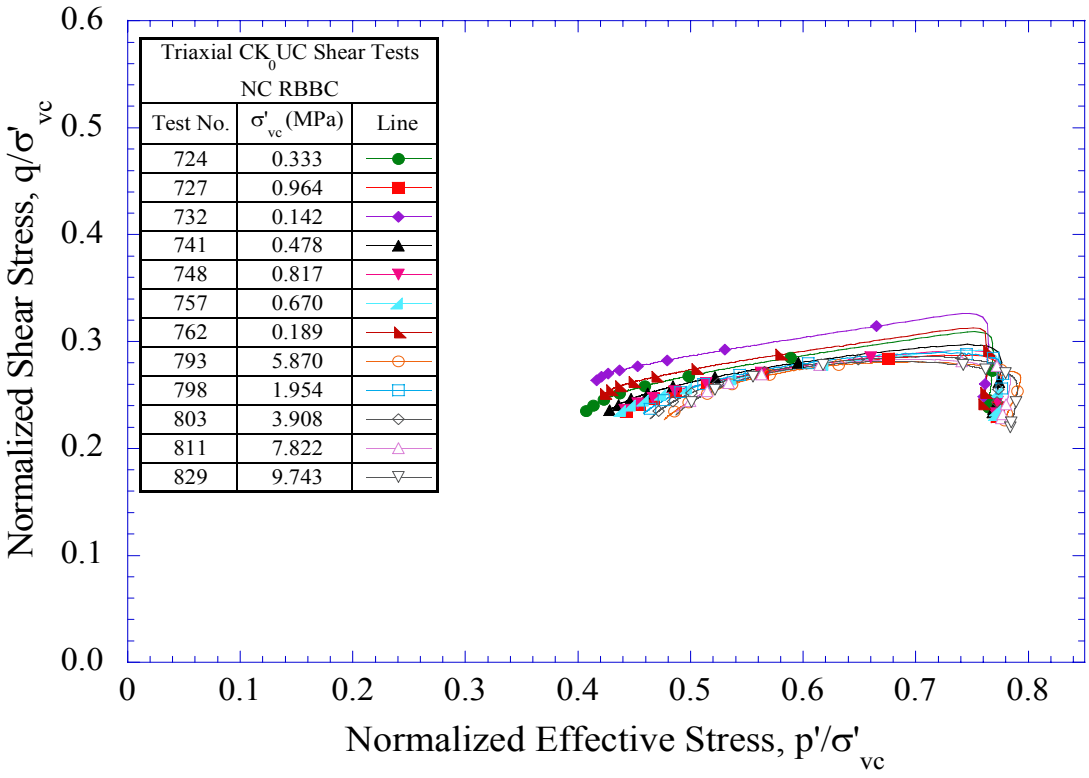

Figure 5-28: Normalized effective stress paths for NC RBBC from CK_0UC triaxial tests

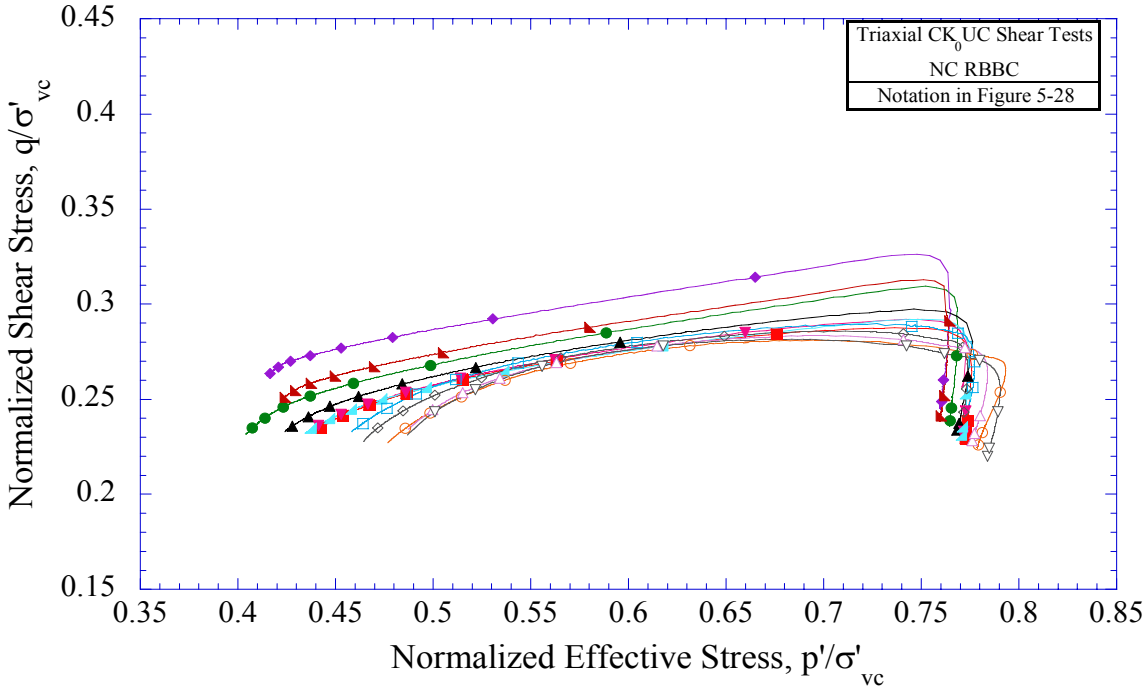

Figure 5-29: Normalized effective stress paths (close up view) for NC RBBC from CK_0UC triaxial tests

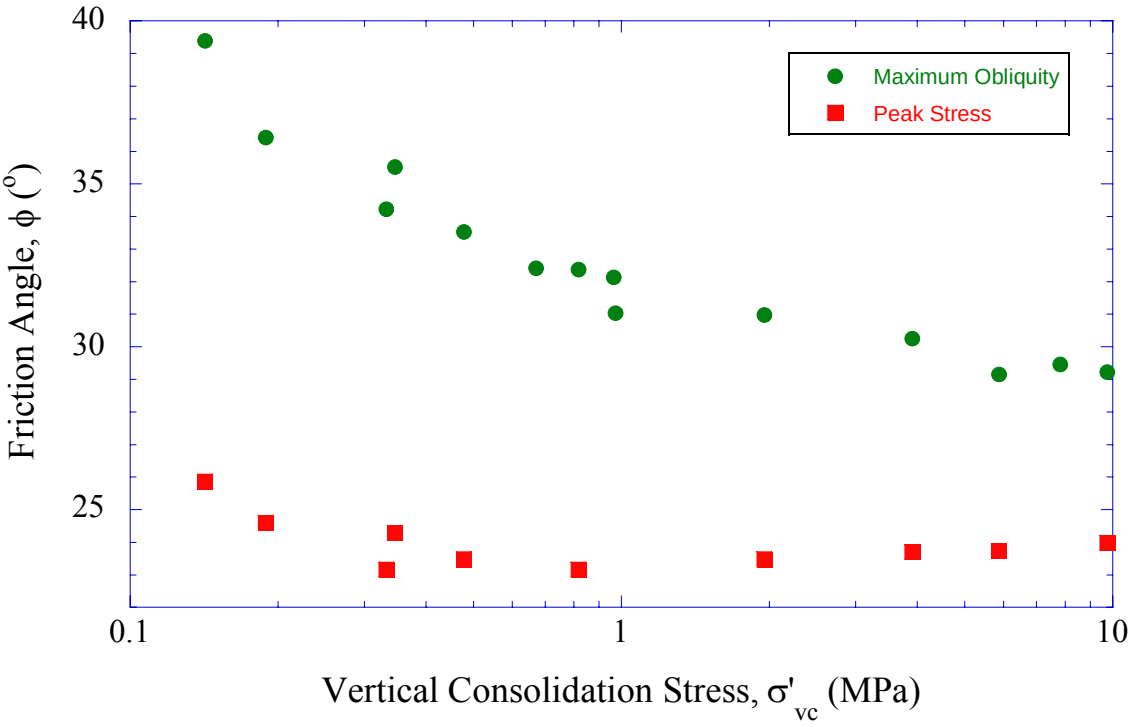

Figure 5-30: Friction angle at peak and maximum obliquity versus stress level for NC RBBC from CK_0UC triaxial tests

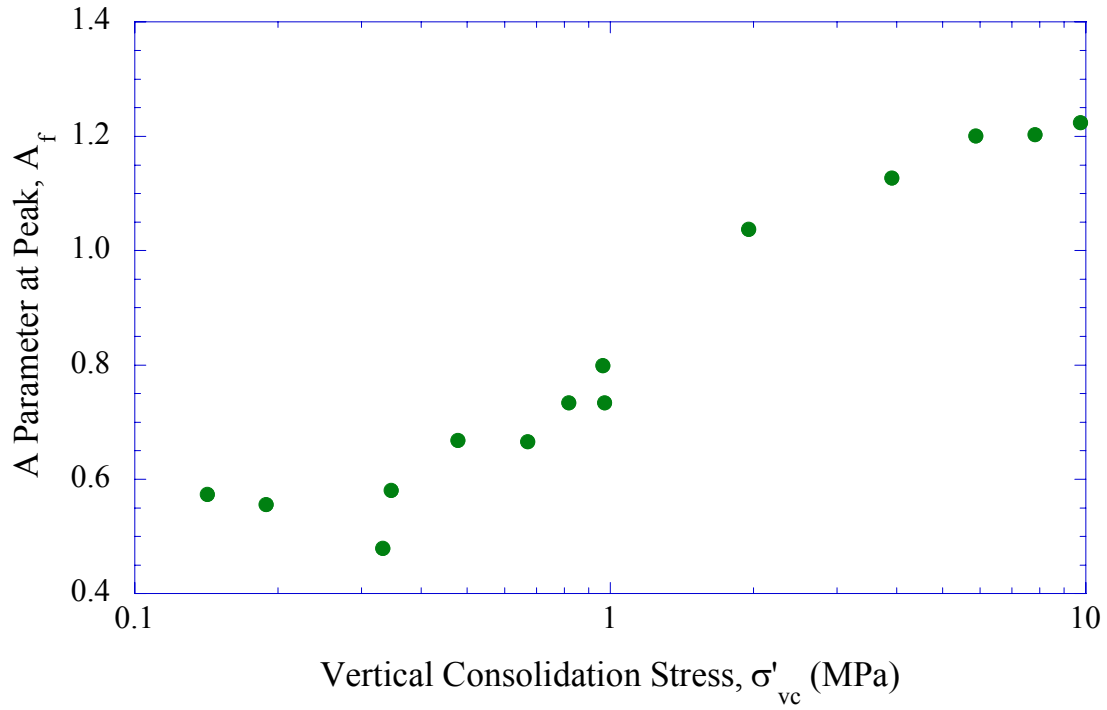

Figure 5-31: Skempton A parameter at peak versus stress level for NC RBBC from CK_0UC triaxial tests

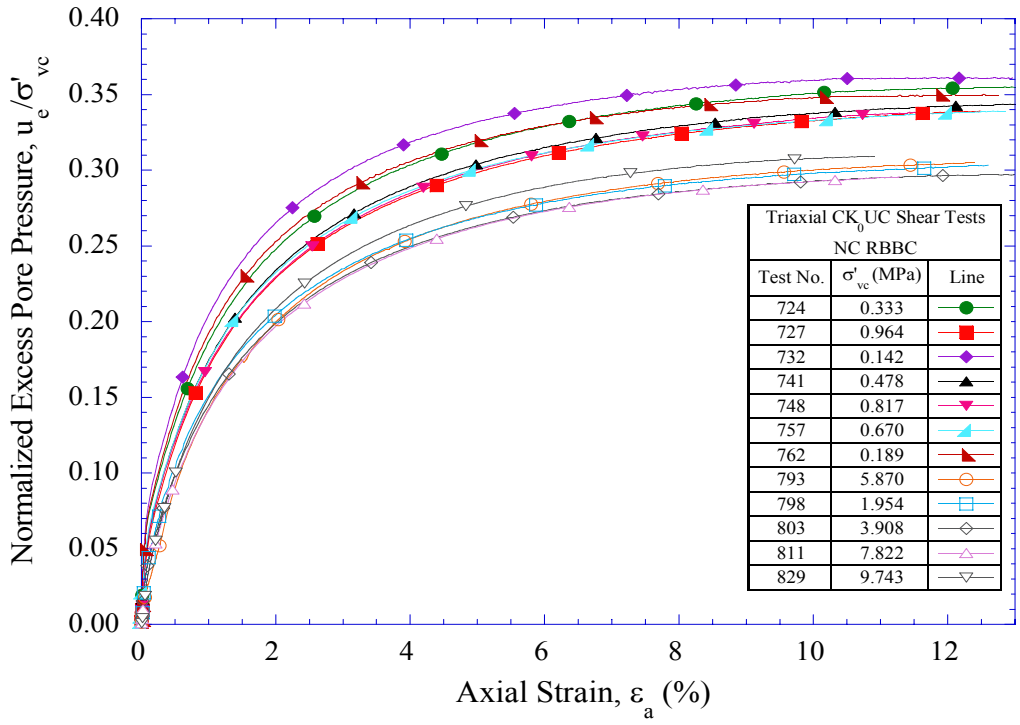

Figure 5-32: Normalized excess pore pressure versus strain for NC RBBC from CK_0UC triaxial tests

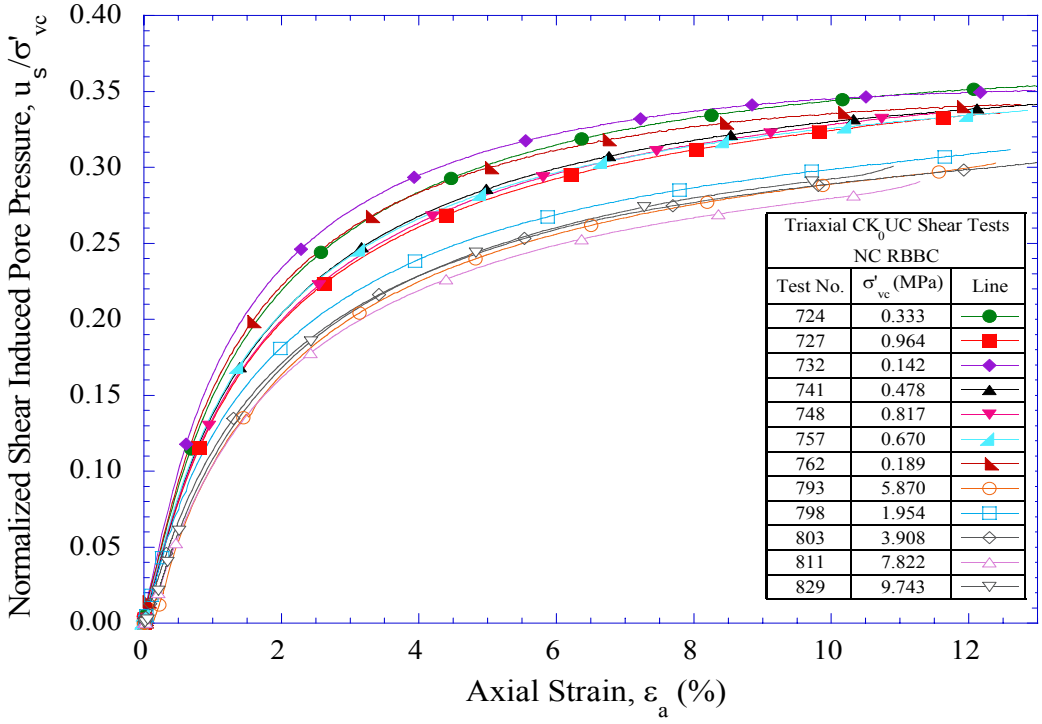

Figure 5-33: Normalized shear induced pore pressure versus strain for NC RBBC from CK_0UC triaxial tests

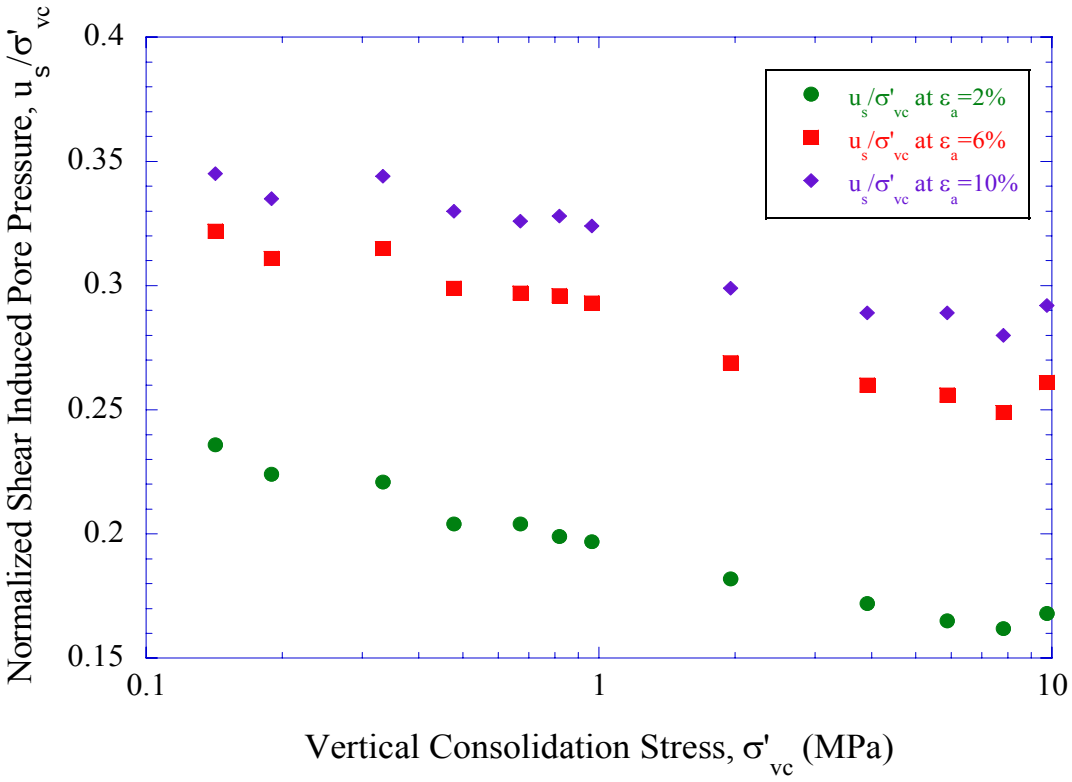

Figure 5-34: Normalized shear induced pore pressure versus stress level for NC RBBC from CK_0UC triaxial tests

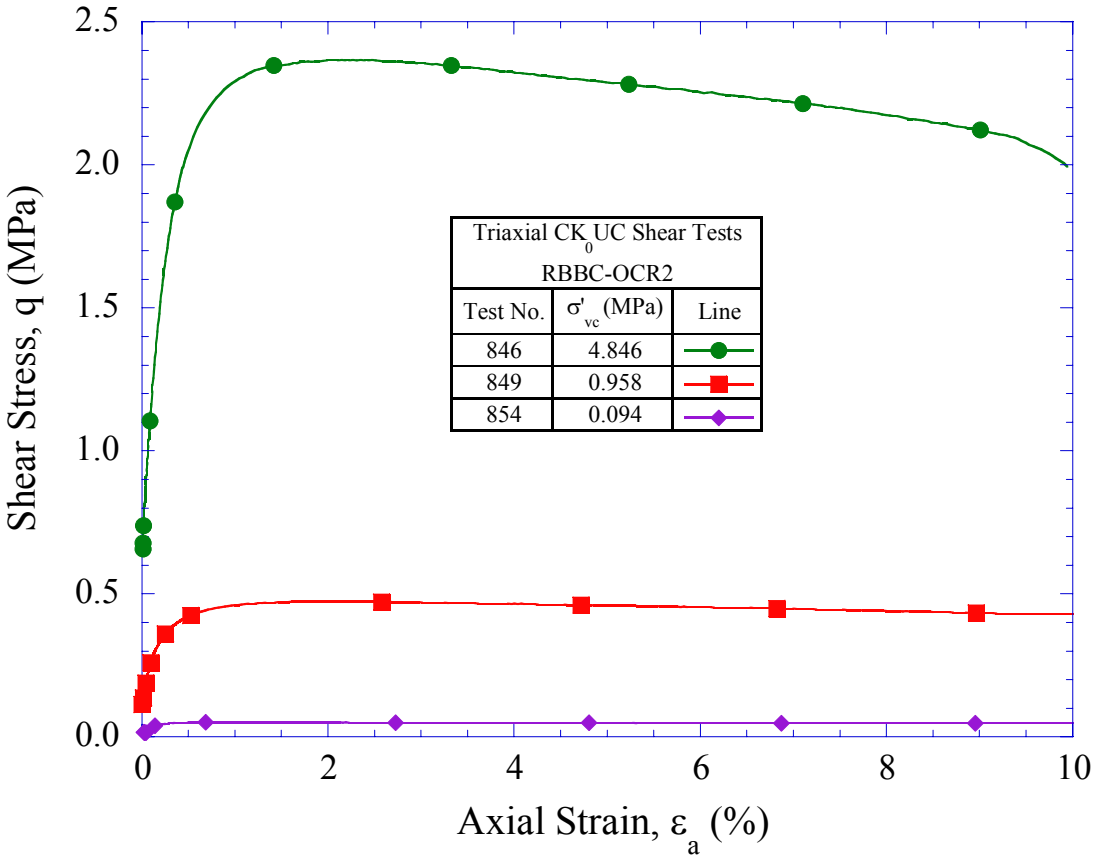

Figure 5-35: Stress-strain curves for OCR=2 RBBC from CK_0UC triaxial tests

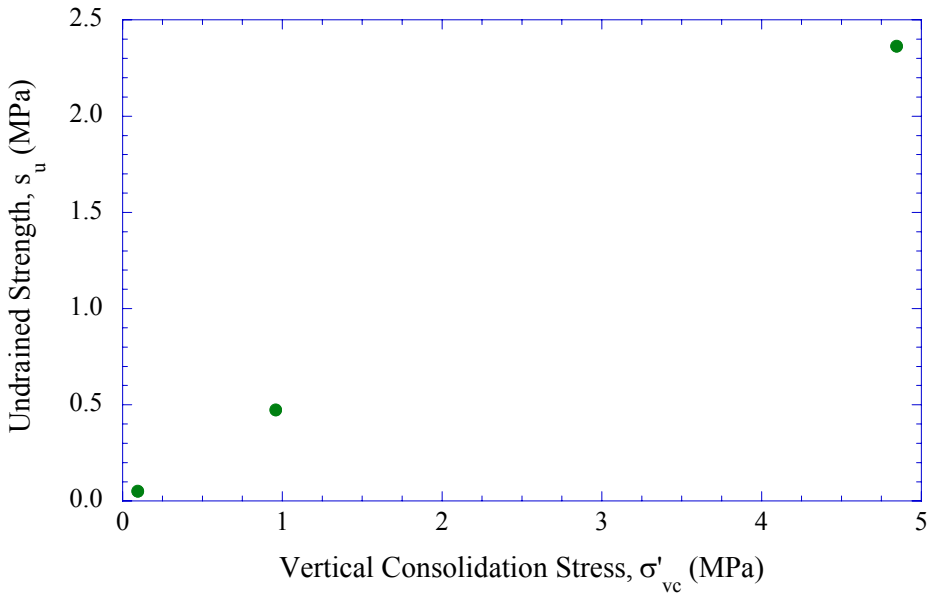

Figure 5-36: Undrained shear strength versus stress level for OCR=2 RBBC from CK_0UC triaxial tests

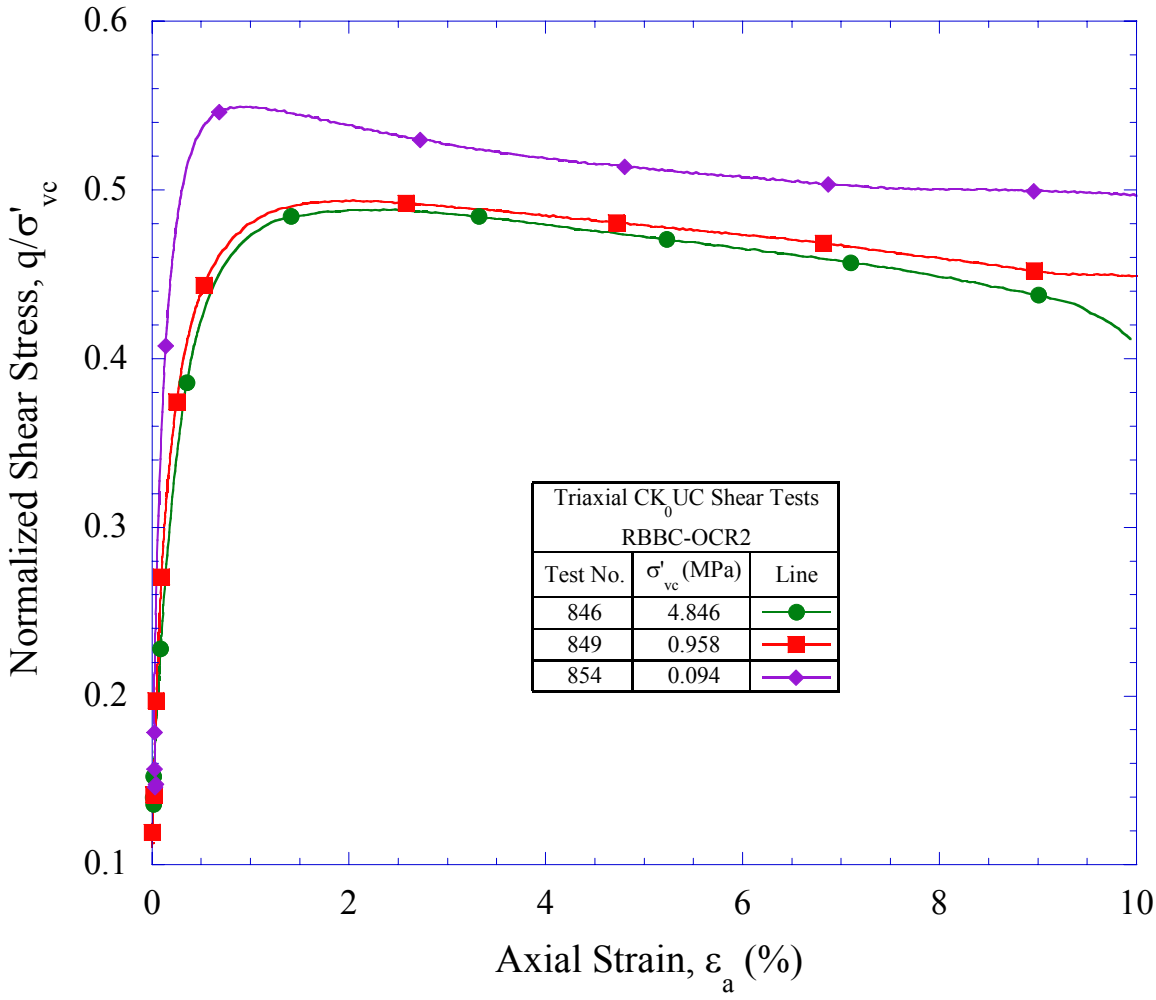

Figure 5-37: Normalized stress-strain curves for OCR=2 RBBC from CK_0UC triaxial tests

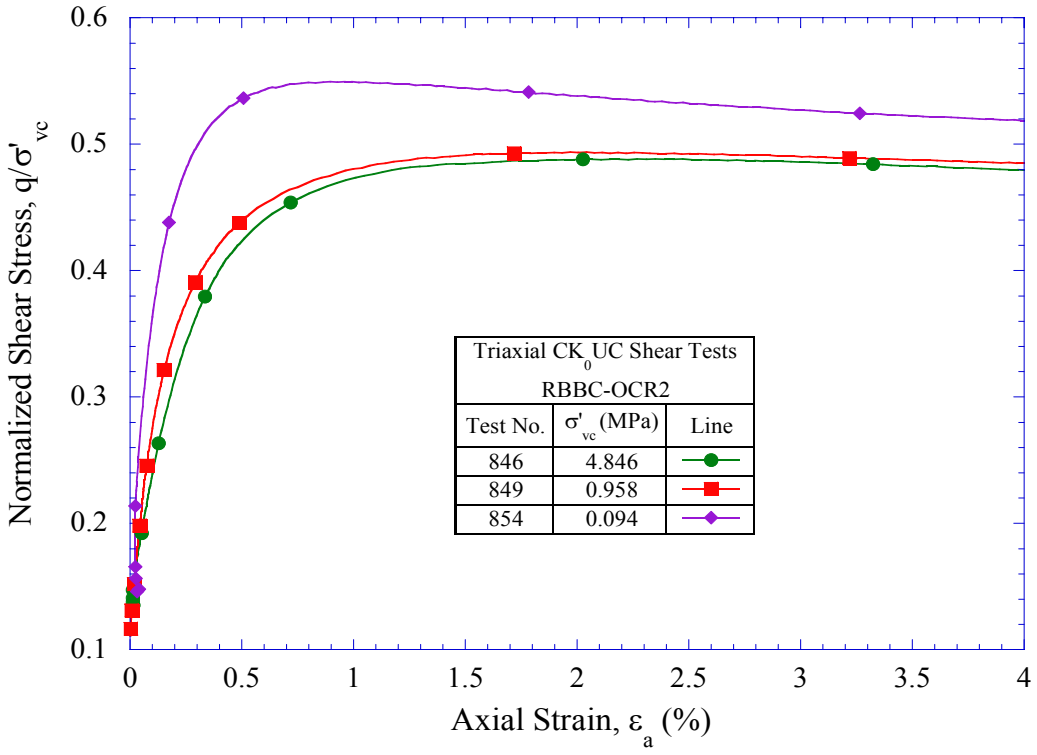

Figure 5-38: Normalized stress-strain curves (up to 4%) for OCR=2 RBBC from CK_0UC triaxial tests

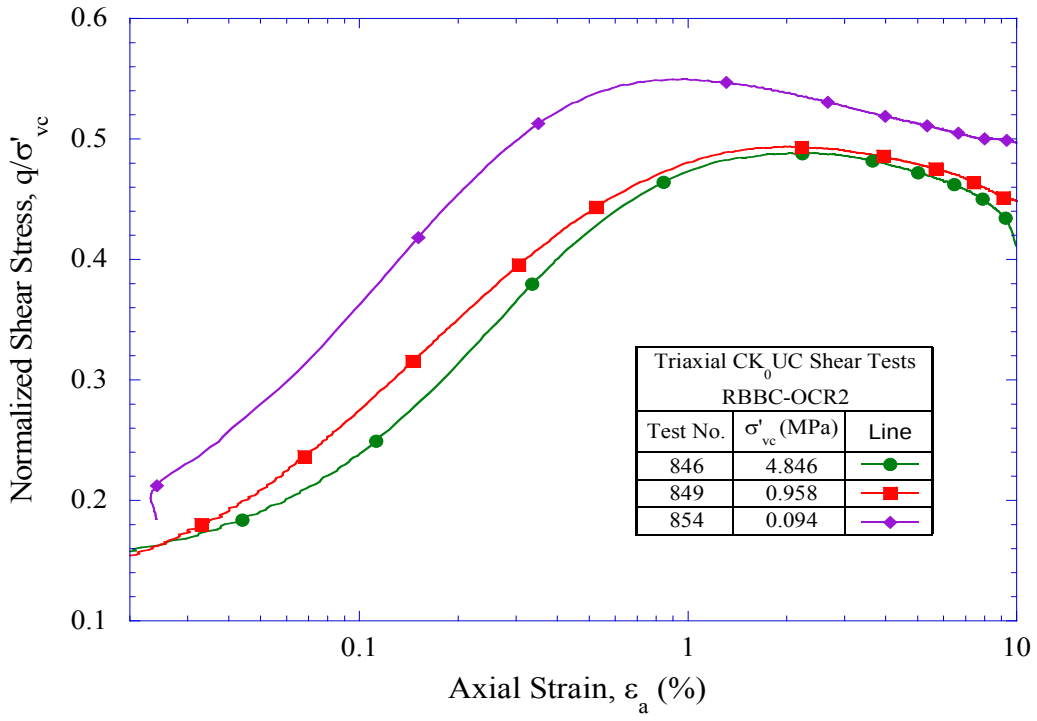

Figure 5-39: Normalized stress-(log) strain curves for OCR=2 RBBC from CK_0UC triaxial tests

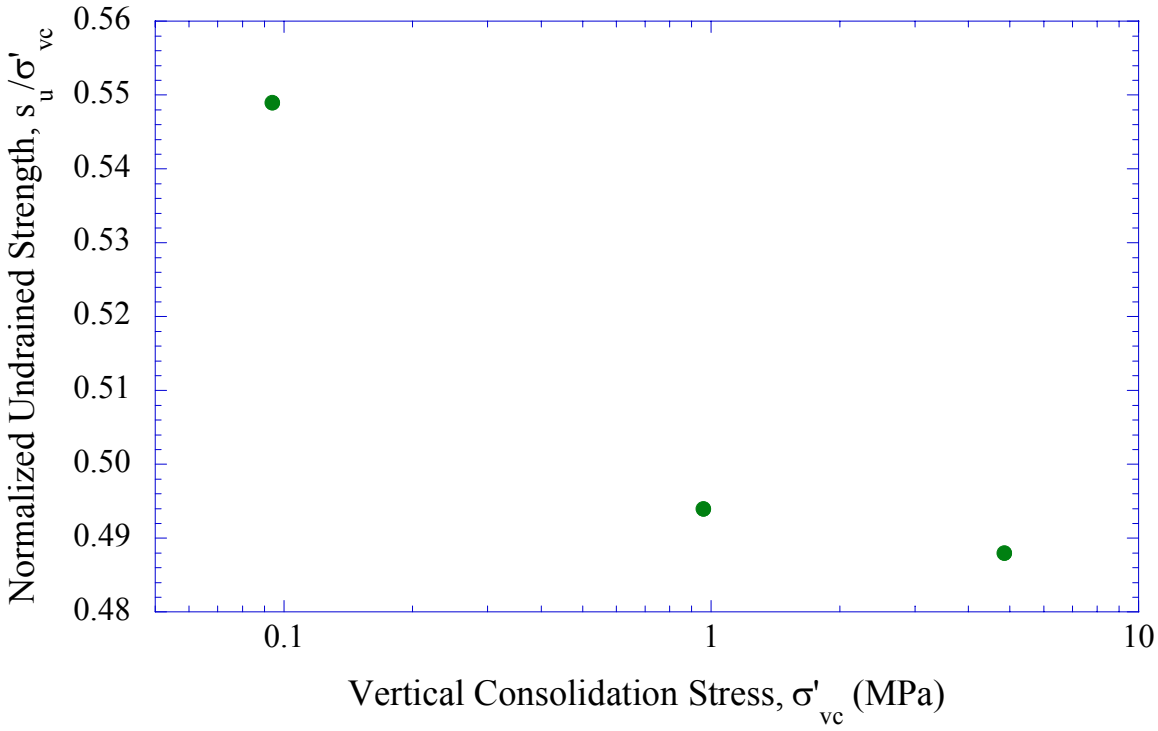

Figure 5-40: Normalized undrained shear strength versus stress level for OCR=2 RBBC from CK_0UC triaxial tests

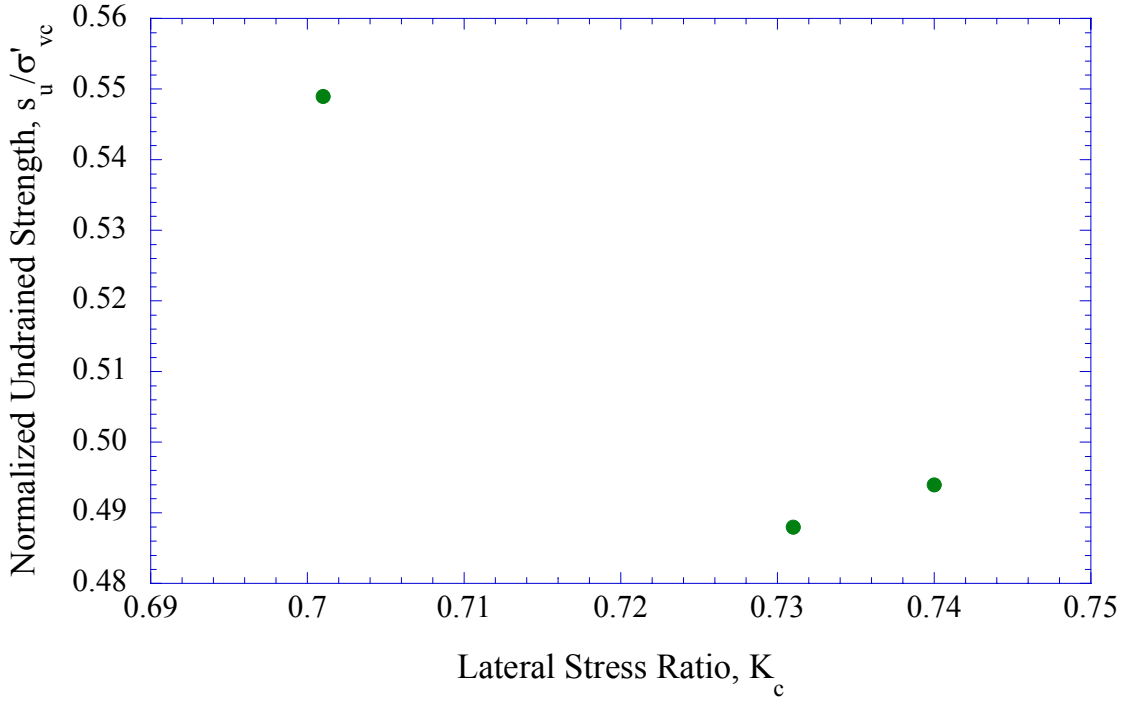

Figure 5-41: Normalized undrained shear strength versus lateral stress ratio for OCR=2 RBBC from CK_0UC triaxial tests

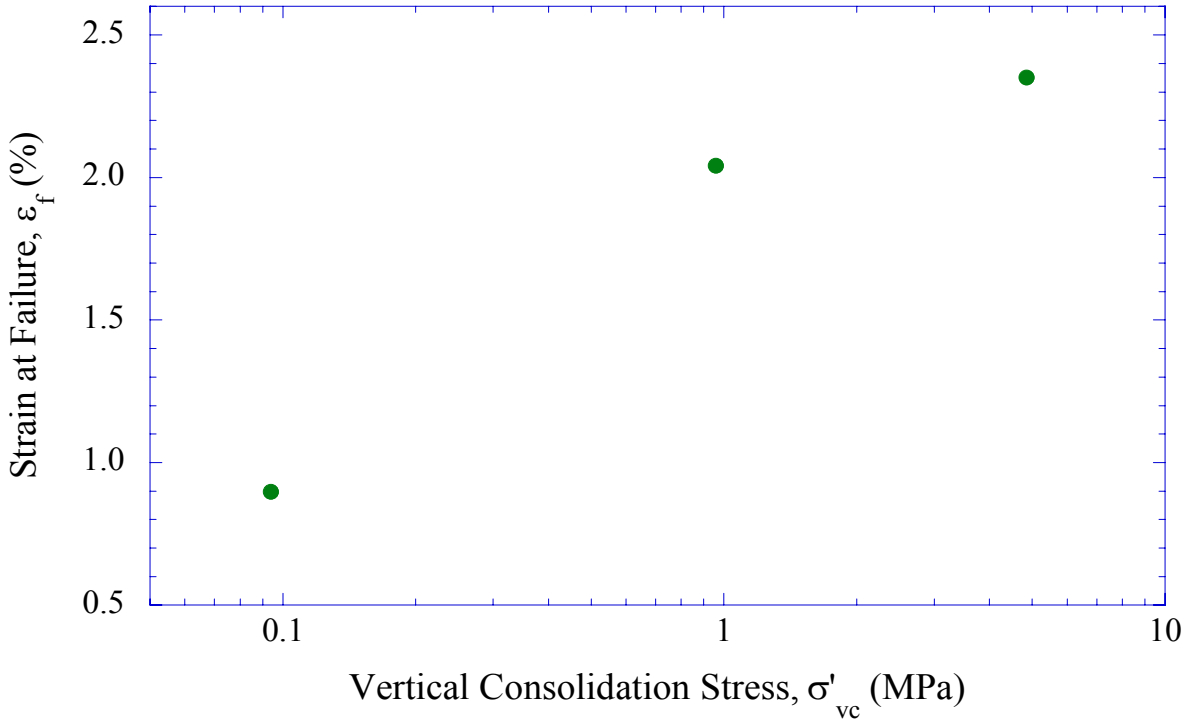

Figure 5-42: Strain at failure versus stress level for OCR=2 RBBC from CK_0UC triaxial tests

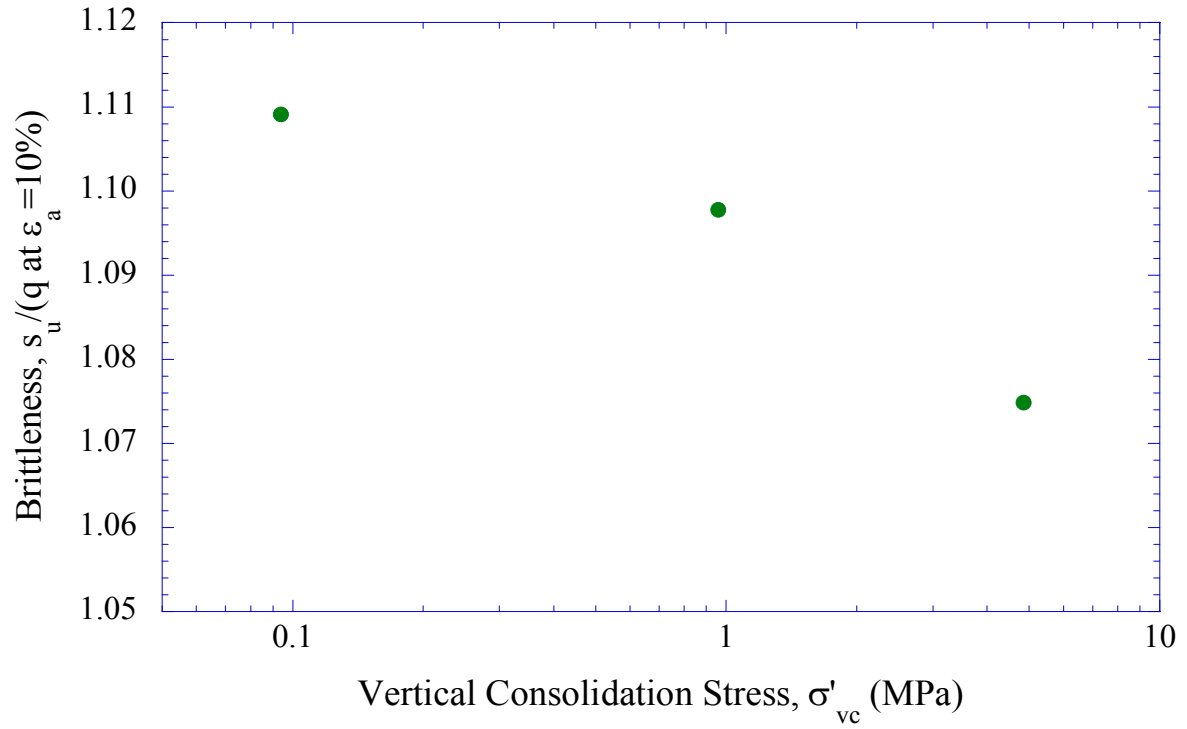

Figure 5-43: Brittleness versus stress level for OCR=2 RBBC from CK_0UC triaxial tests

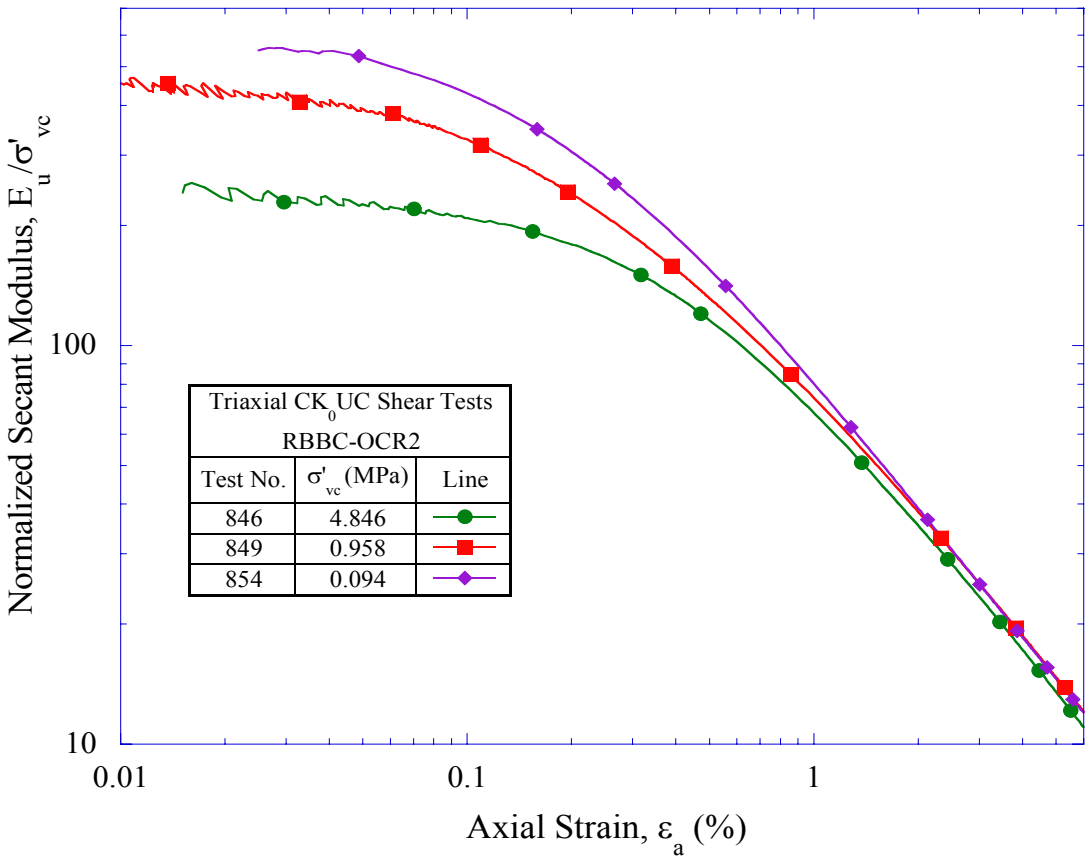

Figure 5-44: Normalized undrained secant modulus versus axial strain for OCR=2 RBBC from CK_0UC triaxial tests

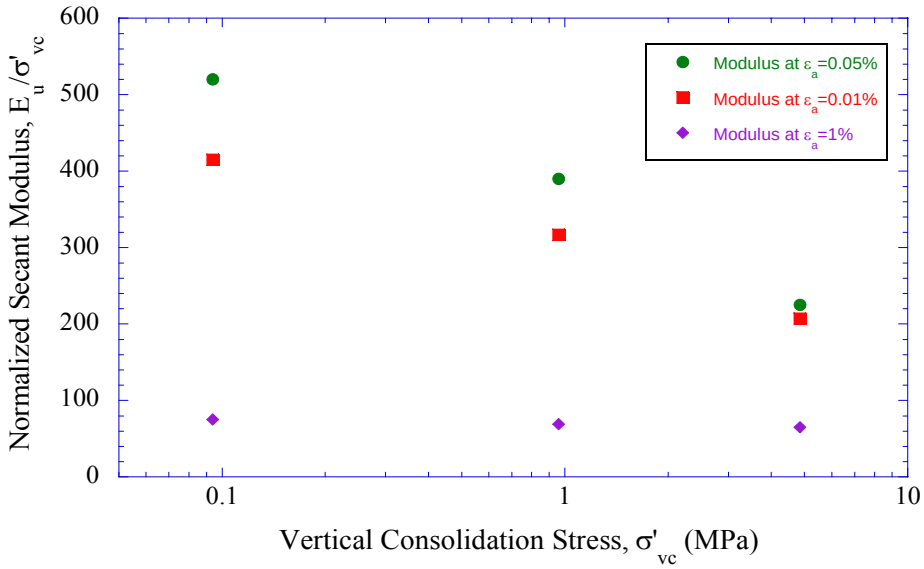

Figure 5-45: Normalized undrained secant modulus versus stress level for OCR=2 RBBC from CK_0UC triaxial tests

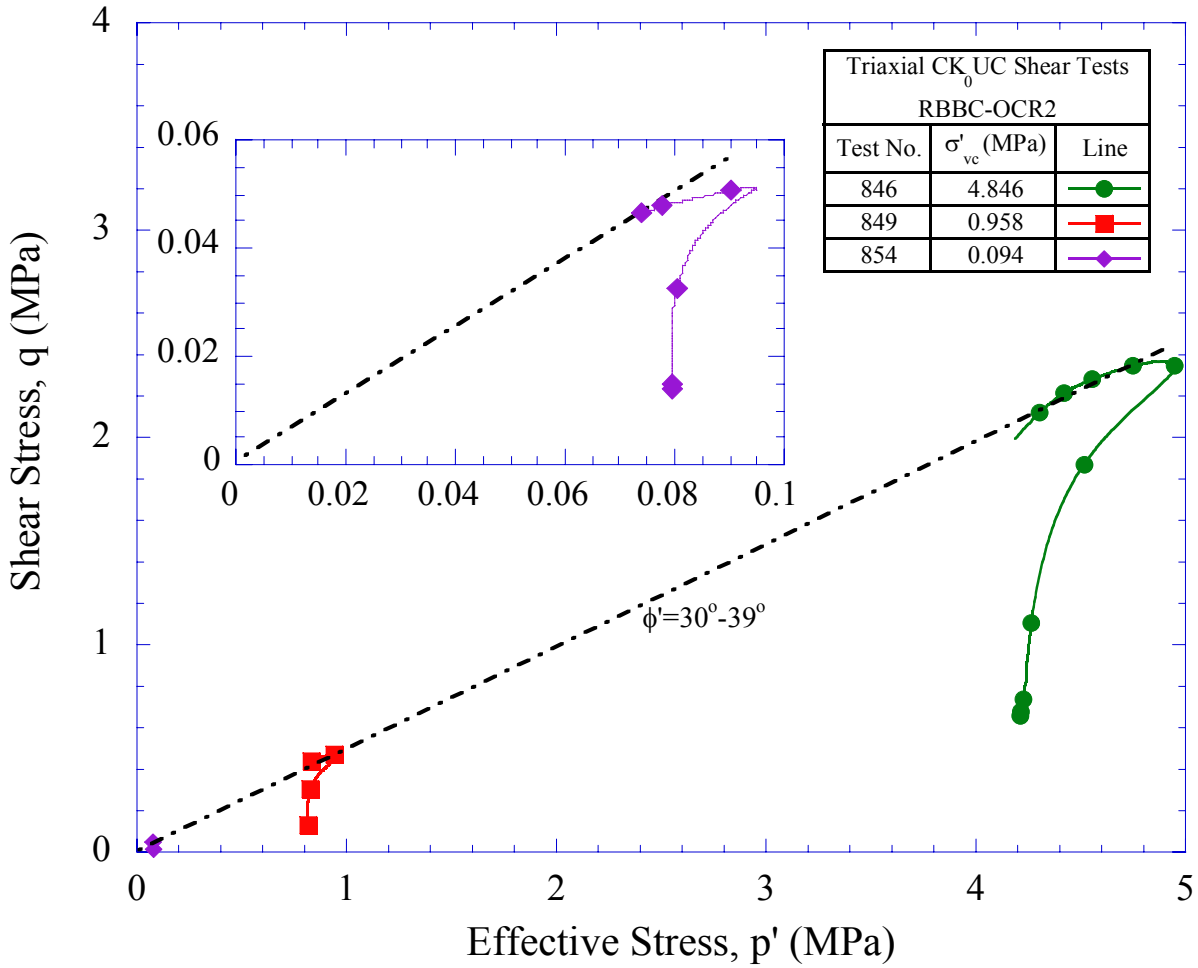

Figure 5-46: Effective stress paths for OCR=2 RBBC from CK_0UC triaxial tests

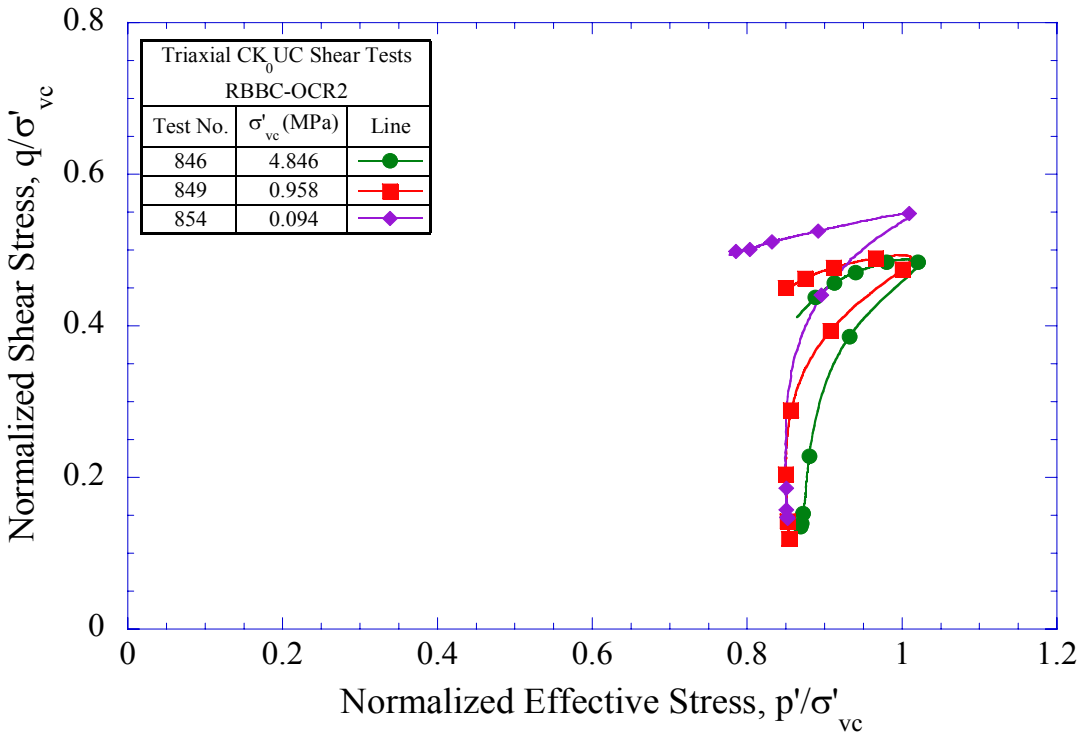

Figure 5-47: Normalized effective stress paths for OCR=2 RBBC from CK_0UC triaxial tests

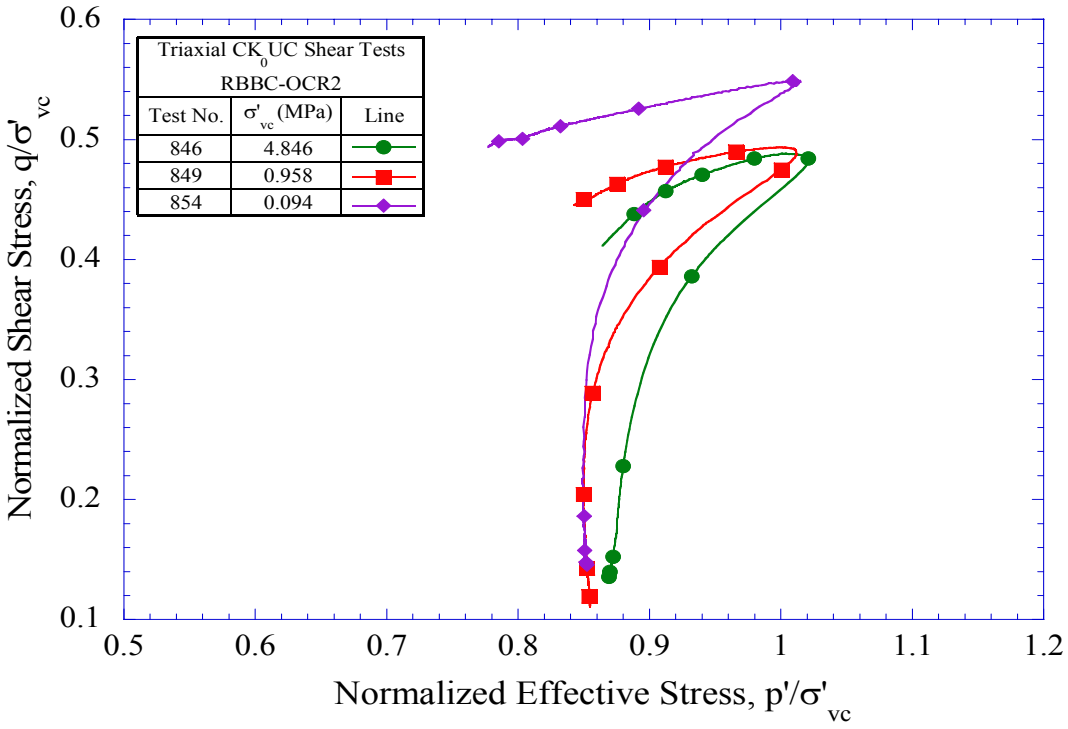

Figure 5-48: Normalized effective stress paths (close up view) for OCR=2 RBBC from CK_0UC triaxial tests

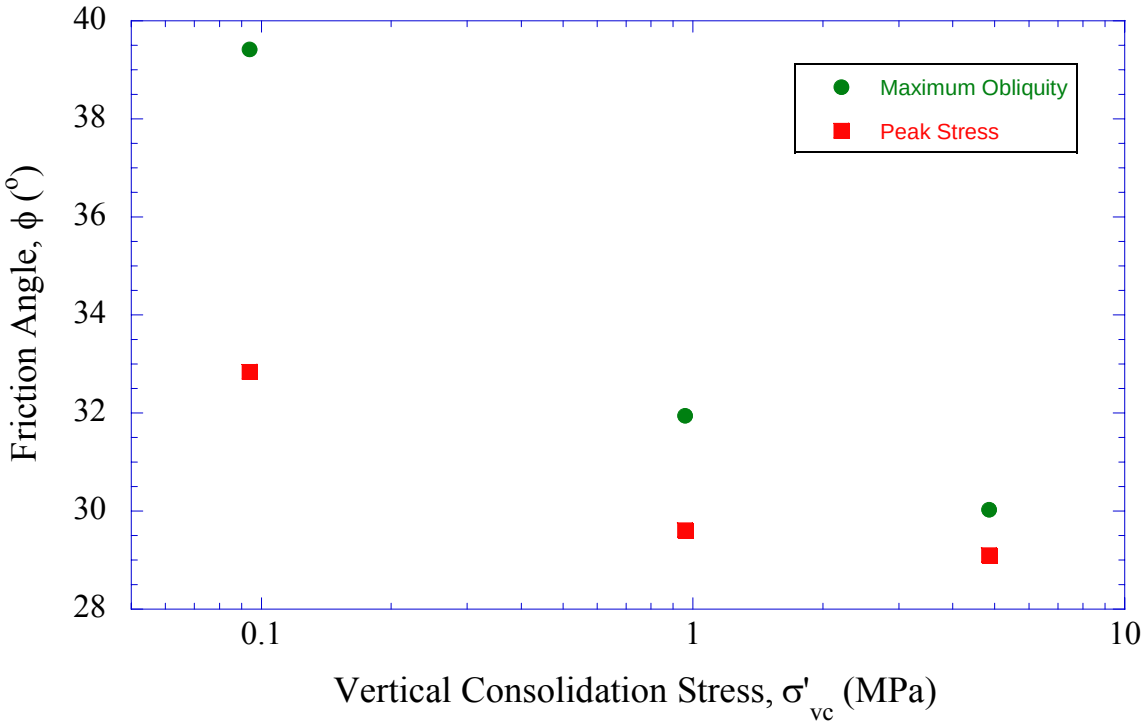

Figure 5-49: Friction angle at peak and maximum obliquity versus stress level for OCR=2 RBBC from CK_0UC triaxial tests

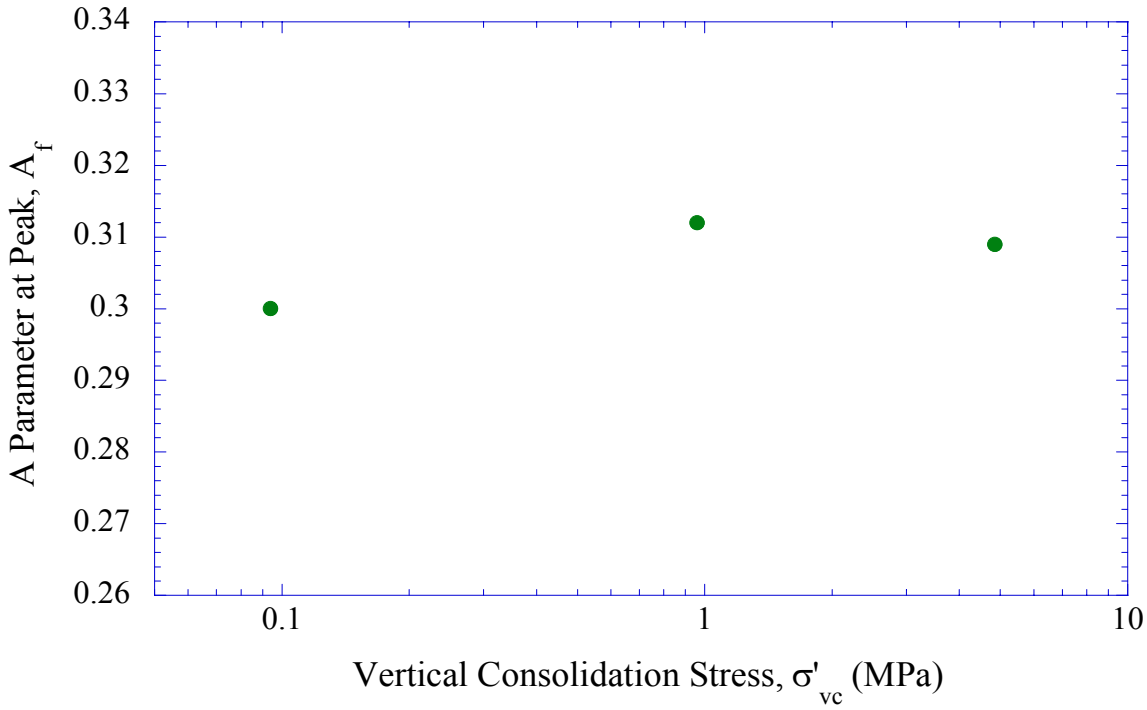

Figure 5-50: Skempton A parameter at peak versus stress level for OCR=2 RBBC from CK_0UC triaxial tests

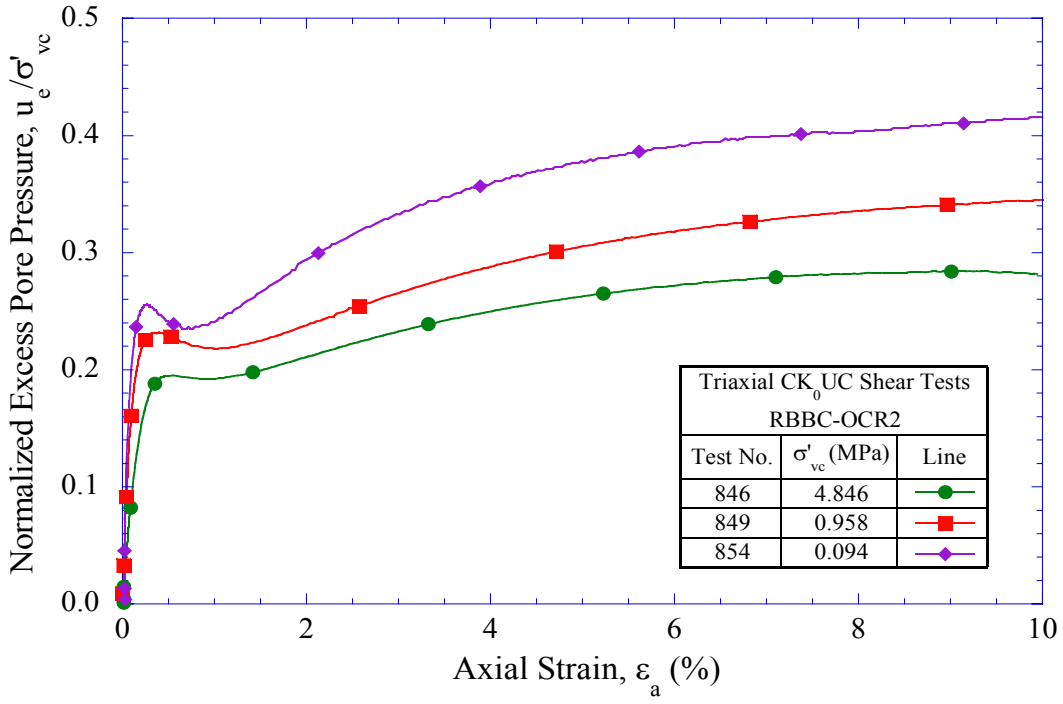

Figure 5-51: Normalized excess pore pressure versus strain for OCR=2 RBBC from CK_0UC triaxial tests

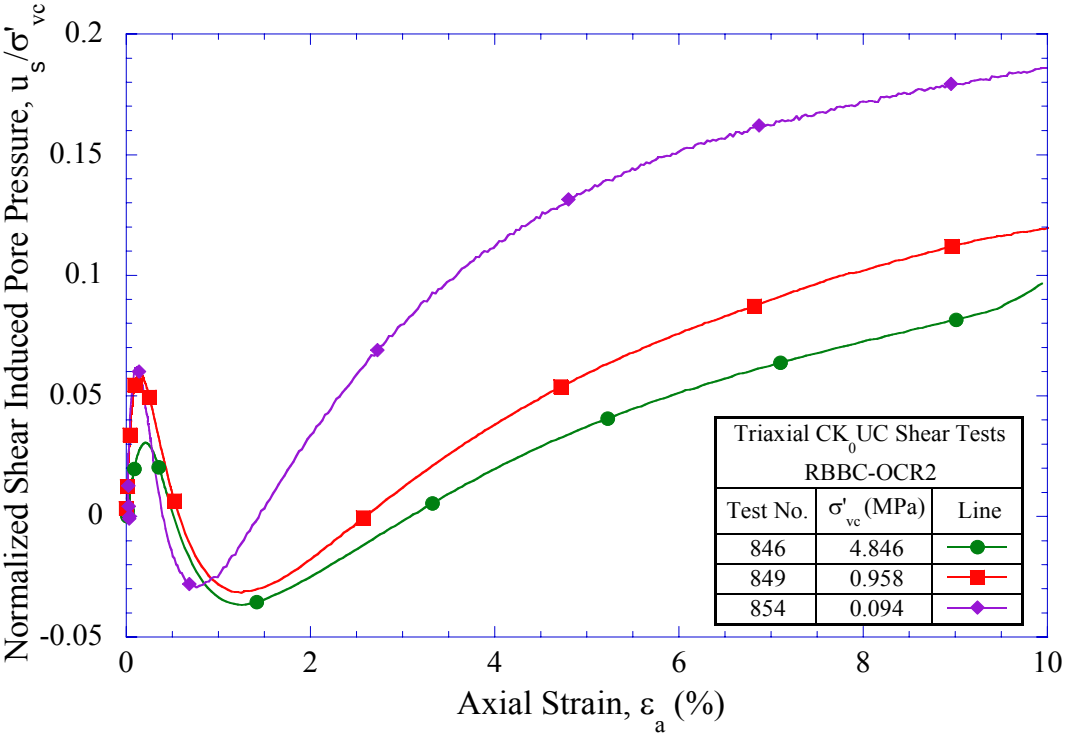

Figure 5-52: Normalized shear induced pore pressure versus strain for OCR=2 RBBC from CK_0UC triaxial tests

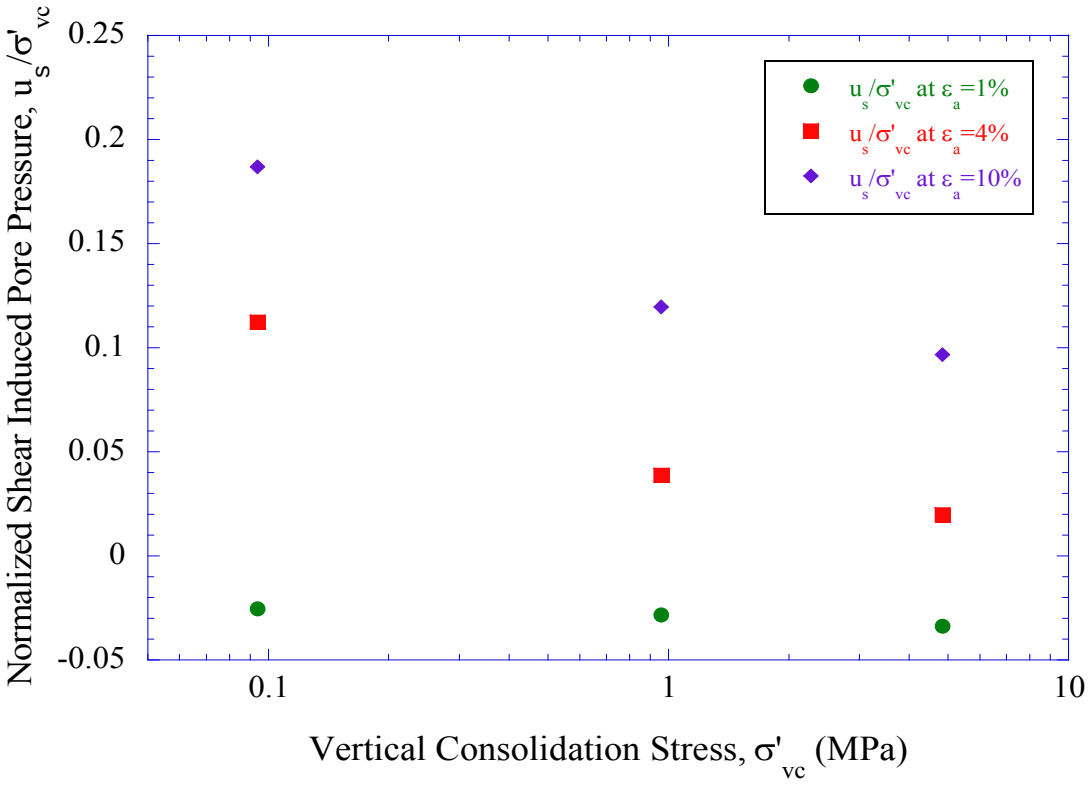

Figure 5-53: Normalized shear induced pore pressure versus stress level for OCR=2 RBBC from CK_0UC triaxial tests

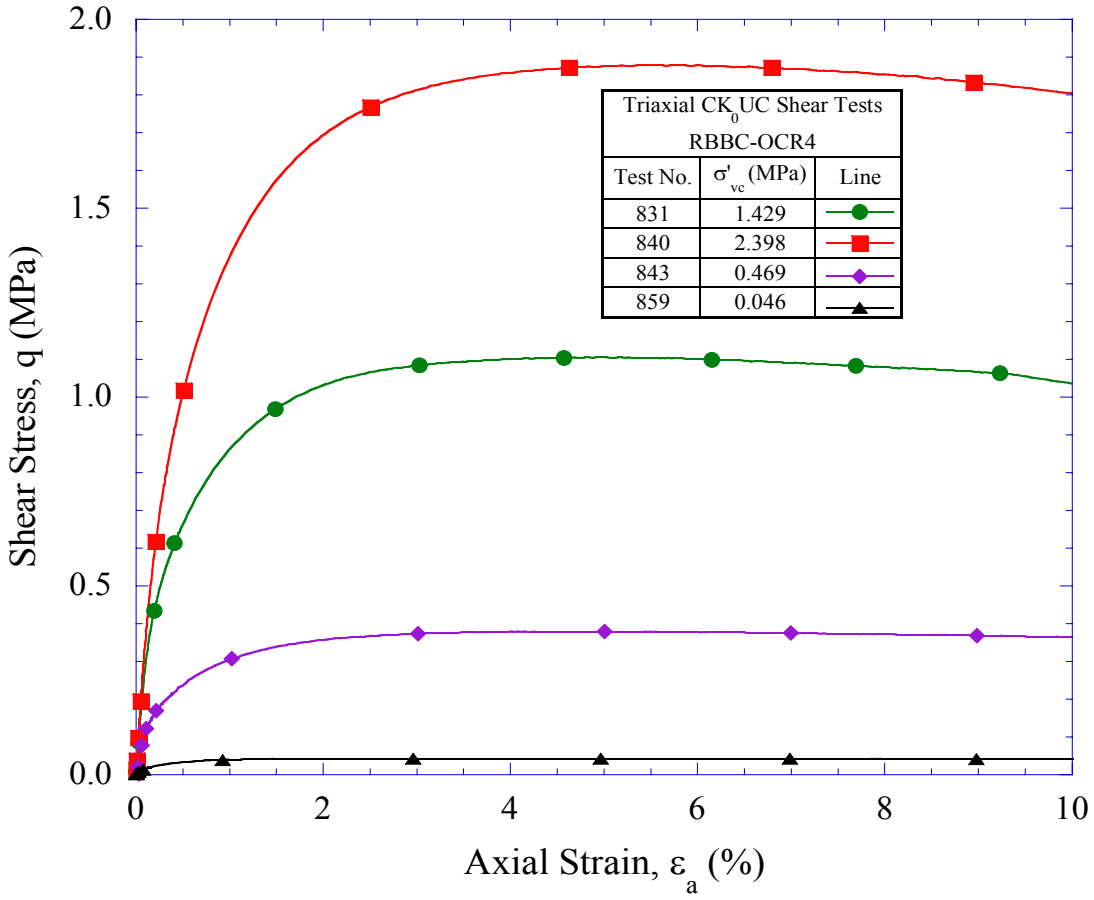

Figure 5-54: Stress-strain curves for OCR=4 RBBC from CK_0UC triaxial tests

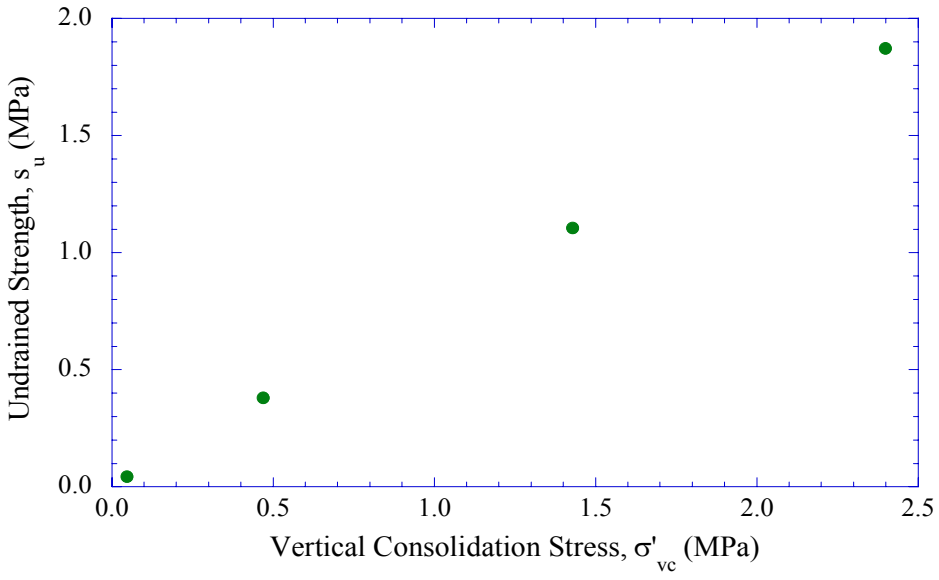

Figure 5-55: Undrained shear strength versus stress level for OCR=4 RBBC from CK_0UC triaxial tests

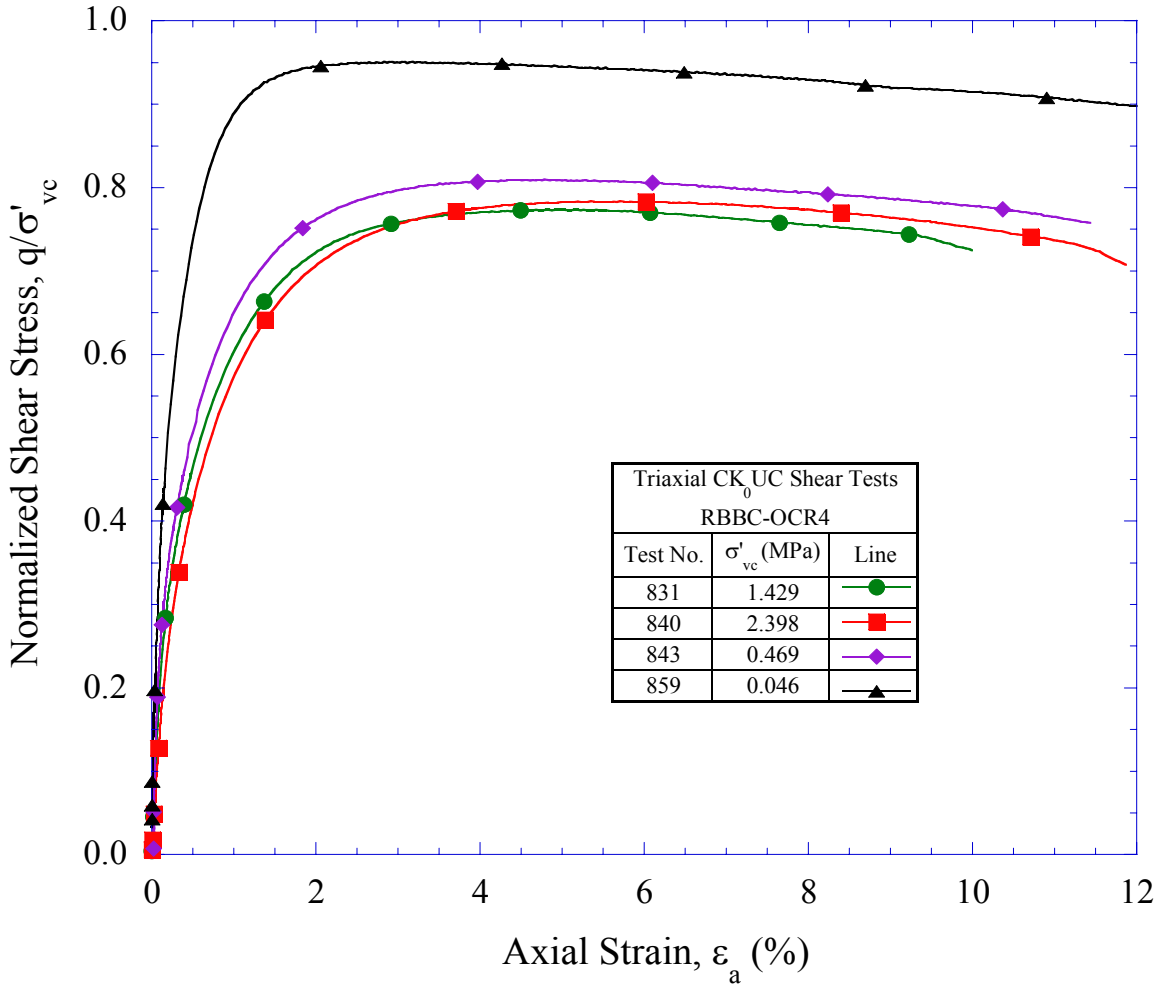

Figure 5-56: Normalized stress-strain curves for OCR=4 RBBC from CK_0UC triaxial tests

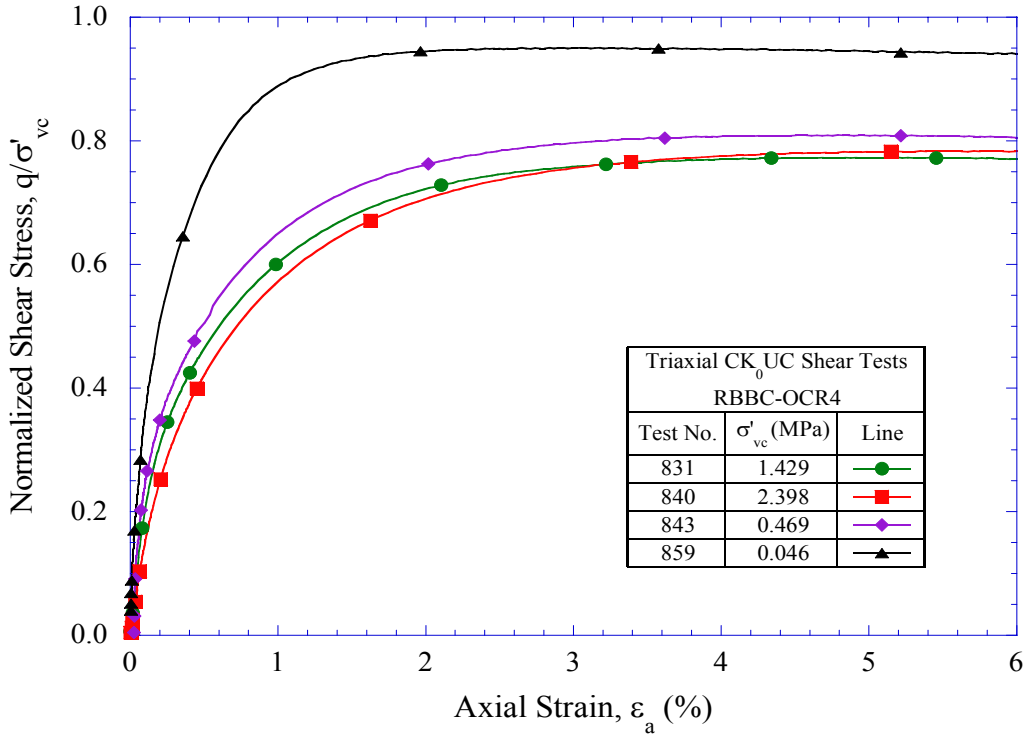

Figure 5-57: Normalized stress-strain curves (up to 6%) for OCR=4 RBBC from CK_0UC triaxial tests

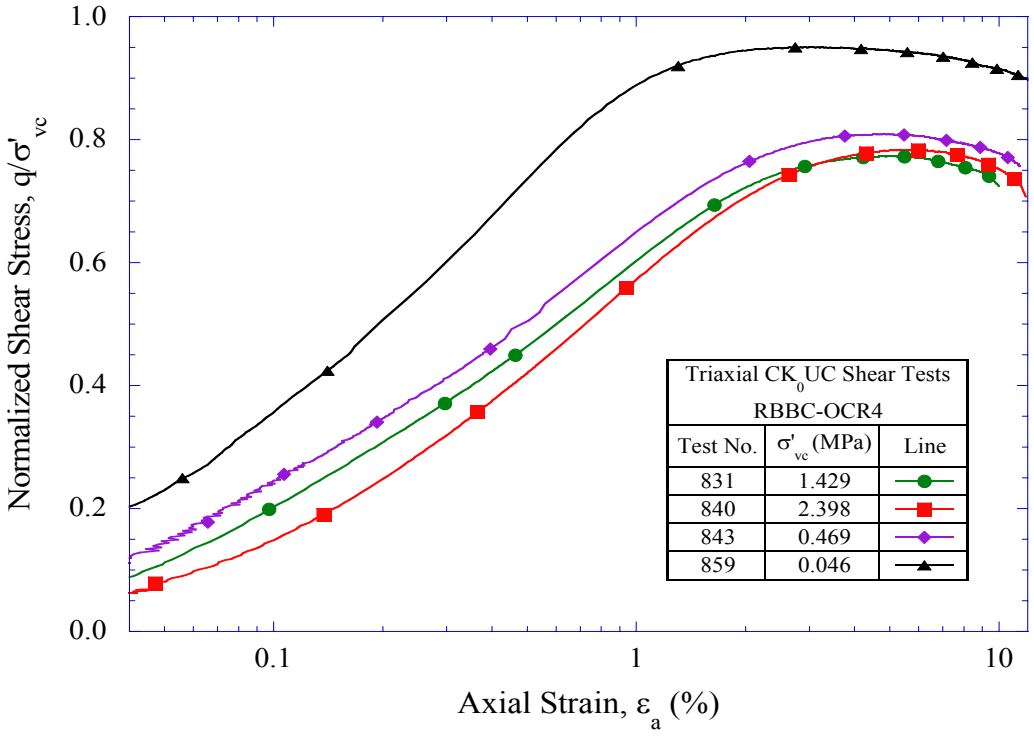

Figure 5-58: Normalized stress-(log) strain curves for OCR=4 RBBC from CK_0UC triaxial tests

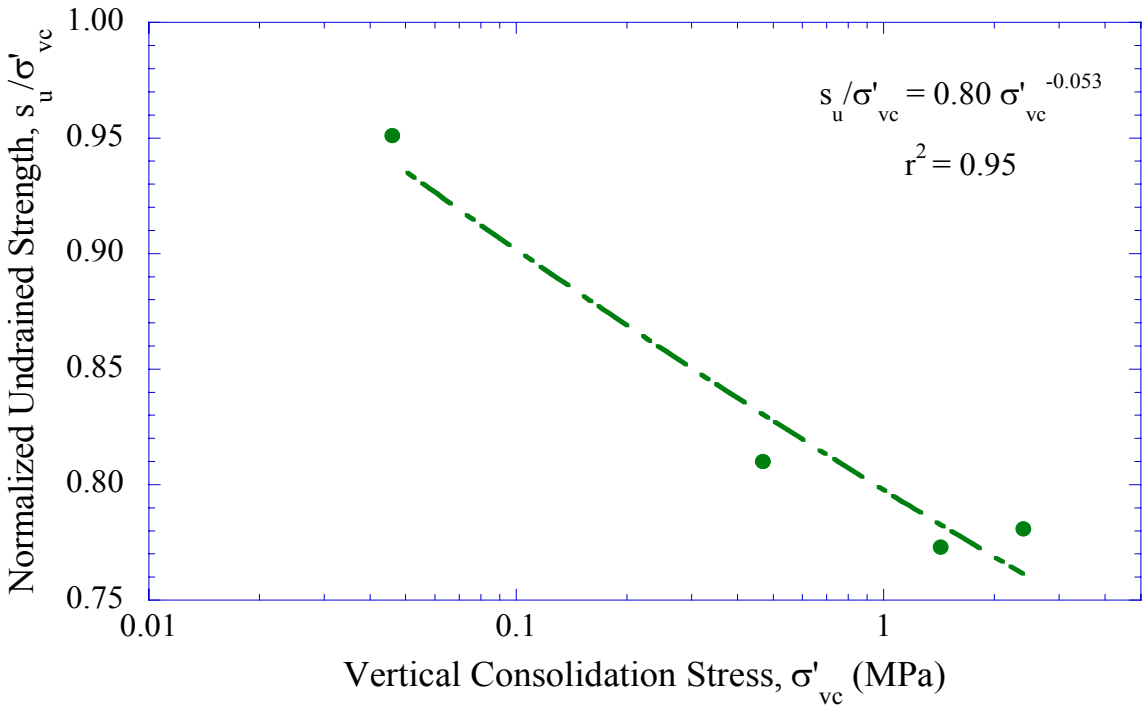

Figure 5-59: Normalized undrained shear strength versus stress level for OCR=4 RBBC from CK_0UC triaxial tests

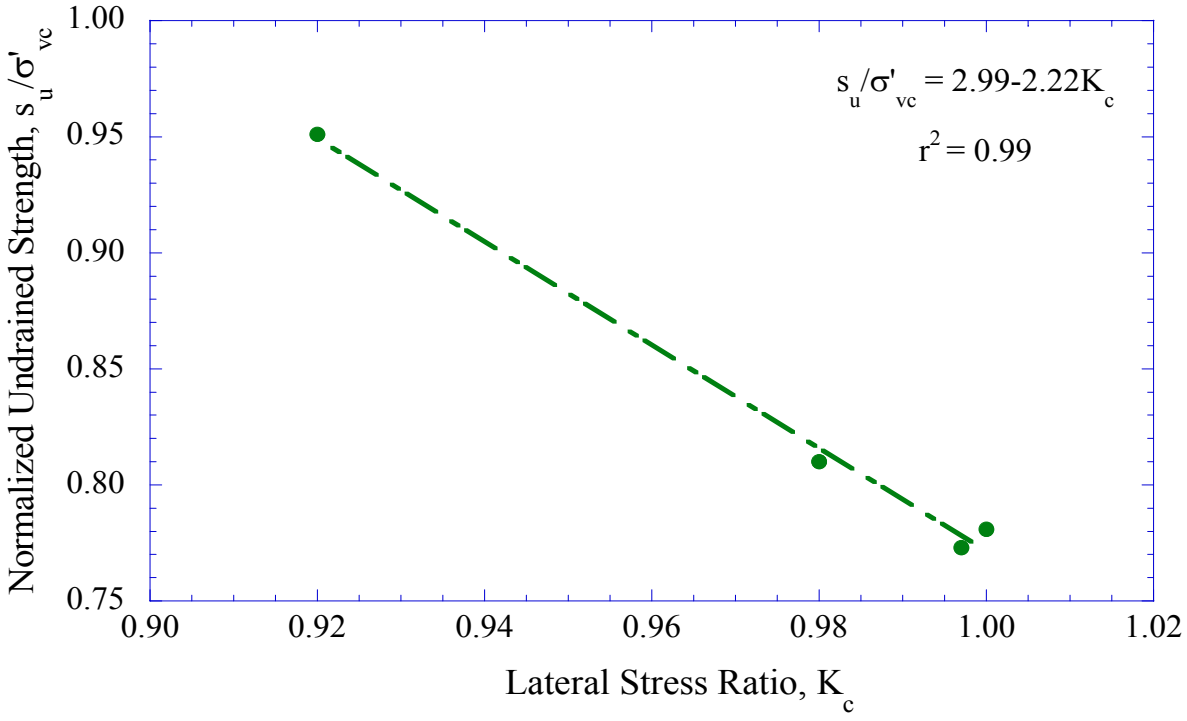

Figure 5-60: Normalized undrained shear strength versus lateral stress ratio for OCR=4 RBBC from CK_0UC triaxial tests

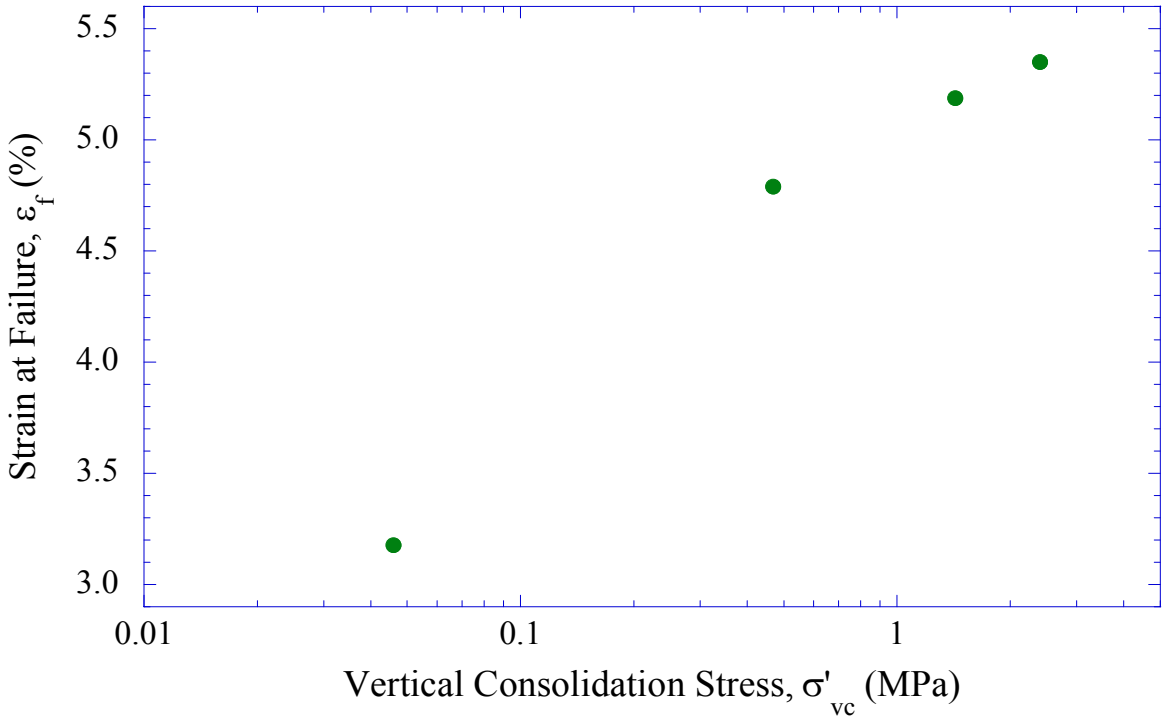

Figure 5-61: Strain at failure versus stress level for OCR=4 RBBC from CK_0UC triaxial tests

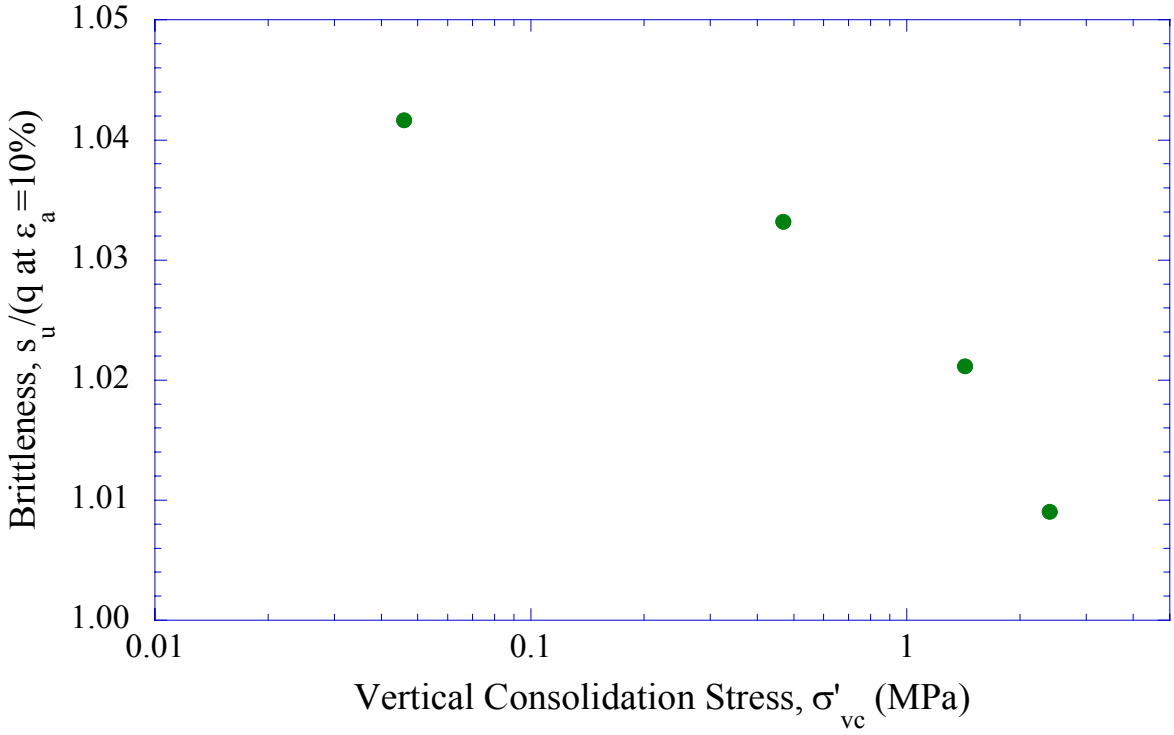

Figure 5-62: Brittleness versus stress level for OCR=4 RBBC from CK_0UC triaxial tests

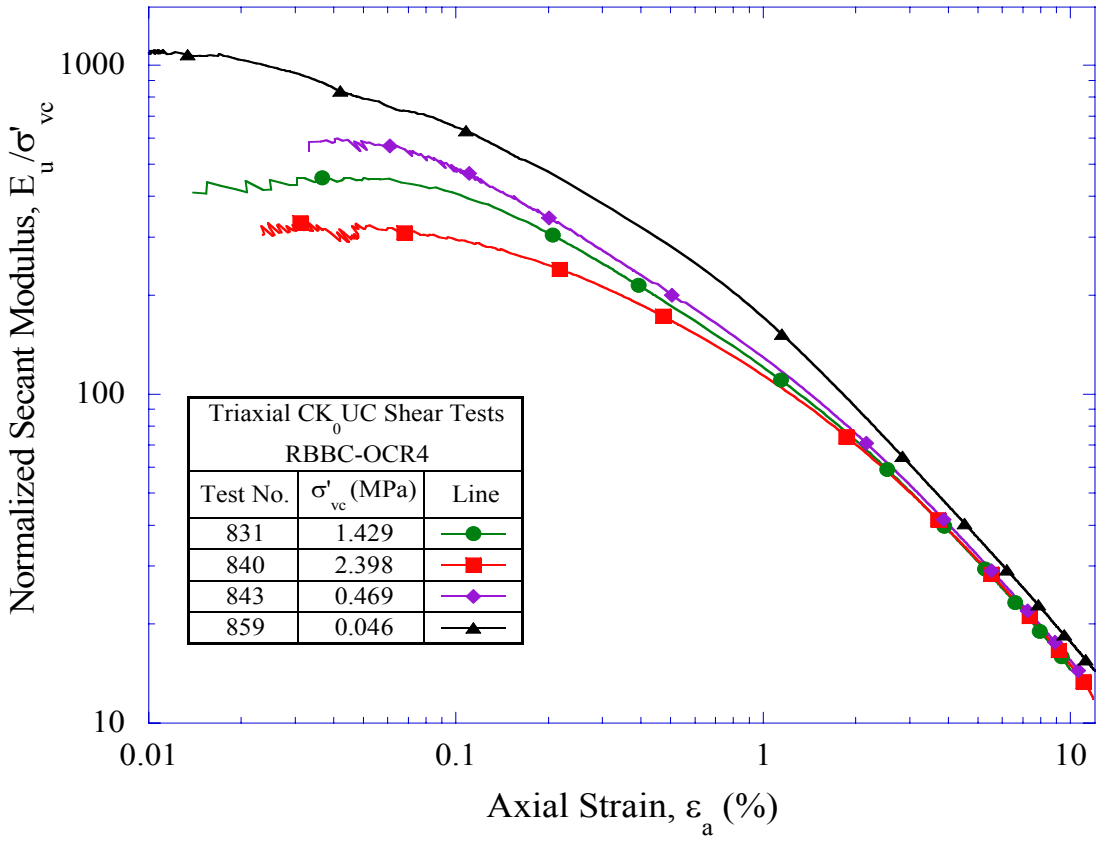

Figure 5-63: Normalized undrained secant modulus versus axial strain for OCR=4 RBBC from CK_0UC triaxial tests

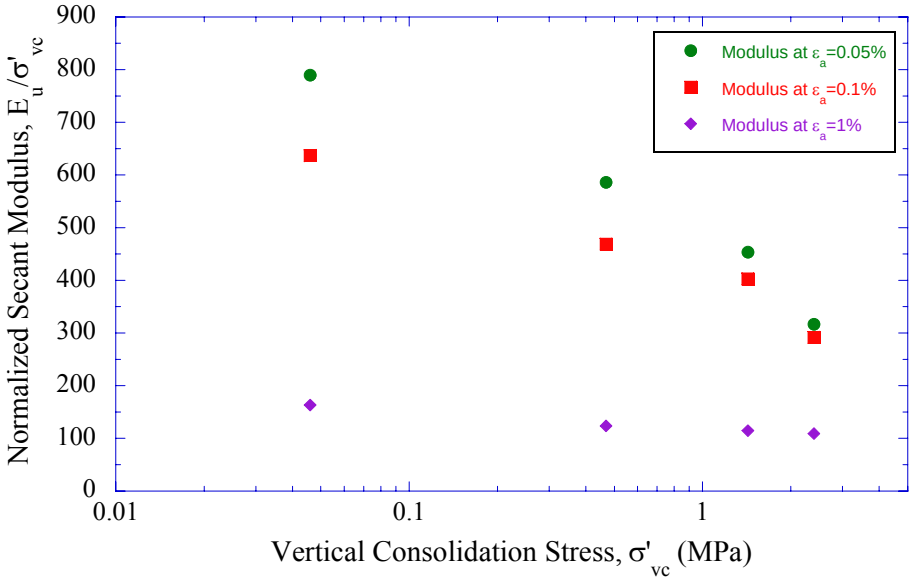

Figure 5-64: Normalized undrained secant modulus versus stress level for OCR=4 RBBC from CK_0UC triaxial tests

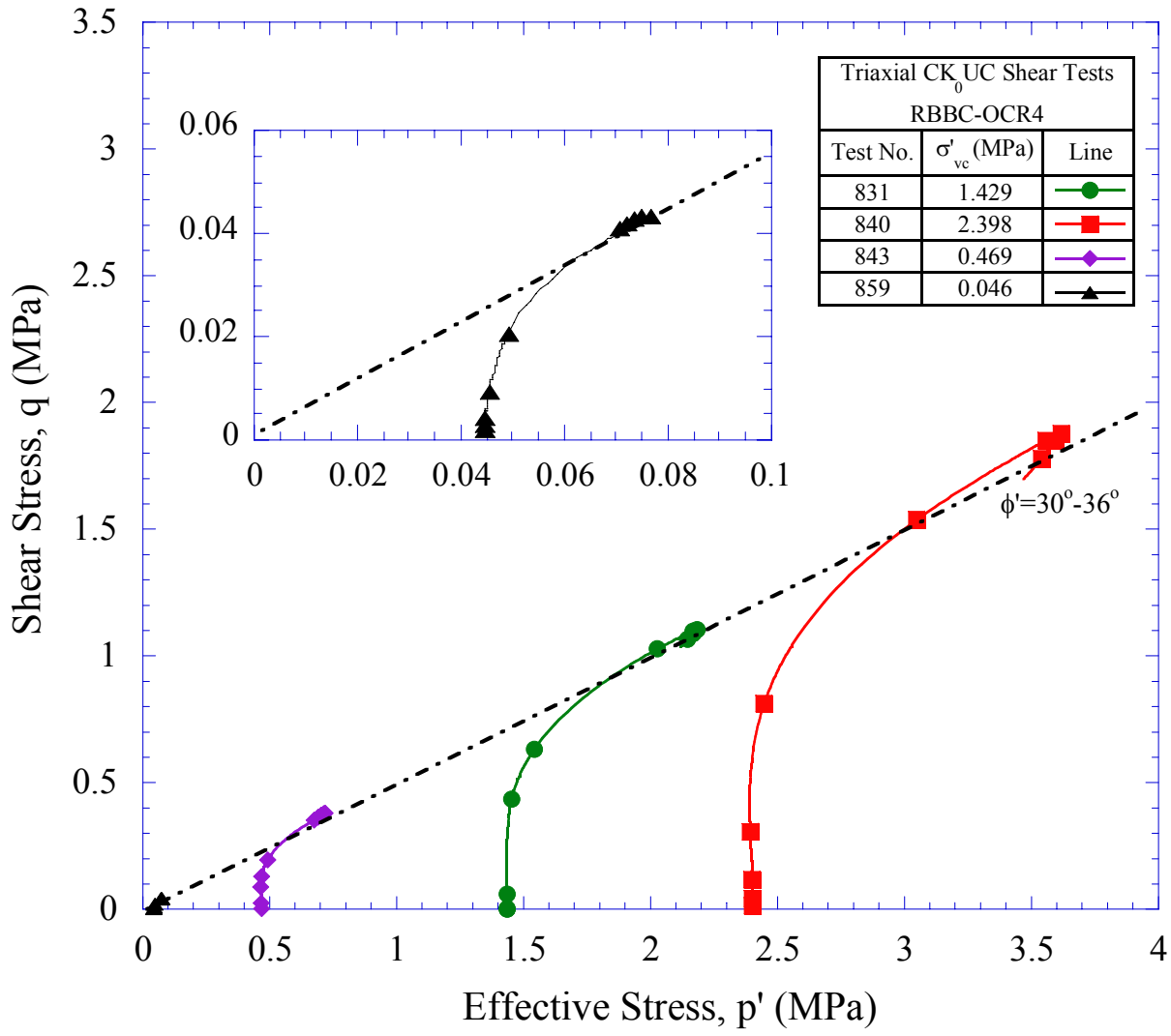

Figure 5-65: Effective stress paths for OCR=4 RBBC from CK_0UC triaxial tests

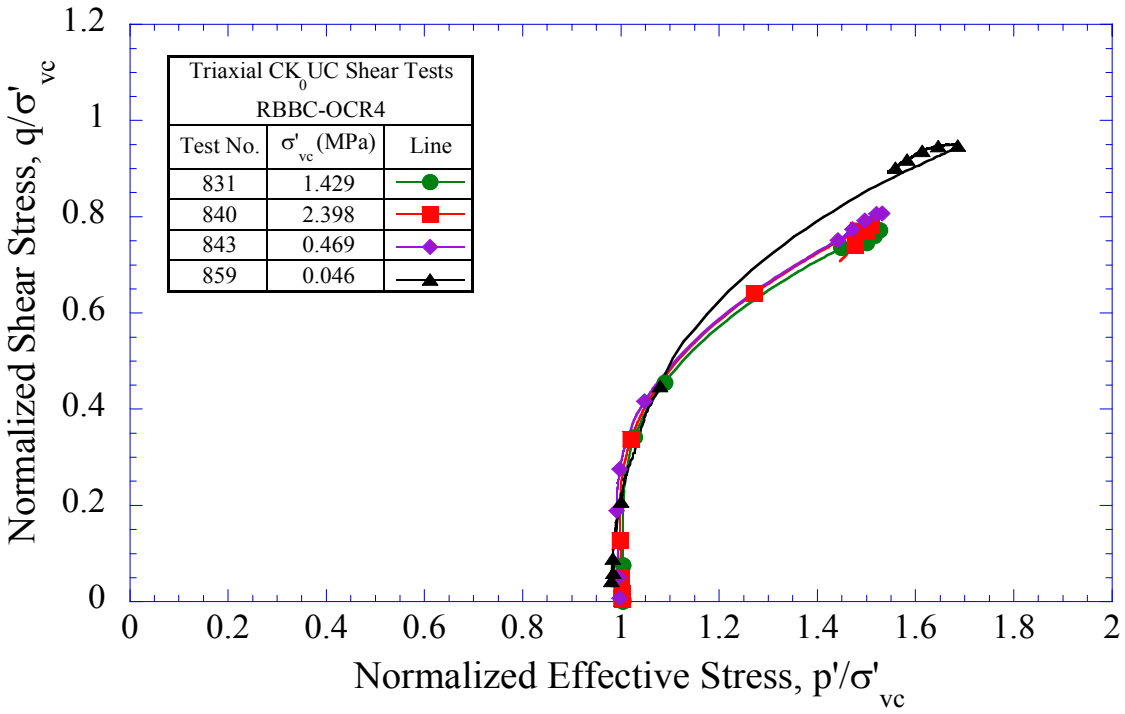

Figure 5-66: Normalized effective stress paths for OCR=4 RBBC from CK_0UC triaxial tests

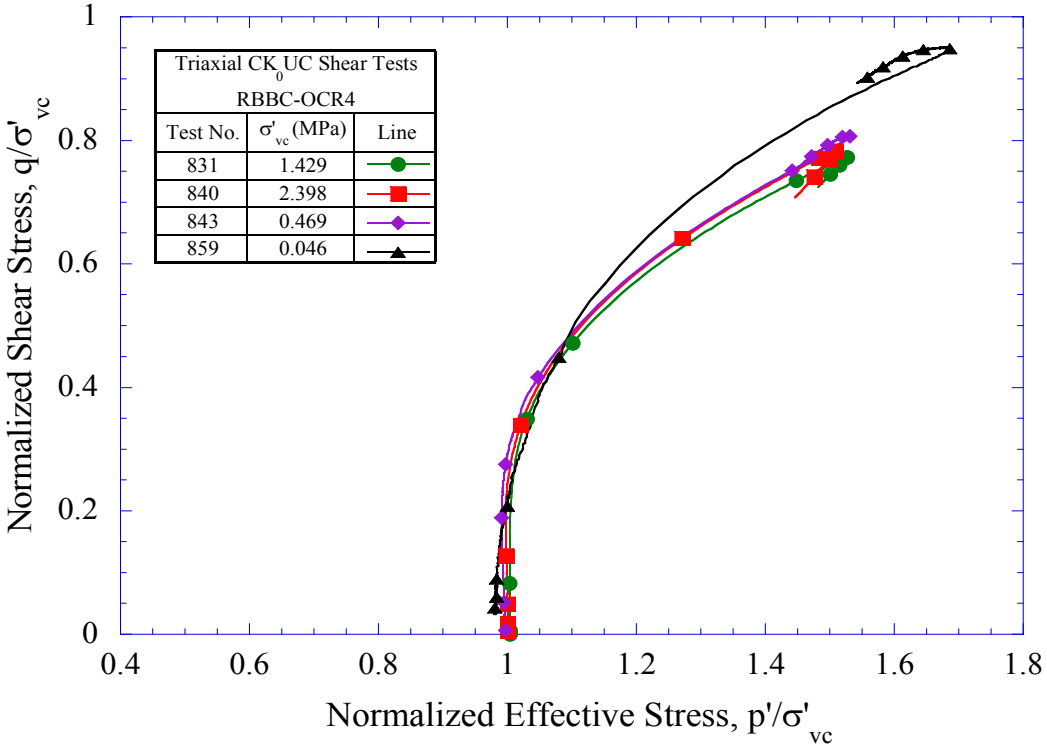

Figure 5-67: Normalized effective stress paths (close up view) for OCR=4 RBBC from CK_0UC triaxial tests

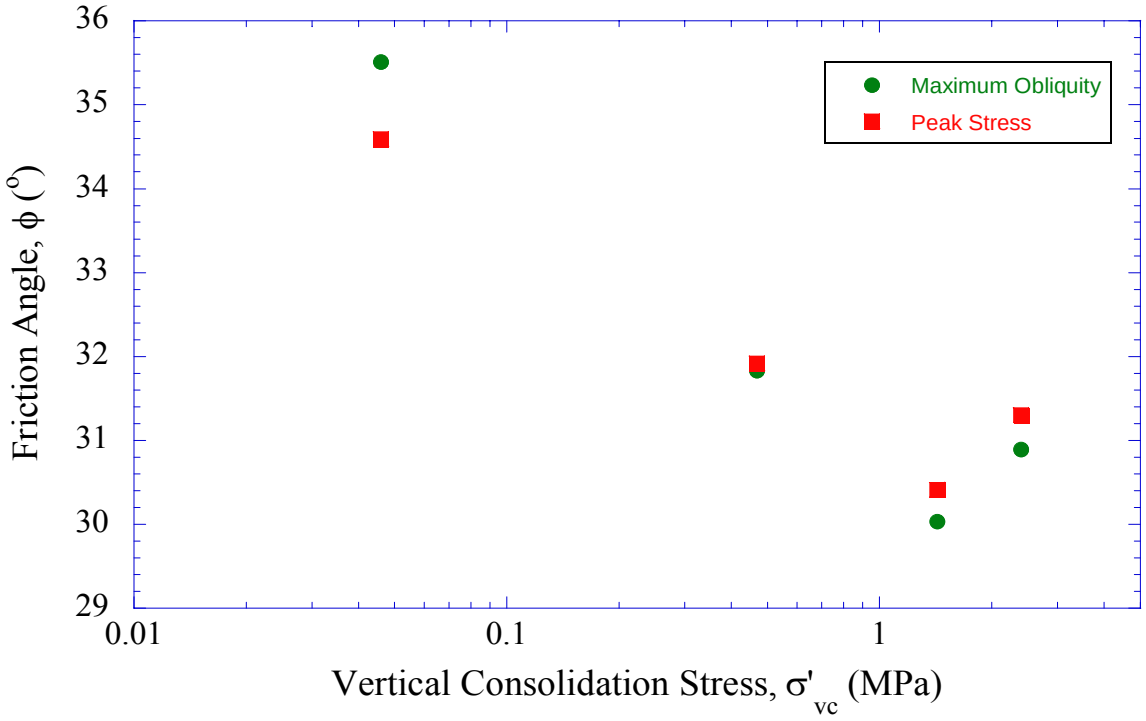

Figure 5-68: Friction angle at peak and maximum obliquity versus stress level for OCR=4 RBBC from CK_0UC triaxial tests

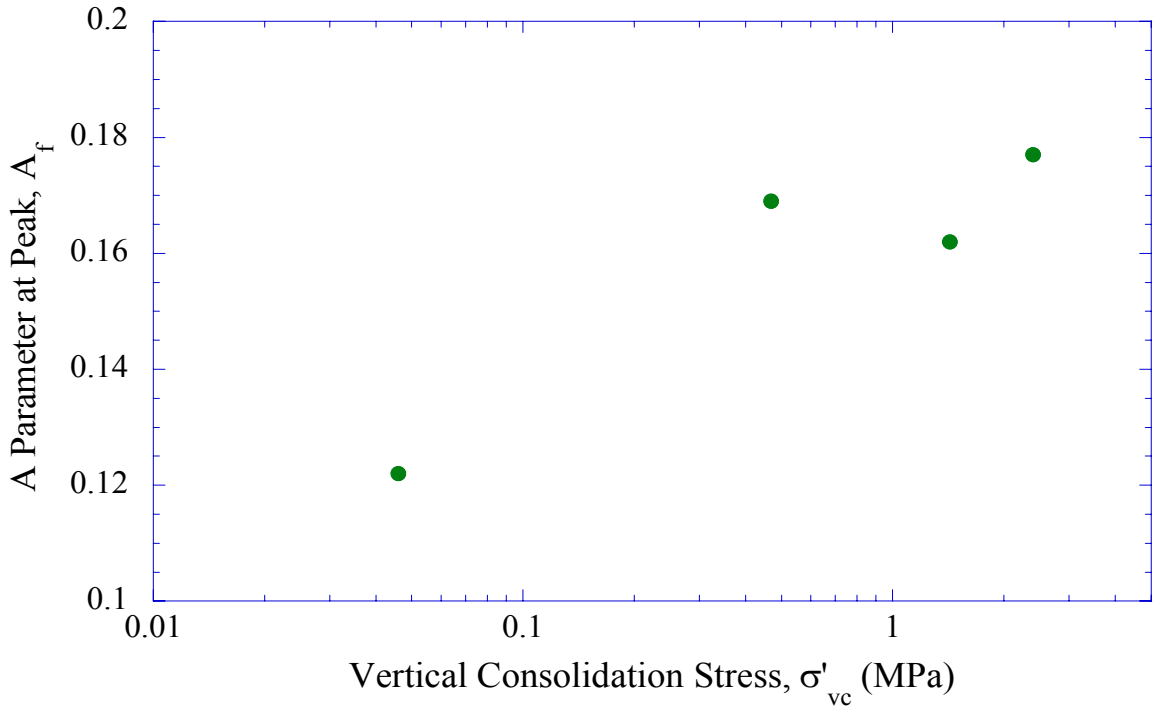

Figure 5-69: Skempton A parameter at peak versus stress level for OCR=4 RBBC from CK_0UC triaxial tests

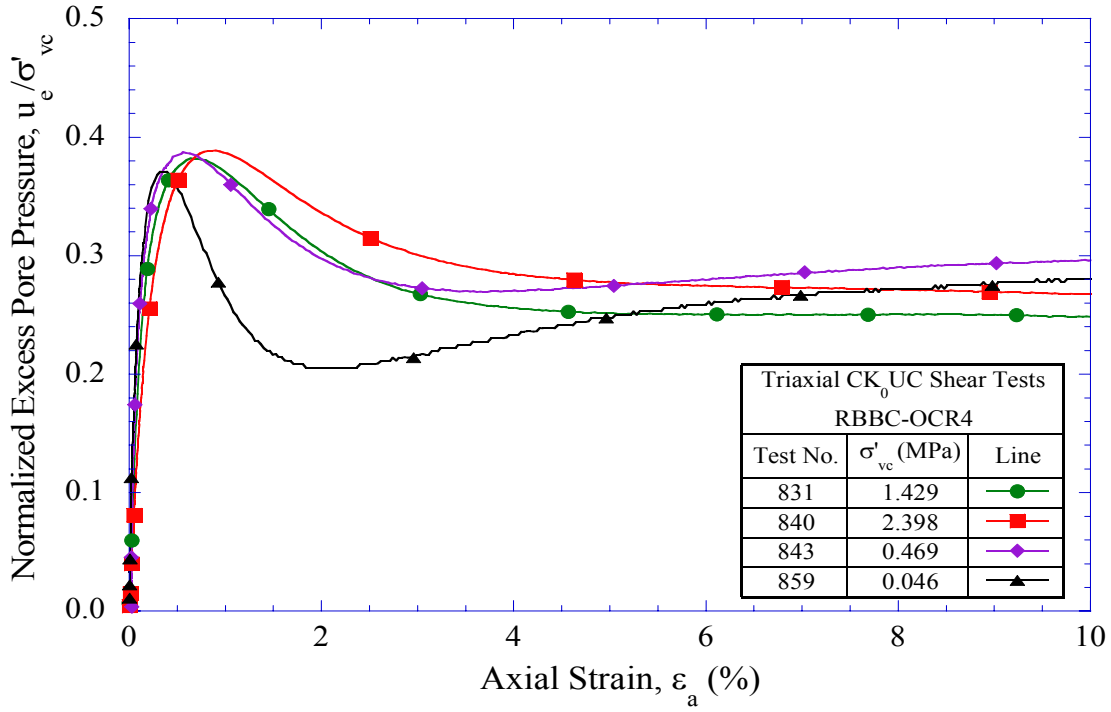

Figure 5-70: Normalized excess pore pressure versus strain for OCR=4 RBBC from CK_0UC triaxial tests

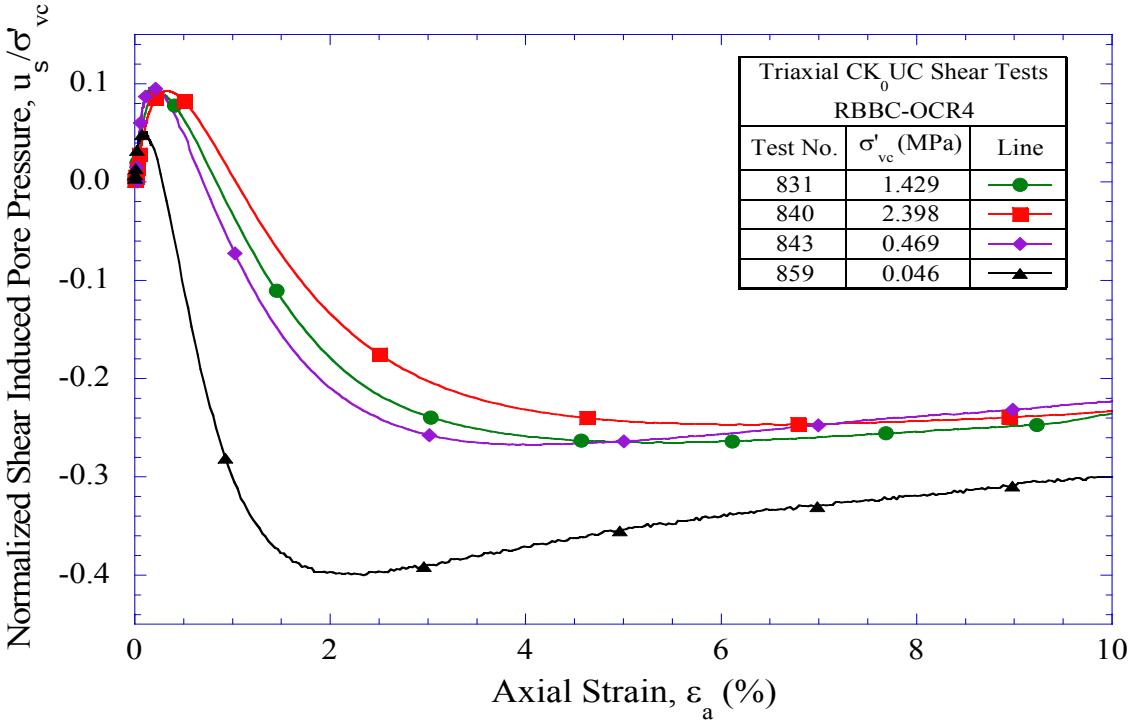

Figure 5-71: Normalized shear induced pore pressure versus strain for OCR=4 RBBC from CK_0UC triaxial tests

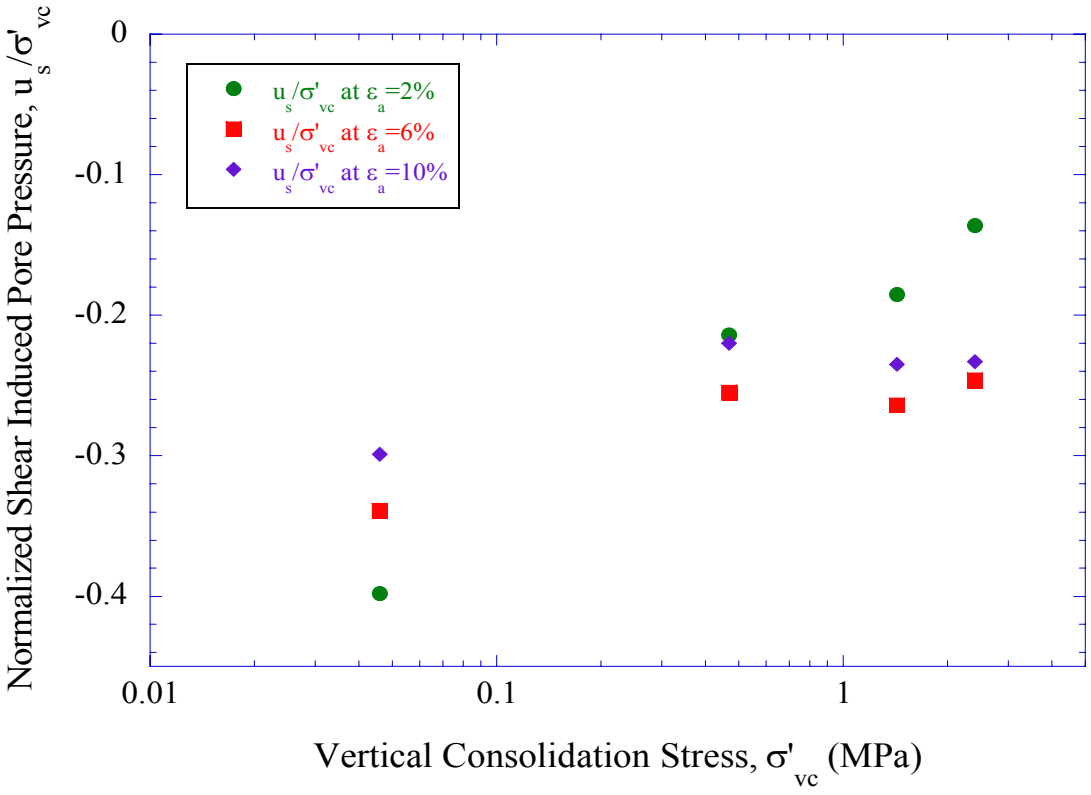

Figure 5-72: Normalized shear induced pore pressure versus stress level for OCR=4 RBBC from CK_0UC triaxial tests

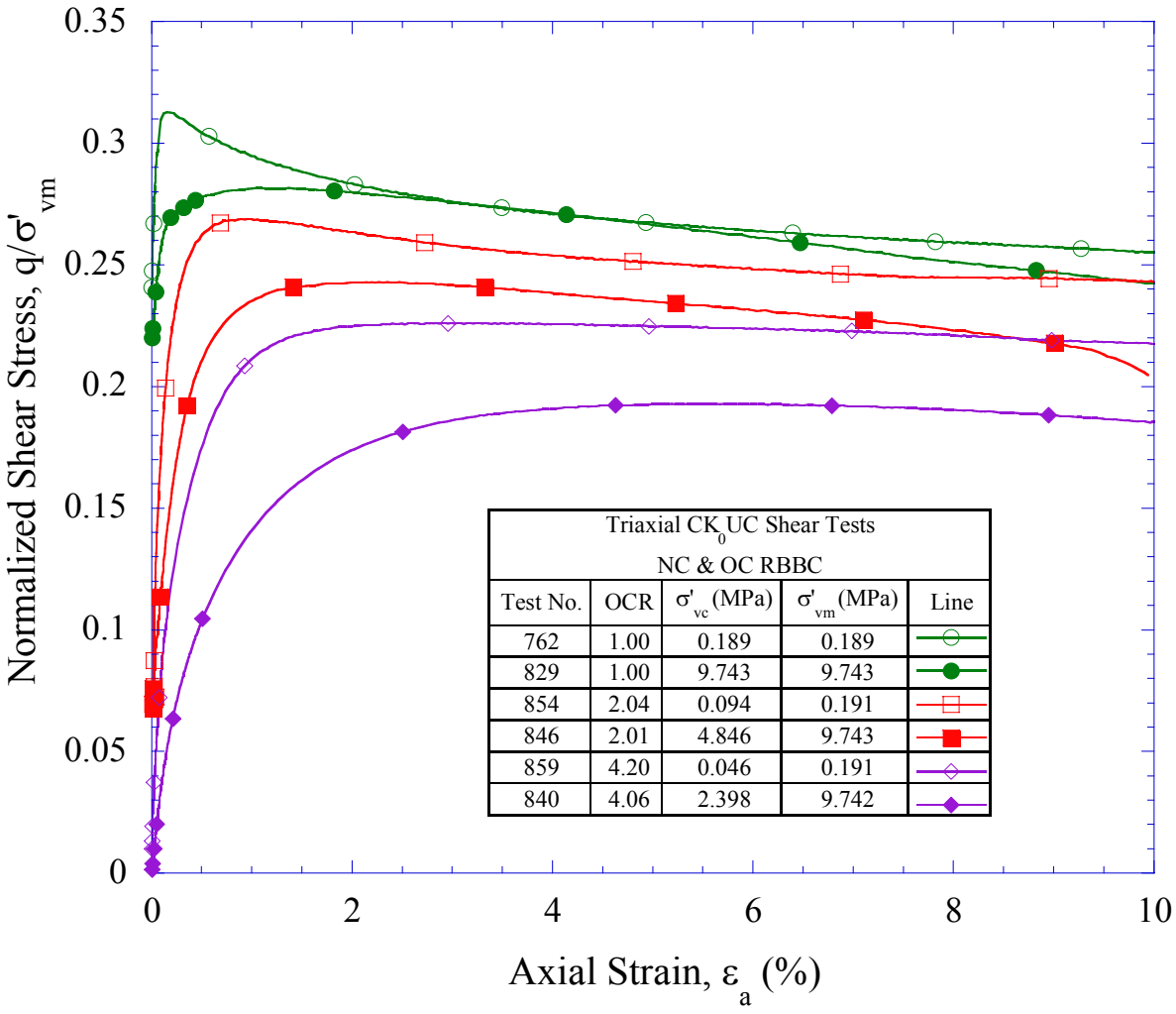

Figure 5-73: Normalized stress-strain curves for RBBC (OCR = 1, 2 & 4) from CK_0UC triaxial tests at low and high stress levels (σ'_{vm} = 0.2 & 10 MPa)

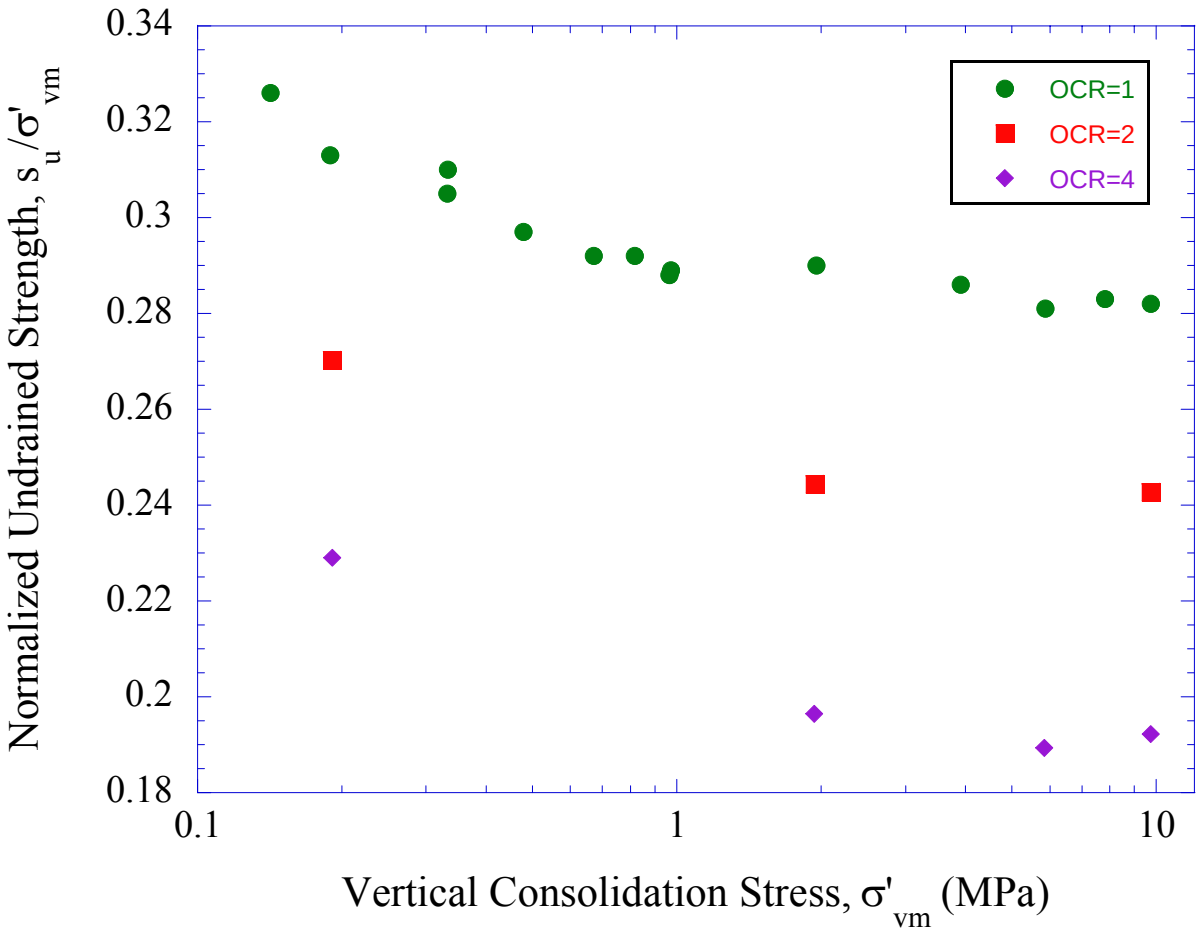

Figure 5-74: Normalized undrained shear strength variations with stress level for RBBC (OCR=1, 2 & 4) from CK_0UC triaxial tests

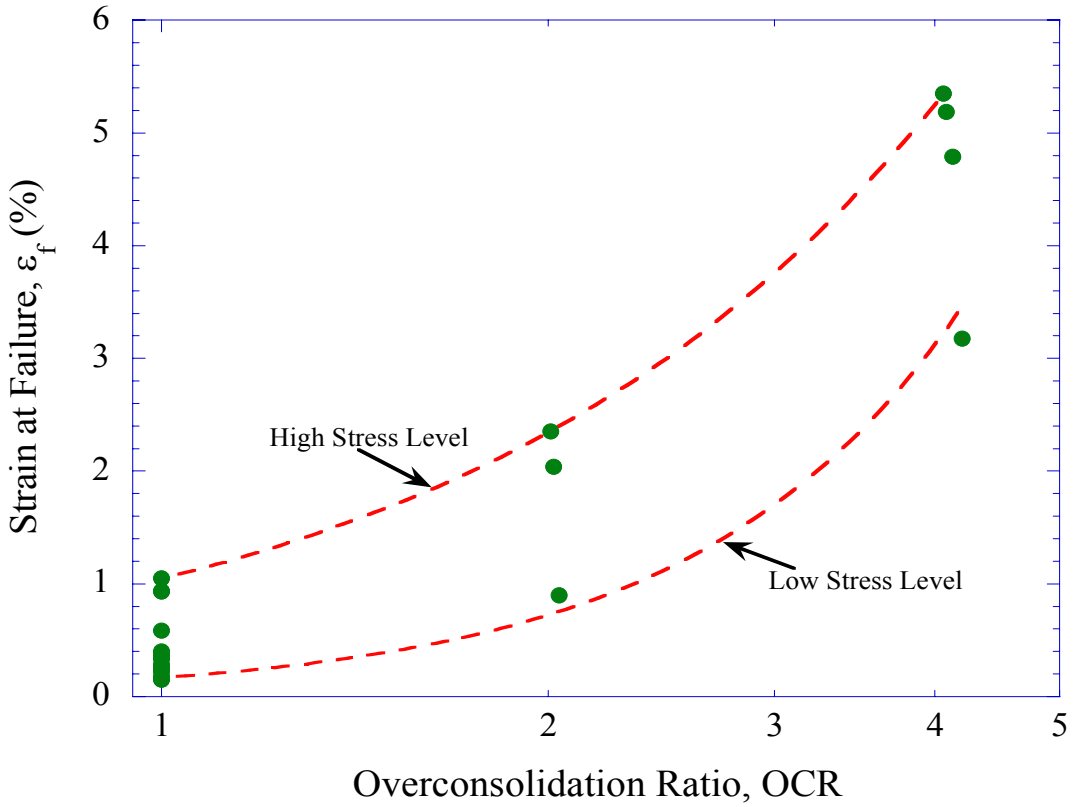

Figure 5-75: Strain at Failure versus OCR for RBBC from CK_0UC triaxial tests

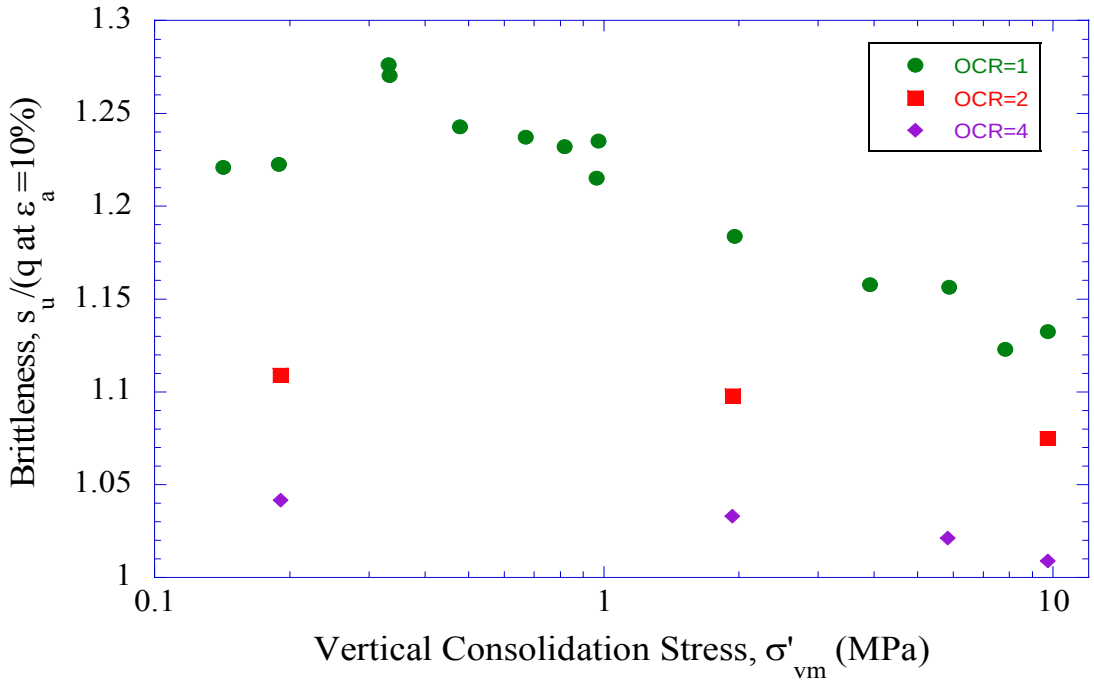

Figure 5-76: Brittleness versus stress level for RBBC (OCR=1, 2 & 4) from CK_0UC triaxial tests

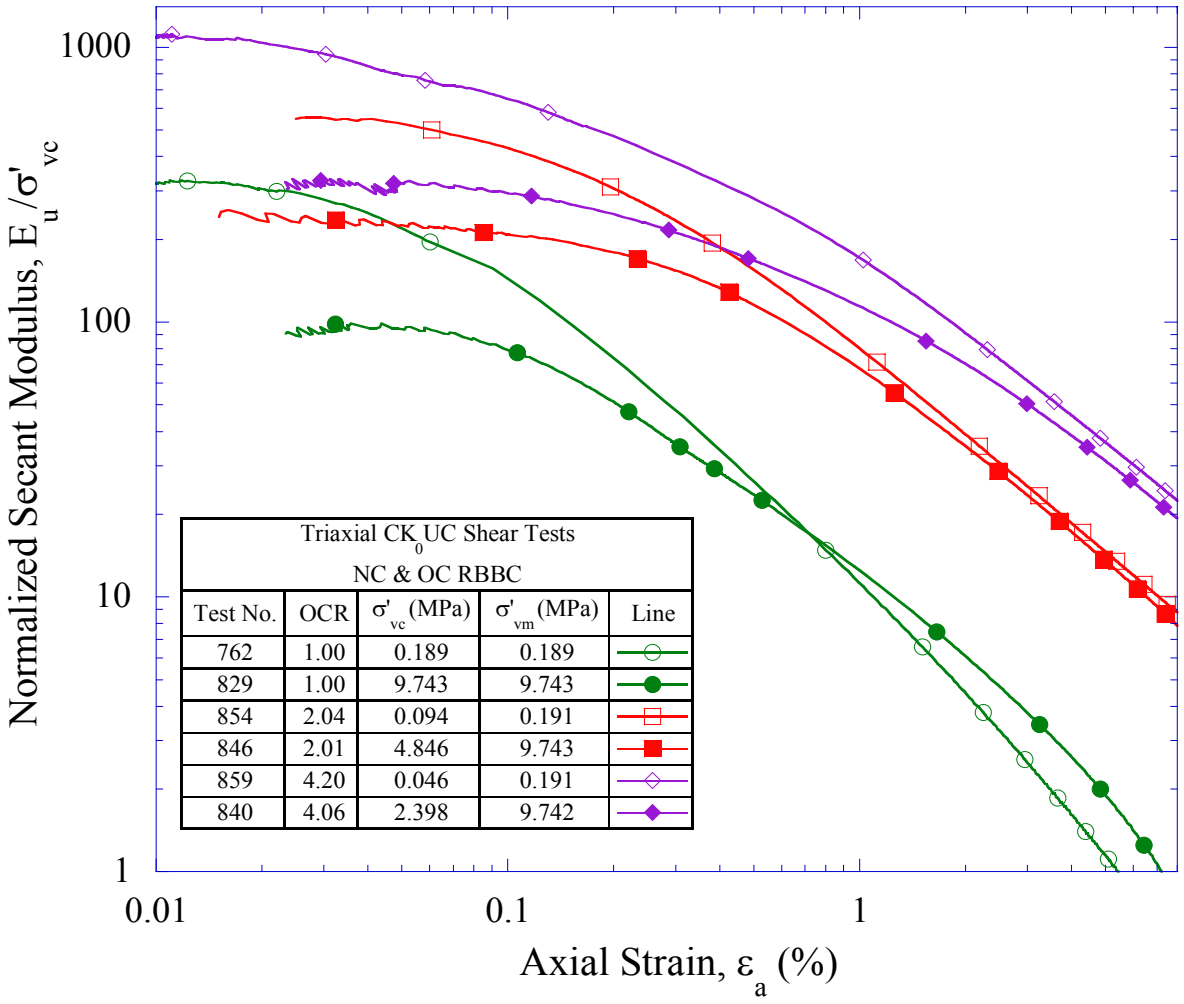

Figure 5-77: Normalized undrained secant modulus (E_u/σ'_{vc}) versus axial strain for RBBC (OCR= 1, 2 & 4) from CK_0UC triaxial tests at low and high stress levels (σ'_{vm} = 0.2 & 10 MPa)

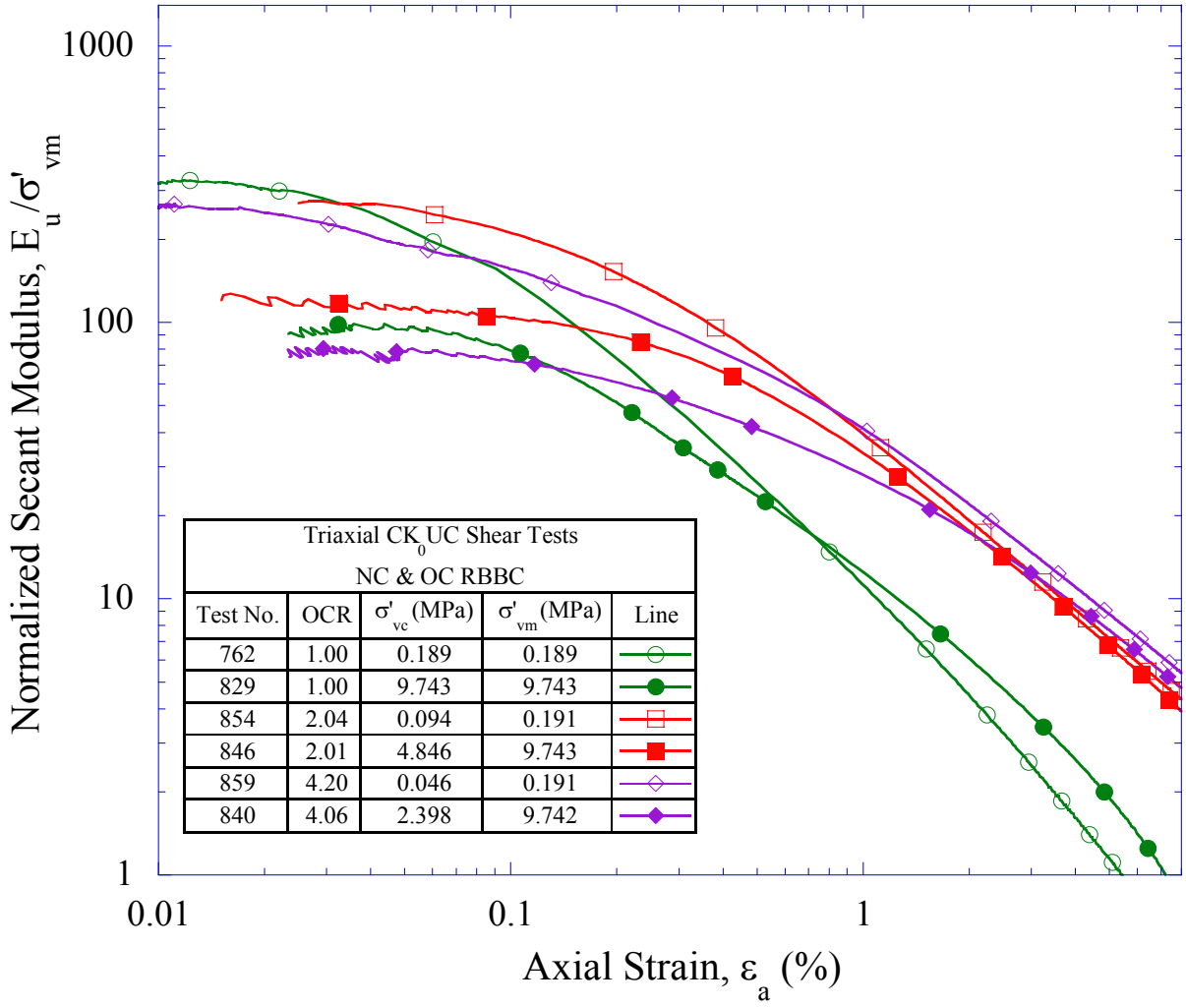

Figure 5-78: Normalized undrained secant modulus (E_u/σ'_{vm}) versus axial strain for RBBC (OCR= 1, 2 & 4) from CK_0UC triaxial tests at low and high stress levels (σ'_{vm} = 0.2 & 10 MPa)

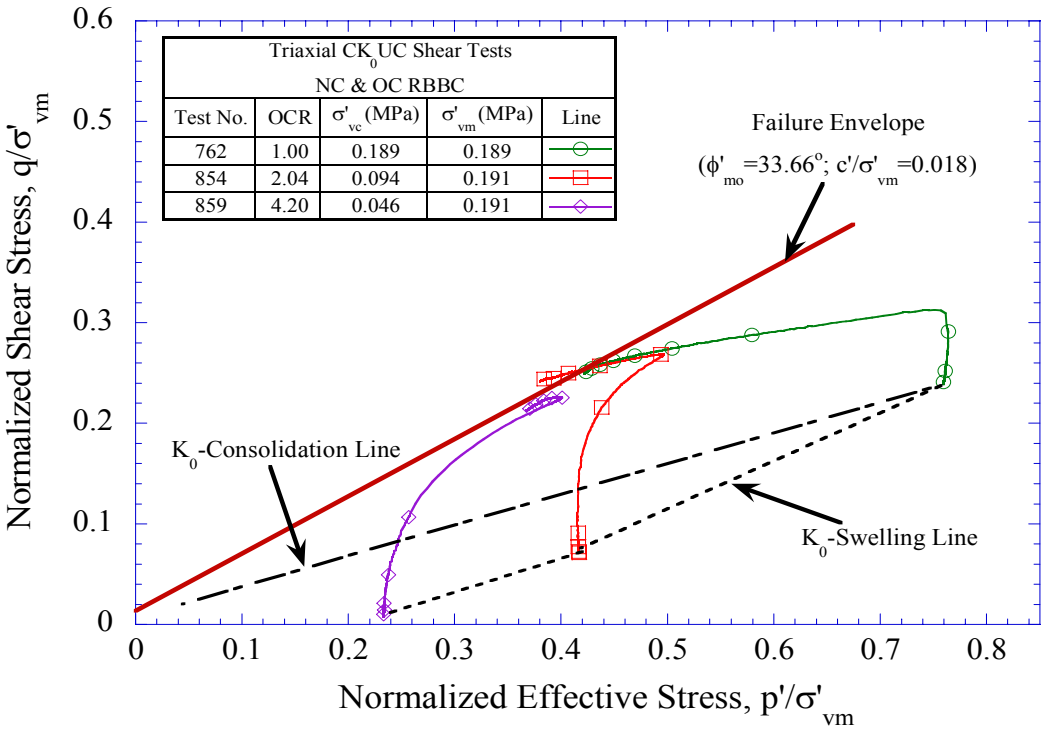

Figure 5-79: Normalized effective stress paths for RBBC (OCR = 1, 2 & 4) from CK_0UC triaxial tests at low stress level (σ'_{vm} = 0.2 MPa)

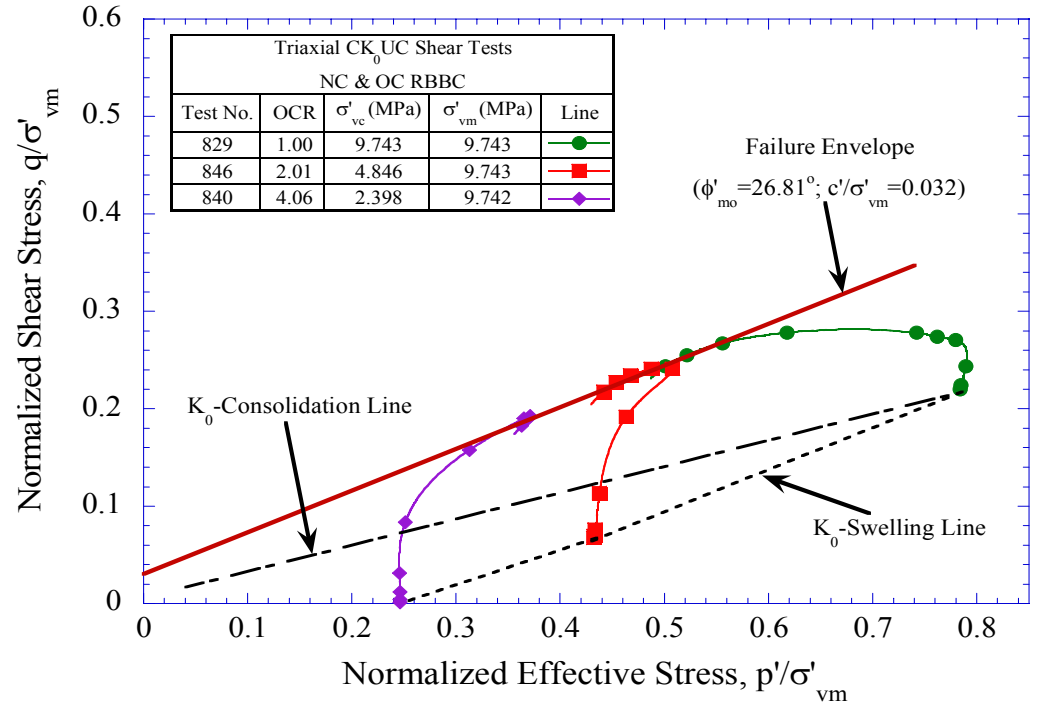

Figure 5-80: Normalized effective stress paths for RBBC (OCR = 1, 2 & 4) from CK_0UC triaxial tests at high stress level (σ'_{vm} = 10 MPa)

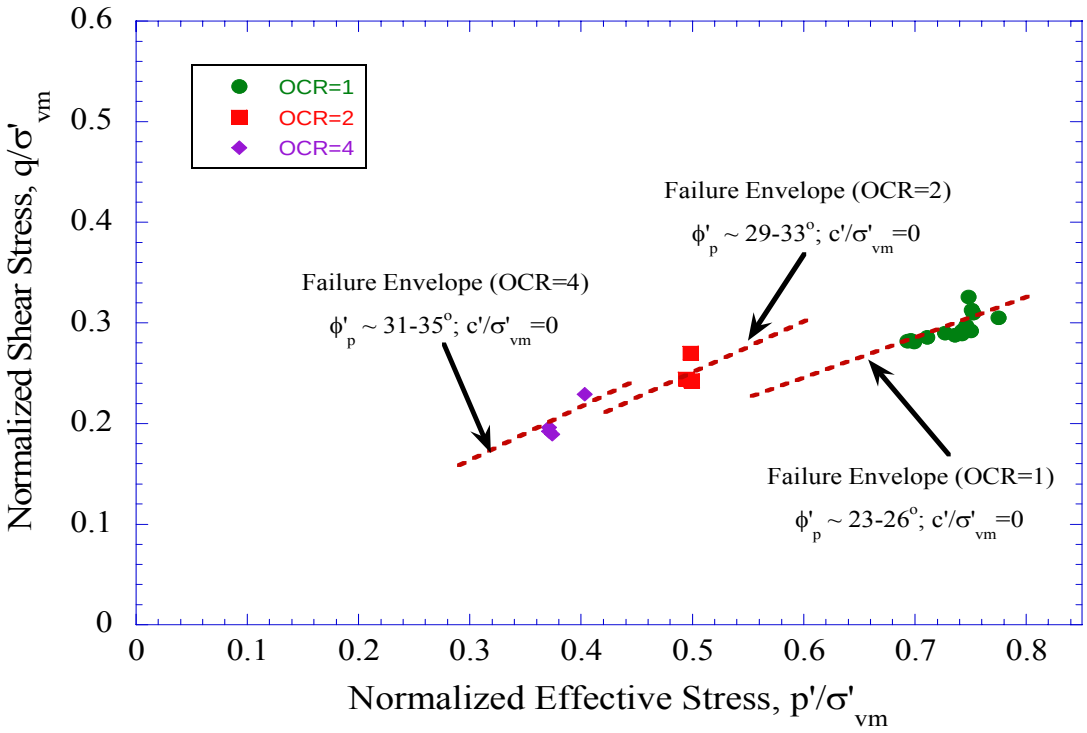

Figure 5-81: Stress states at peak for RBBC (OCR = 1, 2 & 4) from CK_0UC triaxial tests

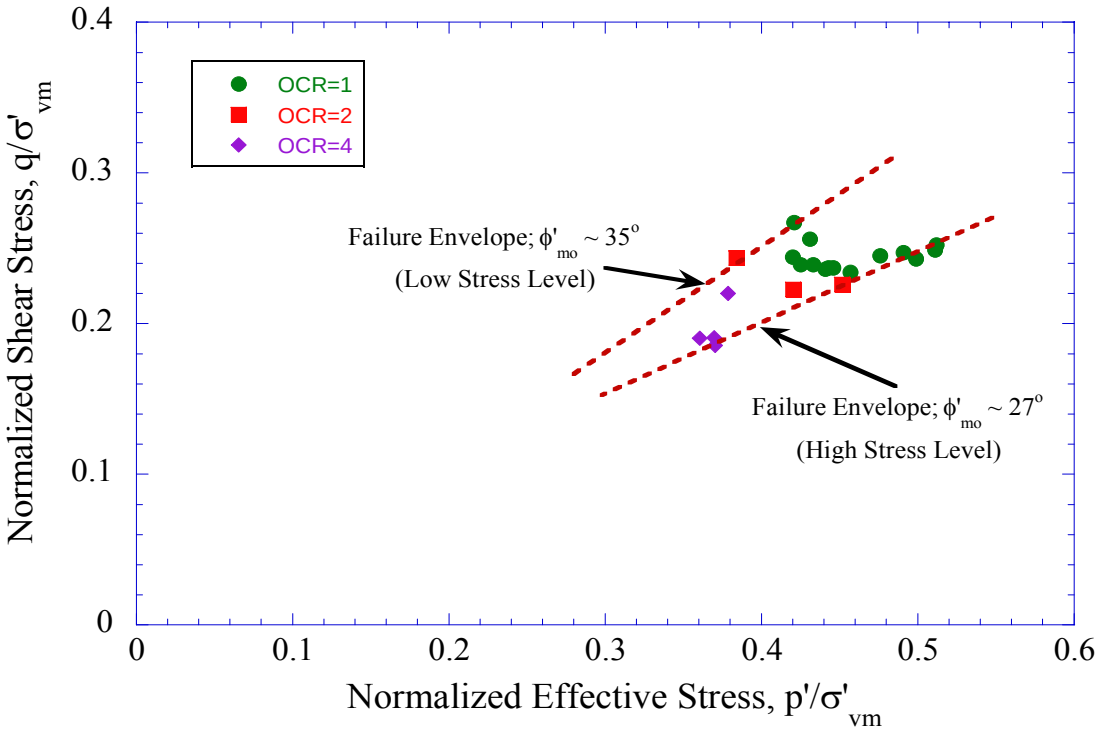

Figure 5-82: Stress states at maximum obliquity for RBBC (OCR = 1, 2 & 4) from CK_0UC triaxial

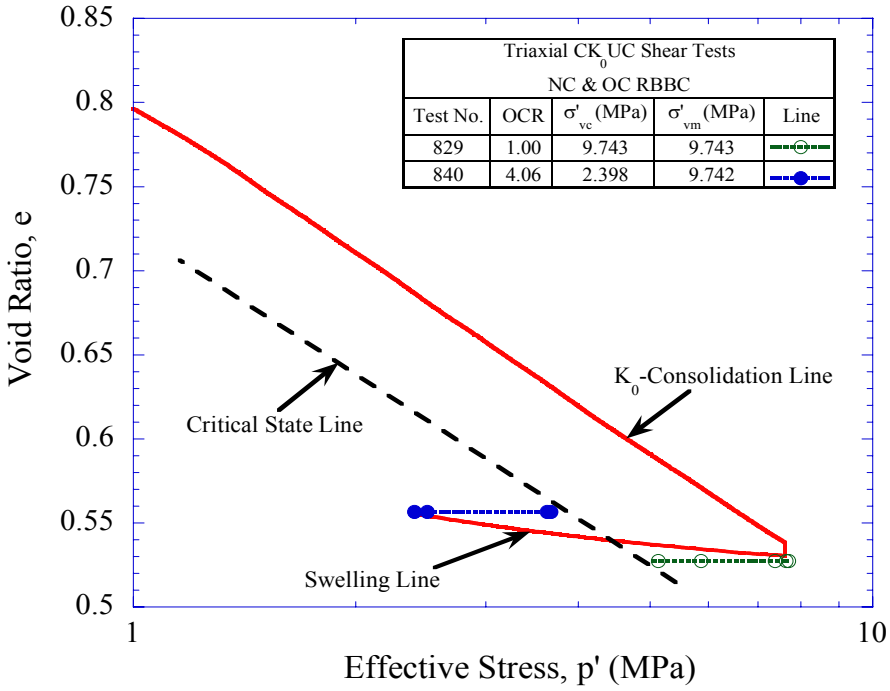

Figure 5-83: Effective stress paths during shearing in e-logp' space for RBBC (OCR = 1 & 4) from CK_0UC triaxial tests at high stress level (σ'_{vm} = 10 MPa)

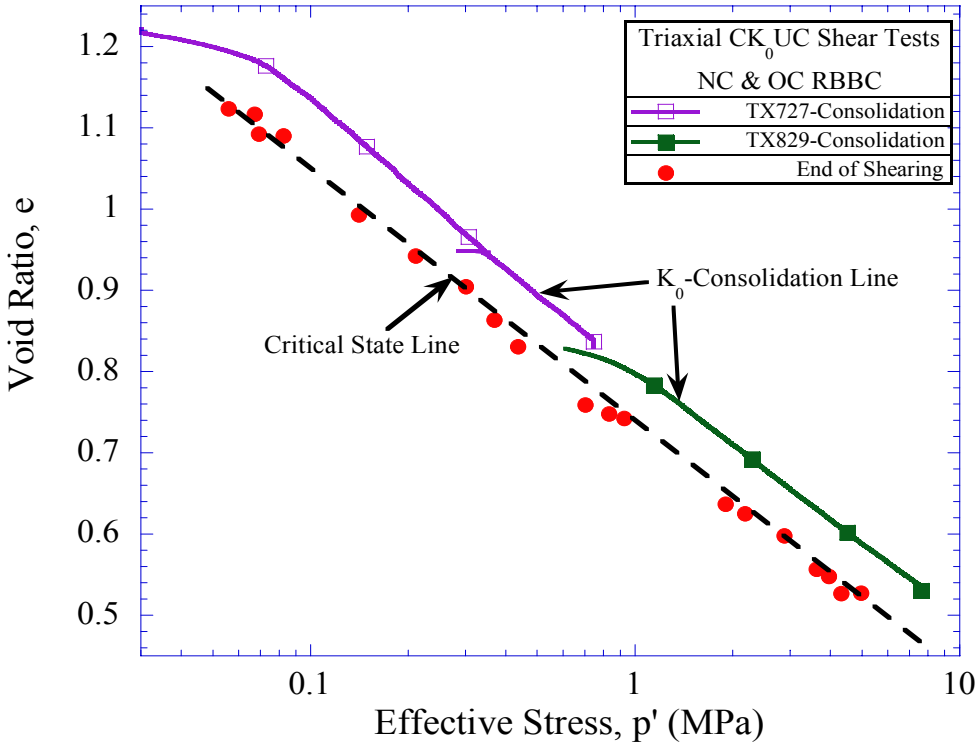

Figure 5-84: Large strain end of shearing stress states in e-logp' space for NC and OC RBBC from all CK_0UC triaxial tests compared with K_0-consolidation line

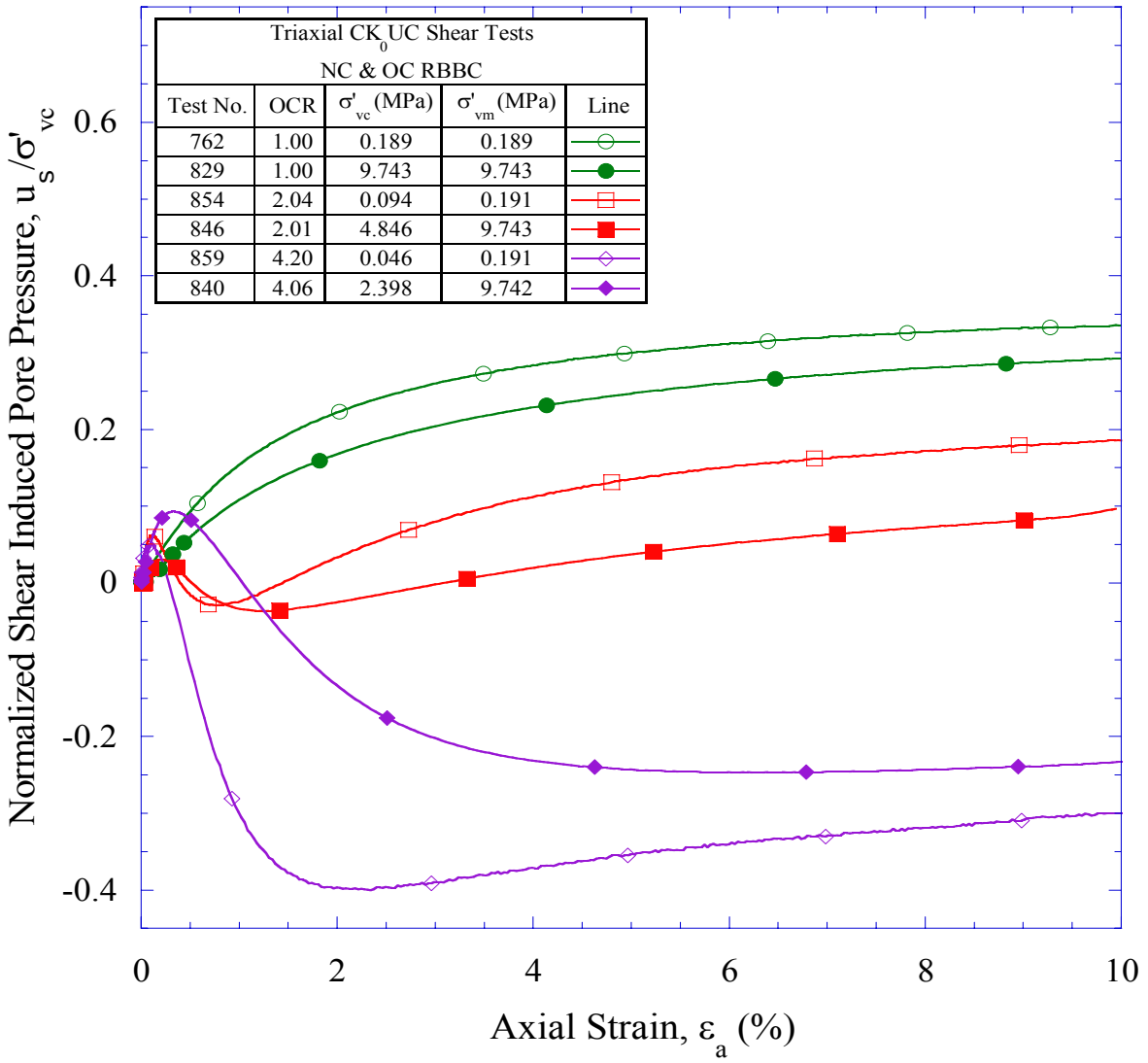

Figure 5-85: Normalized shear induced pore pressure versus strain for RBBC (OCR = 1, 2 & 4) from CK_0UC triaxial tests at low and high stress levels (σ'_{vm} = 0.2 & 10 MPa)

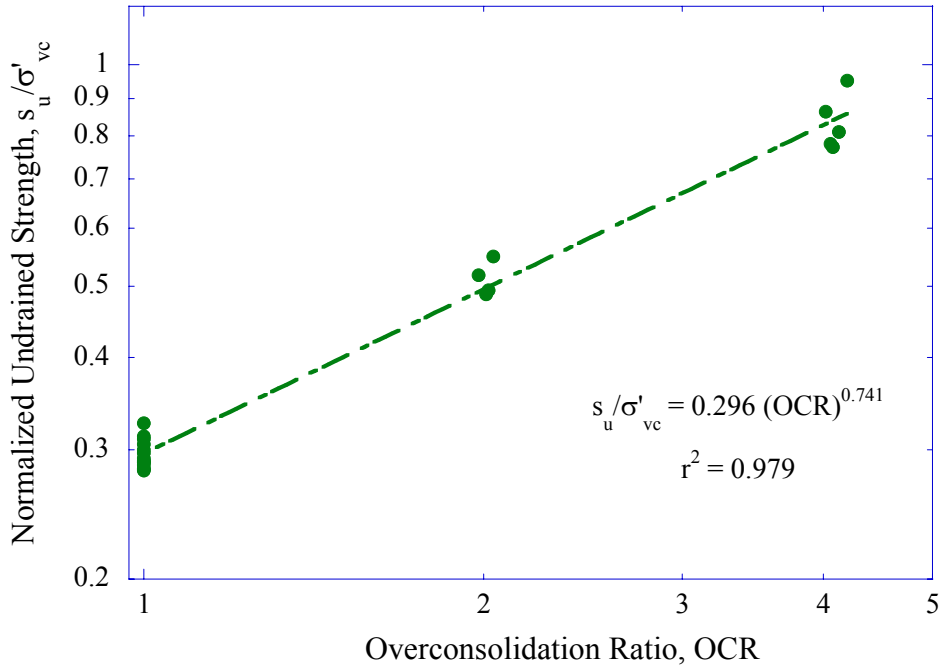

Figure 5-86: Normalized undrained strength versus OCR for RBBC from CK_0UC triaxial tests

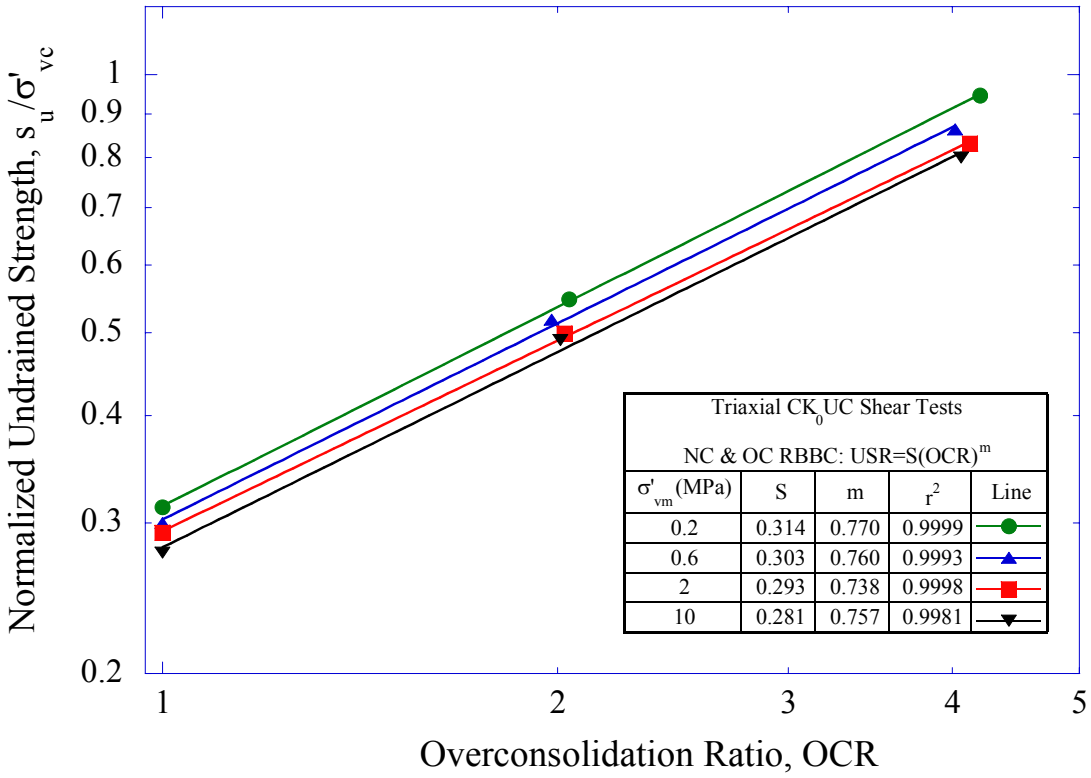

Figure 5-87: Normalized undrained strength versus OCR for RBBC from selected CK_0UC triaxial tests illustrating the effect of stress level

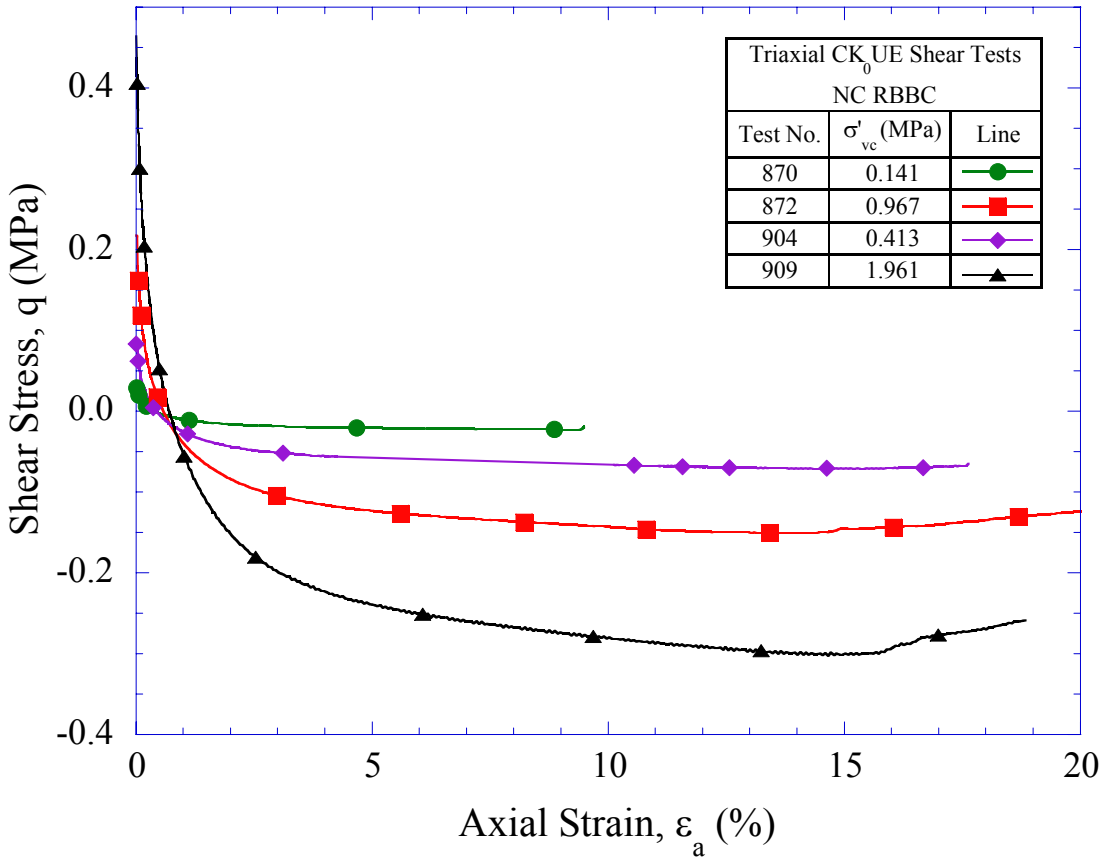

Figure 5-88: Stress-strain curves for NC RBBC from CK_0UE triaxial tests

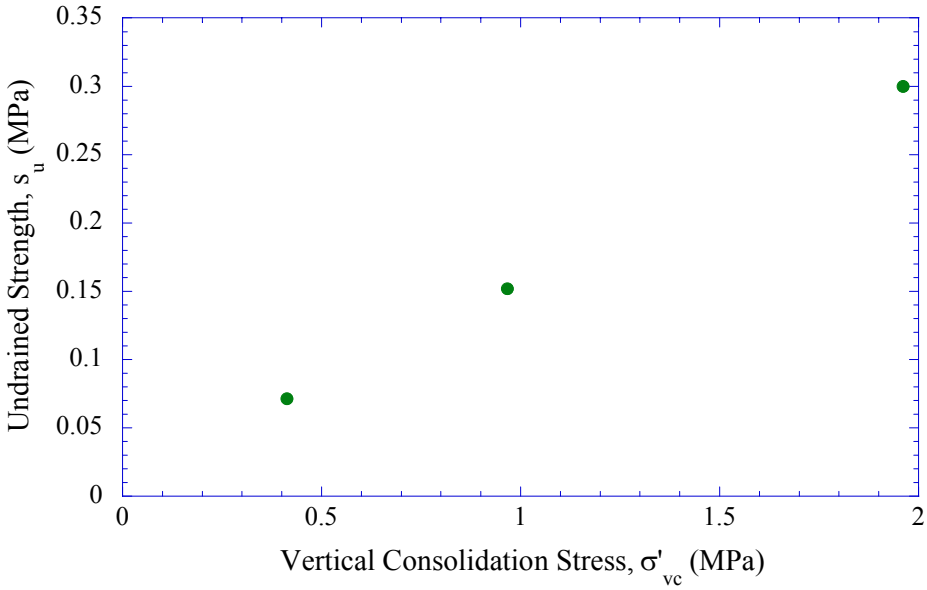

Figure 5-89: Undrained shear strength versus stress level for NC RBBC from CK_0UE triaxial tests

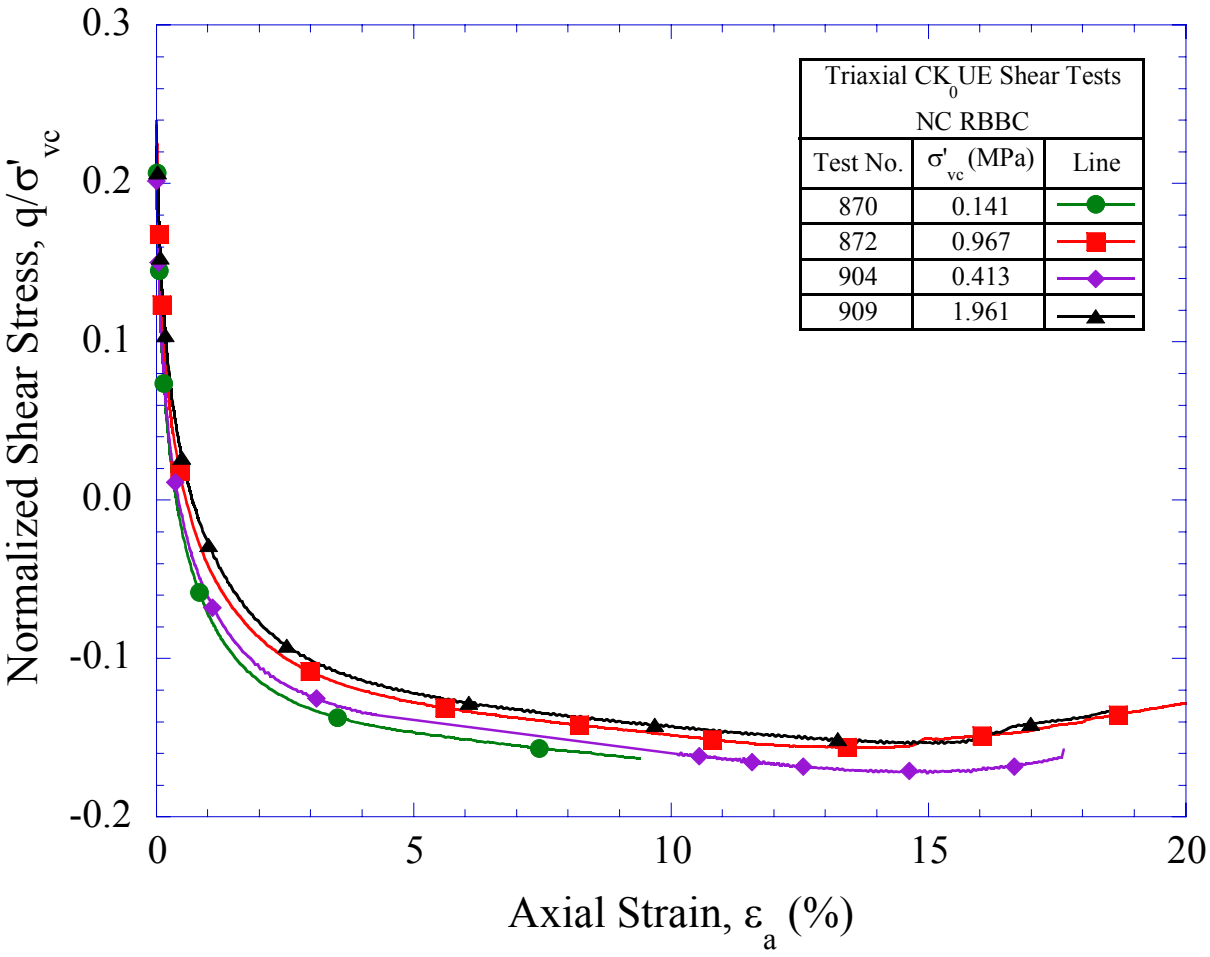

Figure 5-90: Normalized stress-strain curves for NC RBBC from CK_0UE triaxial tests

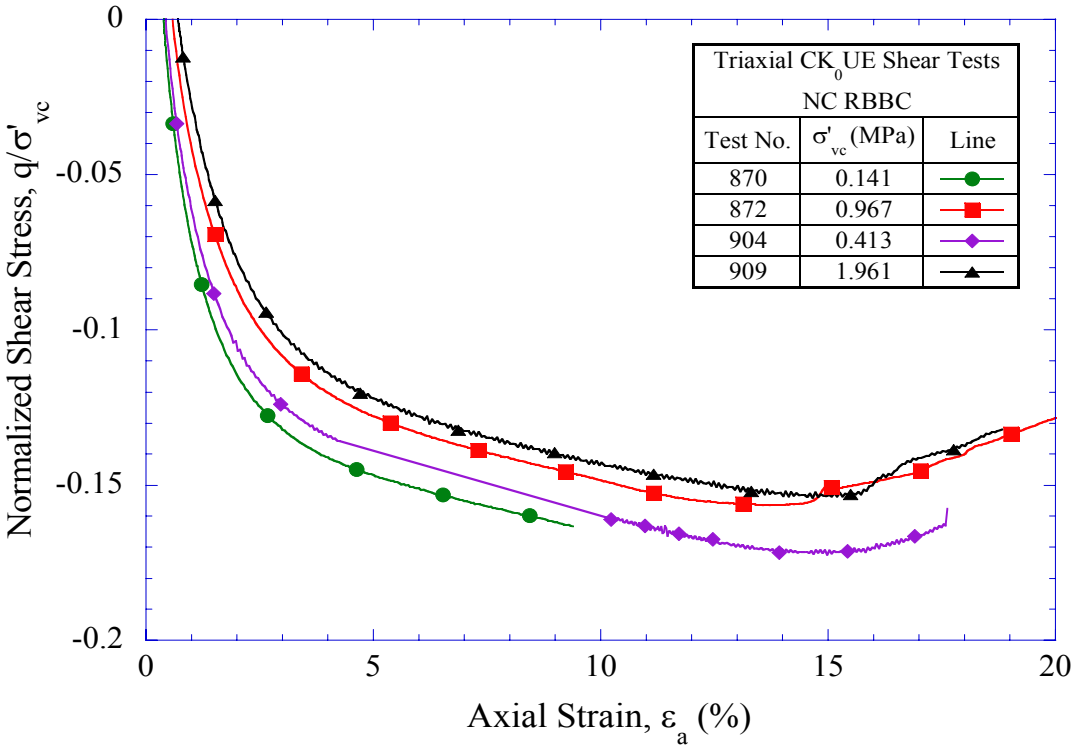

Figure 5-91: Normalized stress-strain curves (close up view) for NC RBBC from CK_0UE triaxial tests

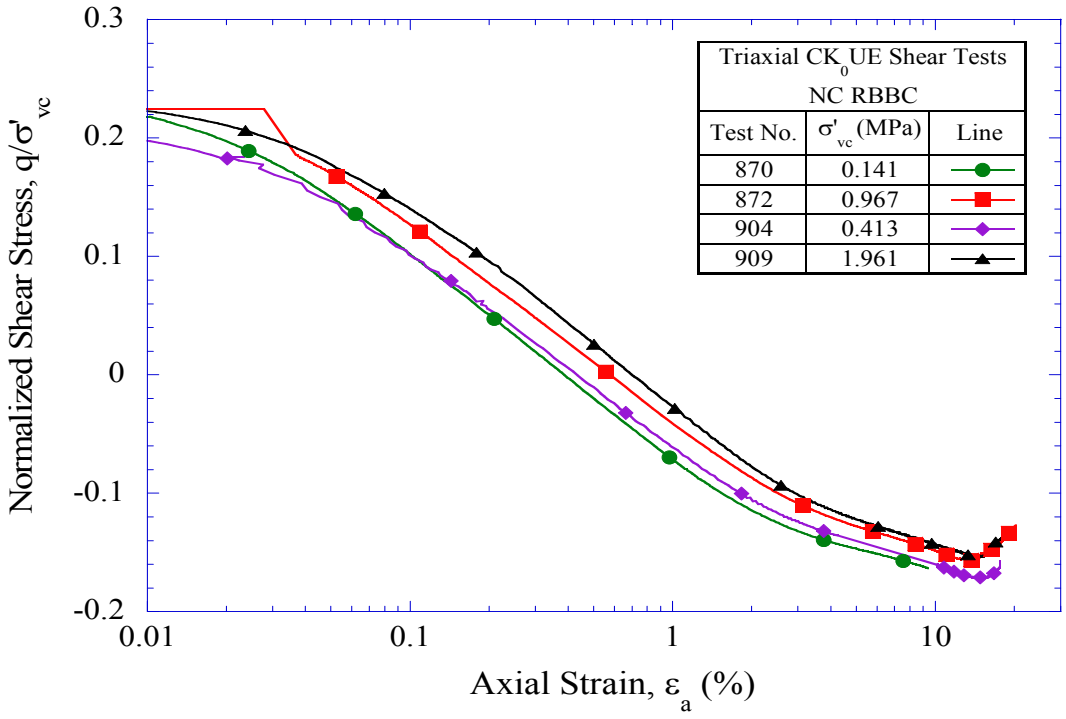

Figure 5-92: Normalized stress-(log) strain curves for NC RBBC from CK_0UE triaxial tests

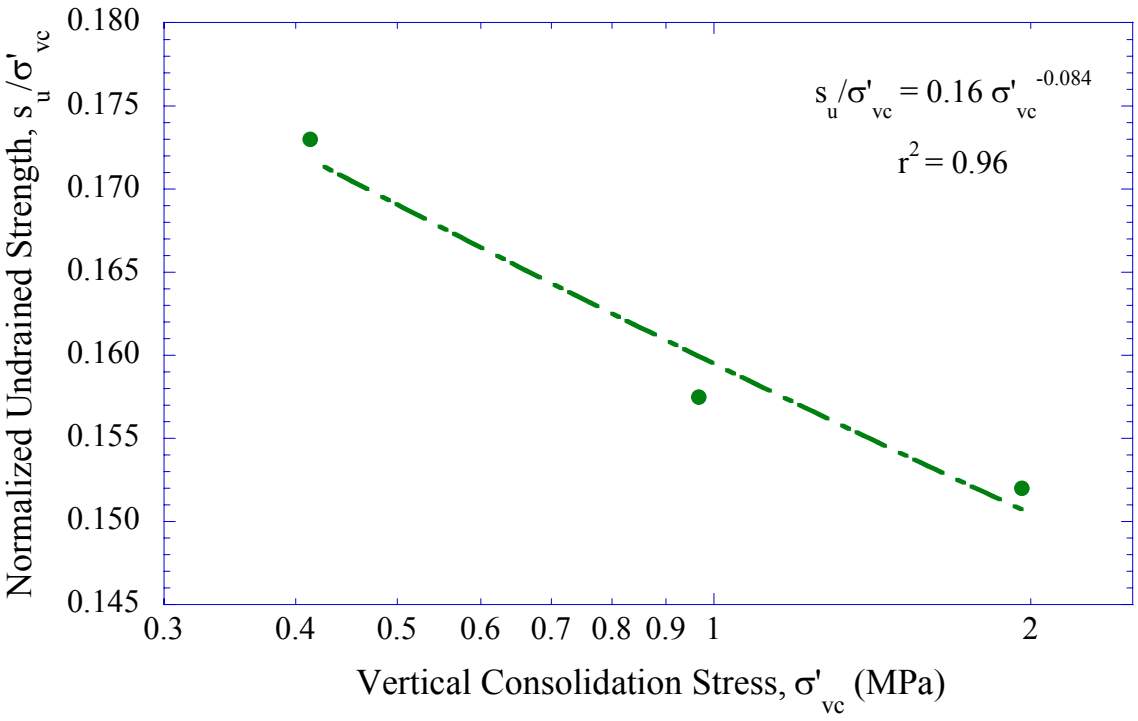

Figure 5-93: Normalized undrained shear strength versus stress level for NC RBBC from CK_0UE triaxial tests

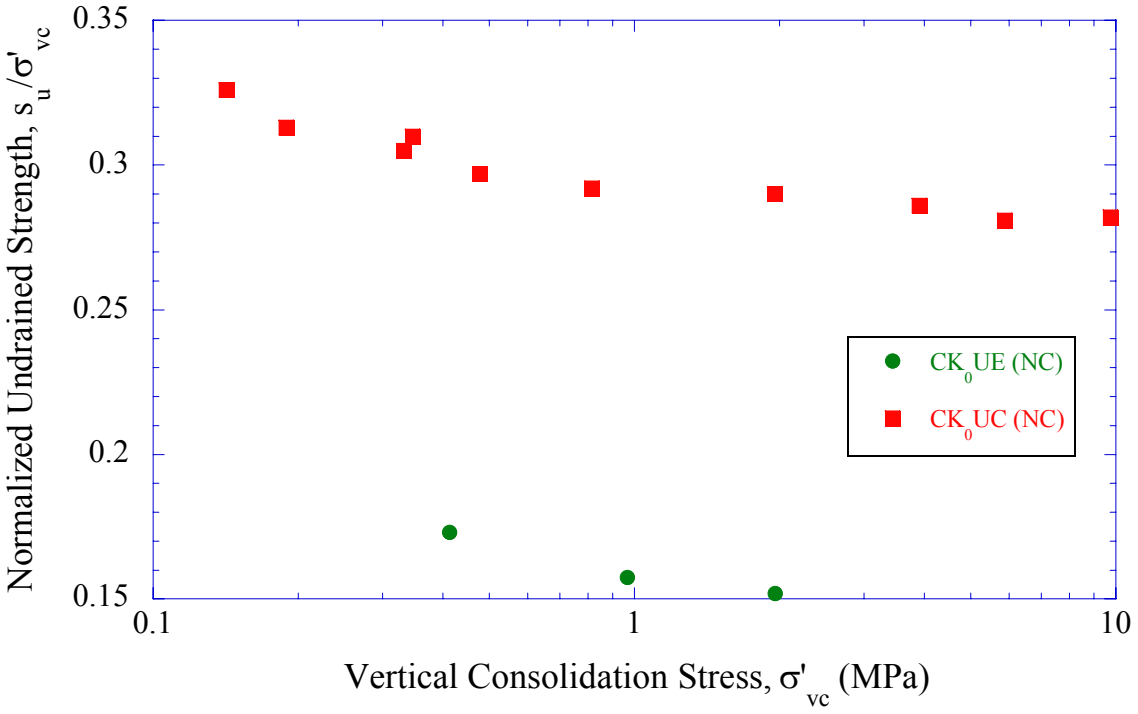

Figure 5-94: Normalized undrained shear strength versus stress level for NC RBBC from CK_0UE and CK_0UC triaxial tests

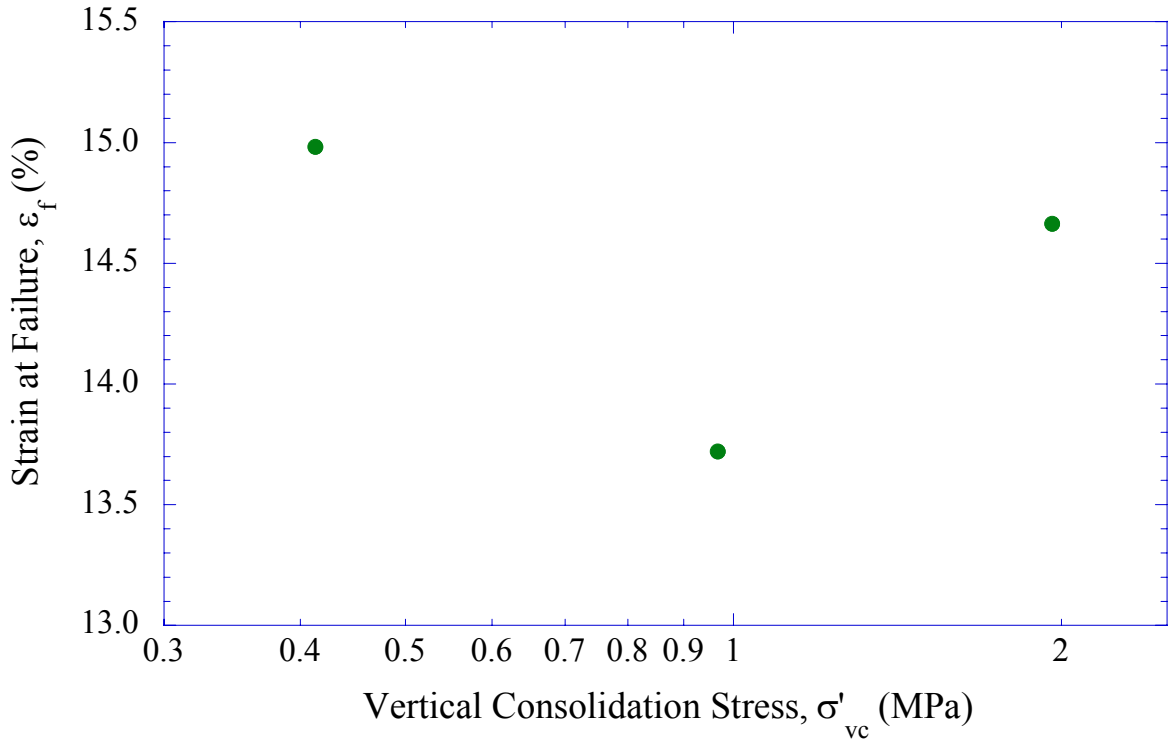

Figure 5-95: Strain at failure versus stress level for NC RBBC from CK_0UE triaxial tests

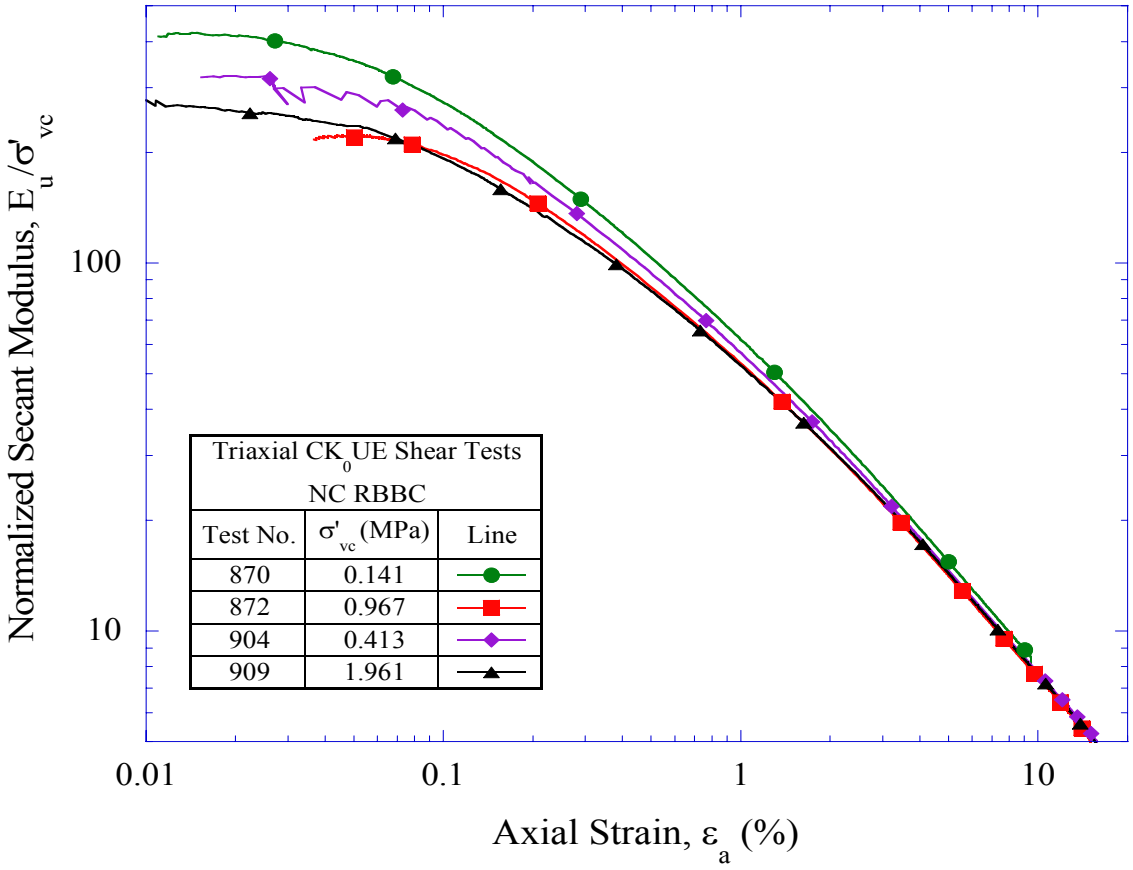

Figure 5-96: Normalized undrained secant modulus versus axial strain for NC RBBC from CK_0UE triaxial tests

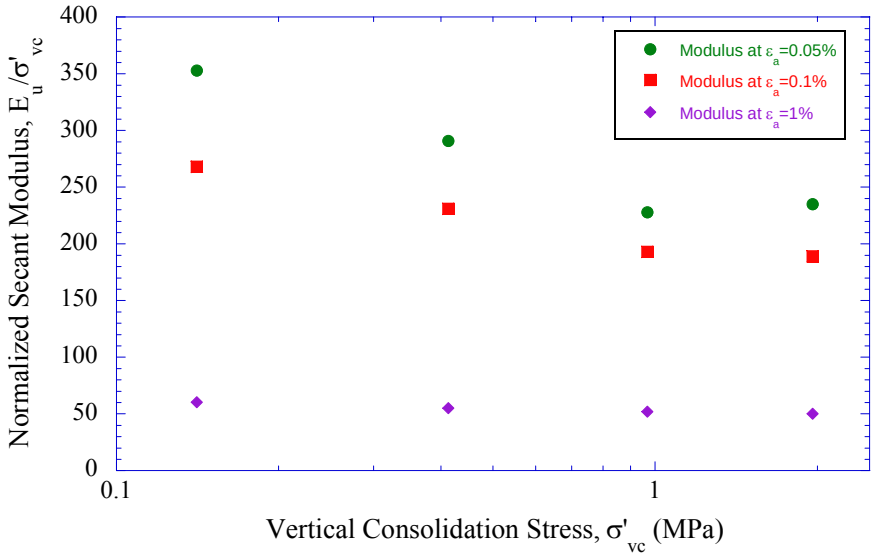

Figure 5-97: Normalized undrained secant modulus versus stress level for NC RBBC from CK_0UE triaxial tests

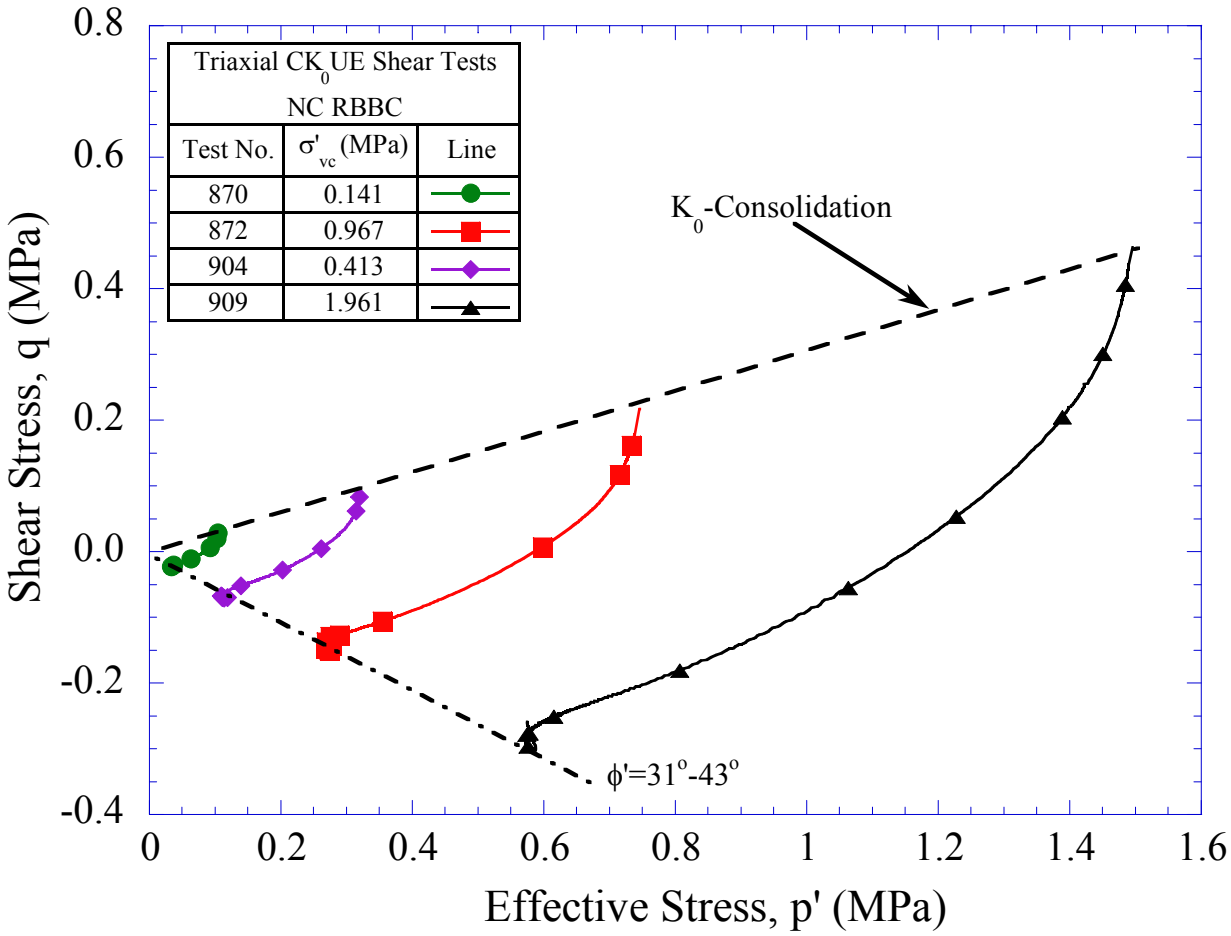

Figure 5-98: Effective stress paths for NC RBBC from CK_0UE triaxial tests

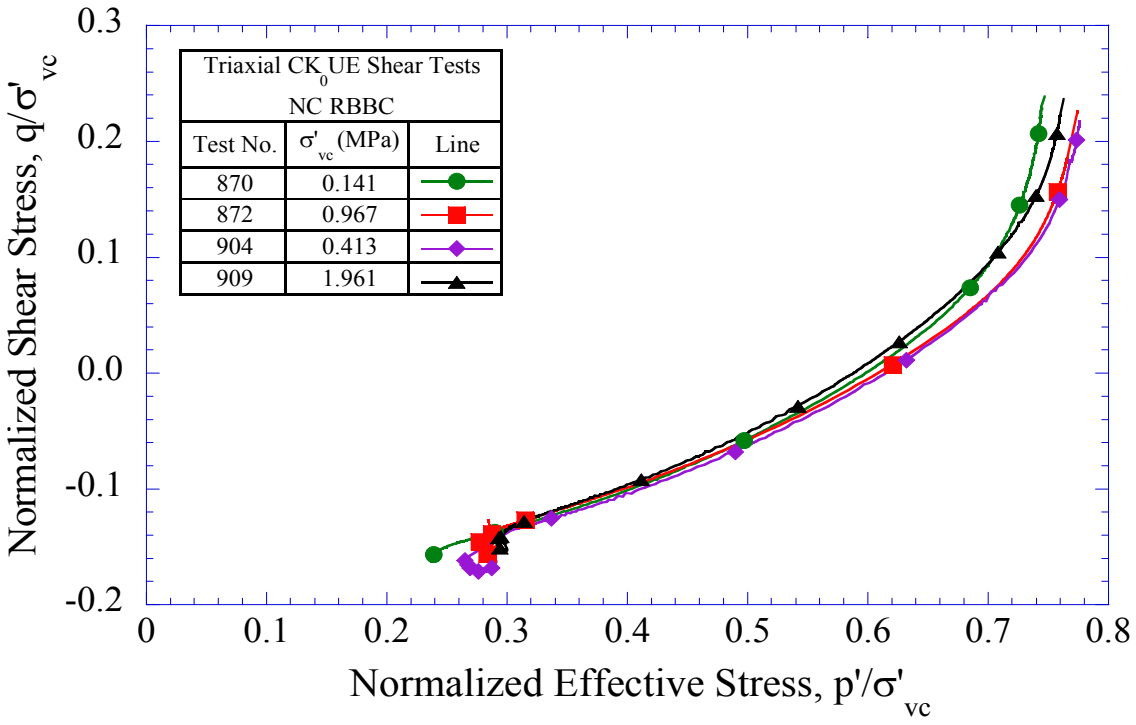

Figure 5-99 Normalized effective stress paths for NC RBBC from CK_0UE triaxial tests

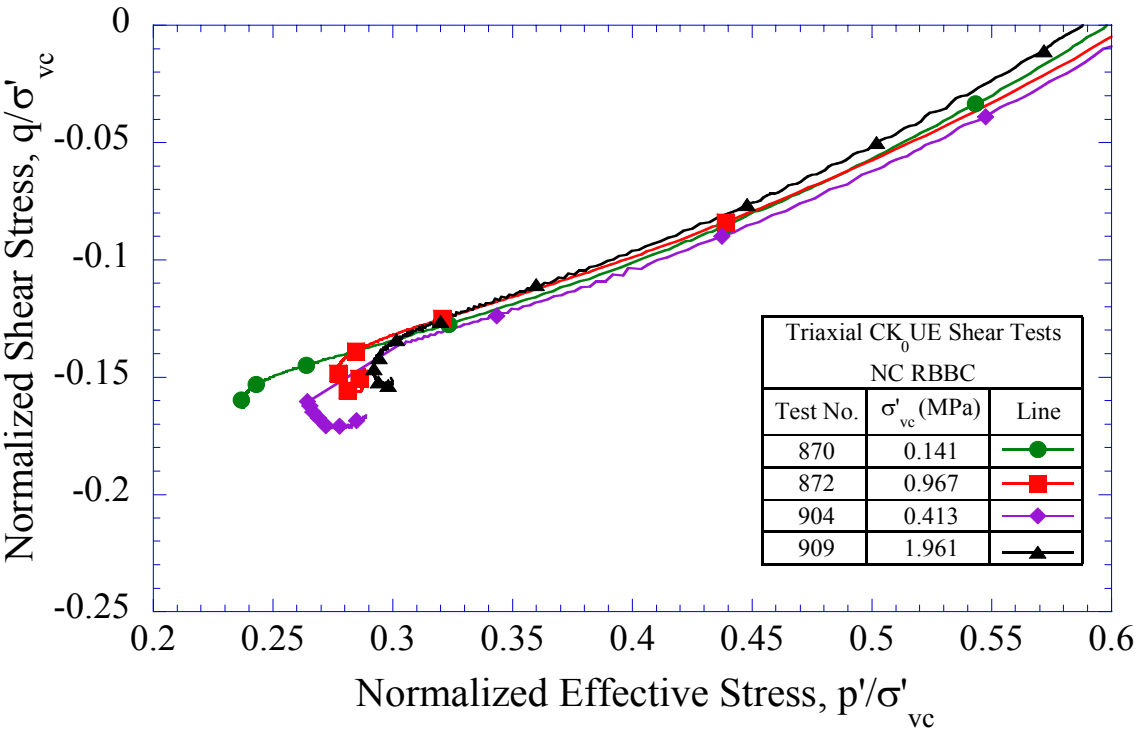

Figure 5-100: Normalized effective stress paths (close up view) for NC RBBC from CK_0UE triaxial tests

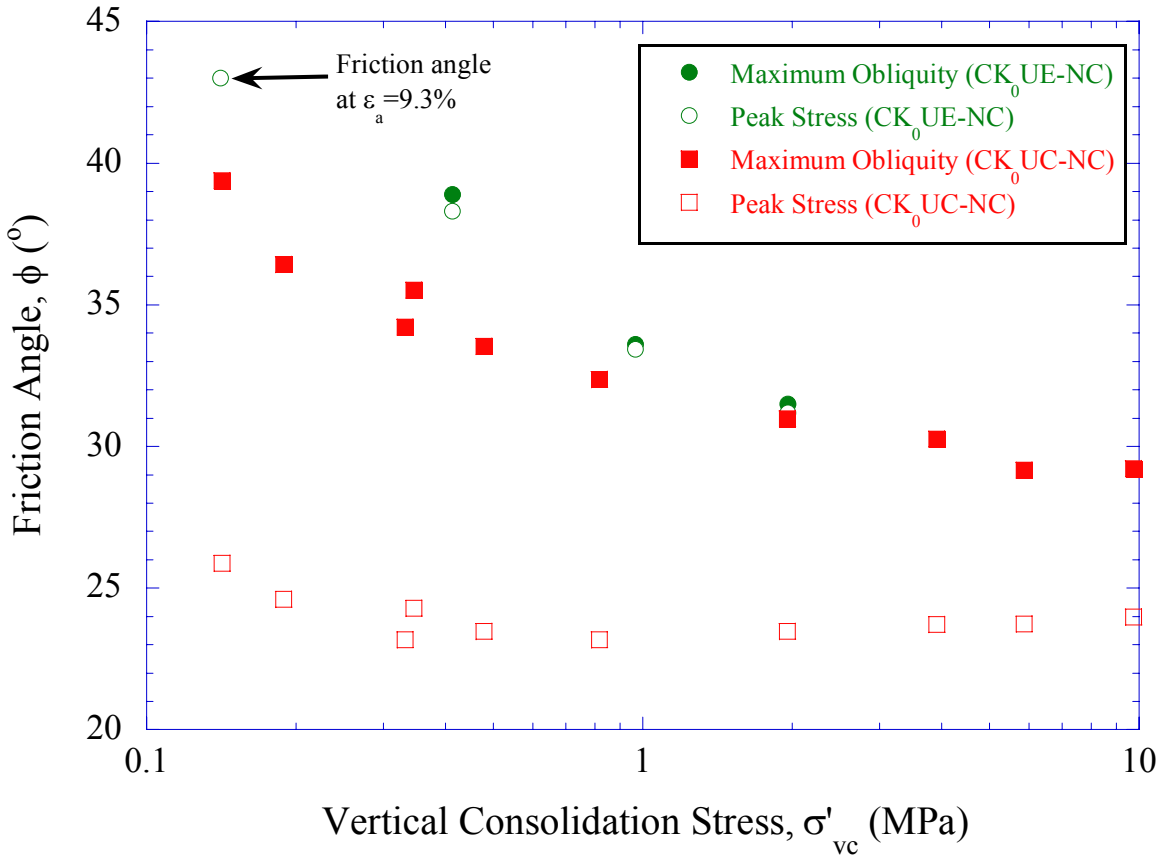

Figure 5-101: Friction angle at peak and maximum obliquity versus stress level for NC RBBC from CK_0UE and CK_0UC triaxial tests

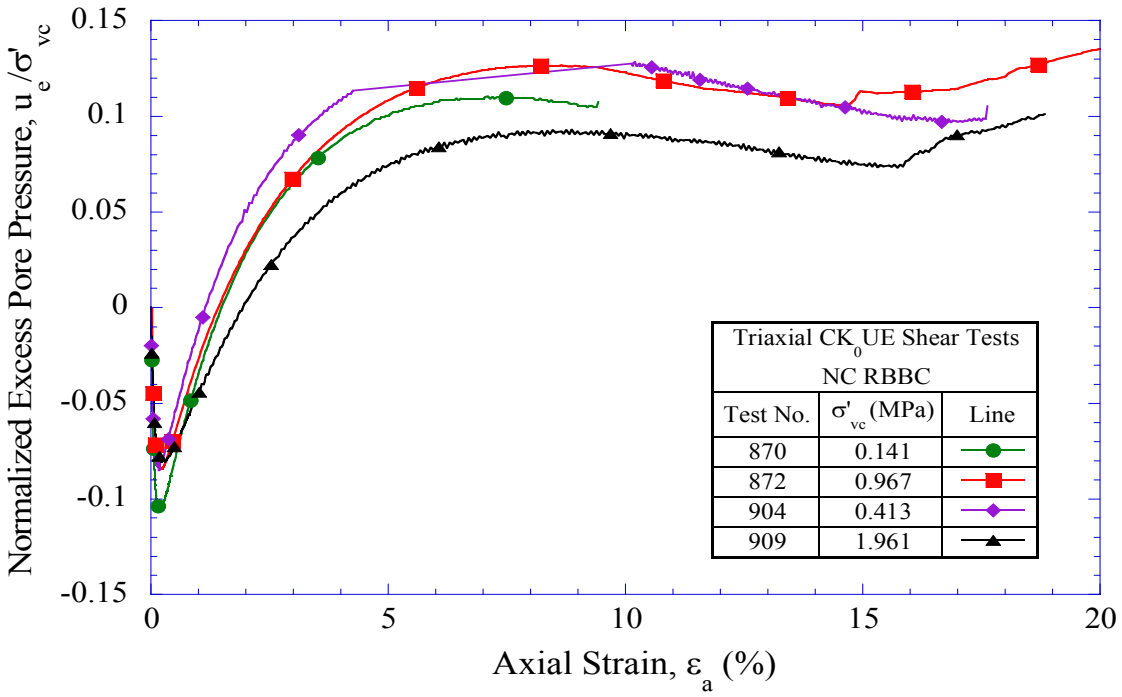

Figure 5-102: Normalized excess pore pressure versus strain for NC RBBC from CK_0UE triaxial tests

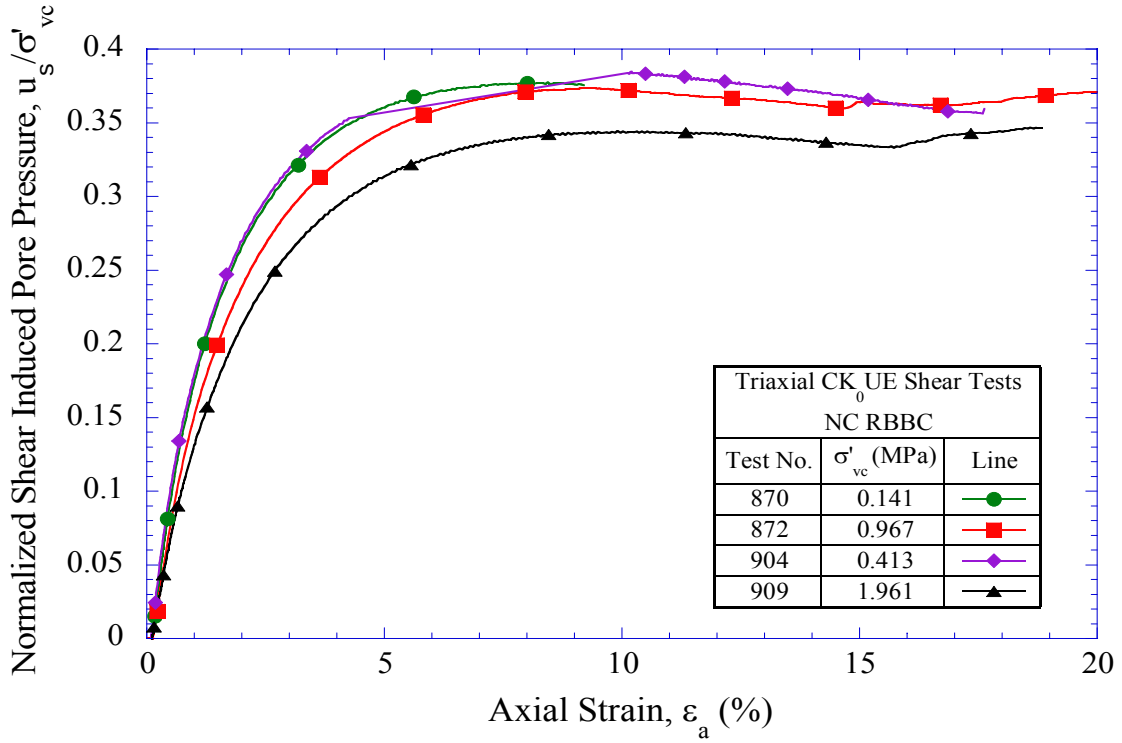

Figure 5-103: Normalized shear induced pore pressure versus strain for NC RBBC from CK_0UE triaxial tests

6 MODEL BOREHOLE BEHAVIOR

6.1 INTRODUCTION

This chapter describes and analyses the results of the model borehole experimental program using the Thick-Walled hollow Cylinder (TWC) apparatus. The main objectives of the TWC testing are to gain insight into the behavior of Resedimented Boston Blue Clay (RBBC) under simulated wellbore conditions and to provide data for comparison with analytical investigations. These objectives will be accomplished by investigating a number of variables which can potentially influence deformations of the model borehole including mode of loading, TWC specimen geometry, consolidation lateral stress ratio, drainage conditions, consolidation stress level, stress history, and strain rate. Most of the data from the TWC test program are presented in this chapter in the form of compilation plots to exhibit characteristics of model borehole behavior.

The chapter is organized to provide the reader first with a summary of the data obtained, then with a discussion and interpretation of the results using principles of soil mechanics and soil behavior. As such, Section 6.2 summarizes the experimental program of model borehole tests and presents the variables investigated. The subsequent section (Section 6.3) describes the results for a reference baseline test illustrating the presentation of the results and key features of a typical TWC test. Section 6.4 presents complete results of the experimental program, treating the effects of each of the aforementioned variables separately. Section 6.5 provides a comprehensive analysis of the data with a discussion of the relative importance of each of the parameters investigated.

6.2 EXPERIMENTAL PROGRAM

The model borehole experimental program comprised a total of 25 TWC tests and has generated a large amount of data regarding model borehole behavior. Of these, 3 tests experienced experimental problems and hence are not included in the analysis. Table 5-2 summarizes the TWC tests in the order in which they were performed. For each test the table provides the most relevant information: initial conditions (specimen dimensions, void ratio,

preconsolidation pressure), preshear consolidation conditions (vertical consolidation stress, OCR, lateral stress ratio, axial and volumetric strains), and borehole closure conditions (mode of loading, drainage conditions, strain rate).

As indicated in Table 5-2, one test (TWC17) was aborted at cavity volumetric strain, ε_{cav}=10.5%, but is reported since the data to that point are considered valuable. Axial loads were not controlled during borehole closure tests at the higher overconsolidation ratios TWC14 and TWC16 (OCR = 4 and 8, respectively). Maintaining constant axial stress requires the axial load to be reduced (to compensate for the reduction in the internal cavity pressure acting on the underside of the top cap). This was not achievable in these tests as the preshear lateral stress ratio, $K_c \approx 1$ (i.e., $\sigma'_h/\sigma'_v \approx 1$), and the current TWC design cannot simulate conditions with $\sigma_v < \sigma_h$ (extension mode). This lack of extension capability also resulted in the classification of TWC16 as a 'pseudo' OCR = 8 test (i.e., although $\sigma'_{vm}/\sigma'_{vc} = 8$ but K = 1 is imposed artificially). Table 5-2 also indicates that the same test specimen for an initial borehole contraction procedure (internal cavity unloading) in TWC22 was then consolidated to a higher effective consolidation stress and an expansion test (internal cavity loading) was carried out (TWC22a). Finally, test TWC23 experienced an internal leak during consolidation which required dismantling the apparatus and cleaning the TWC specimen (cell oil did not penetrate the specimen) before reassembling the test.

The focus of this experimental program was to develop a comprehensive understanding of the factors controlling the behavior of a model borehole. This involved investigating the impact of a number of critical variables. These variables included:

1) Mode of Loading
   a) Internal cavity unloading (contraction) versus external cell loading
   b) Internal cavity unloading (contraction) versus internal cavity loading (expansion)
2) Specimen Geometry
   a) Height
   b) Outer diameter
3) Consolidation lateral Stress Ratio

4) Drainage Conditions

5) Consolidation stress Level

   a) Undrained tests with small diameter TWC specimens

   b) Drained tests with small diameter TWC specimens

   c) Undrained tests with large diameter TWC specimens

6) Stress History

7) Strain Rate

A substantial part of the TWC experimental program has been performed in the small TWC apparatus (MIT06), where the test specimens had an outer diameter, D_o = 7.6 cm, inner diameter, D_i = 2.5 cm, and height, H = 15.2 cm. The 'base' case test configuration comprised the following conditions: OCR = 1, K_c = 0.55, and undrained internal cavity unloading performed at an average cavity volumetric strain rate, $\dot{\varepsilon}_{cav}$ = 10 %/hr. In most cases, investigating the different variables involved varying one of these parameters while keeping the others unchanged. Note that the TWC tests were essentially consolidated in the TWC apparatus to 5 nominal vertical effective stress levels: 0.15, 1.5, 3.0, 6.0, and 10.0 MPa. The effect of varying the specimen height (H = 15.2, 11.5, 8.1 cm) was also evaluated in the small TWC apparatus. Three tests have been performed in the large TWC apparatus (MIT09), where the test specimens had an outer diameter, D_o = 15.2 cm, inner diameter, D_i = 2.5 cm, and height, H= 22.8 cm, to investigate the effect of the outer boundary on the test results (for the internal cavity contraction and expansion cases). The two modes of loading investigated to introduce the mechanisms of instability, other than the 'standard' method of reducing the cavity pressure, are increasing the external cell pressure or increasing the internal cavity pressure (pressuremeter expansion mode). Tests with preshear lateral stress ratio (K_c) of 1.0 and 0.55 were performed as well as drained and undrained borehole closure tests. In addition, the influence of consolidation stress level was evaluated in the small TWC apparatus for the drained and undrained tests and in the large TWC apparatus for the undrained tests. Finally, the effects of varying the preshear stress history (OCR = 1, 2, 4, 8) and the undrained shear strain rate ($\dot{\varepsilon}_{cav}$ = 0.5, 10, 60 %/hr) were investigated.

6.3 OVERVIEW OF THE REFERENCE MODEL BOREHOLE TEST

6.3.1 Introduction

This section presents the consolidation (Section 6.3.2) and borehole closure (Section 6.3.3) results of an anisotropically consolidated undrained (CAU) TWC test (TWC7; see Table 5-2). This reference test satisfies the base conditions listed above (i.e., small diameter NC RBBC specimen, K_c=0.55, undrained borehole closure at an average cavity volumetric strain rate of 10%/hr) and was consolidated to maximum vertical effective stress, σ'_{vm} = 10 MPa.

6.3.2 Stress Path Consolidation

The RBBC specimen was prepared in the consolidometer to stress levels close to those planned for the TWC test ($\sigma'_p = 0.65\ \sigma'_{vm}$) in order to reduce consolidation time in the TWC apparatus and to limit the strains occurring in the test[11]. The reference specimen was initially consolidated to σ'_p = 6.5 MPa in the laboratory consolidometer. After completing the set-up and back pressure saturation[12], the specimen was isotropically consolidated to $\sigma'_v = 0.25\ \sigma'_p$. Thereafter, the soil was consolidated in two stages using stress path consolidation at an axial strain rate of 0.3 %/hr. Figure 2-1 shows the effective stress path during consolidation for reference test TWC7. The first stage of stress path consolidation in the TWC apparatus starts from the isotropic condition and approaches a predefined target value, K = 0.55 at $\sigma'_v = 0.8\ \sigma'_p$ (i.e., σ'_v = 5.2 MPa; σ'_h = 2.9 MPa). This ensures that the specimen does not yield during this first stage of reconsolidation. The second stage involves stress path consolidation at K = 0.55 to the specified stress state ($\sigma'_{vm} = 1.5\ \sigma'_p$ = 10 MPa; σ'_{hm} = 5.5 MPa). The value of K was selected based on information from the triaxial test program (see Chapter 5). Figure 6-2 shows the lateral stress ratio during the consolidation process for the reference test. The figure illustrates that K reduces from 1 to 0.55 during the first stage then remains constant during the second stage. The specimen was then left for 24 - 48 hrs with the stresses held constant to allow full equilibration of volume strain in the specimen. Since the consolidation process in the TWC apparatus is

[11] The TWC apparatus has a rigid top drainage line that cannot accommodate large strains.

[12] Note that the sampling effective stress (σ'_s) measured at the beginning of the test tends to be 0.2 – 0.25 σ'_p.

carried out to stress levels higher than in the consolidometer, effects of the set-up disturbance are minimized.

The compression curves in terms of axial and volumetric strains are shown in Figure 6-3. The figure shows that the compression curves become much steeper once the batch preconsolidation pressure (σ'_p = 6.5 MPa) is reached. Note that the preconsolidation pressure was not determined from the compression curves and the values reported in Table 5-2 are based on the maximum consolidation pressure imposed in the consolidometer. The final volumetric strain reached at the end of the test is 6.77% while the axial strain is 7.48%. Figure 6-3 also shows that the axial and volumetric strains are not identical during consolidation which could indicate that the soil specimen was not consolidated strictly under 1-D (i.e., K_0) conditions. In addition, the 'secondary' compression at the end of the test is fairly large. However, these are believed to be due to the relatively fast axial strain rate[13], which generated excess pore pressures during consolidation and hence, the specimen continued to consolidate even when the maximum stress was reached.

This stress path consolidation procedure was used in all the TWC tests apart from the first three tests (TWC1-3; see Table 5-2) that were isotropically consolidated (K_c=1). For the overconsolidated tests (OCR>1), stress path unloading was performed with strain rate of 0.2%/hr using the empirical method governed by Equation 4.1. In general, the compression curves and the axial and volumetric strains obtained at the end of consolidation for all tests are comparable, as illustrated in Table 5-2. Since the consolidation properties of RBBC were extensively reported for the batch (Chapter 3) and for the triaxial tests (Chapter 5), the following sections will only discuss the shearing phase of the tests.

6.3.3 Undrained Borehole Closure

Mechanisms of instability were introduced in the reference test by reducing the internal pressure in the model borehole while keeping the external cell pressure and axial stress constant. Borehole closure was performed by extracting cavity fluid using the Pressure-Volume Controller (PVC; see Chapter 4) at an average cavity volumetric strain rate, $\acute{\varepsilon}_{cav}$ = 10 %/hr. The tests were typically terminated at ε_{cav} = 20%. The drainage valves were closed to maintain undrained

[13] The axial strain rate employed in the triaxial tests during consolidation was 0.15%/hr.

conditions within the specimen during cavity contraction while pore pressures were measured at the ends.

Figure 6-4 shows the uncorrected and corrected[14] curves of net internal cavity pressure inside the borehole (p_i-u_0; where u_0 is the pore pressure at the start of shearing) versus cavity volumetric strain ($\varepsilon_{cav} = \Delta V/V_0$) for the reference test that was initially consolidated to σ'_{vc} = 10MPa. Figure 6-5 shows a close up view of Figure 6-4 for strains up to ε_{cav} = 5%. The uncorrected curve represents the 'raw' measurement obtained from the cavity PVC. Correcting for system compliance (e.g., compressibility of cavity fluid, tubing etc.) produces a significant shift in the contraction curve. In addition, a correction was made for the axial strain occurring during borehole closure assuming cylindrical deformation (Figure 6-6 shows the axial strain versus cavity volume strain). Figures 6-4 and 6-5 illustrate that the axial strain does not affect the initial pressure drop but implies smaller cavity strains at later stages of the test (the end point shifts by around 0.8% volume strain). This is because the axial strain is minimal during the first 5% cavity volume strain, as illustrated in Figure 6-6, but then increases as the volume strain increases.

The corrected (p_i-u_0) – ε_{cav} curve demonstrates that the bulk of the pressure drop occurs within the first 5% volume strain before the borehole becomes unstable (i.e., deforms without further reduction in cavity pressure). The cavity pressure reaches a minimum of about p_i-u_0 = 1.5MPa at ε_{cav} = 7-8%, then exhibits a very slight increase with continued volume strain through the end of the test. This latter behavior might imply that the specified volume extraction rate is smaller than the specimen deformation rate. A close up view of the corrected results up to ε_{cav}= 5% (Figure 6-5) implies an initial linear cavity stiffness before reaching a 'yield' point at $\varepsilon_{cav} \approx 0.4\%$. However, it must be noted that it is difficult to reliably determine a yield stress by measuring the overall cavity volume strain (as oppose to direct local measurement of the radial strain).

Figure 6-7 shows the net internal cavity pressure (p_i-u_0) as a function of the mid height cavity radial strain ($\varepsilon_r = \Delta r/r_0$), which is computed based on the corrected cavity volume measurements. Here the interpretation of the cavity strain depends on the fixity at the top and bottom platens and the assumed deformation mode shape. The uniform cylindrical radial strain is

[14] Refer to Chapter 4 (Section 4.5.3.7) for the corrections made for the TWC tests.

simply half the cavity volumetric strain after correction ($\varepsilon_{cav} = 2\varepsilon_r$). The parabolic deformation mode shape assumes zero radial deformation at the specimen's ends and maximum deformation at mid height. Therefore, the parabolic assumption shows a higher radial strain at a given cavity pressure than the uniform assumption. However, the measured mid height deformation at the end of the test tends to be somewhat between the two assumed deformation (i.e., corresponding to the end point of the average contraction curve shown in Figure 6-7). Note that all figures of net cavity pressure versus mid height radial strain presented in the following sections are for the average case.

Measurements of the internal cavity volume change and external cell volume change were recorded during the borehole closure test. PVCs mounted with LVDTs were used to measure the volume changes. During an undrained test (i.e., zero volume change in the test specimen), the total volume of the TWC cell should remain constant. Hence, the volume of fluid expelled from the model borehole should balance the increase in volume of fluid in the outer cell (necessary to maintain the constant cell pressure). Figure 6-8 compares the inflow into the external cell with the volume of fluid expelled from the model borehole for the uncorrected and corrected (system compliance correction only) cases. Figure 6-9 shows a close up view of Figure 6-8 at small volume changes (up to 3 cm^3). The results for the uncorrected cavity volume show a relatively large imbalance (more fluid is withdrawn from the model bore). When system compliance is included in the volume calculations there is much better agreement between the two fluid volumes as shown in Figures 6-8 and 6-9.

In the model borehole test, a difference between the internal cavity pressure (p_i) and the external cell pressure (p_o) establishes a gradient of radial stress and circumferential (hoop) stress across the TWC test specimen. In addition, non-uniform stresses can develop due to the effects of wall curvature and end restraints. During undrained shearing, the non-uniformity in stress and strain results in pore pressure non-uniformity (i.e., pore pressure gradient across the specimen wall). The analysis by Gibson (1963) has shown that the extent to which equalization of pore pressure occurs within the sample depends on the permeability and compressibility of the specimen, its dimensions (drainage path length) and the rate of testing. The distribution of pore pressure in the TWC specimen before equalization is very complicated and difficult to calculate

accurately[15]. In the present study, considering the difference in the dimensions and the drainage conditions[16] in the small diameter TWC specimen and standard triaxial specimen, the time to reach 95% equalization of pore pressure within the sample at a given strain rate is shorter in the model borehole tests. However, due to the notably higher shearing rates[17] employed during borehole closure it is likely that the pore pressures are not fully redistributed within the TWC specimen. The measurements at the specimen ends are considered to represent an 'average' pore pressure across the width of the specimen. Figure 6-10 shows the development of excess pore pressure ($u_e = u-u_0$) due to the reduction of the internal cavity pressure. The results show that the pore pressure increases continuously with the cavity volume strain. The pore pressures measured at the minimum net cavity pressure (corresponding to ε_{cav} = 7-8%), u_e = 0.8 MPa and rise to 1.1 MPa at the end of shearing. These changes in pore pressure occur with minimal change in total stress and hence, reflect internal redistribution of the non-uniform pore pressures within the test specimen.

Non-uniform stress and strain conditions within the TWC specimen make reliable interpretation of effective stresses problematic. For example, Figure 6-11 shows the inferred radial effective stress at the inner cavity wall ($\sigma'_{ri} = p_i - u$). Similarly, Figure 6-12 shows the inferred radial effective stress at the outer wall ($\sigma'_{ro} = p_o - u$). These definitions assume that the measured pore pressure is fully redistributed and accurately represent the average conditions at the inner and outer walls of the TWC specimen. The results show that the cavity radial effective stress decreases monotonically with cavity volume strain, but at a decreasing rate. At ε_{cav} = 7-8% (corresponding to the minimum cavity pressure), σ'_{ri} = 0.45 MPa. The external cell pressure is kept constant during the test and the decreasing trend of σ'_{ro} shown in Figure 6-12 is because of the pore pressure generation illustrated in Figure 6-10.

---

[15] The general trend can be inferred from the following equation: $\Delta u = B\{\Delta\sigma_1 - (1\text{-}A)(\Delta\sigma_1 - \Delta\sigma_3)\}$; where Δu is the change in pore pressure corresponding to undrained changes in the minor principal stress σ_3 and the major principal stress σ_1, and A & B are the Skempton pore pressure parameters.

[16] The pore pressures are measured at both ends of the TWC specimen and filter paper is applied to the outer surface to allow radial drainage. No filter paper is applied to the triaxial specimen.

[17] The standard cavity volumetric strain rate, $\dot{\varepsilon}_{cav}$ = 10%/hr employed in the TWC tests is about 10 -15 times faster than the shearing rate used in the triaxial ($\dot{\varepsilon}_a$=0.5%/hr) when compared in terms of shear strains (γ). Note that the effect of strain rate on the TWC results was investigated and the results are presented in Section 6.4.8.

Post-test observations and measurements of the TWC test specimen indicate that the cross-sectional radial deformations are uniform (i.e., there is little distortion of the cross-section). In addition, vertical cracks were observed at the inside wall of the borehole for specimens initially consolidated to maximum vertical effective stresses, $\sigma'_{vm} \geq 6$ MPa.

6.4 RESULTS FROM VARIABLES INVESTIGATED

6.4.1 Introduction

This section presents the results of the model borehole experimental program by discussing each of the variables investigated separately. Table 5-2 summarizes the consolidation and borehole closure conditions for the TWC tests. An interpretation of the results is provided in the subsequent section (Section 6.5).

6.4.2 Mode of Loading

There are several ways to introduce the mechanisms of instability in the TWC specimen. Instabilities can be induced by increasing the boundary stress applied to the external surface of the cylinder, while keeping the internal cavity pressure constant. On the other hand, the internal borehole pressure can be either reduced or increased, while keeping the external cell pressure constant.

Most of the tests in this experimental program were performed by reducing the internal borehole pressure while keeping the external cell pressure and axial stress constant. This procedure is more representative of what happens during and shortly after drilling of a wellbore. However, the other two methods of creating instabilities in the TWC specimen were also investigated and the results were compared. It must be noted that the internal loading tests were carried out to evaluate the pressuremeter cavity expansion mode, since the method employed to analyze the TWC results is based on the pressuremeter mode of shearing. The following subsection (Section 6.4.2.1) compares results from internal unloading and external loading tests. Section 6.4.2.2 compares results from internal cavity unloading and loading tests.

6.4.2.1 Internal Unloading versus External Loading

Investigation of the internal cavity unloading and external cell loading modes was performed on small diameter NC RBBC specimens consolidated isotropically (i.e., K_c=1) to 0.15 MPa. The tests were sheared in undrained conditions with no external drainage from the test specimen (i.e., CIU tests). Note that the nominal cavity volumetric strain rate employed in these tests ($\acute{\varepsilon}_{cav}$=20%/hr) is faster than the 'standard' rate of 10%/hr. Figures 6-13 and 6-14 show the net external cell pressure (p_o-u_0) for test specimen TWC2 and net internal cavity pressure (p_i-u_0) for test specimen TWC1 versus the cavity volumetric strain (ε_{cav}) with ε_{cav} up to 20 and 2%, respectively. The results show that the loading curve appears to be slightly stiffer at low volume strains than the unloading curve. However, both curves increase/decrease rapidly at the beginning before the borehole becomes unstable (i.e., deforms with minute changes in pressure) when p_i-$u_0 \approx$ 0.05 MPa for the unloading test (TWC1) and p_i-$u_0 \approx$ 0.25 MPa for the loading test (TWC2) at volume strain in the range ε_{cav} = 2-4%.

Figure 6-15 depicts the development of excess pore pressure (u_e) measured versus the cavity volumetric strain. The results illustrate that the u_e developed during external loading is considerably greater than the pressures developed during internal unloading (0.15 MPa versus 0.035 MPa at end of the test). During internal unloading and external loading, the specimen deforms inwards as the cavity contracts which results in large circumferential stresses across the wall. However, the total radial stress at the inner cavity wall is decreasing in the internal unloading test (external radial stress constant), while the radial stress at the outer wall is increasing in the external loading test (internal radial stress constant). Therefore, the average total stress in the TWC specimen is significantly higher in the external loading case which explains the higher pore pressures developed during the test.

The inferred radial effective stresses at the inner cavity wall (σ'_{ri}) versus ε_{cav} are shown in Figure 6-16. The figure shows that the radial effective stresses are comparable for both tests. Moreover, Figure 6-17 shows that the inferred radial effective stresses at the outer wall (σ'_{ro}) are also similar. This illustrates that the two modes of loading produce similar radial effective stress distributions across the TWC specimen wall. It should be noted that the resolution of the data for these low pressure tests is not ideal since high pressure capacity transducers were used to make the measurements.

The results indicate that even though the total stress system is fundamentally different between the cavity unloading and cell loading modes, the inferred radial effective stresses are comparable. The borehole closure tests in this study have all been performed by reducing the internal cavity pressure as this method is less affected by the compressibility of the apparatus, easier to control and better simulates the field condition.

6.4.2.2 Internal Unloading versus Internal Loading

An internal cavity loading test was performed, where the borehole was expanded, to simulate the pressuremeter mode of shearing and the results were compared to an internal unloading test. The tests were stress path consolidated (K=0.55) to σ'_{vc} = 3 MPa in the small TWC apparatus before carrying out undrained cavity loading/unloading at average volume strain rate, $\acute{\varepsilon}_{cav}$=10 %/hr. The external cell pressure and axial stress were kept constant during this procedure. Figures 6-18 and 6-19 show the net internal cavity pressure (p_i-u_0) versus the cavity volumetric strain with ε_{cav} up to 20 and 2%, respectively. Figure 6-20 shows the net cavity pressure versus the average cavity radial strain (ε_r) at mid height. Note that the cavity volumetric strains for the internal loading test are plotted positive (in all TWC tests volume contraction is positive) for presentation purposes. The tests start from the same net internal pressure (p_i-u_0 = K σ'_{vc} =1.65 MPa) and the curves appear to have very similar profiles (i.e., evolution of net pressure with strain) even at small strains. The cavity loading test (TWC24) reached a maximum p_i-u_o = 2.7 MPa while the unloading test (TWC9) has a minimum p_i-u_0 = 0.5 MPa. Figure 6-21 shows that the measured average excess pore pressures are alike for both tests (u_e = 0.4 MPa at end of the test). The inferred radial effective stresses at the inner cavity wall versus volume strain are shown in Figure 6-22. The effective stresses are lower than the applied cavity pressures due to the development of pore pressures in the TWC specimen.

The modes of shearing in the cavity contraction and expansion tests are essentially the same; the soil is sheared in the horizontal plane as the cylindrical cavity expands or contracts. During cavity expansion, the radial stress is the maximum stress while the circumferential stress is the minimum stress in the horizontal plane. The reverse situation applies during cavity contraction where the radial stress is the minimum stress while the circumferential stress is the maximum stress. However, the soil exhibits isotropic properties in the horizontal plane due to the 1-D consolidation and hence, the two modes of loading should yield similar shear stress-strain-

strength properties. This explains why the shape of the cavity expansion/contraction curves and the excess pore pressures are similar. The interpreted shear stress-strain behavior and the distribution of principal stresses across the TWC specimen wall for these tests are explained in more detail in Section 6.5.3.

6.4.3 Specimen Geometry

The model borehole testing program was carried out in two phases. Phase 1 TWC tests were performed on relatively small specimens with outer diameter, D_o = 7.6 cm, inner diameter, D_i = 2.5 cm, and height, H = 15.2 cm. These dimensions provide aspect ratios (i.e., D_o/D_i = 3, H/D_o = 2) that are consistent with recommendations by Santarelli & Brown (1989) from prior experience using TWC tests on lithified rock. These Authors show that test specimens with diametral ratio, D_o/D_i = 3 – 4, and height to outer diameter, H/D_o = 2, minimize boundary end effects and provide a reasonable representation of the stress field around a borehole.

Phase 2 tests were carried out on larger specimens (using the large TWC apparatus) with outer diameter, D_o = 15.2 cm, inner diameter, D_i = 2.5 cm, and height, H = 22.8 cm (i.e., D_o/D_i = 6, H/D_o = 1.5). The reason for increasing the diametral ratio (D_o/D_i) was to enhance the boundary conditions of the specimen and examine the effect of wall thickness on the test results. However, the H/D_o ratio is somewhat lower than what is recommended by Santarelli & Brown (1989) in order to produce shorter specimens that will be easier to prepare and test. Experimental tests on specimens with different heights were performed using the small TWC apparatus to investigate the effect of H/D_o ratio on the test results and confirm the testing program for Phase 2. The following subsections present the results of the effects of specimen height as well as the outer diameter.

6.4.3.1 Height

The effect of the vertical boundary was investigated in the small TWC apparatus by testing small diameter specimens (D_o = 7.6 cm) with H = 15.2, 11.5 and 8.2 cm (i.e., H/D_o = 2.0, 1.5 and 1.1). The tests were stress path consolidated (K=0.55) to σ'_{vc} = 3 MPa before shearing undrained through cavity pressure reduction at nominal volume strain rate, $\dot{\varepsilon}_{cav}$ = 10 %/hr. Figures 6-23 and 6-24 compare the net internal cavity pressure versus the cavity volumetric strain with ε_{cav} up to 20 and 3%, respectively, for the three tests. Figure 6-25 shows the net cavity pressure versus the

average cavity radial strain at mid height. The results in general show very good agreement between the three tests with minimum p_i-$u_0 \approx 0.5$ MPa. The short specimen (TWC12) tends to deviate slightly from the other two tests. This also holds for the excess pore pressure development (Figure 6-26), where the curves for tests TWC9 & TWC11 are identical while TWC12 is slightly lower. Figure 6-27 shows that the inferred radial effective stresses at the inner cavity wall are indistinguishable for the three tests ($\sigma'_{ri} = 0.12$ MPa at the end of each test).

These results illustrate that the initial height has minimal impact on the observed borehole response. It seems that the large plastic deformations that the TWC specimen undergoes make the effect of the end conditions on the test results almost negligible. Therefore, the H/D_o ratio of 1.5 employed in the large diameter specimens is considered satisfactory.

6.4.3.2 Outer Diameter

Three tests were performed on large diameter NC RBBC specimens and the results were compared with analogous tests on small diameter specimens in order to investigate the effect of the outer boundary on the TWC tests results. Two of these tests were sheared by decreasing the cavity pressure (cavity contraction) while the third test was sheared by increasing the cavity pressure (cavity expansion). The specimens were anisotropically consolidated to different stress levels prior to introducing the mechanisms of instability under undrained global conditions (i.e., no external drainage from the test specimen). Note that the same test specimen was used in TWC22 and TWC22a; following an internal cavity contraction procedure in TWC22, the specimen was consolidated to a higher effective consolidation stress and an internal cavity expansion test was performed (TWC22a). Although consolidating the specimen to higher effective stresses tends to 'erase' some past disturbances, the results might still be affected by the first shearing phase.

Section 6.4.3.2.1 compares cavity contraction results from small and large TWC specimens consolidated to a common vertical consolidation effective stress, $\sigma'_{vc} = 6$ MPa[18]. Section 6.4.3.2.2 compares cavity expansion results from small and large TWC specimens consolidated

[18] A similar comparison was made between the small and large TWC specimens consolidated to $\sigma'_{vc} = 1.5$ MPa and the results were similar to those presented in Section 6.4.3.2.1. Section 6.4.6.3 compares the two cavity contraction tests performed in the large TWC apparatus to investigate the effect of stress level.

to σ'_{vc} = 3MPa. Apart from the difference in the specimen dimensions, the compared tests were consolidated and sheared under identical conditions.

6.4.3.2.1 Internal Unloading

The net cavity pressure versus the cavity volumetric strain (ε_{cav} up to 20 and 5%) and cavity radial strain are shown in Figures 6-28, 6-29 and 6-30, respectively, for the small and large TWC specimens initially consolidated to σ'_{vc} = 6 MPa. The cavity in both tests was contracted at the standard average volume strain rate, $\dot{\varepsilon}_{cav}$ = 10 %/hr. The figures show that the curves for the large TWC specimen are significantly lower than the small TWC specimen. The small TWC specimen (TWC6) reaches a minimum internal pressure, p_i-u_0 = 0.86 MPa while the large TWC specimen (TWC23) reaches a minimum, p_i-u_0 = 0.28 MPa. This illustrates that the minimum cavity pressure is governed by the outer boundary of the specimen. The initial stiffness is also higher for the large TWC specimen. Figure 6-31 compares the measured average excess pore pressure in both tests. The pore pressures generated in the small specimen are much greater than those generated in the large specimen (0.55 MPa versus 0.24 MPa at the end of each test). However, the drainage path is substantially longer in the large specimen and hence, less pore pressure redistribution is expected to occur than in the small specimen at this rate of shearing. Figure 6-32 shows the inferred radial effective stresses at the inner cavity wall versus volume strain. The effective stress drops to zero in the large specimen while in the small specimen σ'_{ri} = 0.2 MPa at the end of the test. However, this figure is somewhat misleading since the pore pressures measured at the ends of the large TWC specimen are unlikely to represent reliably the pore pressures at the center of the specimen.

The above results demonstrate that the outer boundary has a pronounced effect on the observed borehole response. While most of the borehole closure tests in this research were carried out on small diameter TWC specimens, the method used to interpret the results corrects for the specimen dimensions. The interpreted shear stress-strain behavior for the small and large TWC tests is presented in Section 6.5.4.2.

6.4.3.2.2 Internal loading

Figures 6-33, 6-34 and 6-35 illustrate the effect of the TWC wall thickness for internal loading (cavity expansion) tests that were first consolidated to σ'_{vc} = 3 MPa and then sheared at

volume strain rate, $\dot{\varepsilon}_{cav}$ = 10%/hr. The results show that the large TWC specimen (TWC22a) reaches a higher maximum net cavity pressure than the small specimen TWC24 (3.66 MPa versus 2.71 MPa). Figure 6-36 depicts the measured excess pore pressures developed in both tests. The results illustrate that the pore pressures generated in the large specimen are lower than the small one due to the longer drainage path (less pore pressure redistribution).

6.4.4 Consolidation Lateral Stress Ratio

The first three tests carried out in the model borehole testing program were isotropically consolidated before switching to stress path consolidation with a predefined target value, K=0.55, in order to better simulate the field stress conditions. This allowed a comparison in the borehole response to be made between tests with different preshear lateral stress ratio K_c. This section presents the results of two TWC tests (on small diameter NC RBBC specimens) consolidated under isotropic conditions (K=1; TWC3) or stress path consolidation (K=0.55; TWC13) to a common vertical consolidation effective stress, σ'_{vc} = 1.5 MPa (i.e., the initial preshear cavity pressures are different). The tests were sheared undrained by decreasing the internal cavity pressure at the standard volume strain rate, $\dot{\varepsilon}_{cav}$ = 10 %/hr. Figure 6-37 shows the net internal cavity pressure normalized with respect to the initial radial stress ($[p_i-u_0]/\sigma'_{r0}$; where $\sigma'_{r0} = K\ \sigma'_{vc} = p_o-u_0$) versus cavity volumetric strain. Figure 6-38 shows the normalized net cavity pressure versus volume strain up to ε_{cav} = 5%. Figure 6-39 shows the normalized net cavity pressure versus the average cavity radial strain. The results show that the normalized borehole behavior is similar for the two tests with the bulk of the pressure drop occurring within the first 5% cavity volume strain and the curves reducing to minimum pressure ratio, $(p_i-u_0)/\sigma'_{r0} \approx 0.35$.

Figure 6-40 shows the average excess pore pressure normalized with respect to the vertical consolidation effective stress (u_e/σ'_{vc}). The normalized pore pressure is increasing continuously with volume strain for both tests but is higher for the CIU test (the pore pressures normalized with the initial cavity pressure are almost the same). The normalized pore pressure measured at the end of the borehole closure procedure for the CIU test, u_e/σ'_{vc} = 0.31, while for the CAU test, u_e/σ'_{vc} = 0.14. The inferred cavity radial effective stress normalized with respect to the initial radial effective stress ($\sigma'_{ri}/\sigma'_{r0}$) is shown in Figure 6-41. The results demonstrate that the

different lateral stress ratios produce similar normalized soil response. The effect of the preshear K on the interpreted strengths is discussed later in this chapter.

6.4.5 Drainage Conditions

The effect of drainage conditions during borehole closure was investigated in the small TWC apparatus for NC RBBC specimens. In total, three drained tests were performed at different consolidation stresses in order to simulate the conditions that the borehole experience in the long term and the results were compared with the undrained tests (simulating the conditions shortly after drilling the borehole). This section compares the results for undrained and drained model borehole tests which were initially stress path consolidated (K=0.55) to a nominal σ'_{vc} = 6MPa[19]. The 'undrained' borehole closure test (TWC6) was performed with the drainage lines closed at average cavity volume strain rate, $\acute{\varepsilon}_{cav}$ = 10 %/hr. On the other hand, the fully drained test (TWC21) was sheared very slowly ($\acute{\varepsilon}_{cav}$ = 0.2 %/hr) with the drainage lines open in order to ensure no development of excess pore pressure in the TWC specimen. Measurements of the specimen volumetric strains (ε_v) were taken during this procedure.

Figures 6-42, 6-43 and 6-44 show the net cavity pressure (p_i-u_0) versus the cavity volumetric strains (ε_{cav} up to 20 and 3%) and the average cavity radial strain, respectively, for the drained (CAD) and undrained (CAU) TWC tests. The figures show notably different borehole response for both tests; the drained test has much larger cavity volume strains at a given cavity pressure in the initial unloading portion (up to ε_{cav} = 5%) and then reduces to a lower minimum cavity pressure than the undrained test. The minimum cavity pressure in the drained test is about p_i-u_0 = 0.3 MPa (reached at $\varepsilon_{cav} \approx$ 17%), while the undrained test becomes unstable when p_i-u_0 = 0.9MPa (reached at $\varepsilon_{cav} \approx$ 8%). The initial stiffness is also lower in the drained test.

Figure 6-45 shows the average excess pore pressure measured during the test. The pore pressures increases during undrained borehole closure to a maximum u_e = 0.58 MPa while the measured excess pore pressure in the drained test is zero. Figure 6-46 shows that the specimen volume strain (measured using the specimen PVC) in the CAD test increases continuously with cavity volume strain and reaches ε_v = 0.9% at the end of the test. This result indicates that the

[19] A similar comparison was made between the drained and undrained tests consolidated to σ'_{vc} = 1.5 and 3.0 MPa and the results are similar to those presented in this section. Section 6.4.6.2 compares the three drained tests to investigate the effect of consolidation stress level on the borehole response.

specimen does not undergo significant volume change during the drained borehole closure test. In addition, the positive specimen volume strain (volume decreasing) illustrates the overall contractive behavior of the material. The cavity radial effective stresses are shown in Figure 6-47. Note that the $\sigma'_{ri} - \varepsilon_{cav}$ curve for the CAD test is the same as the $(p_i-u_0) - \varepsilon_{cav}$ relationship shown in Figure 6-42 since $u_e = 0$ MPa. The results again show that the cavity volume strain is greater at a given radial effective stress for the CAD test but the two curves tend to converge at large cavity strains to $\sigma'_{ri} \approx 0.2$-0.3 MPa.

It is apparent that the drainage conditions affect the borehole closure results. The specimen total volume changes in the CAD test since pore water can leave/enter the test specimen and hence, the soil has a greater potential to deform than the CAU test, resulting in larger cavity volumetric strains at the beginning of shearing. This agrees with the behavior observed in the triaxial tests, where the drained test deforms more than the undrained test at a given shear stress. Moreover, the net cavity pressure curve in the CAD test decreases to a lower value than the CAU test. However, this curve also represents the radial effective stress at the inner wall and is reducing to a minimum effective stress value comparable to that obtained from the CAU TWC test.

The main purpose of conducting the drained borehole closure tests was to compare the overall trend with the undrained test and provide data for comparison with analytical investigations. Note that these tests will not be further analyzed in Section 6.5. The method of interpretation used is only applied to the undrained tests of this experimental program.

6.4.6 Consolidation Stress Level

The typical in situ stress levels pertinent to shallow oil field developments (less than 1,000 m) range from 1 to 10 MPa and hence, it is important to evaluate the effect of consolidation stress level on model borehole behavior. As a result, a series of TWC tests have been performed on NC RBBC specimens in the small and large TWC devices at different preshear consolidation stress levels. The small TWC apparatus was employed to perform CAD as well as CAU borehole closure tests while the large TWC apparatus was used to carry out CAU tests at different consolidation stresses. All tests were stress path consolidated (K=0.55) to the required effective stress before shearing the specimen by decreasing the internal cavity pressure.

Section 6.4.6.1 compares CAU borehole closure results from five small diameter TWC specimens consolidated to vertical consolidation effective stresses, σ'_{vc} = 0.15 – 10.0 MPa. Section 6.4.6.2 compares CAD borehole closure results from three small diameter TWC specimens consolidated to σ'_{vc} = 1.5 – 6.0 MPa. Section 6.4.6.3 compares CAU borehole closure results from two large diameter TWC specimens consolidated to σ'_{vc} = 1.5 and 6.0 MPa. Apart from the different preshear consolidation stresses, the compared tests in each section were consolidated and sheared under identical conditions.

6.4.6.1 Undrained Tests Using Small TWC Apparatus

The normalized net cavity pressure ($[p_i-u_0]/\sigma'_{r0}$) versus the cavity volumetric strains (ε_{cav} up to 20 and 3%) and cavity radial strains are shown in Figures 6-48, 6-49 and 6-50, respectively, for the five TWC tests initially consolidated to σ'_{vc} = 0.15 – 10.0 MPa. The cavity in these tests was contracted at the standard volume strain rate, $\acute{\varepsilon}_{cav}$ = 10 %/hr. The results demonstrate that the overall normalized behavior is similar for the five tests; the bulk of the pressure drop occurs within the first 3 – 4% cavity volume strain and the borehole becomes unstable when the normalized net pressure, $(p_i-u_0)/\sigma'_{r0}$ = 0.25 – 0.35 at volume strain in the range ε_{cav} = 5 – 8%. The effect of stress level is evident especially at small strains (Figure 6-49). The figure shows that at the same net pressure ratio, there are larger volume strains for tests at higher consolidation pressures. The initial stiffness also decreases as stress level increases.

Figure 6-51 depicts the normalized average excess pore pressure (u_e/σ'_{vc}). The pore pressure increases with volume strain to a range u_e/σ'_{vc} = 0.10 - 0.14 for all except one test performed at low pressure (σ'_{vc} = 0.15 MPa, TWC8), where the pore pressure goes up in the first 5% strain then drops and remains fairly stable at u_e/σ'_{vc} = 0.04. This is probably related to the internal bore membrane where any wrinkles or yielding in the membrane during internal pressure reduction would have significant effect on the results of this low pressure test. Figure 6-52 shows the inferred cavity radial effective stress normalized with respect to the initial radial effective stress ($\sigma'_{ri}/\sigma'_{r0}$). Apart from TWC8, the results show very good agreement in the cavity contraction data (for σ'_{vc} = 1.5 – 10 MPa). The minimum effective stress attained at large strain, $\sigma'_{ri}/\sigma'_{r0} \approx 0.08$.

The mode of failure in all these tests involved the specimen deforming into the cavity in a uniform manner (i.e., there is minimal distortion of the cross-section). As mentioned previously,

vertical cracks were observed at the inside wall of the borehole in test specimens initially consolidated to maximum vertical effective stress, $\sigma'_{vm} \geq 6$ MPa.

6.4.6.2 Drained Tests Using Small TWC Apparatus

Three CAD borehole closure tests were performed on small diameter TWC specimens at consolidation effective stresses, $\sigma'_{vc} = 1.5 - 6.0$ MPa. The tests were sheared by decreasing the internal cavity pressure at volume strain rate, $\dot{\varepsilon}_{cav} = 0.2$ %/hr, to ensure no excess pore pressure development in the TWC specimen. The figures of normalized net cavity pressure versus cavity strain (Figures 6-53, 6-54 and 6-55) show that the three tests have a comparable trend; continuous reduction in the net cavity pressures with strain (but at a decreasing rate) until reaching $(p_i-u_0)/\sigma'_{r0} = 0.1$ at the end of the test. The test consolidated to $\sigma'_{vc} = 3$ MPa (TWC19) behaves in a strange manner as it begins with a high initial stiffness, yields abruptly at very small strains ($\varepsilon_{cav} \approx 0.2\%$), then crosses the other two tests and remains above them until the end of the test. If this test is disregarded, the trend with stress level is similar to the CAU tests; greater strains at the same net cavity pressure (in the small strain region) and lower initial stiffness as stress level increases.

Figure 6-56 presents the specimen volume strain (ε_v) versus cavity volumetric strain. The figure confirms that test TWC19 behaves in a different fashion as the measured volume strain during the test is lower than the other two tests. Tests TWC18 & TWC21 have almost identical behavior with ε_v increasing as strain increases until reaching $\varepsilon_v = 0.9 - 0.95$ % at the end of the test. Note that Figures 6-53, 6-54 and 6-55 also present the cavity radial effective stress since there are no excess pore pressures generated during the drained borehole closure procedure.

6.4.6.3 Undrained Tests Using Large TWC Apparatus

The effect of stress level was also investigated in the large TWC apparatus by testing two specimens consolidated to $\sigma'_{vc} = 1.5$ and 6.0 MPa. The tests were sheared undrained at a volume strain rate, $\dot{\varepsilon}_{cav} = 10$ %/hr. The figures of normalized net cavity pressure versus cavity strain (Figures 6-57, 6-58 and 6-59) illustrate that both tests drop relatively fast to minimum cavity pressure, $(p_i-u_0)/\sigma'_{r0} = 0.08 - 0.1$ at volume strain in the range $\varepsilon_{cav} = 4 - 6\%$, and then plateaus. Note that these minimum pressures are significantly lower than those obtained in the CAU tests with small diameter TWC specimens. Like the small TWC specimens, the cavity volume strain

increases for the higher pressure test at a given cavity pressure while the initial stiffness decreases, as shown in Figure 6-58.

The excess pore pressures (Figure 6-60) at the beginning of borehole closure procedure decreases slightly to a negative[20] value before increasing as volume strain increases (u_e/σ'_{vc} = 0.04 - 0.045 for both tests at the end of shearing). As discussed earlier, the measured pore pressures in the large TWC specimen are assumed to be non-equilibrated at this rate of cavity unloading due to the relatively long drainage path. This explains why u_e/σ'_{vc} is much lower than those measured in the small TWC specimens (u_e/σ'_{vc} = 0.04 – 0.045 in large TWC specimens versus 0.1-0.14 in the smaller specimens at the end of the test). Also, the pore pressures continue to increase even with minimal changes in total stress and hence confirm that some internal redistribution of the non-uniform pore pressures is taking place within the test specimen. This notwithstanding, Figure 6-61 shows the estimated cavity radial effective stress normalized with respect to the initial radial effective stress ($\sigma'_{ri}/\sigma'_{r0}$). The curves, which are quite similar, ultimately decrease to zero effective stress.

6.4.7 Stress History

As indicated in Table 5-2, the majority of the model borehole tests were performed on NC RBBC. Investigation of the OC behavior of RBBC required additional tests to be conducted at three nominal values of OCR: 2, 4, and 8. Such a range in OCR reflects the typical variation observed in the shallow oil fields considered in this study. For example, sediments in Golf of Mexico are expected to be somewhat normally consolidated (OCR ≈ 1), while North Slope of Alaska soils have been overconsolidated by prior glaciation and typically have OCR ≥ 4. This section presents the results of four model borehole tests on small diameter TWC specimens initially stress path consolidated (K=0.55) to a common maximum vertical effective stress, σ'_{vm} = 6 MPa. Three tests were then unloaded to OCR of 2, 4, and 8. In addition, undrained shear was performed by decreasing the internal cavity pressure at an average volume strain rate, $\dot{\varepsilon}_{cav}$ = 10%/hr. As mentioned in Section 6.2, the axial load was not controlled during borehole closure

[20] The reason for this slight decrease in pore pressures is not known but is believed to be related to the unloading occurring at the inner wall along with the minimal redistribution of pore pressures across the TWC specimen.

for OCR=4 (TWC14) and OCR=8 (TWC16) tests[21]. Keeping the axial stress constant requires the axial load to be reduced in order to compensate for the reduction in the internal cavity pressure acting on the underside of the top cap. This could not be performed as the preshear lateral stress ratio, K≈1 (i.e., $\sigma'_h/\sigma'_v \approx 1$) for these tests and the TWC apparatus does not have extension capabilities. This limitation also prevents 1-D swelling to OCR=8. Instead, TWC16 was unloaded along a specified stress path to K =1 and hence, correspond to a pseudo OCR=8 state.

Figure 6-62 shows the normalized net internal cavity pressure ($[p_i-u_0]/\sigma'_{r0}$) versus cavity volumetric strain. Figure 6-63 shows the normalized net cavity pressure versus volume strain up to ε_{cav} = 3%. Figure 6-64 shows the normalized net cavity pressure versus the cavity radial strain. The results demonstrate that the OCR has a marked effect on the borehole behavior. The curves of cavity pressure shifts downward drastically as OCR increases, and in the cases of the OC tests, the net pressures become negative. The internal bore pressure at the end of the test decreases from $(p_i-u_0)/\sigma'_{r0}$ = 0.25 at OCR=1 to $(p_i-u_0)/\sigma'_{r0}$ = -0.55 at OCR=8. The cavity pressure can decrease to negative values since the excess pore pressure is also decreasing in the OC tests (and hence, the effective stress remains positive), as discussed below. Moreover, OCR=4 and OCR=8 RBBC do not level off even at large volume strains. Figure 6-63 shows that the initial stiffness is higher for the OC tests.

Figure 6-65 shows the average excess pore pressure normalized with respect to the effective vertical consolidation stress (u_e/σ'_{vc}). As OCR increases, the excess pore pressures decrease and become increasingly negative. The pore pressures at the end of the test decline from u_e/σ'_{vc} = 0.10 at OCR=1 to u_e/σ'_{vc} = -0.65 at OCR=8[22]. The results indicate that NC RBBC has a contractive behavior while OC RBBC specimens have a dilatant shear behavior even from the very beginning. The very large decrease in the pore pressure observed in the OC tests is believed to be due to two factors: 1) the soil at the inner wall of the specimen is following an unloading path, and 2) the inherent dilatant behavior of the OC material. The normalized inferred radial effective stresses at the inner wall ($\sigma'_{ri}/\sigma'_{r0}$) and outer wall ($\sigma'_{ro}/\sigma'_{r0}$) are shown in Figures 6-66 and 6-67, respectively. The trends of effective stress at the inner wall are comparable for the four

[21] The resultant increase in axial stress was less than 0.1 MPa in both tests.

[22] Note that OCR=8 (TWC16) test was initially back pressure saturated to u_0 = 1 MPa (all other tests were back pressure saturated to u_0 = 400 kPa) to accommodate the large decrease in pore pressures.

tests. Increasing OCR shifts the curves slightly to the left. Nonetheless, the minimum effective stress is only in the range $\sigma'_{ri}/\sigma'_{r0} = 0.05 - 0.1$. This illustrates that the effective stresses are always positive at the inner wall and that the net cavity pressure profiles are associated with the pore pressures developed in the test specimen. On the other hand, the radial effective stresses at the outer wall are very different ($\sigma'_{ro}/\sigma'_{r0} = 0.8$ for OCR=1 while $\sigma'_{ro}/\sigma'_{r0} = 1.65$ at OCR=8 when $\varepsilon_{cav} = 20\%$) since the pore pressure profiles are dissimilar for the four tests (external cell pressure is kept constant during the borehole closure procedure).

6.4.8 Strain Rate

This research has investigated the effects of cavity volumetric strain rate on the undrained model borehole behavior of NC RBBC in the small TWC apparatus. The main goal of this portion of the experimental program was to determine the strain rate sensitivity of the borehole response and the corresponding interpreted results as well as the measured pore pressures. For undrained tests, the rate of shearing must be sufficiently slow to allow for pore pressure redistribution within the test specimen and hence 'correct' pore pressure measurements. On the other hand, this migration of pore pressures across the TWC wall can violate the undrained assumption locally. This is particularly important for the interpretation of the results since the analysis employed assume undrained conditions.

Three nominal cavity volumetric strain rates were evaluated over approximately two orders of magnitude: very slow rate (0.5%/hr), moderate 'standard' rate (10%/hr), and fast rate (60%/hr). All three tests involved stress path consolidation (K=0.55) to $\sigma'_{vc} = 6$ MPa prior to undrained cavity unloading. Note that the slow test (TWC17) was aborted at cavity volumetric strain, $\varepsilon_{cav} = 10.5\%$, but is reported since the data to that point are considered valuable. Figures 6-68, 6-69 and 6-70 show the net cavity pressure (p_i-u_0) versus the cavity volumetric strains (ε_{cav} up to 20 and 4%) and cavity radial strains respectively for the three tests. The standard and fast rate tests have a comparable borehole behavior while the curve for the slow rate test is higher. The borehole becomes unstable at p_i-$u_0 = 1.2$ MPa for the slow rate test and at p_i-$u_0 = 0.9$ MPa for the standard and fast rate tests, indicating that the faster tests are perhaps slightly stronger. In addition, the initial stiffness increases slightly with increasing strain rate, as illustrated in Figure 6-69.

The average excess pore pressures measured during undrained borehole closure are shown in Figure 6-71. The figure shows that the pore pressure generation increases with decreasing strain rate. At ε_{cav} = 10%, the pore pressure, u_e = 0.8 MPa in the slow rate test, u_e = 0.55 MPa in the standard rate test, and u_e = 0.35 MPa in the fast rate test. The difference between the standard and the slow rate tests is thought to be partly due to the pore water redistribution and partly due to the inherent 'viscosity' of the soil skeleton (i.e., true soil behavior). Research by Sheahan et al. (1996) using the triaxial apparatus indicated that the pore pressure generation increases with decreasing strain rate as a result of soil viscosity[23]. On the other hand, the pore pressure measured in the fast rate test shows that minimal redistribution occurs at the beginning of shearing and then picks up towards the end of the test where it approaches the standard rate curve. In fact, the pore pressure decreases slightly to a negative value before increasing with volume strain, akin to the CAU tests with large diameter TWC specimens. Figure 6-72 shows the inferred radial effective stresses at the inner cavity wall assuming pore pressures are equilibrated at the center of each specimen. The trends in effective stress appear to be comparable for the three cavity strain rates (σ'_{ri} = 0.2 - 0.3 MPa at the end of each test). However, the results for test TWC20 are potentially inaccurate due to the limited time available for internal migration of pore water.

In conclusion, the effect of increasing cavity volumetric strain rate in the model borehole tests is to decrease the minimum net cavity pressure (possibly indicating higher strength), increase initial stiffness and decrease pore pressure development. These trends are consistent with the observations made by Sheahan et al. (1996) using the triaxial device. Furthermore, the pore pressures in the slow rate (0.5%/hr) test are assumed to be fully redistributed, while the fast rate (60%/hr) simulates the closest situation to the 'true' undrained case. The borehole response of the standard rate (10%/hr) test is apparently similar to the fast test, as shown in Figure 6-68. However, the pore pressures are believed to be almost uniform within the specimen when shearing at $\acute{\varepsilon}_{cav}$ = 10%/hr (perhaps 80-90% equilibrated). The effect of cavity volumetric strain rate on the interpreted shear stress-strain results will be discussed in Section 6.5.8.

[23] Increasing strain rates are associated in the case of NC RBBC in triaxial compression with an increase in pore pressures of about 10-15% (at ε_a = 10%) per log cycle of strain rate (Sheahan et al., 1996; see also Chapter 3 (Section 3.4.3.2)).

6.5 INTERPRETATION OF RESULTS

6.5.1 Introduction

The previous section presented the effects of the seven variables investigated (mode of loading, specimen geometry, lateral stress ratio, drainage conditions, stress level, stress history, and strain rate) on the model borehole behavior of RBBC. This section analyzes the results of the experimental program using an analytical framework originally developed for interpreting model pressuremeter tests. This interpretation enables estimation of the stress-strain-strength properties, stress (radial, circumferential, and shear) distribution as well as stress paths followed by soil elements across the TWC specimen wall. Hence, the borehole closure tests can be linked to soil behavior principles and elemental shear properties. Section 6.5.2 introduces the interpretation method by means of analyzing the results of the reference model borehole test (TWC7: small diameter NC RBBC specimen, K_c = 0.55, σ'_{vc} = 10 MPa, undrained borehole closure at an average cavity volumetric strain rate of 10%/hr). The following sections present the analysis of the model borehole experimental program by treating each of the variables investigated separately. Note that the method of interpretation used is only applied to the undrained tests performed in this study.

6.5.2 Reference Test

6.5.2.1 Introduction

The method used to interpret the model borehole tests is based on pressuremeter cavity expansion theory. Silvestri (1998) proposed a method to obtain the exact solution to the problem of expanding cavity in a thick-walled cylinder (TWC) of clay, under plane strain and undrained conditions[24]. For these conditions, the interpretation method is also applicable to cavity contraction, as the problem geometry is fully strain controlled (i.e., strain field is independent of the stress-strain curve).

Before proceeding with the interpretation of the results, it is important to evaluate these two fundamental assumptions for the 'undrained' model borehole tests conducted in this study. As

[24] Refer to Chapter 2 (Section 2.5.3) for interpretation of model pressuremeter tests.

mentioned previously, the axial stress was kept constant during borehole closure procedure and hence some axial deformations occurred. However, these strains were relatively small (less than 1%), as illustrated in Figure 6-6 for the reference test (TWC7). Also, the axial deformations took place mainly when the specimen was deforming with minimal change in cavity pressure while the analysis is more sensitive to the initial evolving portion of the contraction/expansion curve. As for drainage in the TWC specimen, global undrained conditions with no external drainage from the specimen were maintained during cavity contraction. Nonetheless, internal pore water migration can take place to equilibrate the pore pressure gradient generated across the specimen wall from the non-uniform stress conditions, especially if the shearing rate is sufficiently slow. As a result, a series of TWC tests were performed at various rates ranging from very fast ($\acute{\varepsilon}_{cav}$ = 60%/hr; i.e., minimal internal drainage) to very slow ($\acute{\varepsilon}_{cav}$ = 0.5%/hr; i.e., equilibrated pore pressures) to determine the effect of cavity strain rate on the borehole closure data as well as the corresponding interpreted results, as indicated in Section 6.4.8. The results illustrated that the interpreted stress-strain curves[25] for the different tests were very similar signifying that the strain rates investigated have minimal impact on the analysis. The strengths obtained from the model borehole tests also seem to be reasonable. Following this line of reasoning, the method of interpretation is considered to be appropriate for the undrained model borehole experimental program performed in this research.

6.5.2.2 Interpretation of Undrained Borehole Closure Results

The complete stress-strain curve of a saturated clay from undrained plane strain expansion/contraction of a hollow cylinder can be obtained by means of the following relationship (Silvestri, 1998):

$$\tau_a = \chi(\chi - 1)\frac{dp_i}{d\chi} + \frac{\chi}{1 - \beta + \beta\chi}\tau_b \qquad (6.1)$$

where τ_a is the shear stress generated at the inner radius of the hollow cylinder ($=q_{ha}=(\sigma_{\theta i} - \sigma_{ri})/2$; where σ_θ and σ_r are the circumferential and radial stresses, respectively); χ is the distortion parameter ($= (a'/a)^2$; where a' is the inner radius of the hollow cylinder in a deformed state and a is the initial inner radius); $dp_i/d\chi$ is the slope of the expansion/contraction curve, where p_i is the

[25] The effect of strain rate on the interpreted stress-strain behavior is discussed in Section 6.5.8.

internal cavity pressure; $\beta = a^2/b^2$, where b is the initial outer radius of the hollow cylinder; and τ_b is the shear stress generated at the outer radius ($= q_{hb} = (\sigma_{\theta o} - \sigma_{ro})/2$). Figure 6-73 shows the net cavity pressure (p_i-u_0) versus the distortion parameter (χ) for the reference test TWC7 which was initially consolidated to σ'_{vc} = 10 MPa. The distortion parameter is obtained from the cavity volumetric strain, where $\chi = (1+\varepsilon_{cav})$. In order to obtain the shear stress curve of the clay, the slope of the contraction curve in Figure 6-73 was first calculated and then Equation 6.1 was used. Note that the shear stress at the outer boundary (τ_b) is not known at the start of the test, but follows the same stress-strain curve as τ_a. Therefore, an iteration process was performed to obtain the true and unique stress-strain curve of the soil. It is also worth mentioning that the differentiation procedure performed on the experimental contraction pressure-strain relationship often results in fluctuations in the stress-strain curves. This particular behavior is caused by the fact that when differentiation is performed on discrete data points, the procedure is very sensitive to even the smallest variation in the raw data. As a consequence, the resultant stress-strain curves were smoothed using typically a five-point moving window.

The interpreted shear stress-strain results for the reference test (small diameter TWC specimen: $\beta = 0.111$) are presented in Figure 6-74. The y-axis in the plot is the shear stress in the horizontal direction[26] ($q_h = (\sigma_\theta - \sigma_r)/2$), and the x-axis is the natural shear strain ($\gamma = (r'/r)^2$; where r' is the deformed state of the initial radial coordinate r). The results show that the stress-strain curve reaches a maximum shear stress, q_h = 2.1 – 2.2 MPa at $\gamma \approx 3\%$ and exhibit almost perfectly plastic behavior beyond peak shear resistance (i.e., the material does not strain soften). The undrained shear strength (s_u) of the clay is equated to the maximum value of shear stress in the horizontal plane; $s_u = q_{hMAX} = [(\sigma_\theta - \sigma_r)/2]_{MAX}$. This yields a normalized shear strength, s_u/σ'_{vc} = 0.21 – 0.22, which is somewhat between the strengths obtained in triaxial compression and extension tests, and similar to that in a direct simple shear (DSS) mode. These results are consistent with considerations of anisotropic behavior, as discussed in Chapter 2. It must be noted that the initial portion of the stress-strain curve is not well defined and therefore it was not possible to estimate the initial shear modulus (G_i) of the soil.

[26] Note that the vertical stress can be higher than the radial and circumferential stresses in the TWC test, but is not considered here since cavity contraction/expansion causes shearing of the soil in the horizontal (r, θ) plane.

Figure 6-75 presents the stress-strain curves for elements at the inner and outer walls of the hollow cylinder. Figure 6-76 shows a close up view of Figure 6-75 up to $\gamma = 4\%$. These figures illustrate that the stress-strain curve of the soil is unique as both elements follow the same curve. However, when the inner wall element is at $\gamma_a = 16\%$, the outer wall element is only at $\gamma_b = 2\%$, since the strains diminish rapidly as one moves away from the inner core. This is also demonstrated in Figure 6-77, which shows the shear strain distribution across the TWC wall at $\varepsilon_{cav} = 17.5\%$ (i.e., $\gamma_a = 16\%$ and $\gamma_b = 2\%$). This distribution of strain results in shear stress variation across the specimen. The natural shear strains at the inner radius (a), outer radius (b), and r are linked to the distortion parameter (and hence ε_{cav}) through the following expressions:

$$\gamma_a = \ln \chi \tag{6.2}$$

$$\gamma_b = \ln(1 - \beta + \beta\chi) \tag{6.3}$$

$$\gamma_r = \ln(1 - \beta_r + \beta_r \chi) \tag{6.4}$$

where $\beta = a^2/b^2$, $\beta_r = a^2/r^2$ and $\chi = (1+\varepsilon_{cav})$.

The significance of considering the finite lateral extent of the TWC specimen is demonstrated in Figure 6-78. The figure compares the shear stress-strain curve obtained from the above analysis with one which assumes infinite boundary condition[27]. The results show that the behavior is very different for the two boundary assumptions. The curve for the infinite case reaches a peak shear strength, $s_u = 1$ MPa at $\gamma \approx 1\%$ then strain softens drastically. On the other hand, the peak strength almost doubles and the shape of the curve changes to one with perfectly plastic behavior beyond peak shear stress when the finite dimensions of the specimens are taken into account.

Figure 6-79 presents the total stress paths in the horizontal plane followed by elements at the inner and outer walls of the TWC specimen using the MIT stress space ($q_h = (\sigma_\theta - \sigma_r)/2$ versus $p_h = (\sigma_\theta + \sigma_r)/2$). At the end of the consolidation stage for test TWC7, the circumferential and radial stresses are equal; $\sigma_\theta = \sigma_r = 5.5$ MPa. Hence, the stress paths start from a stress state where $q_h = 0$ MPa and $p_h = 5.5$ MPa. During cavity contraction, the element at the outer wall

[27] For the special case of infinite soil medium, $b/a = \infty$ and $\tau_b = 0$, and the second term on the right-hand side of Equation 6.1 also vanishes. As a consequence, Equation 6.1 reduces to essentially the same equation as that obtained by Baguelin et al. (1972), Palmer (1972), and Ladanyi (1972), and which applies to the undrained plane strain expansion around a pressuremeter in clay.

follows a loading stress path with 1:1 slope. This is because the outer cell pressure is kept constant while the circumferential stress continues to increase during shearing. On the other hand, the stress path for an element at the inner wall rises with a slight increase in average stress then continues to shear with decreasing average stress, following an unloading path. Effective stress paths can be also obtained given that accurate pore pressure measurements are available at these locations. For this reference test, the pore pressures in the specimen are believed to be not fully equilibrated. This notwithstanding, the estimated friction angles at the inner and outer walls measured from the inferred effective stresses are 48° and 19° respectively.

Analysis of stress distributions (radial, circumferential, and shear) across the wall of the TWC specimen as a function of cavity strain are particularly valuable for determination of the gradual spreading of failure zones and the stress paths experienced by different soil elements around the bore. Silvestri (1998) developed expressions for radial and circumferential stresses generated from expanding a cavity in thick hollow cylinders (expressions presented in Chapter 2; Section 2.5.3). The following relationships were adapted for the cavity contraction tests:

$$\sigma_r = \sigma_{r0} - \int_{\gamma_b}^{\gamma_r} \frac{\tau d\gamma}{(e^{\gamma} - 1)} \tag{6.5}$$

$$\sigma_\theta = \sigma_r + 2\tau = \sigma_{r0} + \int_{\gamma_b}^{\gamma_r} \frac{\tau d\gamma}{(e^{\gamma} - 1)} + 2\tau \tag{6.6}$$

where σ_{r0} is the initial total radial stress acting both inside and outside the hollow cylinder, τ is the shear stress, and γ is the natural shear strain. Figure 6-80 shows the radial and circumferential stress distributions across the TWC specimen wall at ε_{cav} = 0.2, 2, and 10% (i.e., γ_a = 0.19, 1.98, and 9.5%). As mentioned above, the preshear circumferential and radial stresses, $\sigma_\theta = \sigma_r$ = 5.5 MPa. The results indicate that as the cavity pressure decreases from σ_r = 5.5 MPa to σ_r = 1.5 MPa, the circumferential stress at the inner wall initially increase to σ_θ = 6.7 MPa at ε_{cav} = 0.2% then decrease to σ_θ = 5.6 MPa at ε_{cav} = 10%. On the other hand, the external radial stress remains stable at σ_r = 5.5MPa (since the cell pressure is kept constant) while the circumferential stress at the outer wall continues to increase up to σ_θ = 9.2 MPa at ε_{cav} = 10% during shearing. The figure also shows the spreading of the failure zone from the core towards the external boundary. At ε_{cav} = 10%, the entire specimen has essentially reached failure.

6.5.3 Mode of Loading – Internal Unloading versus Internal Loading

Cavity unloading (contraction) and loading (expansion) tests were performed on NC RBBC in order to evaluate the effect of loading mode on the model borehole response and the corresponding interpreted results. The specimens were consolidated to nominal σ'_{vc} = 3 MPa in the small TWC apparatus before being sheared undrained. Figure 6-81 presents the shear stress-strain behavior for both tests. The figure illustrates that the curves for the contraction and expansion tests are very similar and reach the same maximum shear stress, q_h = ±0.53-0.54 MPa (i.e., $s_u/\sigma'_{vc} \approx 0.185$). Note that since q_h is defined as $(\sigma_\theta - \sigma_r)/2$, the expansion test yields a negative shear stress ($\sigma_r > \sigma_\theta$). These results are significant and confirm that the stress-strain-strength properties are isotropic in the horizontal plane after stress path consolidation. Moreover, the behavior is in agreement with the predictions made by Aubeny (1992) using the MIT-E3 constitutive model for the pressuremeter tests on Boston Blue Clay (BBC). He demonstrated that the undrained strength ratios (s_u/σ'_{vc}) obtained in a pressuremeter shear mode are about 0.2 (i.e., similar to those measured in a DSS mode) and that the predicted stress-strain curves show almost perfectly plastic behavior beyond peak shear resistance. Ladd et al. (1979) also suggested that the pressuremeter undrained shear strength is similar to those of simple shear.

Figure 6-82 shows the total stress paths in the horizontal plane followed by elements at the inner and outer walls of the TWC specimen using the MIT stress space ($q_h = (\sigma_\theta - \sigma_r)/2$ versus $p_h = (\sigma_\theta + \sigma_r)/2$) for the contraction and expansion tests. The starting point for all stress paths is the same with p_h = 0 MPa and q_h = 1.62 MPa. During cavity contraction, an element at the specimen outer wall follows a loading stress path while an element at the inner wall follows an unloading path. In contrast, an element at the inner wall follows a loading stress path (radial stress is now increasing) in the expansion test while an element at the outer boundary follows an unloading path (circumferential stress decreasing with constant radial stress). These expansion stress paths are essentially the same as the contraction stress paths but rotated by 180°. This is because the outer radial stress is kept constant in both tests, whereas the outer circumferential stress and the inner radial and circumferential stresses are reversed (with similar stress increments) in the contraction and expansion tests, as explained below.

The variation in the radial and circumferential stresses across the TWC wall at different cavity strain levels (ε_{cav} = 0.2, 2, and 10%) are shown in Figures 6-83 and 6-84 for the contraction and expansion tests, respectively. Note that the preshear stresses, $\sigma_\theta = \sigma_r$ = 1.62 MPa

for both tests. Figure 6-83 shows that as the cavity pressure reduces to σ_r = 0.5 MPa, σ_θ at the inner wall remains more or less the same while σ_θ at the outer wall continues to increase up to σ_θ = 2.6 MPa at ε_{cav} = 10% (external cell pressure constant). On the other hand, Figure 6-84 shows that when cavity pressure increase to σ_r = 2.7 MPa, σ_θ at the outer boundary eventually falls to σ_θ = 0.7 MPa at ε_{cav} = 10% with practically non changing σ_θ at the inner wall. The spreading of the failure zone from the core to the outer boundary is almost identical in the two tests.

6.5.4 Specimen Geometry

6.5.4.1 Height

As discussed in Section 6.4.3.1, three tests were performed on small diameter TWC specimens (D_o = 7.6 cm) with different height to outer diameter ratios (H/D_o = 2.0, 1.5 and 1.1) to investigate the effect of the vertical boundary on the borehole closure results. The tests were consolidated and sheared under identical conditions; stress path consolidation (K=0.55) to σ'_{vc} = 3 MPa and then undrained shearing through cavity pressure reduction. The tests illustrated that the specimen height has minimal impact on the measured borehole response. Hence, it is not surprising to see that the interpreted stress-strain curves, presented in Figure 6-85, are also comparable. Tests TWC9 & TWC11 (H/D_o = 2.0 & 1.5 respectively) show somewhat identical behavior with peak undrained shear strength, s_u = 0.53 MPa, while the short specimen (TWC12) reaches a slightly higher shear strength, s_u = 0.57 MPa. This is in agreement with the observed contraction curves for these tests, where the short specimen deviated slightly from the other two tests, especially at small cavity strains.

6.5.4.2 Outer Diameter

6.5.4.2.1 Internal Unloading

The effect of the outer diameter was investigated by comparing the results from tests performed on small diameter (D_i = 2.5 cm; D_o = 7.6 cm; H = 15.2 cm) and large diameter (D_i = 2.5 cm; D_o = 15.2 cm; H = 22.8 cm) TWC specimens. The tests were anisotropically consolidated to σ'_{vc} = 6 MPa before carrying out undrained cavity contraction at $\acute{\varepsilon}_{cav}$ = 10%/hr. The interpreted shear stress-strain curves are shown in Figure 6-86. Note that the distortion parameter (β) used in Equation 6.1 to compute the shear stress is equal to β=0.111 for the small

TWC specimen and β=0.0278 for the larger specimen. The figure shows that both tests have comparable stress-strain curves and reach peak undrained strength, s_u = 1.20 – 1.24 MPa (i.e., s_u/σ'_{vc} = 0.20 – 0.21). Test TWC23 (larger specimen) exhibit some strain softening after reaching the peak stress. These results demonstrate that the interpretation method produces a unique stress-strain curve for the soil which is independent on the specimen dimensions. Furthermore, the results confirm that the analysis is not very sensitive to the internal redistribution of pore pressure taking place within the specimen, since more migration should occur in the small specimen due to the shorter drainage path.

Figure 6-87 plots the shear stress-strain curves for an element at the outer boundary of the small and large TWC specimens. These elements follow the same stress-strain curves presented in Figure 6-86, but attain lower shear strains than those at the inner wall. The distribution of shear strain (γ_r) as a function of the radial distance (r/a) at ε_{cav} = 17.5% (i.e., γ_a = 16%) is shown in Figure 6-88 (applies for small and large specimens). At cavity volume strain, ε_{cav} = 17.5% (approximately end of the test), the shear strain at the outer boundary in the small diameter TWC specimen (r/a = 3) is about γ_b = 2%, whereas γ_b = 0.5% in the larger specimen (r/a = 6). Therefore, an element at the outer wall in the small specimen reaches the peak undrained shear strength ($q_{hb} = s_u$ =1.2 MPa) towards the end of the test while an element at the outer boundary in the large specimen does not reach failure (q_{hb} = 0.9 MPa).

The radial and circumferential stress distributions across the TWC wall during borehole closure at different cavity strain levels (ε_{cav} = 0.2, 2, and 10%) are shown in Figures 6-89 and 6-90 for the small and large specimens, respectively. Note that the preshear circumferential and radial stresses, $\sigma_\theta = \sigma_r$ = 3.22 MPa for both tests. The evolvement of stresses in the TWC specimen during cavity contraction is essentially similar to what have been described earlier. Figure 6-89 shows that as cavity pressure reduces to σ_r = 0.9 MPa in the small TWC specimen, σ_θ at the inner wall increases slightly then reduces to σ_θ = 3.4 MPa at ε_{cav} = 10%, while σ_θ at the outer wall continues to increase up to σ_θ = 5.4 MPa at ε_{cav} = 10%. As for the large TWC specimen, the cavity pressure decreases to σ_r = 0.3 MPa, and σ_θ at the inner wall initially increases to σ_θ = 3.7 MPa at ε_{cav} = 0.2% before reducing to σ_θ = 2.4 MPa at ε_{cav} = 10%. The radial stress at the outer wall remains constant whereas the circumferential stress increases to σ_θ = 5.0 MPa at ε_{cav} = 10%. These stress distributions can also infer the initiation and gradual spreading of the failure zone in both specimens. The figures illustrate that the failure zone advances the

same radial distance in both specimens at a given cavity strain (since the shear strain distribution across the specimen wall is the same and the stress-strain behavior is similar) and hence, reaches the outer boundary earlier in the small diameter TWC specimen than the large one.

6.5.4.2.2 Internal Loading

The effect of the outer diameter was also investigated for the internal loading tests. The tests were consolidated to σ'_{vc} = 3 MPa before performing undrained cavity expansion. Figure 6-91 shows the shear stress-strain behavior for the two tests. The small diameter TWC specimen (TWC24) reaches a peak shear strength, s_u = 0.52 MPa, while the large specimen (TWC22a) attain a peak stress, s_u = 0.62 MPa. This variation in strength is believed to be due to the fact that specimen TWC22a was previously sheared through cavity unloading before reconsolidation to higher stress level for this cavity loading test. The first shearing phase generated excess pore pressures which were allowed to drain after the test and hence, the specimen volume decreased (i.e., consolidation occurred). The reconsolidation to higher stresses increased the axial and volumetric strains by only 4-5% which was not enough to 'erase' this perturbation.

The stress distributions for the cavity expansion test TWC24 were discussed in Section 6.5.3 and presented in Figure 6-84. In addition, the effect of the outer diameter in the cavity loading tests is the same as that for the cavity unloading tests discussed above.

6.5.5 Consolidation Lateral Stress Ratio

Section 6.4.4 compared the measured borehole response of two TWC tests on NC RBBC specimens as a function of the preshear value of the lateral stress ratio K. The specimens were consolidated under isotropic (K=1) or anisotropic (K=0.55) conditions to a common vertical consolidation effective stress, σ'_{vc} = 1.5 MPa before being sheared undrained. Figure 6-92 presents the stress-strain behavior of the two tests. The CIU test reaches a maximum shear stress, s_u = 0.36 MPa at about γ = 5%. On the other hand, the peak shear strength, s_u = 0.28 MPa is attained at γ = 3% in the CAU test. Hence the undrained shear strength obtained from the CIU test is approximately 30% greater than the CAU test.

Ladd & Varallyay (1965), Ladd (1965), and Bensari (1981) compared the results from CIU and CAU (K ≈ 0.53-0.55) tests in triaxial compression and extension for NC RBBC. These researchers reported that the normalized strengths (s_u/σ'_{vc}) obtained from CIU tests can be

slightly higher (about 10-15%) than CAU tests during triaxial compression. In addition, the strain at failure decreases drastically and strain softening increases in the CAU tests. Similarly, the normalized strength increases by about 35% going from CAU to CIU in triaxial extension. Therefore, the higher shear strength observed in the CIU model borehole test is fairly consistent with previous work using the triaxial device.

6.5.6 Consolidation Stress Level

6.5.6.1 Undrained Tests Using Small TWC Apparatus

A series of TWC tests have been performed on NC RBBC to investigate the effect of consolidation stress on the undrained borehole closure behavior in the small TWC apparatus. The specimens were stress path consolidated (K=0.55) to vertical consolidation effective stresses, σ'_{vc} = 0.15 – 10 MPa. Figure 6-93 shows the interpreted shear stress-strain behavior. The curves are characterized by a peak undrained shear strength (s_u) reached at γ = 2-3% followed by almost perfectly plastic behavior beyond peak shear resistance. The undrained shear strength increases with stress level, as summarized in Figure 6-94, from s_u = 0.027 MPa at σ'_{vc} = 0.15 MPa to s_u = 2.15 MPa at σ'_{vc} = 10 MPa.

Figure 6-95 presents the normalized shear stress-strain behavior (q_h/σ'_{vc} versus γ) for the same tests. The figure shows that the shape of the curves is similar and that the normalized strength (s_u/σ'_{vc}) range only from 0.18 to 0.215. Figure 6-96 summarizes the normalized strength versus vertical consolidation stress level. The normalized strength tends to increase with increasing stress level from s_u/σ'_{vc} = 0.18 at σ'_{vc} = 0.15 MPa to s_u/σ'_{vc} = 0.215 at σ'_{vc} = 10 MPa. Figure 6-97 compares the normalized strengths obtained from the TWC tests as function of stress level with those measured in K_0-consolidated undrained triaxial compression (CK_0UC) and extension (CK_0UE) tests on NC RBBC (results presented in Chapter 5). The results show that TWC strength ratios are closer to those measured in triaxial extension at low stresses but tend to reach an average value between triaxial extension and compression strength ratios at higher stresses. In addition, the trend in normalized strength with stress level in the TWC is the opposite of that observed in the triaxial results. The reason for this difference in strength trends between the three modes of shearing is unclear.

6.5.6.2 Undrained Tests Using Large TWC Apparatus

Two undrained borehole closure tests were performed on NC RBBC using the large TWC apparatus at consolidation effective stress, σ'_{vc} = 1.5 and 6 MPa. The interpreted shear stress-strain curves (Figure 6-98) demonstrate that the behavior is very similar to the CAU tests with small diameter TWC specimens at the same consolidation stress. The results show a peak strength at shear strain, γ = 3-4% followed by slight strain softening. Figure 6-99 summarizes the peak undrained strength versus the preshear consolidation stress (σ'_{vc}).

The normalized stress-strain behavior (q_h/σ'_{vc} versus γ) is presented in Figure 6-100. The curves for the two tests are similar and reach comparable normalized strengths (s_u/σ'_{vc}), as summarized in Figure 6-101. The normalized shear strength increases slightly from s_u/σ'_{vc} = 0.195 at σ'_{vc} = 1.5 MPa to s_u/σ'_{vc} = 0.21 at σ'_{vc} = 6 MPa. These results also agree with the CAU tests performed on the small TWC specimens.

6.5.7 Stress History

As discussed in Section 6.4.7, the effect of stress history on the model borehole behavior was investigated by performing tests with nominal values of OCR: 1, 2, 4 and 8. The four tests were initially anisotropically consolidated to a common maximum vertical effective stress, σ'_{vm} = 6 MPa. Three tests were then unloaded to OCR of 2, 4, and 8 prior to undrained borehole closure. Figure 6-102 shows the interpreted shear stress-strain curves for the four tests. It can be seen that the peak value of strength decreases with increasing OCR (since the tests were consolidated to the same maximum effective stress). Except for OCR=8 RBBC (TWC16), the undrained shear strength is mobilized at shear strains, γ = 3-5%, and give no indication of post-peak strain softening. Test TWC16 exhibits strain hardening behavior where the shear stress continues to increase during the test. This is linked to the cavity contraction curve which did not level off (i.e., a steady minimum value was not reached) even at high cavity volume strains, as illustrated in Figure 6-62. Also note that the axial load was not controlled during borehole closure for OCR=4 (TWC14) and OCR=8 (TWC16) tests and that TWC16 is a pseudo OCR=8.

Figure 6-103 presents the normalized stress-strain behavior (q_h/σ'_{vm} versus γ) from OCR=1, 2, 4 and 8 tests. The results show that as OCR increases, the peak value of strength normalized to the maximum vertical stress (σ'_{vm}) decreases. However, undrained strength ratios (s_u/σ'_{vc}) increase with increasing OCR (Figure 6-104), as expected. These results can be

interpreted using the SHANSEP power law equation (Equation 2.1). Figure 6-105 demonstrates that s_u/σ'_{vc} can be well described as a function of the OCR with S = 0.21 and exponent m = 0.717 (r^2 = 0.995). These parameters are very similar to those obtained by Ahmed (1990) for RBBC from the DSS test (S = 0.20 and m = 0.74 - 0.82). In addition, the results are in excellent agreement with the predictions made by Aubeny (1992) using the MIT-E3 constitutive model for the pressuremeter tests on BBC at OCR=1, 2 and 4. Figure 6-106 presents the undrained strength ratio (s_u/σ'_{vc}) versus OCR for the TWC and triaxial compression tests performed on RBBC at high consolidation stresses. The figure shows that the value of S is smaller for the TWC tests (0.21 versus 0.29) while m is somewhat comparable (~ 0.72 - 0.74).

6.5.8 Strain Rate

This research included the investigation of the effects of variations in the strain rate over approximately two orders of magnitude on the model borehole behavior of NC RBBC. The three nominal cavity volumetric strain rates investigated are $\acute{\varepsilon}_{cav}$ = 0.5, 10 and 60 %/hr. As mentioned in Section 6.4.8, the pore pressures in the slow rate (0.5%/hr) test are believed to be fully equilibrated, whereas the fast rate (60%/hr) test has minimal internal drainage. On the other hand, the pore pressures in the standard rate (10%/hr) test are assumed to be 80-90% equilibrated. All tests were initially anisotropically consolidated to a common consolidation vertical effective stress, σ'_{vc} = 6 MPa before undrained borehole closure.

The interpreted stress-strain curves are presented in Figure 6-107. The figure shows that the curves are comparable for the three tests indicating that the strain rate (and hence, the degree of internal pore water migration) has a minimal effect on the interpreted stress-strain behavior. The standard rate and fast rate tests reach a peak shear strength, s_u = 1.22-1.26 MPa (i.e., s_u/σ'_{vc} = 0.208 – 0.215), whereas the slow rate test attain a peak strength, s_u = 1.15 MPa (i.e., s_u/σ'_{vc} = 0.196). The slightly lower strength obtained in the slow rate test is in agreement with data presented by Sheahan et al. (1996) using the triaxial apparatus[28].

[28] Increasing strain rates are associated in the case of NC RBBC in triaxial compression with an increase in strength of about 6.5% per log cycle of strain rate (Sheahan et al., 1996; see also Chapter 3 (Section 3.4.3.2)).

Test No. Cell	Initial				Consolidation					Borehole Closure			Comments
	H (cm)	D_o (cm)	e	σ'_p (MPa)	σ'_{vc} (MPa)	OCR	K_c	ε_a (%)	ε_v (%)	Mode of loading	Drainage	Rate (%/hr)	
TWC1 (MIT06)	15.27	7.59	1.34	0.10	0.15	1.00	1.00	-	6.41	Internal unloading	Undrained	~20.0	
TWC2 (MIT06)	15.24	7.59	1.28	0.10	0.15	1.00	1.00	-	6.36	External loading	Undrained	~20.0	
TWC3 (MIT06)	15.24	7.65	0.90	1.01	1.47	1.00	1.00	-	7.32	Internal unloading	Undrained	10.0	
TWC6 (MIT06)	15.26	7.62	0.70	3.99	5.86	1.00	0.55	6.95	5.82	Internal unloading	Undrained	10.0	
TWC7 (MIT06)	15.28	7.63	0.64	6.39	10.2	1.00	0.55	7.48	6.77	Internal unloading	Undrained	10.0	
TWC8 (MIT06)	15.24	7.58	1.32	0.10	0.15	1.00	0.55	7.55	5.43	Internal unloading	Undrained	10.0	
TWC9 (MIT06)	15.27	7.61	0.81	2.00	2.95	1.00	0.55	7.12	5.78	Internal unloading	Undrained	10.0	
TWC11 (MIT06)	11.52	7.59	0.78	1.99	2.93	1.00	0.55	7.88	6.25	Internal unloading	Undrained	10.0	
TWC12 (MIT06)	8.15	7.58	0.77	1.99	2.91	1.00	0.55	6.41	4.88	Internal unloading	Undrained	10.0	
TWC13 (MIT06)	15.25	7.61	0.93	0.99	1.47	1.00	0.55	7.28	5.88	Internal unloading	Undrained	10.0	
TWC14 (MIT06)	15.27	7.62	0.71	3.99	1.47	3.98	0.99	5.44	4.77	Internal unloading	Undrained	10.0	Axial load not controlled during BH closure

Table 6-1: Summary of TWC tests

Test No. Cell	Initial				Consolidation					Borehole Closure			Comments
	H (cm)	D_o (cm)	e	σ'_p (MPa)	σ'_{vc} (MPa)	OCR	K_c	ε_a (%)	ε_v (%)	Mode of loading	Drainage	Rate (%/hr)	
TWC15 (MIT06)	15.26	7.62	0.68	3.99	2.94	2.02	0.74	7.11	5.54	Internal unloading	Undrained	10.0	
TWC16 (MIT06)	15.27	7.62	0.67	3.99	0.73	8.09	0.99	5.09	4.17	Internal unloading	Undrained	10.0	Axial load not controlled during BH closure
TWC17 (MIT06)	15.25	7.62	0.68	3.99	5.87	1.00	0.55	7.22	6.36	Internal unloading	Undrained	0.5	Test aborted at ε_{cav}=10.5%
TWC18 (MIT06)	15.25	7.61	0.89	0.99	1.46	1.00	0.55	6.91	6.11	Internal unloading	Drained	0.2	
TWC19 (MIT06)	15.26	7.59	0.82	2.01	2.92	1.00	0.55	6.43	5.22	Internal unloading	Drained	0.2	
TWC20 (MIT06)	15.25	7.62	0.68	3.99	5.85	1.00	0.55	6.74	6.32	Internal unloading	Undrained	60.0	
TWC21 (MIT06)	15.24	7.61	0.69	3.99	5.85	1.00	0.55	6.92	5.75	Internal unloading	Drained	0.2	
TWC22 (MIT09)	22.85	15.34	0.85	0.98	1.48	1.00	0.55	6.42	5.63	Internal unloading	Undrained	10.0	
TWC22a (MIT09)	22.85	15.34	0.85	0.98	2.96	1.00	0.55	11.76	10.04	Internal loading	Undrained	10.0	Same specimen as TWC22
TWC23 (MIT09)	22.85	15.23	0.73	4.01	5.88	1.00	0.55	7.79	-	Internal unloading	Undrained	10.0	Internal leak during cons. - Dismantled and reassembled
TWC24 (MIT06)	15.14	7.61	0.76	2.01	2.96	1.00	0.55	6.47	5.71	Internal loading	Undrained	10.0	

Table 6-1: (continued) Summary of TWC tests

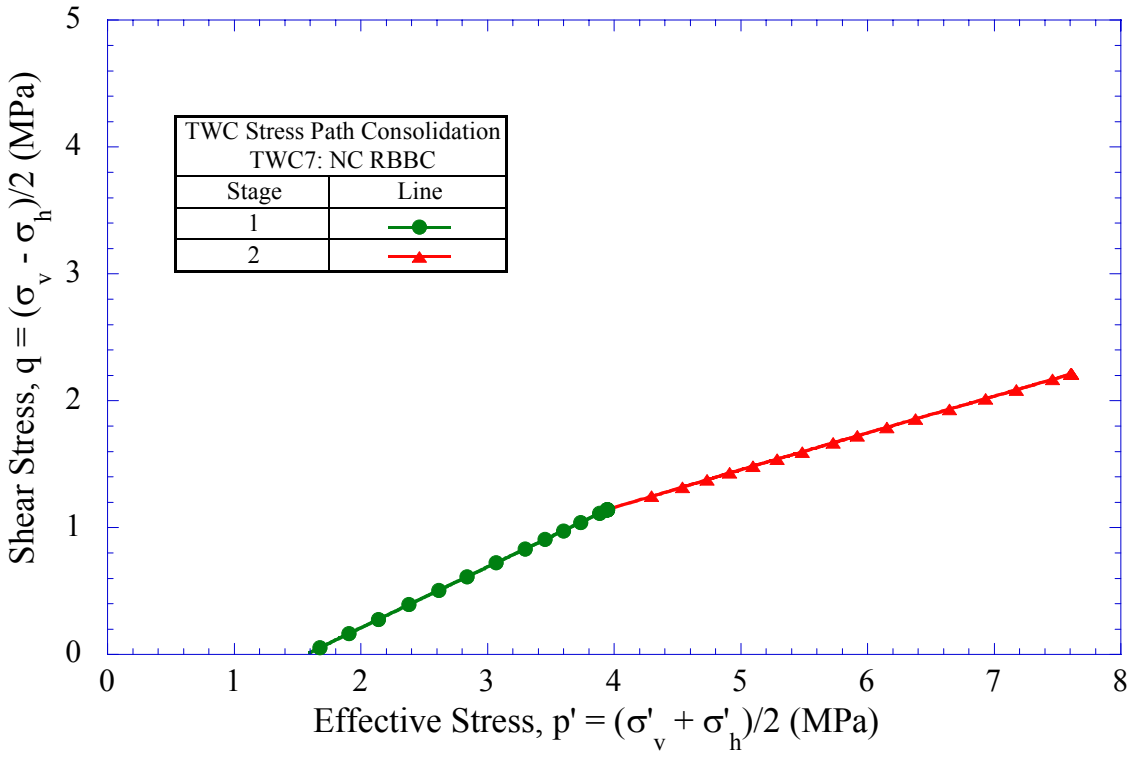

Figure 6-1: Effective stress path during consolidation for test TWC7 on NC RBBC

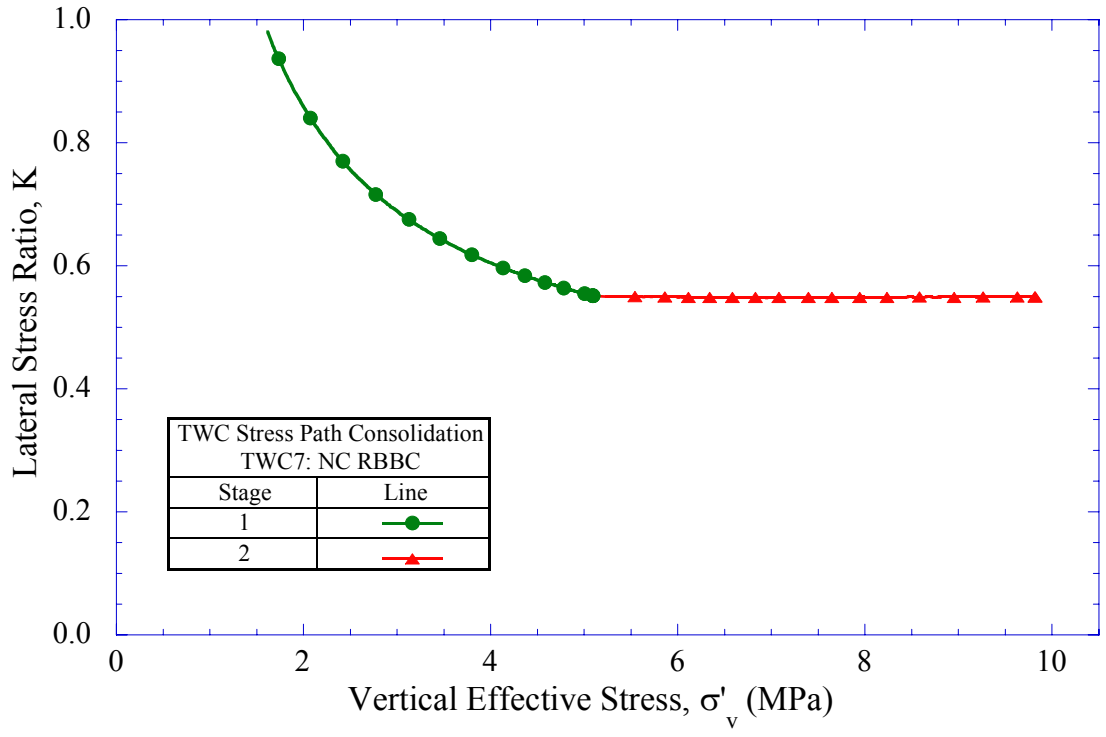

Figure 6-2: Lateral stress ratio versus stress level for test TWC7 on NC RBBC

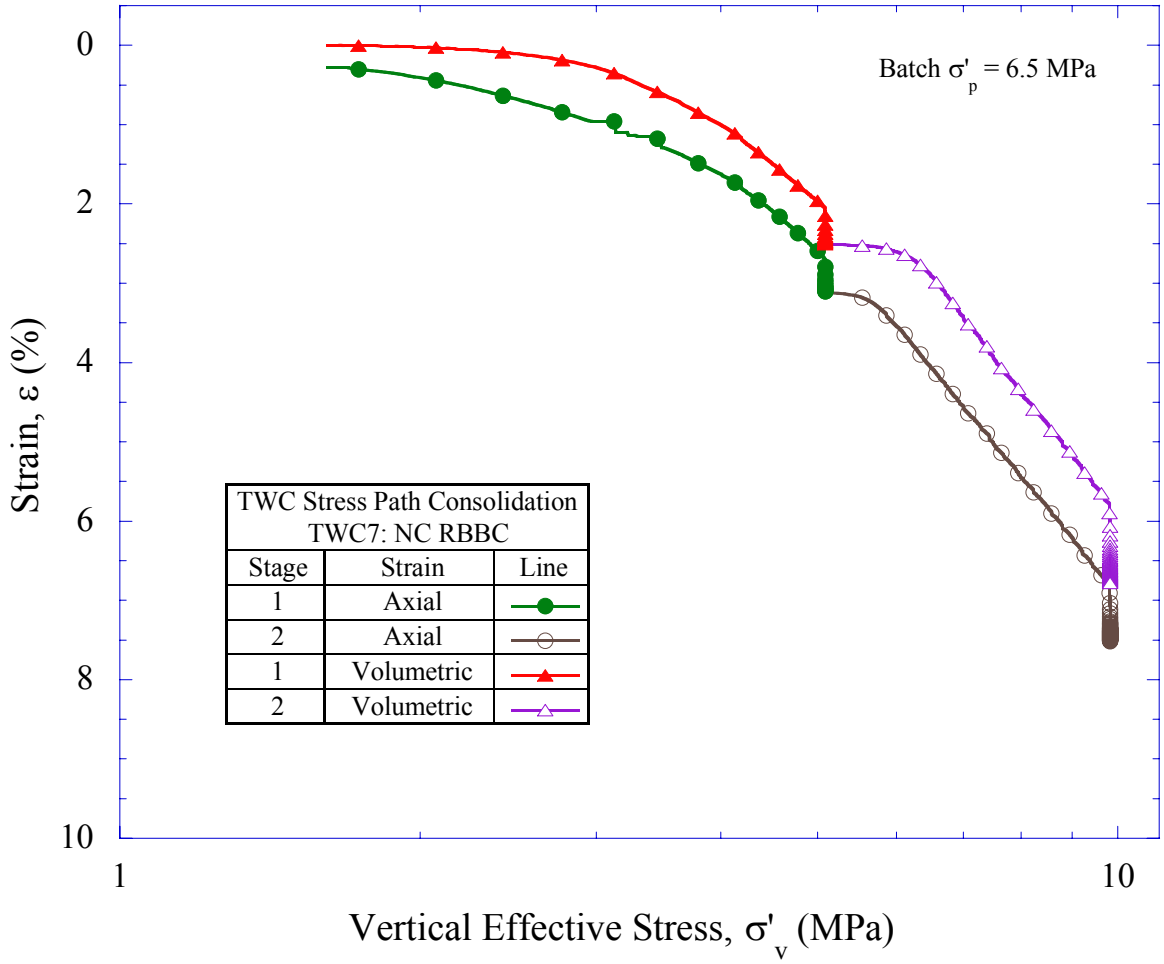

Figure 6-3: Compression behavior for test TWC7 on NC RBBC

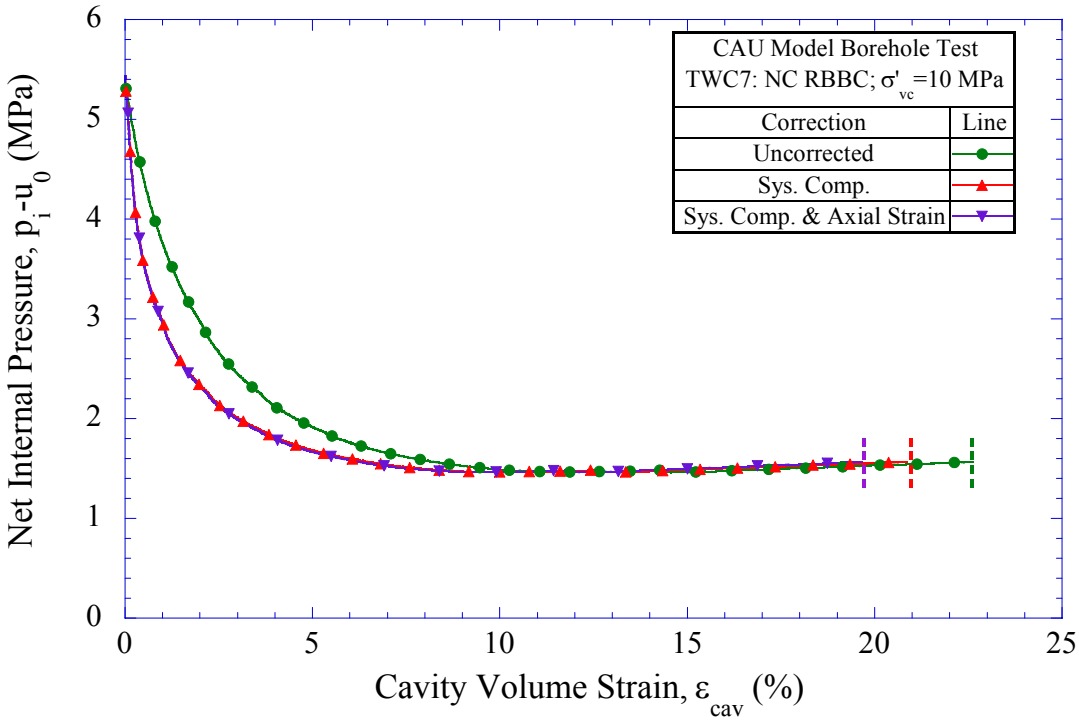

Figure 6-4: Net internal cavity pressure versus cavity volumetric strain for test TWC7 on NC RBBC

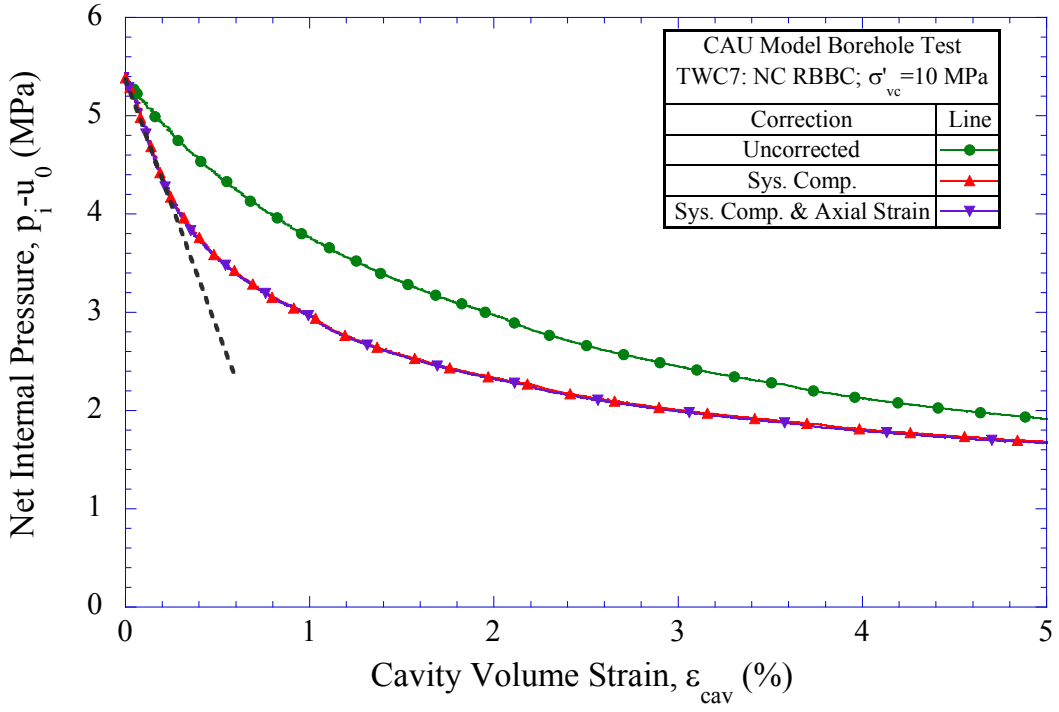

Figure 6-5: Net internal cavity pressure versus cavity volumetric strain (up to 5%) for test TWC7 on NC RBBC

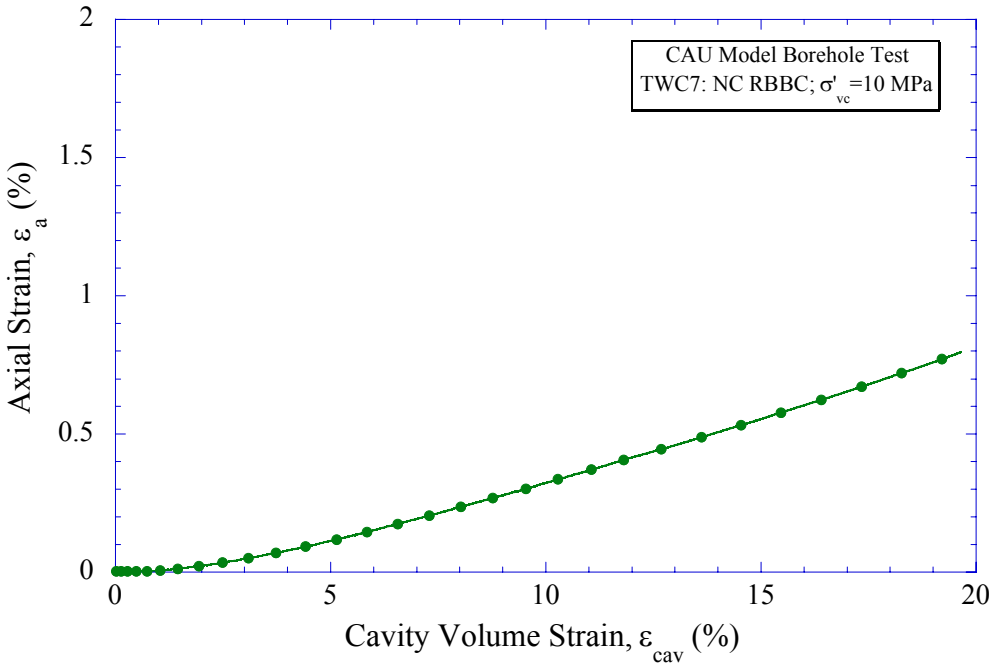

Figure 6-6: Axial strain versus cavity volumetric strain during borehole closure for test TWC7 on NC RBBC

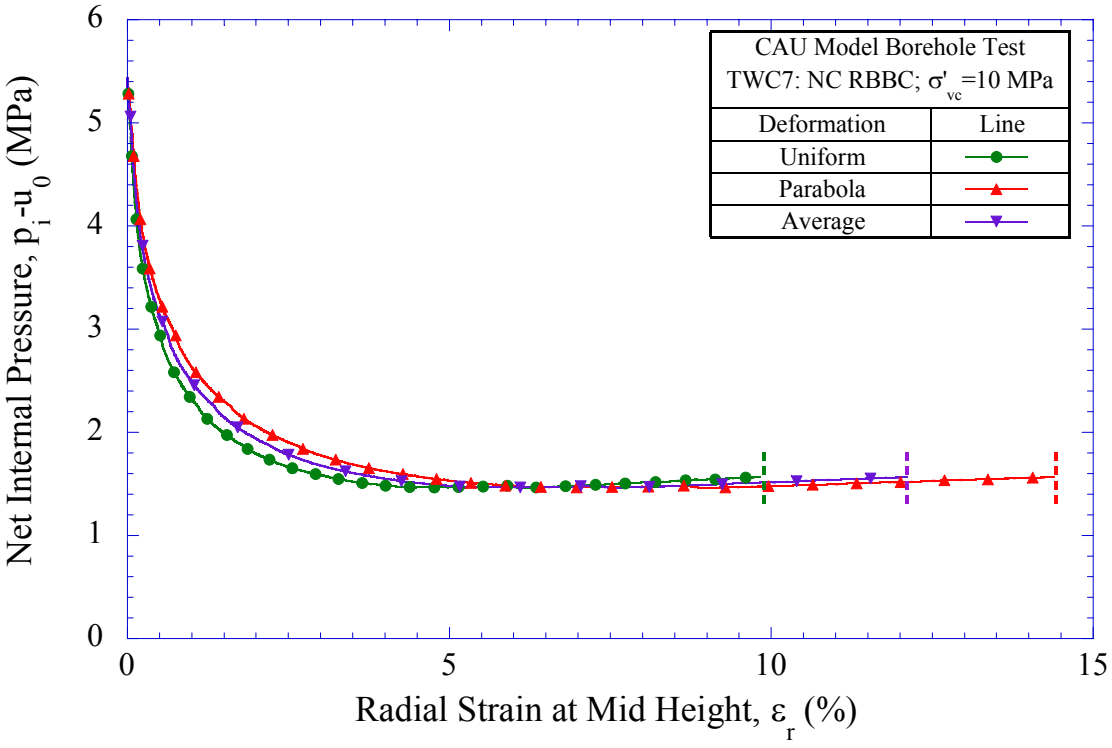

Figure 6-7: Net internal cavity pressure versus mid height cavity radial strain for test TWC7 on NC RBBC

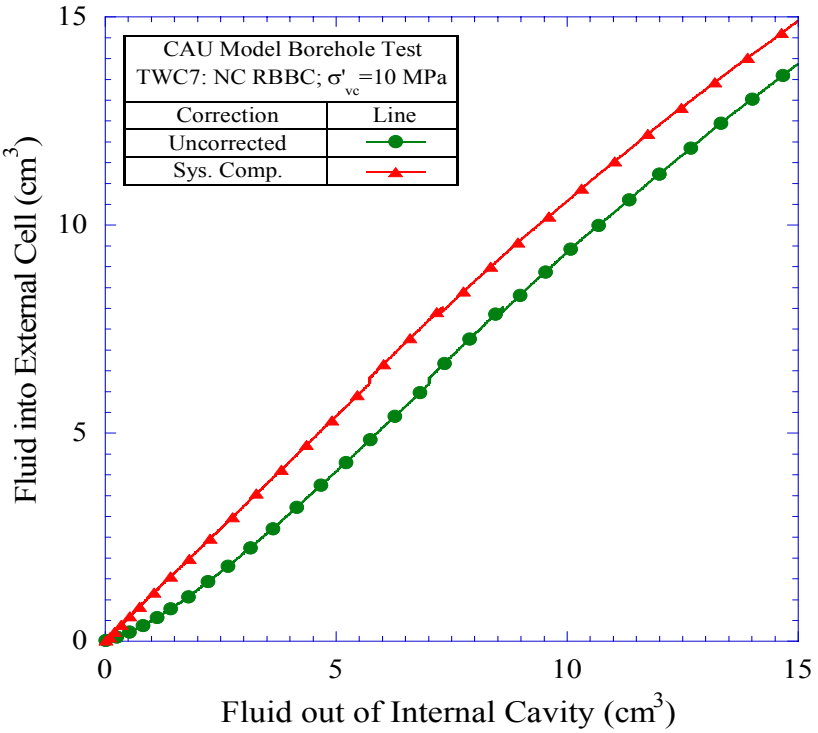

Figure 6-8: Balance of fluid injected into outer cell and withdrawn from inner model borehole for test TWC7 on NC RBBC

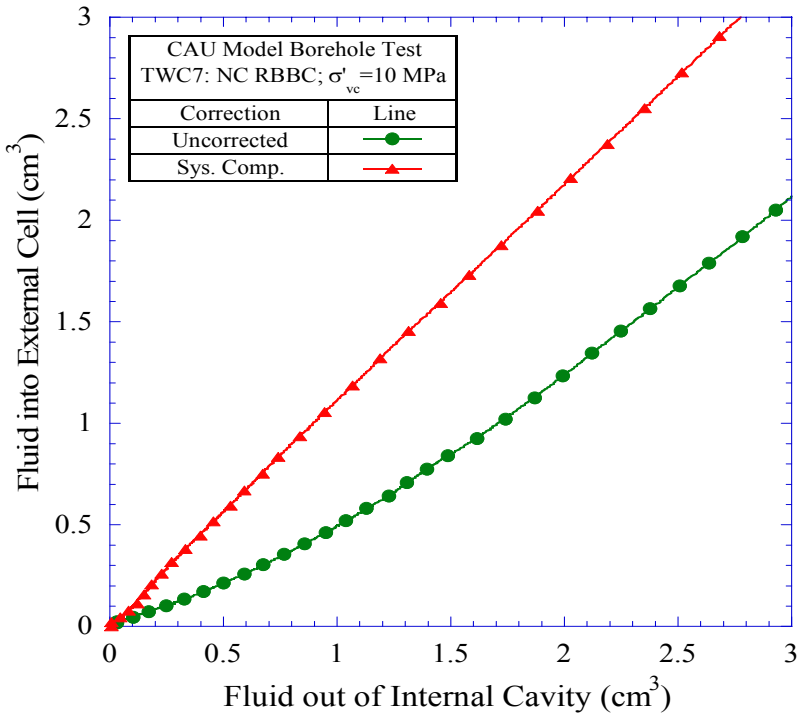

Figure 6-9: Balance of fluid injected into outer cell and withdrawn from inner model borehole (close up view) for test TWC7 on NC RBBC

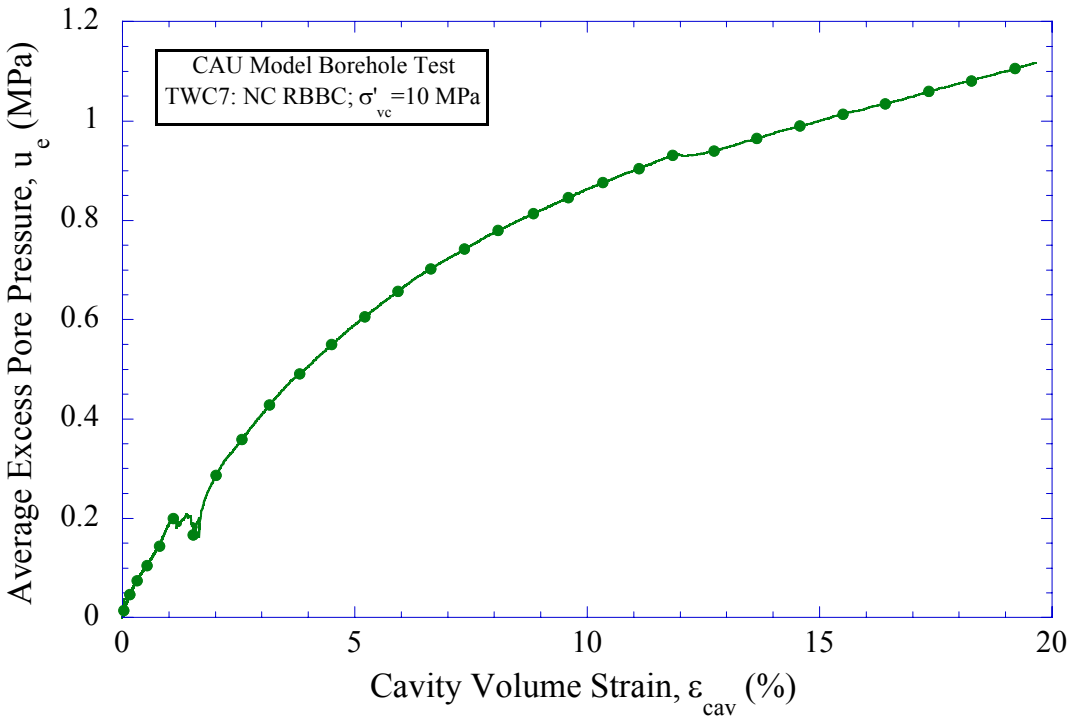

Figure 6-10: Average excess pore pressure versus cavity volumetric strain for test TWC7 on NC RBBC

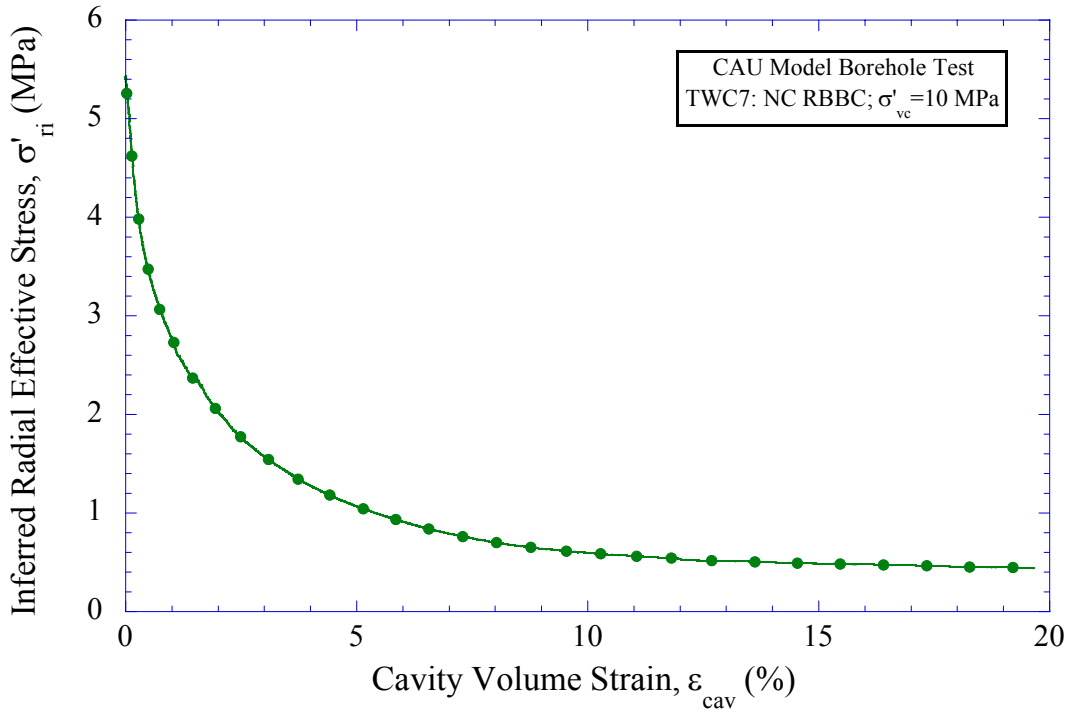

Figure 6-11: Inferred cavity radial effective stress versus cavity volumetric strain for test TWC7 on NC RBBC

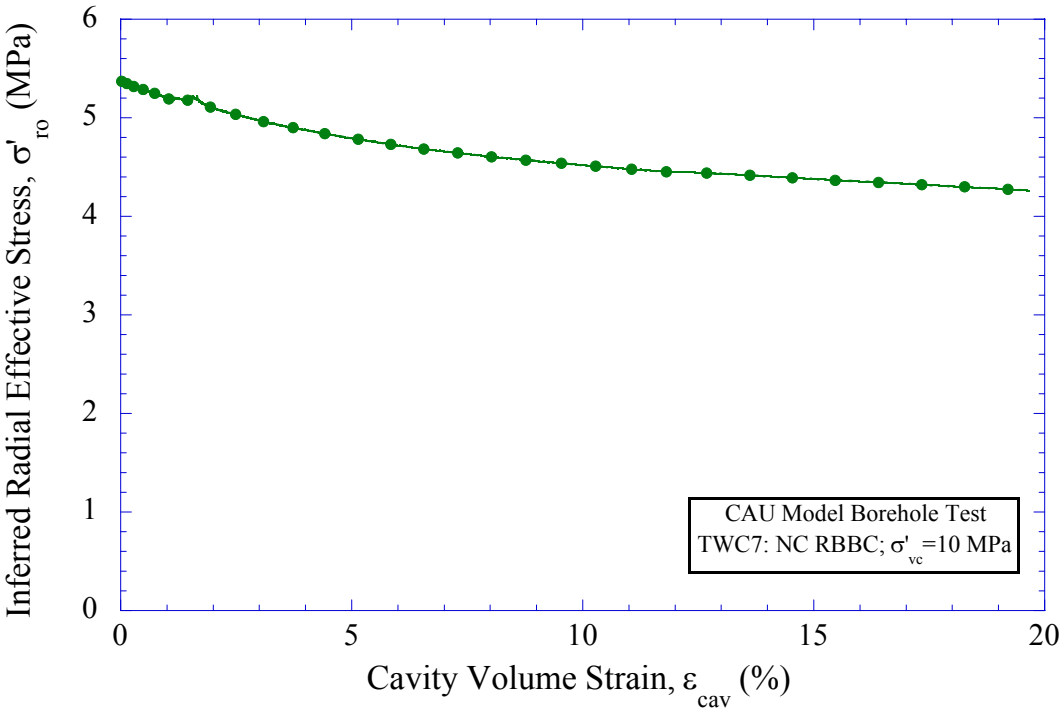

Figure 6-12: Inferred radial effective stress at the outer wall versus cavity volumetric strain for test TWC7 on NC RBBC

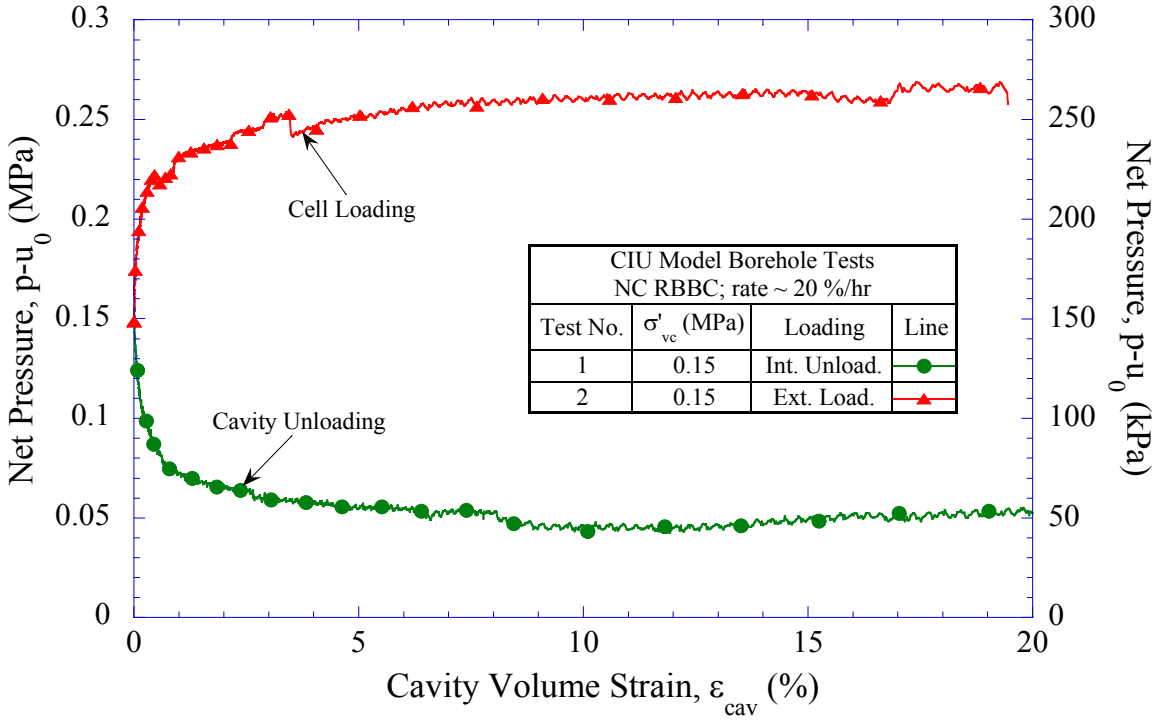

Figure 6-13: Effect of loading mode (internal unloading versus external loading) on net pressure versus cavity volumetric strain for NC RBBC from CIU model borehole tests

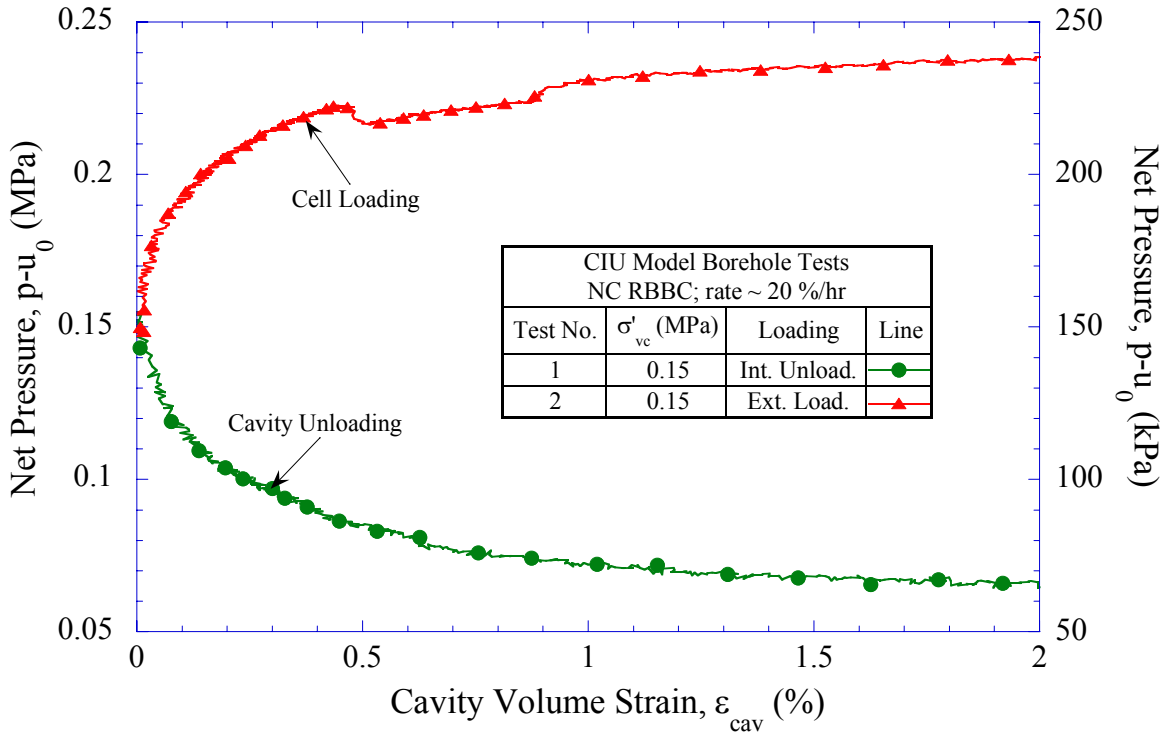

Figure 6-14: Effect of loading mode (internal unloading versus external loading) on net pressure versus cavity volumetric strain (up to 2%) for NC RBBC from CIU model borehole tests

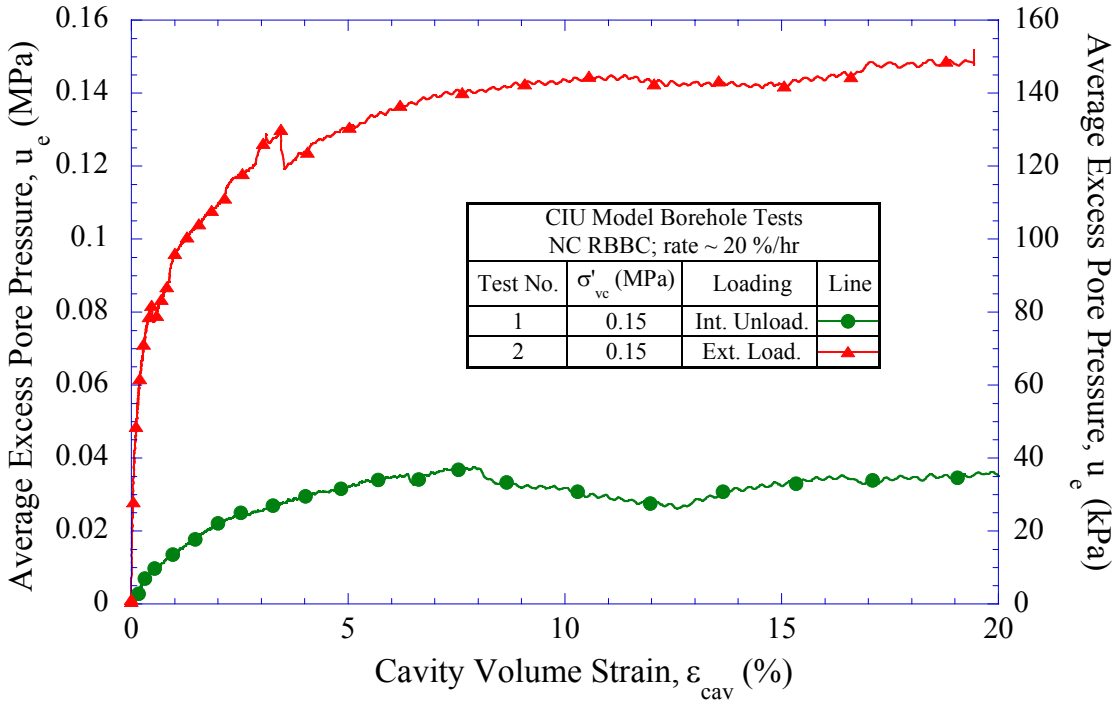

Figure 6-15: Effect of loading mode (internal unloading versus external loading) on average excess pore pressures for NC RBBC from CIU model borehole tests

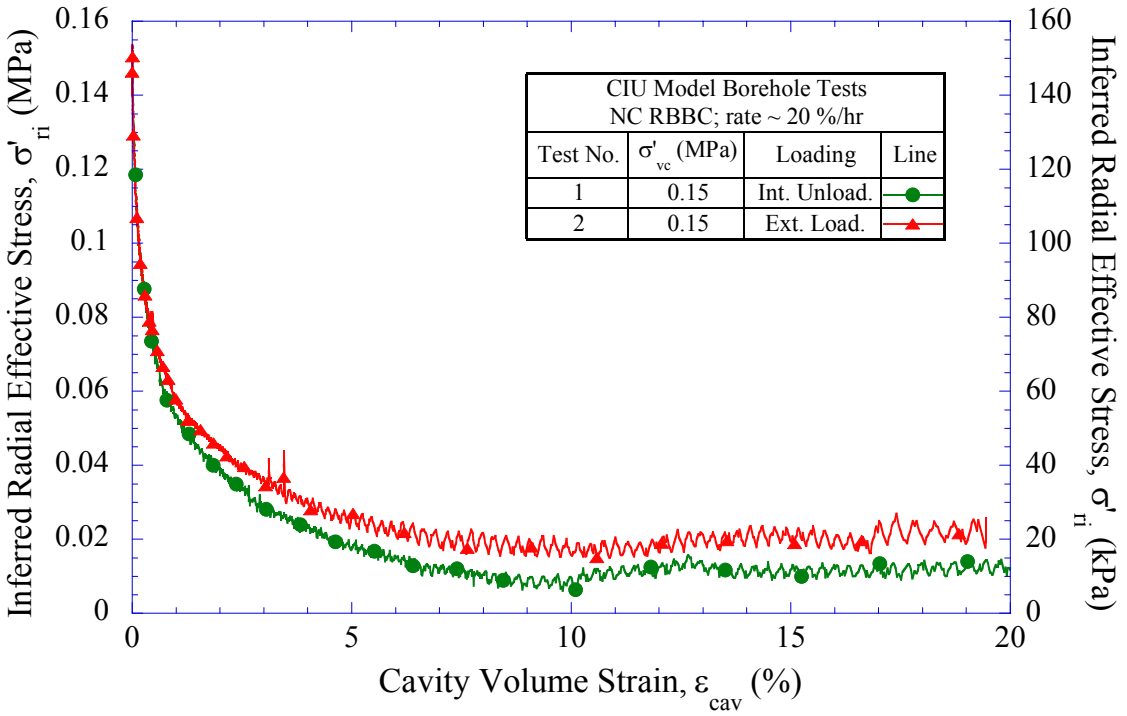

Figure 6-16: Effect of loading mode (internal unloading versus external loading) on inferred cavity radial effective stress for NC RBBC from CIU model borehole tests

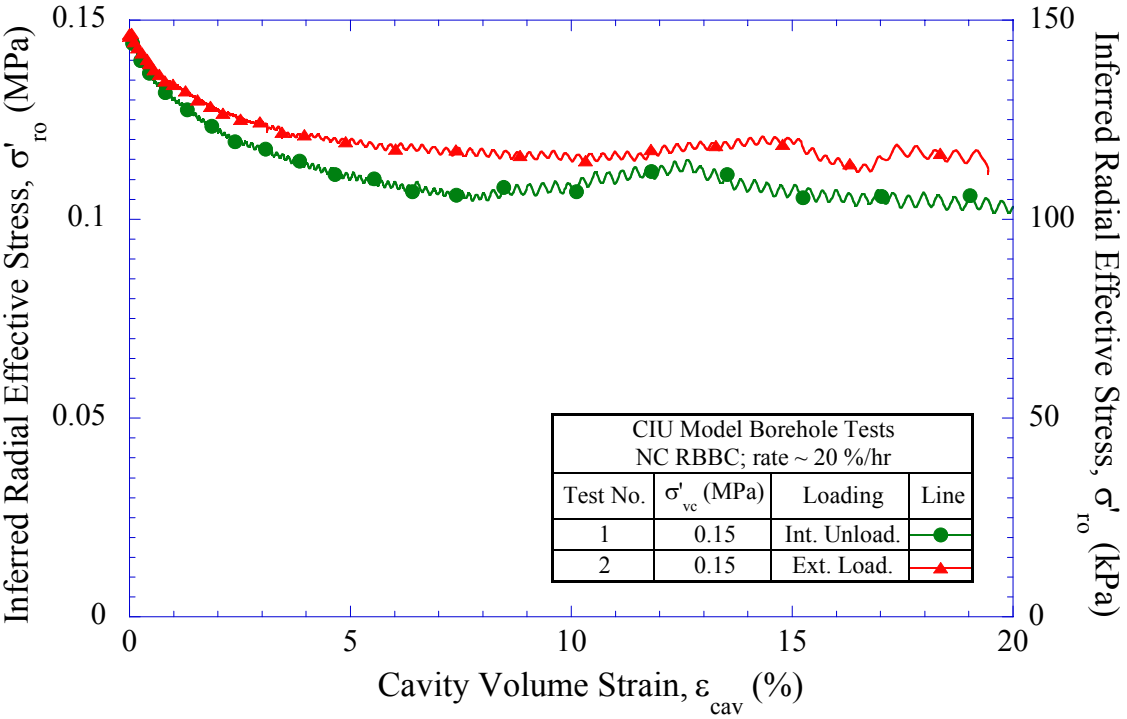

Figure 6-17: Effect of loading mode (internal unloading versus external loading) on inferred radial effective stress at the outer wall for NC RBBC from CIU model borehole tests

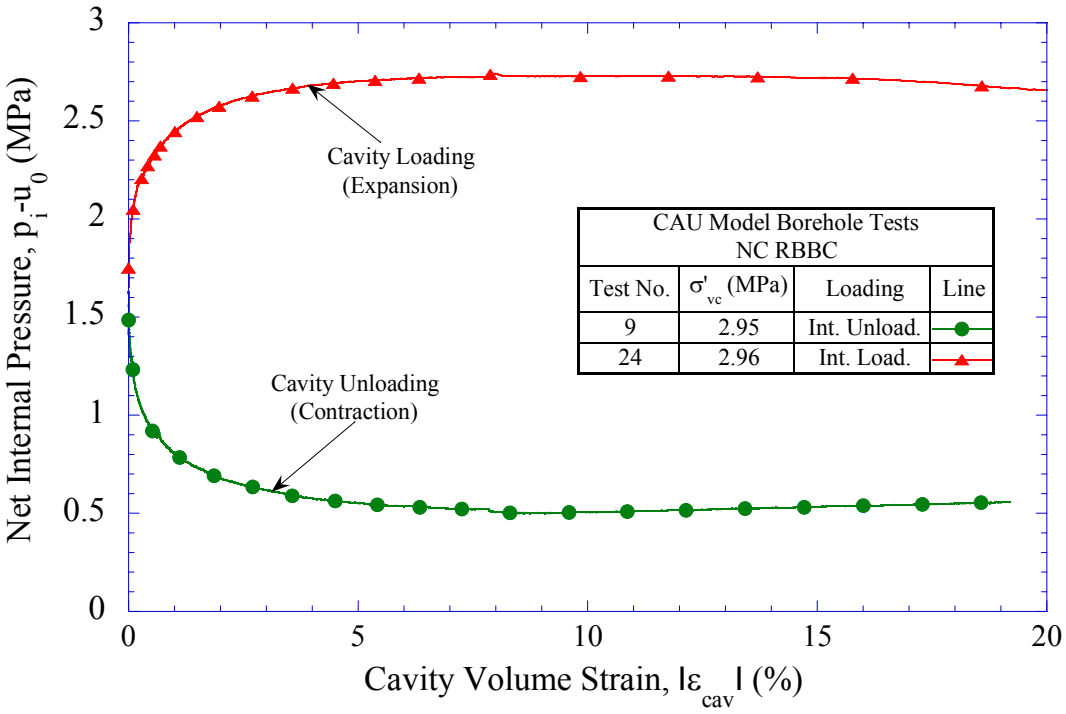

Figure 6-18: Effect of loading mode (internal unloading versus internal loading) on net internal cavity pressure versus cavity volumetric strain for NC RBBC from CAU model borehole tests

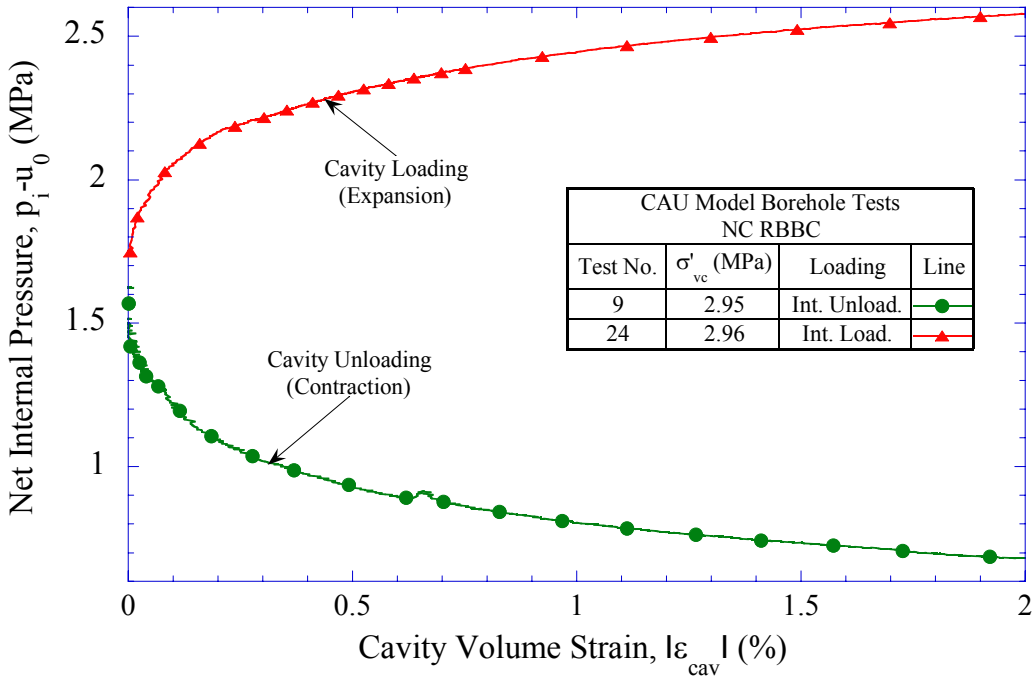

Figure 6-19: Effect of loading mode (internal unloading versus internal loading) on net internal cavity pressure versus cavity volumetric strain (up to 2%) for NC RBBC from CAU model borehole tests

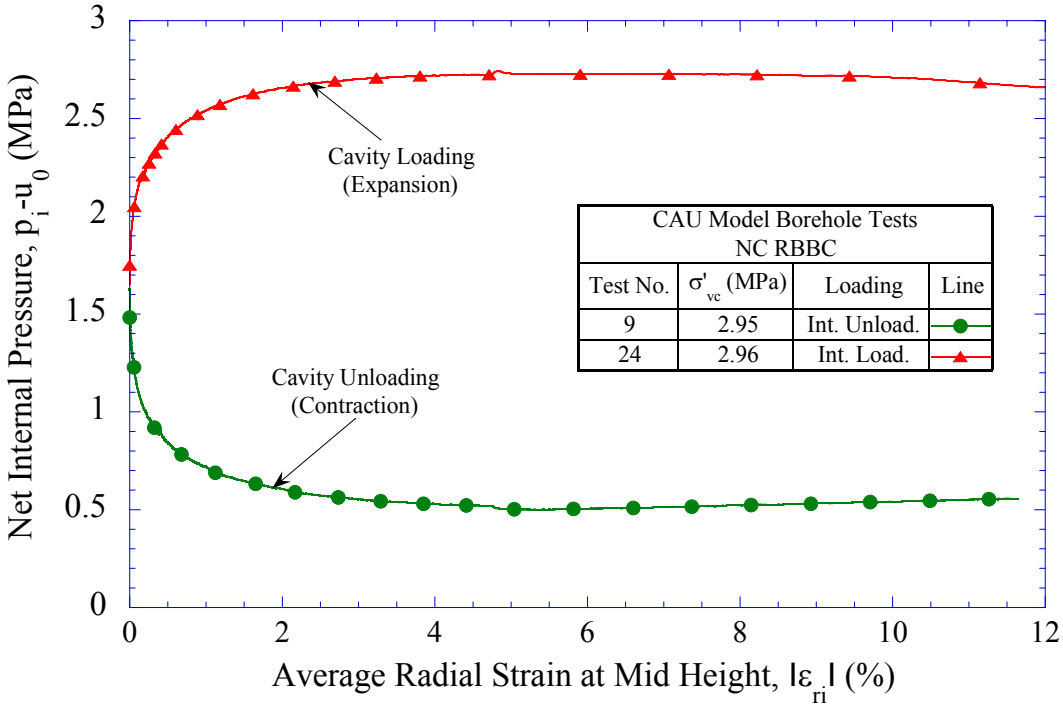

Figure 6-20: Effect of loading mode (internal unloading versus internal loading) on net internal cavity pressure versus mid height average cavity radial strain for NC RBBC from CAU model borehole tests

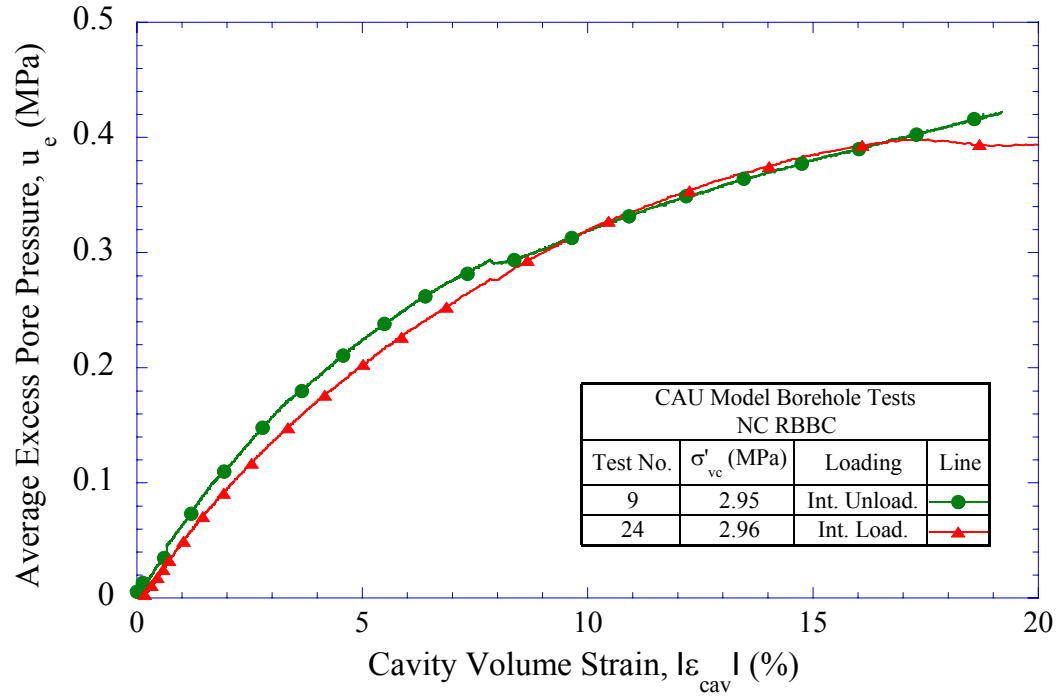

Figure 6-21: Effect of loading mode (internal unloading versus internal loading) on average excess pore pressures for NC RBBC from CAU model borehole tests

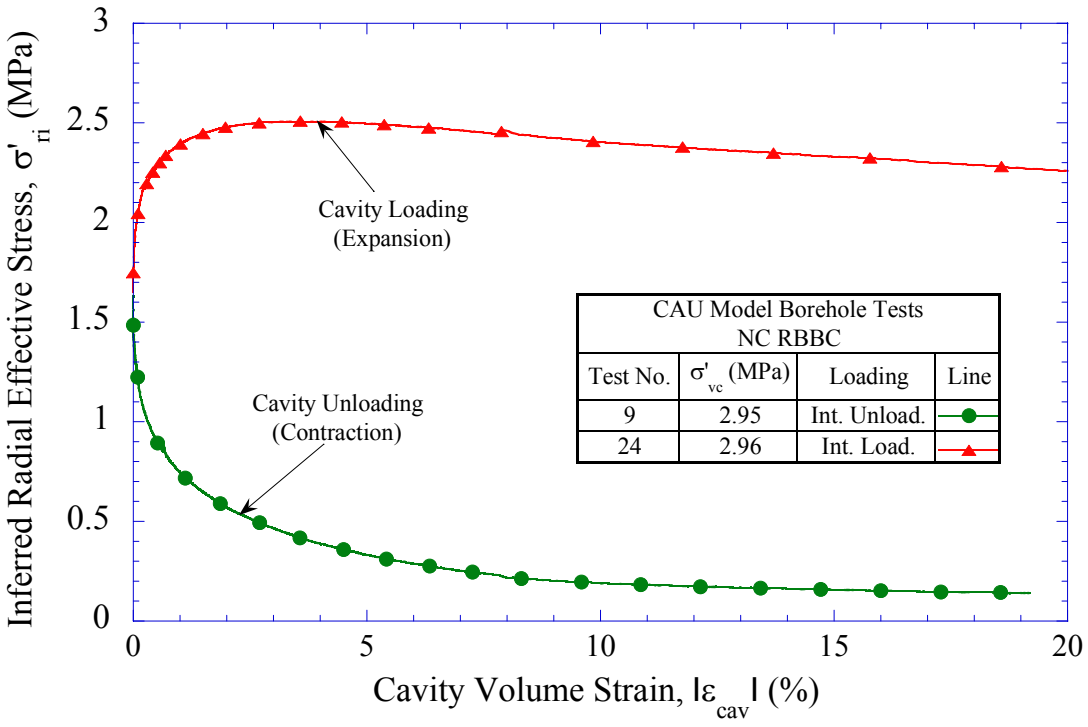

Figure 6-22: Effect of loading mode (internal unloading versus internal loading) on inferred cavity radial effective stress for NC RBBC from CAU model borehole tests

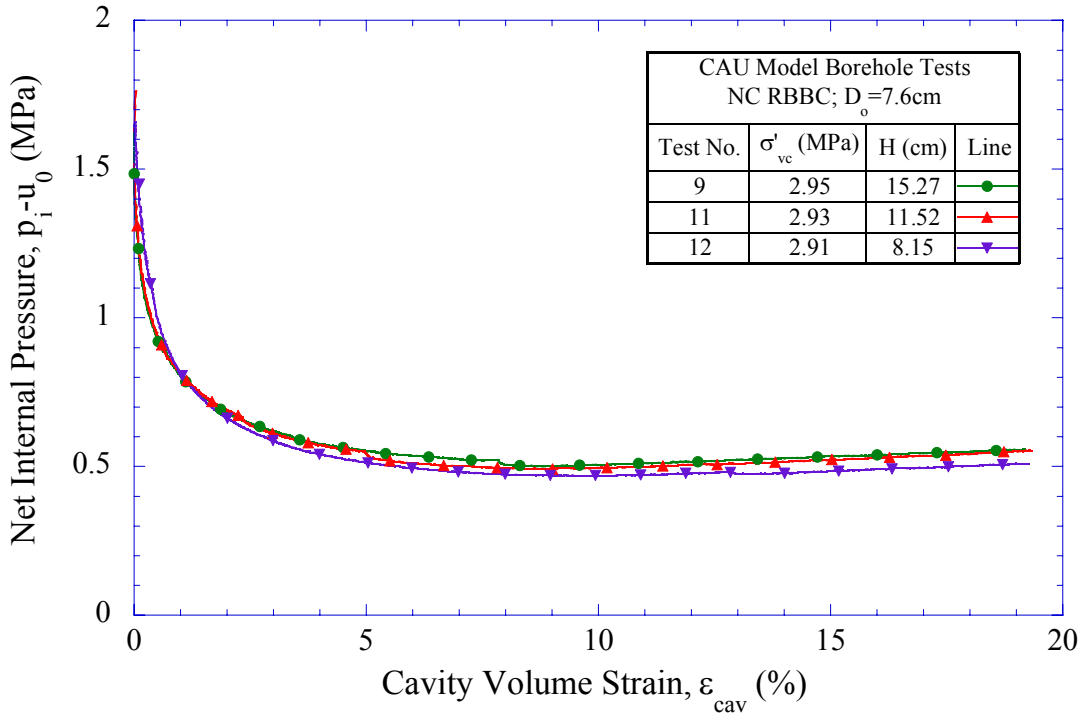

Figure 6-23: Effect of specimen height on net internal cavity pressure versus cavity volumetric strain for NC RBBC from CAU model borehole tests

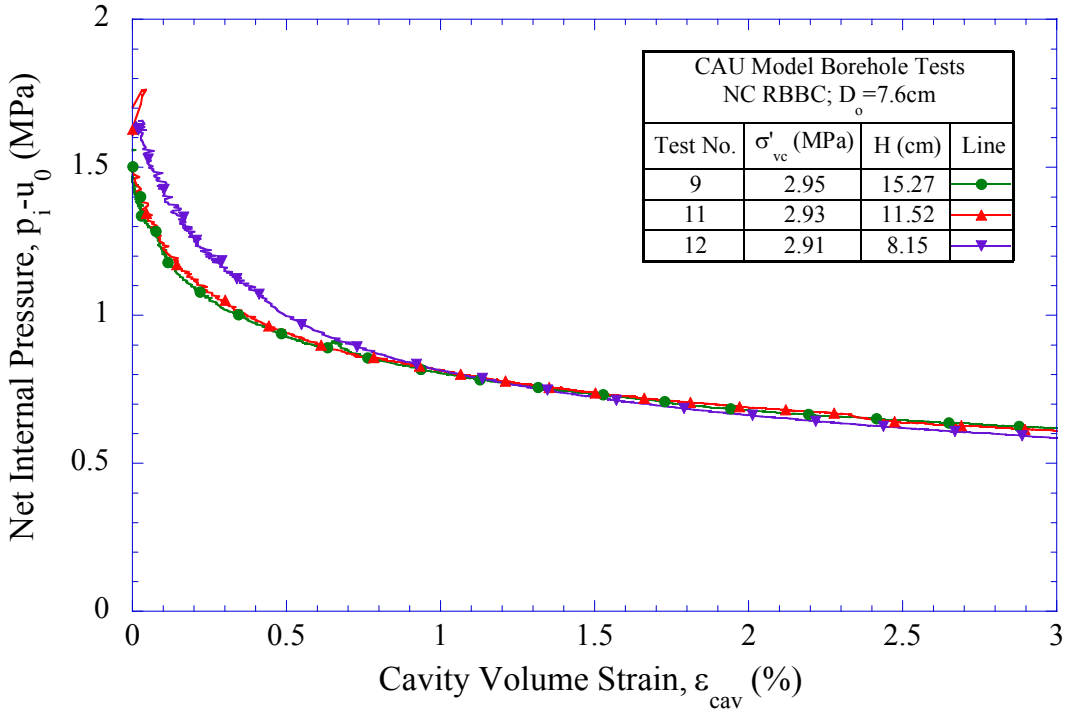

Figure 6-24: Effect of specimen height on net internal cavity pressure versus cavity volumetric strain (up to 3%) for NC RBBC from CAU model borehole tests

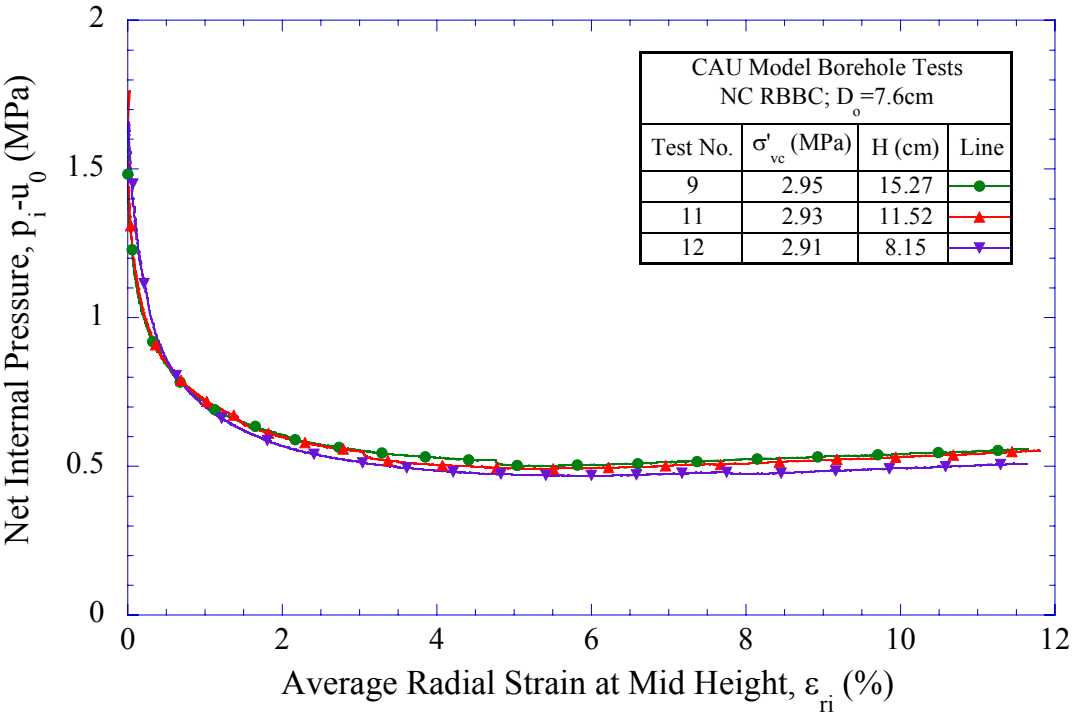

Figure 6-25: Effect of specimen height on net internal cavity pressure versus mid height average cavity radial strain for NC RBBC from CAU model borehole tests

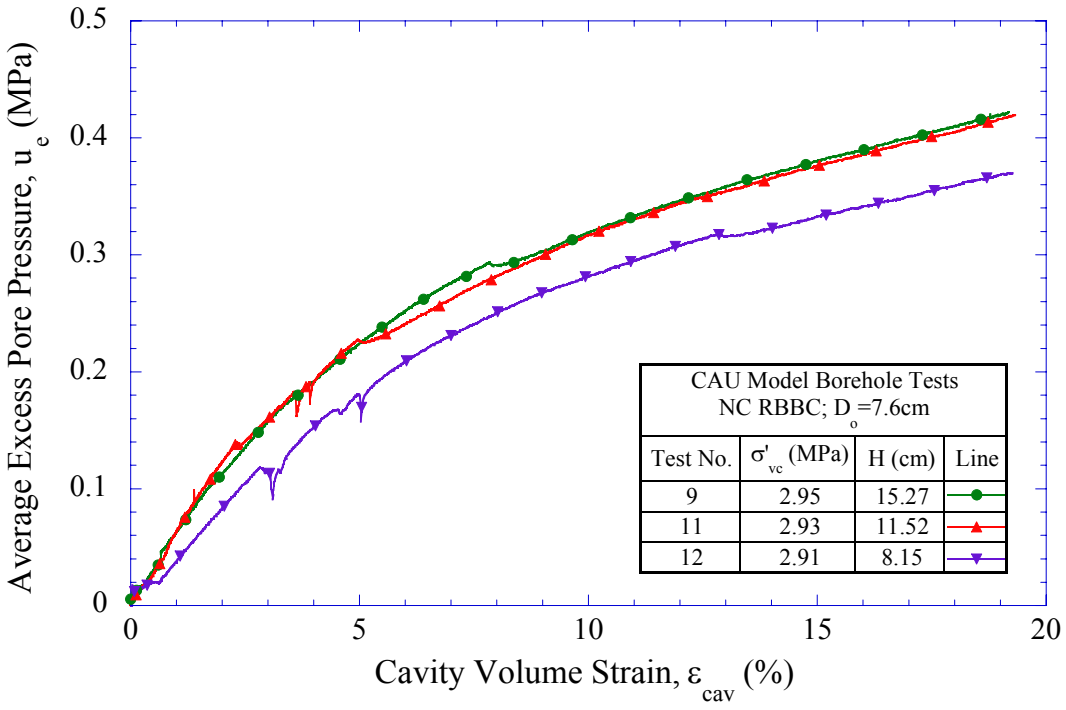

Figure 6-26: Effect of specimen height on average excess pore pressures for NC RBBC from CAU model borehole tests

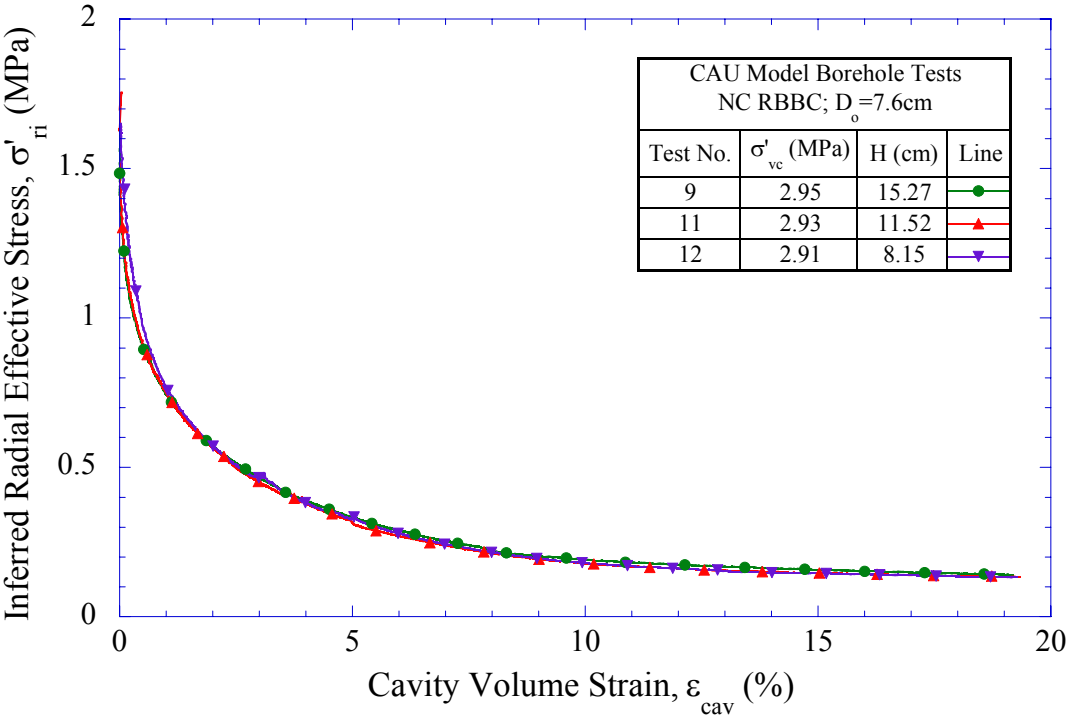

Figure 6-27: Effect of specimen height on inferred cavity radial effective stress for NC RBBC from CAU model borehole tests

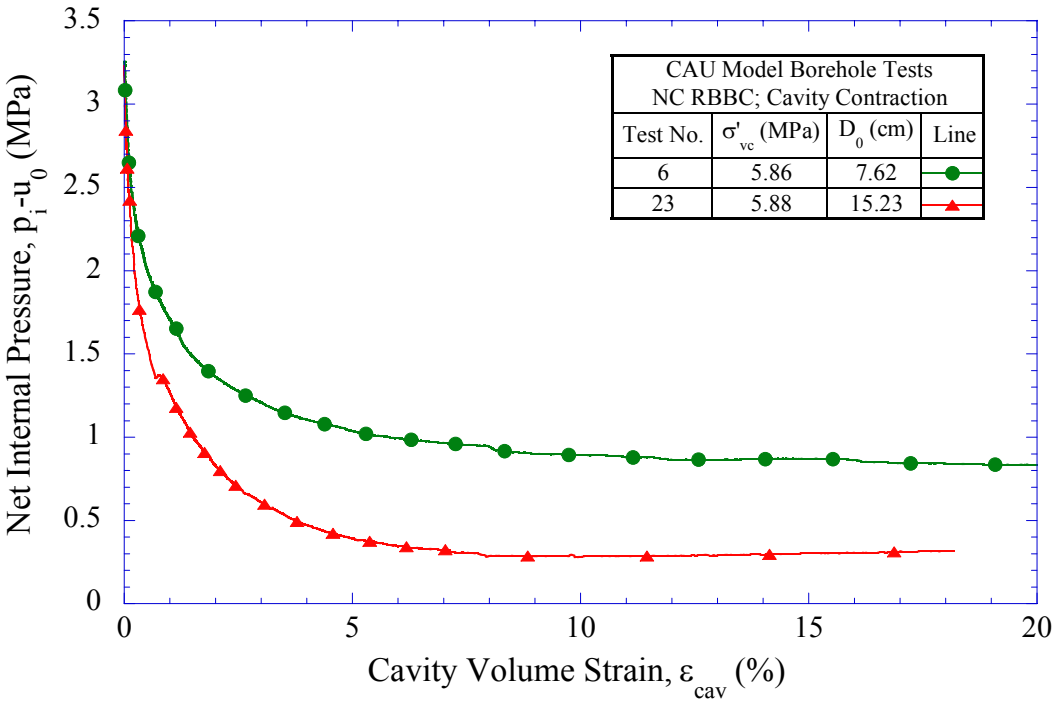

Figure 6-28: Effect of specimen outer diameter on net internal cavity pressure versus cavity volumetric strain during internal unloading for NC RBBC from CAU model borehole tests

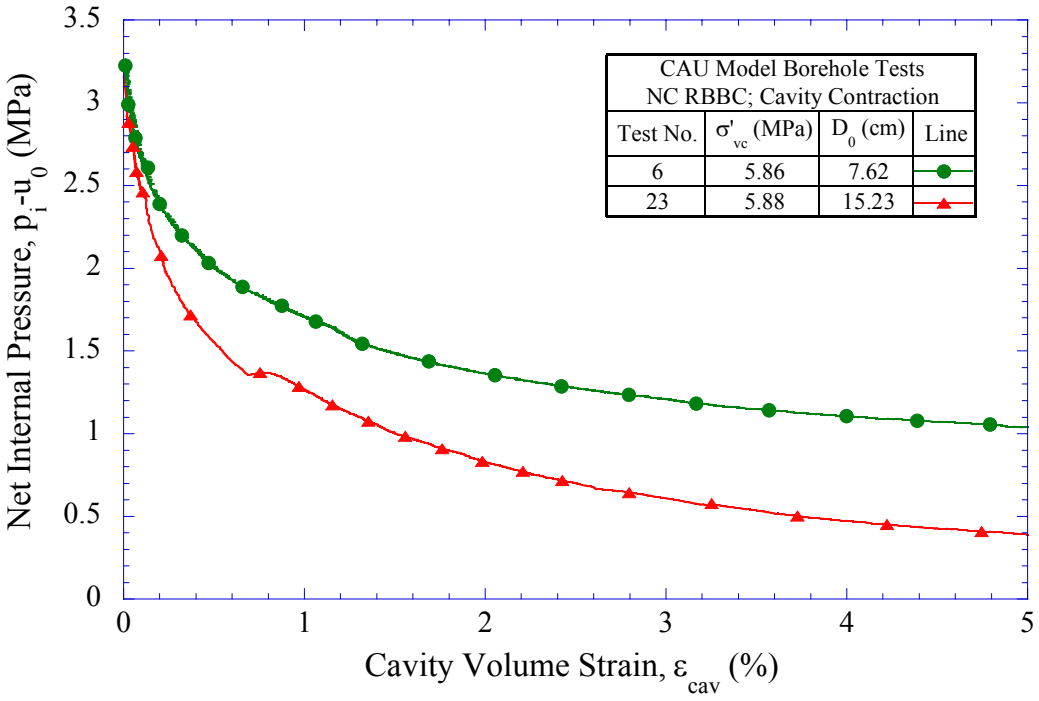

Figure 6-29: Effect of specimen outer diameter on net internal cavity pressure versus cavity volumetric strain (up to 5%) during internal unloading for NC RBBC from CAU model borehole tests

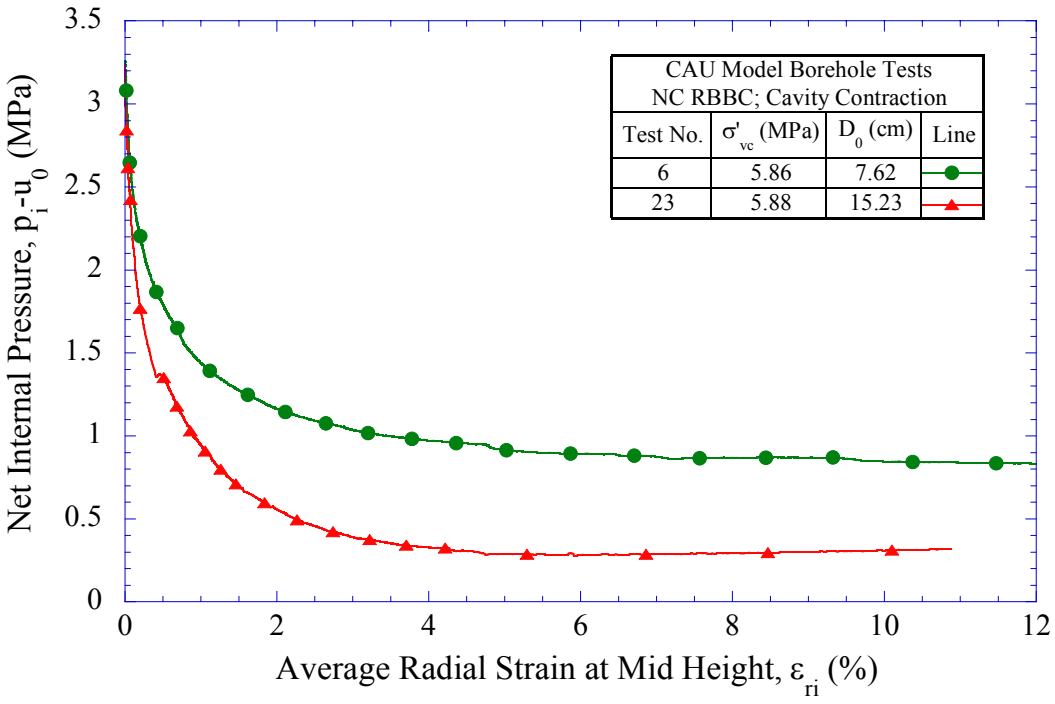

Figure 6-30: Effect of specimen outer diameter on net internal cavity pressure versus mid height average cavity radial strain during internal unloading for NC RBBC from CAU model borehole tests

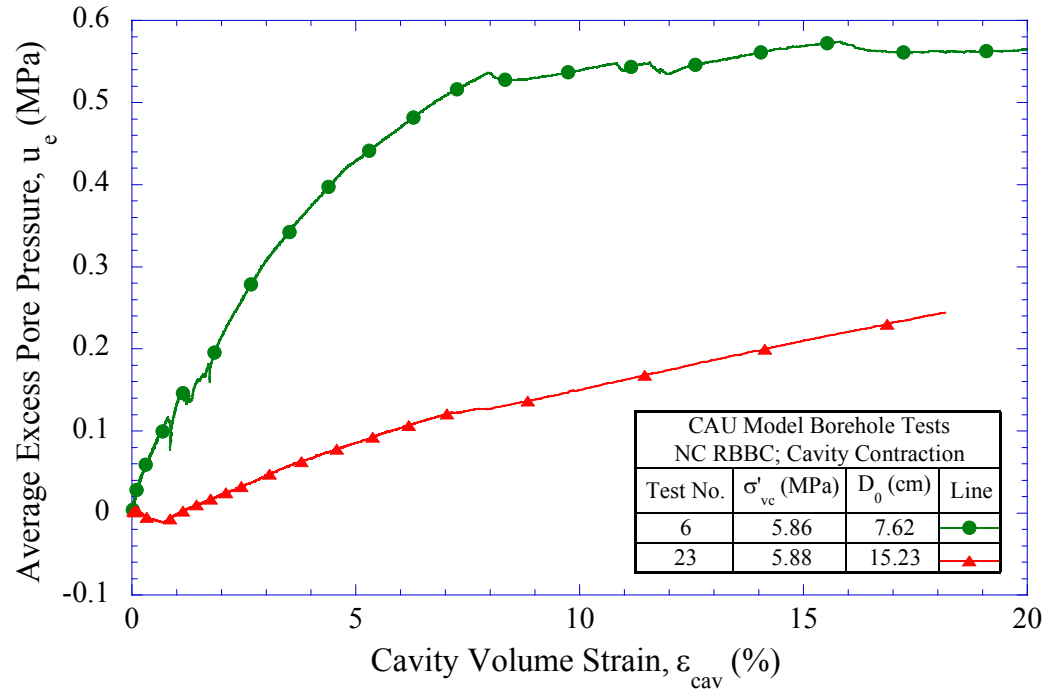

Figure 6-31: Effect of specimen outer diameter on average excess pore pressures during internal unloading for NC RBBC from CAU model borehole tests

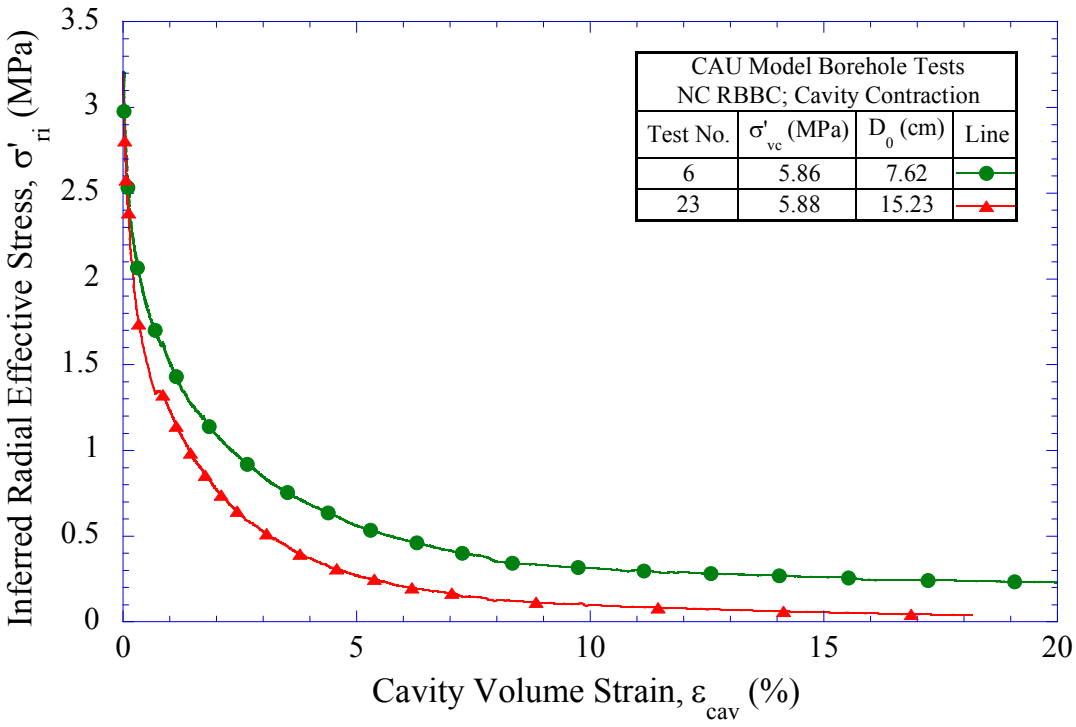

Figure 6-32: Effect of specimen outer diameter on inferred cavity radial effective stress during internal unloading for NC RBBC from CAU model borehole tests

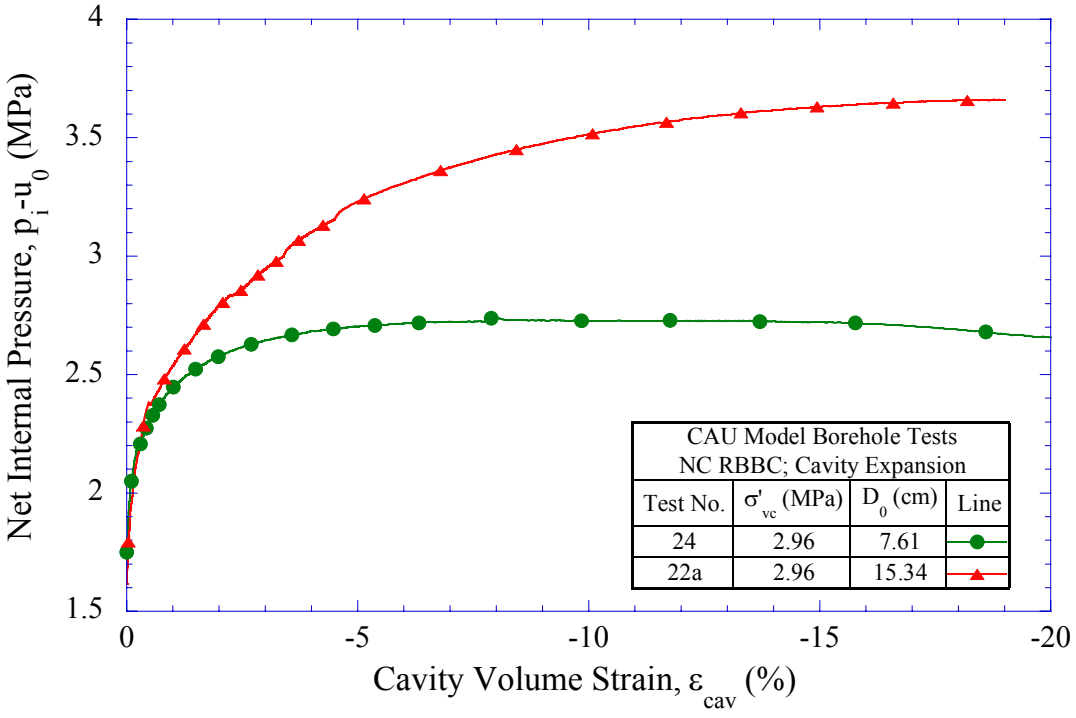

Figure 6-33: Effect of specimen outer diameter on net internal cavity pressure versus cavity volumetric strain during internal loading for NC RBBC from CAU model borehole tests

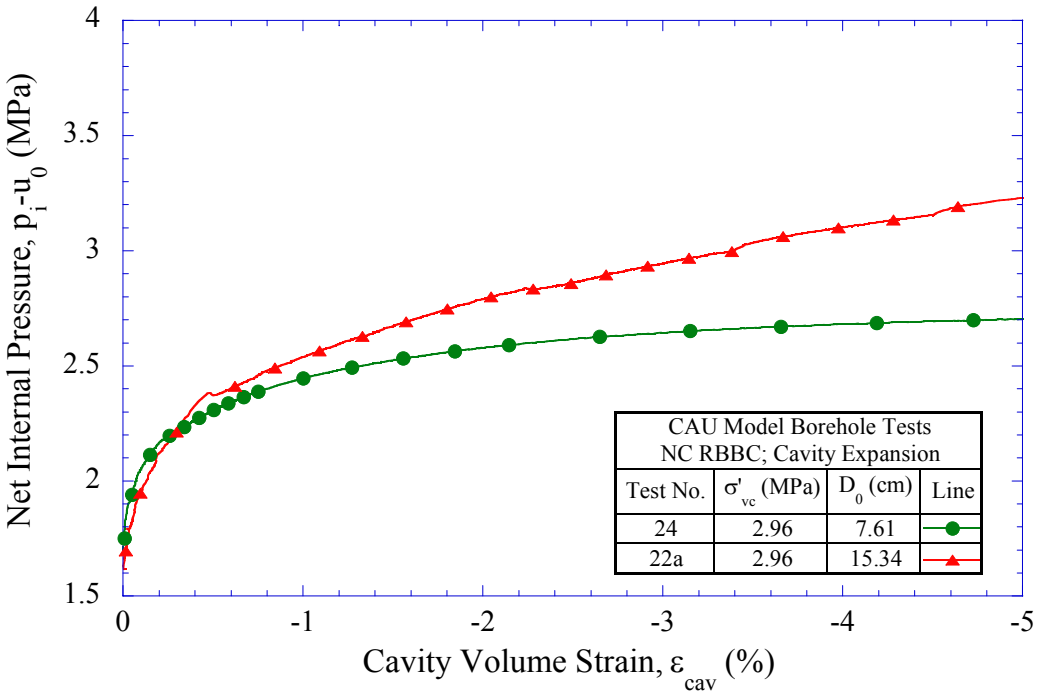

Figure 6-34: Effect of specimen outer diameter on net internal cavity pressure versus cavity volumetric strain (up to 5%) during internal loading for NC RBBC from CAU model borehole tests

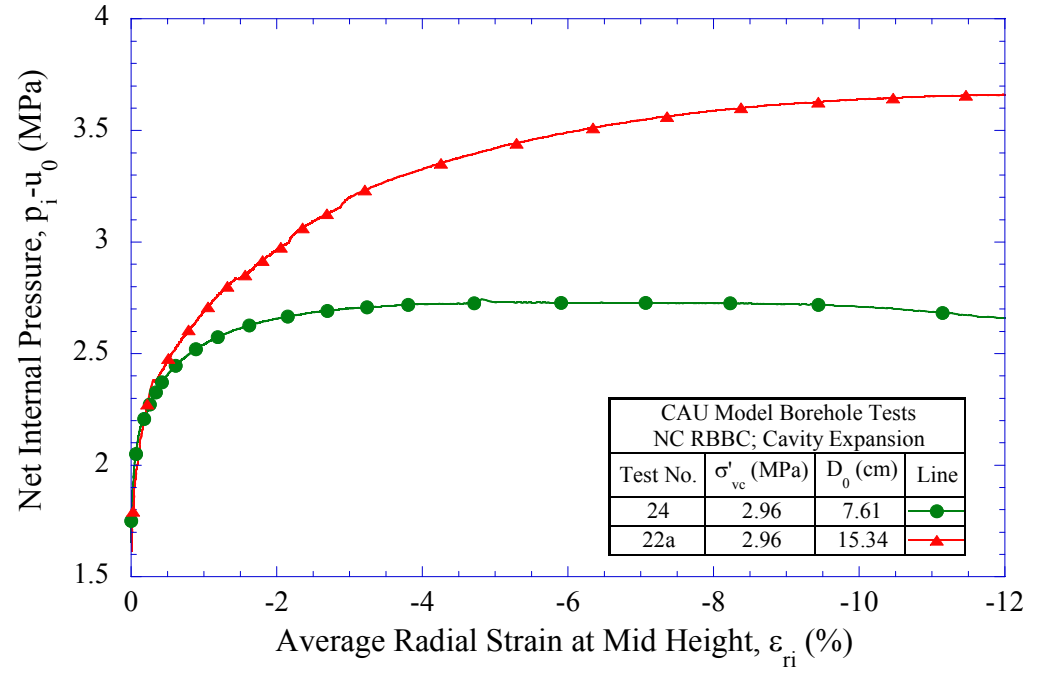

Figure 6-35: Effect of specimen outer diameter on net internal cavity pressure versus mid height average cavity radial strain during internal loading for NC RBBC from CAU model borehole tests

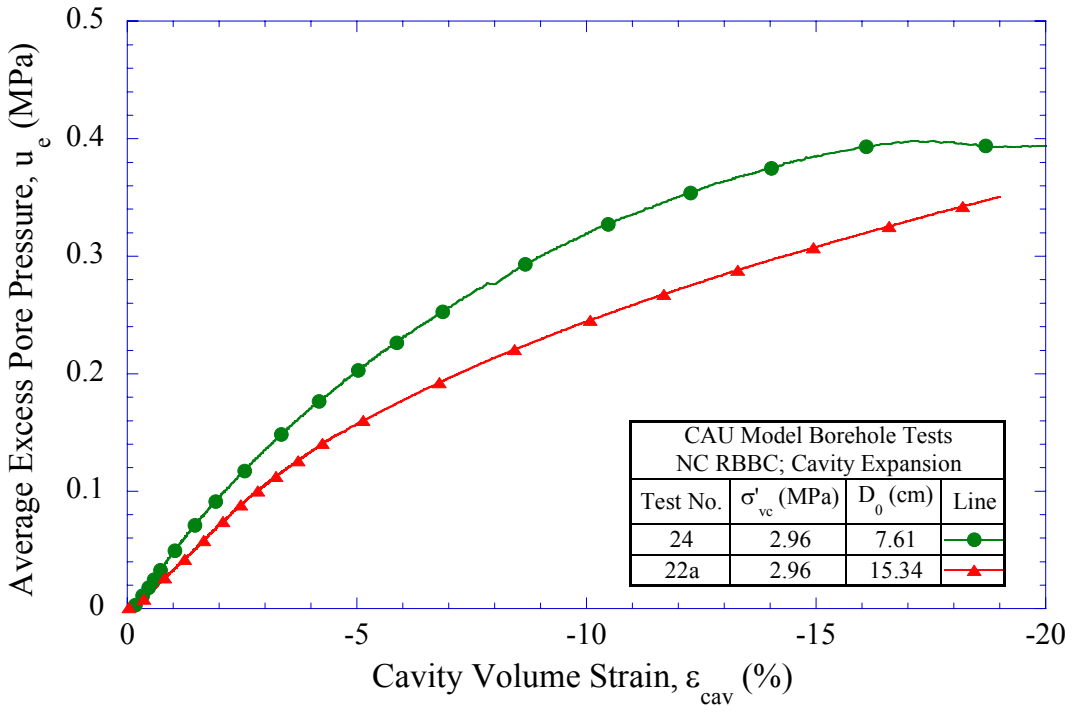

Figure 6-36: Effect of specimen outer diameter on average excess pore pressures during internal loading for NC RBBC from CAU model borehole tests

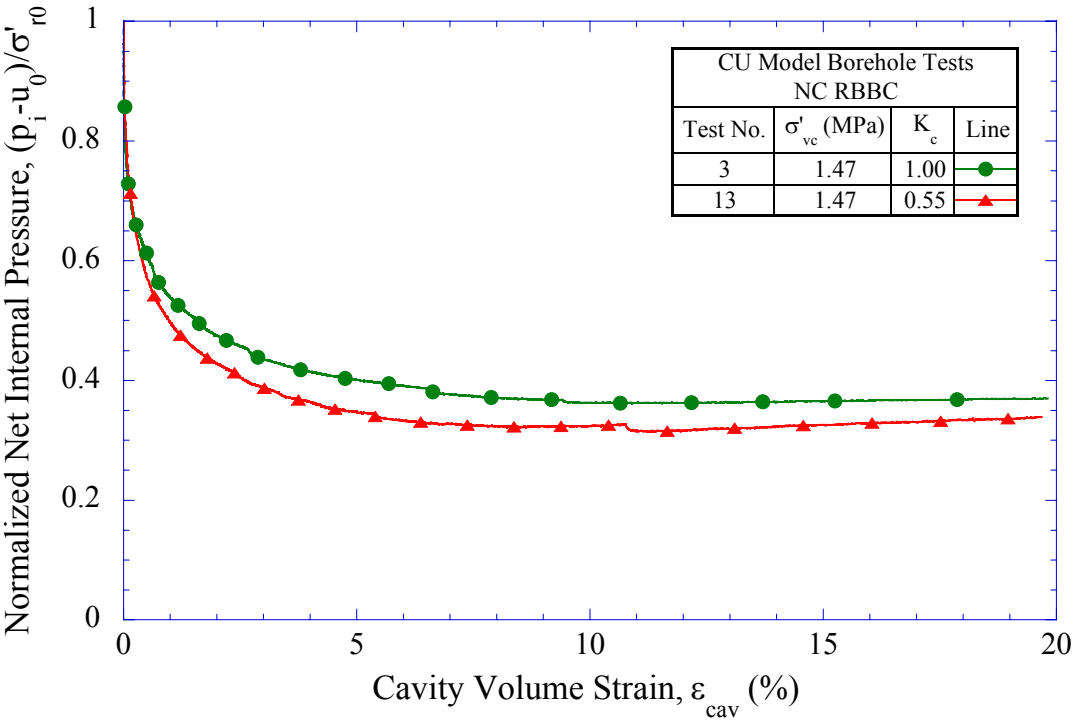

Figure 6-37: Effect of lateral stress ratio on normalized net internal cavity pressure versus cavity volumetric strain for NC RBBC from CU model borehole tests

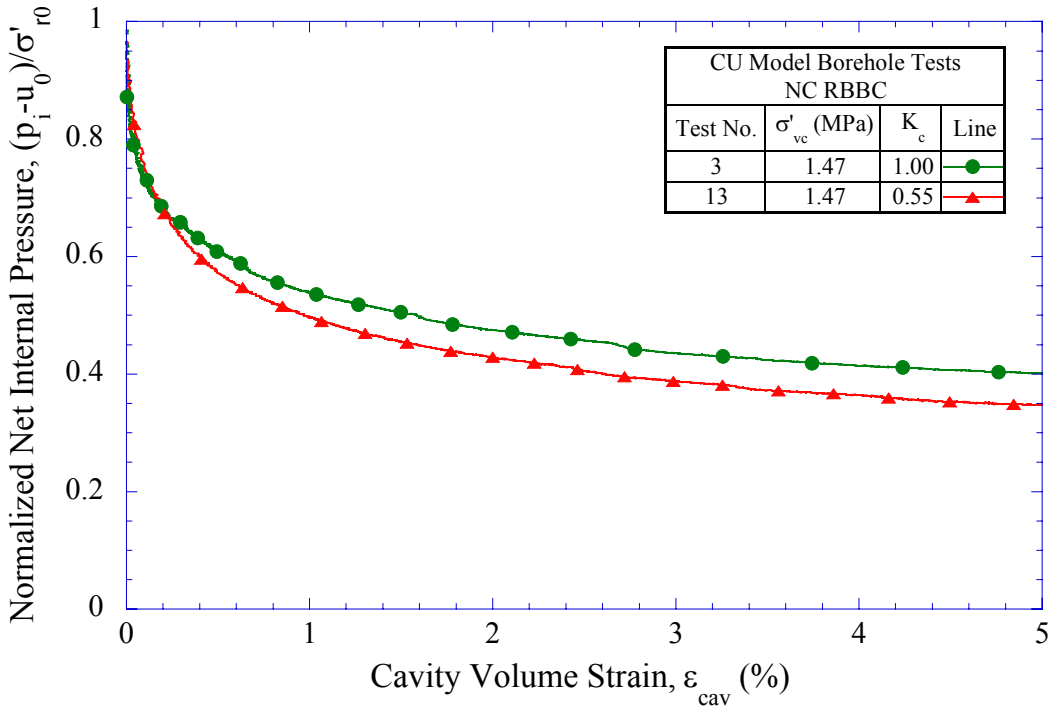

Figure 6-38: Effect of lateral stress ratio on normalized net internal cavity pressure versus cavity volumetric strain (up to 5%) for NC RBBC from CU model borehole tests

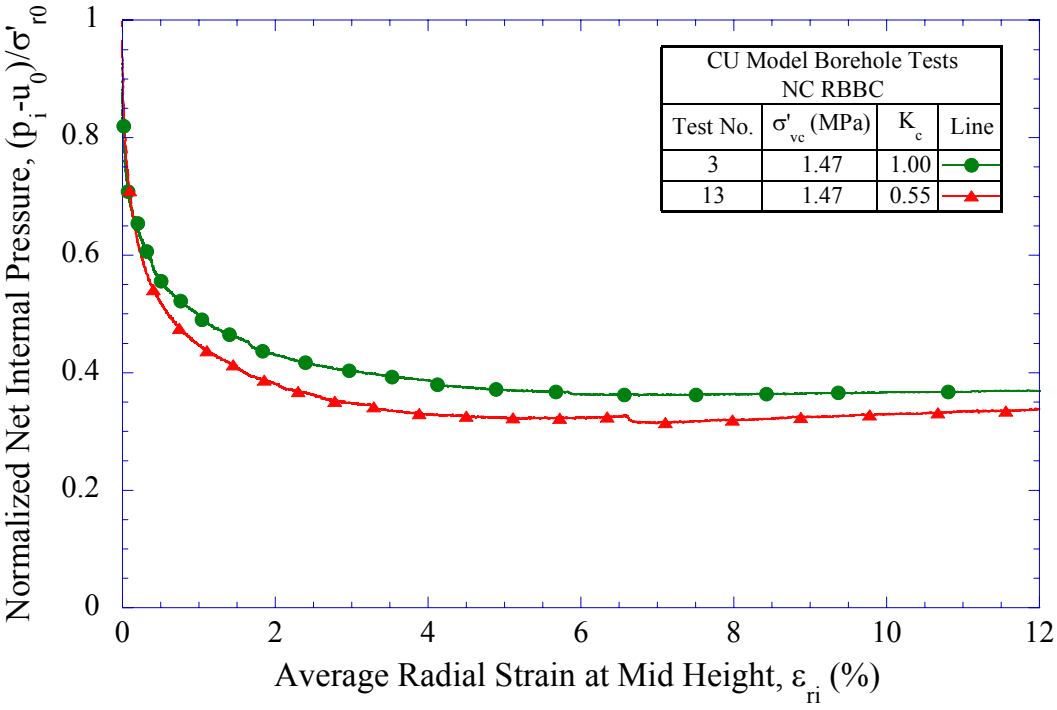

Figure 6-39: Effect of lateral stress ratio on normalized net internal cavity pressure versus mid height average cavity radial strain for NC RBBC from CU model borehole tests

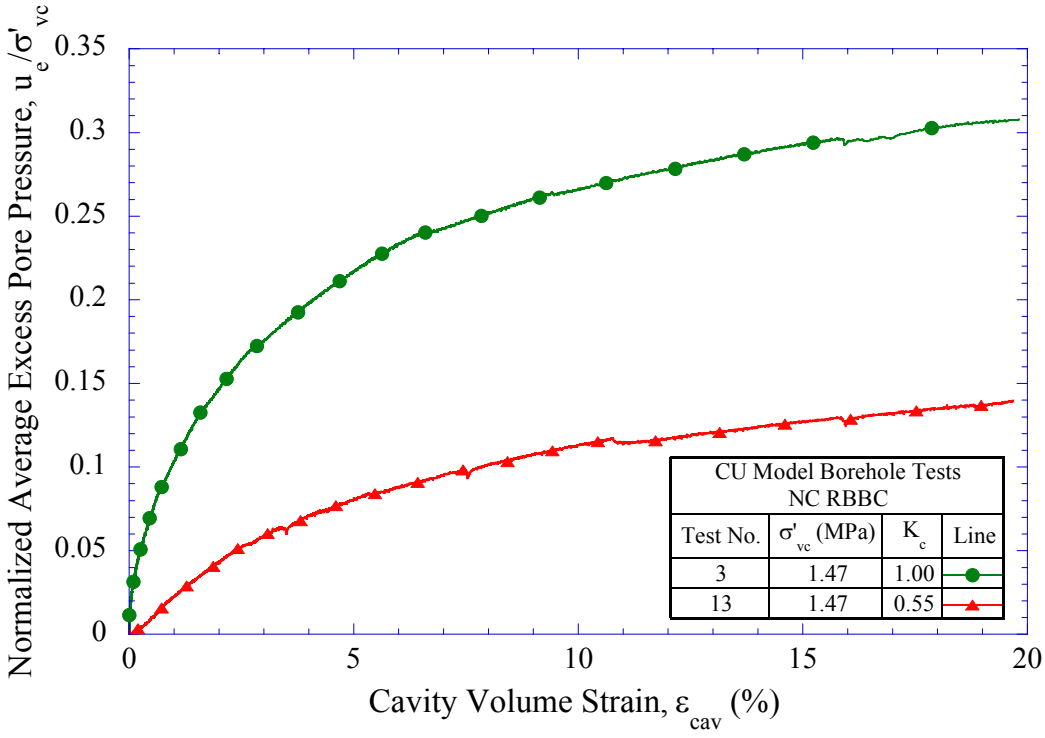

Figure 6-40: Effect of lateral stress ratio on normalized average excess pore pressures for NC RBBC from CU model borehole tests

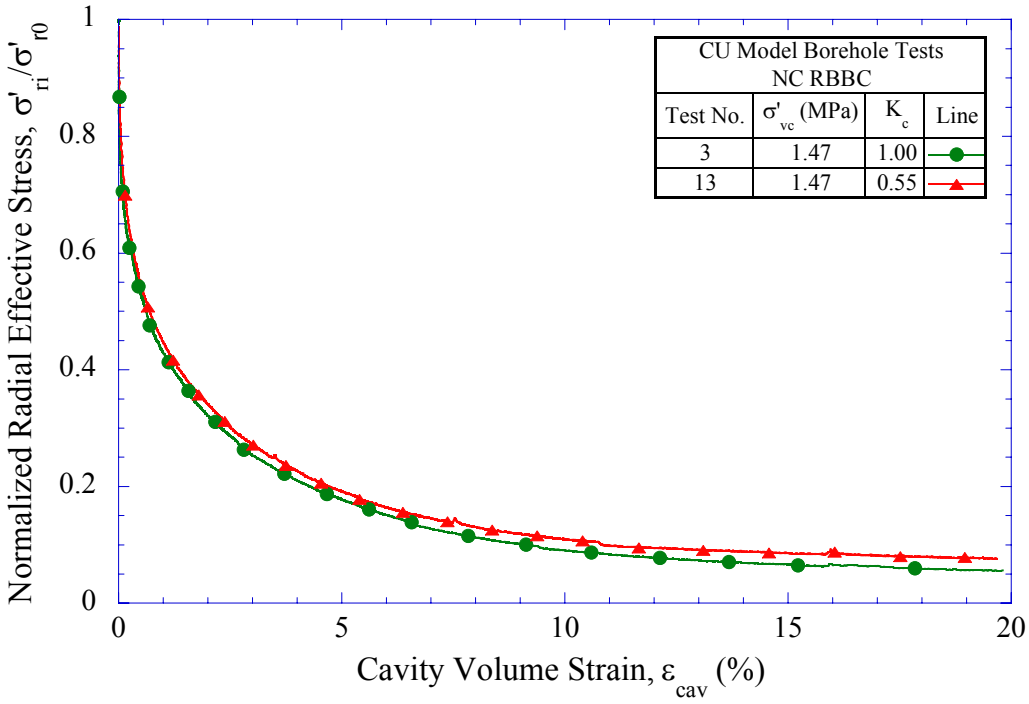

Figure 6-41: Effect of lateral stress ratio on normalized inferred cavity radial effective stress for NC RBBC from CU model borehole tests

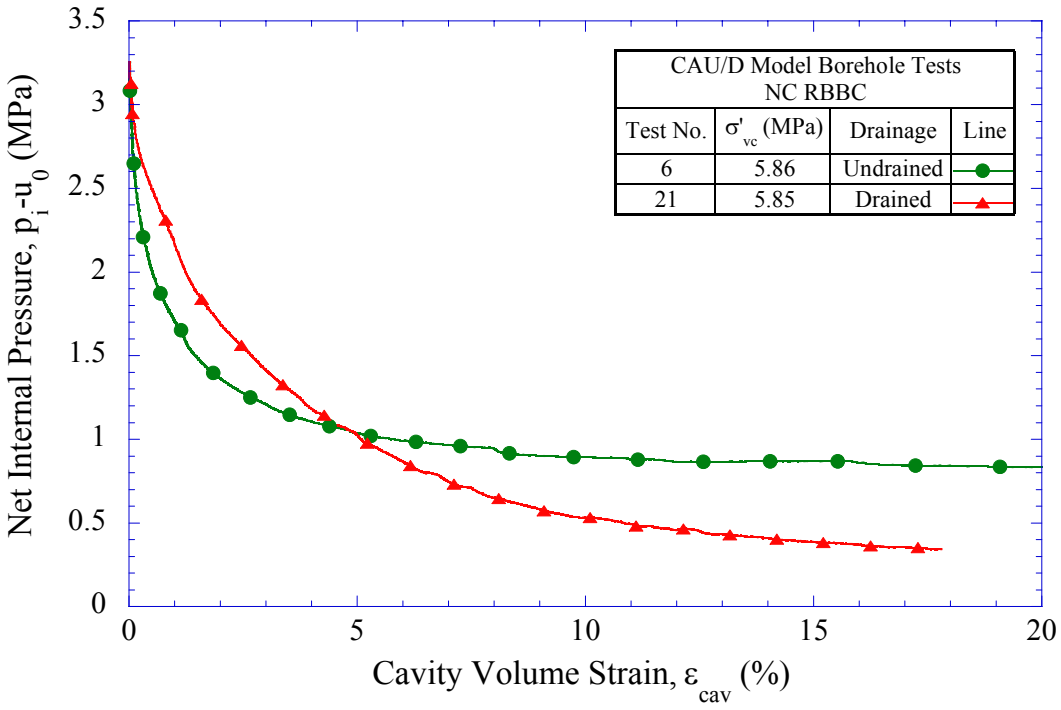

Figure 6-42: Effect of specimen drainage conditions on net internal cavity pressure versus cavity volumetric strain for NC RBBC from CAU/D model borehole tests

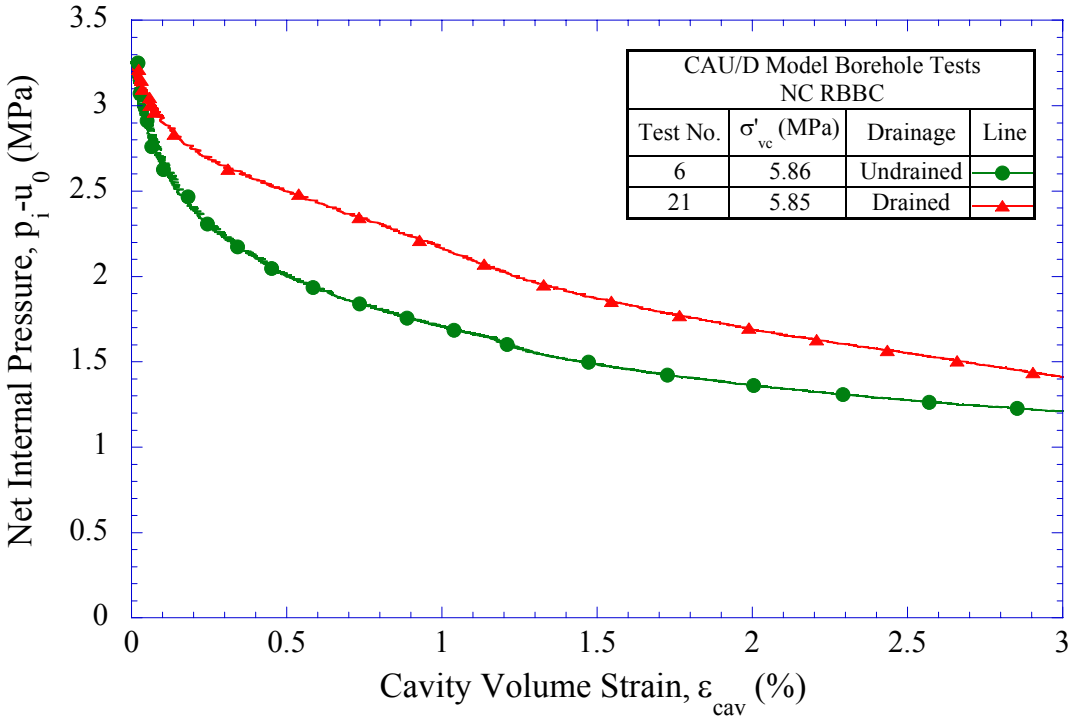

Figure 6-43: Effect of specimen drainage conditions on net internal cavity pressure versus cavity volumetric strain (up to 3%) for NC RBBC from CAU/D model borehole tests

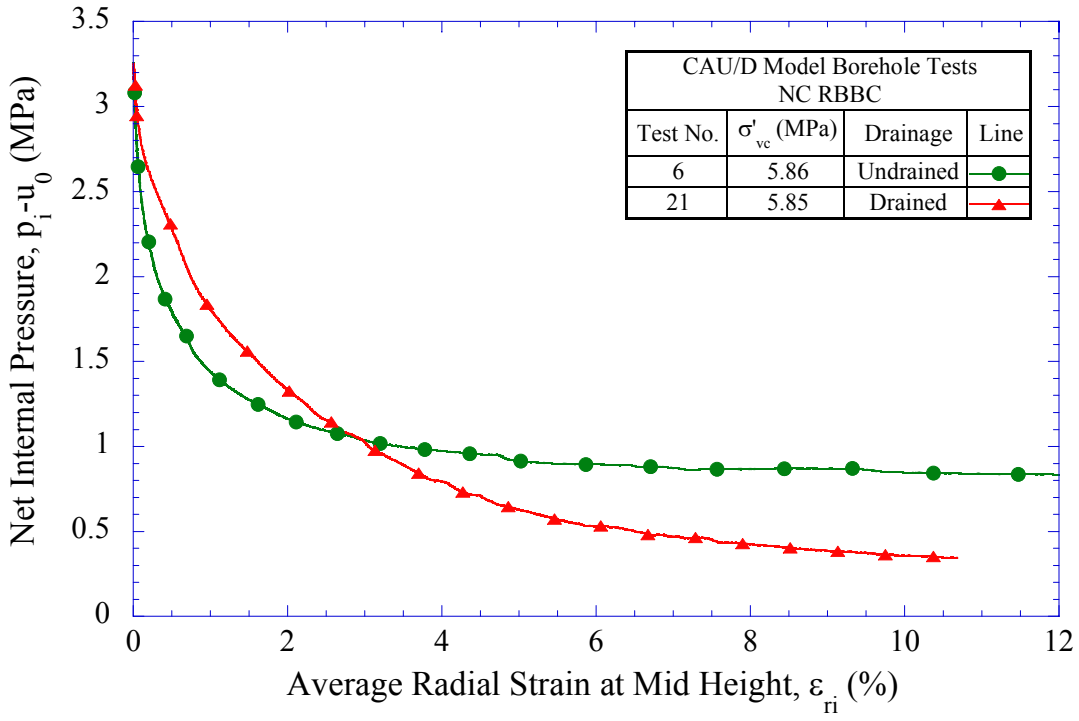

Figure 6-44: Effect of specimen drainage conditions on net internal cavity pressure versus mid height average cavity radial strain for NC RBBC from CAU/D model borehole tests

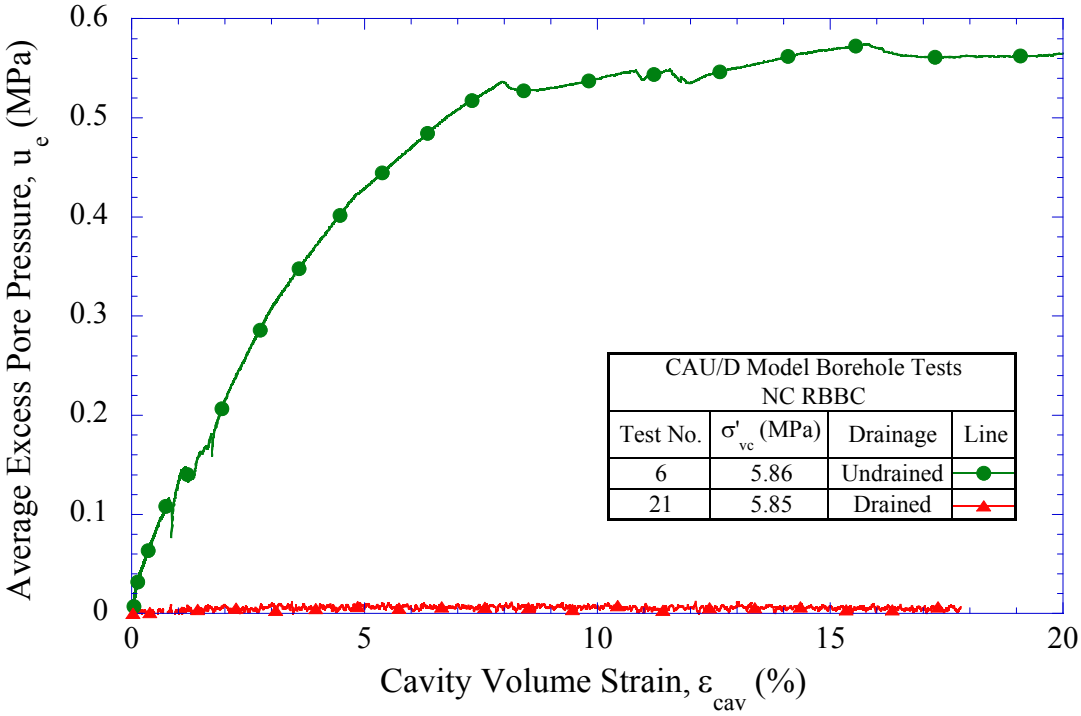

Figure 6-45: Average excess pore pressure versus cavity volumetric strain for NC RBBC from CAU/D model borehole tests

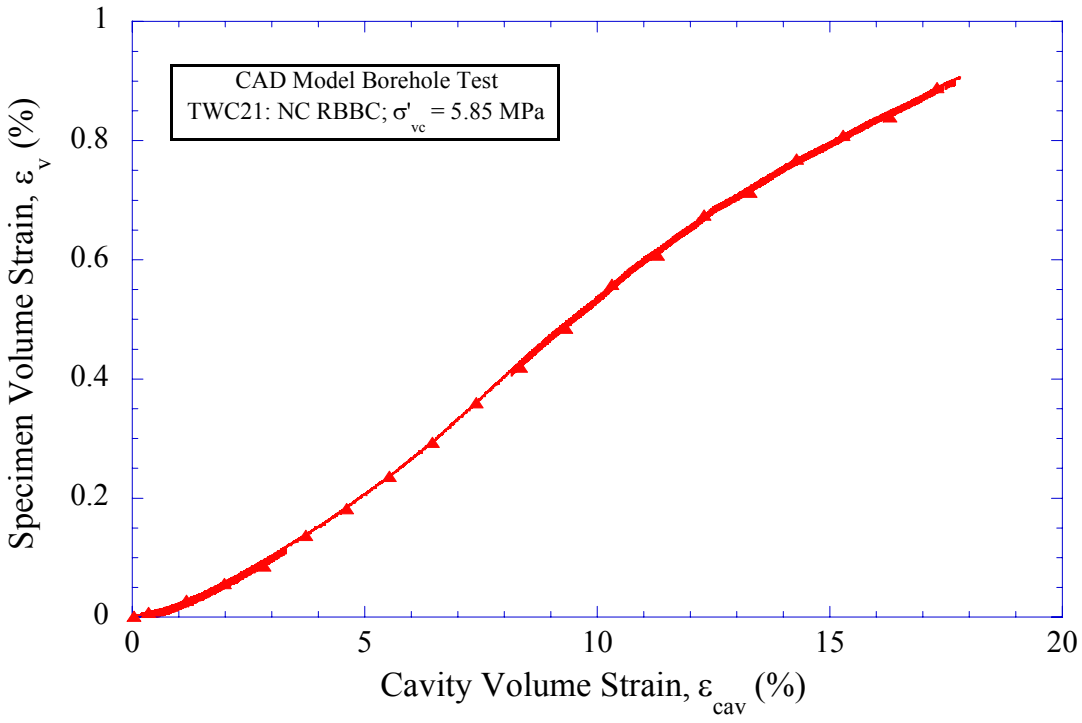

Figure 6-46: Specimen volume strain versus cavity volumetric strain for NC RBBC from CAD model borehole test (TWC21)

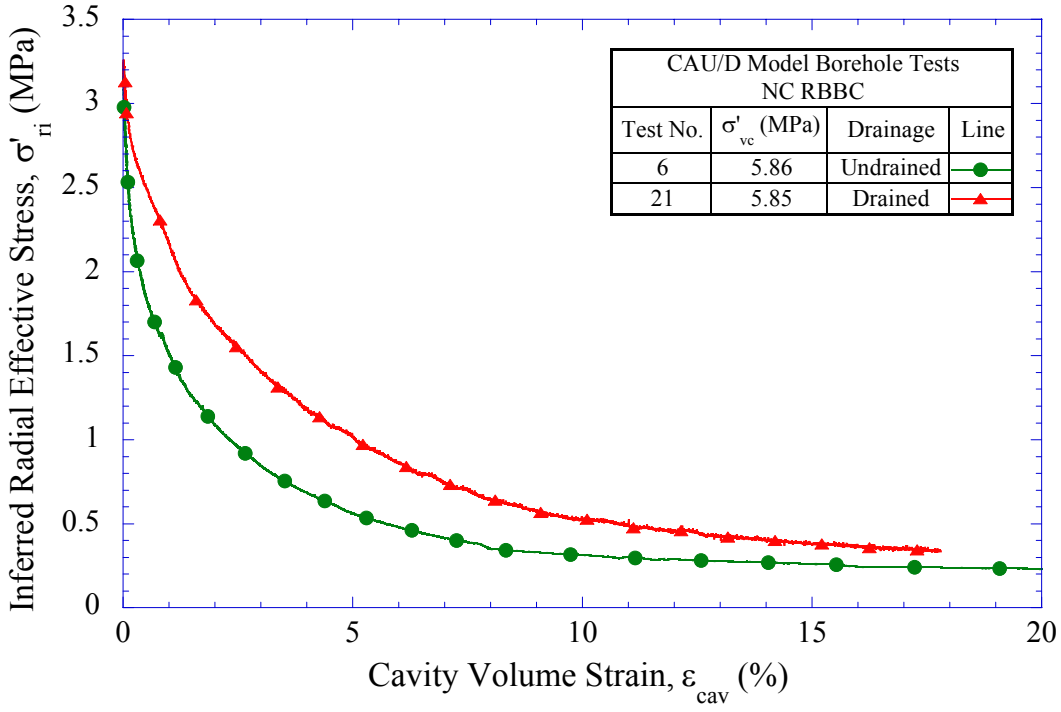

Figure 6-47: Effect of specimen drainage conditions on inferred cavity radial effective stress for NC RBBC from CAU/D model borehole tests

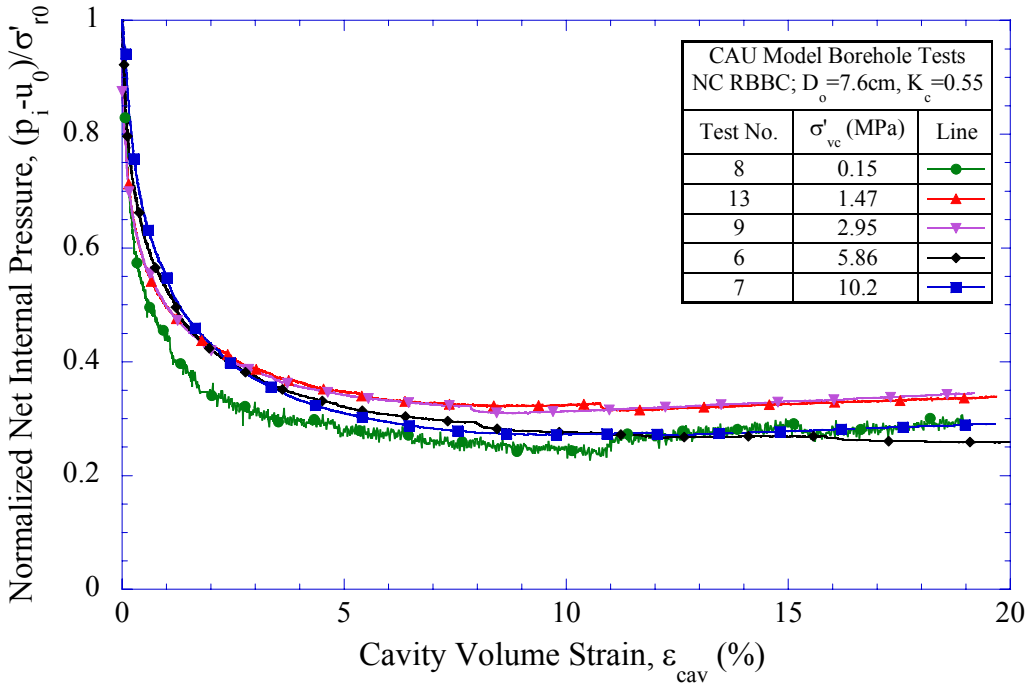

Figure 6-48: Effect of consolidation stress level on normalized net internal cavity pressure versus cavity volumetric strain for NC RBBC from CAU model borehole tests with small diameter TWC specimens

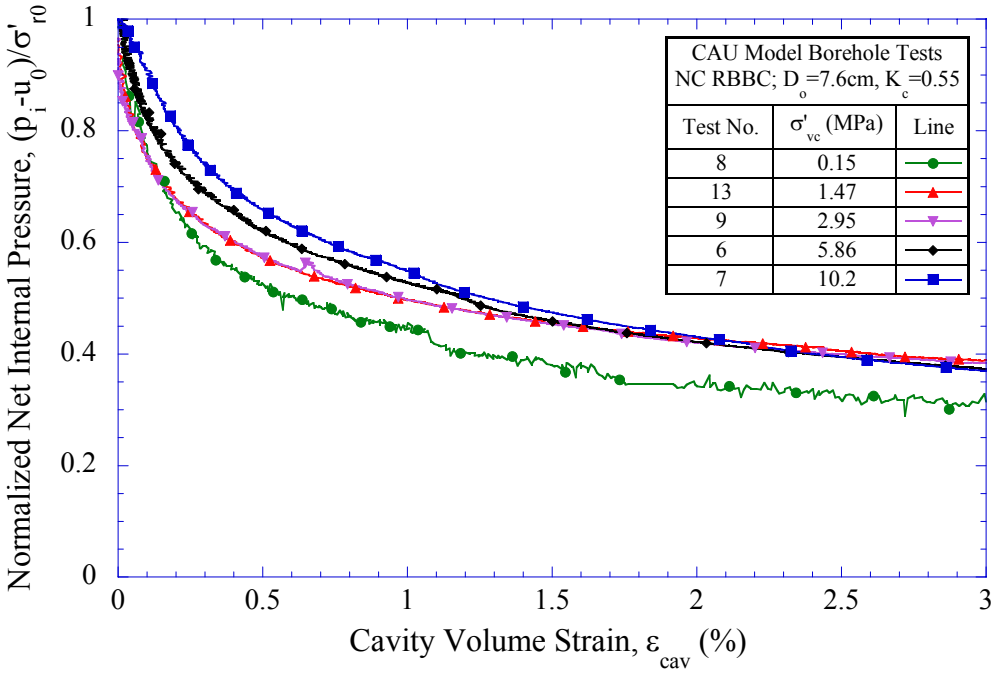

Figure 6-49: Effect of consolidation stress level on normalized net internal cavity pressure versus cavity volumetric strain (up to 3%) for NC RBBC from CAU model borehole tests with small diameter TWC specimens

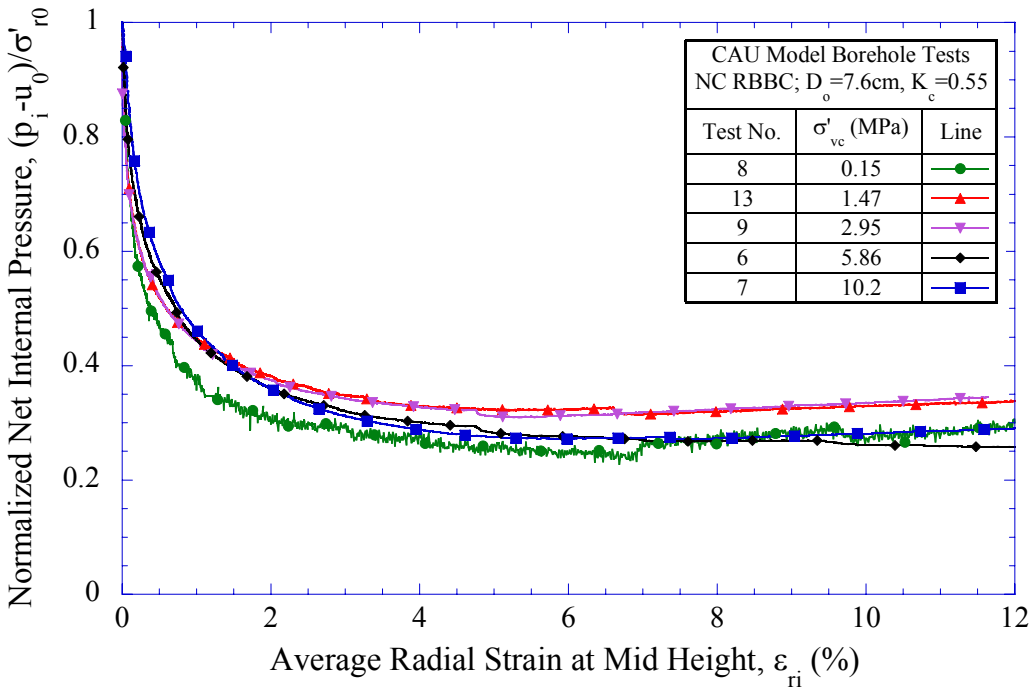

Figure 6-50: Effect of consolidation stress level on normalized net internal cavity pressure versus mid height average cavity radial strain for NC RBBC from CAU model borehole tests with small diameter TWC specimens

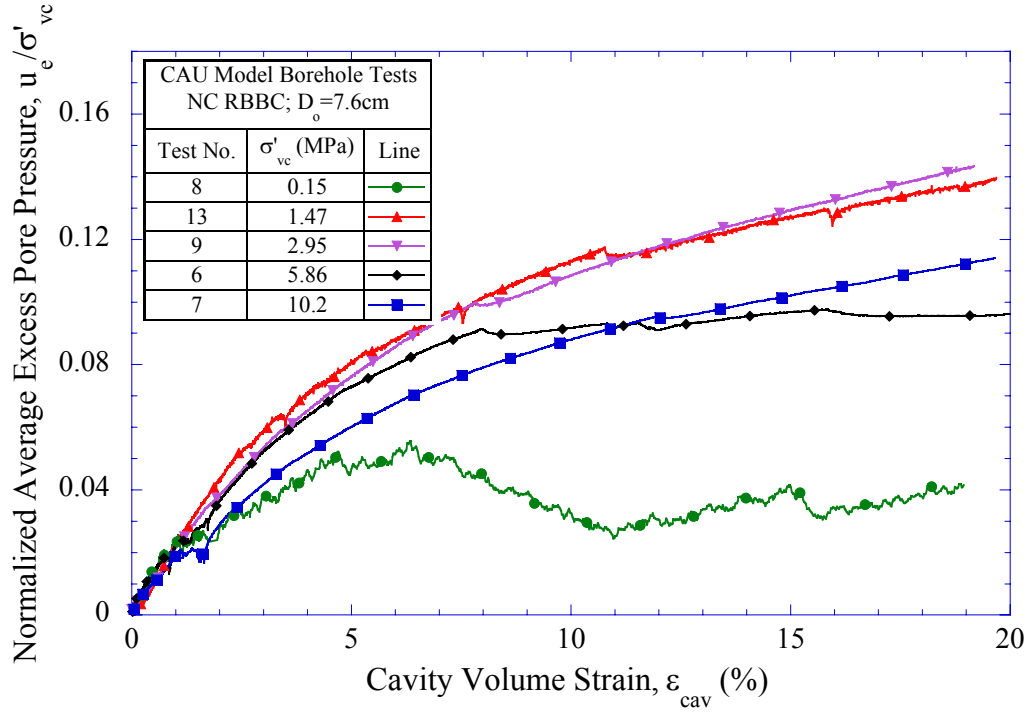

Figure 6-51: Effect of consolidation stress level on normalized average excess pore pressures for NC RBBC from CAU model borehole tests with small diameter TWC specimens

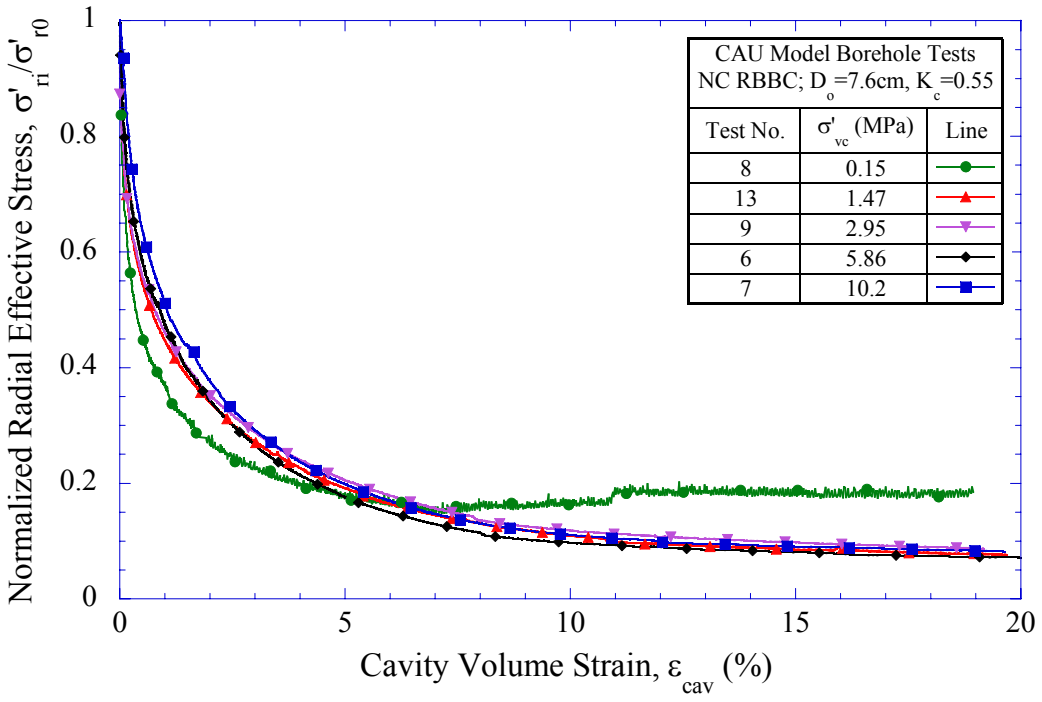

Figure 6-52: Effect of consolidation stress level on normalized inferred cavity radial effective stress for NC RBBC from CAU model borehole tests with small diameter TWC specimens

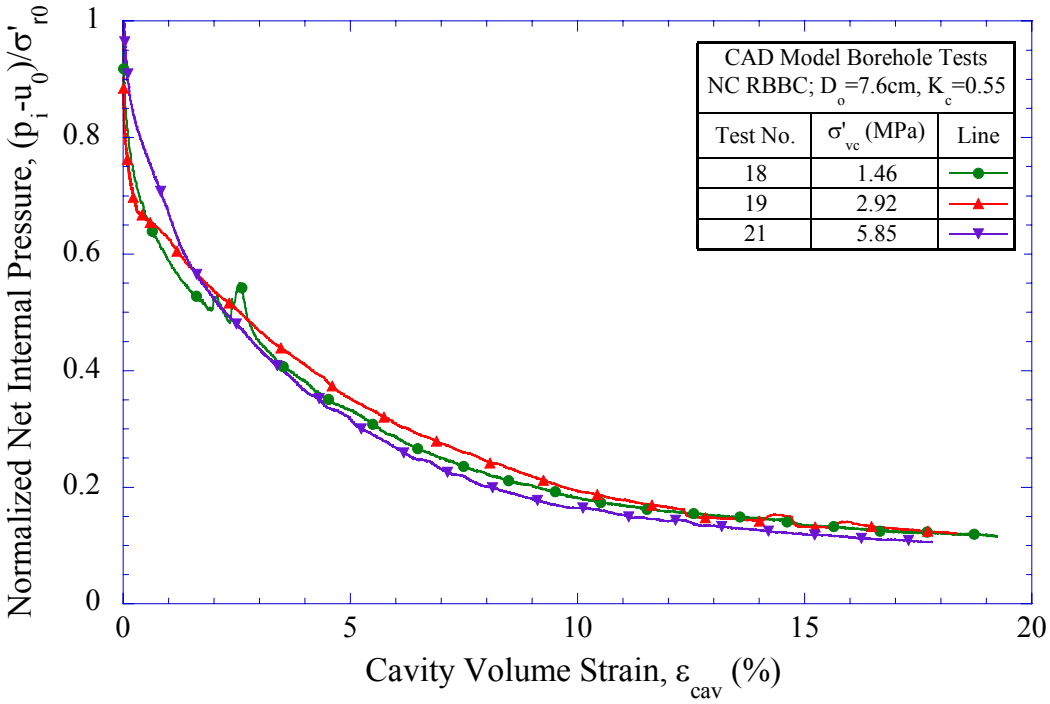

Figure 6-53: Effect of consolidation stress level on normalized net internal cavity pressure versus cavity volumetric strain for NC RBBC from CAD model borehole tests with small diameter TWC specimens

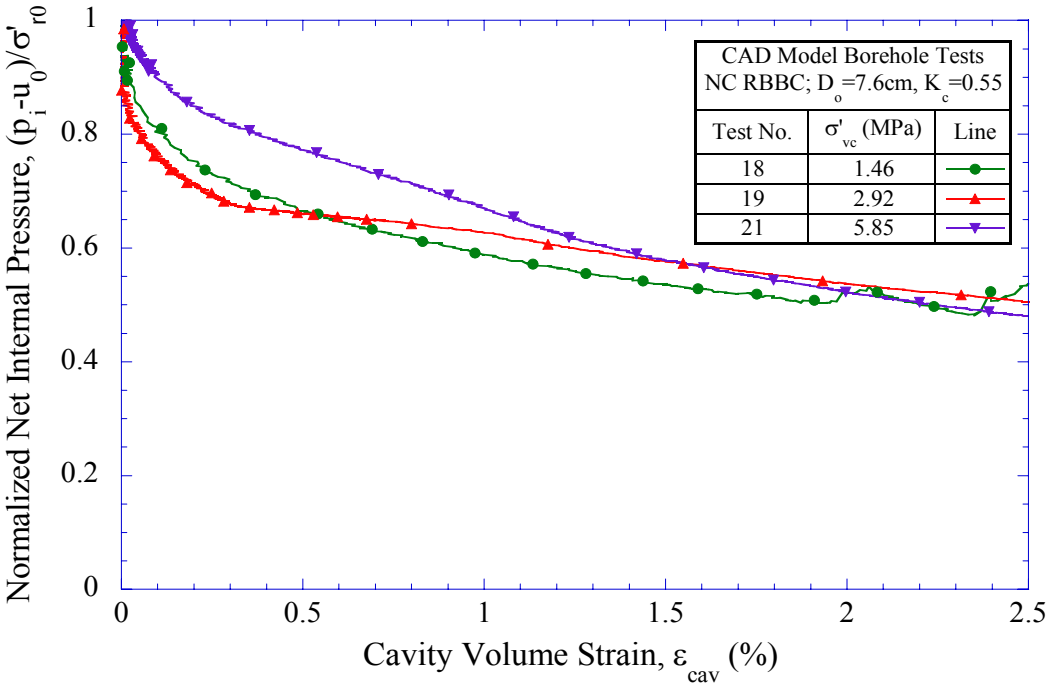

Figure 6-54: Effect of consolidation stress level on normalized net internal cavity pressure versus cavity volumetric strain (up to 2.5%) for NC RBBC from CAD model borehole tests with small diameter TWC specimens

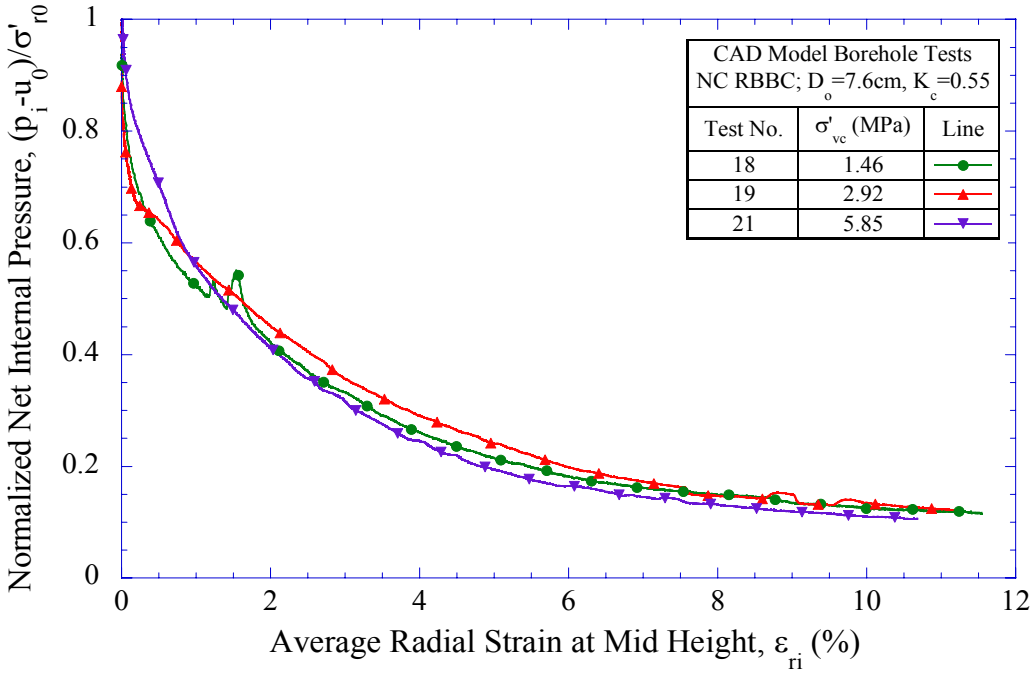

Figure 6-55: Effect of consolidation stress level on normalized net internal cavity pressure versus mid height average cavity radial strain for NC RBBC from CAD model borehole tests with small diameter TWC specimens

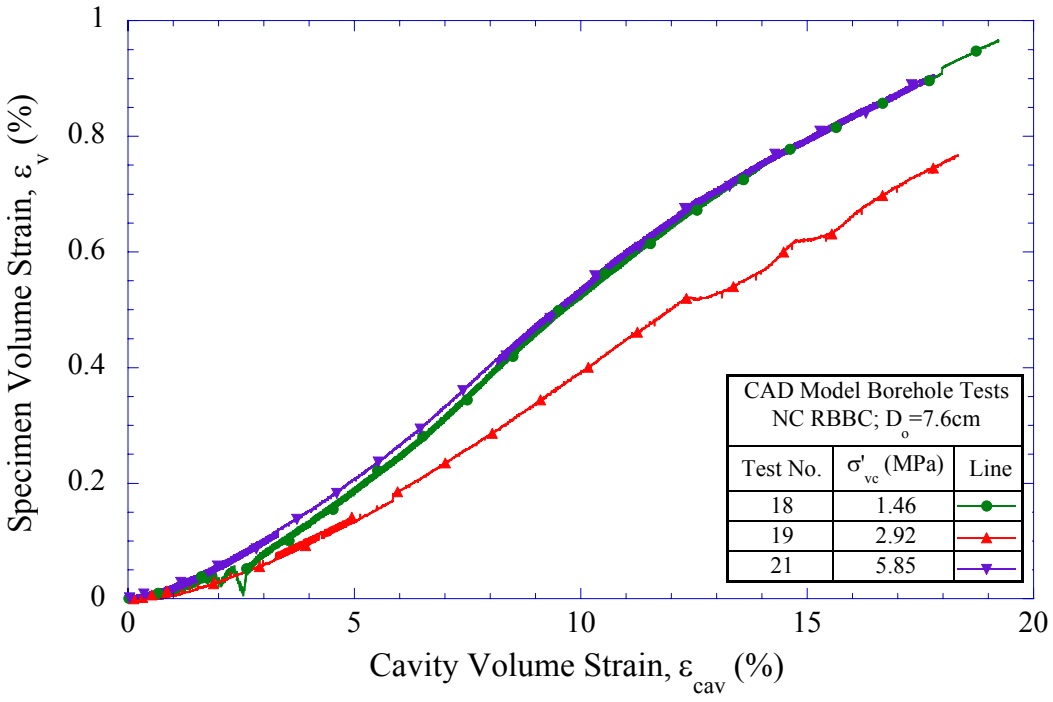

Figure 6-56: Effect of consolidation stress level on specimen volume strain for NC RBBC from CAD model borehole tests with small diameter TWC specimens

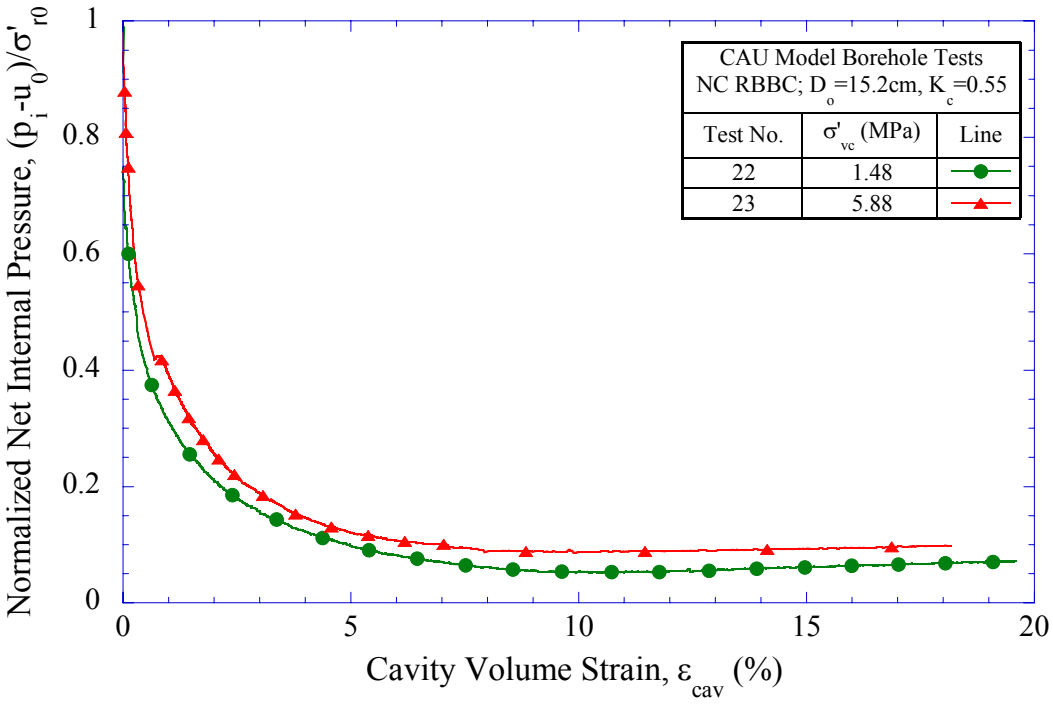

Figure 6-57: Effect of consolidation stress level on normalized net internal cavity pressure versus cavity volumetric strain for NC RBBC from CAU model borehole tests with large diameter TWC specimens

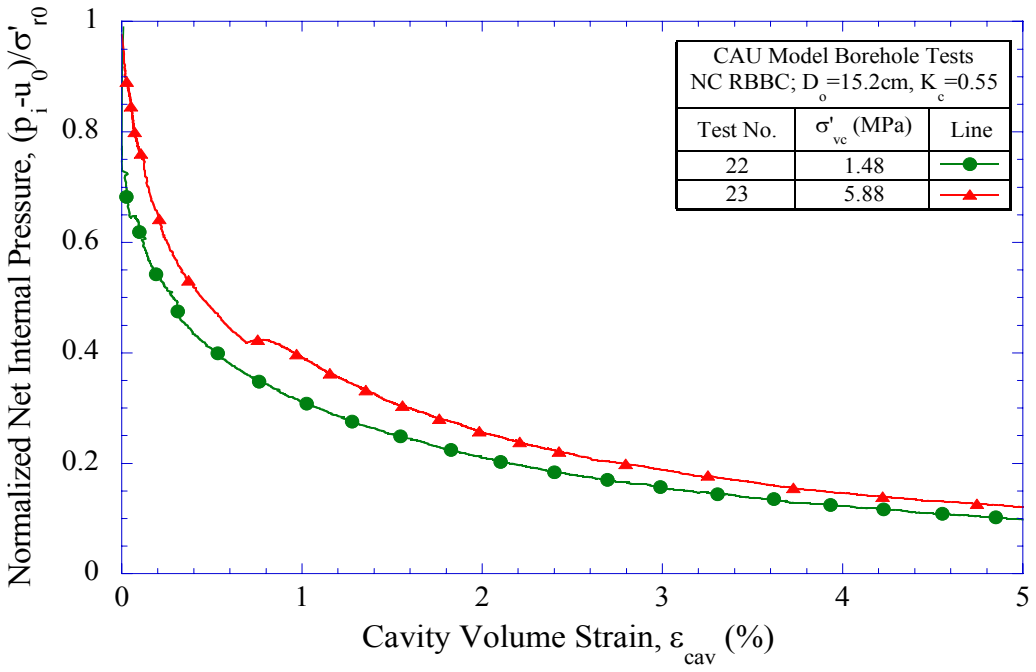

Figure 6-58: Effect of consolidation stress level on normalized net internal cavity pressure versus cavity volumetric strain (up to 5%) for NC RBBC from CAU model borehole tests with large diameter TWC specimens

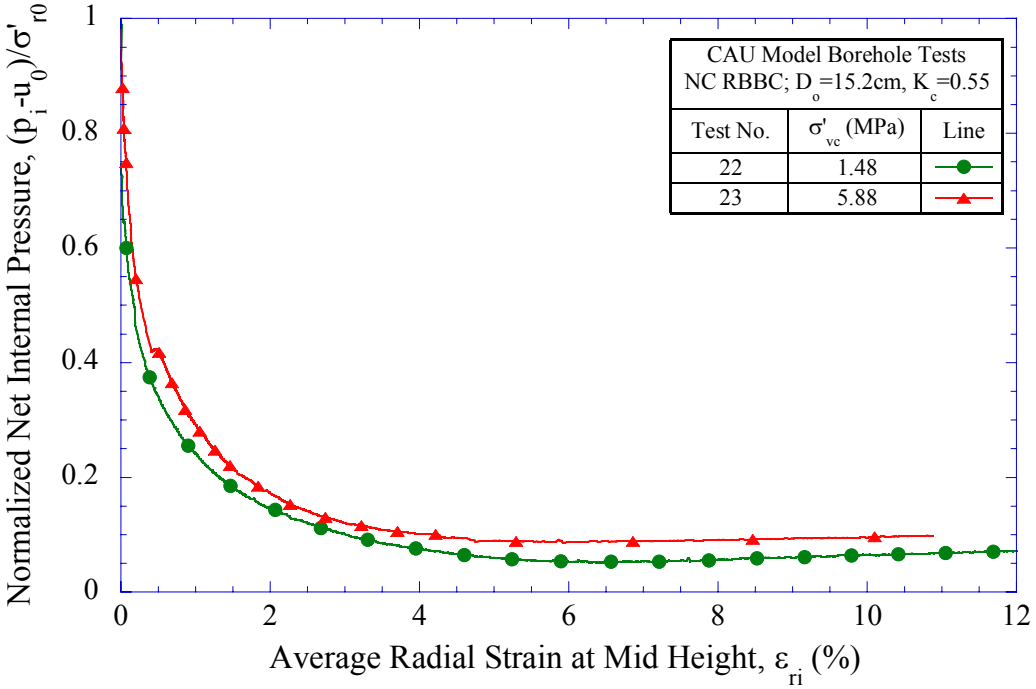

Figure 6-59: Effect of consolidation stress level on normalized net internal cavity pressure versus mid height average cavity radial strain for NC RBBC from CAU model borehole tests with large diameter TWC specimens

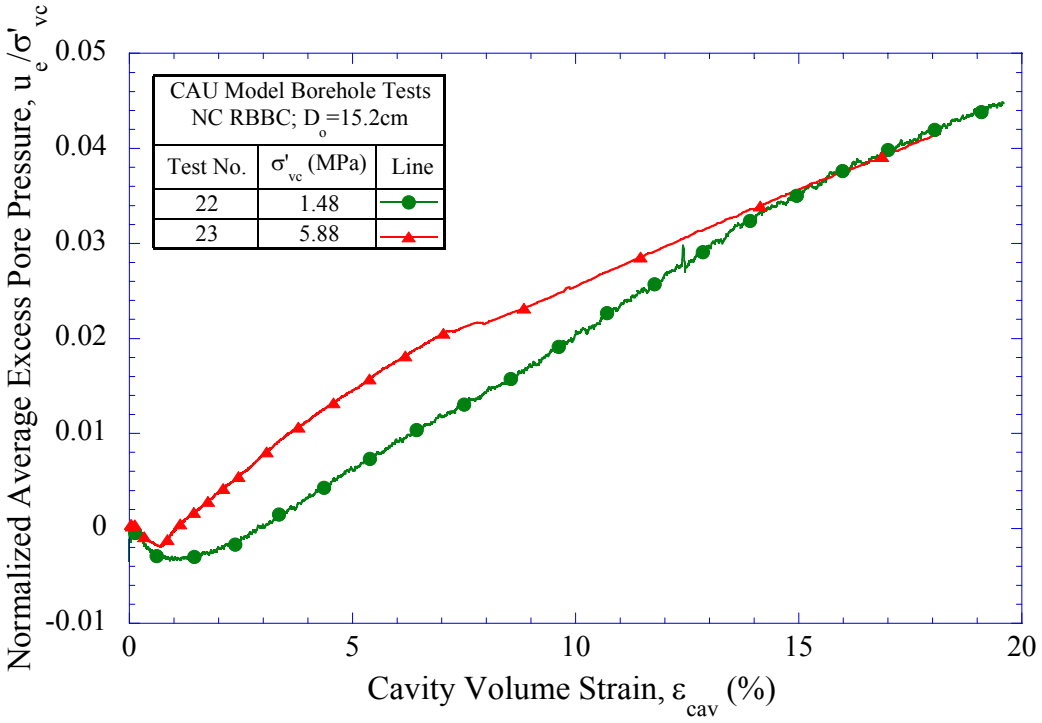

Figure 6-60: Effect of consolidation stress level on normalized average excess pore pressures for NC RBBC from CAU model borehole tests with large diameter TWC specimens

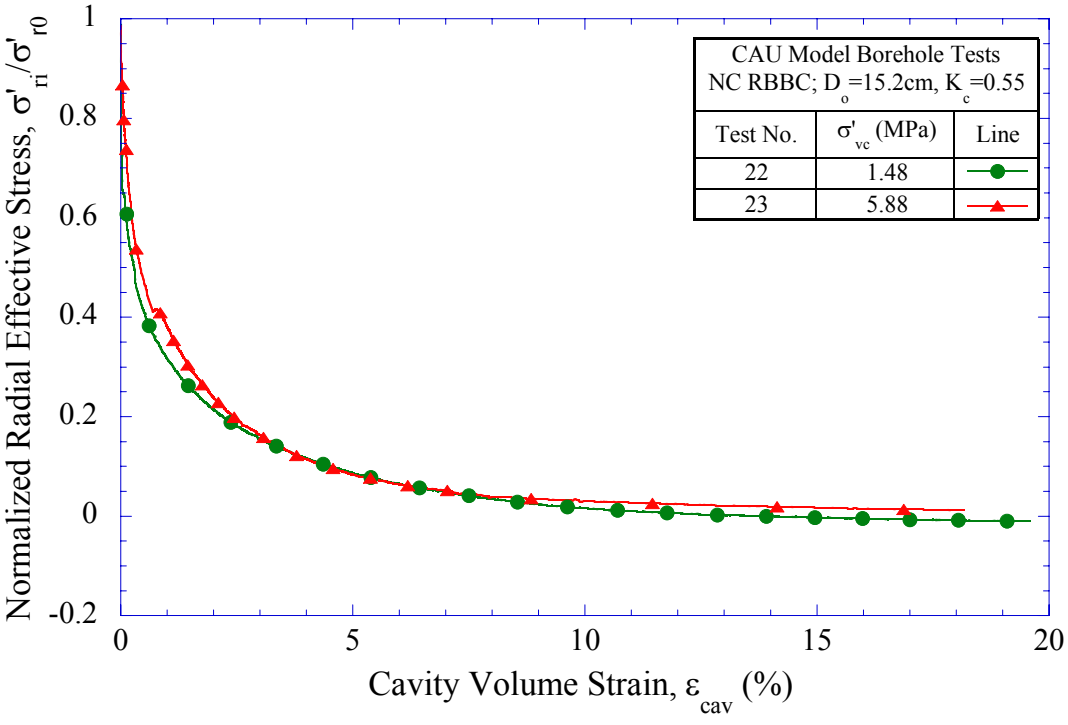

Figure 6-61: Effect of consolidation stress level on normalized inferred cavity radial effective stress for NC RBBC from CAU model borehole tests with large diameter TWC specimens

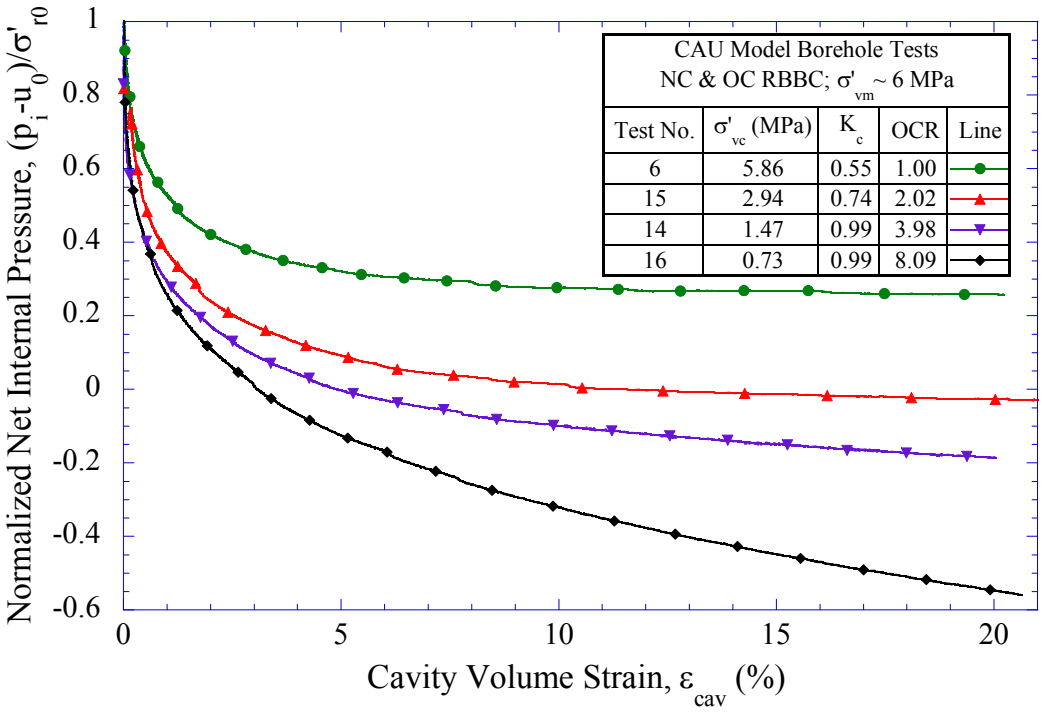

Figure 6-62: Effect of stress history on normalized net internal cavity pressure versus cavity volumetric strain for NC & OC RBBC from CAU model borehole tests

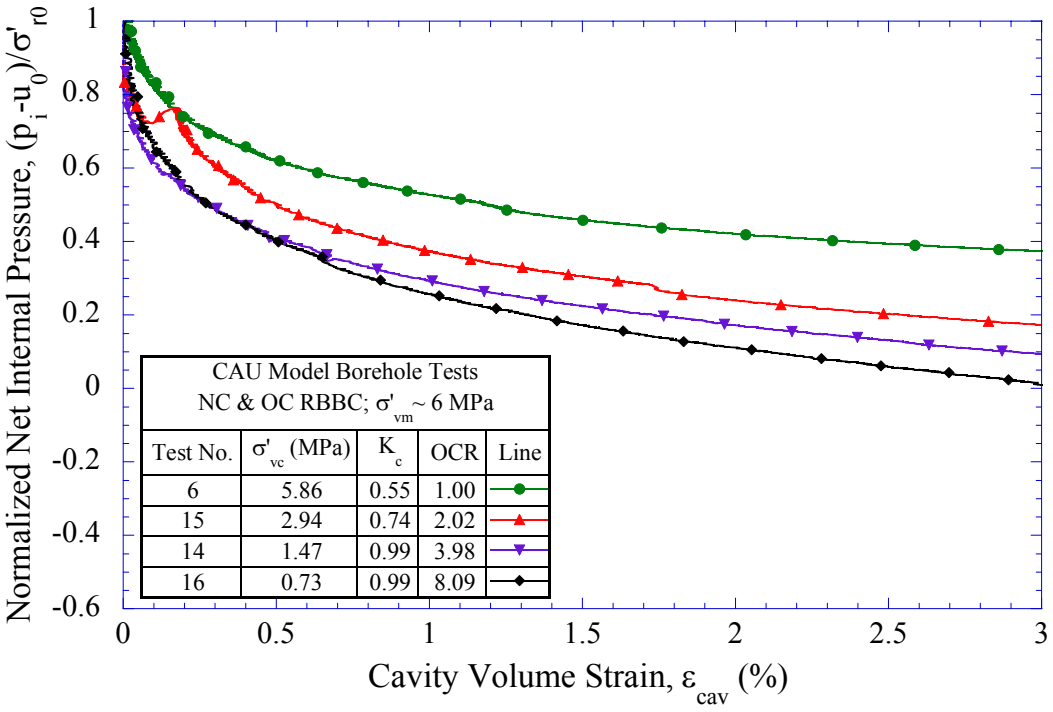

Figure 6-63: Effect of stress history on normalized net internal cavity pressure versus cavity volumetric strain (up to 3%) for NC & OC RBBC from CAU model borehole tests

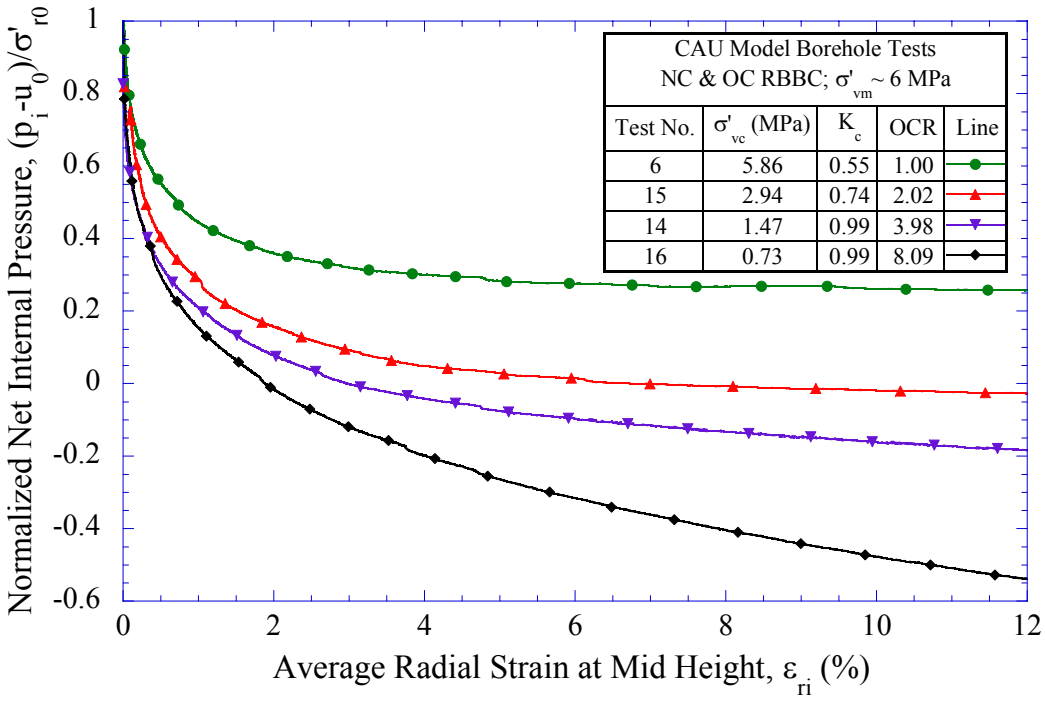

Figure 6-64: Effect of stress history on normalized net internal cavity pressure versus mid height average cavity radial strain for NC & OC RBBC from CAU model borehole tests

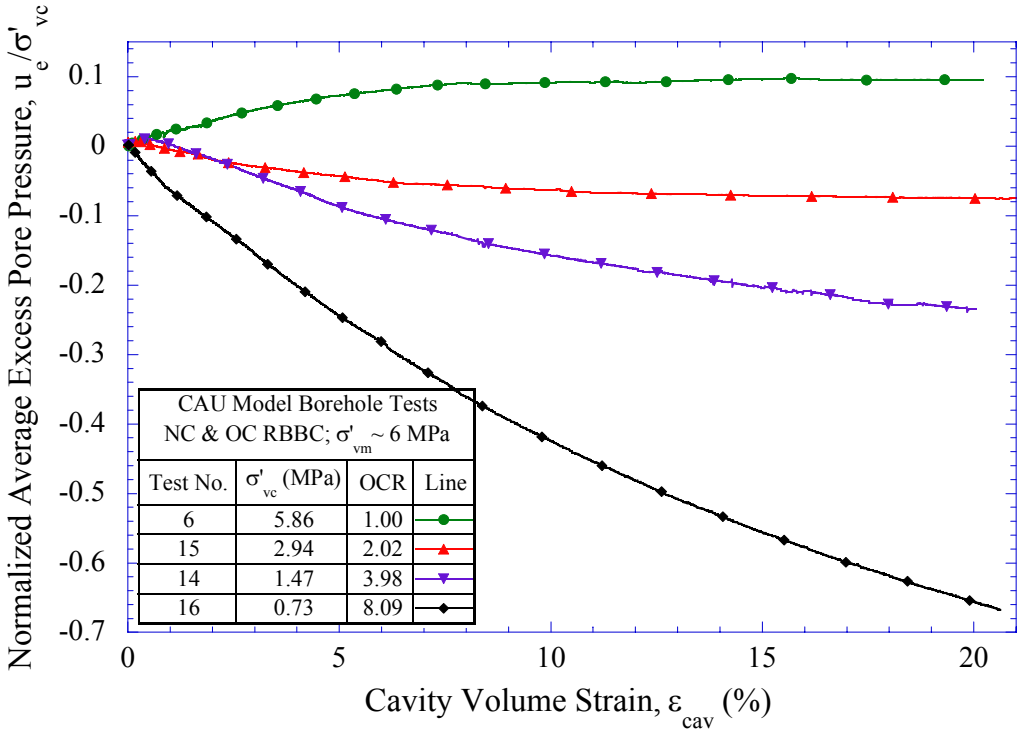

Figure 6-65: Effect of stress history on normalized average excess pore pressures for NC & OC RBBC from CAU model borehole tests

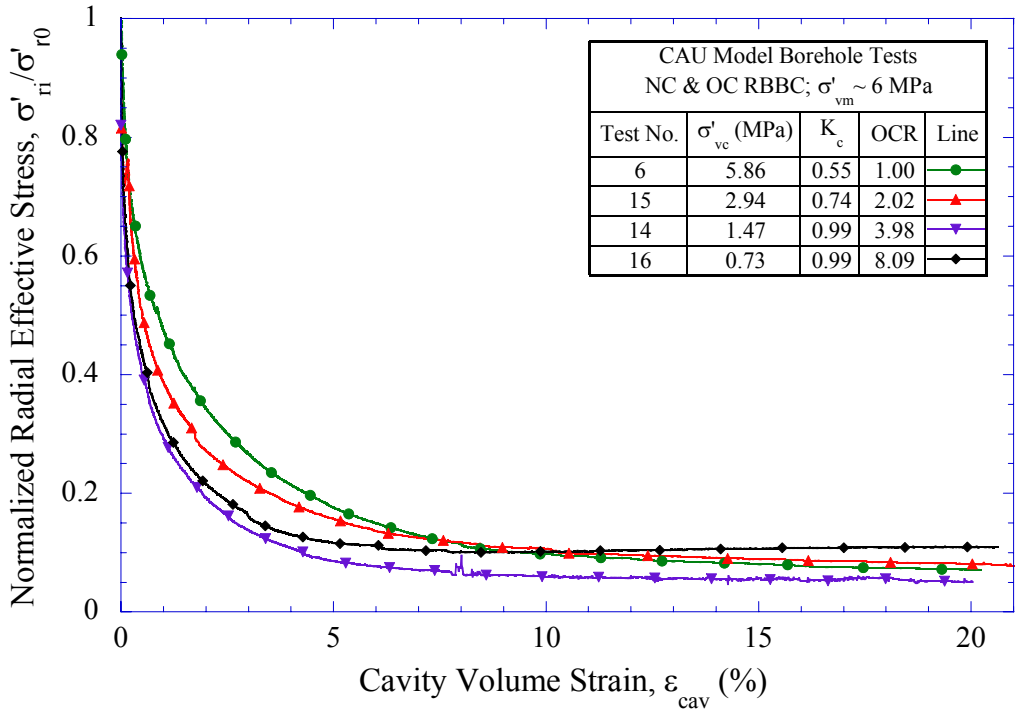

Figure 6-66: Effect of stress history on normalized inferred cavity radial effective stress for NC & OC RBBC from CAU model borehole tests

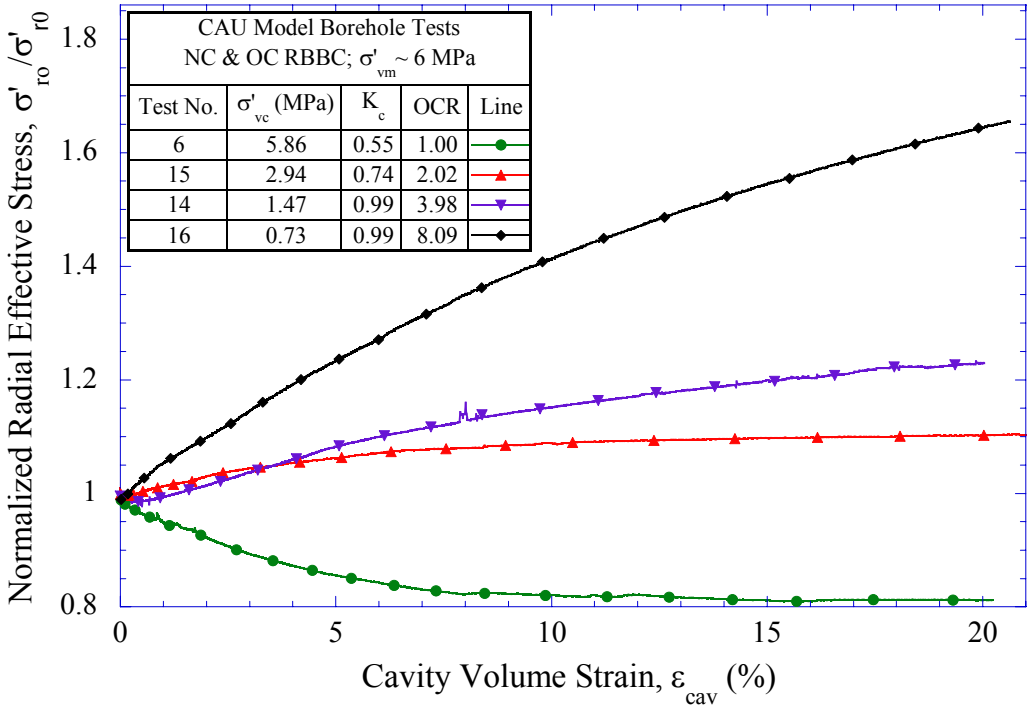

Figure 6-67: Effect of stress history on normalized inferred radial effective stress at the outer wall for NC & OC RBBC from CAU model borehole tests

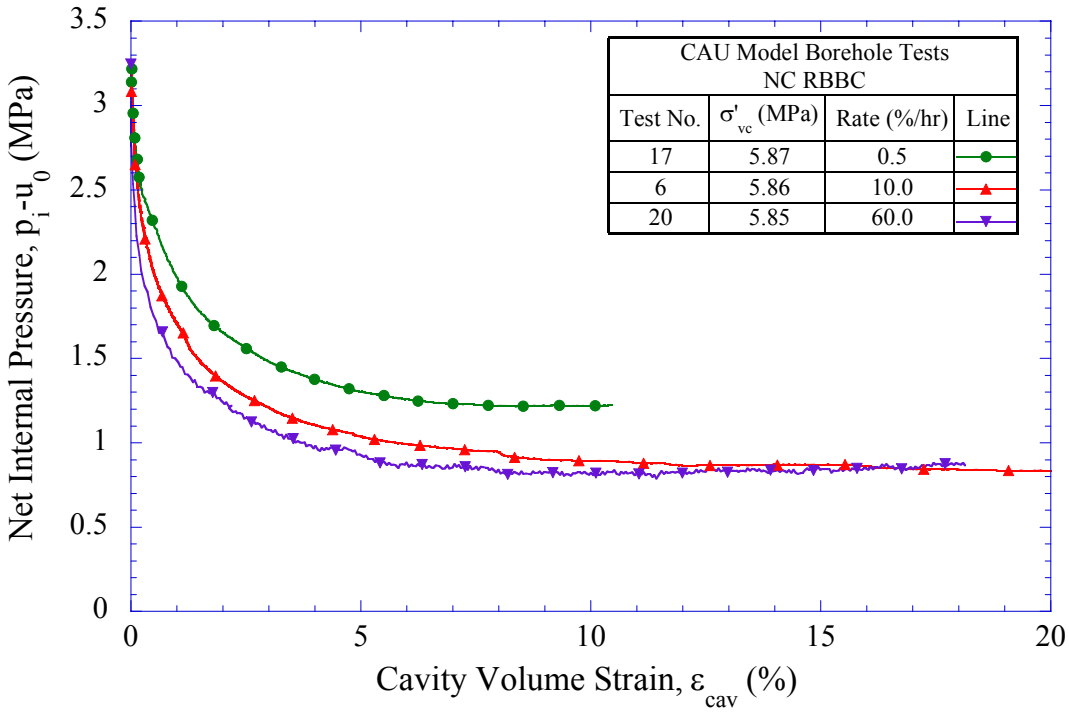

Figure 6-68: Effect of cavity volumetric strain rate on net internal cavity pressure versus cavity volumetric strain for NC RBBC from CAU model borehole tests

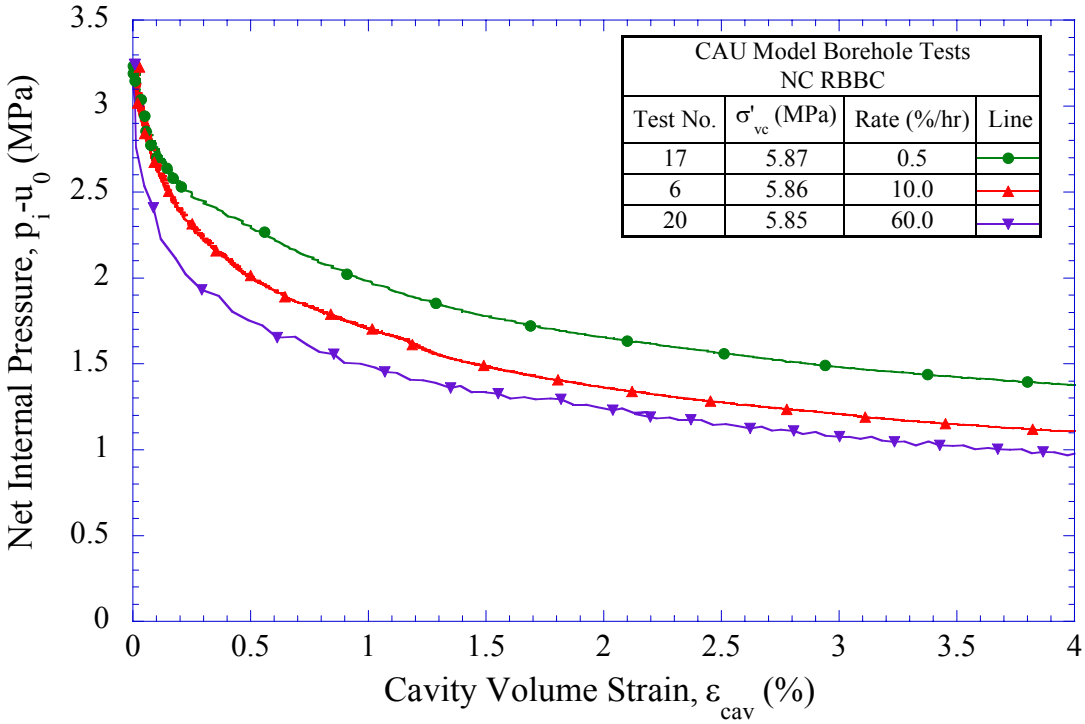

Figure 6-69: Effect of cavity volumetric strain rate on net internal cavity pressure versus cavity volumetric strain (up to 4%) for NC RBBC from CAU model borehole tests

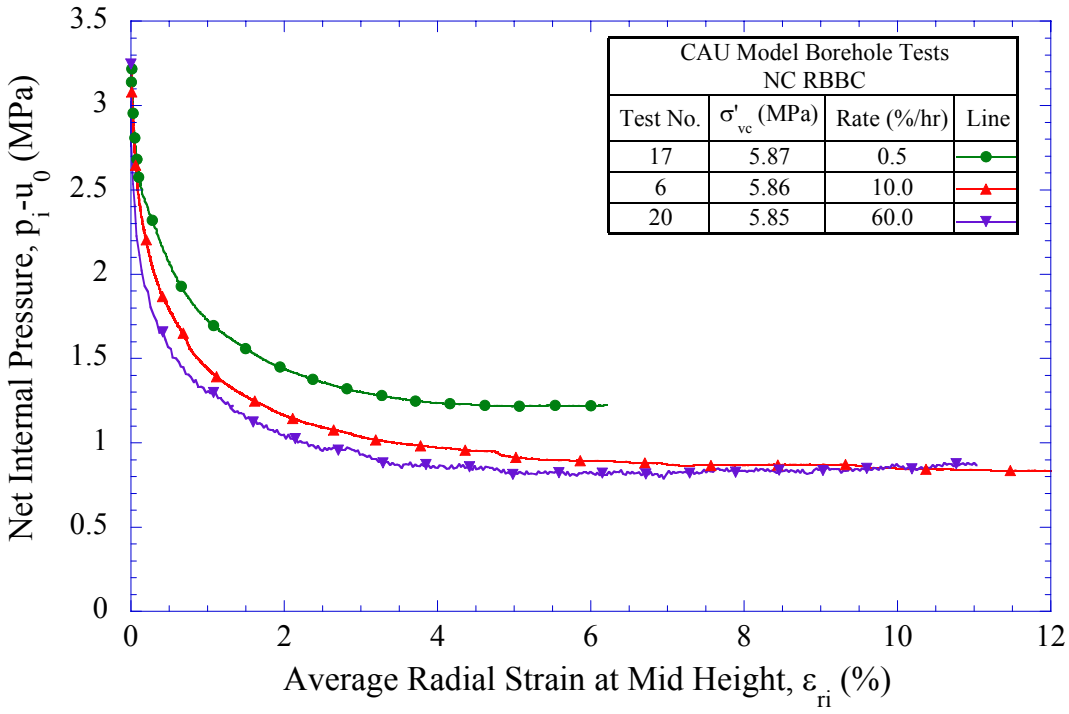

Figure 6-70: Effect of cavity volumetric strain rate on net internal cavity pressure versus mid height average cavity radial strain for NC RBBC from CAU model borehole tests

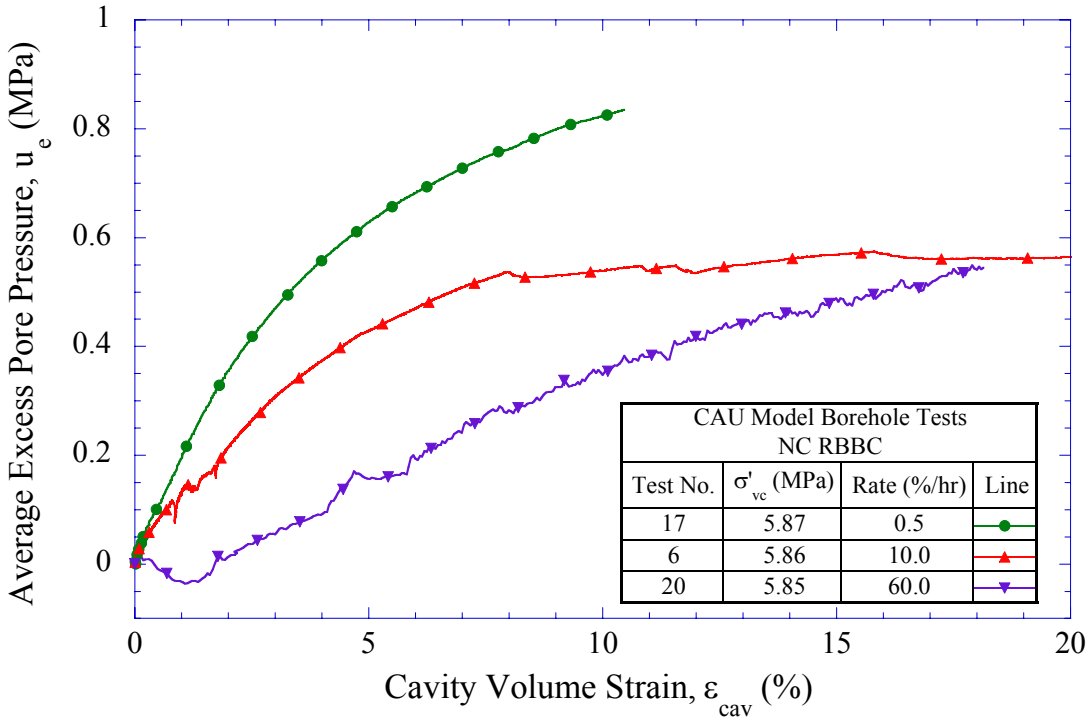

Figure 6-71: Effect of cavity volumetric strain rate on average excess pore pressures for NC RBBC from CAU model borehole tests

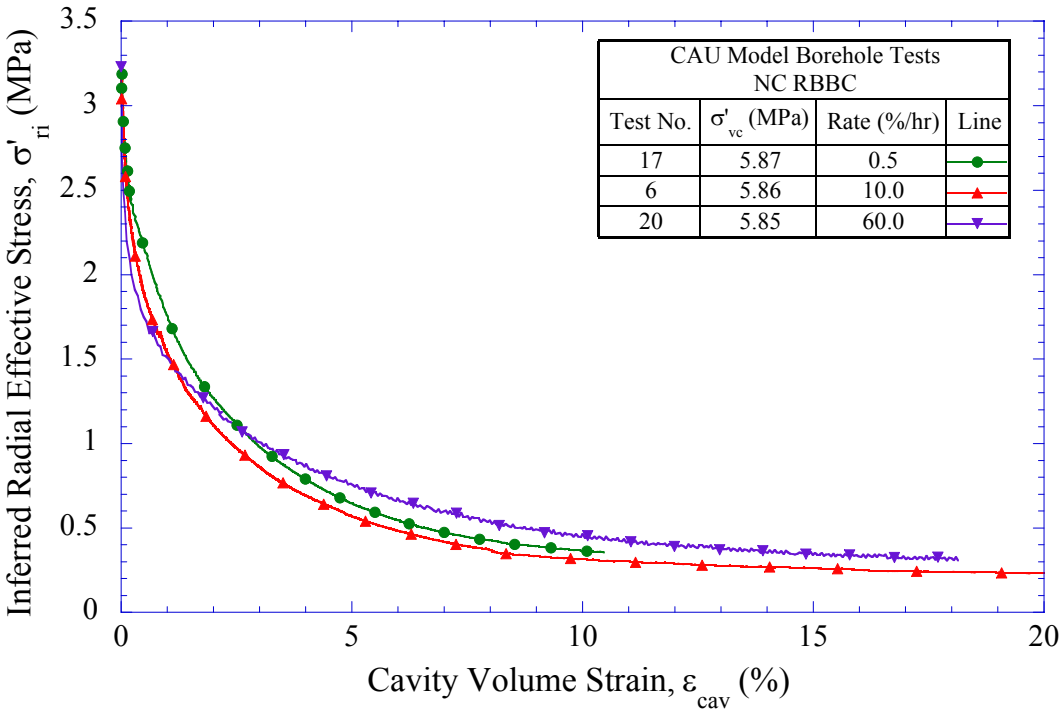

Figure 6-72: Effect of cavity volumetric strain rate on estimated cavity radial effective stress for NC RBBC from CAU model borehole tests

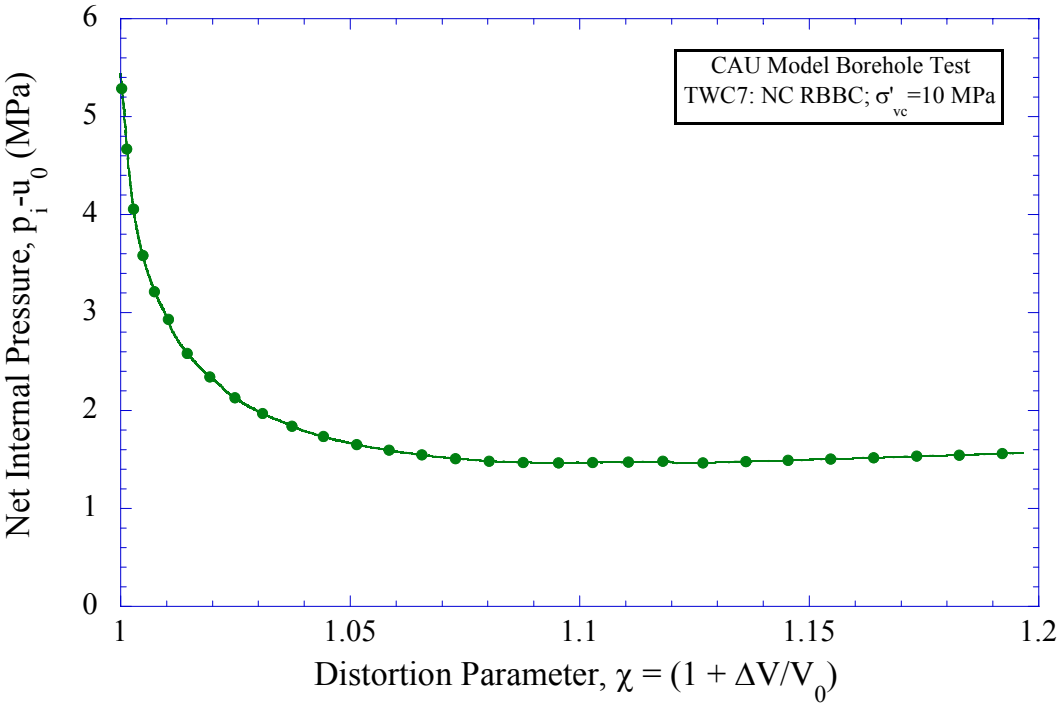

Figure 6-73: Net internal cavity pressure versus distortion parameter for test TWC7 on NC RBBC

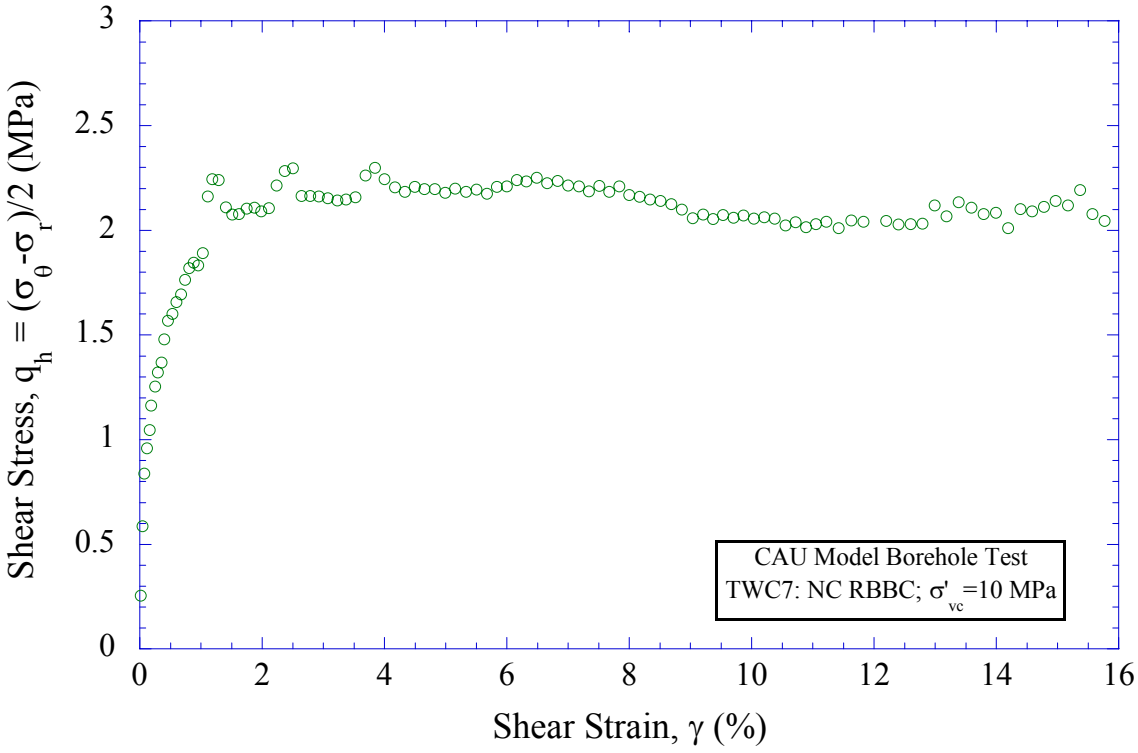

Figure 6-74: Interpreted shear stress-strain behavior for test TWC7 on NC RBBC

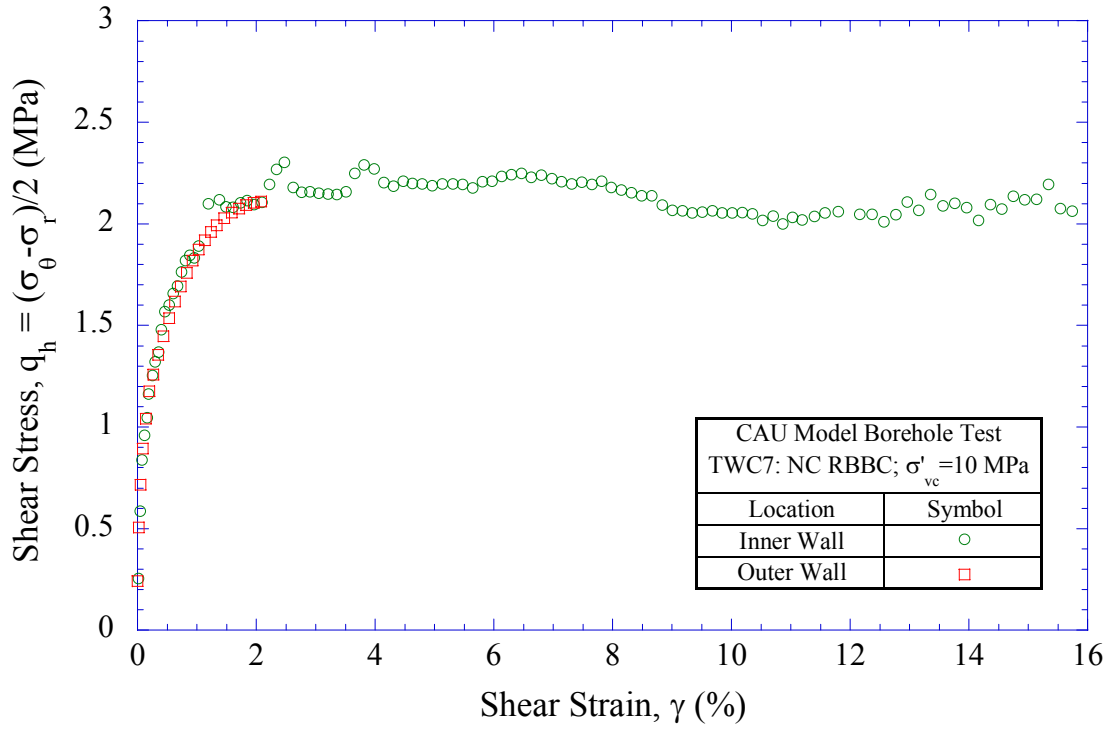

Figure 6-75: Interpreted shear stress-strain behavior for elements at inner and outer walls for test TWC7 on NC RBBC

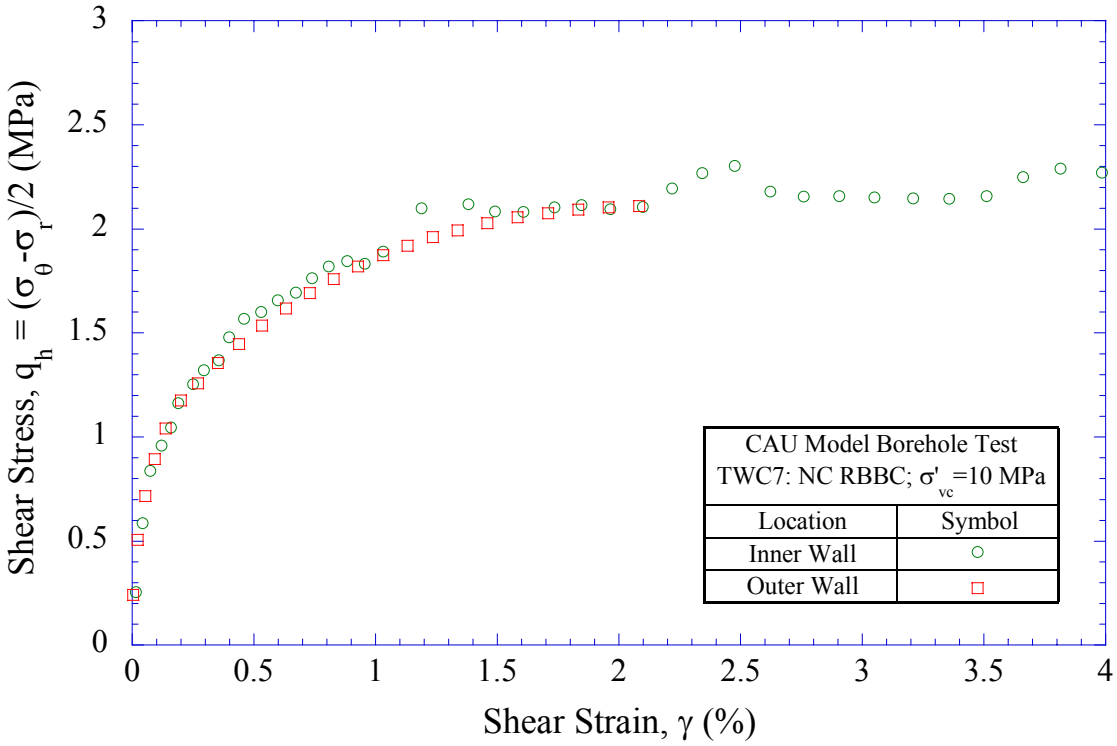

Figure 6-76: Interpreted shear stress-strain (up to 4%) behavior for elements at inner and outer walls for test TWC7 on NC RBBC

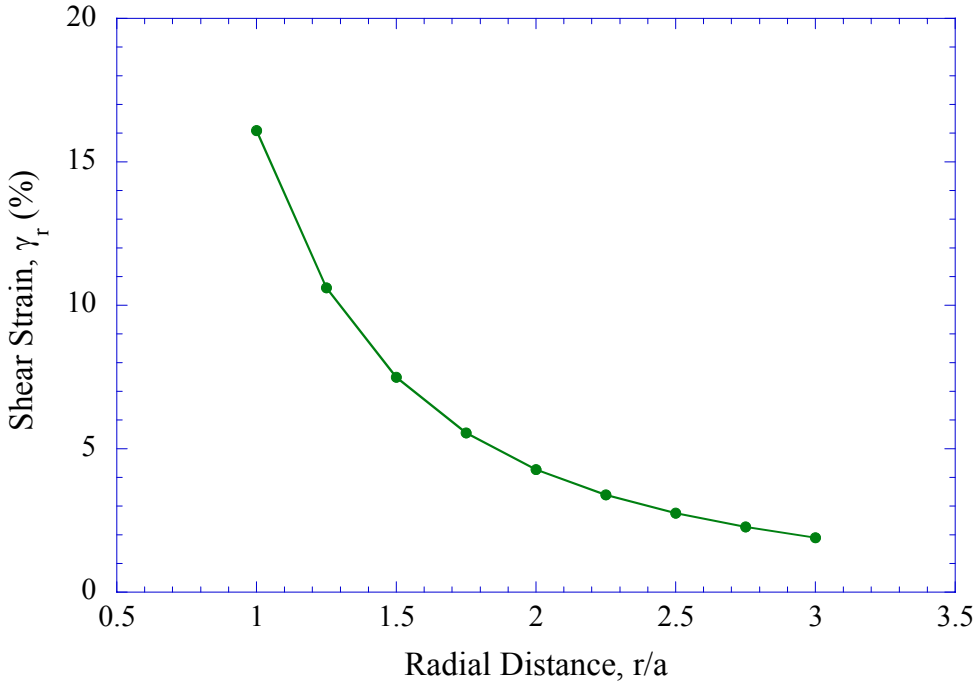

Figure 6-77: Strain distribution across small diameter TWC specimen wall at ε_{cav} = 17.5% (γ_a = 16%)

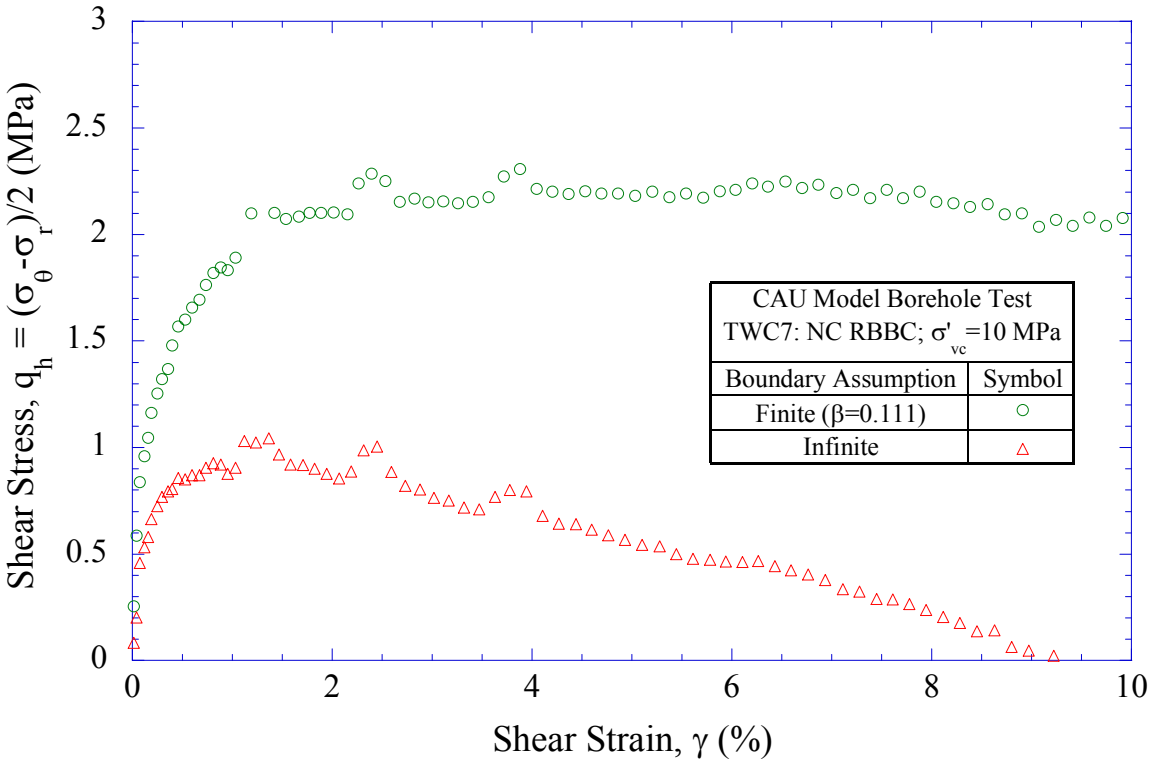

Figure 6-78: Comparison of interpreted shear stress-strain curves for finite (TWC) and infinite boundary assumptions for test TWC7 on NC RBBC

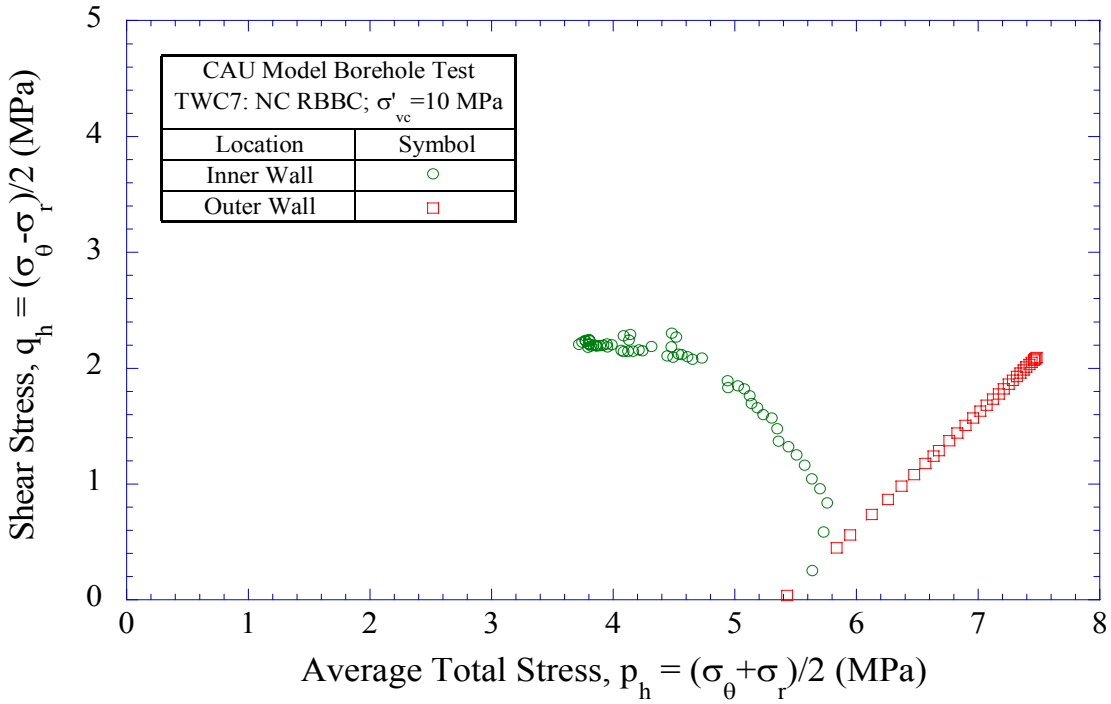

Figure 6-79: Total stress paths for elements at inner and outer walls for test TWC7 on NC RBBC

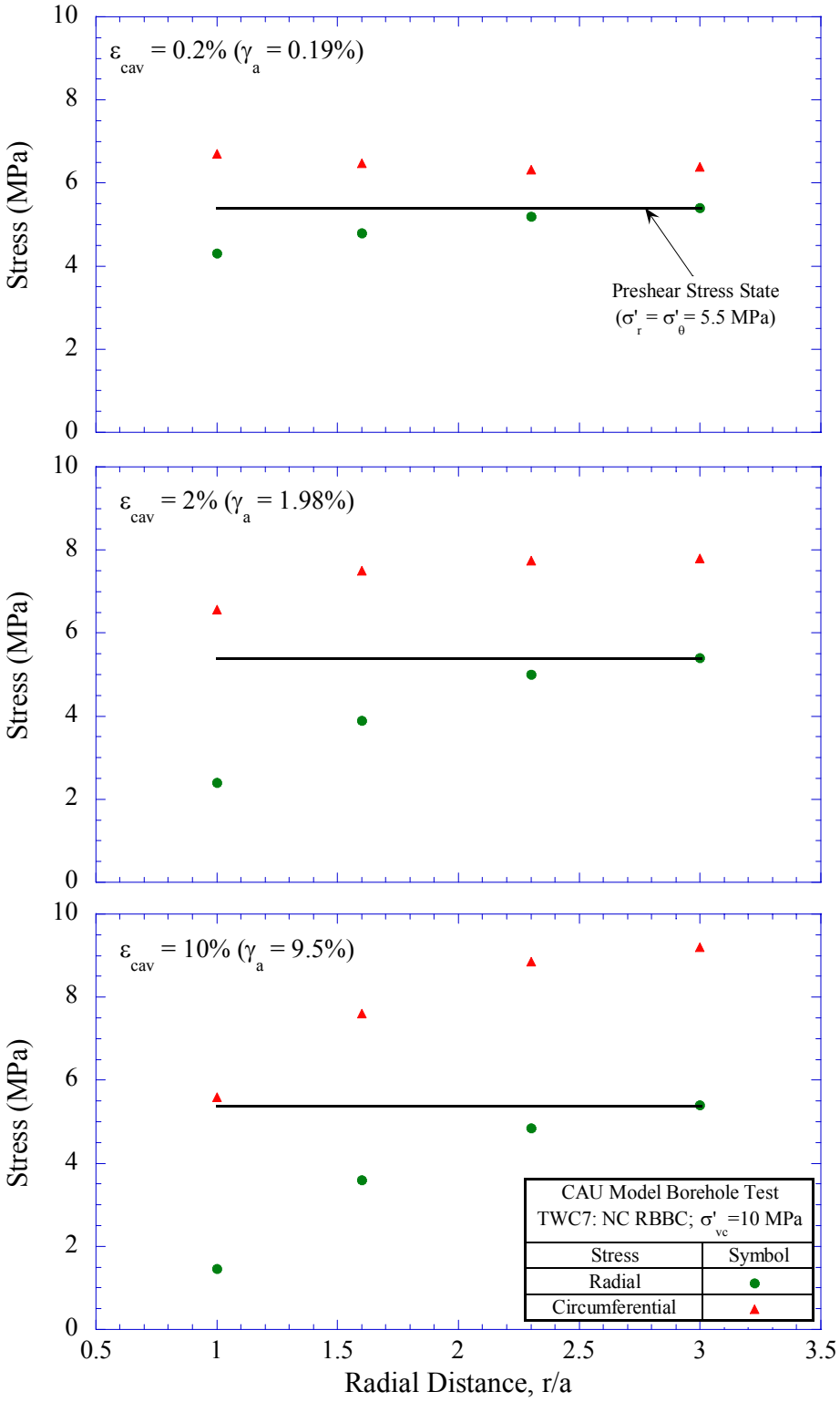

Figure 6-80: Total stress distribution across TWC specimen wall at different strain levels for test TWC7 on NC RBBC

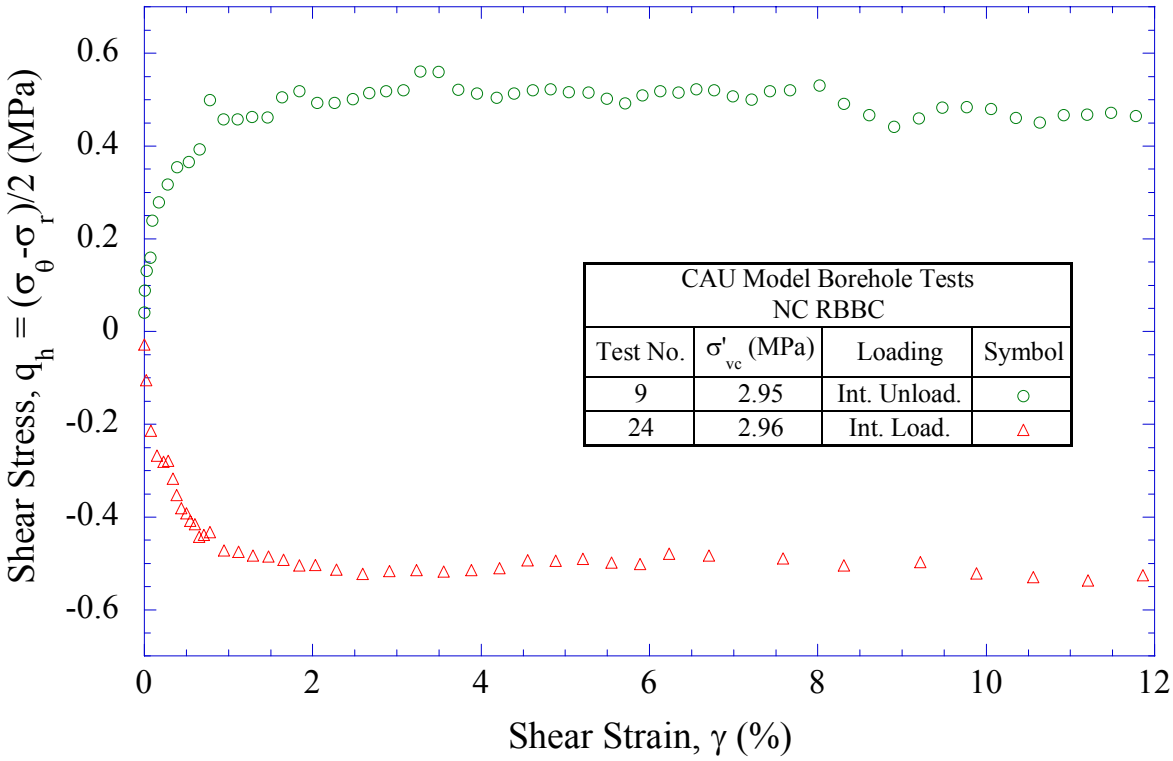

Figure 6-81: Effect of loading mode (cavity contraction versus expansion) on interpreted shear stress-strain behavior for NC RBBC from CAU model borehole tests

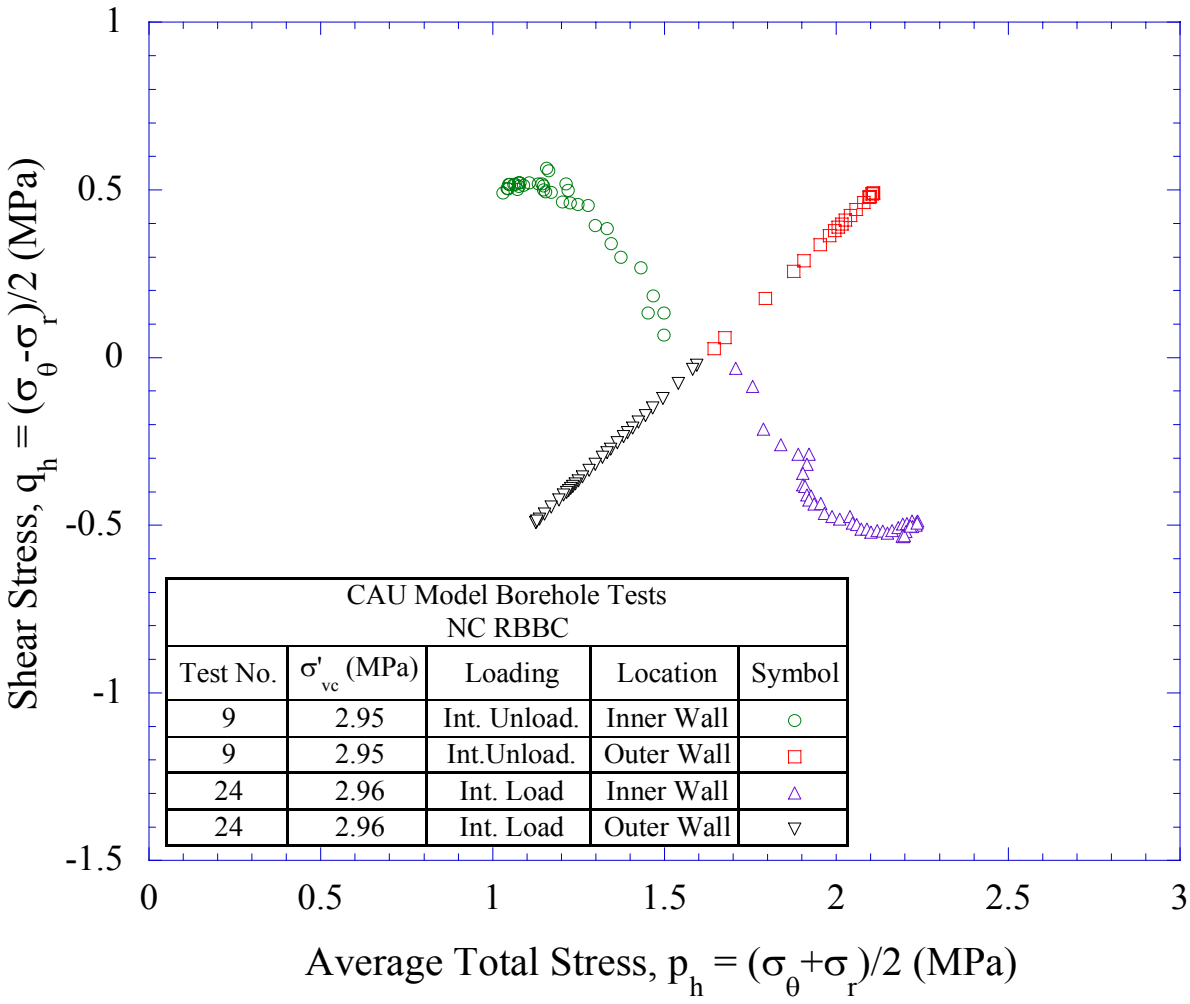

Figure 6-82: Effect of loading mode (cavity contraction versus expansion) on total stress paths for elements at inner and outer walls for NC RBBC from CAU model borehole tests

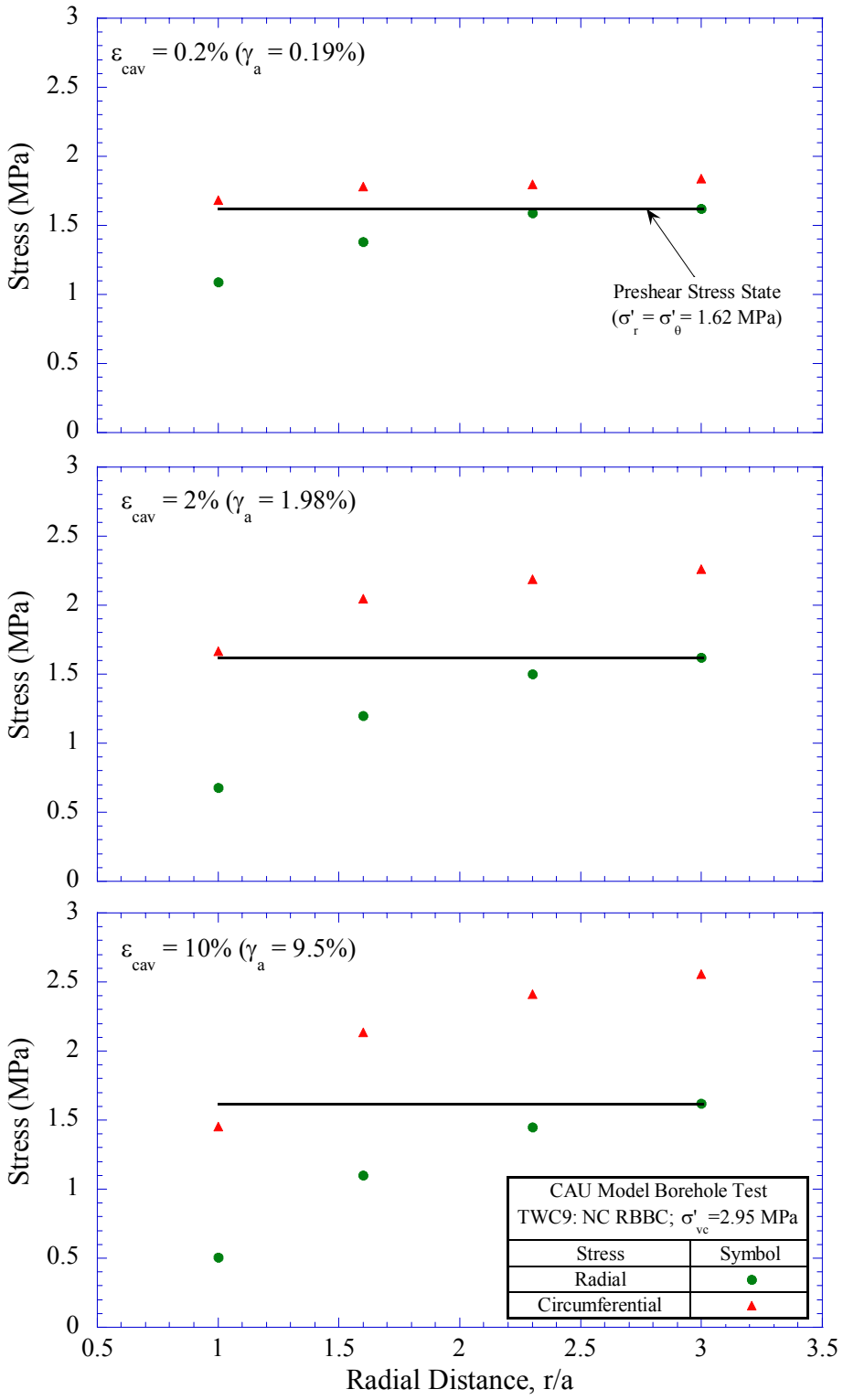

Figure 6-83: Total stress distribution across TWC specimen wall at different strain levels for cavity contraction test TWC9 on NC RBBC

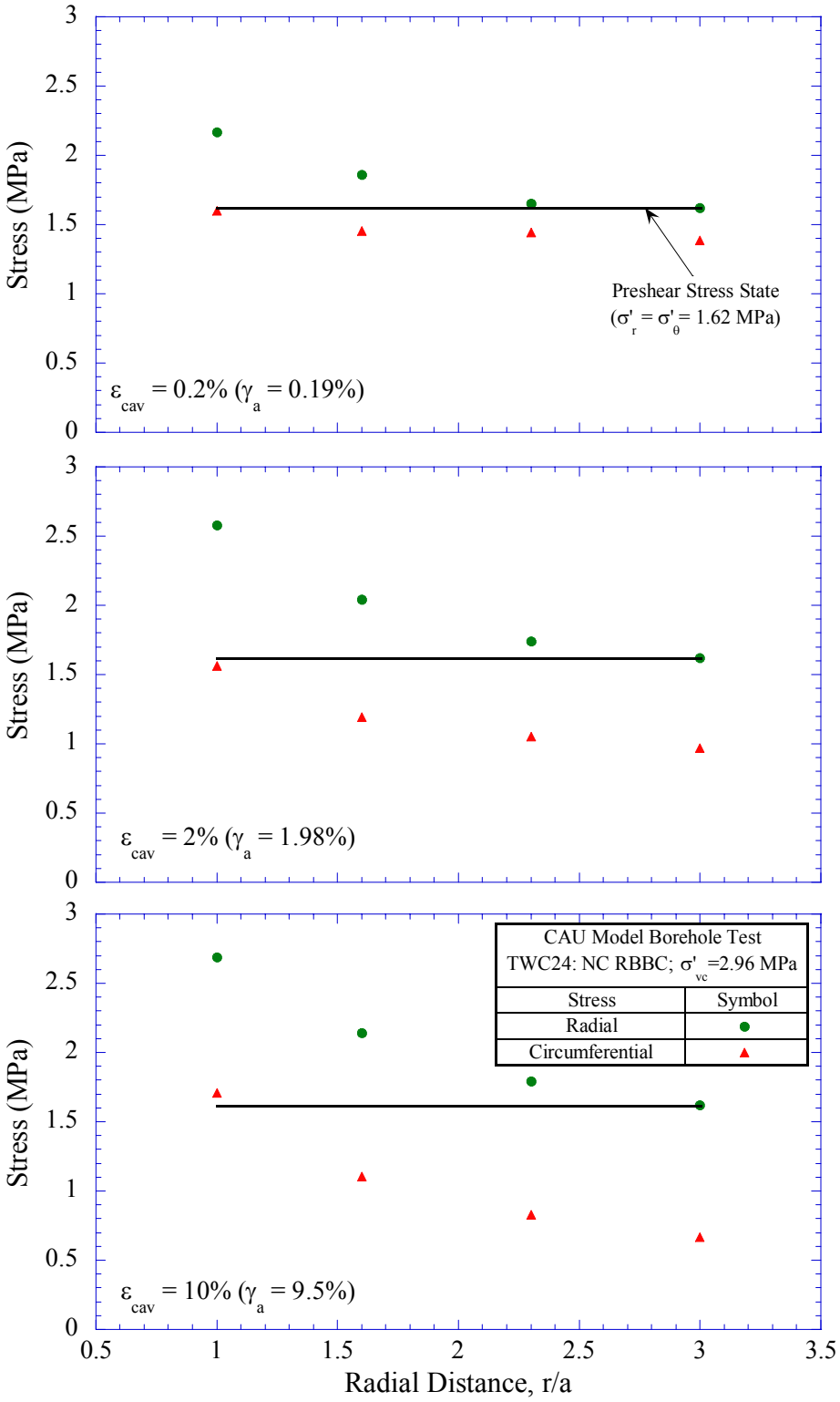

Figure 6-84: Total stress distribution across TWC specimen wall at different strain levels for cavity expansion test TWC24 on NC RBBC

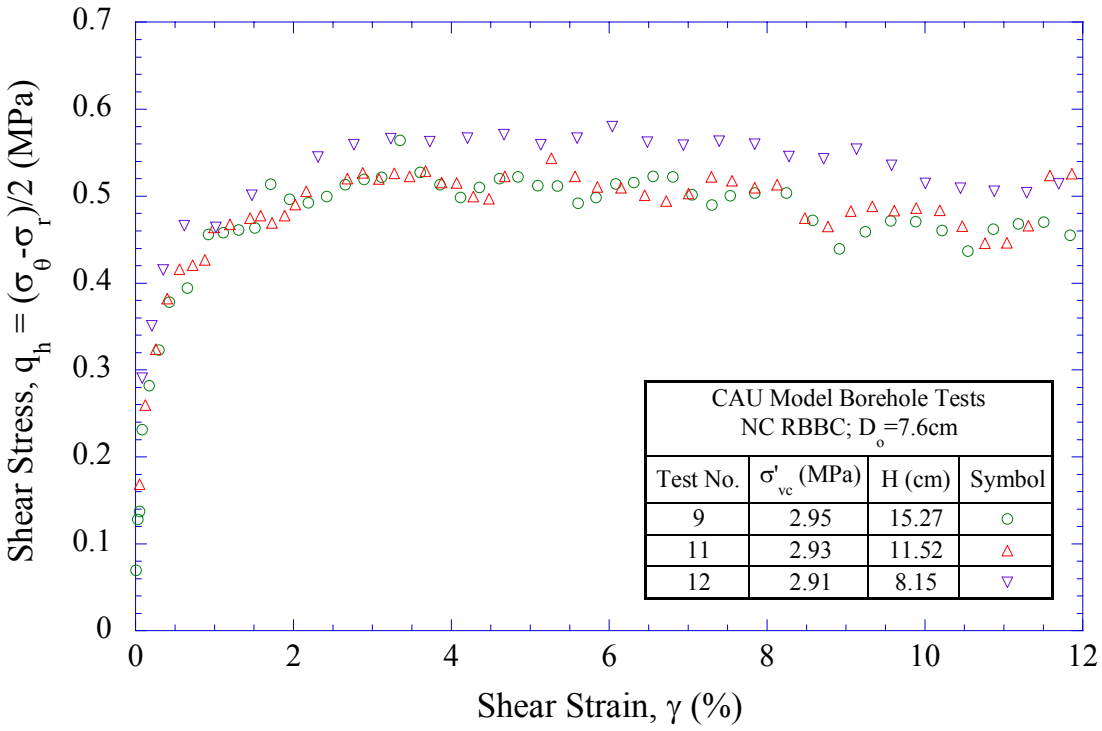

Figure 6-85: Effect of specimen height on interpreted shear stress-strain behavior for NC RBBC from CAU model borehole tests

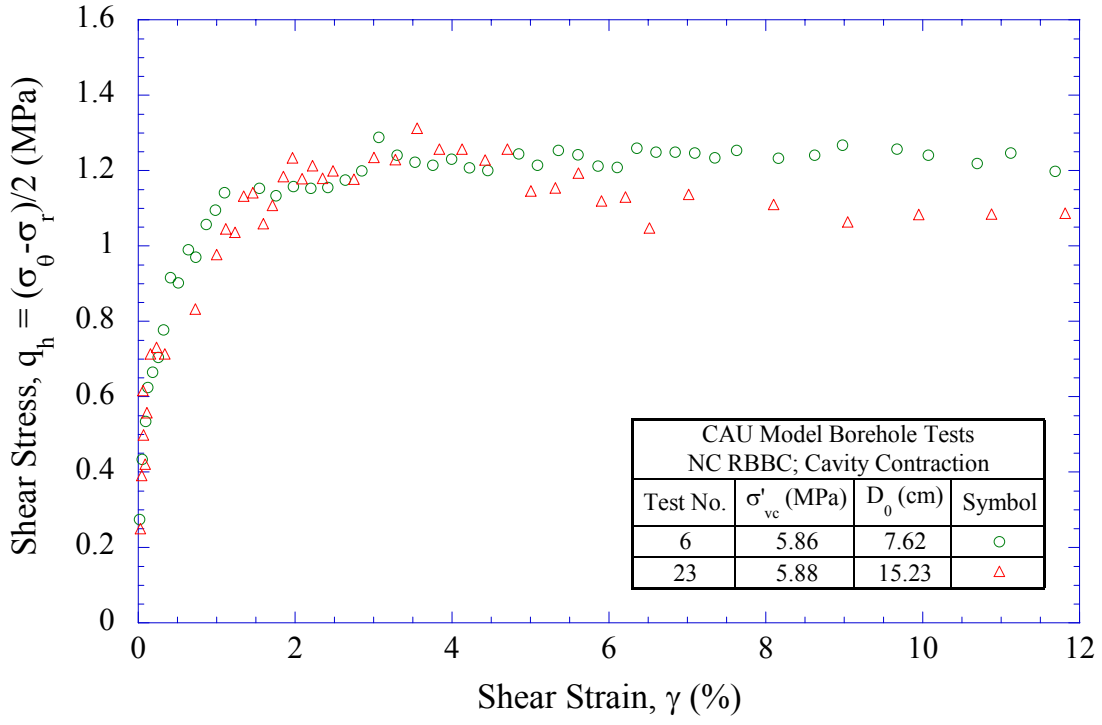

Figure 6-86: Effect of specimen outer diameter on interpreted shear stress-strain behavior during internal unloading for NC RBBC from CAU model borehole tests

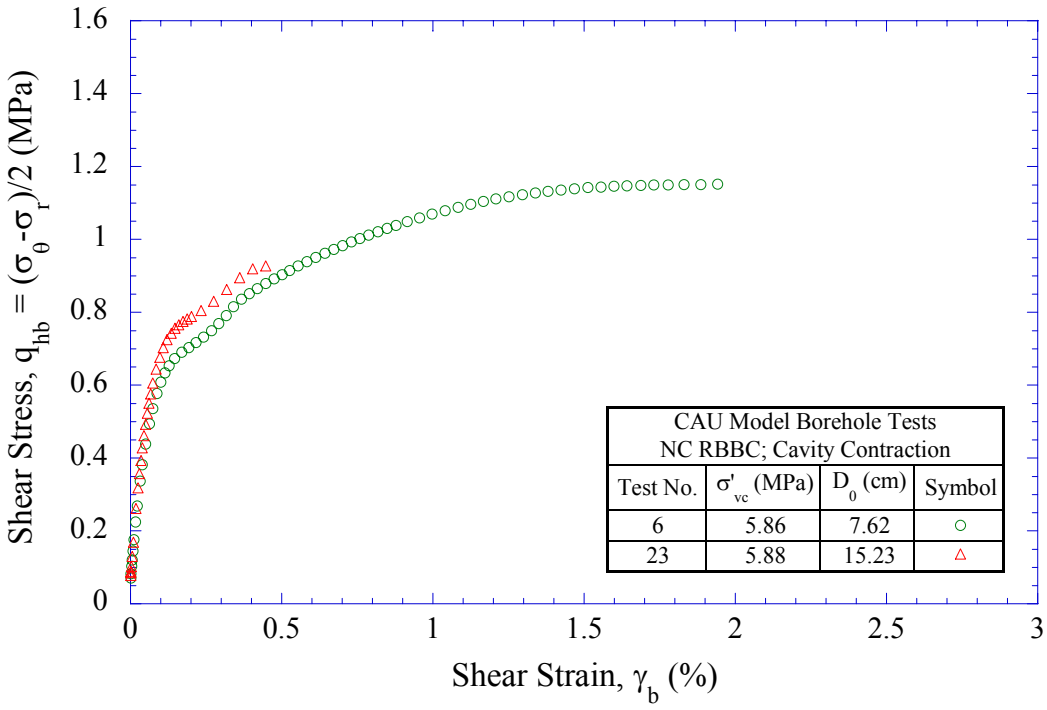

Figure 6-87: Interpreted shear stress-strain behavior for an element at the outer wall for small and large diameter TWC specimens

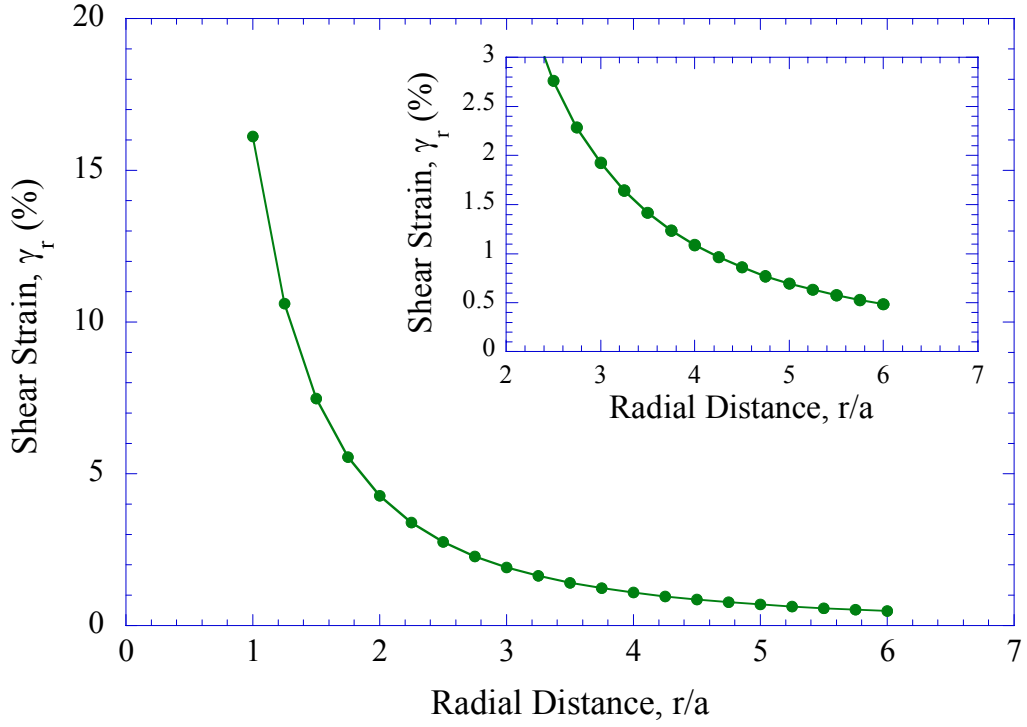

Figure 6-88: Strain distribution as a function of the radial distance across TWC specimen wall at $\varepsilon_{cav} = 17.5\%$ ($\gamma_a = 16\%$)

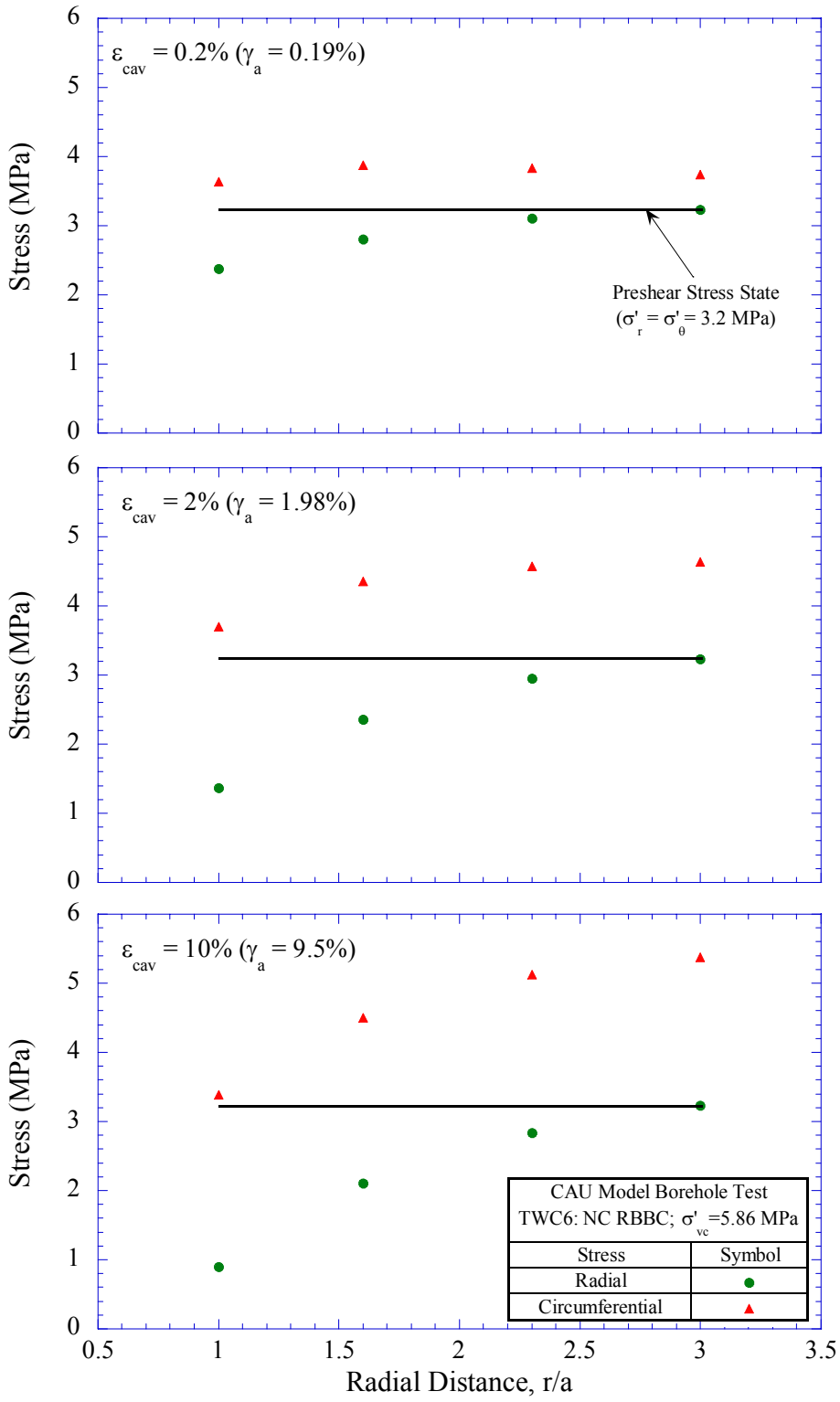

Figure 6-89: Total stress distribution across small diameter TWC specimen wall at different strain levels for test TWC6 on NC RBBC

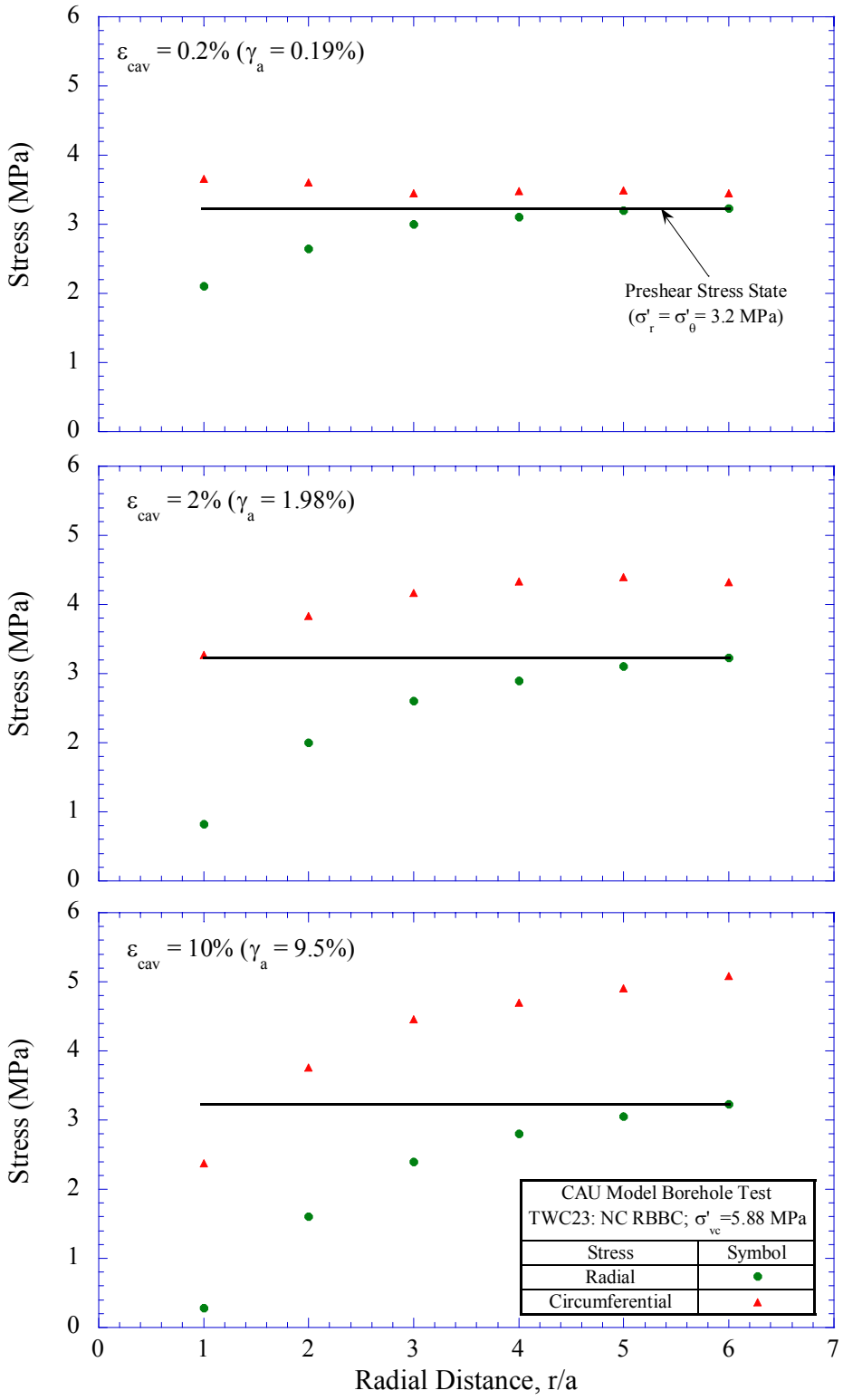

Figure 6-90: Total stress distribution across large diameter TWC specimen wall at different strain levels for test TWC23 on NC RBBC

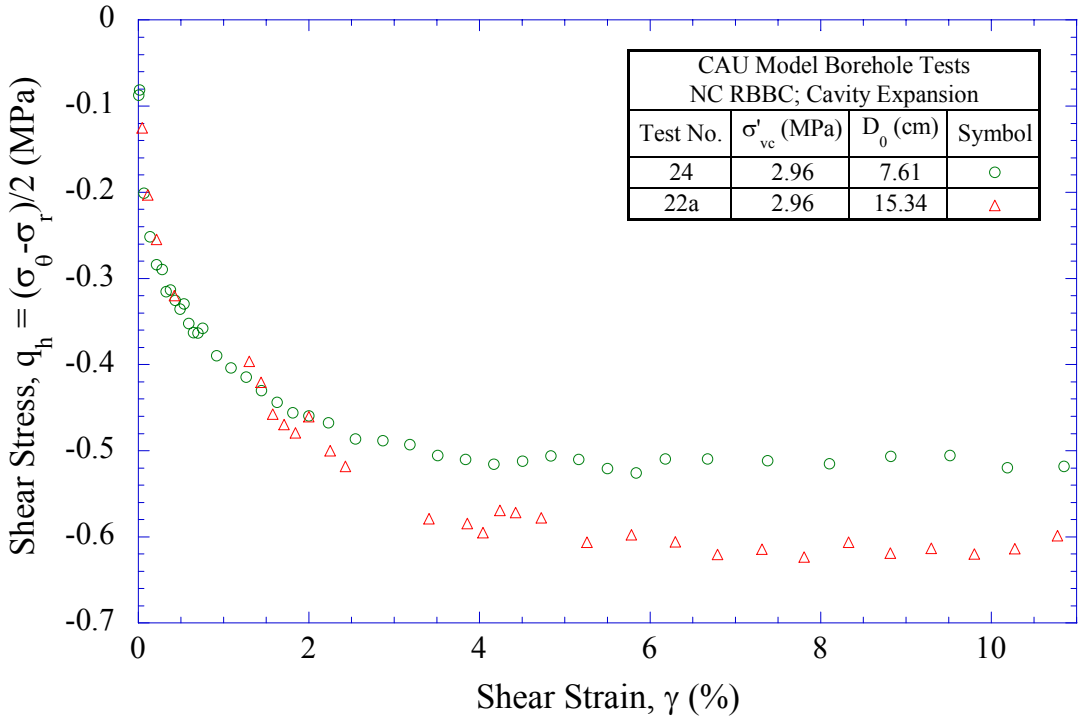

Figure 6-91: Effect of specimen outer diameter on interpreted shear stress-strain behavior during internal loading for NC RBBC from CAU model borehole tests

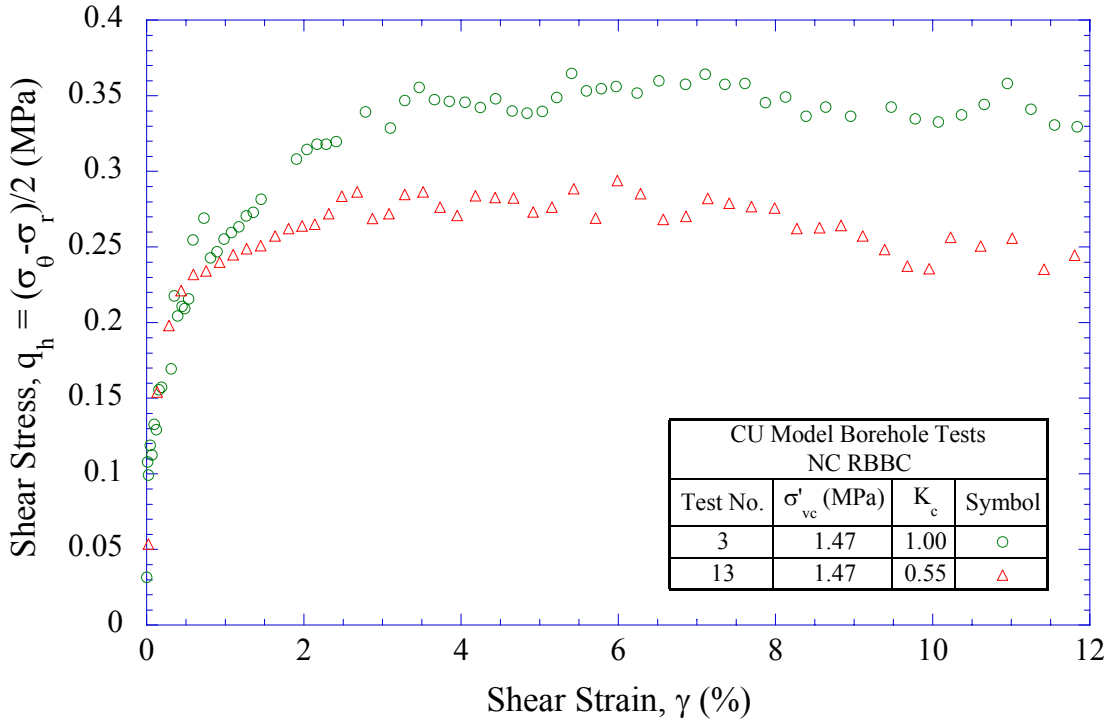

Figure 6-92: Effect of lateral stress ratio on interpreted shear stress-strain behavior for NC RBBC from CU model borehole tests

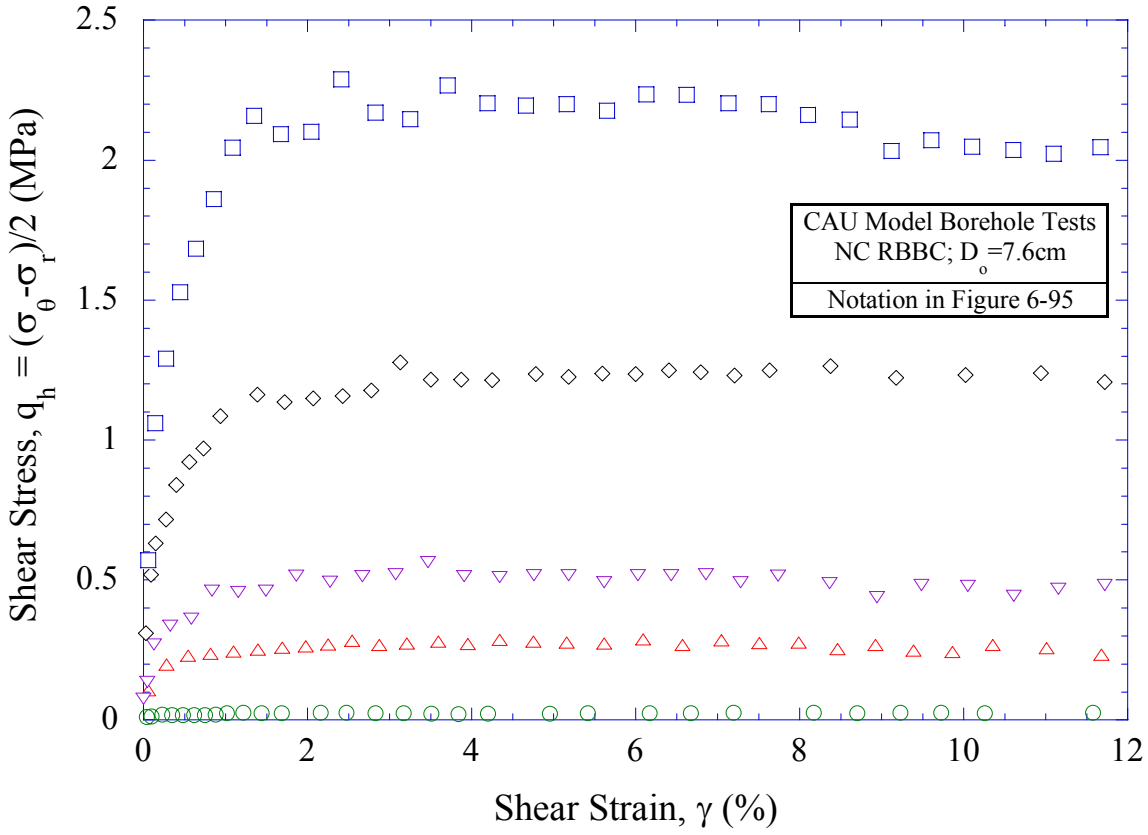

Figure 6-93: Effect of consolidation stress level on interpreted shear stress-strain behavior for NC RBBC from CAU model borehole tests with small diameter TWC specimens

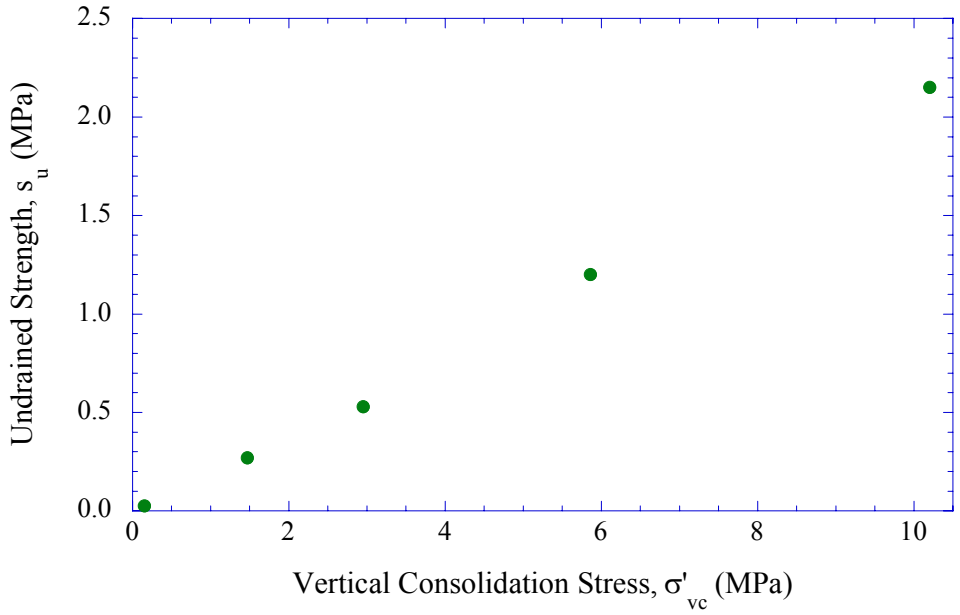

Figure 6-94: Undrained shear strength versus stress level for NC RBBC from CAU model borehole tests with small diameter TWC specimens

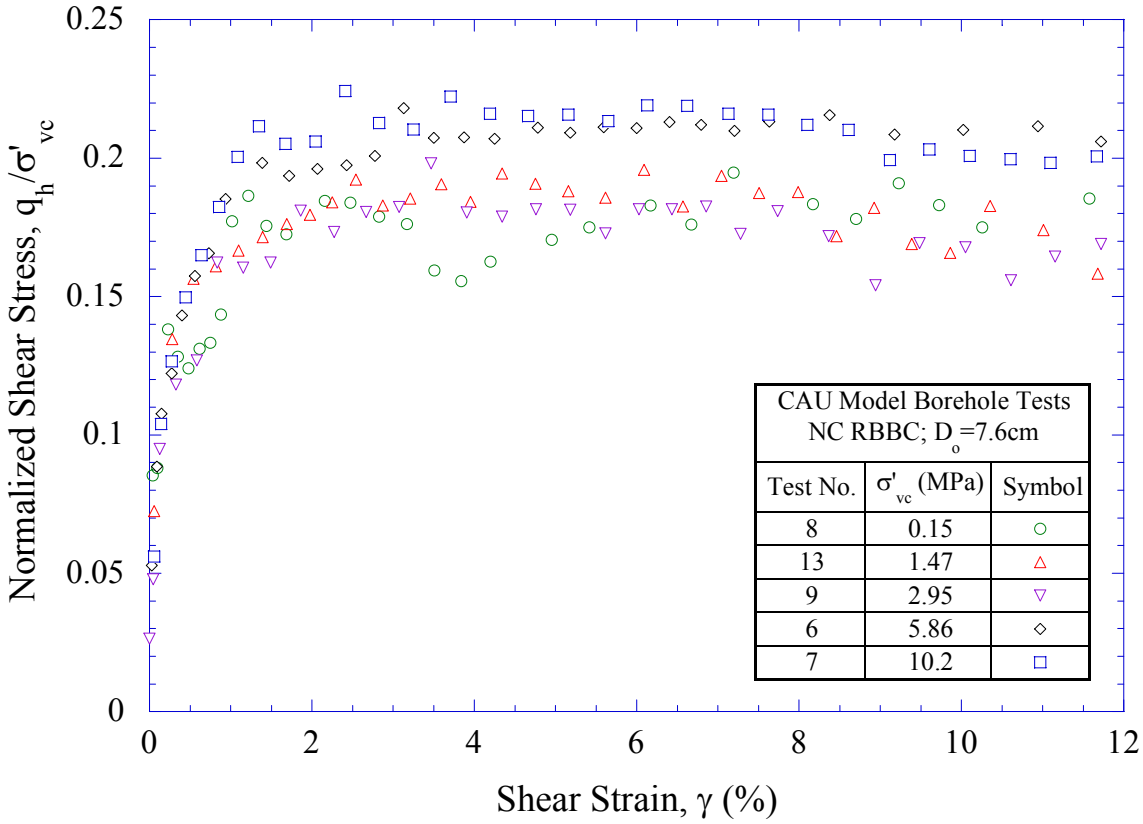

Figure 6-95: Effect of consolidation stress level on normalized stress-strain curves for NC RBBC from CAU model borehole tests with small diameter TWC specimens

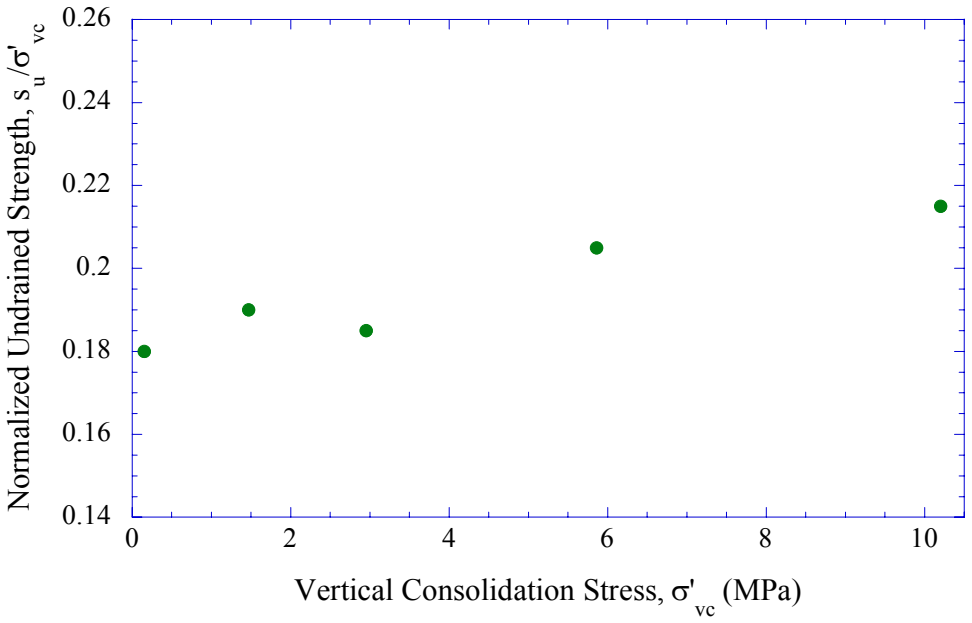

Figure 6-96: Normalized undrained shear strength versus stress level for NC RBBC from CAU model borehole tests with small diameter TWC specimens

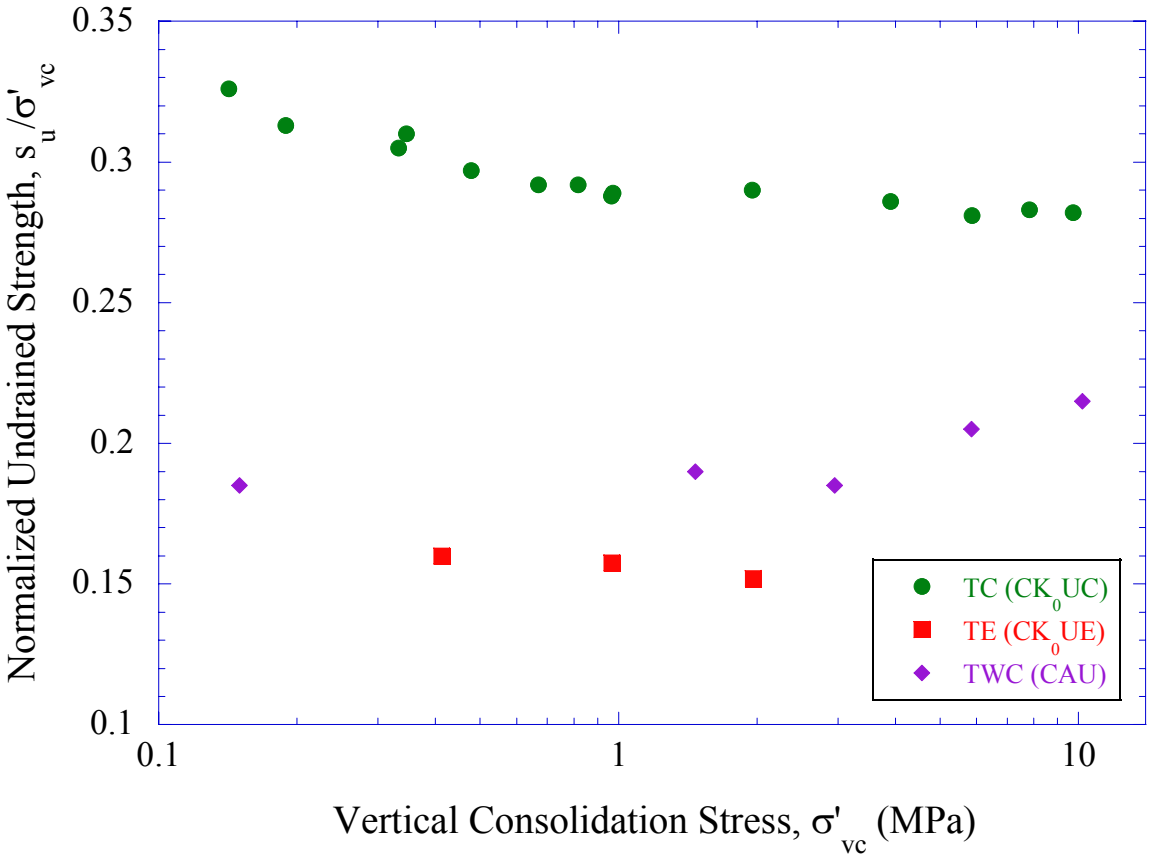

Figure 6-97: Normalized undrained shear strength versus stress level for NC RBBC from model borehole (TWC), triaxial compression (TC), and triaxial extension (TE) tests

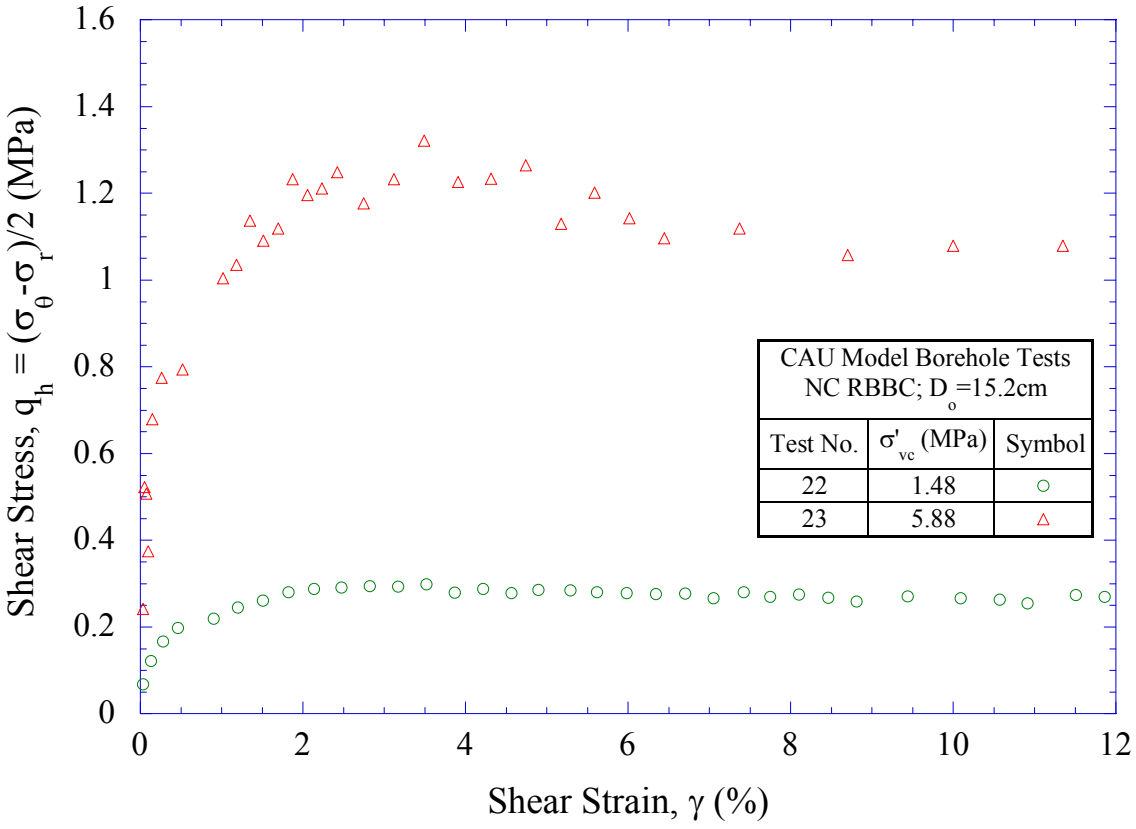

Figure 6-98: Effect of consolidation stress level on interpreted shear stress-strain behavior for NC RBBC from CAU model borehole tests with large diameter TWC specimens

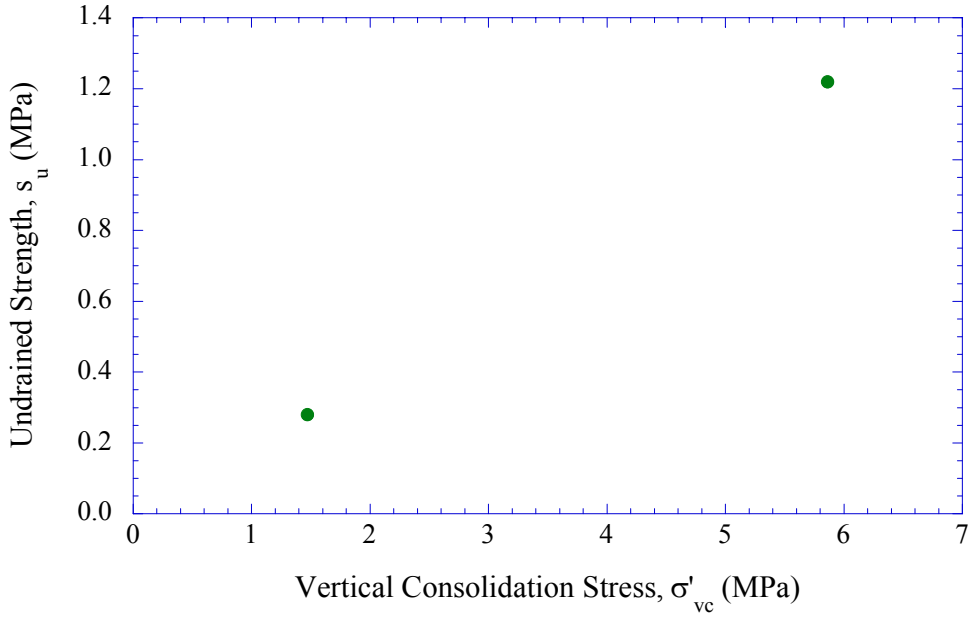

Figure 6-99: Undrained shear strength versus stress level for NC RBBC from CAU model borehole tests with large diameter TWC specimens

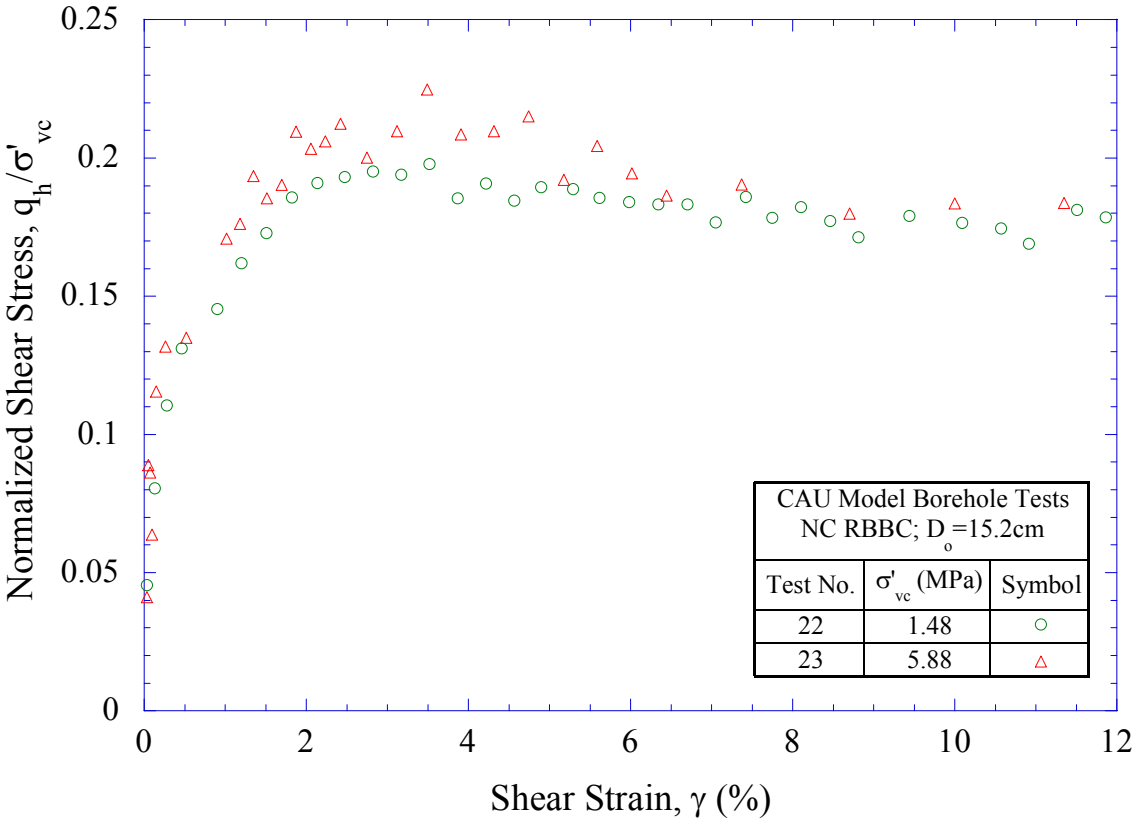

Figure 6-100: Effect of consolidation stress level on normalized stress-strain curves for NC RBBC from CAU model borehole tests with large diameter TWC specimens

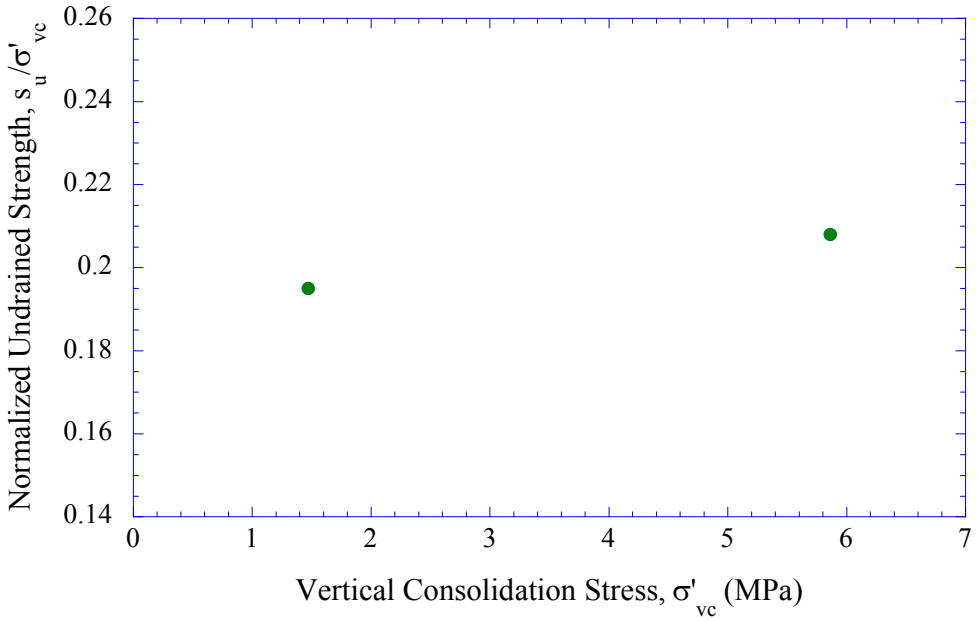

Figure 6-101: Normalized undrained shear strength versus stress level for NC RBBC from CAU model borehole tests with large diameter TWC specimens

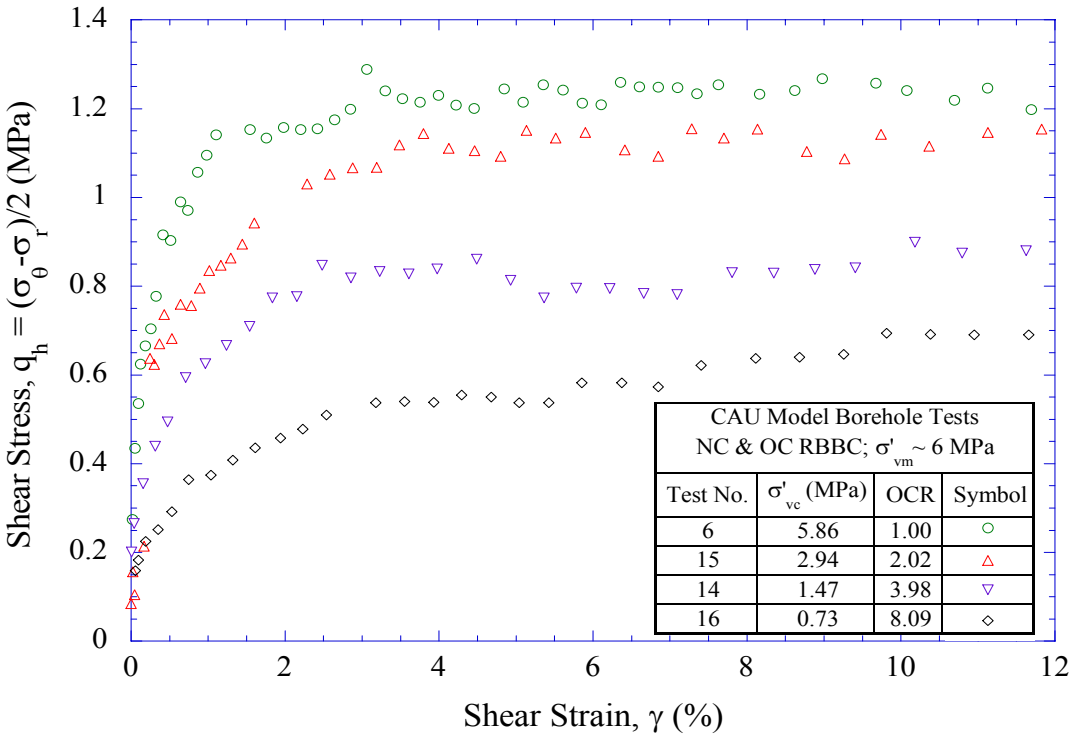

Figure 6-102: Effect of stress history on interpreted shear stress-strain behavior for NC & OC RBBC from CAU model borehole tests

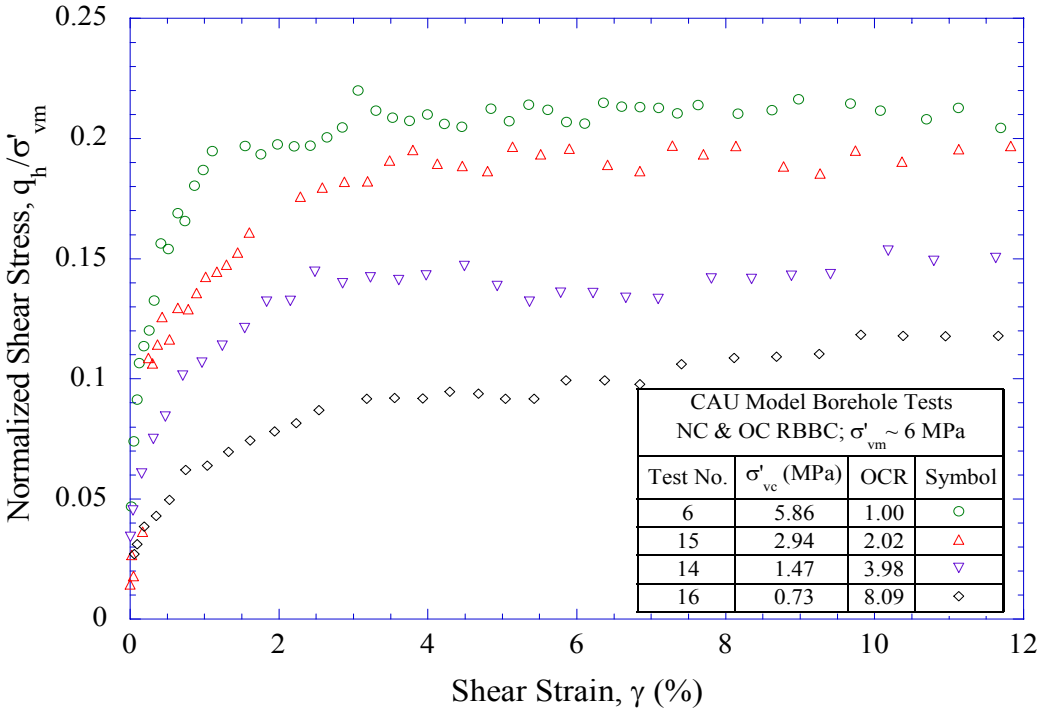

Figure 6-103: Effect of stress history on σ'_{vm}-normalized stress-strain behavior for NC & OC RBBC from CAU model borehole tests

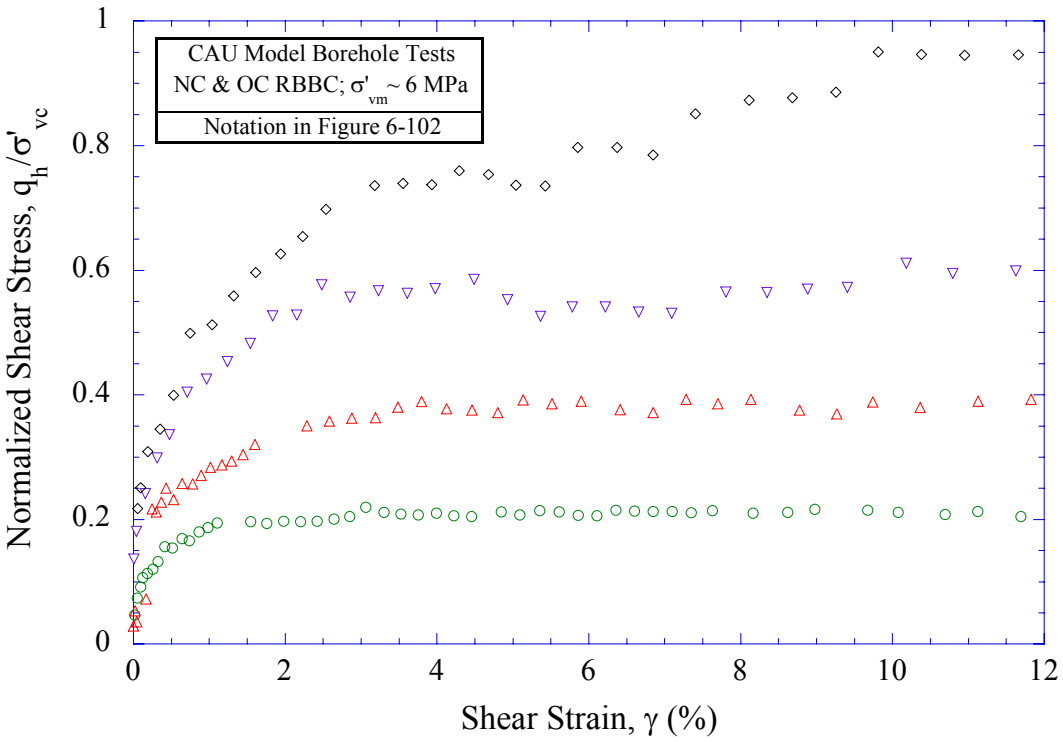

Figure 6-104: Effect of stress history on σ'_{vc}-normalized stress-strain behavior for NC & OC RBBC from CAU model borehole tests

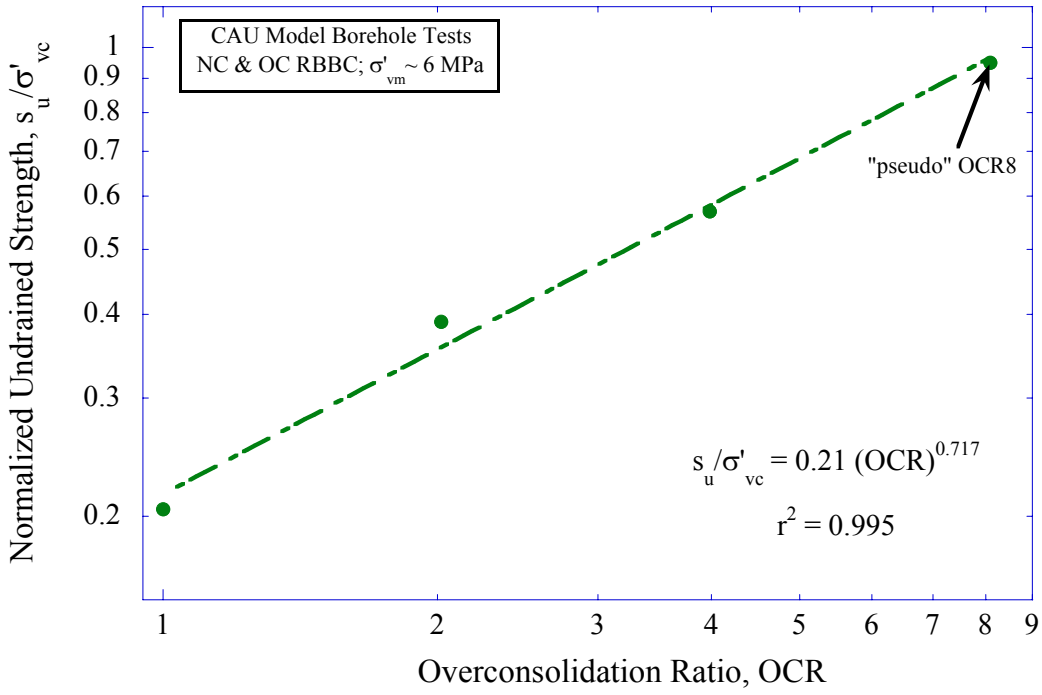

Figure 6-105: Normalized undrained strength versus OCR for RBBC from CAU model borehole tests

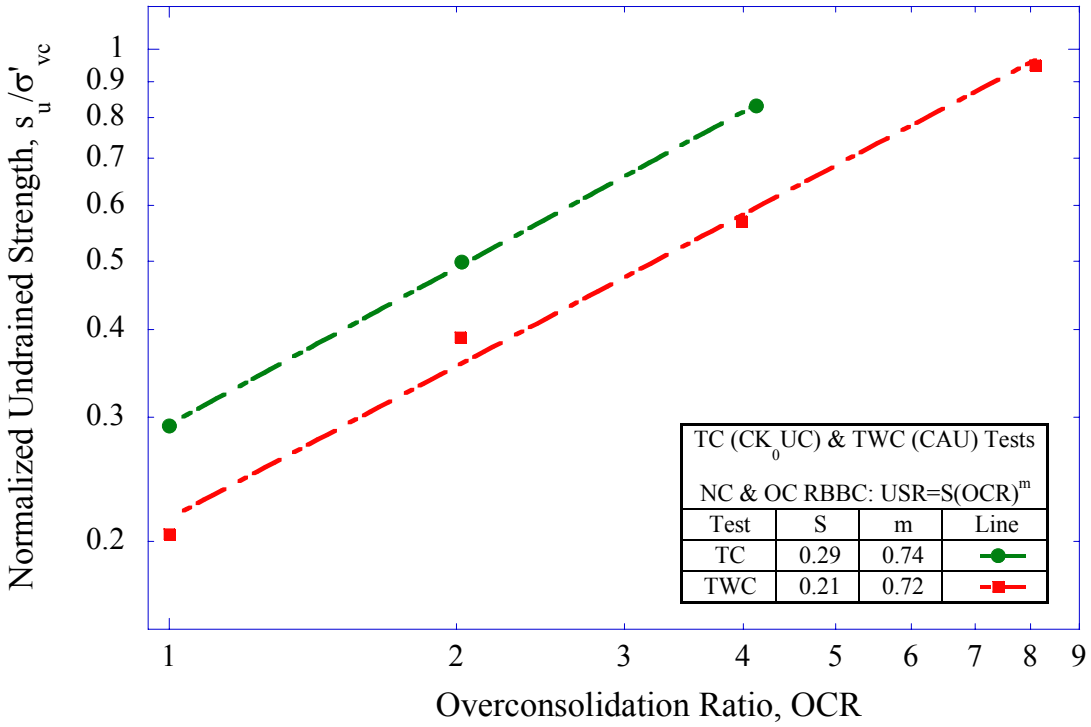

Figure 6-106: Normalized undrained strength versus OCR for RBBC from model borehole (TWC) and triaxial compression (TC) tests at high consolidation pressures

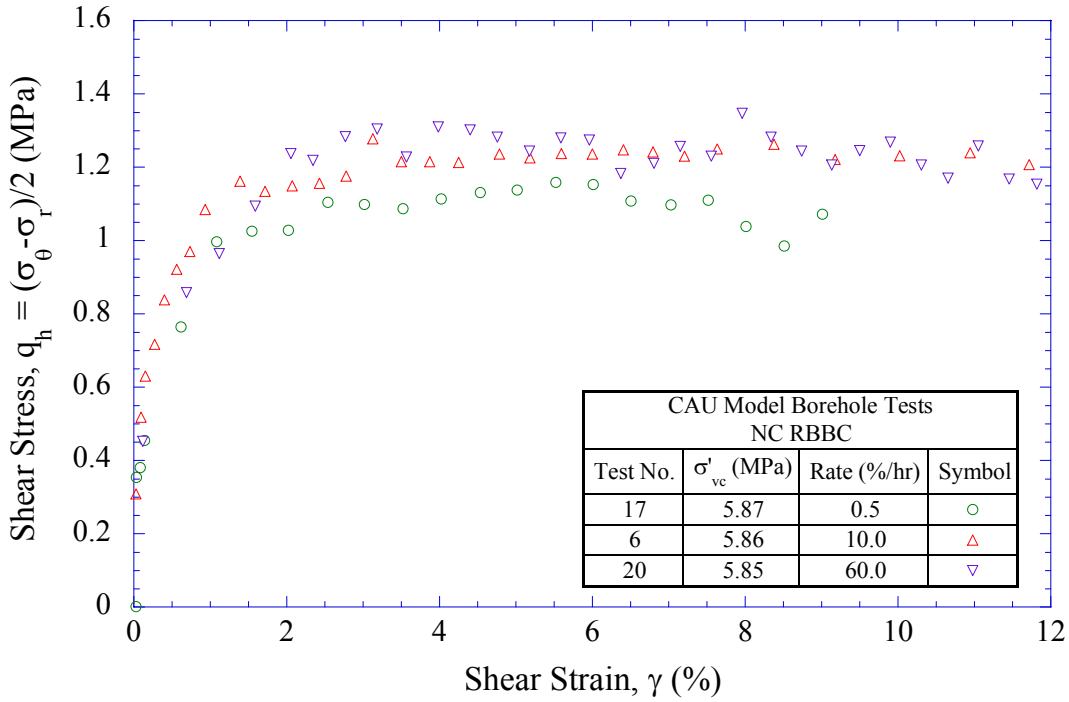

Figure 6-107: Effect of cavity volumetric strain rate on interpreted shear stress-strain behavior for NC RBBC from CAU model borehole tests

7 CONCLUSIONS AND RECOMMENDATIONS

7.1 OVERVIEW

This research comprised a detailed laboratory investigation of the mechanical behavior of cohesive soils over a wide range of consolidation stresses (0.15 – 10 MPa) with reference to the applications of wellbore instabilities in shallow oil field developments. The stress level effects on the elemental undrained shear characteristics have been investigated at three well defined stress histories (OCR = 1, 2, 4) in triaxial compression and one stress history (OCR = 1) in triaxial extension shear modes. The 1-D consolidation behavior from Constant Rate of Strain (CRS) tests and from K_0-consolidation phase in triaxial tests was also analyzed. In addition, Thick-Walled Cylinder (TWC) tests have been performed to study the effects of the following parameters on the model borehole behavior: mode of loading (internal unloading/loading, external loading), specimen geometry (height, outer diameter), preshear lateral stress ratio (K_c = 0.55, 1.0), drainage conditions (undrained, drained), consolidation stress level (0.15 – 10 MPa), stress history (OCR = 1 – 8), and cavity volumetric strain rate (0.5 – 60 %/hr). The program interpreted the measured borehole response to outline the fundamental behavior of a model borehole.

The extensive experimental program was performed on Resedimented Boston Blue Clay (RBBC), a cohesive soil manufactured in the laboratory from natural BBC. The uniformity and reproducibility in the behavior of this clay, established as a result of extensive investigations at MIT over the past 40 years, permitted a detailed study of the mechanical behavior. The present research introduced a new resedimentation procedure where each consolidometer is used to prepare an individual test specimen.

In order to perform the high pressure triaxial tests on cohesive soils, a number of improvements to the triaxial testing system originally developed for testing frozen sand by Anderson (1991) were implemented. These included a system for better strain rate control, as well as modifications to the end platens, load application, and top drainage line.

The stability of a borehole was studied in the laboratory using two computer controlled, high pressure Thick-Walled Cylinder (TWC) devices developed as part of this research. The first small diameter TWC apparatus was employed to test relatively small specimens with outer

diameter, D_o = 7.6 cm, inner diameter, D_i = 2.5 cm, and height, H = 15.2 cm, while the second large diameter TWC apparatus tested larger specimens with dimensions D_o = 15.2 cm, D_i = 2.5 cm, and H = 22.8 cm. Both TWC devices allow for independent control of the vertical stress and the radial pressures acting on the inner and outer walls of the cylinder, as well as pore pressure. Furthermore, reliable testing procedures were established for all phases of testing. A complete description of the equipment and testing procedures was presented in Chapter 4.

7.2 RESULTS AND CONCLUSIONS

7.2.1 Elemental Mechanical Behavior

7.2.1.1 Introduction

Chapter 5 presented the results from 3 CRS consolidation tests and 25 K_0-consolidated undrained triaxial compression and extension tests. The triaxial compression (CK_0UC) test series comprised 21 tests and provided a comprehensive study of cohesive soil stress level effects (σ'_{vm} = 0.15 – 10 MPa) at three overconsolidation ratios (OCR = 1, 2, 4). In addition, four triaxial extension (CK_0UE) tests were performed on normally consolidated (NC) specimens at vertical consolidation stresses, σ'_{vc} = 0.15 – 2 MPa.

7.2.1.2 One-Dimensional Consolidation Behavior

The compression, consolidation, and flow properties of RBBC were obtained from CRS tests as well as the K_0-consolidation phase of each triaxial test prior to undrained shearing. The compression curves from the CRS and triaxial tests were in good agreement. The virgin compression ratio (CR) values ranged from 0.14 to 0.18 over the stress range 0.15 – 10 MPa. The swelling ratio (SR) averaged 0.015 at OCR = 1 – 4 (i.e., approximately one order of magnitude smaller than CR).

The vertical coefficient of consolidation (c_v), interpreted from the CRS tests using the standard linear theory (Wissa et al., 1971), increased in the normally consolidated region from a minimum value of 15×10^{-4} cm^2/sec at σ'_v = 0.2 MPa to a range of 30 - 50×10^{-4} cm^2/sec at σ'_v = 10 MPa. This relatively small change in c_v with stress level indicates that the pore pressure readings in the undrained triaxial shear tests performed at the standard rate of 0.5%/hr are

expected to be reliable at all pressures since the rate of pore pressure equilibration is influenced by the consolidation coefficient.

The vertical hydraulic conductivity (k_v) obtained from the CRS tests decreased with decreasing void ratio (i.e., with increasing consolidation stress) from approximately 1 x 10^{-7} at e = 1.1 (σ'_v = 0.15 MPa) to around 3 x 10^{-9} at e = 0.53 (σ'_v = 10 MPa). The value of C_k (= $\Delta e/\Delta \log k$) was not constant over this stress range and illustrated a decreasing trend with stress level. However, the ratio of C_c/C_k appears to have a relatively narrow range around the value of 1.0.

The coefficient of earth pressure at rest (K_0) was obtained from feedback-controlled 1-D consolidation in the triaxial cell. The general trend of K_0 with vertical stress during consolidation involved a decrease in K_0 during the initial loading within the overconsolidated region until reaching the preconsolidation pressure and then plateaus. The value of K_0 in the virgin compression region (K_{0NC}) tends to increase with stress level from 0.518 at σ'_v = 0.15 MPa to about 0.564 at σ'_v = 10 MPa.

7.2.1.3 Undrained Triaxial Compression

The CK_0UC tests investigated the effect of consolidation stress level at three stress histories (OCR = 1, 2, 4) in the range σ'_{vm} = 0.15 – 10 MPa. The shear stress-strain behavior demonstrated that as stress level increases, the normalized strength decreases and the behavior becomes more ductile (i.e., post peak strain softening decreases and larger strains are required to mobilize peak resistance). Increasing OCR has similar effects; the peak value of strength normalized to the maximum vertical stress decreases, strain softening decreases, and axial strain at failure increases.

The decrease in normalized shear strength with stress level is shown in Figure 5-74 for all OCRs. The undrained strength ratio (s_u/σ'_{vc}) of NC soil decreased from 0.33 at σ'_{vc} = 0.15 MPa to 0.28 at σ'_{vc} = 10 MPa. The strength ratio is also linked to variation in the preshear lateral stress ratio K_c in the case of NC RBBC. This association between the strength ratio and K_c is stronger in the NC specimens than the OC soil since a relatively small shear stress increment is required to attain the peak stress state from the preshear stress state. The relationship between the strength ratio and the preshear K_c is consistent with the observation of Santagata (1994) on NC RBBC.

The strain at peak shear stress (ε_f) increased with increasing stress level and OCR (Figure 5-75), while the degree of post peak strain softening or brittleness, defined as s_u/(q at ε_a=10%), decreased as OCR and stress level increased (Figure 5-76). The increase in axial strain at peak and the decrease in strain softening with increasing stress level are coherent with previous studies at high pressures (e.g., Petley, 1999; Gutierrez et al., 2008).

The undrained secant Young's modulus ratio (E_u/σ'_{vc}) also illustrated stress level dependence, decreasing in magnitude with increased consolidation stress at all three OCRs (Figures 5-25, 5-44 and 5-63). In addition, the high pressure tests showed a larger strain range of linear behavior than from low pressure tests. However, the stiffness ratio curves tend to converge at higher strains indicating that the stress dependence at all OCRs decreased with increasing strains. The OC soil had consistently larger stiffness ratio than NC clay. These results are in agreement with Santagata (1998).

The effective stress paths illustrated that the peak friction angles at peak and maximum obliquity decrease when consolidation stress level increases. The friction angle at peak (φ'_p) decreased slightly with increasing stress level at each OCR, while the average φ'_p increased with increasing OCR (assuming zero cohesion intercept). On the other hand, the friction angle at maximum obliquity (φ'_{mo}) showed a significant stress level dependence with φ'_{mo} decreasing from 36-39° at low stresses to 30˚ at high stresses (Figures 5-30, 5-49, and 5-68). Hence, a linear failure envelope (with constant friction angle and cohesion intercept) is not an accurate representation of the measured non-linear failure envelope. This variation in the large strain maximum obliquity friction angle with stress level has not been previously observed for RBBC and contradicts prior knowledge of soil behavior, where the large strain friction angle of clays is assumed to be constant.

The Skempton A parameter at peak shear stress (A_f) increased with increasing stress level at each OCR (Figures 5-31, 5-50 and 5-69), while the average A_f decreased as OCR increases. The shear induced pore pressures (Figures 5-33, 5-52 and 5-71) indicated that NC soil remains contractive throughout shearing, while OCR = 2 specimens tend to dilate and then contract again with increasing strain. On the other hand, OCR = 4 RBBC ultimately dilates with shearing. As stress level increased, the shear induced pore pressures were suppressed at OCR = 1 and 2, whereas the pore pressures increased (became less negative) for OCR = 4 specimens.

The stress dependence of the SHANSEP equation parameters in triaxial compression was illustrated in Figure 5-87. The undrained strength ratio of NC clay (S) decreased from 0.32 to 0.28 as stress level increased. The parameter S at low stresses agrees with previous results for RBBC in triaxial compression. The value of the exponent m for tests consolidated to the same maximum vertical effective stress (σ'_{vm}) varied only slightly with stress level (m ranges between 0.74 and 0.77) and is somewhat higher than previously quoted values for RBBC. These are the first data to show the reliable trends in S and m in the SHANSEP equation as a function of stress level.

7.2.1.4 Undrained Triaxial Extension

Four CK_0UE tests were performed on NC RBBC specimens at vertical effective consolidation stresses, σ'_{vc} = 0.15 – 2 MPa. The shear stress-strain behavior confirms the decreasing trend of normalized strength with stress level in the extension tests (Figure 5-93). The undrained strength ratio (s_u/σ'_{vc}) decreased from 0.17 at σ'_{vc} = 0.4 MPa to 0.15 at σ'_{vc} = 2 MPa. On the other hand, the strain at failure (ε_f) is not noticeably linked to the consolidation stress.

Like the compression tests, the undrained secant Young's modulus ratio (E_u/σ'_{vc}) is stress level dependent as the curves tend to be suppressed with increasing stress level (Figure 5-96). There is a clear decreasing trend in the maximum stiffness ratio (E_{uMAX}/σ'_{vc}) measured at small strains and then the stress dependence decreases with increasing strain. The modulus values for NC RBBC obtained from extension tests are slightly higher than those obtained from compression tests.

The effective stress paths from the triaxial extension test series on NC RBBC also demonstrated that the failure envelope is stress level dependent. The friction angle at maximum obliquity (φ'_{mo}) decreased from $\varphi'_{mo} = 43^\circ$ at low stresses to $\varphi'_{mo} = 30^\circ$ at high stresses (Figure 5-101). The friction angles at low stresses are higher than those obtained in triaxial compression tests. As consolidation stress level increases (up to 2 MPa), the friction angles in triaxial compression and extension tests tend to converge.

The shear induced pore pressures remain positive for the NC RBBC during extension indicating that the soil has a fully contractive behavior. Increasing stress level tends to push down the normalized shear induced pore pressure curves. The pore pressure generation during shear is in agreement with the compression tests.

7.2.2 Model Borehole Behavior

7.2.2.1 Introduction

The model borehole experimental program consisted of 22 tests and yielded a tremendous amount of data regarding borehole performance. Chapter 6 presented and analyzed the results of the experimental program using the TWC apparatus. The two main objectives of the testing were to gain insight into the fundamental model borehole behavior and provide data for comparisons with analytical predictions. These goals were achieved by investigating the effects of seven major parameters on the borehole response. Prior to highlighting the main conclusions from these parameters, an overview of the results from a reference baseline model borehole test is presented.

7.2.2.2 Reference Model Borehole Test

The reference test was performed on a small diameter NC RBBC specimen initially stress path consolidated (K=0.55) to σ'_{vc} = 10 MPa prior to undrained shearing by reducing the cavity pressure at average cavity volumetric strain rate of 10%/hr (TWC7; see Table 6-1). This test was used to introduce the basic figures and key features of the TWC test. Note that the above conditions satisfy the 'base' case followed in most of the model borehole tests.

Reconsolidation conditions in the TWC apparatus impose higher stress levels than those used for specimen preparation in the consolidometer and hence, the TWC experiment simulates a high quality test with minimal disturbance to the soil around the cavity and unloading starts from an at-rest condition. The axial and volumetric strains during this consolidation phase were somewhat comparable indicating that the soil specimen was consolidated under conditions close to 1-D (i.e., K_0).

The borehole closure data illustrated the non-linear relation between the cavity pressure and volume strain (Figures 6-4 and 6-5). The bulk of the pressure drop occurs within a cavity volume strain, 5-7% before the borehole becomes unstable (i.e., deforms without further reduction in cavity pressure). The measured average pore pressure increased continuously during cavity pressure reduction (Figure 6-10). However, the non-uniform stress and strain conditions do generate large pore pressure gradients across the TWC specimen wall and it is estimated that the pore pressures are only 80-90% equilibrated at the standard rate of shearing ($\dot{\varepsilon}_{cav}$ = 10%/hr).

The undrained borehole response was analyzed using pressuremeter-type interpretation for thick-walled cylinders (Silvestri, 1998). The interpreted shear stress-strain behavior demonstrated that the soil reaches a maximum shear stress in the horizontal plane ($q_{hMAX} = s_u$) at shear strain, $\gamma \approx 3\%$, and exhibit almost perfectly plastic behavior beyond peak shear resistance (Figure 6-74). The backfigured undrained strength ratio, $s_u/\sigma'_{vc} \approx 0.21$ lies between the strengths measured in triaxial compression and extension shear tests, and is similar to that in a direct simple shear (DSS) mode. These results are consistent with prior knowledge of anisotropic strength properties of RBBC (Whittle et al., 1994). The stress distributions across the wall of the TWC specimen as a function of cavity strain (Figure 6-80) illustrated the spreading of the plastic failure zone from the core towards the external boundary of the TWC device.

The mode of failure involved the specimen deforming into the cavity in a uniform manner (i.e., there is minimal distortion of the cross-section). Vertical cracks were observed at the inside wall of the borehole. Note that these cracks were only present in specimens initially consolidated to maximum vertical effective stresses equal or greater than $\sigma'_{vm} = 6$ MPa.

7.2.2.3 Effect of Loading Mode

The effects of loading mode were investigated by comparing the undrained borehole response of internal cavity loading (expansion) and external cell loading modes to the response of the 'standard' cavity unloading (contraction) mode using NC RBBC.

It was found that the pore pressure generation in the internal unloading (decreasing cavity pressure with constant cell pressure) and external loading (increasing cell pressure with constant cavity pressure) modes were very different (external loading generated much greater pore pressures) due to the fundamentally different total stress system (Figure 6-15). However, the inferred radial effective stress distributions across the TWC specimen wall were quite similar (Figures 6-16 and 6-17).

On the other hand, the cavity contraction/expansion curves from the internal unloading/loading tests had very similar profiles (i.e., evolution of pressure with volume strain) even at small strains (Figures 6-18 to 6-20). The pore pressures are observed to be independent of the mode of loading (Figure 6-21). In addition, the interpreted shear stress-strain-strength properties were almost identical, suggesting that the soil exhibits isotropic behavior in the horizontal plane after stress path consolidation (Figure 6-81). The normalized undrained shear

strengths are in agreement with previous studies on pressuremeter tests (e.g., Ladd et al., 1979; Aubeny, 1992). Figure 6-82 presented the stress paths in the horizontal plane followed by elements at the inner and outer walls of the TWC specimen. The stress paths for the expansion and contraction tests lie at approximately 180° with respect to each other (i.e., when one element is following a loading path, the other is following an unloading path). The spreading of the plastic failure zone, inferred from the stress distributions, was identical in both modes (Figures 6-83 and 6-84).

7.2.2.4 Effect of Specimen Geometry

Investigation of the effects of specimen height and outer diameter on the undrained borehole behavior was carried out using NC RBBC.

The effect of the vertical boundary was investigated by testing small diameter TWC specimens (D_o = 7.6 cm) with H = 15.2, 11.5 and 8.2 cm (i.e., H/D_o = 2.0, 1.5 and 1.1). The tests show that the initial height has minimal impact on the observed borehole response and pore pressures (Figures 6-23 to 6-26). Consequently, the interpreted stress-strain curves for these tests were comparable (Figure 6-85).

The effect of the outer diameter was investigated by comparing the results from undrained cavity contraction tests performed on small diameter (D_i = 2.5 cm; D_o = 7.6 cm; H = 15.2 cm) and large diameter (D_i = 2.5 cm; D_o = 15.2 cm; H = 22.8 cm) specimens. The lateral boundary had a pronounced effect on the measured borehole response, producing lower minimum cavity pressure in the larger TWC device (Figures 6-28 to 6-30). In addition, the pore pressures generated in the large TWC specimen were much lower than those generated in the small specimen (Figure 6-31) due to the longer drainage path (less pore pressure redistribution). However, the interpretation method takes into account the lateral extent of the specimen and hence, the shear stress-strain curves yielded comparable results confirming that this stress-strain curve is unique for the soil (Figure 6-86). The results also indicated that the plastic failure zone reaches the outer boundary in the small specimen before the larger one, as expected. Similar trends were observed in the cavity expansion tests.

7.2.2.5 Effect of Lateral Stress Ratio

The undrained borehole behavior of NC RBBC was investigated following isotropic (K_c=1; CIU) and stress path (K_c=0.55; CAU) consolidation. Comparison of the normalized cavity contraction curves indicated that the borehole response was not significantly dependent on the preshear lateral stress ratio (Figures 6-37 to 6-39).

On the other hand, the interpreted undrained shear strength obtained from the CIU test was approximately 30% greater than the CAU test (Figure 6-92). The higher shear strength observed in the CIU model borehole test is fairly consistent with previous work using the triaxial device (e.g., Ladd & Varallyay, 1965; Ladd, 1965; Bensari, 1981).

7.2.2.6 Effect of Drainage Conditions

The effects of drainage conditions during borehole closure were investigated for NC RBBC specimens by comparing the data for the drained case to that of the undrained case. The undrained borehole closure tests were performed with the drainage lines closed at the standard average cavity volumetric strain rate, $\acute{\varepsilon}_{cav}$ = 10 %/hr. On the other hand, the fully drained tests were sheared very slowly ($\acute{\varepsilon}_{cav}$ = 0.2 %/hr) in order to ensure no development of excess pore pressure in the TWC specimen.

It was observed that the drainage conditions significantly impacts the borehole response of NC RBBC. The drained tests had much larger cavity volume strains at a given cavity pressure in the initial unloading portion (up to ε_{cav} = 5%) since the soil has a greater potential to deform than the undrained tests (pore water can leave/enter the test specimen). Moreover, the minimum cavity pressure in the drained tests was lower than the undrained tests (Figures 6-42 to 6-44). However, the net cavity pressure is equal to the radial effective stress in the soil at the inner wall in the drained test (as u_e = 0 MPa). This reduces to a minimum effective stress value comparable to that obtained in the undrained shear tests. The specimen volume strain in the drained tests indicated that the volume does not change significantly (ε_v < 1%) during the test and that the soil has an overall contractive behavior (Figure 6-46).

7.2.2.7 Effect of Stress Level

A series of model borehole tests have been performed on NC RBBC specimens in the small and large TWC apparatuses over a wide range of stresses to evaluate the dependence of the

borehole behavior on consolidation stress level. Borehole closure tests on small diameter TWC specimens were carried out under undrained conditions over a stress range, $\sigma'_{vc} = 0.15 - 10$ MPa, and under drained conditions over a stress range, $\sigma'_{vc} = 1.5 - 6$ MPa. Additionally, undrained borehole closure tests were performed on large diameter TWC specimens consolidated to $\sigma'_{vc} = 1.5 - 6$ MPa.

The effect of stress level on the normalized cavity contraction curves was similar in all tests. At the same net pressure ratio ($[p_i-u_0]/\sigma'_{r0}$), there were larger volume strains for tests at higher consolidation pressures. Also, the initial stiffness ratio decreased as stress level increased. The normalized pore pressures were comparable for the undrained tests on small TWC specimens (Figure 6-51). However, these pore pressures were much greater than those measured in the larger specimens (Figure 6-60) due to the shorter drainage path (normalized pore pressures were more or less the same in the large specimens). The specimen volume strain in the drained tests showed no dependence on the stress level (Figure 6-56).

The normalized shear stress-strain curves were very similar in all undrained tests (small and large diameter TWC specimens) with backfigured undrained strength ratios in the range $s_u/\sigma'_{vc} = 0.18 - 0.21$ (Figures 6-95 and 6-100). The TWC strength ratios are closer to those measured in triaxial extension at low stresses but tend to reach an average value between triaxial extension and compression strength ratios at higher stresses (Figure 6-97). This trend with stress level is in the reverse of that observed in undrained triaxial shear tests.

7.2.2.8 Effect of Stress History

The effect of stress history on the undrained model borehole behavior was investigated by comparing results from tests with nominal values of OCR: 1, 2, 4 and 8. All tests were initially consolidated to the same maximum stress, $\sigma'_{vm} = 6$ MPa.

The observed borehole response was found to be considerably affected by the stress history of the material. As OCR increased, the borehole pressure became more stable, producing smaller cavity volume strain for a given change in net cavity pressure (Figures 6-62 to 6-64). The tests on OC specimens were able to sustain net pressures less than zero (i.e., internal pressure is less than the initial pore pressure). Moreover, the higher OCR tests (OCR = 4 and 8) did not reach a limiting cavity pressure even at large volume strains. The excess pore pressures decreased and become increasingly negative as OCR increased (Figure 6-65). The pore pressures indicated that

NC RBBC has a contractive behavior while OC RBBC specimens have a dilatant shear behavior even from the very beginning. On the other hand, the trends of normalized effective stress at the inner wall were comparable for the four OCRs (Figure 6-66) indicating that the effective stresses remain positive throughout the test and that the net cavity pressure profiles are associated with the pore pressures developed in the test specimen.

Figure 6-104 presented the normalized stress-strain behavior (q_h/σ'_{vc} versus γ) from OCR=1, 2, 4 and 8 tests. The peak mobilized strength ratio increased with OCR. The SHANSEP equation parameters S and m obtained from these tests are consistent with element shear tests where S = 0.21 and m = 0.717 (Figure 6-106). These results are very similar to those obtained by Ahmed (1990) for RBBC from the DSS test and are in excellent agreement with the predictions made by Aubeny (1992) using the MIT-E3 constitutive model for the pressuremeter tests on BBC at OCR = 1, 2, and 4.

7.2.2.9 Effect of Strain Rate

The investigation of the strain rate sensitivity of the borehole behavior of NC RBBC involved undrained shearing at cavity volumetric strain rates varying within approximately two orders of magnitude: slow rate (0.5%/hr), moderate 'standard' rate (10%/hr), and fast rate (60%/hr).

The effect of increasing strain rate in the borehole closure tests on small diameter TWC specimens was to decrease the minimum net cavity pressure, increase initial stiffness and decrease pore pressure development (Figure 6-68 to 6-71). The pore pressures in the slow rate test are believed to be fully equilibrated, whereas the fast rate test has minimal internal drainage. On the other hand, the pore pressures in the standard rate tests are assumed to be 80-90% equilibrated.

The shear stress-strain curves were comparable for the three rates indicating that the strain rate (and hence the degree of internal pore water migration) had minimal effect on the interpreted stress-strain behavior (Figure 6-107). The slow rate test had a slightly lower strength than the other two rates. The trends in pore pressures and strength with strain rate are consistent with the observations made by Sheahan (1996) from triaxial shear tests.

7.3 RECOMMENDATIONS FOR FUTURE RESEARCH

Recommendations for future research are divided into two categories; one related to investigations into the stress dependence of the elemental mechanical properties, and the other to the model borehole work. The suggestions in each category cover equipment modifications as well as additional experimental programs.

7.3.1 Elemental Stress Dependence Investigations

a) The triaxial extension test series presented in this thesis included only four tests on NC RBBC and covered relatively small range in consolidation stresses (σ'_{vc} = 0.15 – 2 MPa). Additional tests should be carried out at this stress range to check the results obtained in the current study, as well as tests at higher consolidation stresses (up to 10 MPa or higher). This work will require modifications to the high pressure triaxial apparatus to incorporate extension capabilities. This can be achieved by integrating a suction cap with the load application system in order to have a better alignment between the test specimen and the top cap.

b) Further triaxial extension tests at higher overconsolidation ratios (OCR = 2 – 8) are required over a wide range of consolidation stresses to understand the stress level dependence of the OC RBBC. This would provide a data base similar to that obtained for the triaxial compression tests and permit the evaluation of the SHANSEP equation parameters as function of stress level.

c) The trends in the normalized strength and stiffness properties with consolidation stress level appeared to level off slightly at high stresses in the triaxial compression tests. A series of tests at consolidation stresses greater than 10 MPa (perhaps up to 100 MPa) should be carried out to examine whether the trend eventually reaches a steady state or if it continues to decrease.

d) Failure planes were observed in NC RBBC at high pressures when sheared in compression and extension although the soil has a fully contractive behavior. The development of failure planes could be related to the specimen non-uniformity created by the fixed ends (i.e., the ends of the specimen are restrained from radial deformations by rough porous stones). Moreover, the non-uniformity and development of failure planes might have also affected the friction angles measured at high strains (and undrained strength in the case of extension tests). This can be investigated by conducting high pressure triaxial tests with lubricated end platens.

Note that these tests would ideally require pore pressure measurements to be taken at the specimen mid-height.

e) All triaxial tests conducted in this thesis were sheared under undrained conditions. It would be beneficial to investigate the effect of consolidation stress level on the drained shear stress-strain-strength properties. The dependence of the high strain friction angle on stress level can also be evaluated with these tests.

f) Additional consolidation tests (CRS and incremental oedometer) conducted at vertical stresses up to 100 MPa would provide useful insights into the compression and flow properties of RBBC at very high pressures. These tests would complement the high pressure triaxial tests (greater than 10 MPa) recommended above.

g) The stress dependence of the mechanical properties should be validated for natural soils, in particular the parent material for RBBC, natural Boston Blue Clay. However, the preconsolidation pressures for Boston Blue Clay tend to be less than 1 MPa (~0.1 – 0.3 MPa) and hence, large consolidation strains will take place in the triaxial apparatus to reach high stresses. Further tests on other clays and mudrocks over a wide consolidation stresses are also recommended.

7.3.2 Model Borehole Investigations

a) The cavity deformations were determined in this thesis by measuring the amount of fluid expelled from the borehole. The mean radial strain was then calculated assuming a deformation mode shape and taking into account the axial strain. A superior method of measuring the radial strain is to have local instrumentation inside the bore. This method would also allow to determine precisely the yield point in the cavity pressure-strain curve if present. It should be noted that local instrumentation introduces significant complexity to the test and will require substantial design challenges due to the very small operational space.

b) The average pore pressures generated in the TWC specimen during undrained shearing were measured by means of annular stones located at both ends of the specimen. In order to get a better understanding of the pore pressure distribution in the test specimen, pore pressure probes at different locations across the TWC wall are needed. These are particularly important for high strain rate tests (performed to simulate ‘true’ undrained conditions locally) carried out on large

specimens where there is very little pore pressure redistribution. In addition, effective stress paths for different elements across the wall can also be determined (since only total stress paths are obtained using the current interpretation method).

c) The current research investigated the stability of axisymmetric borehole in the TWC device. This device only permits independent control of two principal stresses and hence, cannot be readily used to study the effects of anisotropy. To overcome this, a true triaxial borehole stability tests would require control of three principal stresses. These tests are important to simulate stress conditions in anisotropic material as well as deviated boreholes (i.e., orientation of borehole is different to the orientation of principal stresses acting within the surrounding soil mass).

d) Conducting a series of undrained creep borehole tests, where the cavity pressure is held constant after some initial reduction and before reaching failure, would provide useful information on the time-dependent behavior of a borehole. This would in fact simulate the stability control method used in the field by means of the drilling mud.

e) Interpretation of the model borehole tests sheared under drained conditions is needed to obtain shear stress-strain curves analogous to those produced for the undrained tests. A constitutive relationship must be assumed in this case since the condition of unique stress-strain behavior for all locations in the soil mass is no longer valid.

f) The model borehole behavior and the corresponding interpretation method should be verified with other soils, both resedimented and natural. The challenge with testing natural material is the specimen size, whereas resedimented specimens can be easily prepared from wellbore cuttings obtained during the drilling process.

g) Performing additional cavity expansion tests would provide invaluable insights into the pressuremeter performance and interpretation in clays and soft rock. The pressuremeter is a popular geotechnical in situ testing device, but suffers from serious problems such as overpredicting strength parameters. Executing a comprehensive experimental study that investigates various parameters which are believed to affect the strength and deformation properties obtained from the pressuremeter test (such as soil disturbance, strain rate, etc.) could offer very useful answers.

REFERENCES

Abdulhadi, N.O. (2004) "Triaxial Testing on Reconstituted London Clay," MSc Thesis, Imperial College of Science, Technology and Medicine, University of London.

Abdulhadi, N.O., Akl, S.A., Germaine, J.T., & Whittle, A.J. (2009) "Wellbore Instability Mechanisms in Very Hard Clay," 17th International Conference on Soil Mechanics and Geotechnical Engineering, Egypt, October 2009.

Abdulhadi, N.O., Akl, S.A., Germaine, J.T., & Whittle, A.J. (2009) "Wellbore Instability Mechanisms in Soil: Progress Report June 2006 – September 2008," Report submitted to BP America Inc., Cambridge, MA.

Adams, F.D. (1912) "An Experimental Contribution to the Question of the Depth of the Zone of Flow in the Earth's Crust," Journal of Geology, 20, 97-118.

Ahmed, I. (1990) "Investigation of Normalized Behavior of Resedimented Boston Blue Clay using Geonor Direct Simple Shear," SM Thesis, MIT, Cambridge, MA.

Amorosi, A. & Rampello, S. (2007) "An Experimental Investigation into the Mechanical Behavior of a Structured Stiff Clay," Géotechnique, 57 (2), 153-166.

Anderson, G.R. (1991) "Physical Mechanisms Controlling the Strength and Deformation Behavior of Frozen Sand," ScD Thesis, MIT, Cambridge, MA.

Anderson, W.F., Pyrah, I.C., & Haji-Ali, F. (1987) "Rate Effects in Pressuremeter Tests in Clays," Journal of Geotechnical Engineering, ASCE, 113 (11), 1344-1358.

Anderson, W.F., Pyrah, I.C., Pang, L.S., & Haji-Ali, F. (1988) "The Time Dependent Behavior of Normally Consolidated Clay in Thick Hollow Cylinder Tests," Proceedings of the International Conference on Rheology and Soil Mechanics, Coventry, UK, 204-218.

Aubeny, C.P. (1992) "Rational Interpretation of In Situ Tests in Cohesive Soils," PhD Thesis, MIT, Cambridge, MA.

Aubeny, C.P., Whittle, A.J., & Ladd, C.C. (2000) "Effects of Disturbance on Undrained Strengths Interpreted from Pressuremeter Tests," Journal of Geotechnical and Geoenvironmental Engineering, 126 (12), 1133-1144.

Baguelin, F., Jezequel, J.F., Mee, E.L., & Mehaute, A.L. (1972) "Expansion of Cylindrical Probes in Cohesive Soils," Journal of Soil Mechanics and Foundation Division, ASCE, 98 (11), 1129-1142.

Baguelin, F., Jezequel, J.F., & Shields, D.H. (1978) The Pressuremeter and Foundation Engineering, Trans Tech Pblication.

Bailey, W.A. (1961) "Effects of Salt on the Shear Strength of Boston Blue Clay," SM Thesis, MIT, Cambridge, MA.

Barton, N. (1987) "Predicting the Behavior of Underground Openings in Rock," The 4th Manual Rocha Memorial Lecture, Lisbon, Portugal.

Becker, D.E., Crooks, J.H.A., Been, K., & Jefferies, M.G. (1987) "Work as a Criterion for Determining In-Situ and Yield Stresses in Clays," Canadian Geotechnical Journal, 24 (1), 549-564.

Bell, J.S. & Gough, D.I (1979) "Northeast-Southeast Compressive Stress in Alberta: Evidence from Oil Wells," Earth Planet Sci. Lett., 45, 475-482.

Bellwald, P. (1990) "A Contribution to the Design of Tunnels in Argillaceous Rock," ScD Thesis, MIT, Cambridge, MA.

Bensari, J.E. (1984) "Stress-Strain Characteristics from Undrained and Drained Triaxial Tests on Resedimented Boston Blue Clay," SM Thesis, MIT, Cambridge, MA.

Berman, D.R. (1993) "Characterization of the Engineering Properties of Boston Blue Clay at the MIT Campus," SM Thesis, MIT, Cambridge, MA.

Berre, T. (1992) "Geotechnical Properties of Clay-Shales," Report No. 541082-3. Norwegian Geotechnical Institute.

Berre, T. & Bjerrum, L. (1973) "Shear Strength of Normally Consolidated Clays," Proceedings of the 8th International Conference on Soil Mechanics and Foundation Engineering, Moscow, 1, 39-49.

Bishop, A.W. & Henkel, D.J. (1957) The Measurement of Soil Properties in the Triaxial Test, Edward Arnold LTD, London.

Bishop, A.W., Webb, D.L., & Skinner, A.E. (1965) "Triaxial Tests on Soil at Elevated Cell Pressures," Proceedings of the International Conference of Soil Mechanics, Montreal, 1, 170-174.

Bjerrum, L. (1973) "Problems of Soil Mechanics and Construction on Soft Clays and Structurally Unstable Soils Collapsible, Expansive, and Others," Proceedings of the 8th International Conference on Soil Mechanics and Foundation Engineering, Moscow, 3, 109-159.

Bovee, R.B. (1970) "Analysis of Undrained Plane Strain Shear of Boston Blue Clay," SM Thesis, MIT, Cambridge, MA.

Braathen, N.F. (1966) "Investigation of Effects of Disturbance on Undrained Shear Strength of Boston Blue Clay," SM Thesis, MIT, Cambridge, MA.

Bradley, W.B. (1979) “Failure of Inclined Boreholes,” J. Energy Resour. Technol., Trans. Am. Soc. Mech. Engrs., 101, 232-239.

Burland, J.B. (1990) “On the Compressibility and Shear Strength of Natural Soils,” Géotechnique, 40 (3), 329-378.

Burland, J.B., Rampello, S., Georgiannou, V.N., & Calabresi, G. (1996) “A Laboratory Study of the Strength of Four Stiff Clays,” Géotechnique, 46 (3), 491-514.

Casagrande, A. & Carillo, N. (1944) “Shear Failure of Anisotropic Materials,” Journal of Boston Society of Civil Engineers, 31 (2), 74-87.

Cauble, D.F. (1993) “The Behavior of Resedimented Boston Blue Clay at OCR4 in Cyclic and Post-Cyclic Undrained Direct Simple Shear,” SM Thesis, MIT, Cambridge, MA.

Cauble, D.F. (1993) “An Experimental Investigation of the Behavior of a Model Suction Caisson in a Cohesive Soil,” PhD Thesis, MIT, Cambridge, MA.

Chauhan, S. (1995) “Laboratory Measurements of Load-Transfer in Geosynthetic Reinforced Soils,” PhD Thesis, MIT, Cambridge, MA.

Coop, M.R. & Willson, S.M. (2003) “Behavior of Hydrocarbon Reservoir Sands and Sandstone,” ASCE Journal of Geotechnical and Geoenvironmental Engineering, 129 (1), 1010-1019.

Daemen, J.J.K, & Fairhurst, C. (1971) “Influence of Failed Rock Properties on Tunnel Stability,” Proceedings of 12th US Symposium on Rock Mechanics, New York, 855-875.

Da Re, G. (2000) “Constitutive Modeling of Frozen Sand,” PhD Thesis, MIT, Cambridge, MA.

Deere, D.U. & Miller, R.P. (1966) “Engineering Classification and Index Properties for Intact Rock,” US Air Force System Command, Air Force Weapons Laboratory, Kirtland Air Force Base, New Mexico, Technical Report AFWL-TR-65-116.

DeGroot, D.J. (1989) “The Multidirectional Direct Simple Shear Apparatus with Application to Design of Offshore Arctic Structures,” PhD Thesis, MIT, Cambridge, MA.

Degue, K.M. (1998) “Study of Fracture Mechanics in Saturated Clays,” PhD Thesis, Ecole Ploytechnique, Montreal, Quebec, Canada.

Diab, R. (2001) “Undrained Response of a Saturated Clay by means of Hollow Cylinder Triaxial Tests,” PhD Thesis, Ecole Ploytechnique, Montreal, Quebec, Canada.

Dickey, J.W. (1967) “A Plane Strain Shearing Device for Testing Clays,” SM Thesis, MIT, Cambridge, MA.

Dussaeault, M.B. (1994) "Analysis of Borehole Stability," Proceedings of the Eight International Conference on Computer Methods and Advances in Geomechanics, 3, Rotterdam, Balkema, 125-137.

Edwards, S., Matasutruyu, B, & Willson, S.M. (2004) "Real-Time Imaging of Borehole Failures," SPE/IADC 78946, SPE Drilling & Completion Journal, 19 (4), 236-243.

Ewy, R.T. & Cook, N.G. (1989) "Fracture Processes around Highly Stresses Boreholes," 12th Annual Energy-Sources Technol. Conf. & Exhibition, Drilling Symposium ASME, New York, 63-70.

Ewy, R.T. & Cook, N.G. (1990) "Deformation and Fracture around Cylindrical Openings in Rock: II Initiation, Growth and Interaction of Fractures," Int. J. Rock Mech. Min. Sci. & Geomech. Abstr., 27 (5), 409-427.

Fayad, P.H. (1986) "Aspects of the Volumetric and Undrained Behavior of Boston Blue Clay," SM Thesis, MIT, Cambridge, MA.

Fjaer, E., Holt, R.M., Horsrud, R., Raaen, A.M., & Risnes, R. (2008) Petroleum Related Rock Mechanics, 2nd Edition, Elsevier.

Force, E.A. (1998) "Factors Controlling Pore-Pressure Generation during K_0-Consolidation of Laboratory Tests," SM Thesis, MIT, Cambridge, MA.

Gasparre, A. (2005) "Advanced Laboratory Characterization of London Clay," PhD Thesis, Imperial College of Science, Technology and Medicine, University of London.

Gay, N.C. (1973) "Fracture Growth around Openings in Thick Walled Cylinders of Rock Subjected to Hydrostatic Compression," Int. J. Rock Mech. Min Sci. & Geomech. Abstr., 110, 209-233.

Gens, A (1982) "Stress-Strain and Strength Characteristics of a Low Plasticity Clay," PhD Thesis, Imperial College of Science, Technology and Medicine, University of London.

Germaine, J.T. (1980) "Evaluation of Self-Boring Pressuremeter Tests in Soft Cohesive Soils," SM Thesis, MIT, Cambridge, MA.

Germaine, J.T. (1982) "Development of the Directional Shear Cell for Measuring Cross-Anisotropic Clay Properties," ScD Thesis, MIT, Cambridge, MA.

Germaine, J.T. & Germaine, A.V. (2009) Geotechnical Laboratory Measurements for Engineers, John Wiley and Sons, Inc.

Germaine, J.T. & Ladd, C.C. (1988) "Triaxial Testing of Saturated Cohesive Soils: State of the Art Paper," Advanced Triaxial Testing of Soil and Rock, ASTM STP 977, Philadelphia: ASTM, 421-459.

Gibson, R.E. (1963) "An Analysis of System Flexibility and its Effects on Time-Lag in Pore-Water Pressure Measurements," Géotechnique, 13 (1), 1-11.

Gibson, R.E. & Anderson, W.F. (1961) "In-Situ Measurements of Soil Properties with the Pressuremeter," Civ. Engrg. and Public Works Rev., 56 (658), 615-167.

Gonzalez, J.H. (2000) "Experimental and Theoretical Investigation of Constant Rate of Strain Consolidation," SM Thesis, MIT, Cambridge, MA.

Gutierrez, M., Nygard, R., Hoeg, K., & Berre, T. (2008) "Normalized Undrained Shear Strength of Clay Shales," Engineering Geology, 99, 31-39.

Haimson, B.C. & Herrick, C.G. (1985) "In Situ Stress Evaluation from Borehole Breakouts" Experimental Study," Research and Engineering Applications in Rock Masses, Balkema, Rotterdam, 2, 1207-1218.

Haimson, B.C. & Song, I. (1993) "Laboratory Study of Borehole Breakouts in Cardova Cream: A Case Shear Failure Mechanism," Int. J. Rock Mech. Min. Sci. & Geomech. Abstr., 30, 1047-1056.

Haimson, B.C. & Song, I. (1998) "Borehole Breakouts in Berea Sandstone: Tow Porosity-Dependent Distinct Shapes and Mechanisms of Formation," Rock Mechanics and Petroleum Engineering, 229-238.

Handin, J. (1966) "Strength and Ductility," In Handbook of Physical Constant, Revised ed. (Clark ed). Geol. Soc. Am. Memoir, 79.

Handin, J & Hager, R.V. (1957) "Experimental Deformation of Sedimentary Rocks under Confining Pressure: Tests at Room Temperature on Dry Samples," Bull. Am. Assoc. Petrol. Geol., 41, 1-50.

Hansen, J.B. & Gibson, R.E. (1949) "Undrained Shear Strength of Anisotropically Consolidated Clays," Géotechnique, 1 (3), 189-204.

Hornby, B., Schwartz, L., & Hudson, J. (1994) "Anisotropic Effective Medium Modeling of the Elastic Properties of Shales," Geophysics, 59 (10), 1570-1583.

Horseman, S.T., Winter, M.G., & Entwistle, D.C. (1993) "Triaxial Experiments on Boom Clay," The Engineering Geology of Weak Rock, Balkema, Rotterdam.

Hoskins, E.R. (1969) "The Failure of Thick Walled Hollow Cylinders of Isotropic Rock," Int. J. Rock Mech. Min. Sci., 6, 99-125.

Houlsby, G.T. & Whithers, N. (1988) "Analysis of the Cone Pressuremeter Test in Clay," Géotechnique, 38 (4), 575-587.

Huang, A.B., Holtz, R.D., & Chameau, J-L. (1991) "Laboratory Study of Pressuremeter Tests in Clays," Journal of Geotechnical Engineering, 117 (10), 1549-1567.

Jackson, W.T. (1963) "Stress Paths and Strain in a Saturated Clay," SM Thesis, MIT, Cambridge, MA.

Jamiolkowski, M., Ladd, C.C., Lancellotta, R., & Germaine, J.T. (1985) "New Developments in Field and Laboratory testing of Soils," Proceedings of 11th International Conference on Soil Mechanics and Foundation Engineering, San Francisco, 57-153.

Johnston, I.W. & Novello, E.A. (1994) "Soil Mechanics, Rock Mechanics and Soft Rock Technology," Proceedings of Institution of Civil Engineers, Geotechnical Engineering, 107, 3-9.

Juan, A. & BenSaid, M.A. (1987) "Cavity Expansion Tests in a Hollow Cylinder Cell," Geotechnical Testing Journal, 10 (4), 203-212.

Kavvadas, M. (1982) "Non-linear Consolidation around Driven Piles in Clays," ScD Thesis, MIT, Cambridge, MA.

Kenny, T.C. (1964) "Sea-Level Movements and the Geologic Histories of the Postglacial Marine Soils at Boston, Nicolet, Ottawa and Oslo," Géotechnique, 14 (3), 203-230.

King, L.V. (1912) "On the Limiting Strength of Rocks under Conditions of Stress Existing in the Earth's Interior," Journal of Geology, 21, 119-138.

Kinner, E.B. (1970) "Load-Deformation Behavior of Saturated Clay during Undrained Shear," ScD Thesis, MIT, Cambridge, MA.

Koutsoftas, D.C. & Ladd, C.C. (1985) "Design Strengths for an Offshore Clay," ASCE, Journal of Geotechnical Engineering Division, 111 (3), 337-355.

Kutter, H.K. & Rehse, H. (1996) "Laboratory Investigations of Factors Affecting Borehole Breakouts," Proceedings of Eurock96, Balkema, Rotterdam, 751-758.

Ladanyi, B. (1972) "In-Situ Determination of Undrained Stress-Strain Behavior of Sensitive Clays with the Pressuremeter," Canadian Geotechnical Journal, Ottawa, 9 (3), 313-319.

Ladd, C.C. (1960) "Stress-Strain Behavior of Saturated Clay and Basic Strength Principles," Research Report R64-17, Research on Earth Physics, Department of Civil Engineering, MIT, Cambridge, MA.

Ladd, C.C. (1964) "Stress-Strain Behavior of Saturated Clay and Basic Strength Principles," Research Report R65-17, Research on Earth Physics, Department of Civil Engineering, MIT, Cambridge, MA.

Ladd, C.C. (1991) "Stability Evaluation during Staged Construction," ASCE, Journal of Geotechnical Engineering, 117 (4), 540-615.

Ladd, C.C. & Foott, R. (1974) "New Design Procedure for Stability of Soft Clays," Journal of the Geotechnical Engineering Division, ASCE, 100 (7), 763-786.

Ladd, C.C., Foott, R., Ishihara, K., Schlosser, F., & Poulos, H.G. (1977) "Stress-Deformation and Strength Characteristics, State of the Art Report," Proceedings of the 9th International Conference of Soil Mechanics and Foundation Engineering, Tokyo, 2, 421-494.

Ladd, C.C., Germaine, J.T., Baligh, M.M., & Lacasse, S. (1979) "Evaluation of Self-Boring Pressuremeter Tests in Sensitive Clays," Research Report R79-A, Department of Civil Engineering, MIT, Cambridge, MA.

Ladd, C.C., Germaine, J.T., Baligh, M.M., & Lacasse, S. (1980) "Evaluation of Self-Boring Pressuremeter Tests in Boston Blue Clay," Report No. FHWA/RD-80/052, Federal Highway Administration, Washington D.C.

Ladd, C.C. & Lambe, T.W. (1963) "The Strength of Undisturbed Clay Determined from Undrained Tests," Symposium on Laboratory Shear Testing of Soils, ASTM STP. 361, 342-371.

Ladd, C.C. & Varallyay, J. (1965) "The Influence of Stress System on the Behavior of Saturated Clays during Undrained Shear," Research Report R65-11, Soil Publication No. 177, Department of Civil Engineering, MIT, Cambridge, MA.

Ladd, C.C., Young, G.A., Kraemer, S.R., & Burke, D.M. (1998) "Engineering Properties of Boston Blue Clay from Special Testing Program," Geo-Congress 1998, ASCE National Convention, Boston, October.

Ladd, R.S. (1965) "Use of Electrical Pressure Transducers to Measure Soil Pressure," Research Report R65-48, No. 80, Department of Civil Engineering, MIT, Cambridge, MA.

Lambe, T.W. (1951) Soil Testing for Engineers, John Wiley and Sons, New York.

Lambe, T.W. & Whitman, R.V. (1969) Soil Mechanics, John Wiley and Sons, New York.

Leddra, M.J., Petley, D.N., & Jones, M.E. (1991) "Fabric Changes Induced in a Cemented Shale through Consolidation and Shear," Rock Mechanics, Balkema, Rotterdam, 917-926.

Malek, A.M. (1987) "Cyclic Behavior of Clay in Undrained Simple Shearing and Application to Offshore Tension Piles," PhD Thesis, MIT, Cambridge, MA.

Marsden, J.R., Holt, R.M., Nakken, S.J., Raaen, A.M. (1992) "Mechanical and Petrophysical Characterization of Highly Stress Mudstones," Proceedings of Eurock 92 Conference, Balkema, Rotterdam, 51-56.

Marsden, J.R., Dennis, J.W., & Wu, B. (1996) "Deformation and Failure of Thick-Walled Hollow Cylinders of Mudrock: A Study of Wellbore Instability in Weak Rock," Proceedings of Eurock 96 Conference, Balkema, Rotterdam, 759-766.

Martin, R.T. (1970) "Suggested Method of Test for Determination of Soluble Salts in Soil," ASTM STP 476, 288-290.

Mastin, L.G. (1984) "The Development of Wellbore Breakouts in Sandstone," MSc Thesis, Stanford University, CA.

Mesri, G. & Castro, A. (1987) "C_α/C_c Concept and K_0 during Secondary Compression," Journal of the Geotechnical Engineering Division, ASCE, 113 (3), 230-247.

Mitchell, J.K. & Soga, S. (2005) Fundamentals of Soil Behavior, 3rd Edition, John Wiley and Sons, Inc.

Moniz, S. R. (2009) "The Influence of Effective Consolidation Stress on the Normalized Extension Strength Properties of Resedimented Boston Blue Clay," MEng Thesis, MIT, Cambridge, MA.

Nadai, A. (1950) Theory of Flow and Fractures of Solids, McGraw-Hill Book Company, Inc., New York.

Nakken, S.J., Christensen, T.L., Marsden, J.R., & Holt, R.M. (1989) "Mechanical Behavior of Clays at High Stress Levels for Wellbore Stability Applications," Proceedings of International Conference on Rock at Great Depth, Pau, France, 2, 141-148.

O'Niell, D. (1985) "Undrained Strength Anisotropy of an Overconsolidated Thixotropic Clay," SM Thesis, MIT, Cambridge, MA.

Ortega, O.J. (1992) "Computer Automation of the Consolidated-Undrained Direct Simple Shear Test," SM Thesis, MIT, Cambridge, MA.

Palmer, A.C. (1972) "Undrained Plane-Strain Expansion of Cylindrical Cavity in Clay: A Simple Interpretation of the Pressuremeter Test," Géotechnique, 22 (3), 451-457.

Palmer, A.C. & Mitchell, R.J. (1972) "Plane-Strain Expansion of a Cavity in Clay," Proceedings of the Roscoe Memorial Symposium on Stress-Strain Behavior of Soils, Cambridge, 588-599.

Paterson, M.S. (1978) Experimental Rock Deformation: The Brittle Field, Springer Verlog, Beilin.

Pestana, J.M. (1994) "A Unified Constitutive Model for Clays and Sands," ScD Thesis, MIT, Cambridge, MA.

Pestana, J.M. & Whittle, A.J. (1995) "Compression Model for Cohesionless Soils," Géotechnique, 45 (4), 611-633.

Peley, D.N. (1994) "The Deformation of Mudrocks," PhD Thesis, University of London.

Petley, D.N. (1999) "Failure Envelopes of Mudrocks at High Confining Pressures," Geological Society, London, Special Publication 1999, 158, 61-71.

Penumadu, D. & Chameau, J-L (1997) "Strain Rate Effects in Model Pressuremeter Testing," Journal of Geotechnical and Geoenvironmental Engineering, ASCE, 123 (11), 1051-1059.

Penumadu, D. & Chameau, J-L (1999) "Interpretation of Model Pressuremeter Test Using Automated Clay Calibration Chamber Data," Geotechnical Testing Journal, 21 (1), 18-30.

Preston, W.B. (1965) "The Effects of Sample Disturbance on the Undrained Strength Behavior of Boston Blue Clay," SM Thesis, MIT, Cambridge, MA.

Prevost, J.H. & Hoeg, K. (1975) "Analysis of the Pressuremeter in Strain-Softening Soil," J. Geotech. Engrg. Div., ASCE, 101 (8), 717-732.

Rixner, J.J. (1967) "The Influence of Plane Strain Conditions on the Strength Behavior of Saturated Clay," SM Thesis, MIT, Cambridge, MA.

Robertson, E.C. (1955) "Experimental Study of the Strength of Rocks," Bull. Geol. Soc. Am., 66, 1275-1314.

Roscoe, K.H. & Burland, J.B. (1968) "On the Generalized Stress-Strain Behavior of 'Wet' Clay," in Engineering Plasticity, Cambridge University Press, 535-609.

Santagata, M.C. (1994), "Investigation of Sample Disturbance in Soft Clays Using Triaxial Element Tests," SM Thesis, MIT, Cambridge, MA.

Santagata, M.C. (1998), "Factors Affecting the Initial Stiffness and Stiffness Degradation of Cohesive Soils," PhD Thesis, MIT, Cambridge, MA.

Santarelli, F.J. (1987) "Theoretical and Experimental Investigation of the Stability of the Axisymmetric Wellbore," PhD Thesis, Imperial College of Science, Technology and Medicine, University of London.

Santarelli, F.J. & Brown, E.T. (1989) "Failure of Three Sedimentary Rocks in Triaxial and Hollow Cylinder Compression Tests," Int. J. Rock Mech. Min. Sci. & Geomech. Abstr., 26 (5), 401-413.

Schmidt, B. (1966) Discussion of "Earth Pressure at Rest Related to Stress History," Canadian Geotechnical Journal, 3 (4), 239-242.

Schofield, A.N. & Wroth, C.P. (1968) Critical State Soil Mechanics, McGraw-Hill.

Seah, T.H. (1990) "Anisotropy of Resedimented Boston Blue Clay," ScD Thesis, MIT, Cambridge, MA.

Sheahan, T.C. (1988) "Modification and Implementation of a Computer Controlled Triaxial Apparatus," SM Thesis, MIT, Cambridge, MA.

Sheahan, T.C. (1991) "An Experimental Study of the Time-Dependent Undrained Shear Behavior of Resedimented Clay Using Automated Stress-Path Triaxial Equipment," ScD Thesis, MIT, Cambridge, MA.

Sheahan, T.C. & Germaine, J.T. (1992) "Computer Automation of Conventional Triaxial Equipment," Geotechnical Testing Journal, 15 (4), 311-322.

Sheahan, T.C., Ladd, C.C., & Germaine, J.T. (1996) "Rate-Dependent Undrained Shear Behavior of Saturated Clay," Journal of Geotechnical Engineering, ACSE, 122 (2), February, 99-108.

Silvestri, V. (1998) "On the Determination of the Stress-Strain Curve of Clay from Undrained Plane-Strain Expansion of Hollow Cylinders: A Long Forgotten Method," Canadian Geotechnical Journal, 35 (2), 360-363.

Silvestri, V. & Diab R. (2001) "Stress Distributions and Paths in Clays During Pressuremeter Tests," Canadian Geotechnical Journal, 13 (3) 243-249.

Silvestri, V., Diab, R., & Ducharme, A. (2005) "Development of a New Hollow Cylinder Triaxial Apparatus for the Study of Expansion Tests in Clays," Geotechnical Testing Journal, 28 (3). 1-9.

Sinfield, J.V. (1994) "An Experimental Investigation of Sampling Disturbance Effects in Resedimented Boston Blue Clay," SM Thesis, MIT, Cambridge, MA.

Steiger, R.P. & Leung, P.K. (1988) "Quantitative Determination of the Mechanical Properties of Shales," Proceedings of 63rd Ann. Tech. Conf. and Exhib., Houston, TX, 67-76, SPE Paper 18024.

Steiger, R.P. & Lueng, P.K. (1989) "Prediction of Wellbore Stability in shale Formations at Great Depth," Proceedings of International Conference on Rock at Great Depth, Pau, France, 3, 1209-1218.

Steiger, R.P. & Lueng, P.K. (1991) "Critical State Shale Mechanics," Proceedings of 32nd US Symposium on Rock, 293-302.

Swan, C. (1994) "Physical Mechanisms Controlling the Deformation and Strength Behavior of Unfrozen and Frozen Manchester Fine Sand," ScD Thesis, MIT, Cambridge, MA.

Taylor, R.N. & Coop, M.R. (1993) "Stress Path Testing of Boom Clay from Mol, Belgium," The Engineering Geology of Weak Rock, Balkema, Rotterdam, 77-82.

Terzaghi, K. & Peck, R.B. (1948) Soil Mechanics in Engineering Practice, John Wiley and Sons, Inc.

Ting, N.A. (1990) "Effects of Disturbance on Consolidation with Vertical Drains," SM Thesis, MIT, Cambridge, MA.

Varallyay, J. (1964) "The Influence of Stress System Variables on the Undrained Strength of Boston Blue Clay," SM Thesis, MIT, Cambridge, MA.

Walbaum, M. (1998) "Procedure for Investigation of Sample Disturbance using the Direct Shear Apparatus," SM Thesis, MIT, Cambridge, MA.

Whittle, A.J. (1987) "A Constitutive Model for Overconsolidated Clays with Application to the Cyclic Loading of Friction Piles," ScD Thesis, MIT, Cambridge, MA.

Whittle, A.J., DeGroot, D.J., Ladd, C.C., & Seah, T-H (1994) "Model Prediction of the Anisotropic Behavior of Boston Blue Clay," Journal of Geotechnical Engineering, ACSE, 120 (1), 199-224.

Whittle, A.J. & Kavvadas, M. (1994) "Formulation of the MIT-E3 Constitutive Model for Overconsolidated Clays," ASCE Journal of Geotechnical Engineering, 120 (1), 173-198.

Windle, D. & Wroth, C.P. (1977) "The Use of a Self-Boring Pressuremeter to Determine the Undrained Properties of Clays," Ground Engineering, September, 37-46.

Wissa, A.E.Z. (1961) "A Study of the Effects of Environmental Changes on the Stress-Strain Properties of Kaolinite," SM Thesis, MIT, Cambridge, MA.

Wissa, A.E.Z., Christian, J.T., Davis, E.H., & Heiberg, S. (1971) "Consolidation at Constant Rate of Strain," Journal of Soil Mechanics and Foundation, ASCE, Vol. 97, No. SM10, 1393-1413.

Wu, B. (1991) "Investigations into the Mechanical Behavior of Soft Rocks," PhD Thesis, Imperial College of Science, Technology and Medicine, University of London.

Wu, B., Marsden, J.R., & Hudson, J.A. (1990) "Undrained Mechanical Behavior of Mudstones," Proceedings of 26th Ann. Conf. Eng. Group of Geol. Soc., Leeds, 105-114.

Yamamuro, J.A. & Lade, P.V. (1996) "Drained Sand Behavior in Axisymmetric Tests at High Pressures," ASCE Journal of Geotechnical Engineering, 122 (2), 109-119.

Yassir, N. A. (1989) "Mud Volcanoes and the Behavior of Overpressured Clays and Silts," PhD Thesis, University College London, University of London.

Yu, H.S. & Rowe, R.K. (1999) "Plasticity Solutions for Soil Behavior around Contracting Cavities and Tunnels," International Journal for Numerical and analytical Methods in Geomechanics, 23, 1245-1279.

Zoback, M.D., Moos, D., Mastin, L., & Anderson, R.N. (1985) "Wellbore Breakout and In Situ Stress," Journal of Geophys. Res., 90, B7, 5523-5530.

Zreik, D.A. (1994) "Behavior of Cohesive Soils and their Drained, Undrained, and Erosional Strengths at Ultra-Low Stresses," PhD Thesis, MIT, Cambridge, MA.

APPENDIX A

AUTOMATION SOFTWARE FOR HIGH PRESSURE TRIAXIAL TESTING SYSTEM FOR COHESIVE SOIL

```
  'rev 6.2 6/12/08 jtg modifications to PID control
  'rev 6.1 9/4/07 jtg add PID control
  'rev 5.3 5/17/06 change to work with clamp configuration
  'rev 5.2 7/25/05 small edits to make consistent
  'rev 5.1 this has a pressure sensitivity zero adjustment to the internal LC
  'rev 5.0  10/24/00   jtg  major rehaul of the basic program
  'rev 4.0 8/1/00  jtg   converted to quickbasic
  'rev 3.1  8/06/91  jtg
  '
  '  Revision 1 written by Tom Sheahan to control stepper motors.
  '  Revision 2 written by Jack germaine to control dc servo motors.
  '
  ' ****************************************************************
  '
  ' The following hardware is required:
  '        -Strawberrytree d to a converter
  '        -The Sheahan a to d converter
  '        -The MIT three axis dc controller box with;
  '           -channel 1 for axial force
  '           -channel 2 for cell pressure
  '           -channel 3 for pore pressure

  ' Relay switches are used for the following
  '        -1 is to turn off motor 1
  '        -2 is to turn off motor 2
  '        -3 is to turn off motor 3
  '        -4 is to reverse the direction of motor 1 when using the 352 controller
  '        -5 is to turn on and off the input voltage relay


  '***  Information shared with the setup program    ****

   COMMON FILENAME$, DAT$, INITIALS$, TYPE$, WEIGHT, H0, A0, PISTAREA
   COMMON MEMBRANE$, FILTER, AREACORR$, ZLOAD, CFLOAD, ZDCDT, CFDCDT
   COMMON ZCELL, CFCELL, ZPORE, CFPORE, ZVOLDCDT, CFVOLDCDT, LOADCHANNEL
   COMMON DCDTCHANNEL, CELLCHANNEL, PORECHANNEL, VOLDCDTCHANNEL, DUMMY1
   COMMON DUMMY2, VINCHANNEL

    DIM CELL(25), Axial(25), BACK(25), time(25), VOLTS(10)
    DIM MFLAG$(3), control!(3), SGAIN(3), DGAIN(3), mvolts(3), ZVOLTS(3), Amp(6)
    DIM k(3, 5, 2), e(3, 3), mdir(3)

'   ****************************************************************
    AD1170$ = "N"    'used as flag to allow debugging the program
    AD1170$ = "Y"    'comment this line out when card is not in machine
'   ****************************************************************
    MOTOR1$ = "Y"    'use this setting when using reversing relay on motor1
    MOTOR1$ = "N"    'default condition when not using the relay

'***** Constants which are used throughout the program *****
    rev$ = "6.1"
    blk$ = SPACE$(60)                              'line eraser
    H1$ = "TRANSDUCER READINGS in volts"
    H2$ = "      disp      cell      load      pore      volume    input"
    H3$ = "A.Stress       Cell       Back   A.Strain   V.Strain"
    H4$ = "    ksc        ksc        ksc         %          %"
    P1$ = "####.#": P2$ = "###.##": P3$ = "##.###"

    V0 = A0 * H0                  'initial volume
    VINREAD = 10                  'period to read vin & update screen
    VINFLAG = VINREAD             'input voltage counter
    Refreshrate = 3               'number of readings between updating screen
    STEPTIME = 1                  'time for each motor step in sec.
```

```
' ****** Set up function keys and be sure keyboard is set correctly ***
    CLS
    X = 1
    GOSUB 3890                          'lock out keyboard
260 GOSUB 4160                          'set enter key
270 A$ = INKEY$
    IF ENTERFLAG = 1 THEN GOTO 340
    IF A$ <> CHR$(13) THEN GOTO 270
    CLS
    LOCATE 15 + 2 * X, 2
    PRINT "turn off both the NUMBER LOCK and CAPS LOCK keys"
    PRINT "              and"
    X = X + 1
    GOTO 260

340 CLS
    LOCATE 10, 5
    PRINT "This will take two seconds"
    GOSUB 3750                          'calibrate steptime


 '************* SET UP GAINS, ARRAYS, VARIABLES AND CURRENT READINGS *******

    ' set the  A/D converter up and define performance variables
    INTTIME = 21  'to specify the integraion time of the A/D converter
                  'inttime=16+N where N=0   1 msec      N=4  100 msec
                  '                  N=1  10 msec      N=5  166.7 msec
                  '                  N=2  16.7 msec    N=6  300 msec
                  '                  N=3  20 msec
                  ' can set a variable integration time using the EIS command
    INTBIT = 13   ' specify the bit precision    INTBIT=(bit precision-7)
    AD1170 = 768  ' the decimal I/O address of the A/D converter
    MUX! = 776    ' decimal I/O of channel selecter
    '                CORRESPONDS TO SWITCH SETTING 00001

 '******* set default values and flags   *****

    row = 2             ' for what
    Tadjust = 0         ' to adjust time for a change in date during test
    ENTERFLAG = 0       ' for breaking a loop on the enter key
    NUMCHANNELS = 6     ' for input channel loop for data acq card
    MAXINCS = 25        ' for saturation steps
    STARTDATE$ = DATE$  ' get todays date for rate calculations
    GNDCHANNEL = 15     ' location of the ground connection on ad card
    REFCHANNEL = 14     ' location of the 5 volt reference voltage on A/D card
    tolerance = .1      ' stress (ksc) condition to move to next step
    feedback = 0        ' variable to specific equations used to computer error

    GOSUB 10000                 'this sets up the A/D card

'   ************* Setup the DC servo motors *********************

    motors! = 6928              'decimal I/O address of analog out card
    STOPDEVICE! = 0             'varible to specify motors to stop;0=all
    OUT motors! + 4, 0          'open relays and lock all motors

    '******* specify the gain values to control the motors  *****

    FOR i = 1 TO 3                 'k(motor,constant,control type)
    FOR j = 1 TO 4                 'constant=0 step control (1sec)
    k(i, j, 0) = 0                 '        =1 porportional
    NEXT j                         '        =2 differential
```

```
    NEXT i                          '        =3 integration
                                    '        =4  memory

    k(1, 0, 1) = 1   'volt-sec/kg '
    k(1, 1, 1) = .1                '
    k(1, 2, 1) = -.05               ' control type=0 off
    k(1, 3, 1) = .05               '             =1 pressure
    k(1, 4, 1) = .9                 '             =2 displacement
    k(2, 0, 1) = 10   'v-s/ksc   '
    k(2, 1, 1) = .04                '      motor=1  axial
    k(2, 2, 1) = -.03                      '     =2  cell
    k(2, 3, 1) = .1                        '     =3  pore
    k(2, 4, 1) = .8
    k(3, 0, 1) = 1   'v-s/ksc
    k(3, 1, 1) = 1
    k(3, 2, 1) = 0
    k(3, 3, 1) = 0
    k(3, 4, 1) = 0
    k(1, 0, 2) = .0000203  'v-s/cm
    k(1, 1, 2) = 25
    k(1, 2, 2) = -25
    k(1, 3, 2) = 20
    k(1, 4, 2) = .9
    k(2, 0, 2) = 10   'v-s/cm3
    k(2, 1, 2) = 10
    k(2, 2, 2) = 0
    k(2, 3, 2) = 0
    k(2, 4, 2) = 0
    k(3, 0, 2) = .2   'v-s/cm3
    k(3, 1, 2) = .2
    k(3, 2, 2) = 0
    k(3, 3, 2) = 0
    k(3, 4, 2) = 0

'****************** Hardware settings for the interface **************

    Amp(1) = 1                 'amplifier gains on the ad524 by channel
    Amp(2) = 10
    Amp(3) = 10
    Amp(4) = 10
    Amp(5) = 1
    Amp(6) = 1

    DEVICE!(1) = 14               'set motor 1 to axial
    DEVICE!(2) = 13               'set motor 2 to cell
    DEVICE!(3) = 11               'set motor 3 to pore

    mdir(1) = -1                 'program assumes positive sign convention
    mdir(2) = -1                 'so a positive voltage causes increase stress
    mdir(3) = -1                 'and positive strain.  mdir reverses the
                                'convention to account for wiring changes

    ZVOLTS(1) = 0               'voltage offset to stop each motor
    ZVOLTS(2) = 0
    ZVOLTS(3) = 0

    control!(1) = 0               'set axial to off  1=stress, 2=disp
    control!(2) = 0               'set cell to off
    control!(3) = 0               'set pore to off

    Mode(1) = 0                   'determines method of control
    Mode(2) = 0                   '    0=step
    Mode(3) = 0                   '    1=continuous open loop
```

```
                                '    2=continuous PID loop

    Reverse(1) = 0              'prevents the motor from moving in both directions
    Reverse(2) = 0              '  =0 to allow only one direction
    Reverse(3) = 0              '  =1 to allow motion is both directions


    LDZgrad = 0'    .00748 / 5.5    'pressure sensitivity of load zero to cell
pressure



  '*** Reminders to set up the load frame for testing ****


    PRINT "Ensure that "
    PRINT "      -the loadframe lever is down and in the fine position"
    PRINT "      -the coarse wheel moves freely"
    PRINT "      -the back pressure valves are closed"
    PRINT "      -the gear selector is in position 'C'"
    PRINT "      -and the control box is on "
    PRINT
    PRINT "   This is program revision "; rev$
    IF AD1170$ = "N" THEN PRINT "  The AD1170 card is DISABLED"
    IF MOTOR1$ = "Y" THEN PRINT "   The reversing switch for motor 1 is ENABLED"
    INPUT "    press ENTER to continue ", A$

  ' ******  Collect a set of readings and set the target values ****
    GOSUB 3260              'get set of readings
     newcell = CELL         'set target values
     newback = BACK
     newLoad = lode

    '*************************************************************
890 '*****  This is the starting point of the control program *****
    '*************************************************************
    control(1) = 1  'needed to print target values on screen
    control(2) = 1
    control(3) = 1

    feedback = 0
    CLS : GOSUB 4463                    'data set and basic screen
    GOSUB 3880                          'turn off motors and zero control
    PRINT
    PRINT "Please select the next phase of test;": PRINT
    PRINT " 1. Undrained Hydrostatic Initial Stress   7. Ko Consolidation"
    PRINT " 2. Drained Hydrostatic Stress Change      8. Stress Path Consolidation"
    PRINT " 3. Hold Current State of Stress           9. Undrained Shear"
    PRINT " 4. Hold Target State of Stress           10. Sample Disturbance
Simulation"
    PRINT " 5. Enter New Target State of Stress      11. End Program"
    PRINT " 6. Measure 'B' Value"
900 LOCATE 19, 1: PRINT blk$
    LOCATE 19, 1: INPUT "     Enter OPTION number ", CHOICE$
    CH = VAL(CHOICE$)
    IF CH < 1 OR CH > 11 THEN GOTO 900
    ON CH GOTO 930, 1100, 2040, 2050, 2060, 2140, 4700, 6200, 7210, 8500, 2100

    '*********************************************************************
930 '************** PRESSURE-UP TO GET INITIAL EFFECTIVE STRESS ***********
    '*********************************************************************

    control(1) = 1          'stress control
```

```
    control(2) = 1           'stress control
    control(3) = 0           'turned off
    Mode(1) = 0
    Mode(2) = 0                'off between steps
    Mode(3) = 0
    Reverse(1) = 0
    Reverse(2) = 0
    Reverse(3) = 0
    feedback = 1

    KEYFLAG = 0
    LOCATE 23, 1: PRINT blk$
    PRINT "NOTE-Be sure the back pressure valves are closed"
960 INPUT "Initial pressure-up desired (yes or no) ? ", Z$
    IF Z$ = "YES" OR Z$ = "yes" THEN GOTO 990
    IF Z$ = "no" OR Z$ = "NO" THEN GOTO 890 ELSE GOTO 960
990 CLS : GOSUB 4463               'read & basic screen
     LOCATE 16, 1
     INPUT "What cell pressure should be applied (ksc) ? ", newcell
     LOCATE 16, 1: PRINT SPACE$(65)
     INPUT "What deviator load should be applied (kg ) ? ", newLoad
     KEY(1) ON: ON KEY(1) GOSUB 2600

     CLS : LOCATE 25, 1: PRINT blk$
     LOCATE 25, 1: PRINT "<F1> TO END PRESSURE UP";
     LOCATE 25, 65: COLOR 0, 7: PRINT "PRESSURE UP"; : COLOR 3, 8
     GOSUB 4450                          'print screen
     PTRFLAG! = 1

     WHILE (KEYFLAG <> 1)
         GOSUB 2720
     WEND

     GOSUB 3880                      'stop motors and lock relays

     GOTO 890                        ' return home

     '*****************************************************************
1100 '************* DRAINED STRESS STEP APPLICATION *******************
     '*****************************************************************
    control(1) = 1           'stress control
    control(2) = 1           'stress control
    control(3) = 1           'stress control
    Mode(1) = 0
    Mode(2) = 0                'off between steps
    Mode(3) = 0
    Reverse(1) = 0
    Reverse(2) = 0
    Reverse(3) = 0
    feedback = 1

1140 CLS : GOSUB 4465                'readings and basic screen
1150 PRINT
     R = CSRLIN
     LOCATE 23, 1: PRINT blk$
     COLOR 0, 7
     LOCATE R, 11
     PRINT "DRAINED CONSOLIDATION STRESS INCREMENTS"
     COLOR 3, 8
     PRINT "For each STRESS STEP specify the CELL PRESSURE, AXIAL STRESS, BACK
PRESSURE and DURATION"
     PRINT "Enter a '99' for cell pressure when finished."
     PRINT "Enter a '999' for cell pressure to return to MAIN MENU"
```

```
     NUMINCS = 0
     FOR i = 1 TO MAXINCS
       CELL(i) = -1
       Axial(i) = -1
       BACK(i) = -1
       time(i) = -1
     NEXT i
     PRINT "Increment #"; TAB(18); "Cell"; TAB(34); "Axial"; TAB(46); "Back"; TAB(60);
"Time (minutes)"

1250 WHILE (CELL(NUMINCS) <> 999 AND CELL(NUMINCS) <> 99 AND NUMINCS <> MAXINCS)
         NUMINCS = NUMINCS + 1
         row = CSRLIN
         IF row < 24 THEN GOTO 1360
            i = 23 - NUMINCS
            LOCATE 17, 1
            FOR row = 17 TO 22
            PRINT row - i; TAB(18); CELL(row - i); TAB(34); Axial(row - i); TAB(46);
BACK(row - i); TAB(60); time(row - i)
            NEXT row
            PRINT SPACE$(70)

1360     LOCATE row, 1: PRINT NUMINCS; TAB(20); : INPUT CELL(NUMINCS)
         IF CELL(NUMINCS) < 0 THEN 1360
         IF CELL(NUMINCS) = 99 THEN 1250  'Finished entering data
         IF CELL(NUMINCS) = 999 THEN 1250  'Finished entering data
1370     LOCATE row, 34: PRINT ""; : INPUT Axial(NUMINCS)
         IF Axial(NUMINCS) < 0 THEN GOTO 1370
1380     LOCATE row, 46: PRINT ""; : INPUT BACK(NUMINCS)
         IF BACK(NUMINCS) < 0 THEN 1380
         IF BACK(NUMINCS) > CELL(NUMINCS) THEN 1380
         IF BACK(NUMINCS) > Axial(NUMINCS) THEN 1380
1390     LOCATE row, 60: PRINT ""; : INPUT time(NUMINCS)
         IF time(NUMINCS) < 1 THEN 1390
         IF NUMINCS = MAXINCS THEN PRINT "Max # increments ="; MAXINCS: GOTO 1250
       WEND
        IF CELL(NUMINCS) = 99 THEN NUMINCS = NUMINCS - 1
        IF CELL(NUMINCS) = 999 THEN GOTO 890

     CLS : PRINT
     PRINT "Increment #"; TAB(18); "Cell"; TAB(34); "Axial"; TAB(46); "Back"; TAB(60);
"Time (minutes)"
     FOR i = 1 TO NUMINCS
         PRINT i; TAB(20); CELL(i); TAB(34); Axial(i); TAB(46); BACK(i); TAB(60);
time(i)
         time(i) = time(i) * 60
     NEXT i
     LOCATE 24, 1
1550 INPUT "Is this schedule okay (yes or no) ?"; A$
     IF A$ = "yes" OR A$ = "YES" THEN 1560
     IF A$ = "NO" OR A$ = "no" THEN GOTO 1100
     GOTO 1550

1560 FOR i = 1 TO NUMINCS                          'convert to loads
        Axial(i) = (Axial(i) - CELL(i)) * area
     NEXT i

1600 ' ********** APPLY THE DRAINED STRESS INCREMENTS *****************


1650 INCR = 1                         ' loop to apply the large increments

1660 CLS : GOSUB 4450                   'readings & basic screen
```

```
     PTRFLAG! = 1
       GOSUB 4160                       'enter flag for next inc
       GOSUB 4290                       'esc flag to abort inc
       LOCATE 25, 55: COLOR 0, 7: PRINT "STRESS APPLICATION"; : COLOR 3, 8
       OLDCELL = CELL: OLDBACK = BACK: OLDLODE = lode
       LOCATE 16, 57: PRINT "Increasing Pressure "
       LOCATE 18, 57: PRINT "of Increment "; INCR
       DCELL = (CELL(INCR) - CELL) / 10
       DBACK = (BACK(INCR) - BACK) / 10
       DLODE = (Axial(INCR) - lode) / 10
       t0 = TIMER: Tadjust = 0      'set the start time for the increment
       Lasttime = t0
       Deltime = 0
       newcell = OLDCELL: newback = OLDBACK
       newLoad = lode

     '++++++ This section is the minor increment loop +++++++

       CTR = 0
       WHILE (ENTERFLAG = 0 AND CTR <> 10)   'Loop to apply the split increment
         CTR = CTR + 1
         LOCATE 17, 57: PRINT "for Step "; CTR
         newcell = newcell + DCELL
         newback = newback + DBACK
         newLoad = newLoad + DLODE
         IF CTR = 10 THEN
            newcell = CELL(INCR)
            newback = BACK(INCR)
            newLoad = Axial(INCR)
         END IF
1770       GOSUB 2720
           IF ENTERFLAG <> 0 THEN GOTO 1800
           IF ABS(CELL - newcell) > tolerance THEN GOTO 1770   'tolerance check
           IF ABS(BACK - newback) > tolerance THEN GOTO 1770
           IF ABS(lode - newLoad) > tolerance * area THEN GOTO 1770
1800   WEND

      '++++ This section continously monitors cell, pore and load

        IF ENTERFLAG <> 0 THEN GOTO 1960
        LOCATE 16, 57: PRINT "Holding pressure    "
        WHILE (Deltime <= time(INCR) AND ENTERFLAG = 0)
             GOSUB 2720
             now = TIMER
             IF now < Lasttime THEN Tadjust = Tadjust + 86400
             Deltime = now - t0 + Tadjust
             Lasttime = now
             LOCATE 17, 57
             T! = INT(Deltime / 60)
             PRINT "for "; T!; " of "; INT(time(INCR) / 60); " MIN"
        WEND

1960  'Process the end of increment

      IF ENTERFLAG <> 1 THEN GOTO 1970         'not enter key
         ENTERFLAG = 0
         KEY(19) ON: KEY(20) ON                'reset keys
         GOTO 2010                             'next inc
1970  IF ENTERFLAG = 2 THEN GOTO 2015          'abort the mission
         GOSUB 2150                            'Do a B-value check
         control(3) = 1                        'return to stress control
         GOSUB 2720
```

```
2010  IF INCR = NUMINCS THEN GOTO 2050         'goto hold stress
        INCR = INCR + 1
        GOTO 1660                              'continue to next increment

2015 '**** manage action on abort increment ****

     KEY(19) OFF: KEY(20) OFF
     GOSUB 3880                  'close relays
     GOTO 890                    'return to main menu

     '*************************************************************
2040 '******* HOLD CURRENT STRESS SUBROUTINE ************************
     '*************************************************************

     strainrate = 0   'allows axial motor to move in both directions

2042 newback = BACK   'enter if all new values but limit motor direction
2044 newcell = CELL
2046 newLoad = lode


     '*************************************************************
2050 '******* HOLD EXISTING TARGET STATE OF STRESS SUBROUTINE ********
     '*************************************************************

    control(1) = 1           'stress control
    control(2) = 1           'stress control
    control(3) = 1           'stress control
    Mode(1) = 0
    Mode(2) = 0                'off between steps
    Mode(3) = 0
    Reverse(1) = Reverse(1)
    Reverse(2) = 0
    Reverse(3) = 0
    feedback = 1

2053 CLS : GOSUB 4450            'enter using existing control settings
2055 PTRFLAG! = 1
     GOSUB 4290

     LOCATE 25, 65: COLOR 0, 7: PRINT "HOLD STRESS"; : COLOR 3, 8
     t0 = TIMER
     Tadjust = 0
     Lasttime = t0
       WHILE (ENTERFLAG = 0)
          GOSUB 2720
          now = TIMER
          IF now < Lasttime THEN Tadjust = Tadjust + 86400
          INCtime = now - t0 + Tadjust
          Lasttime = now
          LOCATE 17, 56: PRINT "Time (hrs) =";
          PRINT USING " ###.##"; INCtime / 3600!

       WEND

     GOSUB 3880                      'close relay and stop motors
     GOTO 890                        'go to main

     '*************************************************************
2060 '********  Manually set a new set of target values   ***********
     '*************************************************************

     CLS : GOSUB 4463
```

```
     row = 11
     COLOR 0, 7: LOCATE row, 11
     PRINT "Manually Input a NEW SET of TARGET VALUES"
     COLOR 3, 8
     PRINT
     PRINT "The current target values are displayed above"
     PRINT "  You can enter new target values for each stress"
     PRINT "  or press ENTER to keep the current value"
2062 LOCATE 17, 1
     PRINT "  The target LOAD is displayed above but you should"
     INPUT "   Enter the new target axial STRESS (ksc) ", A$
     IF A$ = "" THEN A = newcell + newLoad / area: GOTO 2064
     A = VAL(A$)

2064 LOCATE 17, 1
     PRINT SPACE$(65)
     PRINT SPACE$(65)
     LOCATE 17, 1
     INPUT "   Enter the new cell pressure (ksc) ", A$
     IF A$ = "" THEN b = newcell: GOTO 2066
     b = VAL(A$)

2066 LOCATE 17, 1
     PRINT SPACE$(65)
     PRINT SPACE$(65)
     LOCATE 17, 1
     INPUT "   Enter the new back pressure (ksc) ", A$
     IF A$ = "" THEN c = newback: GOTO 2068
     c = VAL(A$)
     IF c >= b THEN GOTO 2066

2068 LOCATE 12, 1
     FOR i = 1 TO 7
     PRINT SPACE$(65)
     NEXT i
     LOCATE 13, 1
     PRINT "The following values will be used as the new target values"
     PRINT
     PRINT "         Axial Stress  = "; A
     PRINT "         Cell Pressure = "; b
     PRINT "         Back Pressure = "; c
     PRINT
     INPUT "    Is it okay to continue (yes or no) ", A$
     IF A$ <> "yes" THEN GOTO 890
     newLoad = (A - b) * area
     newcell = b
     newback = c
     GOTO 2050

     '-------------------------------------------------------------
     '---- THE FOLLOWING SECTIONS ARE ALL UTILITY ROUTINES -------
     '-------------------------------------------------------------

2100 '************ END PROGRAM ***********************************

     OUT motors! + 4, 0                        'LOCK MOTORS
     LOCATE 10, 1
     FOR j = 1 TO 10
       PRINT blk$
     NEXT j
     LOCATE 13, 1
     PRINT "Enter 'a' to return to the setup program => "
     PRINT "      'b' to continue running this program =>"
```

```
     INPUT " or just press <Enter> to stop program ", Z$
     IF Z$ = "a" OR Z$ = "A" THEN CHAIN "qbsetup6.bas"
     IF Z$ = "B" OR Z$ = "b" THEN GOTO 890
     STOP: END

     '*********************************************************************
2140 '***************** Measurement of B value subroutine *****************
     '*********************************************************************
     GOSUB 2150              'this allows the B value routine to be entered using a
got
     GOTO 890
     ' *************************

2150 FOR i = 1 TO 5: BEEP: NEXT i
    control(1) = 1           'stress control
    control(2) = 1           'stress control
    control(3) = 1           'stress control
    Mode(1) = 0
    Mode(2) = 0                'off between steps
    Mode(3) = 0
    Reverse(1) = 0
    Reverse(2) = 0
    Reverse(3) = 0
    feedback = 1

2190 CLS : GOSUB 4450
2200 LOCATE 25, 65: COLOR 0, 7: PRINT "B-VALUE CHECK"; : COLOR 3, 8
2210 TIMER ON: ON TIMER(60) GOSUB 4230   'Time out ==> set flag
2220 GOSUB 4160                          'set enter flag
2221 GOSUB 4290                          'set esc   flag
2222 PTRFLAG! = 1
2230 WHILE (ENTERFLAG = 0)
2235 GOSUB 2720
2237 WEND
2238 TIMER OFF
2240 IF ENTERFLAG = 1 THEN GOTO 2270     'measure B-value
2250 RETURN                              'time up or esc key
2270 CLS : GOSUB 4465
2271 LOCATE 25, 65: COLOR 0, 7: PRINT "B-VALUE CHECK"; : COLOR 3, 8
2280 LOCATE 14, 1: INPUT "Enter cell pressure increment (ksc) to apply: ", CELLINCR
2290 INPUT "Close pore pressure valves,press <Enter>."; A$
2291 RETURNCELL = CELL: RETURNBACK = BACK' pressures to return to at end
2295 GOSUB 4290                          'set esc   flag
2296 LOCATE 14, 1: PRINT blk$: PRINT blk$
2300 GOSUB 4465                         'new readings
2301 PTRFLAG! = 1
2302 LOCATE 12, 1: PRINT H3$; "     B-value"
2303 row = CSRLIN
2304 LOCATE 21, 20: PRINT H1$: PRINT H2$; "   B-value"
2310 ZROCELL = CELL: ZROBACK = BACK     'start values for b-value

2360 '
2370 ' This is a loop to do the B-value check
     Extraprint$ = "bvalue"
2400    newcell = RETURNCELL + CELLINCR' set the target cell pressure
2405 TIMER ON: ON TIMER(120) GOSUB 4230
     control(3) = 0                            'lock off pore motor
2410 WHILE (ENTERFLAG = 0)
2420    GOSUB 2720
2425    IF (CELL - ZROCELL) <= 0 THEN BVALUE = 0: GOTO 2440
2430    BVALUE = (BACK - ZROBACK) / (CELL - ZROCELL)
2440 '
2460 WEND
```

```
2480 Extraprint$ = ""
2490 TIMER OFF
2491 'LOCATE 12, 1': PRINT H3$; "              "
2492 'FOR i = 1 TO 7: PRINT SPACE$(60): NEXT i
2493 'Row = 13
2500 CLS
     GOSUB 4440
     LOCATE 17, 60: PRINT "The final B-value"
     LOCATE 18, 65: PRINT "is "; : PRINT USING "#.##"; BVALUE
2510 newcell = RETURNCELL
2520 GOSUB 4160
2521 GOSUB 4290
2529 WHILE (ENTERFLAG = 0)
2530    GOSUB 2720
2540 WEND
2550 CLS : PRINT : PRINT
2560 INPUT "OPEN drainage valves and press <ENTER> "; A$

2590 RETURN
2600 '
2610 ' ** SET THE FLAG
2620 '
2630 ' Needed to maintain the syntax of the ON KEY() statements
2640 '
2650  KEYFLAG = 1
2660  RETURN

     '*********************************************************************
2720 '******************** CONTROL THE MOTORS ****************************
     '*********************************************************************


     GOSUB 3260             ' take a set of readings

     '++++++++++++++++++++++++++++++++++++
     IF AD1170$ = "N" THEN     'this is here to allow program development
           FOR i = 1 TO stepinc
           X = X
           NEXT i
           'RETURN
     END IF
     '++++++++++++++++++++++++++++++++++++

     'Calculate the difference between readings and target values

      e(3, 1) = newback - BACK     'use for all situations
      row(3) = 6
      ON feedback GOTO 2730, 2734, 2732

2730  '*** this is feedback 1  (all stress control)
      e(1, 1) = newLoad - lode
      row(1) = 3
      e(2, 1) = newcell - CELL
      row(2) = 5
      GOTO 2760

2732  '*** this is feedback 3 for Ko consolidation
      e(1, 1) = newstrain - Strain
      row(1) = 7
      e(2, 1) = (area - targetarea) * (H0 - DISP)
      row(2) = 8
      GOTO 2760
```

```
2734  '*** this is feedback 2
      e(1, 1) = newstrain - Strain
      row(1) = 7
      e(2, 1) = newcell - CELL
      row(2) = 5

2760 Enable = 7                              'unlocks only motors in use
     IF control(1) = 0 THEN Enable = Enable - 1
     IF control(2) = 0 THEN Enable = Enable - 2
     IF control(3) = 0 THEN Enable = Enable - 4
    ' STOP

     '*************************************************************
     FOR i = 1 TO 3                 'loop over motors
         IF control!(i) <> 0 THEN
           LOCATE row(i), 63
           PRINT "              "
           LOCATE row(i), 63
           PRINT USING P3$; mvolts(i)
         END IF

       'compute the PID constants

         IF Mode(i) <> 2 THEN    'not PID control
                mvolts(i) = 0
                stiff = 0
                PID = 0
                GOTO 2765
         END IF 'not PID control
         stiff = 1
         sume(i) = sume(i) * k(i, 4, control!(i)) + e(i, 1)
         diffe(i) = e(i, 1) - e(i, 2)
         PID = diffe(i) * k(i, 2, control!(i)) + sume(i) * k(i, 3, control!(i))

2765     mvolts(i) = PID + e(i, 1) * k(i, stiff, control(i))
         'STOP
         'mvolts(i) = mvolts(i) + adjust
         IF mvolts(i) > 4.95 THEN mvolts(i) = 4.95
         IF mvolts(i) < -4.95 THEN mvolts(i) = -4.95
         IF control!(i) <> 0 THEN
           LOCATE row(i), 72
           PRINT USING P3$; mvolts(i)
         END IF
         e(i, 2) = e(i, 1)            'e is the error
       NEXT i

     'modify mvolts in case of preventing backward motion
        'the -.01 is a guess and may need to be changed to a variable

     FOR i = 1 TO 3
        IF mvolts(i) * Reverse(i) < -.01 THEN mvolts(i) = -.01 * Reverse(i)
     NEXT i


       FOR i = 1 TO 3
          cvolts(i) = mvolts(i) + ZVOLTS(i)           'apply offset
          IF cvolts(i) > 4.99 THEN cvolts(i) = 4.99   'constrain limits
          IF cvolts(i) < -4.99 THEN cvolts(i) = -4.99
       NEXT i
     'STOP
2800 FOR j = 1 TO 2                       'loop to start, run and stop each motor

       IF MOTOR1$ = "Y" THEN 2820 ELSE 2840               'use reversing relay
```

```
2820   IF cvolts(1) * mdir(1) < 0 THEN Enable4 = 8 ELSE Enable4 = 0'set relay position
       IF cvolts(1) * mdir(1) < 0 THEN cvolts(1) = cvolts(1) * (-1)        'REVERSE
TYPE 356 MOTOR

2840   OUT motors! + 4, Enable + Enable4              'close motor relays and open
relay #4

       GOSUB 2950     'output to the motors

       IF j = 2 THEN GOTO 2900              'skip out of routine

       FOR i = 1 TO stepinc: NEXT i         'run time delay

       ' set voltage for selected motors to stop value

       IF Mode(1) = 0 THEN cvolts(1) = ZVOLTS(1)
       IF Mode(2) = 0 THEN cvolts(2) = ZVOLTS(2)
       IF Mode(3) = 0 THEN cvolts(3) = ZVOLTS(3)

2900  NEXT j

     OUT motors! + 4, Mode(1) + Mode(2) * 2 + Mode(3) * 4 + Enable4'close relays to
lock motors

     RETURN

2950   'this section of code coverts voltage and sends to motor

       ' ***** Calculate the bit output required for each motor
       FOR i = 1 TO 3
          BITS! = INT((cvolts(i) * mdir(i) + 5) * 409.5)
          HIBIT!(i) = INT(BITS! / 256)
          LOBIT!(i) = BITS! - HIBIT!(i) * 256
       NEXT i

       ' Send voltage to motors
       FOR i = 1 TO 3                       'loop over motors
         OUT motors!, LOBIT!(i)             'set voltage register
         OUT motors! + 1, HIBIT!(i)
         OUT motors! + 2, DEVICE!(i)        'activate motor
         OUT motors! + 2, 255               'close register
       NEXT i

       RETURN

     '------------------------------------------------------------------------
3190 ' *************** ADJUST FOR CHANGE IN DATE DURING TEST ***************
3210 '------------------------------------------------------------------------
3220 'Tadjust = 86400! - INCtime + Tadjust
3230 'INCtime = 0: 'WON'T NEED THIS ANYMORE AFTER THE FIRST ADJUSTMENT
3240 'STARTDATE$ = DATE$
3250  STOP'RETURN
3260 '
3270 ' ********** TAKE SET OF READINGS AND CONVERT TO ENGINEERING UNITS *******
3280 '
3290 ' This routine takes the transducer readings from NUMCHANNELS number
3300 ' of channels and converts volts to engineering units.
3310 ' The input voltage should only be checked periodically.
3320 ' Automatic background calibration is enabled whenever this
3330 ' routine is not active.
3340 '
     '++++++++++++++++++++++++++++++++++++++++++++++++++++++
     '+++++++++ Create readings when no card in computer  +
```

```
     '++++++++++++++++++++++++++++++++++++++++++++++++++++
     IF AD1170$ = "Y" THEN GOTO 3350
       FOR L = 1 TO NUMCHANNELS
       VOLTS(L) = 1'SIN(TIMER)
       NEXT L
       VOLTS(VINCHANNEL) = 1
     GOTO 3500
     '++++++++++++++++++++++++++++++++++++++++++++++++++++

3350 OUT AD1170, 184: WAIT AD1170, 1, 1        'disable the background calibration
3370 FOR L = 1 TO NUMCHANNELS                  'all channels plus ground
3380    CHANNEL = (L - 1)
3390    OUT MUX!, CHANNEL                      'select the mux channel
3400    IF VINFLAG = VINREAD AND L = VINCHANNEL THEN GOTO 3600
3410    IF L = VINCHANNEL THEN GOTO 3490       'skip the loop and keep old value
3420    OUT AD1170, INTTIME: WAIT AD1170, 1, 1 'conversion using preset time
3430    OUT MUX!, GNDCHANNEL                   'ground the input to the AD1170
3440    ' read the three data bytes
3450    LOWBYTE = INP(AD1170 + 1): MIDBYTE = INP(AD1170 + 2): HIBYTE = INP(AD1170 + 3)
3460    CTS = LOWBYTE + 256 * MIDBYTE + 65536! * HIBYTE  ' total number of bits
3470    VTS = (CTS * 10 / 2 ^ (INTBIT + 7) - 5)          ' convert to volts
3480    VOLTS(L) = VTS / Amp(L)
3485    IF VINFLAG = -1 AND L = VINCHANNEL THEN VOLTS(L) = VOLTS(L) + 5
3490 NEXT L
3492 OUT AD1170, 176: WAIT AD1170, 1, 1        'reenable background calibration
3495
3500 LOCATE 23, 1: PRINT SPACE$(80);
3510 LOCATE 23, 7: PRINT USING "#.#####   "; VOLTS(DCDTCHANNEL); VOLTS(CELLCHANNEL);
VOLTS(LOADCHANNEL); VOLTS(PORECHANNEL); VOLTS(VOLDCDTCHANNEL); VOLTS(VINCHANNEL);
     IF Extraprint$ = "bvalue" THEN PRINT USING "#.##   "; BVALUE;
3530 '
3540 ' convert to engineering units
3550 '
3555 DISP = (VOLTS(DCDTCHANNEL) / VOLTS(VINCHANNEL) - ZDCDT) * CFDCDT
3560 CELL = (VOLTS(CELLCHANNEL) / VOLTS(VINCHANNEL) - ZCELL) * CFCELL
3565 BACK = (VOLTS(PORECHANNEL) / VOLTS(VINCHANNEL) - ZPORE) * CFPORE
     ZLD = LDZgrad * CELL + ZLOAD     ' adjust load zero for cell pressure
3570 lode = (VOLTS(LOADCHANNEL) / VOLTS(VINCHANNEL) - ZLD) * CFLOAD - PISTAREA * CELL
+ WEIGHT
3575 VOLU = (VOLTS(VOLDCDTCHANNEL) / VOLTS(VINCHANNEL) - ZVOLDCDT) * CFVOLDCDT
3580 VOLSTRN = VOLU / V0
3581 Strain = DISP / H0
3582 area = (V0 - VOLU) / (H0 - DISP)
3584 STRESS = lode / area + CELL
3585 'someday add corrections

     IF PTRFLAG! > 0 THEN GOTO 3590             'no screen display for is step
     GOSUB 4500
     row = row + 1: IF row = 20 THEN row = 13
     LOCATE row + 1, 1: PRINT SPACE$(53);
     IF Extraprint$ = "bvalue" THEN PRINT SPACE$(10);
     PRINT
     LOCATE row, 1: PRINT USING "  ###.##   "; STRESS; CELL; BACK; Strain * 100;
VOLSTRN * 100;
     IF Extraprint$ = "bvalue" THEN PRINT USING "  #.##"; BVALUE;
3590 PTRFLAG! = PTRFLAG! - 1
     VINFLAG = VINFLAG + 1
     RETURN
3600 '
3610 'nested subroutine to read the input voltage of the transducers

3620 OUT MUX!, REFCHANNEL                   'mux to AD1170 reference voltage
3630 OUT AD1170, 112: WAIT AD1170, 1, 1     'measure the null signal
```

```
3640 OUT AD1170, 120: WAIT AD1170, 1, 1     'enable the null
3650 OUT MUX!, CHANNEL                      'set mux to input voltage channel
3660 OUT AD1170, INTTIME: WAIT AD1170, 1, 1 'convert using preset time
3670 OUT AD1170, 128: WAIT AD1170, 1, 1     'disable the null
3680 VINFLAG = -1                           'reset the flag
3730 GOTO 3430

3750 '********** Set counter for delay loop **********
     '***********************************************
     'this is done only once
     i = 1
     ON TIMER(2) GOSUB 3810    '2 second sample
     TIMER ON
3800 i = i + 1: GOTO 3800
3810 stepinc = (i / 2) * STEPTIME
     TIMER OFF
     RETURN 3870

3870 '*****  generic return center *****

     RETURN

3880 '****** Set the control functions to off **************
     control(1) = 0
     control(2) = 0
     control(3) = 0
     cvolts(1) = ZVOLTS(1)
     cvolts(2) = ZVOLTS(2)
     cvolts(3) = ZVOLTS(3)
     GOSUB 2950         'send zero command to motors
     GOSUB 4430         'reset PID values to zero
     OUT motors + 4, 0
     RETURN


3890 '************ Subroutine to set soft function keys ******

      KEY OFF: FOR i = 1 TO 10: KEY i, "": NEXT i      'disable F-keys
      KEY 15, CHR$(0) + CHR$(&H45)      'pause key
      KEY 16, CHR$(0) + CHR$(&H3A)
      KEY 17, CHR$(0) + CHR$(70)        'control break   changwe 0 to 4
      KEY 18, CHR$(12) + CHR$(83)       'reset sequence
      KEY 19, CHR$(0) + CHR$(&H1C)      'ENTER KEY
      KEY 20, CHR$(0) + CHR$(&H1)       'ESC   KEY
       ON KEY(1) GOSUB 4380               '/
       ON KEY(2) GOSUB 4390               '/
       ON KEY(3) GOSUB 4400               '\ motor stop/start keys
       ON KEY(10) GOSUB 4410              '\
       ON KEY(15) GOSUB 3870
       ON KEY(16) GOSUB 3870
       ON KEY(17) GOSUB 3870
       ON KEY(18) GOSUB 3870
       ON KEY(19) GOSUB 4100
       ON KEY(20) GOSUB 4230
     FOR i = 15 TO 19: KEY(i) ON: NEXT i
     RETURN

4100 ' ******** GENERIC enter deactivation ****

     ENTERFLAG = 1
     KEY(19) OFF
     KEY(20) OFF
     RETURN
```

```
4160 ' ********* generic enter activation *****
4170 '
4175 LOCATE 25, 1
4180 PRINT "ENTER to continue";
4190 ENTERFLAG = 0
4200 KEY(19) ON
4210 RETURN
4220 '
4230 ' ******** generic ESC deactivation ****
4240 '
4250 ENTERFLAG = 2
4260 KEY(20) OFF
4265 KEY(19) OFF
4270 RETURN
4280 '
4290 ' ********* generic ESC activation *****
4300 '
4305 LOCATE 25, 20
4310 PRINT "ESC to abort";
4320 ENTERFLAG = 0
4330 KEY(20) ON
4340 RETURN
4350 '
4360 '******* toggle to turn on and off motors with f-keys *****

4380 II = 1: GOTO 4420
4390 II = 2: GOTO 4420
4400 II = 3: GOTO 4420
4410 FOR II = 1 TO 3: GOSUB 4420: NEXT II
4420 IF MFLAG$(II) = "start" THEN MFLAG$(II) = "stop " ELSE MFLAG$(II) = "start"
     RETURN

4430 '******* routine to reset the PID registers **********

     FOR i = 1 TO 3
        e(i, 1) = 0
        e(i, 2) = 0
        sume(i) = 0
        mvolts(i) = 0
        PID = 0
     NEXT i
     RETURN

4440 '*****************************************************
4450 '****** print basic screen and collect readings*******
4460 '*****************************************************

4461 LOCATE 11, 1: PRINT H3$: PRINT H4$
4462 row = CSRLIN
4463 LOCATE 21, 20: PRINT H1$: PRINT H2$
4465 'PTRFLAG! = 0
4470 VINFLAG = VINREAD                ' get an initial input voltage
4480 GOSUB 3260   '   get an initial set of readings and convert to eng. units
     '*********************************
4500 '******* print screen only ********
     '*********************************
     PTRFLAG! = Refreshrate
4502 LOCATE 1, 1
4503 FOR i = 1 TO 10: PRINT blk$: NEXT i
4504 LOCATE 1, 1
4510 PRINT
```

```
4520 PRINT "    CURRENT READINGS    TARGET VALUES       GAIN RATES      CONTROL
SIGNALS (V) "
4530 PRINT " A.Load  = "; : PRINT USING P2$; lode; : PRINT " Kg    ";
     IF control(1) = 1 THEN
              PRINT USING P2$; newLoad; : PRINT " Kg       ";
              IF feedback > 0 THEN
                PRINT USING P3$; k(1, 0, 1); : PRINT " v-sec/kg   ";
              END IF
     END IF
     PRINT
4551 '
4560 PRINT " A.Stress= "; : PRINT USING P2$; STRESS; : PRINT " Ksc   ";
     ' IF Control(1) = 1 THEN
4565 '         PRINT USING P2$; NEWSTRESS; : PRINT " Ksc        ";
4566 '         PRINT USING P3$; DGAIN(1); : PRINT "cm/v-sec     ";
4570 ' END IF
     PRINT

     PRINT " Cell    = "; : PRINT USING P2$; CELL; : PRINT " Ksc   ";
     IF control(2) = 1 THEN
            PRINT USING P2$; newcell; : PRINT " Ksc      ";
            IF feedback > 0 THEN
              PRINT USING P3$; k(2, 0, 1); : PRINT " v-sec/ksc   ";
            END IF
     END IF
     IF control(2) = 2 THEN
            PRINT "             ";

4586 END IF
     PRINT

4590 PRINT " Pore    = "; : PRINT USING P2$; BACK; : PRINT " Ksc   ";
     IF control(3) = 1 THEN
         PRINT USING P2$; newback; : PRINT " Ksc      ";
         IF feedback > 0 THEN
           PRINT USING P3$; k(3, 0, 1); : PRINT " v-sec/ksc   ";
         END IF
     END IF
     PRINT

4620 PRINT " A.Strain= "; : PRINT USING P2$; Strain * 100; : PRINT " %     ";
     IF control(1) = 2 THEN
4625     PRINT USING P2$; newstrain * 100; : PRINT " %        ";
4632     PRINT USING P3$; k(1, 0, 2); : PRINT " v-sec/cm    ";
4640 END IF
     PRINT
4641
4650 PRINT " V.Strain= "; : PRINT USING P2$; VOLSTRN * 100; : PRINT " %     ";
     IF control(2) = 2 THEN
4655     PRINT USING P2$; NEWVOLSTRN * 100; : PRINT " %        ";
4662     PRINT USING P3$; k(2, 0, 2); : PRINT " v-sec/cm^3  ";
4670 END IF
     PRINT

     RETURN

     '*************************************************************
4700 '********  Ko  Consolidation To Target stress ******************
     '*************************************************************

4710 CLS : GOSUB 4463
4720 row = 11
4730 COLOR 0, 7: LOCATE row, 11
```

```
4740 PRINT "Ko CONSOLIDATION PARAMETER SELECTION"
4750 COLOR 3, 8
4760 PRINT
     PRINT "This algorithm will apply a constant axial strain rate and"
4770 PRINT "  adjust the cell pressure to maintain a constant area"
4780 PRINT "You have three options for the target area"
4790 PRINT "  a  -initial specimen area   = "; A0
4800 PRINT "  b  -current specimen area   = "; area
4810 PRINT "  c  -you enter the numerical value"

     INPUT "Please Enter you selection (a,b or c) ", A$
     IF A$ = "a" THEN targetarea = A0: GOTO 4870
     IF A$ = "b" THEN targetarea = area: GOTO 4870
     INPUT "Please Enter the target area (cm2): ", targetarea
4870 FOR i = row + 1 TO row + 9: LOCATE i, 1: PRINT SPACE$(79): NEXT i
4875 LOCATE row + 3, 1
4880 PRINT "enter the axial strain rate (%/hr) "
4890 PRINT "      positive for consolidation"
4900 INPUT "      negative for swelling     "; strainrate
4910 VOLTS = strainrate / 360000! * H0 / k(1, 0, 2)
4920 IF ABS(VOLTS) < .01 THEN PRINT "This rate is too slow for the gear setting": GOTO
4950
4930 IF ABS(VOLTS) > 4.9 THEN PRINT "This rate is too fast for the gear setting": GOTO
4950
4940 GOTO 5010
4950 PRINT "You must change the rate or return to setup program"
4960 LOCATE 19, 10: PRINT SPACE$(50)
4970 LOCATE 19, 10: INPUT "Do you want to change rate (yes or no) ", A$
4980 IF A$ = "no" THEN GOTO 890
4990 IF A$ <> "yes" THEN GOTO 5010
5000 GOTO 4870
5010 FOR i = row + 1 TO row + 9: LOCATE i, 1: PRINT SPACE$(79): NEXT i
5020 LOCATE row + 3, 1
5030 INPUT "enter the final axial EFFECTIVE Stress (ksc) "; finalstress
5035 finalstress = finalstress + BACK
5040 del = finalstress - STRESS
5050 IF del * strainrate < 0 THEN PRINT "stress not compatable with rate!"
     INPUT "enter the final axial STRAIN (%) "; finalstrain
     del = finalstrain - Strain
     IF del * strainrate < 0 THEN PRINT "strain not compatable with rate!"
5060 LOCATE 19, 10: PRINT SPACE$(50)
5070 LOCATE 19, 10: INPUT "Is it okay to continue (yes or no) ", A$
5080 IF A$ = "no" THEN GOTO 890
5085 '****** prepare to start Ko loading *******

    control(1) = 2           'strain control
    control(2) = 2           'volume control
    control(3) = 1           'stress control
    Mode(1) = 2               'PID control of axial
    Mode(2) = 0                'off between steps
    Mode(3) = 0
    IF strainrate > 0 THEN Reverse(1) = 1 ELSE Reverse(1) = -1
    Reverse(2) = 0
    Reverse(3) = 0
    feedback = 3
    GOSUB 4430                'reset PID values

5090 CLS : GOSUB 4450                        'setup screen
5091 LOCATE 25, 65: COLOR 0, 7: PRINT "Ko CONSOLIDATION"; : COLOR 3, 8
5094 PTRFLAG! = 1

     LOCATE 11, 56: PRINT "Limiting Conditions"
     LOCATE 12, 57: PRINT "A.Eff.Sts. (ksc) =";
```

```
     PRINT USING "##.##"; finalstress - newback
     LOCATE 13, 57: PRINT "Axial Strain =";
     PRINT USING "##.##"; finalstrain
     LOCATE 16, 56: PRINT "Axial Strain Rate (%/hr)"
     LOCATE 17, 57: PRINT "Target =";
     PRINT USING "##.##"; strainrate

     GOSUB 4290                        'set esc key
     STRN0 = Strain
     t0 = TIMER
     Lasttime = t0
     Tadjust = 0

     WHILE (ENTERFLAG = 0)
       now = TIMER
       IF now < Lasttime THEN Tadjust = Tadjust + 86400    'add one day
       Deltime = now - t0 + Tadjust
       Lasttime = now
       newstrain = STRN0 + (strainrate * Deltime / 360000)
       GOSUB 2720
       LOCATE 18, 57: PRINT "Current =";
       IF Deltime < 1 THEN GOTO 5100
       PRINT USING "##.##"; (Strain - STRN0) / Deltime * 360000!
5100   IF strainrate * (finalstress - STRESS) <= 0 THEN ENTERFLAG = 3
       IF strainrate * (finalstrain - Strain) <= 0 THEN ENTERFLAG = 4
     WEND

5210 GOSUB 3880                                  'lock all motors
     newcell = CELL
     newLoad = lode

5215 IF ENTERFLAG = 2 THEN GOTO 890              'return to home

5220 GOTO 2050                                   'hold stress


     '*****************************************************************
6200 '************** Stress Path Consilidation ************************
     '*****************************************************************

6230 CLS : GOSUB 4463
6240 row = CSRLIN + 1
6250 COLOR 0, 7: LOCATE row, 11
6260 PRINT "Stress Path Consolidation Parameter selection"
6270 COLOR 3, 8
     PRINT
6280 PRINT "This algorithm will apply a constant axial strain rate and"
6290 PRINT "  adjust the cell pressure to follow a linear stress path"
6300 'PRINT "Please verify the following values"
6310 PRINT "    -current specimen height = "; H0 - DISP
6320 PRINT "    -current specimen area   = "; area
6330 PRINT "If these values are not correct you must modify the initial"
6340 PRINT "   specimen dimensions in the setup program"
6350 LOCATE 19, 10: PRINT SPACE$(50)
6360 LOCATE 19, 10: INPUT "Is it okay to continue (yes or no) ", A$
6370 IF A$ = "no" THEN GOTO 890
6380 IF A$ <> "yes" THEN GOTO 6350
6390 FOR i = row + 1 TO row + 9: LOCATE i, 1: PRINT blk$: NEXT i
6400 LOCATE row + 3, 1
6410 PRINT "Enter the axial strain rate (%/hr) "
6420 PRINT "      positive for consolidation"
6430 INPUT "      negative for swelling     "; strainrate
6440 'VOLTS = strainrate / 360000! * H0 / DGAIN(1)
```

```
6450 'IF ABS(VOLTS) < .05 THEN PRINT "This rate is too slow for the gear setting":
GOTO 6480
6460 'IF ABS(VOLTS) > 4.9 THEN PRINT "This rate is too fast for the gear setting":
GOTO 6480
6470 GOTO 6540
6480 PRINT "You must change the rate or return to setup program"
6490 LOCATE 19, 10: PRINT SPACE$(50)
6500 LOCATE 19, 10: INPUT "Do you want to change rate (yes or no) ", A$
6510 IF A$ = "no" THEN GOTO 890
6520 IF A$ <> "yes" THEN GOTO 6540
6530 GOTO 6390
6540 FOR i = row + 1 TO row + 9: LOCATE i, 1: PRINT blk$: NEXT i
6550 LOCATE row + 3, 1
6552 INPUT "Enter the final axial EFFECTIVE stress (ksc) "; newstress
6553 INPUT "Enter the final radial EFFECTIVE stress (ksc) "; newhstress
     finalstress = newstress
     finalrstress = newhstress
6554 ALTFLAG = 0
6555 newstress = newstress + BACK
6556 newhstress = newhstress + BACK
6557 DELV = newstress - STRESS
6558 DELH = newhstress - CELL
6559 IF DELV = 0 THEN GOTO 6562
6560 SLOPE = DELH / DELV
6561 IF ABS(SLOPE) < 1.5 THEN GOTO 6570
6562 ALTSLOPE = DELV / DELH
6563 STRESSREF = STRESS - ALTSLOPE * CELL
6564 PRINT : PRINT "        Stress slope = "; ALTSLOPE
6565 PRINT "       Axial reference stress = "; STRESSREF
6566 ALTFLAG = 1
6567 GOTO 6573
6570 CELLREF = CELL - SLOPE * STRESS
6571 PRINT : PRINT "        Stress slope = "; SLOPE
6572 PRINT "       Horizontal reference stress = "; CELLREF
6573 STPLIMIT = DELV ^ 2 + DELH ^ 2
6580 IF DELV * strainrate < 0 THEN PRINT "Stress may not be compatable with rate"
6590 LOCATE 19, 10: PRINT SPACE$(50)
6600 LOCATE 19, 10: INPUT "Is it okay to continue (yes or no) ", A$
6610 IF A$ = "no" THEN GOTO 890
6620 '****** prepare to start loading *******

    control(1) = 2           'strain control
    control(2) = 1           'stress control
    control(3) = 1           'stress control
    Mode(1) = 2
    Mode(2) = 0               'off between steps
    Mode(3) = 0
    IF strainrate > 0 THEN Reverse(1) = 1 ELSE Reverse(1) = -1
    Reverse(2) = 0
    Reverse(3) = 0
    feedback = 2
    GOSUB 4430               'reset PID values


6662 STRTSTRESS = STRESS
6664 STRTCELL = CELL
6670 CLS : GOSUB 4450                       'setup screen
6680 LOCATE 25, 65: COLOR 0, 7: PRINT "Drained STS Path"; : COLOR 3, 8
6700 PTRFLAG! = 1
     LOCATE 11, 56: PRINT "Limiting Conditions"
     LOCATE 12, 57: PRINT "A.Eff.Sts. (ksc) =";
     PRINT USING "##.##"; finalstress
     LOCATE 13, 57: PRINT "R.Eff.Sts. (ksc) =";
```

```
     PRINT USING "##.##"; finalrstress
     LOCATE 16, 56: PRINT "Axial Strain Rate (%/hr)"
     LOCATE 17, 57: PRINT "Target =";
     PRINT USING "##.##"; strainrate


6750 GOSUB 4290                        'set esc key
     STRN0 = Strain
     t0 = TIMER
     Lasttime = t0
     Tadjust = 0

6800 WHILE (ENTERFLAG = 0)
       IF ALTFLAG = 0 THEN newcell = CELLREF + SLOPE * STRESS
6825   IF ALTFLAG = 1 THEN newcell = CELL - STRESS + STRESSREF + ALTSLOPE * CELL
6850   now = TIMER
       IF now < Lasttime THEN Tadjust = Tadjust + 86400!
       INCtime = now - t0 + Tadjust
       Lasttime = now
       newstrain = STRN0 + (strainrate * INCtime / 360000)
       GOSUB 2720
       IF INCtime < 1 THEN GOTO 6880
       LOCATE 17, 57: PRINT "Current rate ="; (Strain - STRN0) / INCtime * 360000!
6880   IF ((STRESS - STRTSTRESS) ^ 2 + (CELL - STRTCELL) ^ 2) >= STPLIMIT THEN
ENTERFLAG = 3
     WEND

6960 GOSUB 3880                                    'stop motors
6970 IF ENTERFLAG = 2 THEN GOTO 890                'return to home
6980 GOTO 2040                                     'hold stress

     '*****************************************************************
7210 '********************** Undrained Shear  ************************
     '*****************************************************************

7230 CLS : GOSUB 4463
7240 row = CSRLIN + 1
7250 COLOR 0, 7: LOCATE row, 11
7260 PRINT "Undrained Shear  PARAMETER SELECTION"
7270 COLOR 3, 8
     PRINT
7280 PRINT "This algorithm will apply a constant axial strain rate ,  "
7290 PRINT "  hold the cell pressure constant and turn off back pressure"
7300 'PRINT "Please verify the following values"
7310 PRINT "    -current specimen height = "; H0 - DISP
7320 PRINT "    -current specimen area   = "; area
7330 PRINT "If these values are not correct you must modify the initial"
7340 PRINT "   specimen dimensions in the setup program"
7350 LOCATE 19, 10: PRINT SPACE$(50)
7360 LOCATE 19, 10: INPUT "Is it okay to continue (yes or no) ", A$
7370 IF A$ = "no" THEN GOTO 890
7380 IF A$ <> "yes" THEN GOTO 7350
7390 FOR i = row + 1 TO row + 9: LOCATE i, 1: PRINT blk$: NEXT i
7400 LOCATE row + 3, 1
7410 PRINT "enter the axial strain rate (%/hr) "
7420 PRINT "      positive for compression  "
7430 INPUT "      negative for extension    "; strainrate
7440 VOLTS = strainrate / 360000! * H0 / k(1, 0, 2)
7450 IF ABS(VOLTS) < .05 THEN PRINT "This rate is too slow for the gear setting": GOTO
7480
7460 IF ABS(VOLTS) > 4.9 THEN PRINT "This rate is too fast for the gear setting": GOTO
7480
7470 GOTO 7540
```

```
7480 PRINT "You must change the rate or return to setup program"
7490 LOCATE 19, 10: PRINT SPACE$(50)
7500 LOCATE 19, 10: INPUT "Do you want to change rate (yes or no) ", A$
7510 IF A$ = "no" THEN GOTO 890
7520 IF A$ <> "yes" THEN GOTO 7540
7530 GOTO 7390

7540 FOR i = row + 1 TO row + 9: LOCATE i, 1: PRINT blk$: NEXT i
     LOCATE row + 3, 1
7550 INPUT "Enter the axial TOTAL stress (ksc) LIMIT"; finalstress
     del = finalstress - STRESS
     IF del * strainrate < 0 THEN PRINT "stress not compatable with rate": GOTO 7550

     FOR i = row + 1 TO row + 9: LOCATE i, 1: PRINT blk$: NEXT i
     LOCATE row + 3, 1
7560 INPUT "Enter the axial STRAIN (%) LIMIT"; finalstrain
     DELstrain = finalstrain - Strain
     IF DELstrain * strainrate < 0 THEN PRINT "Strain limit not compatable with rate":
GOTO 7560


     LOCATE 19, 10: PRINT SPACE$(50)
     LOCATE 19, 10: INPUT "Is it okay to continue (yes or no) ", A$
     IF A$ = "no" THEN GOTO 890

    '****** prepare to start shearing   *******
    control(1) = 2           'strain control
    control(2) = 1           'stress control
    control(3) = 0           'turned off
    Mode(1) = 2
    Mode(2) = 0               'off between steps
    Mode(3) = 0
    IF strainrate > 0 THEN Reverse(1) = 1 ELSE Reverse(1) = -1
    Reverse(2) = 0
    Reverse(3) = 0
    feedback = 2
    GOSUB 4430               'reset PID values


7670 CLS : GOSUB 4450                       'setup screen
7680 LOCATE 25, 65: COLOR 0, 7: PRINT "Undrained Shear "; : COLOR 3, 8
7700 PTRFLAG! = 1

     LOCATE 11, 56: PRINT "Limiting Conditions"
     LOCATE 12, 57: PRINT "A.Tot.Sts. (ksc) =";
     PRINT USING "##.##"; finalstress
     LOCATE 13, 57: PRINT "Axial Strain =";
     PRINT USING "##.##"; finalstrain
     LOCATE 16, 56: PRINT "Axial Strain Rate (%/hr)"
     LOCATE 17, 57: PRINT "Target =";
     PRINT USING "##.##"; strainrate

     GOSUB 4290                      'set esc key
     STRN0 = Strain
     t0 = TIMER
     Lasttime = t0
     Tadjust = 0

     WHILE (ENTERFLAG = 0)
       now = TIMER
       IF now < Lasttime THEN Tadjust = Tasjust + 86400
       Deltime = now - t0 + Tadjust
       Lasttime = now
```

```
       newstrain = STRN0 + (strainrate * Deltime / 360000)
       GOSUB 2720
       LOCATE 18, 57: PRINT "Current rate =";
       IF Deltime < 1 THEN GOTO 7890
       PRINT USING "##.##"; (Strain - STRN0) / Deltime * 360000!
7890   IF strainrate * (finalstress - STRESS) <= 0 THEN ENTERFLAG = 3
       IF strainrate * (finalstrain - Strain) <= 0 THEN ENTERFLAG = 4
     WEND

     GOSUB 3880                                    'stop motors
     IF ENTERFLAG = 2 THEN GOTO 890                'return to home
     GOTO 2040                                     'hold stress

     '*****************************************************************
8500 '*****************  Ideal Sample Disturbance Simulation  **********
     '*****************************************************************

     CLS : GOSUB 4463
     row = CSRLIN + 1
     COLOR 0, 7: LOCATE row, 11
     PRINT "Sampling Disturbance PARAMETER SELECTION"
     COLOR 3, 8
     PRINT
     PRINT "This algorithm will apply one cycle of undrained loading at"
     PRINT "  constant strain rate between the specified strain increment"
     'PRINT "Please verify the following values"
     PRINT "  and then return the state of stress back to the hydrostatic"
     PRINT "  condition. Control will then proceed to the hold stress routine"
     'RINT "If these values are not correct you must modify the initial"
     'RINT "   specimen dimensions in the setup program"
8510 LOCATE 19, 10: PRINT SPACE$(50)
     LOCATE 19, 10: INPUT "Is it okay to continue (yes or no) ", A$
     IF A$ = "no" THEN GOTO 890
     IF A$ <> "yes" THEN GOTO 8510
8520 FOR i = row + 1 TO row + 9: LOCATE i, 1: PRINT blk$: NEXT i
     LOCATE row + 3, 1
     PRINT "enter the axial strain rate (%/hr) "
     PRINT "      positive for compression  "
     INPUT "      negative for extension    "; strainrate
     VOLTS = strainrate / 360000! * H0 / k(1, 0, 2)
     IF ABS(VOLTS) < .05 THEN PRINT "This rate is too slow for the gear setting": GOTO
8530
     IF ABS(VOLTS) > 4.9 THEN PRINT "This rate is too fast for the gear setting": GOTO
8530
     GOTO 8540
8530 PRINT "You must change the rate or return to setup program"
     LOCATE 19, 10: PRINT SPACE$(50)
     LOCATE 19, 10: INPUT "Do you want to change rate (yes or no) ", A$
     IF A$ = "no" THEN GOTO 890
     IF A$ <> "yes" THEN GOTO 8520

8540 FOR i = row + 1 TO row + 9: LOCATE i, 1: PRINT blk$: NEXT i
     LOCATE row + 3, 1
     PRINT "enter the strain increment for the distrubance cycle  "
     PRINT "      this is the strain based on the current height  "
     INPUT "      the value is in %    "; STRAININC
     ZDISP = DISP              'record the current displacement
     DELTAH = (H0 - DISP) * STRAININC / 100

     '****** prepare to start shearing   *******
    control(1) = 2           'strain control
    control(2) = 1           'stress control
    control(3) = 0           'turned off
```

```
    Mode(1) = 2
    Mode(2) = 0               'off between steps
    Mode(3) = 0
    IF strainrate > 0 THEN Reverse(1) = 1 ELSE Reverse(1) = -1
    Reverse(2) = 0
    Reverse(3) = 0
    feedback = 2
    GOSUB 4430               'reset PID values


     CLS : GOSUB 4450                'setup screen
     LOCATE 25, 55: COLOR 0, 7: PRINT "Undrained Disturbance"; : COLOR 3, 8
     PTRFLAG! = 1
     LOCATE 16, 57: PRINT "Target rate ="; strainrate; "%/hr"
     GOSUB 4290                      'set esc key
     STRN0 = Strain
     t0 = TIMER
     Tadjust = 0
     Lasttime = t0

8570 WHILE (ENTERFLAG = 0)           'step one compression
       now = TIMER
       IF now < Lasttime THEN Tadjust = Tadjust + 86400
       INCtime = now - t0 + Tadjust
       Lasttime = now
       newstrain = STRN0 + (strainrate * INCtime / 360000)
       GOSUB 2720
       IF INCtime > 1 THEN GOTO 8575
       LOCATE 17, 57: PRINT "Current rate ="; (Strain - STRN0) / INCtime * 360000!
8575   IF (ZDISP + DELTAH - DISP) <= 0 THEN ENTERFLAG = 3
     WEND

     IF ENTERFLAG = 2 THEN GOSUB 3880: GOTO 890     'stop motors and return to home
     ENTERFLAG = 0
     strainrate = -strainrate                       'reverse axial motor
     STRN0 = Strain
     t0 = TIMER
     Tadjust = 0
     Lasttime = t0
     GOSUB 4430               'reset PID values

8580 WHILE (ENTERFLAG = 0)                          'step two extension
       now = TIMER
       IF now < Lasttime THEN Tadjust = Tadjust + 86400
       INCtime = now - t0 + Tadjust
       Lasttime = now
       newstrain = STRN0 + (strainrate * INCtime / 360000)
       GOSUB 2720
       IF INCtime < 1 THEN GOTO 8585
       LOCATE 17, 57: PRINT "Current rate ="; (Strain - STRN0) / INCtime * 360000!
8585   IF (ZDISP - DELTAH - DISP) >= 0 THEN ENTERFLAG = 3
     WEND

     IF ENTERFLAG = 2 THEN GOSUB 3880: GOTO 890     'stop motors and return to home
     ENTERFLAG = 0
     strainrate = -strainrate                       'reverse axial motor
     STRN0 = Strain
     t0 = TIMER
     Tadjust = 0
     Lasttime = t0
     GOSUB 4430               'reset PID values

8590 WHILE (ENTERFLAG = 0)           'step three return to starting strain
```

```
       now = TIMER
       IF now < Lasttime THEN Tadjust = Tadjust + 86400
       INCtime = now - t0 + Tadjust
       Lasttime = now
       newstrain = STRN0 + (strainrate * INCtime / 360000)
       GOSUB 2720
       IF INCtime < 1 THEN GOTO 8595
       LOCATE 17, 57: PRINT "Current rate ="; (Strain - STRN0) / INCtime * 360000!
8595   IF (ZDISP - DISP) <= 0 THEN ENTERFLAG = 3
     WEND

     IF ENTERFLAG = 2 THEN GOSUB 3880: GOTO 890     'stop motors and return to home
     ENTERFLAG = 0
     strainrate = -strainrate * lode / ABS(lode)    'set strainrate direction
     STRN0 = Strain
     t0 = TIMER
     Tadjust = 0
     Lasttime = t0
     GOSUB 4430                'reset PID values

8600 WHILE (ENTERFLAG = 0)            'step four return to hydrostatic stress
       now = TIMER
       IF now < Lasttime THEN Tadjust = Tadjust + 86400
       INCtime = now - t0 + Tadjust
       Lasttime = now
       newstrain = STRN0 + (strainrate * INCtime / 360000)
       GOSUB 2720
       IF INCtime < 1 THEN GOTO 8605
       LOCATE 17, 57: PRINT "Current rate ="; (Strain - STRN0) / INCtime * 360000!
8605   IF (lode * strainrate) >= 0 THEN ENTERFLAG = 3
     WEND

     IF ENTERFLAG = 2 THEN GOSUB 3880: GOTO 890     'stop motors and return to home
     GOTO 2044                                      'hold stress


10000 'this is the setup routine for the a/d converter

     IF AD1170$ = "N" THEN RETURN    'No card in computer

     OUT AD1170, 60: WAIT AD1170, 1, 1'set the default calibration time
     OUT AD1170 + 1, INTBIT 'load the data format into the 2nd byte
     OUT AD1170, 48: WAIT AD1170, 1, 1 ' lock in the data format loaded
     OUT AD1170, 176: WAIT AD1170, 1, 1 '  begin background calibration
     OUT MUX!, GNDCHANNEL         ' set input to AD1170 to ground
     RETURN

10100 '************ END PROGRAM *********************************

     OUT motors! + 4, 0                       'LOCK MOTORS
     LOCATE 10, 1
     FOR j = 1 TO 10
       PRINT blk$
     NEXT j
     LOCATE 13, 1
     PRINT "Enter 'a' to return to the setup program => "
     PRINT "      'b' to continue running this program =>"
     INPUT " or just press <Enter> to stop program ", Z$
     IF Z$ = "a" OR Z$ = "A" THEN CHAIN "qbsetup3.bas"
     IF Z$ = "B" OR Z$ = "b" THEN GOTO 890
     STOP: END
```

APPENDIX B

AUTOMATION SOFTWARE FOR THICK-WALLED CYLINDER TESTING SYSTEM

```
  'rev 7.1 9/5/06 NOA cavity pressure reduction
  'rev 5.3 5/17/06 change to work with clamp configuration
  'rev 5.2 7/25/05 small edits to make consistent
  'rev 5.1 this has a pressure sensitivity zero adjustment to the internal LC
  'rev 5.0  10/24/00   jtg  major rehaul of the basic program
  'rev 4.0 8/1/00  jtg   converted to quickbasic
  'rev 3.1  8/06/91  jtg
  '
  '  Revision 1 written by Tom Sheahan to control stepper motors.
  '  Revision 2 written by Jack germaine to control dc servo motors.
  '
  ' ********************************************************************
  '
  ' The following hardware is required:
  '        -Strawberrytree d to a converter
  '        -The Sheahan a to d converter
  '        -The MIT three axis dc controller box with;
  '           -channel 1 for axial force
  '           -channel 2 for cell pressure
  '           -channel 3 for pore pressure

  ' Relay switches are used for the following
  '        -1 is to turn off motor 1
  '        -2 is to turn off motor 2
  '        -3 is to turn off motor 3
  '        -4 is to reverse the direction of motor 1 when using the 352 controller
  '        -5 is to turn on and off the input voltage relay


  '***  Information shared with the setup program    ****

   COMMON FILENAME$, DAT$, INITIALS$, TYPE$, weight, H0, A0, PISTAREA
   COMMON MEMBRANE$, FILTER, AREACORR$, ZLOAD, CFLOAD, ZDCDT, CFDCDT
   COMMON ZCELL, CFCELL, ZPORE, CFPORE, ZVOLDCDT, CFVOLDCDT, LOADCHANNEL
   COMMON DCDTCHANNEL, CELLCHANNEL, PORECHANNEL, VOLDCDTCHANNEL, DUMMY1
   COMMON DUMMY2, VINCHANNEL

'   ********************************************************************
'    AD1170$ = "N"    'used as flag to allow debugging the program
    AD1170$ = "Y"    'comment this line out when card is not in machine
'   ********************************************************************
'    MOTOR1$ = "Y"    'use this setting when using reversing relay on motor1
    MOTOR1$ = "N"    'default condition when not using the relay

'***** Constants which are used throughout the program *****
    rev$ = "5.3"
    blk$ = SPACE$(79)                                  'line eraser
    H1$ = "TRANSDUCER READINGS in volts"
    H2$ = "      disp      cell      load      pore      volume    input"
    H3$ = "A.Stress       Cell       Back   A.Strain   V.Strain"
    H4$ = "    ksc        ksc        ksc         %          %"
    P1$ = "####.#": P2$ = "###.##": P3$ = "##.###"

    V0 = A0 * H0                 'initial volume
    VINREAD = 10                 'period to read vin & update screen
    VINFLAG = VINREAD            'input voltage counter
    Refreshrate = 3                  'number of readings between updating screen
    STEPTIME = 1                 'time for each motor step in sec.

' ****** Set up function keys and be sure keyboard is set correctly ***
    CLS
    X = 1
    GOSUB 3890                       'lock out keyboard
```

```
260 GOSUB 4160                          'set enter key
270 a$ = INKEY$
    IF ENTERFLAG = 1 THEN GOTO 340
    IF a$ <> CHR$(13) THEN GOTO 270
    CLS
    LOCATE 15 + 2 * X, 2
    PRINT "turn off both the NUMBER LOCK and CAPS LOCK keys"
    PRINT "              and"
    X = X + 1
    GOTO 260

340 CLS
    LOCATE 10, 5
    PRINT "This will take two seconds"
    GOSUB 3750                          'calibrate steptime


 '************* SET UP GAINS, ARRAYS, VARIABLES AND CURRENT READINGS *******

    ' set the  A/D converter up and define performance variables
    INTTIME = 21  'to specify the integraion time of the A/D converter
                  'inttime=16+N where N=0   1 msec      N=4  100 msec
                  '                   N=1  10 msec      N=5  166.7 msec
                  '                   N=2  16.7 msec    N=6  300 msec
                  '                   N=3  20 msec
                  ' can set a variable integration time using the EIS command
    INTBIT = 13   ' specify the bit precision    INTBIT=(bit precision-7)
    AD1170 = 768  ' the decimal I/O address of the A/D converter
    MUX! = 776    ' decimal I/O of channel selecter
    '                 CORRESPONDS TO SWITCH SETTING 00001

 '******* set default values and flags   *****

    Row = 2             ' for what
    Tadjust = 0         ' to adjust time for a change in date during test
    ENTERFLAG = 0       ' for breaking a loop on the enter key
    NUMCHANNELS = 6     ' for input channel loop for data acq card
    MAXINCS = 25        ' for saturation steps
    STARTDATE$ = DATE$  ' get todays date for rate calculations
    GNDCHANNEL = 15     ' location of the ground connection on ad card
    REFCHANNEL = 14     ' location of the 5 volt reference voltage on A/D card

    DIM CELL(MAXINCS), Axial(MAXINCS), BACK(MAXINCS), time(MAXINCS), VOLTS(10)
    DIM MFLAG$(3), Control!(3), SGAIN(3), DGAIN(3), MVOLTS(3), ZVOLTS(3), Amp(6)

    GOSUB 10000                 'this sets up the A/D card

'   ************* Setup the DC servo motors *********************

    motors! = 6928              'decimal I/O address of analog out card
    STOPDEVICE! = 0             'varible to specify motors to stop;0=all
    OUT motors! + 4, 0          'open relays and lock all motors

    '******* specify the gain values to control the motors  *****

    SGAIN(1) = 100              'KG/VOLT-SEC         axial motor 1
    DGAIN(1) = .003             'cm/volt-sec       axial motor 1
    ZVOLTS(1) = 0               'zero voltage that stops motor

    SGAIN(2) = .5               'ksc/volt-sec      cell  motor 2
    DGAIN(2) = .5
    ZVOLTS(2) = 0
```

```
    SGAIN(3) = 2.5               'ksc/volt-sec      pore  motor 3
    DGAIN(3) = .05               'cm^3/volt-sec     pore  motor 3
    ZVOLTS(3) = 0

    tolerance = .1             'stress (ksc) condition to move to next step

    Amp(1) = 1                 'amplifier gains on the ad524 by channel
    Amp(2) = 10
    Amp(3) = 100
    Amp(4) = 10
    Amp(5) = 1
    Amp(6) = 1

    DEVICE!(1) = 14               'set motor 1 to axial
    DEVICE!(2) = 13               'set motor 2 to cell
    DEVICE!(3) = 11               'set motor 3 to pore

    Control!(1) = 0               'set axial to off  1=stress, 2=disp
    Control!(2) = 0               'set cell to off
    Control!(3) = 0               'set pore to off

    Mode1 = 0                     'controls set or continuous 1=cont, 0=step
    Mode2 = 0                     'for motor 2   2=cont, 0=step
    Mode3 = 0                     'for motor 3   4=cont, 0=step

    LDZgrad = 0'    .00748 / 5.5    'pressure sensitivity of load zero to cell
pressure

  '*** Reminders to set up the load frame for testing ****


    PRINT "Ensure that "
    PRINT "      -the loadframe lever is down and in the fine position"
    PRINT "      -the coarse wheel moves freely"
    PRINT "      -the back pressure valves are closed"
    PRINT "      -the gear selector is in position 'C'"
    PRINT "      -and the control box is on "
    PRINT
    PRINT "   This is program revision "; rev$
    IF AD1170$ = "N" THEN PRINT "  The AD1170 card is DISABLED"
    IF MOTOR1$ = "Y" THEN PRINT "   The reversing switch for motor 1 is ENABLED"
    INPUT "    press ENTER to continue ", a$

  ' ******  Collect a set of readings and set the target values ****
    GOSUB 3260               'get set of readings
     NEWCELL = CELL          'set target values
     NEWBACK = BACK
     newload = LODE

    '************************************************************
890 '*****  This is the starting point of the control program *****
    '************************************************************
    GOSUB 3880                              'turn off motor control
    CLS : GOSUB 4463                        'data set and basic screen
    PRINT
    PRINT "Please select the next phase of test;": PRINT
    PRINT " 1. Undrained Hydrostatic Initial Stress   7. Ko Consolidation"
    PRINT " 2. Drained Hydrostatic Stress Change      8. Stress Path Consolidation"
    PRINT " 3. Hold Current State of Stress           9. Undrained Shear"
    PRINT " 4. Hold Target State of Stress           10. Sample Disturbance
Simulation"
    PRINT " 5. Enter New Target State of Stress      11. Cavity Pressure Reduction"
    PRINT " 6. Measure 'B' Value                     12. End Program"
```

```
900 LOCATE 19, 1: PRINT blk$
    LOCATE 19, 1: INPUT "     Enter OPTION number ", CHOICE$
    CH = VAL(CHOICE$)
    IF CH < 1 OR CH > 12 THEN GOTO 900
    ON CH GOTO 930, 1100, 2040, 2050, 2060, 2140, 4700, 6200, 7210, 8500, 9000, 2100

    '*********************************************************************
930 '************** PRESSURE-UP TO GET INITIAL EFFECTIVE STRESS ***********
    '*********************************************************************

    Control(1) = 1           'stress control
    Control(2) = 1           'stress control
    Control(3) = 0           'turned off
    Mode1 = 1                'off between steps
    Mode2 = 0
    STRAINRATE = 0           'allows bidirectional axial control

    KEYFLAG = 0
    LOCATE 23, 1: PRINT blk$
    PRINT "NOTE-Be sure the back pressure valves are closed"
960 INPUT "Initial pressure-up desired (yes or no) ? ", Z$
    IF Z$ = "YES" OR Z$ = "yes" THEN GOTO 990
    IF Z$ = "no" OR Z$ = "NO" THEN GOTO 890 ELSE GOTO 960
990 CLS : GOSUB 4463               'read & basic screen
     LOCATE 16, 1
1001 INPUT "What cell pressure should be applied (ksc) ? ", NEWCELL
1002 LOCATE 16, 1: PRINT SPACE$(65)
1003 INPUT "What deviator load should be applied (kg ) ? ", newload
1030 KEY(1) ON: ON KEY(1) GOSUB 2600
1040 CLS : LOCATE 25, 1: PRINT blk$
1050 LOCATE 25, 1: PRINT "<F1> TO END PRESSURE UP";
1060 LOCATE 25, 65: COLOR 0, 7: PRINT "PRESSURE UP"; : COLOR 3, 8
1065 GOSUB 4450                 'print screen
1066 PTRFLAG! = 1

1070 WHILE (KEYFLAG <> 1)
1080     GOSUB 2720
1090 WEND

     GOSUB 3880                    'stop motors and lock relays

1095 GOTO 890

     '*********************************************************************
1100 '************** DRAINED STRESS STEP APPLICATION *********************
     '*********************************************************************
     Control(1) = 1                 'all stress control
     Control(2) = 1
     Control(3) = 1
     Mode1 = 1                     'all turned off between steps
     Mode2 = 0
     Mode3 = 0
     STRAINRATE = 0

1140 CLS : GOSUB 4465                'readings and basic screen
1150 PRINT
     R = CSRLIN
     LOCATE 23, 1: PRINT blk$
     COLOR 0, 7
     LOCATE R, 11
     PRINT "DRAINED CONSOLIDATION STRESS INCREMENTS"
     COLOR 3, 8
```

```
     PRINT "For each STRESS STEP specify the CELL PRESSURE, AXIAL STRESS, BACK
PRESSURE and DURATION"
     PRINT "Enter a '99' for cell pressure when finished."
     PRINT "Enter a '999' for cell pressure to return to MAIN MENU"
     NUMINCS = 0
     FOR i = 1 TO MAXINCS
       CELL(i) = -1
       Axial(i) = -1
       BACK(i) = -1
       time(i) = -1
     NEXT i
     PRINT "Increment #"; TAB(18); "Cell"; TAB(34); "Axial"; TAB(46); "Back"; TAB(60);
"Time (minutes)"

1250 WHILE (CELL(NUMINCS) <> 999 AND CELL(NUMINCS) <> 99 AND NUMINCS <> MAXINCS)
         NUMINCS = NUMINCS + 1
         Row = CSRLIN
         IF Row < 24 THEN GOTO 1360
            i = 23 - NUMINCS
            LOCATE 17, 1
            FOR Row = 17 TO 22
            PRINT Row - i; TAB(18); CELL(Row - i); TAB(34); Axial(Row - i); TAB(46);
BACK(Row - i); TAB(60); time(Row - i)
            NEXT Row
            PRINT SPACE$(70)

1360     LOCATE Row, 1: PRINT NUMINCS; TAB(20); : INPUT CELL(NUMINCS)
         IF CELL(NUMINCS) < 0 THEN 1360
         IF CELL(NUMINCS) = 99 THEN 1250  'Finished entering data
         IF CELL(NUMINCS) = 999 THEN 1250  'Finished entering data
1370     LOCATE Row, 34: PRINT ""; : INPUT Axial(NUMINCS)
         IF Axial(NUMINCS) < 0 THEN GOTO 1370
1380     LOCATE Row, 46: PRINT ""; : INPUT BACK(NUMINCS)
         IF BACK(NUMINCS) < 0 THEN 1380
         IF BACK(NUMINCS) > CELL(NUMINCS) THEN 1380
         IF BACK(NUMINCS) > Axial(NUMINCS) THEN 1380
1390     LOCATE Row, 60: PRINT ""; : INPUT time(NUMINCS)
         IF time(NUMINCS) < 1 THEN 1390
         IF NUMINCS = MAXINCS THEN PRINT "Max # increments ="; MAXINCS: GOTO 1250
       WEND
        IF CELL(NUMINCS) = 99 THEN NUMINCS = NUMINCS - 1
        IF CELL(NUMINCS) = 999 THEN GOTO 890

     CLS : PRINT
     PRINT "Increment #"; TAB(18); "Cell"; TAB(34); "Axial"; TAB(46); "Back"; TAB(60);
"Time (minutes)"
     FOR i = 1 TO NUMINCS
         PRINT i; TAB(20); CELL(i); TAB(34); Axial(i); TAB(46); BACK(i); TAB(60);
time(i)
         time(i) = time(i) * 60
     NEXT i
     LOCATE 24, 1
1550 INPUT "Is this schedule okay (yes or no) ?"; a$
     IF a$ = "yes" OR a$ = "YES" THEN 1560
     IF a$ = "NO" OR a$ = "no" THEN GOTO 1100
     GOTO 1550
1560 FOR i = 1 TO NUMINCS                          'convert to loads
        Axial(i) = (Axial(i) - CELL(i)) * area
     NEXT i
1600 ' ********** APPLY THE DRAINED STRESS INCREMENTS *****************

1650 INCR = 1                         ' loop to apply the large increments
```

```
1660 CLS : GOSUB 4450                    'readings & basic screen
     PTRFLAG! = 1
       GOSUB 4160                        'enter flag for next inc
       GOSUB 4290                        'esc flag to abort inc
       LOCATE 25, 55: COLOR 0, 7: PRINT "STRESS APPLICATION"; : COLOR 3, 8
       OLDCELL = CELL: OLDBACK = BACK: OLDLODE = LODE
       LOCATE 16, 57: PRINT "Increasing Pressure "
       LOCATE 18, 57: PRINT "of Increment "; INCR
       DCELL = (CELL(INCR) - CELL) / 10
       DBACK = (BACK(INCR) - BACK) / 10
       DLODE = (Axial(INCR) - LODE) / 10
       INCTIME = TIMER: Tadjust = 0      'set the start time for the increment
       NEWCELL = OLDCELL: NEWBACK = OLDBACK
       newload = LODE

     '++++++ This section is the minor increment loop +++++++

       CTR = 0
       WHILE (ENTERFLAG = 0 AND CTR <> 10)   'Loop to apply the split increment
         CTR = CTR + 1
         LOCATE 17, 57: PRINT "for Step "; CTR
         NEWCELL = NEWCELL + DCELL
         NEWBACK = NEWBACK + DBACK
         newload = newload + DLODE
         IF CTR = 10 THEN
            NEWCELL = CELL(INCR)
            NEWBACK = BACK(INCR)
            newload = Axial(INCR)
         END IF
1770       GOSUB 2720
           IF ENTERFLAG <> 0 THEN GOTO 1800
           IF ABS(CELL - NEWCELL) > tolerance THEN GOTO 1770   'tolerance check
           IF ABS(BACK - NEWBACK) > tolerance THEN GOTO 1770
           IF ABS(LODE - newload) > tolerance * area THEN GOTO 1770
1800   WEND

       '++++ This section continously monitors cell, pore and load

         NEWTIME = TIMER
         IF ENTERFLAG <> 0 THEN GOTO 1960
         LOCATE 16, 57: PRINT "Holding pressure    "
         WHILE (NEWTIME + Tadjust - INCTIME <= time(INCR) AND ENTERFLAG = 0)
              GOSUB 2720
              NEWDATE$ = DATE$
              IF NEWDATE$ <> STARTDATE$ THEN GOSUB 3190
              NEWTIME = TIMER
              LOCATE 17, 57
              T! = INT((NEWTIME + Tadjust - INCTIME) / 60)
              PRINT "for "; T!; " of "; INT(time(INCR) / 60); " MIN"
         WEND

1960   'Process the end of increment

       IF ENTERFLAG <> 1 THEN GOTO 1970         'not enter key
          ENTERFLAG = 0
          KEY(19) ON: KEY(20) ON                'reset keys
          GOTO 2010                             'next inc
1970   IF ENTERFLAG = 2 THEN GOTO 2015          'abort the mission
          GOSUB 2150                            'Do a B-value check
          Control(3) = 1                        'return to stress control
          GOSUB 2720

2010   IF INCR = NUMINCS THEN GOTO 2050         'goto hold stress
```

```
        INCR = INCR + 1
        GOTO 1660                              'continue to next increment

2015 '**** manage action on abort increment ****

     KEY(19) OFF: KEY(20) OFF
     GOSUB 3880                  'close relays
     GOTO 890                    'return to main menu

     '*****************************************************************
2040 '******* HOLD CURRENT STRESS SUBROUTINE ************************
     '*****************************************************************

     STRAINRATE = 0   'allows axial motor to move in both directions

2042 NEWBACK = BACK   'enter if all new values but limit motor direction
2044 NEWCELL = CELL
2046 newload = LODE


     '*****************************************************************
2050 '******* HOLD EXISTING TARGET STATE OF STRESS SUBROUTINE ********
     '*****************************************************************

     Control(1) = 1
     Control(2) = 1
     Control(3) = 1
     Mode1 = 1
     Mode2 = 0
     Mode3 = 0

2053 CLS : GOSUB 4450            'enter using existing control settings
2055 PTRFLAG! = 1
     GOSUB 4290
     LOCATE 25, 65: COLOR 0, 7: PRINT "HOLD STRESS"; : COLOR 3, 8
       WHILE (ENTERFLAG = 0)
          GOSUB 2720
       WEND

     GOSUB 3880                      'close relay and stop motors
     GOTO 890                        'go to main

     '*****************************************************************
2060 '********  Manually set a new set of target values   ***********
     '*****************************************************************

     CLS : GOSUB 4463
     Row = 11
     COLOR 0, 7: LOCATE Row, 11
     PRINT "Manually Input a NEW SET of TARGET VALUES"
     COLOR 3, 8
     PRINT
     PRINT "The current target values are displayed above"
     PRINT "  You can enter new target values for each stress"
     PRINT "  or press ENTER to keep the current value"
2062 LOCATE 17, 1
     PRINT "  The target LOAD is displayed above but you should"
     INPUT "   Enter the new target axial STRESS (ksc) ", a$
     IF a$ = "" THEN a = NEWCELL + newload / area: GOTO 2064
     a = VAL(a$)

2064 LOCATE 17, 1
     PRINT SPACE$(65)
```

```
     PRINT SPACE$(65)
     LOCATE 17, 1
     INPUT "   Enter the new cell pressure (ksc) ", a$
     IF a$ = "" THEN b = NEWCELL: GOTO 2066
     b = VAL(a$)

2066 LOCATE 17, 1
     PRINT SPACE$(65)
     PRINT SPACE$(65)
     LOCATE 17, 1
     INPUT "   Enter the new back pressure (ksc) ", a$
     IF a$ = "" THEN c = NEWBACK: GOTO 2068
     c = VAL(a$)
     IF c >= b THEN GOTO 2066

2068 LOCATE 12, 1
     FOR i = 1 TO 7
     PRINT SPACE$(65)
     NEXT i
     LOCATE 13, 1
     PRINT "The following values will be used as the new target values"
     PRINT
     PRINT "         Axial Stress  = "; a
     PRINT "         Cell Pressure = "; b
     PRINT "         Back Pressure = "; c
     PRINT
     INPUT "    Is it okay to continue (yes or no) ", a$
     IF a$ <> "yes" THEN GOTO 890
     newload = (a - b) * area
     NEWCELL = b
     NEWBACK = c
     STRAINRATE = 0
     GOTO 2050
     '-------------------------------------------------------------
     '---- THE FOLLOWING SECTIONS ARE ALL UTILITY ROUTINES -------
     '-------------------------------------------------------------

2100 '************ END PROGRAM ***********************************

     OUT motors! + 4, 0                       'LOCK MOTORS
     LOCATE 10, 1
     FOR j = 1 TO 10
       PRINT blk$
     NEXT j
     LOCATE 13, 1
     PRINT "Enter 'a' to return to the setup program => "
     PRINT "      'b' to continue running this program =>"
     INPUT " or just press <Enter> to stop program ", Z$
     IF Z$ = "a" OR Z$ = "A" THEN CHAIN "qbsetup3.bas"
     IF Z$ = "B" OR Z$ = "b" THEN GOTO 890
     STOP: END

     '*********************************************************************
2140 '***************** Measurement of B value subroutine *****************
     '*********************************************************************
     GOSUB 2150              'this allows the B value routine to be entered using a
got
     GOTO 890
     ' *************************

2150 FOR i = 1 TO 5: BEEP: NEXT i
     Control(1) = 1
     Control(2) = 1
```

```
     Control(3) = 1
     Mode1 = 0
     Mode2 = 0
     STRAINRATE = 0

2190 CLS : GOSUB 4450
2200 LOCATE 25, 65: COLOR 0, 7: PRINT "B-VALUE CHECK"; : COLOR 3, 8
2210 TIMER ON: ON TIMER(60) GOSUB 4230   'Time out ==> set flag
2220 GOSUB 4160                          'set enter flag
2221 GOSUB 4290                          'set esc   flag
2222 PTRFLAG! = 1
2230 WHILE (ENTERFLAG = 0)
2235 GOSUB 2720
2237 WEND
2238 TIMER OFF
2240 IF ENTERFLAG = 1 THEN GOTO 2270     'measure B-value
2250 RETURN                              'time up or esc key
2270 CLS : GOSUB 4465
2271 LOCATE 25, 65: COLOR 0, 7: PRINT "B-VALUE CHECK"; : COLOR 3, 8
2280 LOCATE 14, 1: INPUT "Enter cell pressure increment (ksc) to apply: ", CELLINCR
2290 INPUT "Close pore pressure valves,press <Enter>."; a$
2291 RETURNCELL = CELL: RETURNBACK = BACK' pressures to return to at end
2295 GOSUB 4290                          'set esc   flag
2296 LOCATE 14, 1: PRINT blk$: PRINT blk$
2300 GOSUB 4465                         'new readings
2301 PTRFLAG! = 1
2302 LOCATE 12, 1: PRINT H3$; "     B-value"
2303 Row = CSRLIN
2304 LOCATE 21, 20: PRINT H1$: PRINT H2$; "   B-value"
2310 ZROCELL = CELL: ZROBACK = BACK     'start values for b-value

2360 '
2370 ' This is a loop to do the B-value check
     Extraprint$ = "bvalue"
2400    NEWCELL = RETURNCELL + CELLINCR' set the target cell pressure
2405 TIMER ON: ON TIMER(120) GOSUB 4230
     Control(3) = 0                              'lock off pore motor
2410 WHILE (ENTERFLAG = 0)
2420    GOSUB 2720
2425    IF (CELL - ZROCELL) <= 0 THEN BVALUE = 0: GOTO 2440
2430    BVALUE = (BACK - ZROBACK) / (CELL - ZROCELL)
2440 '
2460 WEND
2480 Extraprint$ = ""
2490 TIMER OFF
2491 'LOCATE 12, 1': PRINT H3$; "              "
2492 'FOR i = 1 TO 7: PRINT SPACE$(60): NEXT i
2493 'Row = 13
2500 CLS
     GOSUB 4440
     LOCATE 17, 60: PRINT "The final B-value"
     LOCATE 18, 65: PRINT "is "; : PRINT USING "#.##"; BVALUE
2510 NEWCELL = RETURNCELL
2520 GOSUB 4160
2521 GOSUB 4290
2529 WHILE (ENTERFLAG = 0)
2530    GOSUB 2720
2540 WEND
2550 CLS : PRINT : PRINT
2560 INPUT "OPEN drainage valves and press <ENTER> "; a$
2590 RETURN
2600 '
2610 ' ** SET THE FLAG
```

```
2620 '
2630 ' Needed to maintain the syntax of the ON KEY() statements
2640 '
2650  KEYFLAG = 1
2660  RETURN

     '*********************************************************************
2720 '******************** CONTROL THE MOTORS ****************************
     '*********************************************************************

2750 ' The big control loop
2760 '
2770    GOSUB 3260 ' take a set of readings
     '++++++++++++++++++++++++++++++++++++
     IF AD1170$ = "N" THEN     'this is here to allow program development
           FOR i = 1 TO stepinc
           X = X
           NEXT i
           RETURN
     END IF
     '++++++++++++++++++++++++++++++++++++

2790 '  Calculate the difference between readings and target values
     'take out 12/01/05
    ' FOR I = 1 TO 3
     '    MVOLTS(I) = 0
    ' NEXT I

      IF Control!(1) = 1 THEN MVOLTS(1) = (newload - LODE) / SGAIN(1)
      IF Control!(1) = 2 THEN MVOLTS(1) = STRAINRATE / 360000! * H0 / DGAIN(1)
      IF Control!(2) = 1 THEN MVOLTS(2) = (NEWCELL - CELL) / SGAIN(2)
      IF Control!(2) = 2 THEN MVOLTS(2) = (area - targetarea) * (H0 - DISP) / DGAIN(2)
      IF Control!(3) = 1 THEN MVOLTS(3) = (NEWBACK - BACK) / SGAIN(3)
      IF Control!(3) = 2 THEN MVOLTS(3) = (NEWVOLSTRN - VOLSTRN) / DGAIN(3)

     Enable = 7                              'unlocks only motors in use
     IF Control(1) = 0 THEN Enable = Enable - 1
     IF Control(2) = 0 THEN Enable = Enable - 2
     IF Control(3) = 0 THEN Enable = Enable - 4

     'IF STRAINRATE * (newLoad - lode) < 0 THEN Enable = Enable - 1: MOVLTS(1) = 0

     FOR i = 1 TO 3
        MVOLTS(i) = MVOLTS(i) + ZVOLTS(i)
     NEXT i


     FOR i = 1 TO 3
        IF MVOLTS(i) < -5 THEN MVOLTS(i) = -5
        IF MVOLTS(i) > 5 THEN MVOLTS(i) = 5
     NEXT i

     Mvolts1 = MVOLTS(1)
     Mvolts2 = MVOLTS(2)
     Mvolts3 = MVOLTS(3)

     Enable4 = 0
     IF MOTOR1$ = "Y" THEN 2890 ELSE 2917   'use reversing relay
2890 IF MVOLTS(1) < 0 THEN Enable4 = 8 ELSE Enable4 = 0
     IF MVOLTS(1) < 0 THEN MVOLTS(1) = MVOLTS(1) * (-1)          'REVERSE TYPE 356
MOTOR
     'OUT motors! + 4, Enable + 8            'close all relays including relay #4
     'GOTO 2950
```

```
2917 OUT motors! + 4, Enable + Enable4              'close motor relays and open relay
#4

2950 FOR j = 1 TO 2                        'loop to start, run and stop each motor

       ' Calculate the bit output required for each motor

       FOR i = 1 TO 3
         BITS! = INT((MVOLTS(i) + 5) * 409.5)
         HIBIT!(i) = INT(BITS! / 256)
         LOBIT!(i) = BITS! - HIBIT!(i) * 256
       NEXT i

       ' Send voltage to motors

       FOR i = 1 TO 3                        'loop over motors
         OUT motors!, LOBIT!(i)              'set voltage register
         OUT motors! + 1, HIBIT!(i)
         OUT motors! + 2, DEVICE!(i)         'activate motor
         OUT motors! + 2, 255                'close register
       NEXT i

       IF j = 2 THEN GOTO 3090               'skip out of routine

       FOR i = 1 TO stepinc: NEXT i          'run time

       ' set voltage to selected motors to stop value

       IF Mode1 = 0 THEN MVOLTS(1) = ZVOLTS(1)
       IF Mode2 = 0 THEN MVOLTS(2) = ZVOLTS(2)
       IF Mode3 = 0 THEN MVOLTS(3) = ZVOLTS(3)

3090  NEXT j

     OUT motors! + 4, Mode1 + Mode2 + Mode3 + Enable4   'close relays to lock motors

     RETURN

3190 ' *************** ADJUST FOR CHANGE IN DATE DURING TEST ****************
3210 '
3220 Tadjust = 86400! - TINC + Tadjust
3230 TINC = 0: 'WON'T NEED THIS ANYMORE AFTER THE FIRST ADJUSTMENT
3240 STARTDATE$ = DATE$
3250 RETURN
3260 '
3270 ' ********** TAKE SET OF READINGS AND CONVERT TO ENGINEERING UNITS *******
3280 '
3290 ' This routine takes the transducer readings from NUMCHANNELS number
3300 ' of channels and converts volts to engineering units.
3310 ' The input voltage should only be checked periodically.
3320 ' Automatic background calibration is enabled whenever this
3330 ' routine is not active.
3340 '
     '+++++++++++++++++++++++++++++++++++++++++++++++++++++
     '+++++++++ Create readings when no card in computer  +
     '+++++++++++++++++++++++++++++++++++++++++++++++++++++
     IF AD1170$ = "Y" THEN GOTO 3350
       FOR L = 1 TO NUMCHANNELS
       VOLTS(L) = SIN(TIMER)
       NEXT L
       VOLTS(VINCHANNEL) = 1
     GOTO 3500
     '+++++++++++++++++++++++++++++++++++++++++++++++++++++
```

```
3350 OUT AD1170, 184: WAIT AD1170, 1, 1        'disable the background calibration
3370 FOR L = 1 TO NUMCHANNELS                  'all channels plus ground
3380    CHANNEL = (L - 1)
3390    OUT MUX!, CHANNEL                      'select the mux channel
3400    IF VINFLAG = VINREAD AND L = VINCHANNEL THEN GOTO 3600
3410    IF L = VINCHANNEL THEN GOTO 3490       'skip the loop and keep old value
3420    OUT AD1170, INTTIME: WAIT AD1170, 1, 1 'conversion using preset time
3430    OUT MUX!, GNDCHANNEL                   'ground the input to the AD1170
3440    ' read the three data bytes
3450    LOWBYTE = INP(AD1170 + 1): MIDBYTE = INP(AD1170 + 2): HIBYTE = INP(AD1170 + 3)
3460    CTS = LOWBYTE + 256 * MIDBYTE + 65536! * HIBYTE  ' total number of bits
3470    VTS = (CTS * 10 / 2 ^ (INTBIT + 7) - 5)          ' convert to volts
3480    VOLTS(L) = VTS / Amp(L)
3485    IF VINFLAG = -1 AND L = VINCHANNEL THEN VOLTS(L) = VOLTS(L) + 5
3490 NEXT L
3492 OUT AD1170, 176: WAIT AD1170, 1, 1        'reenable background calibration
3495
3500 LOCATE 23, 1: PRINT SPACE$(80);
3510 LOCATE 23, 7: PRINT USING "#.#####   "; VOLTS(DCDTCHANNEL); VOLTS(CELLCHANNEL);
VOLTS(LOADCHANNEL); VOLTS(PORECHANNEL); VOLTS(VOLDCDTCHANNEL); VOLTS(VINCHANNEL);
     IF Extraprint$ = "bvalue" THEN PRINT USING "#.##   "; BVALUE;
3530 '
3540 ' convert to engineering units
3550 '
3555 DISP = (VOLTS(DCDTCHANNEL) / VOLTS(VINCHANNEL) - ZDCDT) * CFDCDT
3560 CELL = (VOLTS(CELLCHANNEL) / VOLTS(VINCHANNEL) - ZCELL) * CFCELL
3565 BACK = (VOLTS(PORECHANNEL) / VOLTS(VINCHANNEL) - ZPORE) * CFPORE
     ZLD = LDZgrad * CELL + ZLOAD     ' adjust load zero for cell pressure
3570 LODE = (VOLTS(LOADCHANNEL) / VOLTS(VINCHANNEL) - ZLD) * CFLOAD - PISTAREA * CELL
+ weight
3572 'LODE = LODE + ((CELL - BACK) * 5)
3575 VOLU = (VOLTS(VOLDCDTCHANNEL) / VOLTS(VINCHANNEL) - ZVOLDCDT) * CFVOLDCDT
3580 VOLSTRN = VOLU / V0
3581 STRAIN = DISP / H0
3582 area = (V0 - VOLU) / (H0 - DISP)
3584 STRESS = LODE / area + CELL
3585 'someday add corrections

     IF PTRFLAG! > 0 THEN GOTO 3590             'no screen display for is step
     GOSUB 4500
     Row = Row + 1: IF Row = 20 THEN Row = 13
     LOCATE Row + 1, 1: PRINT SPACE$(53);
     IF Extraprint$ = "bvalue" THEN PRINT SPACE$(10);
     PRINT
     LOCATE Row, 1: PRINT USING "  ###.##   "; STRESS; CELL; BACK; STRAIN * 100;
VOLSTRN * 100;
     IF Extraprint$ = "bvalue" THEN PRINT USING "  #.##"; BVALUE;
3590 PTRFLAG! = PTRFLAG! - 1
     VINFLAG = VINFLAG + 1
     RETURN
3600 '
3610 'nested subroutine to read the input voltage of the transducers

3620 OUT MUX!, REFCHANNEL                   'mux to AD1170 reference voltage
3630 OUT AD1170, 112: WAIT AD1170, 1, 1     'measure the null signal
3640 OUT AD1170, 120: WAIT AD1170, 1, 1     'enable the null
3650 OUT MUX!, CHANNEL                      'set mux to input voltage channel
3660 OUT AD1170, INTTIME: WAIT AD1170, 1, 1 'convert using preset time
3670 OUT AD1170, 128: WAIT AD1170, 1, 1     'disable the null
3680 VINFLAG = -1                           'reset the flag
3730 GOTO 3430
```

```
3750 '********** Set counter for delay loop ***********
     '*********************************************
     'this is done only once
     i = 1
     ON TIMER(2) GOSUB 3810    '2 second sample
     TIMER ON
3800 i = i + 1: GOTO 3800
3810 stepinc = (i / 2) * STEPTIME
     TIMER OFF
     RETURN 3870

3870 '*****  generic return center *****

     RETURN

3880 '****** Set the control functions to off **************
     Control(1) = 0
     Control(2) = 0
     Control(3) = 0
     OUT motors + 4, 0
     RETURN


3890 '************ Subroutine to set soft function keys ******

      KEY OFF: FOR i = 1 TO 10: KEY i, "": NEXT i      'disable F-keys
      KEY 15, CHR$(0) + CHR$(&H45)      'pause key
      KEY 16, CHR$(0) + CHR$(&H3A)
      KEY 17, CHR$(0) + CHR$(70)        'control break   changwe 0 to 4
      KEY 18, CHR$(12) + CHR$(83)       'reset sequence
      KEY 19, CHR$(0) + CHR$(&H1C)      'ENTER KEY
      KEY 20, CHR$(0) + CHR$(&H1)       'ESC   KEY
       ON KEY(1) GOSUB 4380               '/
       ON KEY(2) GOSUB 4390               '/
       ON KEY(3) GOSUB 4400               '\ motor stop/start keys
       ON KEY(10) GOSUB 4410              '\
       ON KEY(15) GOSUB 3870
       ON KEY(16) GOSUB 3870
       ON KEY(17) GOSUB 3870
       ON KEY(18) GOSUB 3870
       ON KEY(19) GOSUB 4100
       ON KEY(20) GOSUB 4230
     FOR i = 15 TO 19: KEY(i) ON: NEXT i
     RETURN

4100 ' ******** GENERIC enter deactivation ****

     ENTERFLAG = 1
     KEY(19) OFF
     KEY(20) OFF
     RETURN

4160 ' ********* generic enter activation *****
4170 '
4175 LOCATE 25, 1
4180 PRINT "ENTER to continue";
4190 ENTERFLAG = 0
4200 KEY(19) ON
4210 RETURN
4220 '
4230 ' ******** generic ESC deactivation ****
4240 '
4250 ENTERFLAG = 2
```

```
4260 KEY(20) OFF
4265 KEY(19) OFF
4270 RETURN
4280 '
4290 ' ********* generic ESC activation *****
4300 '
4305 LOCATE 25, 20
4310 PRINT "ESC to abort";
4320 ENTERFLAG = 0
4330 KEY(20) ON
4340 RETURN
4350 '
4360 '******* toggle to turn on and off motors with f-keys *****
4370 '
4380 II = 1: GOTO 4420
4390 II = 2: GOTO 4420
4400 II = 3: GOTO 4420
4410 FOR II = 1 TO 3: GOSUB 4420: NEXT II
4420 IF MFLAG$(II) = "start" THEN MFLAG$(II) = "stop " ELSE MFLAG$(II) = "start"
4430 RETURN

4440 '*****************************************************
4450 '****** print basic screen and collect readings*******
4460 '*****************************************************

4461 LOCATE 11, 1: PRINT H3$: PRINT H4$
4462 Row = CSRLIN
4463 LOCATE 21, 20: PRINT H1$: PRINT H2$
4465 'PTRFLAG! = 0
4470 VINFLAG = VINREAD                ' get an initial input voltage
4480 GOSUB 3260   '   get an initial set of readings and convert to eng. units
     '*********************************
4500 '******* print screen only ********
     '*********************************
     PTRFLAG! = Refreshrate
4502 LOCATE 1, 1
4503 FOR i = 1 TO 10: PRINT blk$: NEXT i
4504 LOCATE 1, 1
4510 PRINT
4520 PRINT "    CURRENT READINGS       TARGET VALUES        GAIN RATES      CONTROL
SIGNALS "
4530 PRINT " A.Load  = "; : PRINT USING P2$; LODE; : PRINT " Kg      ";
     IF Control(1) = 2 THEN GOTO 4550
     PRINT USING P2$; newload; : PRINT " Kg         ";
4541 IF Control(1) <> 1 THEN GOTO 4550
4542 PRINT USING P3$; SGAIN(1); : PRINT " kg/volt-sec    ";
4544 PRINT USING P3$; Mvolts1; : PRINT " Volts";
4550 PRINT
4551 '
4560 PRINT " A.Stress= "; : PRINT USING P2$; STRESS; : PRINT " Ksc     ";
     IF Control(1) <> 2 THEN GOTO 4570
4565 PRINT USING P2$; newstress; : PRINT " Ksc        ";
4566 ' PRINT USING P3$; DGAIN(1); : PRINT "cm/volt-sec     ";
     ' PRINT USING P3$; MVOLTS1; : PRINT "Volts";
4570 PRINT
     PRINT " Cell    = "; : PRINT USING P2$; CELL; : PRINT " Ksc     ";

4575 PRINT USING P2$; NEWCELL; : PRINT " Ksc        ";
4580 IF Control(2) = 0 THEN GOTO 4586
     PRINT USING P3$; SGAIN(2); : PRINT " ksc/volt-sec   ";
4585 PRINT USING P3$; Mvolts2; : PRINT " volts";
4586 PRINT
```

```
4590 PRINT " Pore    = "; : PRINT USING P2$; BACK; : PRINT " Ksc     ";

4595 PRINT USING P2$; NEWBACK; : PRINT " Ksc        ";
4602 IF Control(3) = 0 THEN GOTO 4610
     PRINT USING P3$; SGAIN(3); : PRINT " ksc/volt-sec   ";
4604 PRINT USING P3$; Mvolts3; : PRINT " Volts";
4610 PRINT
4611 '
4620 PRINT " A.Strain= "; : PRINT USING P2$; STRAIN * 100; : PRINT " %       ";
     IF Control(1) <> 2 THEN GOTO 4640
4625 PRINT USING P2$; NEWSTRAIN * 100; : PRINT " %          ";

4632 PRINT USING P3$; DGAIN(1); : PRINT " cm/volt-sec    ";
4634 PRINT USING P3$; Mvolts1; : PRINT " Volts";
4640 PRINT
4641 '
4650 PRINT " V.Strain= "; : PRINT USING P2$; VOLSTRN * 100; : PRINT " %       ";
     IF Control(3) <> 2 THEN GOTO 4670
4655 PRINT USING P2$; NEWVOLSTRN * 100; : PRINT " %          ";

4662 PRINT USING P3$; DGAIN(3); : PRINT " cm^3/volt-sec  ";
4664 PRINT USING P3$; Mvolts3; : PRINT " Volts";
4670 PRINT
4680 RETURN

     '************************************************************
4700 '********  Ko  Consolidation To Target stress ******************
     '************************************************************

4710 CLS : GOSUB 4463
4720 Row = 11
4730 COLOR 0, 7: LOCATE Row, 11
4740 PRINT "Ko CONSOLIDATION PARAMETER SELECTION"
4750 COLOR 3, 8
4760 PRINT
     PRINT "This algorithm will apply a constant axial strain rate and"
4770 PRINT "  adjust the cell pressure to maintain a constant area"
4780 PRINT "You have three options for the target area"
4790 PRINT "  a  -initial specimen area   = "; A0
4800 PRINT "  b  -current specimen area   = "; area
4810 PRINT "  c  -you enter the numerical value"

     INPUT "Please Enter you selection (a,b or c) ", a$
     IF a$ = "a" THEN targetarea = A0: GOTO 4870
     IF a$ = "b" THEN targetarea = area: GOTO 4870
     INPUT "Please Enter the target area (cm2): ", targetarea
4870 FOR i = Row + 1 TO Row + 9: LOCATE i, 1: PRINT blk$: NEXT i
4875 LOCATE Row + 3, 1
4880 PRINT "enter the axial strain rate (%/hr) "
4890 PRINT "      positive for consolidation"
4900 INPUT "      negative for swelling     "; STRAINRATE
4910 VOLTS = STRAINRATE / 360000! * H0 / DGAIN(1)
4920 IF ABS(VOLTS) < .04 THEN PRINT "This rate is too slow for the gear setting": GOTO
4950
4930 IF ABS(VOLTS) > 4.9 THEN PRINT "This rate is too fast for the gear setting": GOTO
4950
4940 GOTO 5010
4950 PRINT "You must change the rate or return to setup program"
4960 LOCATE 19, 10: PRINT SPACE$(50)
4970 LOCATE 19, 10: INPUT "Do you want to change rate (yes or no) ", a$
4980 IF a$ = "no" THEN GOTO 890
4990 IF a$ <> "yes" THEN GOTO 5010
5000 GOTO 4870
```

```
5010 FOR i = Row + 1 TO Row + 9: LOCATE i, 1: PRINT blk$: NEXT i
5020 LOCATE Row + 3, 1
5030 INPUT "enter the final axial EFFECTIVE Stress (ksc) "; newstress
5035 newstress = newstress + BACK
5040 DEL = newstress - STRESS
5050 IF DEL * STRAINRATE < 0 THEN PRINT "stress not compatable with rate"
5060 LOCATE 19, 10: PRINT SPACE$(50)
5070 LOCATE 19, 10: INPUT "Is it okay to continue (yes or no) ", a$
5080 IF a$ = "no" THEN GOTO 890
5085 '****** prepare to start Ko loading *******
     Control!(1) = 2                 'Displacement
     Control!(2) = 2                 'displacement control
     Control!(3) = 1                 'stress
     Mode1 = 1
     Mode2 = 0
     Mode3 = 0
     STOPDEVICE! = 1                 'keep axial moving
5089 NEWCELL = 0                     'for display only
5090 CLS : GOSUB 4450                      'setup screen
5091 LOCATE 25, 65: COLOR 0, 7: PRINT "Ko CONSOLIDATION"; : COLOR 3, 8
5094 PTRFLAG! = 1
5095 DELT = .1 / STRAINRATE * 3600   'sec for .1% strain
5096 LOCATE 16, 57: PRINT "Target rate ="; STRAINRATE; "%/hr"
5105 STRTSTRAIN = STRAIN
5125 GOSUB 4290                      'set esc key
5136 STRN0 = STRAIN: T0 = TIMER
5140 '
5150 WHILE (ENTERFLAG = 0)
5160   'MVOLTS(2) = (AREA - targetarea) * (H0 - DISP) / DGAIN(2)
5170   GOSUB 2720
5172   IF VINFLAG <> 0 THEN GOTO 5180
5173   TINC = TIMER - T0
5174   IF TINC <= 0 THEN GOTO 5180
5175   LOCATE 17, 57: PRINT "Current rate =": PRINT USING " #.##"; (STRAIN - STRN0) /
TINC * 360000!
5176   STRN0 = STRAIN: T0 = TIMER
5180   IF STRAINRATE * (newstress - STRESS) <= 0 THEN ENTERFLAG = 3
5182 WEND
5183 TIMER OFF
5185 IF ENTERFLAG = 1 THEN GOSUB 6000: GOTO 5105    'adj. rate

5210 GOSUB 3880                                    'lock all motors
     NEWCELL = CELL
     newload = LODE

5215 IF ENTERFLAG = 2 THEN GOTO 890                'return to home

5220 GOTO 2050                                     'hold stress
5999 '
6000 '******* adjust voltage for constant rate *****
6001 '
6005 GOSUB 4470                     'get current readings
6010 TIMER OFF
6012 IF ABS(STRAIN - STRTSTRAIN) < .0005 THEN GOTO 6020
6015 MVOLTS(1) = MVOLTS(1) * STRAINRATE / 360000! / (STRAIN - STRTSTRAIN) * DELT
6020 STRTSTRAIN = STRAIN
6025 RETURN

     '*****************************************************************
6200 '************** Stress Path Consilidation ************************
     '*****************************************************************

6230 CLS : GOSUB 4463
```

```
6240 Row = CSRLIN + 1
6250 COLOR 0, 7: LOCATE Row, 11
6260 PRINT "Stress Path Consolidation Parameter selection"
6270 COLOR 3, 8
     PRINT
6280 PRINT "This algorithm will apply a constant axial strain rate and"
6290 PRINT "  adjust the cell pressure to follow a linear stress path"
6300 'PRINT "Please verify the following values"
6310 PRINT "    -current specimen height = "; H0 - DISP
6320 PRINT "    -current specimen area   = "; area
6330 PRINT "If these values are not correct you must modify the initial"
6340 PRINT "   specimen dimensions in the setup program"
6350 LOCATE 19, 10: PRINT SPACE$(50)
6360 LOCATE 19, 10: INPUT "Is it okay to continue (yes or no) ", a$
6370 IF a$ = "no" THEN GOTO 890
6380 IF a$ <> "yes" THEN GOTO 6350
6390 FOR i = Row + 1 TO Row + 9: LOCATE i, 1: PRINT blk$: NEXT i
6400 LOCATE Row + 3, 1
6410 PRINT "Enter the axial strain rate (%/hr) "
6420 PRINT "      positive for consolidation"
6430 INPUT "      negative for swelling     "; STRAINRATE
6440 VOLTS = STRAINRATE / 360000! * H0 / DGAIN(1)
6450 'IF ABS(VOLTS) < .05 THEN PRINT "This rate is too slow for the gear setting":
GOTO 6480
6460 'IF ABS(VOLTS) > 4.9 THEN PRINT "This rate is too fast for the gear setting":
GOTO 6480
6470 GOTO 6540
6480 PRINT "You must change the rate or return to setup program"
6490 LOCATE 19, 10: PRINT SPACE$(50)
6500 LOCATE 19, 10: INPUT "Do you want to change rate (yes or no) ", a$
6510 IF a$ = "no" THEN GOTO 890
6520 IF a$ <> "yes" THEN GOTO 6540
6530 GOTO 6390
6540 FOR i = Row + 1 TO Row + 9: LOCATE i, 1: PRINT blk$: NEXT i
6550 LOCATE Row + 3, 1
6552 INPUT "Enter the final axial EFFECTIVE stress (ksc) "; newstress
6553 INPUT "Enter the final radial EFFECTIVE stress (ksc) "; newhstress
6554 ALTFLAG = 0
6555 newstress = newstress + BACK
6556 newhstress = newhstress + BACK
6557 DELV = newstress - STRESS
6558 DELH = newhstress - CELL
6559 IF DELV = 0 THEN GOTO 6562
6560 SLOPE = DELH / DELV
6561 IF ABS(SLOPE) < 1.5 THEN GOTO 6570
6562 ALTSLOPE = DELV / DELH
6563 STRESSREF = STRESS - ALTSLOPE * CELL
6564 PRINT : PRINT "        Stress slope = "; ALTSLOPE
6565 PRINT "       Axial reference stress = "; STRESSREF
6566 ALTFLAG = 1
6567 GOTO 6573
6570 CELLREF = CELL - SLOPE * STRESS
6571 PRINT : PRINT "        Stress slope = "; SLOPE
6572 PRINT "       Horizontal reference stress = "; CELLREF
6573 STPLIMIT = DELV ^ 2 + DELH ^ 2
6580 IF DELV * STRAINRATE < 0 THEN PRINT "Stress may not be compatable with rate"
6590 LOCATE 19, 10: PRINT SPACE$(50)
6600 LOCATE 19, 10: INPUT "Is it okay to continue (yes or no) ", a$
6610 IF a$ = "no" THEN GOTO 890
6620 '****** prepare to start loading *******
6630 Control!(1) = 2                  'disp control
6640 Control!(2) = 1                  'stress control
     Control(3) = 1
```

```
     Mode1 = 1
     Mode2 = 0
     Mode3 = 0

6650 STOPDEVICE! = 1                      'keep axial moving
6660 'NEWBACK = BACK
6662 STRTSTRESS = STRESS
6664 STRTCELL = CELL
6670 CLS : GOSUB 4450                       'setup screen
6680 LOCATE 25, 65: COLOR 0, 7: PRINT "Drained STS Path"; : COLOR 3, 8
6700 PTRFLAG! = 1
6710 DELT = .1 / STRAINRATE * 3600   'sec for .1% strain
6720 LOCATE 16, 57: PRINT "Target rate ="; STRAINRATE; "%/hr"
6730 IF DELT > 86400! THEN DELT = 86400!
6740 STRTSTRAIN = STRAIN
6750 GOSUB 4290                       'set esc key
6780 STRN0 = STRAIN: T0 = TIMER
6790 '
6800 WHILE (ENTERFLAG = 0)
6810   'MVOLTS(1) = MVTS1
6820   IF ALTFLAG = 0 THEN NEWCELL = CELLREF + SLOPE * STRESS
6825   IF ALTFLAG = 1 THEN NEWCELL = CELL - STRESS + STRESSREF + ALTSLOPE * CELL
6830   GOSUB 2720
6840   IF VINFLAG <> 0 THEN GOTO 6890
6850   TINC = TIMER - T0
6860   IF TINC <= 0 THEN GOTO 6890
6870   LOCATE 17, 57: PRINT "Current rate ="; (STRAIN - STRN0) / TINC * 360000!
6880   STRN0 = STRAIN: T0 = TIMER
6890   IF ((STRESS - STRTSTRESS) ^ 2 + (CELL - STRTCELL) ^ 2) >= STPLIMIT THEN
ENTERFLAG = 3
6900 WEND
6910 TIMER OFF
6920 IF ENTERFLAG = 1 THEN GOSUB 7000: GOTO 6740    'adj. rate
6930 Control!(1) = 1                                'stress control
6940 Control!(2) = 1
6950 STOPDEVICE! = 0                                'stop all motors
6960 GOSUB 3880
6970 IF ENTERFLAG = 2 THEN GOTO 890                 'return to home
     NEWCELL = newhstress
     newload = (newstress - NEWCELL) * area

6980 GOTO 2050                                      'hold stress
6990 '
7000 '******* adjust voltage for constant rate *****
7010 '
7020 GOSUB 4470                      'get current readings
7030 TIMER OFF
7040 IF ABS(STRAIN - STRTSTRAIN) < .0005 THEN GOTO 7060
7050 MVOLTS(1) = MVOLTS(1) * STRAINRATE / 360000! / (STRAIN - STRTSTRAIN) * DELT
7060 STRTSTRAIN = STRAIN
7070 RETURN

7200 '*****************************************************************
7210 '********************** Undrained Shear  ************************
7220 '*****************************************************************

7230 CLS : GOSUB 4463
7240 Row = CSRLIN + 1
7250 COLOR 0, 7: LOCATE Row, 11
7260 PRINT "Undrained Shear  PARAMETER SELECTION"
7270 COLOR 3, 8
     PRINT
7280 PRINT "This algorithm will apply a constant axial strain rate ,  "
```

```
7290 PRINT "  hold the cell pressure constant and turn off back pressure"
7300 'PRINT "Please verify the following values"
7310 PRINT "    -current specimen height = "; H0 - DISP
7320 PRINT "    -current specimen area   = "; area
7330 PRINT "If these values are not correct you must modify the initial"
7340 PRINT "   specimen dimensions in the setup program"
7350 LOCATE 19, 10: PRINT SPACE$(50)
7360 LOCATE 19, 10: INPUT "Is it okay to continue (yes or no) ", a$
7370 IF a$ = "no" THEN GOTO 890
7380 IF a$ <> "yes" THEN GOTO 7350
7390 FOR i = Row + 1 TO Row + 9: LOCATE i, 1: PRINT blk$: NEXT i
7400 LOCATE Row + 3, 1
7410 PRINT "enter the axial strain rate (%/hr) "
7420 PRINT "      positive for compression  "
7430 INPUT "      negative for extension    "; STRAINRATE
7440 VOLTS = STRAINRATE / 360000! * H0 / DGAIN(1)
7450 'IF ABS(VOLTS) < .05 THEN PRINT "This rate is too slow for the gear setting":
GOTO 7480
7460 'IF ABS(VOLTS) > 4.9 THEN PRINT "This rate is too fast for the gear setting":
GOTO 7480
7470 GOTO 7540
7480 PRINT "You must change the rate or return to setup program"
7490 LOCATE 19, 10: PRINT SPACE$(50)
7500 LOCATE 19, 10: INPUT "Do you want to change rate (yes or no) ", a$
7510 IF a$ = "no" THEN GOTO 890
7520 IF a$ <> "yes" THEN GOTO 7540
7530 GOTO 7390

7540 FOR i = Row + 1 TO Row + 9: LOCATE i, 1: PRINT blk$: NEXT i
     LOCATE Row + 3, 1
7550 INPUT "Enter the axial TOTAL stress (ksc) LIMIT"; newstress
     DEL = newstress - STRESS
     IF DEL * STRAINRATE < 0 THEN PRINT "stress not compatable with rate": GOTO 7550

     FOR i = Row + 1 TO Row + 9: LOCATE i, 1: PRINT blk$: NEXT i
     LOCATE Row + 3, 1
7560 INPUT "Enter the axial STRAIN (%) LIMIT"; FINALSTRAIN
     DELstrain = FINALSTRAIN - STRAIN
     IF DELstrain * STRAINRATE < 0 THEN PRINT "Strain limit not compatable with rate":
GOTO 7560


     LOCATE 19, 10: PRINT SPACE$(50)
     LOCATE 19, 10: INPUT "Is it okay to continue (yes or no) ", a$
     IF a$ = "no" THEN GOTO 890
     '****** prepare to start shearing   *******
     Control!(1) = 2                 'disp control
     Control!(2) = 1                 'stress control
     Control!(3) = 0
     Mode1 = 1
     Mode2 = 0

7650 STOPDEVICE! = 1                 'keep axial moving
7660 'NEWCELL = CELL
7670 CLS : GOSUB 4450                      'setup screen
7680 LOCATE 25, 65: COLOR 0, 7: PRINT "Undrained Shear "; : COLOR 3, 8
7700 PTRFLAG! = 1
7710 DELT = .1 / STRAINRATE * 3600   'sec for .1% strain
7720 LOCATE 16, 57: PRINT "Target rate ="; STRAINRATE; "%/hr"
7730 IF DELT > 86400! THEN DELT = 86400!
7740 STRTSTRAIN = STRAIN
7750 GOSUB 4290                      'set esc key
7780 STRN0 = STRAIN: T0 = TIMER
```

```
7790 '
7800 WHILE (ENTERFLAG = 0)
7810   'MVOLTS(1) = MVTS1
7830   GOSUB 2720
7840   IF VINFLAG <> 0 THEN GOTO 7890
7850   TINC = TIMER - T0
7860   IF TINC <= 0 THEN GOTO 7890
7870   LOCATE 17, 57: PRINT "Current rate ="; (STRAIN - STRN0) / TINC * 360000!
7880   STRN0 = STRAIN: T0 = TIMER
7890   IF STRAINRATE * (newstress - STRESS) <= 0 THEN ENTERFLAG = 3
       IF STRAINRATE * (FINALSTRAIN - STRAIN) <= 0 THEN ENTERFLAG = 3
7900 WEND
7910 TIMER OFF
7920 IF ENTERFLAG = 1 THEN GOSUB 8000: GOTO 7740    'adj. rate
7960 GOSUB 3880                                     'stop motors
7970 IF ENTERFLAG = 2 THEN GOTO 890                 'return to home
7980 GOTO 2040                                      'hold stress
7990 '
8000 '******* adjust voltage for constant rate *****
8010 '
8020 GOSUB 4470                      'get current readings
8030 TIMER OFF
8040 IF ABS(STRAIN - STRTSTRAIN) < .0005 THEN GOTO 8060
8050 MVOLTS(1) = MVOLTS(1) * STRAINRATE / 360000! / (STRAIN - STRTSTRAIN) * DELT
8060 STRTSTRAIN = STRAIN
8070 RETURN

     '*****************************************************************
8500 '*****************  Ideal Sample Disturbance Simulation  **********
     '*****************************************************************

     CLS : GOSUB 4463
     Row = CSRLIN + 1
     COLOR 0, 7: LOCATE Row, 11
     PRINT "Sampling Disturbance PARAMETER SELECTION"
     COLOR 3, 8
     PRINT
     PRINT "This algorithm will apply one cycle of undrained loading at"
     PRINT "  constant strain rate between the specified strain increment"
     'PRINT "Please verify the following values"
     PRINT "  and then return the state of stress back to the hydrostatic"
     PRINT "  condition. Control will then proceed to the hold stress routine"
     'RINT "If these values are not correct you must modify the initial"
     'RINT "   specimen dimensions in the setup program"
8510 LOCATE 19, 10: PRINT SPACE$(50)
     LOCATE 19, 10: INPUT "Is it okay to continue (yes or no) ", a$
     IF a$ = "no" THEN GOTO 890
     IF a$ <> "yes" THEN GOTO 8510
8520 FOR i = Row + 1 TO Row + 9: LOCATE i, 1: PRINT blk$: NEXT i
     LOCATE Row + 3, 1
     PRINT "enter the axial strain rate (%/hr) "
     PRINT "      positive for compression  "
     INPUT "      negative for extension    "; STRAINRATE
     VOLTS = STRAINRATE / 360000! * H0 / DGAIN(1)
     IF ABS(VOLTS) < .05 THEN PRINT "This rate is too slow for the gear setting": GOTO
8530
     IF ABS(VOLTS) > 4.9 THEN PRINT "This rate is too fast for the gear setting": GOTO
8530
     GOTO 8540
8530 PRINT "You must change the rate or return to setup program"
     LOCATE 19, 10: PRINT SPACE$(50)
     LOCATE 19, 10: INPUT "Do you want to change rate (yes or no) ", a$
     IF a$ = "no" THEN GOTO 890
```

```
     IF a$ <> "yes" THEN GOTO 8520

8540 FOR i = Row + 1 TO Row + 9: LOCATE i, 1: PRINT blk$: NEXT i
     LOCATE Row + 3, 1
     PRINT "enter the strain increment for the distrubance cycle  "
     PRINT "      this is the strain based on the current height  "
     INPUT "      the value is in %    "; STRAININC
     ZDISP = DISP              'record the current displacement
     DELTAH = (H0 - DISP) * STRAININC / 100

     '****** prepare to start shearing   *******
     Control!(1) = 2                 'disp control
     Control!(2) = 1                 'stress control
     Control!(3) = 0
     Mode1 = 1
     Mode2 = 0


     STOPDEVICE! = 1                 'keep axial moving
     CLS : GOSUB 4450                'setup screen
     LOCATE 25, 55: COLOR 0, 7: PRINT "Undrained Disturbance"; : COLOR 3, 8
     PTRFLAG! = 1
     DELT = .1 / STRAINRATE * 3600   'sec for .1% strain
     LOCATE 16, 57: PRINT "Target rate ="; STRAINRATE; "%/hr"
     IF DELT > 86400! THEN DELT = 86400!
     STRTSTRAIN = STRAIN
     GOSUB 4290                      'set esc key
     STRN0 = STRAIN: T0 = TIMER
     '
8570 WHILE (ENTERFLAG = 0)           'step one compression
       'MVOLTS(1) = MVTS1
       GOSUB 2720
       IF VINFLAG <> 0 THEN GOTO 8575
       TINC = TIMER - T0
       IF TINC <= 0 THEN GOTO 8575
       LOCATE 17, 57: PRINT "Current rate ="; (STRAIN - STRN0) / TINC * 360000!
       STRN0 = STRAIN: T0 = TIMER
8575   IF (ZDISP + DELTAH - DISP) <= 0 THEN ENTERFLAG = 3
     WEND
     TIMER OFF
     IF ENTERFLAG = 1 THEN GOSUB 8610: GOTO 8570    'adj. rate
     IF ENTERFLAG = 2 THEN GOSUB 3880: GOTO 890     'stop motors and return to home
     ENTERFLAG = 0
     STRAINRATE = -STRAINRATE                       'reverse axial motor

8580 WHILE (ENTERFLAG = 0)                          'step two extension
       'MVOLTS(1) = MVTS1
       GOSUB 2720
       IF VINFLAG <> 0 THEN GOTO 8585
       TINC = TIMER - T0
       IF TINC <= 0 THEN GOTO 8585
       LOCATE 17, 57: PRINT "Current rate ="; (STRAIN - STRN0) / TINC * 360000!
       STRN0 = STRAIN: T0 = TIMER
8585   IF (ZDISP - DELTAH - DISP) >= 0 THEN ENTERFLAG = 3
     WEND
     TIMER OFF
     IF ENTERFLAG = 1 THEN GOSUB 8610: GOTO 8570    'adj. rate
     IF ENTERFLAG = 2 THEN GOSUB 3880: GOTO 890     'stop motors and return to home
     ENTERFLAG = 0
     STRAINRATE = -STRAINRATE                       'reverse axial motor

8590 WHILE (ENTERFLAG = 0)           'step three return to starting strain
       'MVOLTS(1) = MVTS1
```

```
      GOSUB 2720
      IF VINFLAG <> 0 THEN GOTO 8595
      TINC = TIMER - T0
      IF TINC <= 0 THEN GOTO 8595
      LOCATE 17, 57: PRINT "Current rate ="; (STRAIN - STRN0) / TINC * 360000!
      STRN0 = STRAIN: T0 = TIMER
8595  IF (ZDISP - DISP) <= 0 THEN ENTERFLAG = 3
    WEND
    TIMER OFF
    IF ENTERFLAG = 1 THEN GOSUB 8610: GOTO 8570    'adj. rate
    IF ENTERFLAG = 2 THEN GOSUB 3880: GOTO 890     'stop motors and return to home
    ENTERFLAG = 0
    STRAINRATE = -STRAINRATE * LODE / ABS(LODE)    'set strainrate direction

8600 WHILE (ENTERFLAG = 0)            'step four return to hydrostatic stress
      'MVOLTS(1) = MVTS1
      GOSUB 2720
      IF VINFLAG <> 0 THEN GOTO 8605
      TINC = TIMER - T0
      IF TINC <= 0 THEN GOTO 8605
      LOCATE 17, 57: PRINT "Current rate ="; (STRAIN - STRN0) / TINC * 360000!
      STRN0 = STRAIN: T0 = TIMER
8605  IF (LODE * STRAINRATE) >= 0 THEN ENTERFLAG = 3
    WEND
    TIMER OFF
    IF ENTERFLAG = 1 THEN GOSUB 8610: GOTO 8570    'adj. rate
    IF ENTERFLAG = 2 THEN GOSUB 3880: GOTO 890     'stop motors and return to home
    GOTO 2044                                      'hold stress
    '
8610 '******* adjust voltage for constant rate *****
    '
    GOSUB 4470                      'get current readings
    TIMER OFF
    IF ABS(STRAIN - STRTSTRAIN) < .0005 THEN GOTO 8620
    MVOLTS(1) = MVOLTS(1) * STRAINRATE / 360000! / (STRAIN - STRTSTRAIN) * DELT
8620 STRTSTRAIN = STRAIN
    RETURN

    '*****************************************************************
9000 '****************** CAVITY PRESSURE REDUCTION ********************
    '*****************************************************************

    CLS : GOSUB 4463
    Row = CSRLIN + 1
    COLOR 0, 7: LOCATE Row, 11
    PRINT "Cavity Pressure Reduction PARAMETER SELECTION"
    COLOR 3, 8
    PRINT
    PRINT "Please switch pore control motor to cavity control motor"
    INPUT "Press ENTER to continue"; a$
    PRINT "Please switch pore pressure transducer to cavity pressure transducer"
    INPUT "Press ENTER to continue"; a$
    INPUT "Please enter Calibration Factor for cavity pressure transducer"; CFPORE
    INPUT "Please enter Zero Value for cavity pressure transducer (v/v)"; ZPORE
9010 LOCATE 19, 10: PRINT SPACE$(50)
    LOCATE 19, 10: INPUT "Is it okay to continue (yes or no) ", a$
    IF a$ = "no" THEN GOTO 890
    IF a$ <> "yes" THEN GOTO 9010
9015 FOR i = Row + 1 TO Row + 9: LOCATE i, 1: PRINT blk$: NEXT i
    LOCATE Row + 3, 1

    CLS : GOSUB 4463
    Row = CSRLIN + 1
```

```
     COLOR 0, 7: LOCATE Row, 11
     PRINT "Cavity Pressure Reduction PARAMETER SELECTION"
     COLOR 3, 8
     PRINT
     PRINT "Please switch specimen volume transducer to cavity volume transducer"
     INPUT "Press ENTER to continue"; a$
     INPUT "Please enter Calibration Factor for cavity volume transducer"; CFVOLDCDT
     INPUT "Please enter Zero Value for cavity volume transducer (v/v)"; ZVOLDCDT
     INPUT "please enter cavity volume (cm3)"; V0
9017 LOCATE 19, 10: PRINT SPACE$(50)
     LOCATE 19, 10: INPUT "Is it okay to continue (yes or no) ", a$
     IF a$ = "no" THEN GOTO 890
     IF a$ <> "yes" THEN GOTO 9017
9019 FOR i = Row + 1 TO Row + 9: LOCATE i, 1: PRINT blk$: NEXT i
     LOCATE Row + 3, 1

     CLS : GOSUB 4463
     Row = CSRLIN + 1
     COLOR 0, 7: LOCATE Row, 11
     PRINT "Cavity Pressure Reduction PARAMETER SELECTION"
     COLOR 3, 8
     PRINT
     PRINT "This algorithm will apply a constant cavity strain rate,"
     PRINT "  hold the cell pressure and axial stress constant"
9020 LOCATE 19, 10: PRINT SPACE$(50)
     LOCATE 19, 10: INPUT "Is it okay to continue (yes or no) ", a$
     IF a$ = "no" THEN GOTO 890
     IF a$ <> "yes" THEN GOTO 9020
9025 FOR i = Row + 1 TO Row + 9: LOCATE i, 1: PRINT blk$: NEXT i
     LOCATE Row + 3, 1
     PRINT "Enter the cavity strain rate (%/hr)"
     PRINT "      posituve for increase"
     INPUT "      negative for reduction"; STRAINRATE

9030 FOR i = Row + 1 TO Row + 9: LOCATE i, 1: PRINT blk$: NEXT i
     LOCATE Row + 3, 1
9035 INPUT "Enter the final cavity strain (%)"; FINALSTRAIN
     NEWVOLSTRN = VOLSTRN
     DEL = FINALSTRAIN - NEWVOLSTRN
     'IF DEL * STRAINRATE < 0 THEN PRINT "stress not compatable with rate": GOTO 9035

     LOCATE 19, 10: PRINT SPACE$(50)
     LOCATE 19, 10: INPUT "Is it okay to continue (yes or no) ", a$
     IF a$ = "no" THEN GOTO 890
     '****** prepare to start shearing   *******
     Control!(1) = 1                 'stress control
     Control!(2) = 1                 'stress control
     Control!(3) = 2                 'strain control
     Mode1 = 1
     Mode2 = 0
     Mode3 = 0

     STOPDEVICE! = 0
     NEWCELL = CELL
     newload = LODE
     NEWBACK = BACK
     INITIALBACK = NEWBACK
     NEWVOLSTRN = VOLSTRN
     INITIALVOLSTRN = NEWVOLSTRN

     CLS : GOSUB 4450                'setup screen
     LOCATE 25, 55: COLOR 0, 7: PRINT "Cavity Pressure Reduction"; : COLOR 3, 8
     PTRFLAG! = 1
```

```
     DELT = .1 / STRAINRATE * 3600   'sec for .1% strain
     LOCATE 16, 57: PRINT "Target rate ="; STRAINRATE; "%/hr"
     IF DELT > 86400! THEN DELT = 86400!
     GOSUB 4290       'set esc key
     'TIMER = 86100
     T0 = TIMER
     Lasttime = T0
     Tadjust = 0
     '
9050 WHILE (ENTERFLAG = 0)
     now = TIMER
     IF now < Lasttime THEN Tadjust = Tadjust + 86400     'add one day
     Deltime = now - T0 + Tadjust
     Lasttime = now
     NEWVOLSTRN = INITIALVOLSTRN + ((Deltime * STRAINRATE) / 360000)
     GOSUB 2720
     'IF VINFLAG <> 0 THEN GOTO 9055
     'IF TINC <= 0 THEN GOTO 9055
     IF Deltime < 1 THEN GOTO 9055
     LOCATE 17, 57: PRINT "Current rate ="; (VOLSTRN - INITIALVOLSTRN) / Deltime *
360000!
9055 IF NEWVOLSTRN * 100 < FINALSTRAIN THEN ENTERFLAG = 3
     WEND
     TIMER OFF
     'IF ENTERFLAG = 1 THEN GOSUB 9060: GOTO 7740    'adj. rate
     GOSUB 3880                                     'stop motors
     IF ENTERFLAG = 2 THEN GOTO 890                 'return to home
     GOTO 2040                                      'hold stress
     '
9060 '******* adjust voltage for constant rate *****
     '
     GOSUB 4470                      'get current readings
     TIMER OFF
     IF ABS(STRAIN - STRTSTRAIN) < .0005 THEN GOTO 9065
     MVOLTS(1) = MVOLTS(1) * STRAINRATE / 360000! / (STRAIN - STRTSTRAIN) * DELT
9065 STRTSTRAIN = STRAIN
     RETURN

10000 'this is the setup routine for the a/d converter

     IF AD1170$ = "N" THEN RETURN    'No card in computer

     OUT AD1170, 60: WAIT AD1170, 1, 1'set the default calibration time
     OUT AD1170 + 1, INTBIT 'load the data format into the 2nd byte
     OUT AD1170, 48: WAIT AD1170, 1, 1 ' lock in the data format loaded
     OUT AD1170, 176: WAIT AD1170, 1, 1 '  begin background calibration
     OUT MUX!, GNDCHANNEL         ' set input to AD1170 to ground
     RETURN

10100 '************ END PROGRAM *********************************

     OUT motors! + 4, 0                       'LOCK MOTORS
     LOCATE 10, 1
     FOR j = 1 TO 10
       PRINT blk$
     NEXT j
     LOCATE 13, 1
     PRINT "Enter 'a' to return to the setup program => "
     PRINT "      'b' to continue running this program =>"
     INPUT " or just press <Enter> to stop program ", Z$
     IF Z$ = "a" OR Z$ = "A" THEN CHAIN "qbsetup3.bas"
     IF Z$ = "B" OR Z$ = "b" THEN GOTO 890
     STOP: END
```